EU COST C13 FINAL REPORT

GLASS & INTERACTIVE BUILDING ENVELOPES

Research in Architectural Engineering Series
Volume 1
ISSN 1873-6033

EU COST C13 FINAL REPORT

GLASS & INTERACTIVE BUILDING ENVELOPES

Edited by Michel Crisinel, Mick Eekhout, Matthias Haldimann, Ronald Visser

IOS PRESS

Published and distributed by IOS Press under the imprint Delft University Press
PRINTED IN THE NETHERLANDS

Publisher & Distributor
IOS Press
Nieuwe Hemweg 6b
1013 BG Amsterdam
Netherlands
fax: +31-20-687 0019
email: info@iospress.nl
www.iospress.nl
www.dupress.nl

ISBN
978-1-58603-709-3

Editors
Michel Crisinel, Mick Eekhout, Matthias Haldimann, Ronald Visser

Contents

Mick Eekhout, Ulrich Knaack, Ronald Visser, Michel Crisinel, Matthias Haldimann
Foreword 3

Michel Crisinel
Scientific Report 5

Working Group 1 – Architecture and Design Integration

Mick Eekhout
'Zappi' Structures And Constructions In 'Blob' Architecture 19

Michael Wigginton
Glass Architecture and the Interactive Building Envelope: Principles and Precedent 27

Working Group 2 – Quality of Interior Space

Marcelo Blasco
Acoustical Performances of Ventilated Double Glass Façades 33

Henk De Bleecker, Marc Zobec, Alberto Franceschet
From Energy Rating towards a more Holistic Approach for the Selection of the most Suitable Advanced Façade System 41

Jan Hensen, Martin Bartak, Frantisek Drkal
Modeling and Simulation of a Double-Skin Façade System 49

Aleš Krainer, Živa Kristl
Harmonization of Optical and Thermal Behaviour of Buildings 57

Aleš Krainer, Jože Peternelj, Živa Kristl, Vito Lampret
Luminous Efficacy Based on Fuzzy Controlled Roller Blind Positioning 67

A. Simonella, A. Franceschet, H. De Bleecker, M. Zobec
Carbon Emissions Calculation for Non-Residential Buildings: Integration of Daylighting Analysis in Dynamic Energy Simulation Software 75

Annemie Wyckmans, Øyvind Aschehoug, Anne Grete Hestnes
Intelligent Building Envelopes – Application in the Field of Daylighting 85

Working Group 3 – Structural Aspects of Glass

Fabrice Bernard, Laurent Daudeville
Is Prestressing Control Possible for Tempered Glass Structures? 95

Martina Eliášová, Sébastien Floury, František Wald
Glass in Contact with Different Inserts 101

Matthias Haldimann
Design of Glass Members – A Critical Review of the Present Knowledge 109

Alexander Kott, Thomas Vogel
Structural Behaviour of Broken Laminated Safety Glass 123

Jørgen Munch-Andersen, Randi Kruse Vestergaard
Proposal for a code calibration procedure 133

Jürgen Neugebauer
To Increase the Residual Bearing Capacity of Glass with a Local Reinforcement 141

Frank Schneider, J.-D. Wörner
Inelastic Material Behaviour of Soda-Lime-Silica Glass 149

Jens Schneider
Glass Strength in the Borehole Area of Annealed Float Glass and Tempered Float Glass 157

Jan Belis, Rudy Van Impe
Buckling-related problems of glass beams 169

Ruth Kasper, Gerhard Sedlacek
Stability of Laminated Glass Beams 177

Klaus Kreher
Contribution to the Use of Reinforced Glass Loaded on its Strong Axis 189

Andreas Luible, Michel Crisinel
Stability of Load Carrying Elements of Glass 195

Peter Hof, Jens Schneider
Fastening of Glass Panes with Undercut Anchors – FEA and Experimental Investigations 209

Ruth Kasper, Gerhard Sedlacek
Point Bearing Elements – Research Investigations 215

Jürgen Neugebauer
Pre-design of Discretely Supported Glass under Uniform Loading with the Help of Interpolation 221

Frank Wellershoff, Gerhard Sedlacek
Glued Joints in Glass Structures 229

Charalambos C. Baniotopoulos, Konstantinos T. Chatzinikos
Glass Façades of Mid-rise Steel Buildings under Seismic Excitation 239

Mick Eekhout
Design, Engineering, Production & Realisation of Glass Structures for 'Free-Form' Architecture 247

Rudolf Hess
Glass Canopy for the Office Center of the DZ Bank in Berlin 255

Wilfried Laufs
All-Glass Staircase, Notting Hill, London 265

Hans Schober, Hannes Gerber, Jens Schneider
Glass House Badenweiler 271

Olavi Tenhunen, Sini Uuttu, Aki Vuolio
Designing Double Glazed Façade Constructions 277

Ture Wester
Shaping Glass Plate Structures 287

Philip Wilson
Construction Practice in Glass Structures 295

APPENDIX

Working Group 3 Activity Report 303

EU COST C13 Glass and Interactive Building Envelopes. M. Crisinel, et al. (Eds.). IOS Press, 2007.

Foreword

The main objective of the COST Action C13 was to increase the knowledge of properties and possibilities of glazing in order to increase the performance of building envelopes, to reduce the energy consumption and to improve the quality of life with respect to interior space, impact on the environment and human welfare.

This collection of papers presented at meetings and workshops of the COST C13 working groups 1 (Architectural Aspects and Design Integration), 2 (Quality of Interior Space) and 3 (Structural Aspects of Glass) are the result of 5 years of exchange of ideas, experiences and know-how between members, delegates and experts. It represents the body of knowledge from a restricted but representative group of professionals in Europe on the subject of glass building envelopes.

The Steel Structures Laboratory at Ecole Polytechnique Fédérale de Lausanne (CH) and the research group 'Façades' of the faculty of Architecture at Delft University of Technology (NL) have taken the initiative to publish these COST C13 papers in order to disseminate the knowledge to the world of glass façade professionals and to contribute to the development of a new generation of high-performance glass building envelopes.

One of the main conclusions of COST Action C13 is that the three worlds of Architecture, Building Physics and Structural Engineering are today by far not sufficiently integrated. Additional efforts are clearly required to align these three worlds into a holistic entity that is able to design building envelopes that are optimised with regard to all three points of view.

The reader is encouraged to read the separate articles, to reflect on the content and to contribute to the future development of innovative building envelopes by writing novel contributions in the field. Preferably these contributions are interdisciplinary and try to integrate all facets of the subject, from fundamental research topics via technology development issues through to the application in architecture. All of these domains are supposed to stimulate each other rather than living apart together.

Delft, August 2006

Prof. Dr. Mick Eekhout, Prof. Dr. Ulrich Knaack, Ronald Visser
Delft University of Technology, the Netherlands

Lausanne, August 2006

Michel Crisinel, Matthias Haldimann
Ecole Polytechnique Fédérale de Lausanne (EPFL), Switzerland

EU COST C13 Glass and Interactive Building Envelopes. M. Crisinel, et al. (Eds.). IOS Press, 2007.

Scientific Report

Michel Crisinel, Chairman COST C13 WG3
Ecole polytechnique fédérale de Lausanne (EPFL)
Steel Structures Laboratory (ICOM) CH-1015 Lausanne, Switzerland

I. WORKING GROUP 1 ARCHITECTURE AND DESIGN INTEGRATION

The main activity of Working Group 1 of COST Action C13 was dedicated to consideration of the design processes involved in interactive building envelopes made of glass, in the functional design of the facade as well as the overall architectural implications of glazed facades on the local environment.

Presentations were made during the working group meetings by members, delegates and experts on topics that can be classified in three categories: design methodology, case studies and smart materials. This report comprises the original programme of the working group as described in the Technical Annex of the Memorandum of Understanding for Working Group 1 and the list of the papers reflecting the work of the group during the action period.

The programme described in the technical annex of the *Memorandum of Understanding* for the Working Group 1 was very ambitious and consequently not followed strictly. Here are some extracts from the programme.

(...) « It can be said safely that the rapid development of glass has not allowed architects to gain experience and to analyse the possibilities thoroughly. Consequently, there is a need to establish a databank of examples of glass buildings – individual buildings or galleries and atriums covering public or semi public urban spaces, glass walls as protection against noise, wind, etc. – to evaluate and discuss their architectural quality and their visual impact on the surroundings. Modern glass buildings may stand individually or as parts of existing urban environments. Often these buildings are located in old, sometimes even historical urban areas where the urban architecture is vulnerable to the special architectural properties of glass buildings. Typical areas of cities where glass buildings are located should be studied and recorded, and criteria for the different kinds of settings and the architectural expression of different types of glass buildings should be established. The purpose of this is to establish architectural guidelines for the use and design of glass buildings, to develop appropriate methods of architectural evaluation and to disseminate the experience gathered concerning glass building envelopes for new applications. »

TABLE 1:
FINAL REPORT PAPERS WG1

Mick Eekhout
‘Zappi’ Structures And Constructions In ‘Blob’ Architecture
Michael Wigginton
Glass Architecture and the Interactive Building Envelope: Principles and Precedent

II. WORKING GROUP 2
QUALITY OF INTERIOR SPACE

The main activity of Working Group 2 of COST Action C13 was dedicated to give answers concerning building performance and comfort aspects in buildings with glass facades

Presentations were made during the working group meetings by members, delegates and experts on topics that can be classified in the two above mentioned categories: building performance and comfort aspects. This report comprises the original programme of the working group as described in the Technical Annex of the Memorandum of Understanding for Working Group 2 and the list of the papers reflecting the work of the group during the action period.

The programme described in the technical annex of the *Memorandum of Understanding* for the Working Group 2 was very ambitious and consequently not followed strictly. Here are some extracts from the programme.

(...) « In order to improve the comfort of the occupants by an increase in the quality of interior space and optimisation of natural resources, it is necessary to conceive of a building with an "interactive" envelope. The control over these natural resources is dependent upon building usage and results in a minimisation of the resources used for construction, maintenance and demolishing. This can be done by means of the tools for Life Cycle Analysis that is presently dealt with all over the world. The term "interactive" building implies an "interactive" building envelope. There must be numerous further developments in order to establish the "interactive" envelope concept:

– definition of spatial, social and environmental problems,
– definition of the type of construction (renovation or new construction),
– definition of physics and energy problems,
– definition of building automation, which includes the "interactive" envelope.

These developments will result in the formulation of theoretical models that integrate notions of energy and building automation, as well as space, comfort and environmental impact, while permitting the conception and analysis of a basic "interactive" building envelope.

The foreseeable technological advances is further improvement of the thermal insulation of glass, smart glazing with adjustable transmissivity, and integration of solar cells in the glass envelope. Also transparent insulation material will become available soon. These new technologies will greatly improve the possibilities to create glazed building envelopes with low environmental impact and high comfort, contributing significantly to the possibilities of ensuring good quality of life.

Mechanical solar shading will presumably still be one of the major issues when attempting to reduce the need for cooling. The development of simple but effective systems will therefore be of great importance.

Research is needed both to improve the technologies on their own but especially in developing concepts for building envelopes where the properties of glass are used in the optimal way, with respect to both economy and environmental impact on a life cycle basis. Future developments must not increase the life cycle energy consumption, and neutral waste products with respect to environmental impacts must be ensured. The concept of double skin envelopes is already being used, but the potentials need to be further investigated, together with other concepts, perhaps not yet invented.

Promotion of daylight conscious building design has large energy saving potentials through greater utilisation of natural light. Such fenestration systems should seek to cover visual, architectural and environmental aspects. Utilisation of daylight in new and exciting buildings can aggregate large electric saving potentials in all types of buildings and thereby reduce the need for active cooling.

Test, evaluation and development of different innovative systems for daylight utilisation and solar control should be subject to massive R&D over the coming years. It is important that the new glazing and window technologies do not conflict with user requirements. As existing knowledge about user preferences is very limited, this area clearly needs to be refined. Links to the ongoing European research programmes will be ensured.

High insulating glazing suffers from outside condensation during cold nights and cold bridges that form along the edges of the glazing. These phenomena need to be solved in order to improve the utility value of the windows.

Furthermore, it should be insured that the extensive use of glazed facades does not cause noise problems inside the building. »

TABLE 2:
FINAL REPORT PAPERS WG2

Marcelo Blasco
Acoustical Performances of Ventilated Double Glass Façades
Henk De Bleecker, Marc Zobec, Alberto Franceschet
From Energy Rating towards a more Holistic Approach for the Selection of the most Suitable Advanced Façade System
Jan Hensen, Martin Bartak, Frantisek Drkal
Modeling and Simulation of a Double-Skin Façade System
Aleš Krainer, Živa Kristl
Harmonization of Optical and Thermal Behaviour of Buildings
Aleš Krainer, Jože Peternelj, Živa Kristl, Vito Lampret
Luminous Efficacy Based on Fuzzy Controlled Roller Blind Positioning
A. Simonella, A. Franceschet, H. De Bleecker, M. Zobec
Carbon Emissions Calculation for Non-Residential Buildings: Integration of Daylighting Analysis in Dynamic Energy Simulation Software
Annemie Wyckmans, Øyvind Aschehoug, Anne Grete Hestnes
Intelligent Building Envelopes – Application in the Field of Daylighting

III. Working Group 3 Structural Aspects of Glass

The main activity of Working Group 3 of COST Action C13 was dedicated to establish the present state of research on glass as a structural element. Presentations were made during the working group meetings by members, delegates and experts on topics that can be classified in four categories: glass (material) strength, design of members, glass connections and applications & systems. They represent the different topics of research ongoing in Europe on glass used as load-carrying members and structures. This report comprises the original programme of the working group as described in the Technical Annex of the Memorandum of Understanding for Working Group 3, the list of the papers reflecting the work of the group during the action period and a conclusion containing a list of future research needs on glass as a structural element.

Keywords: structural aspect, glass material, glass strength, design of members, glass connections, applications, systems

A. Introduction

The general objective of COST C13 WG3 (Structural Aspects of Glass Working Group) was to coordinate the research on glass as a structural element in the field of building envelopes. Secondary objectives were to increase knowledge on glass construction within the group, to prepare a design guide and propose a course on structural glass at a master level.

Initial initiative was to invite members to present the state of knowledge and research in each member country of COST C13. During the first meetings, presentations were made on the following topics:

- Design considerations
- Similarities/differences with steel codes
- Stability of glass elements,
- Connections.

Many other presentations were made on general subjects like: case studies and built examples, current structures, design of glass façades, European standardization, double skin façades, glass and wood in structural glazing, remaining structural capacity, numerical modelling, glass girders, etc. At the end of the action, a list of research needs in the framework of glass as structural elements was established. Thank to the intensive work done during the meetings, several collaborations were initiated between members and groups of researchers that were followed by new research projects.

The papers contained in this report reflect most of the presentations made during the working group meetings. They are classified in four categories:

- Glass (material) strength,
- Design of members,
- Glass connections
- Applications & systems

The following table give the titles and the author's names of the 25 papers.

TABLE 3:
FINAL REPORT PAPERS WG3

Category	Contribution
1 Glass strength (Material)	Bernard Fabrice, Daudeville Laurent (FR) Is prestressing control possible for tempered glass structures? Eliášová Martina, Floury Sébastien, Wald Frantisek (CZ) Glass in Contact with Different Inserts Haldimann Matthias (CH) Design of Glass Members – A Critical Review of the Present Knowledge Kott Alexander (CH) Structural Behaviour of Broken Laminated Safety Glass Munch-Andersen Jørgen, Vestergaard Randi Kruse (DK) Proposal for a code calibration procedure Neugebauer Jürgen (AT) To increase the residual bearing capacity of glass with a local reinforcement Schneider Frank, Wörner J.-D. (DE) Inelastic material behaviour of Soda-Lime-Silica Glass Schneider Jens (DE) Glass Strength in the Borehole Area of Annealed Float Glass and Tempered Float Glass
2 Design of Members	Belis Jan, Van Impe Rudy (BE) Buckling-related problems of glass beams Kasper Ruth, Sedlacek Gerhard (DE) Stability of laminated glass beams Kreher Klaus (CH) Contribution to the use of reinforced glass loaded on its strong axis Luible Andreas, Crisinel Michel (CH) Stability of load-carrying elements of glass
3 Glass Connections	Hof Peter, Schneider Jens (DE) Fastening of Glass Panes with Undercut Anchors – FEA and experimental investigations Kasper Ruth, Sedlacek Gerhard (DE) Point bearing elements - Research investigations Neugebauer Jürgen (AT) Pre-design of discrete supported glass under uniform loading with the help of interpolation Wellershoff Frank, Sedlacek Gerhard (DE) Glued Joints in Glass Structures
4 Applications / Systems	Baniotopoulos C. C., Chatzinikos, K. T. (GR) Glass façades of mid-rise steel buildings under seismic excitation Eekhout Mick (NL) Design, Engineering, Production & Realisation of Glass Structures for 'Free-Form' Architecture Hess Rudolf (CH) Glass Canopy for the Office Center of the DZ Bank in Berlin Laufs Wilfried (DE) All-Glass Staircase, Notting Hill, London Schober Hans, Gerber Hannes, Schneider Jens (DE) Glass House Badenweiler Tenhunen Olavi, Uuttu Sini, Vuolio Aki (FIN) Designing Double Glazed Façade Constructions Wester Ture (DK) Shaping Glass Plate Structures Wilson Philip (UK) Construction Practice in Glass Structures

B. Programme

The programme described in the technical annex of the *Memorandum of Understanding* for the Working Group 3 was very ambitious and consequently not followed strictly. Here are some extracts from the programme.

(...) « A structural study of façades must be initiated through a clear definition of the effects acting on the façade; this would include the determination of load models and a subsequent risk analysis. In the interest of uniformity with the structural design philosophies used for other building components, it will be necessary to outline the ultimate and serviceability limit states for façades. Also the effect that the façade might have on the design of secondary or support elements must be examined.

Other research on the development of probabilistic design models for window systems (glass layers, coatings) will also be indispensable. Design models will allow for a quasi-infinite combination of the various window sub-systems, and also for the direct definition of the global behaviour of a window. Furthermore, the development of new envelope materials, such as glass and carbon fibre composites, possessing physical and mechanical capacities with more potential than those of glass and giving more flexibility to the conception process must be envisioned.

Research on the realisation of the structural support and framework for the façade will also be necessary, as well as the study of tubular, cold formed and cable structures. This also includes the investigation of new, lighter materials that are geometrically flexible, as well as the development of new, more flexible industrial production procedures—especially for steel and aluminium sections. The aforementioned research and development is necessary in order to achieve an "interactive" envelope and to circumvent industrial and construction constraints presently associated with the realisation of façades.

Research must also address new connection methods that will allow for the flexible conception of the façade and structural framework while, at the same time, reducing costs. The focus of this research must be directed towards mechanical connections, friction fastener systems or cast elements—all of which facilitate inspection of the structure and result in increased levels of safety and durability. Furthermore, connections between the building envelope and the structural framework play a crucial role in the conception of façades. Studies are required in order to define the behaviour of these connections, which must be characterised by a maximal capacity to adapt to different geometric forms. The research must define the global behaviour of the connections and the type of material to be used, and determine the local forces in the detail. »

C. Conclusions and Future Needs

Comparison between the list of papers and the initial proposed programme shows that most of the envisaged research topics have been studied in Europe or are under studies at this moment. But it also appears clearly that future research must be conducted, particularly in two directions:

- Towards a better knowledge of the glass material, glass elements and glass structures,
- Towards the development of structural analysis and safety concepts for global systems made of glass acting compositely with other materials.

The discussion concerning the future researches to be conducted in these two directions led to the following, not exhaustive list:

- Lifetime prediction model for load carrying glass structures
- Development of a design concept for glass structures
- Stability: different boundary conditions and the influence of silicon joints, point wise fixings

- Stability: plate buckling behaviour of shear panels made of glass
- Durability of glass structures
- Sustainability of glass structures
- Different supporting systems for glass
- Glued glass connections (point and linear fixing)
- Design concept concerning residual stresses (edge, borehole, surface)
- Long term behaviour of structural load introductions
- Other interlayers than PVB (e.g. Sentry Glass by Dupont)
- Possible stress control during fabrication for the purpose of a quality control
- Use of glass together with other materials (concrete, steel, composite materials)
- Load carrying behaviour of glass in combination with plastic/ductile materials
- Development of composite structural elements made with steel and glass
- Interaction between steel and glass in façades
- Residual resistance of façades
- Extreme loading (impact, explosion, earth quakes) on glass structures or façades
- Special applications: glass floors, glass stair cases, bridges
- Safety concepts for glass structures and perception of safety by users
- Fail safe design
- Application of research results in practice, practical approach to design.

Concerning the dissemination of the results of the WG3 work, two initiatives have been proposed:

- To prepare a design guide for glass structures construction,
- To establish a postgraduate programme for courses on façade engineering.

The provisional table of contents of the design guide is the following:

1. Glass products
2. Load cases
3. Glass strength
4. Stability
5. Connections
6. Special applications
7. Erection on site
8. General design principles
9. Glass structures based on 3D-design
10. Software
11. Normative rules
12. Teaching guide

D. Acknowledgments

The chairman of the Working Group 3 would like to express his gratitude to all the members, delegates, substitutes, guests, hosts and experts who have contributed to the work presented in this report. He would like to thank Dr Stephen Ledbetter, chairman of the management committee of the action COST C13, Wilfried Laufs, chairman of WG3 at the beginning of the action, as well as the three Scientific Officers, Franck Charmaison, Ilias Samaras and Jan Spousta, for their support during the five year action.

A particular thank is due to his two collaborators Andreas Luible and Matthias Haldimann who were in charge of the minutes of the working group meetings and of the production of the present Final Report.

The ***Activity Report*** of COST C13 WG3 is given in Appendix to the present Final Report.

E. References

List of scientific papers written by the members of COST C13 WG3 in connection to the action.

Austria

[Freytag. 2000]
FREYTAG, B., *Glass-Concrete-composite Members*, Proceedings of 3rd PhD Symposium in Civil Engineering, pp. 163-173, Vienna, Austria, 2000.

[Freytag. 2002]
FREYTAG, B., *Glas-Beton-Verbund –Eine Anwendung von Ductal® (UHPC) in der modernen Architektur*, Kolloquium Zement+Beton, Sonderheft 2002.

[Freytag. 2004]
FREYTAG, B., *Glass-Concrete Composite Technology*, Structural Engineer International, Journal of IABSE, Volume 14, pp. 111-114, May 2004.

[Freytag. 2004]
FREYTAG, B., *The Use of UHPC in Composites – Ideas and realisations* Proceedings of International Symposium on Ultra High Performance Concrete, Kassel 2004.

[Leicht und Glasbau, 2002]
Bemessung von Glaskonstruktionen, Institut für Stahlbau, Holtbau und Flächentragwerke, Technische Universität Graz, 2002.

[Neugebauer. 2004]
NEUGEBAUER, J., *Methods to increase the residual bearing capacity of glass*, Proceedings 5th International PhD Symposium in Civil Engineering, pp. 575-580, Delft, The Netherlands, 2004.

[Neugebauer. 2005]
NEUGEBAUER, J., *Broken laminated Glass has a risk of falling down*, Proceedings of International Conference Glass in Building, pp. 109-117, Bath, UK, 7/8 April 2005.

[Neugebauer. 2005]
NEUGEBAUER, J., *A special fixation with which the broken laminated safety glass is prevent from falling down,* Conference proceedings 9th Glass processing days, pp. 105-109, Tampere, Finland, 17-20 June 2005.

Czech Republic

[Eliášová et al. 2003]
ELIÁŠOVÁ, M., WALD, F., SOKOL, Z., *Šroubované přípoje konstrukcí ze skla*, Proceeding 20. česko-slovenské konference „Ocelové konstrukce a mosty 2003“, September 2003, pp. 101-106, Praha, Czech Republic, ISBN 80-01-02747-3.

[Eliášová et al. 2004]
ELIÁŠOVÁ, M., WALD, F., *Pevnost skla v kontaktu s jinými materiály*, Proceeding Česko - Slovenská konference „Experiment ´04“, 14.-16. October 2004, pp. 81-86, Brno, CERM s.r.o., ISBN 80-7204-354-4.

[Eliášová et al. 2005]
ELIÁŠOVÁ, M., FLOURY, S., WALD, F., *Resistance of glass in contact to different materials*, Proceeding “Glass in Buildings ②”, 7/8 April 2005, pp. 89-97, Centre for Window & Cladding Technology, University of Bath, UK, ISBN 18-74-00335-1.

France

[Bernard et al. 2005a]
BERNARD, F., DAUDEVILLE, L., GY, R., *Une mesure des contraintes pour le contrôle en service des structures en verre*, Mécanique et Industries, Vol. 6, No. 1, pp. 55-64, 2005.

[Bernard et al. 2005b]
BERNARD, F., DAUDEVILLE, L., GY, R., *Calcul des contraintes résiduelles dans les zones d’assemblage de plaques en verre trempé,* Instrumentation Mesures Métrologie, Vol. 4, No. 3-4, pp. 89-104, 2005.

[Bernard et al. 2004a]
BERNARD, F., DAUDEVILLE, L., GY, R., *Load bearing capacity of connections in tempered glass structures*, Structural Engineering International, Vol. 14, No. 2, pp. 107-110, 2004.

[Bernard et al. 2004b]
BERNARD, F., DAUDEVILLE, L., GY, R., *La biréfringence du verre : une propriété remarquable pour l’ingénieur*, Photonique, Vol. 16, pp. 46-49, 2004.

[Bernard et al. 2004c]
BERNARD, F., DAUDEVILLE, L., GY, R., *Vers une procédure de contrôle des structures en verre trempé*, Mécanique et Industries, Vol. 5, No. 3, pp. 267-273, 2004.

[Bernard et al. 2004d]
BERNARD, F., DAUDEVILLE, L., GY, R., *La photoélasticité : un moyen de contrôle des structures en verre*, Photomécanique 2004, 4-6 May 2004, Albi, France, 2004.

[Daudeville et al. 2003]
DAUDEVILLE, L., BERNARD, F., GY, R., *Analyse de la rupture des zones de connexion dans les structures en verre*, Congrès Français de Mécanique CFM 2003, 1-5 September 2003, Nice, France, 2003.

[Bernard et al. 2003a]
BERNARD, F., DAUDEVILLE, L., GY, R., *Calcul par Eléments Finis des contraintes résiduelles près des bords et des trous dans les plaques de verre trempé*, Congrès Français de Mécanique CFM 2003, 1-5 September 2003, Nice, France, 2003.

[Bernard et al. 2003b]
BERNARD, F., DAUDEVILLE, L., GY, R., *Prediction of the load bearing capacity of joints in tempered glass structures*, Glass Days 2003, 4-5 November 2003, Eindhoven, The Netherlands, 2003.

[Bernard et al. 2003c]
BERNARD, F., DAUDEVILLE, L., GY, R., *On the design of mechanical joints in tempered glass structures*, Glass Processing Days, 15-18 June 2003, pp. 754-757, Tampere, Finland, 2003.

[Daudeville et al. 2002]
DAUDEVILLE, L., BERNARD, F., GY, R., *Residual stresses near holes in tempered glass plates*, Materials Science Forum, Vol. 404-407, pp. 43-48, 2002.

[Bernard et al. 2002a]
BERNARD, F., DAUDEVILLE, L., GY, R., *Finite element computation of residual stresses near holes in tempered glass plates*, Glass Technology, Vol. 43C, pp. 290-295, 2002.

[Bernard et al. 2002b]
BERNARD, F., DAUDEVILLE, L., GY, R., *Sur le dimensionnement des structures en verre trempé*, Revue Française de Génie Civil, Vol. 6, No. 7-8, pp. 1359-1380, 2002.

[Bernard et al. 2002c]
BERNARD, F., DAUDEVILLE, L., GY, R., *Finite element computation of residual stresses near holes and straight edges in tempered glass plates*, Modelling of Glass Forming and Tempering MGFT 2002, 23-25 January 2002, pp. 234-240, Valenciennes, France, 2002.

Finland

[Mäkeläinen et al. 2002]
MÄKELÄINEN, P., TENHUNEN, O., VUOLIO, A., LINTULA, K., VILJANEN, M., BERGMAN, J., HÄNNINEN, J., ALINIKULA, T., PALMI, P., *Kaksoisjulkisivun suunnitteluohjeet.* Espoo 2003: Helsinki University of Technology, Laboratory of Steel Structures, P.O. Box 2100, FIN-02015 HUT. Publications 26. 166 p. ISBN 951-22-6649-0. ISSN 1456-4327. http://www.hut.fi/Yksikot/Rakennus/Teras/Julkaisut/jsarj.html

[Mäkinen 2002]
MÄKINEN, H., *Korroosiomuodot ja -riskit kaksoisjulkisivujärjestelmissä.* Espoo, 29.11.2002: Helsinki University of Technology, Department of Civil and Environmental Engineering, Laboratory of Steel Structures, Erikoistyö. http://www.hut.fi/Yksikot/Rakennus/Teras/Tutkimus/HM-etyo-mod.pdf

[Tenhunen et al. 2001.1]
TENHUNEN, O., LEHTINEN, T., LINTULA, K., LEHTOVAARA, J., VUOLIO, A., UUTTU, S., ALINIKULA, T., KESTI, J., VILJANEN, M., SÖDERLUND, J., HALONEN, L., MÄKELÄINEN, P., *Metalli-lasirakenteet kaksoisjulkisivuissa, Esitutkimus.* Espoo 2001: Helsinki University of Technology, Laboratory of Steel Structures, P.O. Box 2100, FIN-02015 HUT. Publications 21. 91 p. + appendices 16 p. ISBN 951-22-5528-6. ISSN 1456-4327. http://www.hut.fi/Yksikot/Rakennus/Teras/Julkaisut/jsarj.html

[Tenhunen et al. 2001.2]
TENHUNEN, O., LINTULA, K., LEHTINEN, T., LEHTOVAARA, J., VILJANEN, M., KESTI, J., MÄKELÄINEN, P., *Double skin Facades - Structures and Building Physics*, Glass Processing Days, 18-21 June 2001, pp. 306-310, Tampere, Finland, 2001. ISBN 952-91-3526-2.

[Tenhunen et al. 2001.3]
TENHUNEN, O., LINTULA, K., LEHTINEN, T., LEHTOVAARA, J., VILJANEN, M., KESTI, J., MÄKELÄINEN, P., *Double skin Facades - Structures and Building Physics*, 9th Nordic Steel Construction Conference, Helsinki, Finland. Proceedings book: NSCC 2001 Proceedings, Edited by: Mäkeläinen, P., Kesti, J., Jutila, A., Kaitila, O., pp. 141-148, 2001.

[Tenhunen et al. 2001.4]
TENHUNEN, O., VUOLIO, A., PALMI, P., *Metallilasirakenteet julkisivuissa*, Teräsrakentamisen tutkimus- ja kehityspäivät, 13.-14.6.2002, 7 p., Mikkeli, Mikkelin AMK, 2002.

[Tenhunen 2003.1]
TENHUNEN, O., *Metalli-lasirakenteisen kaksoisjulkisivun materiaalien soveltamiskriteerit.* Espoo 2003: Helsinki University of Technology, Laboratory of Steel Structures, P.O. Box 2100, FIN-02015 HUT. Publications 28. 104 p. + appendices 43 p. ISBN 951-22-6780-2. ISSN 1456-4327. http://www.hut.fi/Yksikot/Rakennus/Teras/Julkaisut/jsarj.html

[Tenhunen 2003.2]
TENHUNEN, O., *Rakenneteknisiä mittauksia kaksoisjulkisivussa*, Rakenteiden Mekaniikka, Vol. 36, No. 2, pp. 41-45, 2003. ISSN 0783-6104.

[Tenhunen et al. 2004.1]
TENHUNEN, O., VUOLIO, A., *Kaksoisjulkisivurakenteiden suunnittelu*, Lasirakentaja, No. 3, pp. 4-13, 2004.

[Tenhunen et al. 2004.2]
TENHUNEN, O., VUOLIO, A., *Kaksoisjulkisivurakenteiden suunnittelu*, Teräsrakenne, No. 1, pp. 38-41, 2004.

[Uuttu 2001]
UUTTU, S., *Study of Current Structures in Double-Skin Façades.* Espoo, 21.8.2001: Helsinki University of Technology, Department of Civil and Environmental Engineering, Laboratory of Steel Structures, Master´s Thesis. 62 p. + appendices 39 p. http://www.hut.fi/Yksikot/Rakennus/Teras/Tutkimus/tproj_mela.htm http://www.glassfiles.com/library

[Vuolio 2001]
VUOLIO, A., *Kaksoisjulkisivujärjestelmien rakennetekniikka.* Espoo 2001: Helsinki University of Technology, Laboratory of Steel Structures, P.O. Box 2100, FIN-02015 HUT. Publications 22. 72 p. ISBN 951-22-5624-X. ISSN 1456-4327. http://www.hut.fi/Yksikot/Rakennus/Teras/Julkaisut/jsarj.html

[Vuolio 2003]
VUOLIO, A., *Structural Behaviour of Glass Structures in Facades.* Espoo 2003: Helsinki University of Technology, Laboratory of Steel Structures, P.O. Box 2100, FIN-02015 HUT. Publications 27. 127 p. + appendices 34 p. ISBN 951-22-6843-4. ISSN 1456-4327. http:// www.hut.fi/Yksikot/Rakennus/Teras/Julkaisut/jsarj.html

Germany

[Kasper 2005]
KASPER, R., *Tragverhalten von Glasträgern,* Dissertation, Shaker Verlag, Heft 55, 2005.

[Kasper et al. 2004]
KASPER, R., SCARPINO, P. SEDLACEK, G., *Saint Venantsche Torsionswiderstände von Querschnitten in Sandwichbauweise,* Bauingenieur 79, Heft 10, S. 167-175, 2004.

[Kasper et al. 2003]
KASPER, R., SEDLACEK, G., *Structural Use of Glass Beams*, Glass Processing Days, 15-18 June 2003, pp. 312-315, Tampere, Finland, 2003.

[Laufs et al. 2002]
LAUFS, W., KASPER, R., SEDLACEK, VÖLLING, W., *Structural Use of Glass – Stress Distribution in tempered glass panels*, 2nd International Colloquium on Modelling of glass – Forming and Tempering 2002.

[Mohren et al. 2001]
MOHREN, R., LAUFS, W., *Neuartige Stahl-Glas-Konstruktionen mit Tragwirkung in der Scheibenebene,* Bautechnik 78, Heft 10, S. 716-723, 2001.

[Platzer et al. 2005]
PLATZER, W., HUBE, W., ADELMANN, W., CRISINEL, M., VOLLMAR, T., *Development of a Glass Facade with Internal Fluid Flow*. In: Proceedings of Glass Processing Days 2005, 17-20 June, Tampere, Finland, pp. 303-307, 2005.

[Schneider et al. 2001]
WÖRNER, J. D., SCHNEIDER, J., *Konstruktiver Glasbau.* Bau-Zeitung, Heft 3, S. 42 – 45, Heft 4, S. 51-54, Heft 5 S. 61 – 63, 2001.

[Wörner et al. 2001]
WÖRNER, J. D., SCHNEIDER, J., FINK, A., *Konstruktiver Glasbau. gs,* ISBN 3540668810. Springer-Verlag, Berlin.

[Schneider et al. 2001]
SCHNEIDER, J., WÖRNER, J. D., *Impact Loading on Glass Panes by Soft Body Impact.* Proceedings 7th Glass Processings Days 2001, Tampere Finland, pp 638., 2001.

[Schneider et al. 2001]
SCHNEIDER, J., WÖRNER, J. D., *Glass Strength of Annealed and Tempered Structural Glass in the Area of Drilled Holes.* Proceedings 7th Glass Processings Days 2001, Tampere Finland, pp 157, 2001.

[Schneider 2001]
SCHNEIDER, J., *Festigkeit und Bemessung punktgelagerter Gläser und stoßbeanspruchter Gläser.* Dissertation (PhD-thesis), Institut für Statik, TU Darmstadt, 2001.

[Schneider 2002]
SCHNEIDER, J., *Gussglas mit Profil. Hochwertige Fassaden aus billigem Profilglas.* Deutsche Bauzeitung (db) Nr. 3/2002, Seite 89-96, 2002.

[Schneider et al. 2002]
SCHNEIDER, J., BOHMANN, D., *Glasscheiben unter Stoßbelastung – Experimentelle und theoretische Untersuchungen für absturzsichernde Verglasungen bei weichem Stoß.* Bauingenieur Nr. 77, H. 12, S. 581 – 592, 2002.

[Schneider et al. 2002]
SCHNEIDER, J., HOF, P., BLOCK, C., *Fastening of Glass Panes with Undercut Anchors. Numerical tempering simulation, experiments, load-bearing capacity.* Proceedings of the 2nd International Colloquium on Modelling of Glass Forming and Tempering (M.G.F.T.), University of Valenciennes, France, 23.01.-25.01.2002, pp.247-254, 2002.

[Schneider 2002]
SCHNEIDER, J., *Glass Strength in the Borehole Area.* Proceedings of the 2nd International Colloquium on Modelling of Glass Forming and Tempering (M.G.F.T.), University of Valenciennes, France, 23.01.-25.01.2002, , pp.224-241, 2002.

[Schneider et al. 2002]
SCHNEIDER, J., HOF, P., *Fastening of Glass Panes with Undercut Anchors.* IABSE Symposium Report - Melbourne 2002, Vol. 86., 2002.

[Schneider 2002]
SCHNEIDER, J., *Façade Structures with Channel Shaped Glass.* IABSE Symposium Report - Melbourne 2002, Vol. 86., 2002.

[Schneider 2004]
SCHNEIDER, J., *Glass Strength in the Borehole Area of Annealed Float Glass and Tempered Float Glass.* International Journal of Forming Processes (IJFP), Special Issue on Glass, Vol. 7, No.4, pp. 523-541, 2004.

[Schneider et al. 2005]
SCHNEIDER, J., SCHOBER, H., KÜRSCHNER, K., *Innovative Applications of Glass in Structures.* Plenary speech at Glass Processing Days (GPD) 2005, Tampere, Finland, 2005.

[Schneider et al. 2005]
SCHNEIDER, J., SIEGELE, K., *Glasecken. Konstruktion, Gestaltung, Beispiele.* ISBN 3-421-03414-1, DVA-Verlag, München, 2005.

[Schneider 2005]
SCHNEIDER, J., *150 Kilo auf Zehenspitzen. Konstruktion von Überkopfverglasungen.* Deutsche Bauzeitung (db) Nr. 6, Juni 2005.

[Schneider 2005]
SCHNEIDER, J., *Auf den Punkt gebracht. Konstruktion punktgehaltener Glasfassaden.* Fachmagazin phase5 Nr. 1, Juni 2005.

[Schneider 2005]
SCHNEIDER, J., *Joseph Paxton - Ingenieurporträt* Deutsche Bauzeitung (db) Nr. 12, Dezember 2005.

[Schober et al. 2003]
SCHOBER, H., SCHNEIDER, J., *Ganzglaskonstruktion Glaspool Cyberhelvetia. Glas als interaktives Medium.* GLAS 04/2003, S.5 – 7, 2002.

[Schober et al. 2004]
SCHOBER, H., SCHNEIDER, J., *Developments in Structural Glass and Glass Structures.* Structural Engineering International, Vol. 14, No. 2, pp. 84-87, 2004.

[Schober et al. 2004]
SCHOBER, H., SCHNEIDER, J., *There – Not there. Structural Glass and Glass Structures.* Proceedings Symposium on transparency in architectural and structural design. Faculty of Architecture, TU Delft, November 2004.

[Schober et al. 2004]
SCHOBER, H., GERBER, H., SCHNEIDER, J., *Ein Glashaus für die Therme in Badenweiler.* Stahlbau Nr. 73, H.11, S. 886-892, 2004.

[Seldacek et al. 2001]
SEDLACEK, G., LAUFS, W., WELLERSHOFF, F., *Reliability Aspects for Glass in Structural Design,* IABSE Report "Safety, Risk and Reliability – Trends in Engineering", pp. 143-147, 2001.

[Sedlacek et al. 2004.1]
SEDLACEK, G., WELLERSHOFF, F., KASPER, R., *Basis of design and codes for glass structures,* Intelligent Publication Limited, Intelligent Glass Solutions, Issue 1-2004, pp. 47-49, 2004.

[Sedlacek et al. 2004.2]
SEDLACEK, G., WELLERSHOFF, F., NAUMES, J., *Development of hybrid steel-glass-beams in respect to structural and architectural criteria,* KICT research report 09-2004, 2004.

[Sedlacek et al. 2004.3]
SEDLACEK, G., WELLERSHOFF, F., KASPER, R., *Basis of design and codes for glass structures,* ISAAG Conference Proceedings Chapter 4, Munich, 2004.

[Wellershoff et al. 2003.1]
WELLERSHOFF, F., STIEF, U., *Lehrter Bahnhof Berlin – Zustimmung im Einzelfall der Glasanwendungen,* Ernst & Sohn Verlag, Heft 1 - 2003, Seite 29-33, 2003.

[Wellershoff et al. 2003.2]
WELLERSHOFF, F., SEDLACEK, G., *Characteristic Strength and Failure Probability of Channel Shaped Glass,* Glass Processing Days 2003, pp. 94-98, Tampere Finland, 2003.

[Wellershoff et al. 2003.3]
WELLERSHOFF, F., SEDLACEK, G., *Glass Pavilion Rheinbach – Stability of Glass Columns,* Glass Processing Days 2003, pp. 316-318, Tampere Finland, 2003.

[Wellershoff et al. 2003.4]
WELLERSHOFF, F., SEDLACEK, G., *Structural Use of Glass in Hybrid Elements: Steel-Glass-Beams, Glass-GFRP-Plates,* Glass Processing Days 2003, pp. 268-270, Tampere Finland, 2003.

[Wellershoff et al. 2003.5]
WELLERSHOFF, F., SEDLACEK, G., *Steel and Glass – Transparency and Openness,* Window Days Rosenheim 2003, pp. 131-135, 2003.

[Wellershoff et al. 2003.6]
WELLERSHOFF, F, SEDLACEK, G., DÜSTER, H., *Bemessungsschubmodul für PVB-Folien in Verbundsicherheitsglas,* Forschungsbericht G 2003/10-06 Lehrstuhl für Stahlbau, RWTH Aachen, 2003.

[Wellershoff et al. 2003.7]
WELLERSHOFF, F., SEDLACEK, G., *Wirtschaftliche Aussteifung von Stahlkonstruktionen mit Glas zur Schubübertragung und zur Erhöhung der Filigranität der Konstruktion,* AIF Forschungsbericht 12474, 19.11.2003.

[Wellershoff et al. 2004.1]
WELLERSHOFF, F., SEDLACEK, G., *Große gläserne Gebäudehüllen,* Cubus Verlag, Fassadentechnik, Heft 1-2004, Seite 14-18, 2004.

[Wellershoff et al. 2004.2]
WELLERSHOFF, F., SEDLACEK, G., *Fassadentechnik, Multifunktionalität als Herausforderung,* Bau Verlag, Metallbau, Heft 2-2004, Seite 16-18, 2004.

[Wellershoff et al. 2004.3]
WELLERSHOFF, F., SEDLACEK, G., KASPER, R., *Design of joint, members and hybrid elements for glass structures,* ISAAG Conference Proceedings Chapter 5, Munich, 2004.

[Wellershoff et al. 2005.1]
WELLERSHOFF, F., SEDLACEK, G., *Glued joints in glass structures,* Proceedings of Glass in Buildings 2; 7-8.05.2005, Bath, UK, pp. 159-168, 2005.

[Wellershoff et al. 2005.2]
WELLERSHOFF, F., SEDLACEK, G., *Employing the glazing for the stabilisation of building envelopes,* Proceedings of Glass in Buildings 2; 7-8.05.2005, Bath, UK, pp. 343, 2005.

[Wellershoff et al. 2005.3]
WELLERSHOFF, F., SEDLACEK, G., *Glued connections for new steel glass structures,* Proceedings of Glass Processing Days 2005, pp. 340-343, Tampere Finland, 2005.

[Wellershoff et al. 2005.4]
WELLERSHOFF, F., SEDLACEK, G., *Stabilisation of building envelopes with the use of the glazing,* Proceedings of Glass Processing Days 2005, pp. 281-283, Tampere Finland, 2005.

[Wurm et al. 2004]
WURM, J., WELLERSHOFF, F., *Glas-GFK-Sandwichplatten im Fassadenbau; Entwurf, Konstruktion und Prüfung von Glas-GFK-Sandwichplatten für den Einsatz als Fassadenelemente,* Glas Architektur und Technik, Heft 2-2004, Seite 44-48, 2004.

The Netherlands

[Nijsse 2003]
NIJSSE, R., *Glass in structures*, Birkhauser, Basel, Switzerland, ISBN 3-7643-6439-4.

[Nijsse 2003.1]
NIJSSE, R., *Tragendes Glass*, Birkhauser, Basel, Switzerland, ISBN 3-7643-6440-8.

[Nijsse et al. 2005]
NIJSSE, R., BOS, F., VEER,F., ROMEIN,T., *The evaluation of the all transparent Pavilion project*, Glass Processing Days, 17-20 June 2005 pp. 396-400, Tampere, Finland, 2005.

[Nijsse et al. 2005]
NIJSSE,R., BOS, F., VEER, F., ROMEIN, T., BELIS, J., LOUTER, C., VAN NIEUWENHUYZEN, E., *Designing and planning the World's Biggest Experimental Glass structure*, Glass Processing Days, 17-20 June 2005, pp. 401-405, Tampere, Finland, 2005.

[Nijsse 2004]
NIJSSE, R., *Special Steel and Adhesively Bonded Connections for Glass Structures*, Structural Engineering International, Volume 14, number 2, May 2004, pp. 104-107, IABSE, Zurich, Switzerland.

Switzerland

[Crisinel 2004]
CRISINEL, M., *Structures en verre – Recherches en cours à l'ICOM-EPFL*. Tracés, No. 17, pp. 14-18, Société des éditions des associations techniques universitaires SEATU, 2004.

[Crisinel et al. 2005]
CRISINEL, M., VOLLMAR, T., HUBE, W., PLATZER, W., *Glass Facade Elements with internal Fluid Flow*. In: Proceedings of Glass in Buildings 2, 7-8 April 2005, pp. 303-311, Centre for Window & Cladding Technology (CWCT), Bath, UK, 2005.

[Haas et al. 2004]
HAAS, Ch., HALDIMANN, M., *Entwurf und Bemessung von Tragelementen aus Glas – Wissensstandsbericht*. Rapport ICOM 493, Ecole polytechnique fédérale de Lausanne (EPFL), 2004. URL http://icom.epfl.ch/publications/pubinfo.php?pubid=493.

[Haldimann 2005]
HALDIMANN, M., *Fracture Mechanics Modelling and time-dependent Reliability of Structural Glass Elements*. In: Proceedings of Glass in Buildings 2, 7-8 April 2005, Centre for Window & Cladding Technology (CWCT), Bath, UK, 2005. URL http://icom.epfl.ch/publications/pubinfo.php?pubid=519.

[Haldimann 2005.2]
HALDIMANN, M., *Flexible, Consistent and Safe Design of Structural Glass Elements*. In: Proceedings of Glass Processing Days 2005, 17-20 June, Tampere, Finland, pp. 515-519, 2005. URL http://icom.epfl.ch/publications/pubinfo.php?pubid=526.

[Haldimann et al. 2006]
HALDIMANN, M., HIRT, M.A., *Extending the Field of Application of Structural Glass Design Concepts*. In: Proceedings of the IABSE Symposium 2006 "Responding to Tomorrow's Challenges in Structural Engineering", 13-15 Sept., Budapest, Hungary, 2006.

[Hess 2004]
HESS, R., *Einführung in den Baustoff Glas, Bemessungshilfen für Vertikal- und Überkopfverglasungen*, Entwurfshilfen für Architekten und Bauingenieure, pp. 115 - 139 Bauwerk Verlag GmbH, Berlin 2004, ISBN 3-934369-03-0.

[Hess 2004]
HESS, R., *Material Glass,* Structural Engineering, SEI Vol. 14, No. 8, pp. 76 - 79.

[Hess et al. 2005]
HESS, R., SCHADOW T., WELLER B., *Glasbau-Praxis in Beispielen,* Bauwerk Verlag GmbH, Berlin 2005, ISBN 3-934369-47-2.

[Laufs et al. 1999]
LAUFS, W., LUIBLE, A., MOHREN, R., *Voruntersuchung zur konstruktiven Typisierung von Gebäudehüllen aus Glas*. Rapport ICOM 403, Ecole polytechnique fédérale de Lausanne (EPFL), 1999.

[Laufs et al. 2001.2]
LAUFS, W., LUIBLE, A., MOHREN, R., *Étude préliminaire sur le verre comme élément de construction dans le bâtiment*. Rapport ICOM 403F, Ecole polytechnique fédérale de Lausanne (EPFL), 2001.

[Laufs et al. 2003]
LAUFS, W., LUIBLE, A., *Introduction on Use of Glass in Modern Buildings*. Rapport ICOM 462, Ecole polytechnique fédérale de Lausanne (EPFL), 2003.

[Laufs et al. 2003.1]
LAUFS, W., LUIBLE, A., CRISINEL, M., *Introduction à l'utilisation du verre comme élément porteur dans les bâtiments*. Construction métallique, No. 2, pp. 15-32, Centre Technique Industriel de la Construction Métallique (CTICM), St-Rémy-lès-Chevreuse, 2003.

[Luible 2002]

LUIBLE, A., *Stability of Load Carrying Elements of Glass*. In: Proceedings of the 4th International Ph.D. Symposium in Civil Engineering, 19-21 September, Munich, pp. 493-498, Springer-VDI-Verlag GmbH & Co. KG, Düsseldorf, 2002.

[Luible 2004.1]
LUIBLE, A., *Stabilität von Tragelementen aus Glas*. Thèse EPFL 3014, Ecole polytechnique fédérale de Lausanne (EPFL), 2004. URL http://icom.epfl.ch/publications/pubinfo.php?pubid=499.

[Luible 2004.2]
LUIBLE, A., *Lasteinleitungsversuche in Glaskanten*. Rapport ICOM 463, Ecole polytechnique fédérale de Lausanne (EPFL), 2004.

[Luible 2004.3]
LUIBLE, A., *Beulversuche an quadratischen Gläsern*. Rapport ICOM 477, Ecole polytechnique fédérale de Lausanne (EPFL), 2004.

[Luible 2004.4]
LUIBLE, A., *Kippversuche an Glasträgern*. Rapport ICOM 478, Ecole polytechnique fédérale de Lausanne (EPFL), 2004.

[Luible 2004.5]
LUIBLE, A., *Knickversuche an quadratischen Glasscheiben*. Rapport ICOM 479, Ecole polytechnique fédérale de Lausanne (EPFL), 2004.

[Luible et al. 2002.1]
LUIBLE, A., CRISINEL, M., *Auf Biegen und Brechen*. tec21 Nr. 12/2002, pp. 29-36, SIA, Zürich, 2002.

[Luible et al. 2002.2]
LUIBLE, A., *Stabilität von tragenden Glaselementen*. In: Informationstagung Stahl und Glas, 19-20. März 2002, ETH Hönggerberg, Zürich, 2002.

[Luible et al. 2004]
LUIBLE, A., CRISINEL, M., *Buckling Strength of Glass Elements in Compression*. Structural Engineering International, Vol. 2, No. 14, pp. 120-125, IABSE, 2004.

[Luible et al. 2005.1]
LUIBLE, A., CRISINEL, M., *Design for Structural Stability of Glass Compression Members*. In: Proceedings of the 4th European Conference on Steel and Composite Structures, 8-10 June, Maastricht, The Netherlands, 2005.

[Luible et al. 2005.2]
LUIBLE, A., CRISINEL, M., *Plate Buckling of Glass Panels*. In: Proceedings of Glass Processing Days 2005, 17-20 June, Tampere, Finland, pp. 476-479, 2005.

[Luible et al. 2005.3]
LUIBLE, A., CRISINEL, M., *Stability of Load Carrying Elements of Glass*. In: Proceedings of the Conference Eurosteel 2005, 8-10 June, Maastricht, Volume B, Paper 172, 2005.

[Luible et al. 2005.4]
LUIBLE, A., CRISINEL, M., *Design for Structural Stability of Glass Compression Members*. In: Proceedings of the Conference Eurosteel 2005, 8-10 June, Maastricht, Volume B, Paper 173, 2005.

[Luible et al. 2005.5]
LUIBLE, A., CRISINEL, M., *Plate Buckling of Structural Glass Panels*. In: Proceedings of Glass in Buildings 2, 7-8 April 2005, pp. 39-48, Centre for Window & Cladding Technology (CWCT), Bath, UK, 2005.

[Luible et al. 2006.1]
LUIBLE, A., CRISINEL, M., *Design of Glass Beams Subjected to Lateral Torsional Buckling*. In: Proceedings of the IABSE Symposium 2006 "Responding to Tomorrow's Challenges in Structural Engineering", 13-15 Sept., Budapest, Hungary, 2006.

[Luible et al. 2006.2]
LUIBLE, A., CRISINEL, M., *Lateral Torsional Buckling of Glass Beams*. In: Proceedings of the 11th International Conference on Metal Structures (ICMS'2006), 14-16 June, Rzeszow, Poland, 2006.

EU COST C13 Glass and Interactive Building Envelopes. M. Crisinel, et al. (Eds.). IOS Press, 2007.

'Zappi' Structures And Constructions In 'Blob' Architecture

Mick Eekhout, Delft University of Technology, the Netherlands

In 1992 I introduced 'Zappi' (Eekhout, 1992) as the yet unknown, fully transparent, structural reliable material for safe structural design in architecture. I have worked in my chair of Product Development in the faculty of Architecture with my staff and students on this topic, which was initiated by the graduation project of Civil Engineering student Rik Grashoff, nowadays alderman in Delft. Since roughly that time I designed numerous experimental glass structures in my design & build company Octatube Space Structures BV. This paper displays the different 'Zappi' techniques that have been developed in the different design, development and research processes and particularly for the architectural 'Blob' designs of late. The listing contains a mixture of realistic short-term design & development projects I supervised in Octatube and the medium/long term research & developments undertaken in the department of Building Technology.

I. Introduction

In 2001 Karel Vollers completed his dissertation 'Twist & Build' (Vollers, 2001), containing simultaneous studies on urban design, architecture, building technology, production design and material research. It all related to twisted facades of buildings. This dissertation was a prime example of 'design by research'. In the mean time the topic of fluid building designs in architecture, also called 'Blob' designs, came into the picture not only in the international architectural magazines but also in real projects at Octatube. The gap between dreaming architects with new digital skills and the building industry with its traditional orthogonal building systems and materials opened progressively. The department of building industry realized it had to start to close the gap by inventing new technologies to realize these 'fluid' designs. Up to then the building industry saw them as 'fluid design nightmares'. We could start by transfer of technology from the nautical and aeronautical engineering industries, where fluid forms always have been very functional. Fluid designs in architecture are more a change in fashion of design, provoked by the possibilities of the new 3D computer design programs. On the faculty of architecture the 'Blob' research group was started with staff members, PhD students and graduates around the many building technical subjects on the realization of 'Blob' designs.

II. Relationship between Fundamental Research & Application Design

For the Design Platform of the TU Delft I proposed a scheme, inspired by the graphs of prof.dr. Guus Berkhout (Berkhout, 2000) displaying the connections between the two extremes of Fundamental Research and Artistic Design. This figure indicates that the intermediate domains of Fundamental Technical Research, Research by Design, Design by Research, and Technical Application Design all have a mutual relationship with their neighbouring domains of fundamental to the left side and application to the right. Each domain, like an arena, has its own laws, set of rules, habits and players.

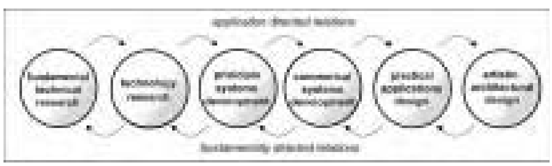

Figure 1: The Relation between Research and Design

III. STRUCTURAL USE OF GLASS

The structural use of glass was one of the items of my work as a scientific designer in the last 15 years of designing, research & development. I have called this quest to unveil and develop ever newer possibilities of using glass as structural components in architectural engineering for the end goal of a structural transparent and unbreakable material and elements and components made of this material: the quest for 'Zappi'. The origin of this quest was the question of the late professor Dick Dicke (1924-2003), my static analysis professor at TU Delft, who asked me during my promotion session in 1989 (Eekhout, 1989) to describe the ideal transparent structural material. As a professor for 4th year students he proposed to design a structure with an imaginary material 'X' having a confusing set of characteristics, derived from those of the well-known materials.

Some 30 years later, in 2002/2003 I have indeed developed a cardboard dome of 28 m span after the design of the Japanese architect Shigeru Ban, taking this 'gingerbread'-principle as a guideline. The quest for Zappi was officially announced in my inauguration as a professor at the TU Delft in 1992 (Eekhout, 1992). In line with our management and marketing dominated times 'Zappi' had a name before it had designer properties and a firm material identity.

In 2001 the 'Zappi' research project was complemented by the 'Blob designing & research' project, which indicates a field of research of 'fluid' designed buildings and more applications of special building components with specific 3D-forms, fitting in the total composition of a Blob building. These Blob designs directly relate to the new 3D-design programs of a select group of avant-garde 'Blob'-architects and designers. They originate from the introduction and use of new computer presentation and design programs like Maya, Rhino, 3D-Studio Max and so on. Within a few hours a skilled computer designer can generate such complex forms of buildings that the collective engineers of the building team have years of work. Understandably these 3D-programs widen the gap between the ambitions and wishes of the architects and the capacities of the largely 2D-producing building industry. The growing gap between these 3D-design programs on the one side and the customary mechanical engineering programs plus the usual, certified production technologies has to be bridged. This is the main goal of the Blob research group at TU Delft under my supervision, existing of post-doc Karel Vollers, 3 PhD students (Martijn Veltkamp, Bige Tunçer and Tuba Kocaturk) and some 10 Master students in Building Technology.

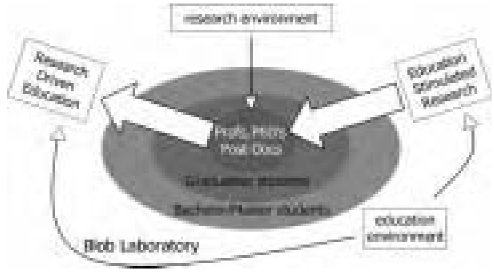

Figure 2: Collaboration research/education in study

The practical design & development projects and issues of my company design office are usually short and medium term directed, although in dialogue with avant-garde technical architects in the Netherlands usually we are amongst the first to pick up a tendency in design and to prepare the material solutions for it. This was the case in space frames in the late 70-ies and frameless glazing in the late 80-ies. In the last 5 years, however, we have turned to the subject of designing building components for Blob designs and we became heavily involved in developing 3D-structures and 3D-claddings, like the GRP stressed skin structures on foam cores for large free spans up to 30m.

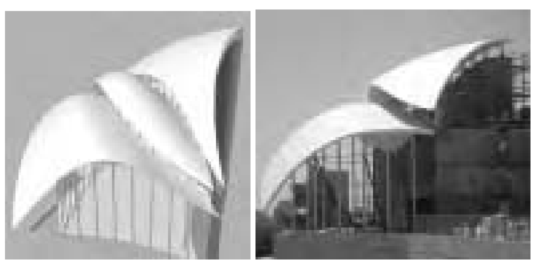

Figure 3/4: The Great Hall of the Rabin Center, Tel Aviv and (right) the Library under construction.

IV. Bending, Compression and Tension Forces in Glass Panels

A. Bending, Compression and Tension Forces in Glass Panels

PhD student Jan Wurm from RHTW Aachen designed, engineered and built as a research fellow on TU Delft in 2002 a prototype of an all-glass dome. He worked with 5 Building Technology students on a frameless glass dome without steel structure or external/internal nodes in a shallow silhouette of 20m span. The detailing was the main point of study. The prototype model was made scale 1 to 5. The connections between the glass panels were made in metal between the joints for the mock-up and the design detail for the full size dome. The detail connection would be primarily based upon the glued connection of the metal strips to the core of the glass panel in the seal area. The actual dome would have insulated glass panels of which the laminated lower panes in heat strengthened glass would have the developed frameless structural connection. The weather seal between the upper panes would ensure the complete water tightness over the structural joint in the sealant area.

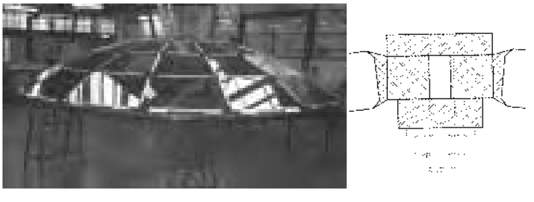

Figure 5/6: Dome scale 1:5 trial erected in the laboratory (left) and detail (right)

B. Bending and twisting in large flexible glass panels

Architects have a tendency to claim visual technical innovations without having an idea on their consequences. Glass panels are designed to be larger and larger. The limitations are restrictions from the production plants, limitations because of deflections by wind and snow loads of ever growing spans and the growing glass thickness and more complicated details. The limitations put forward by the glass industry of 2.140mm width and 3.600mm length of the tempering oven and the lamination autoclave (oven) no longer seem to withhold them to design wider and larger glass panels. Glass panels for one-storey high panels grow to a size of 3.6m length. The initial solution would be to support the 3.6m long panels on l/5th of their spans from both ends (720mm), so that they have a cantilevering scheme. For a width of 1.8 to 2.0m the thickness under 1.0 kN wind pressure would be 10mm. (Fig. 7).

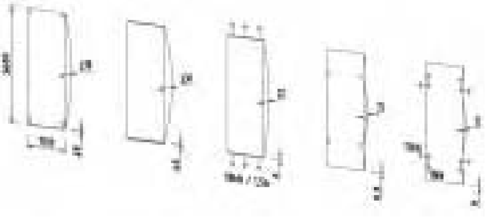

Figure 7: Modes of structural connections and stiffness of one-storey-high glass panels, each 1500mm wide

If on the other hand the span would be a blunt 3.6m in height, the deflection on a 10 mm tick panel would be 200mm, which could be reduced by fixing the panel connectors in the corners, so that in stead of 200 mm deflection, the deflection would only be 50 mm and considerable vertical stresses on the connection points.

An example of a large frameless glass façade without a stiff load bearing sub-structure is the famous Kempinski Hotel in München Airport, designed by architect Helmut Jahn, Chicago. These facades are 30m wide and 12 m high, are filled by panels 1,8x1,8m^2. The load bearing structure is a single pre-stressed cable structure. This structural idea was engineered by Jörgen Schlaich & Partners allowed for large horizontal deflections and special dilatation connection details to the side of the glass façade and the stiff building parts. On some spots due to large deformations, the fully tempered glass panels would get a twisting deformation.

To my knowledge the project never got a building permit, thanks to the cloud of Slaich, but was widely published and copied all over the world.

V. Theoretical Research on New Structural Possibilities of Glass

A. Glass tubular columns

From 1992 onwards this quest for Zappi involved the work of several graduation students in Building Technology at the faculty of Architecture. Most of them were guided by dr. Fred Veer, material scientist in the chair of Product Development. The most exciting work has been done by student Joost Pastunnik in 1998. (Fig. 8). He developed compression tests on laminated tubes of borosilicate laboratory glass. The inner glass tube was loaded under compression. The outer tube was a little shorter, not loaded by compression and acting as the fracture shield of the inner tube. The space between both tubes was filled by clear acrylic resin. From the tests appeared that even fully broken tubes could resist a compression force of 110 kN. They would break and buckle around 120kN. We estimated that a break-through was made in safety engineering of the use of glass ad structural compression elements. After the work of this student the phase of upscaling the columns to real building sizes would follow. We negotiated with Schott and it was a few years later that we learned that Schott found other partners In Germany to follow this line of work. In 2003 Norman Foster realised a building in London using this 'cited' technique. We learned that our principal research had a positive application.

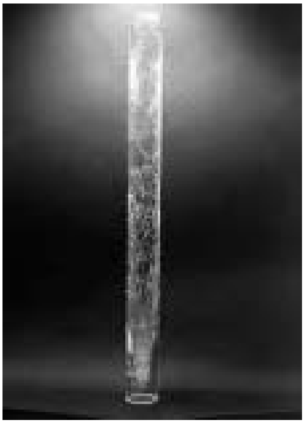

Figure 8: Glass compression test: fully broken inner tube still takes 110KN of compression force

VI. Super Slender Load Supporting Steel Systems

A. The Flying Glass Saucer in Madrid

For a 30m diameter circular roof, designed by New York architect Kevin Roche for the Bancopolis headquarters near Madrid, we designed a radial arrangement of tensile trusses, surrounded by a steel ring of RHS 350x350. The upper and lower rods to be 30mm and post stressed for the required stiffness. The vertical elements in stainless steel as well, although the alternative in glass bars had been offered but was received by the representatives of the client as maybe too experimental for a bank.

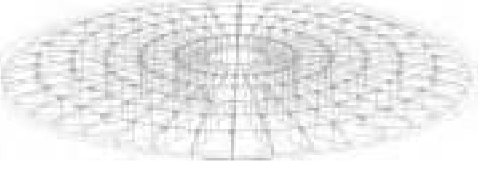

Figure. 9. Drawing of the glass roof of the Bancopolis

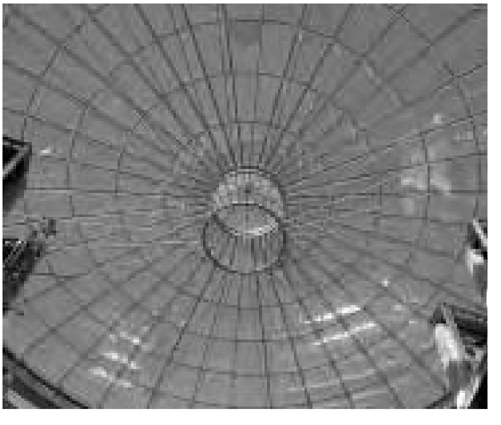

Figure. 10. Photo taken after completion in 2004

Research fellow Li Zhang (Li Zhang, 2002) worked one year on the comparison between glass and steel compression studs in these types of tensegrity arrangements and concluded that glass tubes are perfectly trustworthy structural components. Architect Kevin Roche judged my technical proposals with the stainless steel tubes so favourably ('excellent work') that I did not bother experimenting with glass tubes in order to convince him. (Fig. 9,10).

In the circular roof for a large Spanish Bank near Madrid, designed by 80 years-old architect Kevin Riche from New York, the top had to be filled with an all glass sphere (diameter 3m). Designed to consist of 9 identical insulated glass units, they all had the shape of a spherical segment and smooth curvature all over also on the edges. The fist producer in Holland struggled with the mould for 6 weeks and gave up. The job was reassigned to Cricursa, Spain where they produced the 9 insulated glass units with acceptable deviations from the theoretical model.

VII. Research and Development in Liquid Designs of Buildings

A. *Blob Research Group*

Karel Vollers accelerated further studies as the post-doctorate head of the 'Blob' research group of my chair of Product Development within the department of Building Technology. Yearly some 10 students are joining this master program. In the figures some of the most remarkable studies are represented.

B. *Floating Fluid Pavilion of Sieb Wichers*

One of the Blob graduation students was Sieb Wichers, who designed a shell structure with curved glass in the front (Fig. 13). He developed from a building brief a functional program, a sculptural architectural form that subsequently was translated into a self-supporting structure with an intelligent dual stressed skin structure. The spatial effect of this architectural and technical design is surprising. These students mastered design, drawing, structural design and analysis as well as building technical design. He now calls himself an 'archineer', a contraction of architect and engineer.

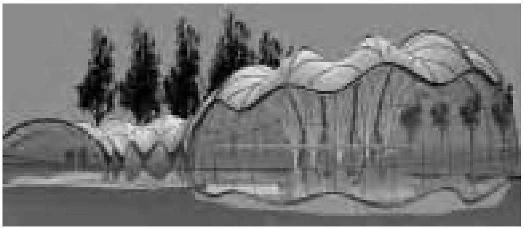

Figure 13: Design of 3D curved glass façades in a fluid pavilion

C. *Glued connections by Barbara van Gelder*

Barbara van Gelder did her final thesis at Octatube and developed a glued connection for a multi-facetted façade. This design was flexible in its corners so that polygonal bodies of buildings could be accommodated. She also did a project with glued nodes in frameless glazing in this same period in Brussels and currently works as the head of the sales department of Octatube and as a design engineer.

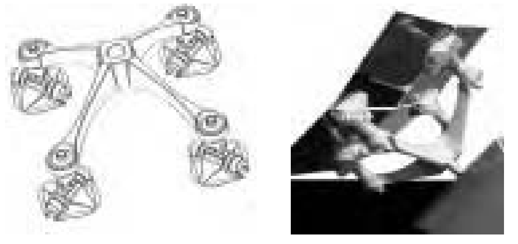

Figure 14/15: Quattro glued-connection developed by Barbara van Gelder

D. *Regularities of cold twisting of glass by Dries Staaks*

The cold twisted double and laminated glass panels in the Town hall of Alphen aan den Rijn (see 10.4) was taken up by TU Eindhoven student Dries Staaks as a point of departure to discover, research and develop the regularities of cold twisting of glass (2003). He discovered that glass panels can be cold twisted elastically, deforming in a symmetrical way into a hypar surface as long as the enforced deformation out-of-plane is less than 16 times the panels' thickness. More twisting will evoke a change of deformation pattern resulting in unidirectional bending along the shortest (stiffest) diagonal axis. (Fig. 16,17). This change in deformation is caused by an instability phenomenon. The double curvature of a twisted plate causes membrane forces: pressure in the middle and tension along the edges. For increase of twisting the membrane forces increase exponentially until the pressure causes the plate to buckle, resulting in the change of deformation. The amount of twisting at which instability occurs proved to be linear related to the panels' thickness, independent of material and size except for the length/width ratio.


Figure 16 Cold twisted glass panels by Dries Staaks (left).

Figure 17.Cold deformation between elastic behaviour and buckling by Dries Staaks (right).

For small amounts of twisting ('plates' thickness) stresses are uniformly distributed. This stress is linear related to the plates' thickness. A thinner plate will cause equally lower stress. For increasing twisting the stress will increase more than linear due to the growing influence of the membrane forces. In general twisted geometries with a deformation up to 10% of the panels' width are possible using pre-stressed glass.

E. Production mould for 3D glass by Kay Verkaaik

The hot deformation of glass panels using a flexible mould usable without materials waste was studied by Building Technology student Kay Verkaaik (2003). He developed a moulding system of parallel axis in a grid with circular saucers on the top which form the desired 3D mould, on which the glass can be heated and deformed and developed the necessary engineering tools for it.

F. Research & development of structural systems for liquid designed buildings

PhD student Martijn Veltkamp works since 2002 on the development of structural systems applicable for liquid designs for buildings. The free form of these liquid designs and the deviations from good professional practice gained from decades of development of lightweight structures (from 1960ies up to 1990-ies). Even the most logical errors that had to be avoided in those days, seem to be more of a standard rule these days. Between these conflicting rules of material efficiency and sculptural 'manierism', Veltkamp will develop new structural systems, for short spans (3 to 10m, for medium range spans 10-50m and for large spans 50 to 100m. A quite impractical but visionary conceptual idea of the London based Auckett architects for using oversized dress dolls as building forms is used as a base for his studies in this moment. (Fig. 20)

VIII. Application Experiments for Liquid Designs in Glass

In the last years a number of 'liquid design' buildings have been realized with typical very complex 3D-geometries and in some of them I was able to experiment with glass applications like:

A. Water pond for the Floriade pavilion

The glass water pond of the municipal Floriade pavilion in 2002, is loaded with 14 kN water weight/m² was originally designed as a 3D-curved frameless glass composition. The glass would have been heated, curved in pairs, chemically prestressed and laminated with epoxy or acrylic resin. Due to time limits it was realized only as flat laminated glass panels; this technical composition was awared with the Du Pont Benedictus Award 2003.


Figure 18: 'Design parallel to model making' to visualize alternatives for the DO Bubble by Auckett Architects

Figure 19: Glass water pond of Floriade building in the Haarlemmermeer

B. Cold bent laminated glass on points supported

In the south side of the same pavilion there are 3 large window glazings, each 6x6m², composed of 9 glass panels of roughly 2x2m². The south windows are flat. The 2 side windows have a large curvature which was attained by cold bending of flat laminated and fully tempered glass panels from their 4 corner connectors by screwing out 2 rubber pushers on the upper and lower edge, fixed on the steel curved steel CHS beam on the inside. Lamination was thought to be a safety precaution against sudden explosion in the face of the workers on the outside when stressing up the panels. No panel broke. The analysis resulted in high bending stresses: up to 50% of the allowable bending stresses. The other 50% were good enough for stresses from wind loading. Thus a system with an economical purchase price and a curvature was realized. The maximum radium to be attained in this way is 4.5m.

Figure 20: Cold bent glass laminated panels in the Floriade building in the Haarlemmermeer

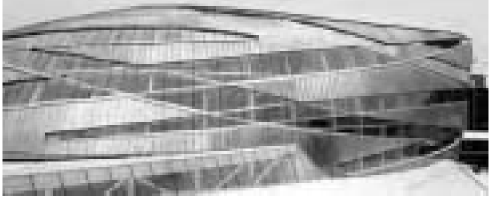

Figure 21: Construction phase of spaghetti facade with cold twisted glass in the Town Hall of Alphen a/d Rijn

C. Cold twisted glass panels in Alphen aan den Rijn

The back part of the town hall of Alphen aan den Rijn had a double curved surface over which glass lintels were designed by the architect EEA. As these glass lintels did not run concentrically, many of the composing glass panels had to be twisted. This was solved by cold twisting of the glass panels on site. Upper and lower profiles were U-channels. The insulated glass panels were maximally 900x2000mm large and consisted of 8 mm outer blade fully tempered and inner blade of also fully tempered 4.4.2. The silicone seals were normal butt seals. The glass was twisted out of its plane maximally 40mm. This work proved to be realizable at very economical costs, with larger risks than normal (300% breaking of panels on site compared to the normal practice). After having completed the job, we wondered what we had done. It took student Dries Staaks one full year to discover and describe the regularity's of cold twisting of glass panels (Fig. 24).

D. Superyacht in London

For a hotel consortium in London naval architect Tim Saunders designed a floating 5-star hotel in the form of a super yacht of 170m length, in the best of the Mediterranean design fashions. The structure will be built on a steel pontoon as a skeleton with steel beams and columns, the hotel rooms will be completely furnished and prefabricated in Dubai and the cladding with 2D / 2.5D-aluminium and 3D-glass fibre reinforced polyester (GRP) panels plus flat glazing (2D), bent glazing (2,5D) and some 3D pieces of glazing are to be made to the latest state of the art by Octatube in Delft. The experiences in 3D cladding deformation, frameless glass structures and bent and twisted glass panels come together in this masterpiece.

Figure 22: Superyacht, design for a five star hotel in London. Rendering by the naval architect: Tim Saunders

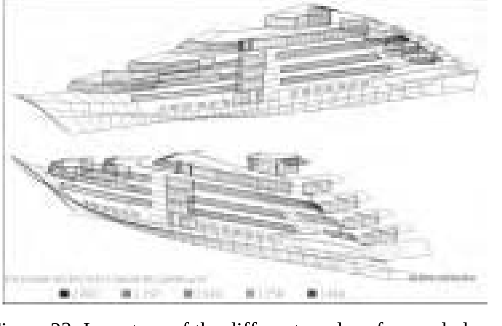

Figure 23: Inventory of the different modes of curved glass.

IX. CONCLUSION FOR THE FUTURE

The more research, developments and designs are made, the more it becomes clear that we do not know enough. The quest goes on. In the case of Zappi, the quest started with a market-directed intriguing description of an unattainable mix of characteristics. In the case of the Blob designs the market provoked us: practising architects dared to throw projects on the market without comprehending or mastering the issues involved that should lead to its realisation. This caused a staggering technology vacuum in which the Blob research group stepped in, to bridge the gap between design & realisation. Yet we must remain vigilant, without an internal cohesion in subject and material the outside and inside world cannot profit much from our research activities. Then, they remain the sole joy of occasional participants of conferences. Therefore our practice projects always depart from design and need research and development to be realised. The idea came up to draw a 'designer fata morgana' for Zappi in the form of a redesign of the former 'Paleis voor Volksvlijt', burned down in Amsterdam 1929, as the most famous of the Dutch glass structures; to be redesigned into a future ambition. The new Guggenheim (Fig. 27) serves a similar purpose.

Safety in design and safety in use are major topics for Zappi, but perhaps the best remedy, for the disease of sterile research is joy in design, joy in performance, vigor and wit.

Figure 24: Design for a New Guggenheim New York. Architect: Frank O. Gehry

REFERENCES

[1] Eekhout, Mick (1992) 'Architectuur tussen traditie en technologie', Publicatiebureau Bouwkunde, Delft, ISBN 9052691134

[2] Vollers, Karel (2001) 'Twist&Build creating non-orthogonal architecture', 010 publishers, Rotterdam, ISBN 9064504105

[3] Berkhout, Guus (2000) 'The dynamic Role of Knowledge in Innovation', Delft University Press Science, Delft, ISBN 9040720770

[4] Eekhout, Mick (1989) 'Architecture in Space Structures', 010 Publishers, Rotterdam, 1989, ISBN 9064500800

[5] Zang, Li, Wardenier, Jaap, Eekhout, Mick (2002) "Analysis of various Types of tensegrity Steel/Glass Roof Structures" and "Analysis of Various Types of Tensegrity Steel Roof Structures in Space Structures 5", Parke, Disney ed., Thomas Telford, London, ISBN 0727731734

EU COST C13 Glass and Interactive Building Envelopes. M. Crisinel, et al. (Eds.). IOS Press, 2007.

Glass Architecture and the Interactive Building Envelope Principles and Precedent

Michael Wigginton

I. Introduction

The issue of whether new architecture will in some way diminish life and culture as it replaces old architecture is a necessary but essentially misplaced consideration. New art has always replaced old art, but generally been able to coexist with it. This is the basis of concerts (although concerts themselves are comparatively new phenomena, as are art galleries).

Buildings pose a problem in that they occupy three dimensional space, are large and are usually owned by the people who also own the land on which they sit. Replacing them has historically been considered to be largely the prerogative of the owner. In the last few hundred years the social aspect of building has led many nations to pass laws about replacement, as well as the construction of something new on a place previously unoccupied by a building. More recently sentiment has added considerations of conservation, which are entirely reasonable: we do not destroy the Bach Magnificat or the works of Beethoven or Mozart simply because Stravinsky and Bartok wrote great works later.

The issue with buildings is different given that two objects cannot occupy the same location at the same time.

Our task then is to determine what we want to keep, which may be an individualwork or a whole contextual environment. However, this too, poses great problems, of land use and functional appropriateness. Where density and constructional appropriateness allow, we do not need to rebuild. The Georgian terrace in Britain exemplifies this.

However, many countries have devised a situation where, in the 20th Century, "natural" evolution and replacement stopped. In the UK the danger is partly addressed by differentiating between conservation, which includes the words "preserve and enhance", and "preservation" on its own. It is accepted that the new can sit next to the old, just as in Cambridge Gibbs Fellows Building of the early 18th century sits next to King's College Chapel completed 200 years before.

Our ideas about sustainability may support the idea of arresting change. It may be argued that the best way of conserving resources is not to continue to build new buildings if old ones suffice. In nations such as the USA this is not a great problem. The old architecture is not very old, and is confined to comparatively small pockets of land. However, in the USA as elsewhere, particularly in developing countries, the idea of technological advance driving architectural change is considered central. The development of technology since the Industrial Revolution has provided opportunities for the improvement of human life that we do not allow old buildings to thwart. To a large degree we can insinuate technology into old buildings: we can rewire them and relight them, and discreetly improve their thermal properties. Wholesale replacement is more socially sensitive, so we have created principles by which we can decide whether a particular building can be replaced or not, and have installed experts to decide the criteria.

This is all comparatively new, and arguments and theoretical positions are now being developed which worry about the large scale freezing of urban contexts as museums: how many Bruges do we want, and what will the people who populate them do other than act as curators? It is in this context that we must worry about the development of new forms of architecture in old cities, with Graz perhaps providing an excellent example in the new project by Peter Cook.

The idea of an epoch creating its own architecture is a founding principle of the so-called Modern Movement which we may, or may not, accept. However, developing technologies, diminishing resources, new materials, new ways of living and working, and new politics, will surely over the next century or more mean the replacement of buildings in very large quantities.

The evolution of glass architecture is simply an example of what needs to be considered. How to consider it, and any other form of architecture is a matter for conjecture. I do not believe this should be by design guides unless these have very short lives. The presumption of the value of expert opinion is too risky. Design guides simply result in more experts dictating more control.

Artists do not refer to Design Guides which remind us of the Nazi and Stalinist dictats on aesthetic taste.

My instinct here is to have faith in people rather than experts, and in technology rather than sentiment, although I accept that such a proposition needs careful argument.

We need to consider the future of the glass interactive facade is in the context of architectural evolution.

II. History

If you want to know where to go, it can help to know how you got to where you are.

People have probably been building, in one form or another, for up to 200,000 years. The history of known architecture and building in the Euro-Mediterranean area (where glass was invented) can be said to go back 5,000 years or more. Progress in tectonics was slow. The Egyptians building at Saqqara in 3000 BC were thought not quite confident enough to risk building stone columns. Although the Egyptians traded in glass objects, the appearance of glass in building does not seem to have occurred until 3,000 years later, 2,000 years ago, being used by the Romans, in greenhouses as well as buildings.

It took a further 1,000 years for the evolution of the idea that flat sheets of glass could be used to create large areas of transparent, light giving, weather shields, perhaps not so necessary in the Mediterranean countries, but very necessary in northern Europe.

Although large sheets of glass were not technically possible in 1100 AD, small blown sheets could be used for domestic windows, and about 250,000 small pieces could be assembled to make up the 300 sq m or so of a window such as the great window at York Minster.

Seen externally, the glass architecture of the Middle Ages was opaque and effectively solid. The elevations of King Henry VII's Chapel at Westminster Abbey built from 1503 to 1509, and Kings College Chapel completed in 1515, show what the real purpose of glass in these very large buildings was: the provision of light and day lit imagery, in places where light and weather protection were both essential.

Glass was an expensive commodity in the first 600 or 700 years of the Second Christian Millennium. A lot of skill and energy was required to make it. In the 1580s in Britain, for example) glass was put in large areas into buildings as a demonstration of wealth. The Client for Hardwick Hall in the middle of England, Elizabeth Countess of Shrewsbury (Bess of Hardwick) owned the forests and coal necessary to fire the furnaces in her own glassworks to make the glass in her palace. The importing of Renaissance symmetry superimposed on an internal organisation which was rather less formally arranged, led to windows being in front of fire places and staircases.

About 100 years later Louis XIV of France became so frustrated with the quality of glass available that he issued a challenge to his own glass technologists to invent a glass strong enough to be located in carriages. Without this sponsored drive, we would not have plate glass, licensed in 1687 to Bernard Perrot. Under the King's patronage the casting tables were moved to Chateau St Gobain in 1693.

The use of glass became much more widespread over the following 200 years, with the builders of domestic and commercial architecture were generally happy with holes in walls filled with glass, preferably opening, and the retailers being naturally drawn to the possibilities of shop windows.

Then idea of using glass to control climate, other than in a rather rudimentary way of keeping the weather out, originates in horticulture. Both the Dutch and British use of glass houses is well documented, but the idea of glass architecture developing from this was an 18th and 19th century creation. The Bicton Glass House in Devon of 1825 (by an unknown designer) and the Great Palm House at Kew by Richard Turner (an Engineer) of 1845 are both early examples, and the Palm House is an Icon.

The Plant Houses embodied the essential ideas which we in COST C13 are now working on. The idea that the control of radiation, the use of mass, with a little help from fossil fuels, could create an indoor climate which replicated a climate from a different place.

Paxton's Crystal Palace was the first great architectural outcome of this horticultural beginning. The Crystal Palace, hailed by Konrad Wachsmann as the building which marks the break between old and new architecture, was only the first great example of many Exhibition buildings in Europe and America which used glass to provide light and enclosure to the great volumes which were built to house the output of the Industrial Revolution, and the means of transporting it.

The idea that glass had some intrinsic aesthetic quality of its own did not appear in an overt way until Paul Scheerbart wrote about it in "Glasarchitektur" of 1914. This book, and the propositions by architects such as Mies van der Rohe and Walter Gropius in the 1920s suggested that a new architecture could be developed with glass at its heart. Unfortunately, they missed a very important point: that glass was just as capable of creating environmentally leaky buildings as buildings which typified modernity, and the transparency of the new socialism.

This defect led to 50 years of insecure evolution in the development of glass architecture, and the all-pervading banality of the glass curtain wall. This was a great shame, because in "Glasarchitektur" itself lay the seed of a new way of thinking about glass, which was taken up (probably unconsciously) in Europe and America, in different ways.

Le Corbusier's Cite de Refuge (Salvation Army Hospital) in Paris of 1931 and George and William Keck's Crystal Pavilion in Chicago of 1934 both embodied the ideas which serve the idea of "Glass and the Interactive Building envelope".

Le Corbusier's building took the idea of the "mur neutralisant" which he had tried in a few domestic projects, and developed the principle of the double wall as the carrier of air to change the interior temperature of the building: warm air in winter and (crucially) cold air in the summer. The idea was to use the comparatively newly invented air conditioning technology to cool air within the cavity of the space. Unfortunately the air conditioning was omitted as a result Of cost savings being necessary, and the building was extremely uncomfortable.

The Keck Brothers work was (in a typically American way) rather more pragmatically derived. The Kecks had realised how hot it got in a glass house in comparatively cold weather if the sun shone through a glass wall, and their great interest in glass led them to use the Crystal Pavilion as an experimental building, using different glasses for different purposes.

It is very sad that the interest shown by a few architects in the 1930s was buried beneath the huge interest in evolving thin, cheap, poorly performing, and easily buildable, (albeit sometimes visually elegant) building skins.

One impact of this was to create uniformity of architecture, independent of climate across the planet, as global communications accelerated the spread of new international style. Another impact was to distort the whole financial balance of buildings as between building services and the building envelope.

It is this issue which COST C13 must address.

III. NEW TYPOLOGIES

The book "Intelligent Skins" set out some of the principles which might inform the evolution of interactive architecture, and also described some Case Studies. The Case Study content of the book is (as was stated in the book) the first stage of a 10 stage programme to investigate the Intelligent Skin, and evaluate its viability. This was intended to avoid value judgements concerning aesthetic, but was guided by the essential aesthetic principal that Form follows Function.

In this brief paper, I will consider three projects which exemplify the type.

A. The Occidental Chemcial Center

This building was designed, and built in 1980, by Canon Design, led by Mark Mendell. It came to light in research work carried out in the early 1980s for the book *Glass in Architecture* into the then current evolution of glass buildings, which identified several buildings which incorporated complex assemblies of glass derived from considerations of climate. The designers put forward several competing designs, and claimed the eventual fully glazed building as the preferred solution in terms of costs and energy consumption. As a paradigm it was usefully located, on the eastern side of the USA with enormously different winter and summer climates. The designers incorporated within the design a self-monitoring system which, in principle, enabled the building to be studied in use. We saw the computers in the basement. During our first visit the building was not behaving quite as the designers expected, but at least the designers were finding out about it. The glazing systems were controlled by cost as well as environmental principle, which is why both the internal and external systems are not double glazed. The environmental systems as incorporated in the double skin are essentially naturally driven, but the hostility of the climate, and the envelope: floor area ratio involve the necessary assistance (as then considered) of plant and energy consuming environmental systems.

B. The Lloyds Building

The Lloyds building was designed by John Young of Rogers Partnership and Tom Barker of ARUP between 1978 and 1982, and completed in 1986. The principles are those set out by Le Corbusier in his Salvation Army Hostel 50 years earlier. The cavity is considered as a “mur neutralisant”, but on this occasion the Architect had the benefit of a sophisticated engineer to devise the environmental system.

C. Duisburg

The Duisburg building was designed by Stefan Behling of Foster and Partners and ARUP between 1988 and 1992. The configuration is significantly different from that proposed for the Occidental Chemical Center and for the Lloyds Building. The cavity is much smaller, and the assumptions about how the exchanges of air and heat are also very different. How these three buildings work in practice in terms of the relationship between their metabolism, their energy consumption, and their delivery of comfort is not published, and may not even be known. Neither is that of most of the other Case Studies considered in the book “Intelligent Skins”. We can probably rely on the fact that the buildings are, in the end, comfortable, and affordable: otherwise they would be empty. However each of them presents an attitude to metabolic effectiveness which is questionable, and unhelpful as we seek to establish the evolutionary potential of the type.

It is for this reason that my colleagues and I are developing ways of considering these sorts of buildings from first principles (ie how to design them), rather than relying on some sort of evolutionary evaluation. Optimisation is the key to this design process, and will be considered by the two other papers in this session.

IV. URBANISM

A. Evolution and functionalism: can we accept glass architecture

The issue of how glass architecture might complement or improve our cities visually and in terms of sensory perception generally is too large an issue to be dealt with in a paper like this.

However, it is generally recognised by all those who have through about the subject that the globalisation of technology considered at a simple level might normalise architecture in a way which would produce the technical and aesthetic equivalent of the loss of biodiversity which is generally considered inimical to the future of the life forms (although this is more metaphorical than real).

The idea of regionalism as a basis for typological differentiation is derived from climate, informed by history and familiarity as well as by economics and resources. One of the benefits of bioclimatic architecture is the variety of architectural form which it can produce. This variety is as implicit in terms of glass architecture, given the advances being made in high technology glasses, as it has been in vernacular architecture.

The development of new bioclimatic paradigms as between (for example) Malaysia, Greece, Middle Europe, and Northern Europe, could be a significant eventual output for any COST C13 outcome. The introduction of nanometric technologies and intelligence may be in competition with the instinct to conserve architectural contexts. History tells which is likely to prevail.

A significant consideration is the nature of bioclimatic architecture, and the impact of the building envelope itself.

Most buildings which were identified in the research work which led to the publication of “Intelligent Skins” were freestanding buildings, with each externally bounding surface operating as the interface between the internal climate and the external climate.

Much city development in the historic European cities is concerned with buildings which share up to 50% of their perimeter with adjacent buildings, and probably have a “front and a back”. Their orientation will be dictated by the existing urban fabric rather than any desire for optimising free environmental exchange. The envelope: floor ratio will be pre-set rather than carefully derived from environmental considerations. The potential benefit of bioclimatic optimisation will be significantly constrained.

In my view we had better let intelligent and sensitive designers evolve solutions one at a time, location by location, rather than try to develop paradigms for city planners or urban designers. We should be Darwinists rather than Stalinists.

This may not be as bland or normative a future as we think. The butterfly's wing and the dichroic coating say otherwise.

EU COST C13 Glass and Interactive Building Envelopes. M. Crisinel, et al. (Eds.). IOS Press, 2007.

Acoustical Performances of Ventilated Double Glass Façades

Marcelo Blasco, Construction Physics and Indoor Climate Department,
Belgian Building Research Institute

Modern Architecture and Ventilated Double Glass Façades (VDGF) are often related with each other: the use of enormous quantities of glass, steel and concrete are essential ingredients. VDGF could be briefly defined as façades consisting of two skins (completely transparent or not) with a very particular ventilation strategy. The acoustical European standard EN 12354 (2000) offers the possibility to predict façade insulation and insulation between rooms inter connected with a cavity. It has been concluded from this study that VDGF have an acoustical façade insulation that is far better (up to 10 dB) than that of traditional façades (office buildings). The special ways of ventilating the building and the 'doubling' of the skin of the façade play an important role. On the other hand due to transmission of sound through the cavity of a double façade, the acoustical insulation between rooms (on different floors) situated at the façade side, is lower compared to buildings with the same internal construction but with no cavity (values up to 8 dB), when no special measures are taken to prevent the (airborne) indirect transmission. To achieve good calculation matches, some modifications were introduced in the standard, i.e. the calculation per frequency band, taking into account either the "Mass-Spring-Mass" or the "Three Rooms model" depending on the frequency band and adaptations concerning free field conditions.

We refer to: www.bbri.be/activefacades.

I. Parameters Of Performances

When determining (simulation) the acoustical performance of a VDGF, one starts from the acoustical performances of the various (constituent) elements measured in the laboratory. By combining these data and applying one or several prediction models, one can (by approximation) do a correct acoustical performance determination. Usually one is interested in knowing what impact changing one of the elements of a façade has on the overall acoustical performances (e.g. changing the outer façade from type A glazing to type B). Mathematical models can provide an answer to this, but (still) only by approximation, since they are prepared for infinite walls and generally do not contain an entirely correct formulation of the various junction points (ref. the new European standard EN 12354) and edge effects. A great deal of research can still be performed here. The question arises whether, with pragmatic resources, one cannot arrive at a range of solutions: this means, on the basis of fundamental acoustical principles and their impact on the overall performances, making a forecast which yields no precise values, but rather a series of results fluctuating between a minimum and maximum value. This could be called a type of preliminary calculation.

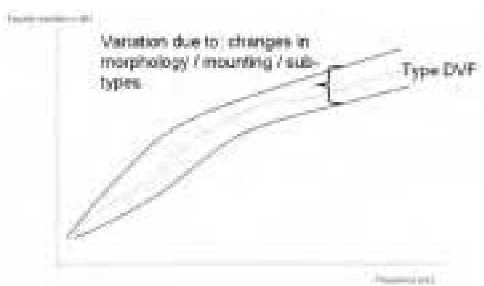

Figure 1

Using the models described further, this kind of evaluation could be implemented. Giving an effective tool for quickly evaluating the mutual impact of different configurations on the acoustical façade insulation. This approach is the next phase in this research, and is very important for approvals and economic studies of façade design.

The acoustical performances will depend on the materials used in the structure and on the configuration (geometrical arrangement) of these parts. The materials used for VDGF will primarily be: glass, steel and concrete. If one wishes to calculate a façade insulation, one bases oneself on measurements performed in the laboratory on the glazings and wall parts. Yet the insulation of these glazings is measured in the laboratory for specific (standard) dimensions according to the standard EN ISO 140-3 (1995). These dimensions are: 1.23 m x 1.48 m. This is small if one compares this with the dimensions used in the practical cases. The fact of using larger dimensions in practice already entails a reduction of the acoustical performances. Other parameters - such as air impermeability of the façade, absorption cavity, flanking (through the construction), user conditions of the inner façade, and so on - will also determine the ultimate performances on-site. Under the acoustical performances of a VDGF can be understood:

- the façade insulation
- the acoustical insulation between rooms located on the active façade side (indirect airborne transmission via the cavity)

II. Acoustical Measurements

A. Overview of some results of measurement campaigns for façade insulation of VDGF

Below we find several acoustical results from a number of measurement campaigns performed by the BBRI within the framework of the Active Façades project (financed by the Ministry of Economic Affairs in Belgium[1]). The most important typologies of VDGF were measured in the areas of acoustics, ventilation, thermal aspects and day lighting.

[1] This project was originally called "Active façades". As the project evolved this name became one of the categories in the typology of VDGF. For the typology of these façades see also our website: www.bbri.be/activefacades.

III. Measurement Campaign 1 (Climate Façade)

A. Measurement campaign 1 (Climate Façade)

The façade element of the measured room includes two modules (2 x 1.5 m width) composed of a glass outer and inner façade. The glass inner façade is hinged and can be opened. In the closed state the inner façade has at the bottom a ventilation slit of 1.5 cm in height over the entire width of the module (the air in the room is extracted via the slit into the cavity and upwards via the false ceiling). The inner façade is only opened for maintenance reasons.

Figure 2: Interior view office
Figure 3: Typology climate façade

volume of room : 50 m³
$D_{ls,2m,n,w}$ (C;C_{tr}) = 38 (-2;-5)dB (inner façade open)
$D_{ls,2m,n,w}$ (C;C_{tr}) = 43 (-2;-5) dB (inner façade closed)
inner façade : single glazing 6 mm
outer façade : double glazing 6-12-8
cavity depth : 12.5 cm

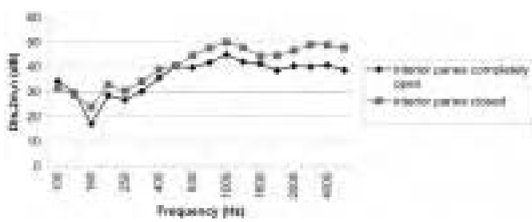

Figure 4: Façade insulation small bureau

B. Measurement campaign 2 (Double Window)

The façade which separates the room from the street side contains a double window. Both windows can be opened. In the measurement campaign a comparison was made between the situation with both windows closed and the situation where the inner window stands completely open. In the completely closed state the inner window has along the bottom a ventilation slit (extraction via the cavity and upwards) with a height of 1.5 cm over the entire width of the window (1.35 m).


Figure 5: Interior view office
Figure 6: Typology Double window

volume of room : 47 m³
$D_{ls,2m,n,w}$ ($C;C_{tr}$) = 41 (-3;-5) dB (inner window open)
$D_{ls,2m,n,w}$ ($C;C_{tr}$) = 47 (-2;-5) dB (inner window closed)
inner window: 10 mm single glazing
outer window: 6-12-8
cavity depth: 7 cm

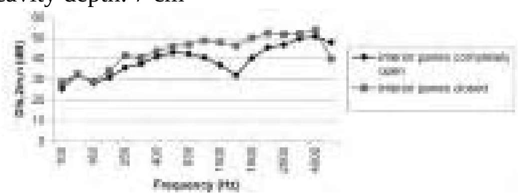

Figure 7: Façade insulation small bureau

C. Measurement campaign 3 (Double façade)

This concerns a façade insulation measurement, expressed in $D_{ls,2m,nT,w}$ ($C;C_{tr}$), of a meeting room on the first storey (V = 93.1 m³). All windows were completely closed.


Figure 8: Interior view cavity
Figure 9: Typology double façade

Volume of room: 93.1 m³
$D_{ls,2m,nT,w}$ ($C;C_{tr}$) = 50 (-1;-5) dB
inner façade: double glazing : 8-12-6
outer façade: single glazing : 6mm
cavity depth: 130 cm

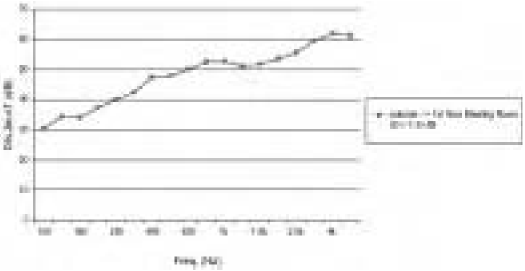

Figure 10: Façade insulation

D. Comparison with traditional façades

In Belgium the average façade insulation for residential construction lies at about 35 dB(A), taking into account the share of glazing, ventilation grid, roof, etc. In office buildings, the requirements for façade insulations (according to NBN S01-400:1977) are identical to those for residences, taking the underlying functions of the room into consideration. The requirements vary from 26 dB(A) to 41 dB(A), depending on the prevailing noise level outside. It is clear that with the use of VDGF one obtains performances which meet the highest requirements of the Belgian standard. It is also evident that the "non-VDGF" demand a thorough acoustical study and effort in order to obtain performances equivalent to those of the VDGF. The acoustical façade insulation of VDGF (based on the measurement campaigns) lies above 43 dB. This can be compared to the acoustical performance of 14 cm of brick (180 kg/m²). The acoustical performance of the double façade (as in measurement campaign 3) of 54 dB corresponds to the acoustical insulation of 14 cm of poured concrete (350 kg/m²) or 19 cm of concrete blocks (285 kg/m²). A typical façade from an office building gives 6 dB less acoustical façade insulation than the poorest performing VDGF. There are quite a few parameters which influence the acoustical performances of a VDGF. These are: type of façade system / type of glass / size of glazed surfaces / properties of receiving room / openings / cavity depth / resonance of one and two layers / source properties Most of these parameters are also applicable to traditional façades. In the extended version of this article, these parameters are more closely looked at.

E. Indirect sound transmission

This concept is important when considering the acoustical insulation between the rooms located on the façade side. It includes the sound which goes from one room to the other via the cavity of the VDGF, especially when the (glass) inner façade can be opened. The impact of this on the acoustical insulation between the rooms is less important between two rooms on the same storey than between two rooms situated above one another. This is because in most cases, with these buildings (generally office buildings), the vertical partition walls are made of light materials, while the floors are made of (heavy) concrete. The light vertical partition walls provide less acoustic insulation, and thus the sound that comes in via the cavity (from the adjoining room) will be less noticeable. Such acoustical insulations are computed by using formulas which are based on the formulas for indirect airborne sound transmission (in analogy with suspended ceilings) via the cavity. Specific formulas for this have been established in the European standard EN 12354-1 (appendix F) (2000):

$$D_{n,s} = D_{n,h} = R_{h,s} + R_{hr} + 10\log\frac{A_h A_0}{S_{hs} S_{hr}} + C_{positiongaps}$$

Ao = 10 m² (reference)

C : depends on the position of the opening relative to one another. If the openings are at a 90° angle to one another and less than 1 m apart, then this term amounts to -2 dB. If the openings are coplanar or further than 1m from one another, then this term amounts to 0 dB. In determining Rhr or Rhs lab data are taken, and the composite insulation has to be taken into account if there are several (different) materials or openings.

F. Measurement campaign F1

For this measurement the indirect transmission was measured, thus including the impact of the cavity for a double façade. Given the volumes of the offices (< 100 m³) we preferred to determine Dn rather than DnT.

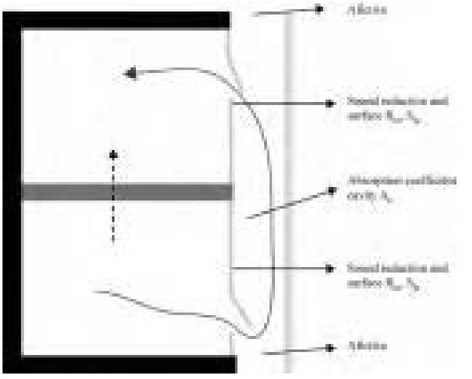

Figure 11

G. Measurement acoustical indirect airborne transmission through the cavity for a double façade

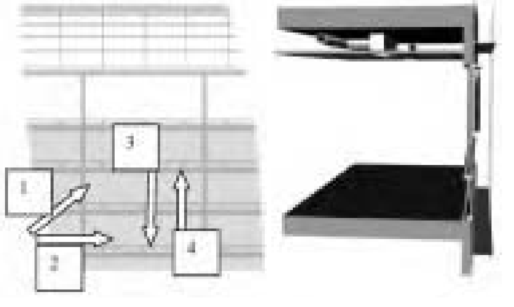

Figure 12: Longitudinal section building
Figure 13: Typology Double Façade

1. $D_{n,s,w}$ (C;C_{tr}) = 56 (-1;-5) dB
2. $D_{n,s,w}$ (C;C_{tr}) = 35 (-1;-5) dB
3. $D_{n,s,w}$ (C;C_{tr}) = 50 (-1;-3) dB / 37 (0;-1) dB
4. $D_{n,s,w}$ (C;C_{tr}) = 49 (-1;-3) dB

inner façade: single glazing 8 mm
outer façade: double glazing 10-12-8
cavity depth: 90 cm

The background noise was also measured in the respective offices (= 28 dB(A)). In the cavity of the double façade the background noise amounted to 44 dB(A). At street level, outside the building, the background noise amounts to values between 65 dB(A) and 70 dB(A).

The most important indirect path between 2 stories is along this cavity. All measurements where undertaken with all windows closed, that is including the windows from the inner façade, except where mentioned.

1) *Discussion measurement 1: Dn,s,w (C;Ctr) = 56 (-1;-5) dB*

This measurement always yields the best results. The direct transmission surface is reduced to one line. Flanking via the vertical walls is very limited since they are disconnected in the vertical direction, in other words there is no vertical continuity, except by the cavity, though here the path through the cavity is longer than for measurements 3 or 4.

2) *Discussion measurement 2: Dn,s,w (C;Ctr) = 35 (-1;-5) dB*

For this configuration, i.e. between offices in the horizontal direction, the impact of the cavity is limited. This is because the vertical walls are light (system) walls. Thus intrinsically they have an airborne sound insulation which is fairly limited. One must also examine whether or not there is a suspended ceiling which connects the two rooms; this can also influence the acoustic insulation. Here this was not the case.

3) *Discussion measurements 3 and 4: Dn,s,w (C;Ctr) = 50 (-1;-3) dB / 37 (0;-1) dB and Dn,s,w (C;Ctr) = 49 (-1;-3) dB*

The results are symmetrical for both from above to below and vice versa. We expect a limitation of the airborne sound insulation due to acoustical insulation losses through the cavity. For the measurement from above to below (measurement 3) we measured the impact of the opening of a window: the opening of a single window in a single office leads to a reduction of 13 dB for the airborne sound insulation. One can expect that the result achieved then corresponds to the airborne sound insulation of one single glazing (8 mm), equal to approximately 32 dB, increased by the screen effect of the cavity, which approximately comes down to an airborne sound insulation of 37 to 40 dB (note: the standard EN 12354-1 appendix F takes this into account with the introduction of the C coefficient).

IV. Application of Standards For The Prediction of the Acoustical Façade Insulation and Indirect Airborne Transmission Compared to the Measurement Campaigns

The acoustic "Eurocode" for façade insulation is the EN 12354-3 (2000). This proceeds from laboratory measurements of the various components in order to determine the façade insulation on-site, taking into account the 3-dimensional character of the façade (projecting parts,...) and any openings in the façade (composite insulation). The problem with this standard is that double-walled systems are not yet implemented; this means that it does not take into consideration the specific properties of a double-walled system (MSM or 3 chamber model). This will be the subject of research in the near future. Yet one should be able to use the standard by regarding the 2 cavity wall skins as being independent and applying the standard separately for each cavity wall skin. This implies that one assumes the 3 chamber model (superposition principle). This will be correct as of the frequency where the 3 chamber model applies.

The European standard EN 12354-1 (annex F) (2000) offers a solution for calculating the indirect transmission. Generally this requirement will not be a limiting factor for the choice of the inner glazing, the façade insulation will be a stricter requirement. However, the positioning of the possible openings in the inner façade is important. The indirect transmission vertically (between rooms on different stories) will be relatively more important than horizontally (between rooms located on the same storey) since the floors display a greater acoustical insulation than the (lighter, movable) partition walls. The following summarizes a number of ideas for applying the model described in EN 12354-3 (2000) and EN 12354-1 annex F. This prediction is compared with the on-site measurements.

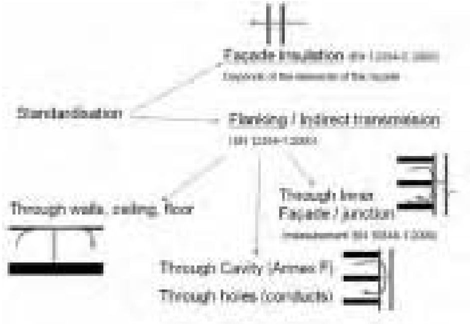

Figure 14

V. Determination In Accordance With EN 12354-3 (2000) for the Façade Insulation

A. Single-number method (calculation is only available in the extended version of this article)

Conclusions: Using the Mass-Spring-Mass model and the 3 Chamber model and direct field conditions we have: A single-number rating is largely determined by the performances in the low frequencies. We thus see that the application of this method with single-number ratings is not precise: this method yields a major overestimation or underestimation of the performances (measured on-site: 45 dB). A spectral approach can yield a more precise result (based on one third octave bands).

B. Spectral method (calculation is only available in the extended version of this article)

Conclusions: Using the Mass-Spring-Mass model and the 3 Chamber model and direct field conditions we have: On-site we had measured 45 dB (for $D_{ls,2m,nT,w}$). The prediction with the aid of the spectral values (= 44 dB) in first instance gives a good and much better approximation than with the single-number ratings alone, because we can make a distinction between the different ways of sound transmission (MSM or 3 chamber transmission). The spectral approach requires more calculation than the single number approach.

VI. Determination in accordance with EN 12354-1 appendix F for indirect airborne transmission (in closed state conditions)

A. Spectral method (indirect airborne transmission through cavity)

Conclusions: The prediction with the spectral method gives a single-number rating: $D_{n,s,w} = 52$ dB. On-site we measured $D_{n,s,w} = 50$ dB. Assembly errors and air leaks can further reduce the performances on-site compared with pre-calculations. This means that one must take this into account when making predictions. In this case, the prediction corresponds well with the measured value if we subtract 2 dB for air leaks and assembly errors. One must take into account a reduction of the performances because of the larger surface areas of the glass (than in the laboratory). This can lead to reductions of 3 dB, and is particularly important when the surface exceeds 10 m². Air leaks between inside and outside additionally lower the insulation (up to 2 dB). The screening effect of the elements that can be opened in the inner façade will play a role in the overall acoustical insulation: thus, two openings which “look” at one another will be less favourable. The sound reduction indices R_h are determined proceeding from the sound reduction indices of the elements from which the wall is composed (composite insulation). The sealant joints are also taken into account with the aid of a sound reduction index. In the case of double façades where longitudinal transmission applies, the cavity (between the inner and outer façade) will spread out over a large number of rooms. In other words, the cavity is not limited to 2 rooms positioned next to one another or above one another. In order to take account of this when determining the indirect transmission through the cavity between 2 rooms, one will have to take into account an additional fictive equivalent absorption surface area.

VII. SUMMARY

We have seen that VDGF perform very well in the field of acoustical façade insulation. Generally no complaints have been heard concerning indirect transmission through the cavity of the façade (only possible for passive or interactive façades). This can be explained due to the fact that these buildings are office buildings, no dwellings. The choice of the type of the façade (active, passive or interactive) depends primarily on the climate conditions of the region. The actual standards permit a good evaluation of the façade insulation and indirect transmission of VDGF. Although more case studies are needed to validate the results. A next step in the research is to evaluate the impact of the frames of the façade on the acoustical façade insulation, the impact of inner junctions and connections in the façade and to model this impact. For this the standards EN 10848 and EN 12354 will be examined, and several tests will be realized in the coming months. Link: *www.bbri.be/activefacades*



From the left to the right:

Figure 15: Bürohaus am Halensee
H. Léon & K. Wohlage, arch.
Passive façade
Germany

Figure 16: Médiathèque Vénissieux
Dom. Perrault, arch.
Passive façade
France

Figure 17: Airport Gardens
KPF & Jaspers/Eyers, arch.
Active façade
Belgium

ACKNOWLEDGEMENTS

We would like to express our gratitude to the Ministry of Economic Affairs of Belgium for financing this study.

REFERENCES

[1] Faist, A.P. La façade double peau. EPFL Architecture Department 1998
[2] Oesterle.Lieb.Lutz.Heusler. Double Skin Façades - 2001
[3] BBRI Construction Physics Department. Jaarrapport Actieve Gevels – MEZ 2001
[4] Vermeir, G. Hogere cursus akoestiek-Bouwakoestiek. KUL. Applied Sciences Department 2000.
[5] Renckens, J. De tweedehuid façade. Adviesbureau Renckens 2000.
[6] Mayerowitz, M. (CEBTP). Performances acoustiques des façades et des couvertures. CATED June 1993

EU COST C13 Glass and Interactive Building Envelopes. M. Crisinel, et al. (Eds.). IOS Press, 2007.

From Energy Rating towards a more Holistic Approach for the Selection of the most Suitable Advanced Façade System

Henk De Bleecker, Senior Engineer, Research and Engineering, Permasteelisa
Marc Zobec, Group Director of Research and Engineering, Permasteelisa
Alberto Franceschet, Project Engineer, Research and Engineering, Permasteelisa

This paper demonstrates how advanced façade systems can comply with energy regulations and advocates for a more holistic approach to the selection of the most suitable façade system based on project specific requirements. The impact of different advanced façade systems on the yearly office energy consumption can be determined by using whole building simulation models. A whole building simulation, applied on an office situated in London, demonstrated that double skin façades are able to deliver easier compliance with the new UK energy regulations compared to the more traditional wall systems. The UK energy regulations have incorporated a carbon emission calculation method, which is a flexible method for demonstrating the compliance of offices build with new building materials or innovative envelope systems. This paper highlights that a lot of national regulations do not have such an appropriate assessment methodology, which therefore forms an obstacle of the development and use of innovative building materials and envelope systems. This paper also warns about issues for performing proper building energy comparison such as the choice of the reference façade, the risk of over-estimating the functionality of specific façade components and the progressive impact of the selection of a façade configuration on other façade performance criteria and costs. Finally, the authors urge researchers to use more holistic approaches for the assessment of the ideal façade system. Façade configurations are rarely optimised for one sole parameter but many - and sometimes conflicting - requirements have to be taken into account, e.g. energy performance; acoustic-visual-thermal comfort; initial costs and long-term maintenance and repair costs; architectural appearance; structural performance; durability of façade components; fire resistance and many more. For every new project with its own specific critical requirements, a decision-making matrix and a prediction tool can be used in order to facilitate the optimisation of the most suitable façade system early in the design process.
Keywords: Advanced Double Skin Façade (DSF); Energy and Carbon Emission Calculation; Compliance with Energy Regulations Part L2, Selection of most suitable façade system, Decision-Making Matrix for different performance criteria

I. Introduction

Within the current architectural trend, there is a significant increasing demand for high transparent façades with glazed elements consisting of clear glass over the full height of the façade, i.e. from floor to ceiling. Conventional façade systems with high transparent glazing and large glass areas can cause the following difficulties: - excessive heating demand during the winter; - overheating of the building and/or high cooling requirements during the summer; - a difference in surface temperature of external and internal walls resulting in discomfort for the occupant placed near the façade, e.g. drafts and asymmetric radiation; - difficulties in demonstrating compliance with ever more stringent energy regulations and comfort requirements. Double skin façade (DSF) technology has been developed that not only allows for high transparency but also can deliver an increased energy performance and positive effects on the indoor comfort compared with façade systems with internal shading devices. The DSF technique is based on providing movable shading devices within a ventilated cavity. The strength of most double skin façade systems is that the façade can be designed to have variable properties so that both solar gain and heat loss through the façade can be optimised by the use of a building management system (BMS). For advanced façades currently no international standard, agreed calculation procedures or benchmarks exist. In order to allow for and encourage new advanced materials and double skin façade constructions for the 21st century, it is necessary to set up internationally agreed assessment methods for the thermal and energy performance prediction. Some design considerations for innovative DSF are highlighted in another paper of the same authors [1]. Detailed finite element analysis tools were applied for different examples of DSF to check the performance criteria under critical steady state environmental conditions. However, it is very difficult to use conventional steady state parameters to predict the overall yearly energy consumption of innovative DSFs. This paper demonstrates how dynamic building simulation tools are more suitable for the prediction of the impact of the advanced façade type on the energy use and carbon emission production of a building. Furthermore, advice is given on how energy calculations can be part of a holistic approach for the selection of the most suitable advanced façade configuration for a specific project.

II. THE IMPACT OF THE FAÇADE CHOICE ON THE YEARLY ENERGY CONSUMPTION OF AN OFFICE ROOM

In order to reduce the national carbon emission produced by buildings, the UK energy regulations for office buildings (Part L2 [2]) has been revised and is now one of the most stringent regulations in Europe. The regulations set acceptable levels of carbon emission for offices and define minimum required performance parameters for typical envelope components (target elemental values). A Notional Wall consists of different façade components with defined target values such as a maximum U-value for windows and panels (2.2 W/m2.K and 0.35 W/m2.K respectively) and a g-value of the glazing (0.70) in combination with a maximum glazed area (limited to 40%). The reduced window area is set as target for the limitation of heat loss in the winter and solar gain in the summer. The Notional Wall is defined as the current good-practice construction. Usually, modern high transparent façades will not comply directly with the required target values mainly because the client usually prefers a higher percentage of glazed area (usually much larger than 40%) for visual comfort. Part L2 has therefore included a Carbon Emission Calculation method, which allows the designers to demonstrate that their proposed façade/building configuration (which might be completely different than the Notional Wall) produces less carbon emission than a building with the same geometrical shape and fitted with the Notional Wall elements. An illustrative assessment of the yearly energy consumption of an office room (see Figure 1), fitted with different façade systems, has been performed for a building situated in London. The energy consumption is calculated using a dynamic building energy model CAPSOL [3] and hourly yearly local weather data (KEW, London) is chosen. The office room has only one external façade (West orientated).

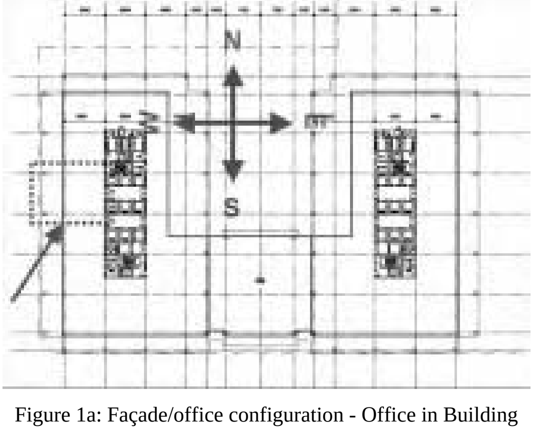

Figure 1a: Façade/office configuration - Office in Building

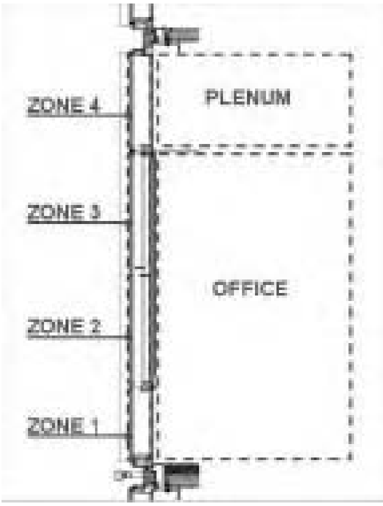

Figure 1b: Façade/office configuration - Wall configuration

The yearly energy consumption of the same room is simulated for various external façade systems:

- A curtain wall with 100% clear glass;
- An Active Wall with 100% clear glass;
- An Active Wall with 100% high performance glazing;
- An Interactive Wall with 100% clear glass.

An additional wall/room configuration is added to this study: the same office room fitted with a Notional Wall consisting of 40% clear glass with a U_g-value of 2.2W/m^2.K (target values of the UK building regulations Part L2). The office fitted with the Notional Wall is therefore also the reference case for this comparative study as it will indicate which façade configuration will give direct compliance with the UK energy regulations.

Although Part L2 allows to trade-off between façade performance and other building elements (such as HVAC system performance), the non-façade elements are kept the same for all different cases in this comparative study. Further, the following input parameters have been assumed: high internal loads (people, PCs, lights), the use of a building management system in which the blinds are down when the solar radiation on the façade exceeds 200W/m2 and the ventilation rate is equal to 2.5ACH during the office hours but turned-off during the night. The influence of available daylight (in direct relation to the percentage of glazed area) on the energy consumption of the room is excluded from this study, although the authors are currently carrying out research in that area [4]. Figure 2 shows the difference in heating and cooling energy consumption of the façade/room configuration in comparison with the reference case. The energy consumption of each room, with the different façade configurations, has been deducted from the energy consumption of the reference office. The latter represents the reference configuration, i.e. the Y=0 line in the graph.

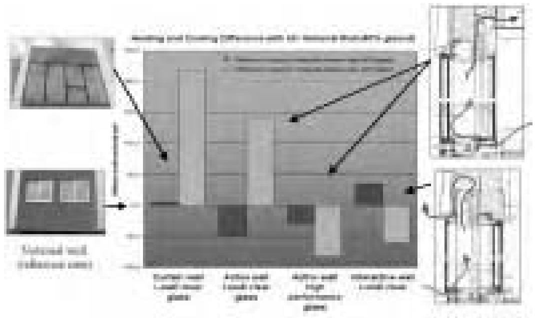

Figure 2: Difference in energy use for heating and cooling compared with reference case (40% glazing)

The following conclusions can be drawn from the above analysis:

- For the room fitted with a curtain wall of 100% clear glass, the heating consumption is nearly identical to the reference room but the energy use for cooling is significantly higher. This is due to the higher glazed area of the curtain wall, resulting in higher solar gain, which is beneficial in the winter but has negative effects in the summer period when a lot of cooling is needed.
- The room configuration with an Active Wall with 100% clear glass has a lower heating demand than the traditional wall with 40% glazing and curtain wall with 100% glazing. This is due to the additional glass pane in the double skin, which gives a higher thermal resistance than the curtain wall with double-glazing. The cooling demand is also less than the curtain wall with 100% glass because a part of the solar energy can be reflected and absorbed by the blinds and extracted via the ventilated cavity in the double skin façade. The energy

needed for cooling is higher than for the reference case (40% glazed wall). In order to achieve compliance with Part L2, higher reflective blinds or effective integration with HVAC can be established.

- An Active Wall® with 100% high performance glass fitted in the same room, results in a lower heating consumption than the reference case and is also successful in terms of reducing the energy consumption for cooling. This demonstrates that it is possible to construct a fully glazed double skin façade and at the same time deliver direct compliance with the UK energy regulations.
- For the room constructed with the Interactive Wall (100% glass), the ventilation in the double skin façade happens from the outside to the outside. The façade is particularly efficient in reducing the solar heat gain and thus also the cooling load. Assuming that the same cavity ventilation rate is used during the whole year (conservative approach as the ventilation is usually switched off during the winter), the heating consumption is higher than for the reference case. However, Part L2 states that a gas burner for heating delivers half of the carbon emission production of an electrical cooling equipment. Thus, the interactive wall can give direct compliance with the UK energy regulations Part L2. This is particularly attractive to architectural practices as complete transparency is achieved by delivering a glazed façade with 100% clear glass.

The above building energy assessment demonstrates that double skin façades can be effective to reduce energy consumption or carbon emission consumption compared with typical conventional façade systems and gives easier compliance with the regulations. It should be clear that for every specific case, an energy assessment should be done as results may differ for other types of façade/building properties, other geographical location, different orientation of the façade, glazing type, ventilation flow

As shown in the above-presented example, the methodology for demonstrating compliance with the UK energy regulations is very flexible and useful for buildings with innovative façades. Unfortunately, other countries prefer to develop Energy Performance Regulations for buildings, which are based on equations using parameters and coefficients for every new developed system. The downfall is that it is nearly impossible to include and update the regulations continuously for every new innovative envelope system that is developed. It might be possible to provide coefficients for dynamic façades with variable properties in time, but it will remain difficult to predict the whole building energy consumption in the same accurate way as dynamic building simulation tools. The industry feels that such simplified methods are not flexible enough and do not encourage the use and development of innovative building envelope systems. The authors feel that preference could be given to the carbon emission calculation method when developing new energy regulations.

III. Critical considerations about façade design for optimal energy performance and influence on other façade performance criteria

In the above energy comparison, it was shown that double skin façades can be beneficial to reduce the whole building energy consumption. However, in the literature, controversial generalised statements and results can be found, ranging from double skin façades are the perfect system for environmental control to double skin façades do not work at all. As highlighted above, an energy assessment ought to be done for every specific façade and building configuration. In this context, such general statements are difficult to justify. Moreover, one needs to be very careful with applying the results from one research to another project case. When interpreting the results of other researchers, all their assumptions should be carefully studied. In the following some common mistakes in energy comparison studies are highlighted.

A. Is the chosen reference façade appropriate for the energy comparison?

Some researchers take the fully glazed (100% glazed curtain wall) as the standard façade configuration for the study of double skin façade configurations. As the above example assessment illustrated, this would lead to the conclusion that all double skin façades result in superior energy performance of the building. Other researchers use a standard curtain wall system with fully external movable shading devices as the reference case in their energy comparison studies. External shading devices are able to emit and convect the absorbed solar radiation directly to the external environment and thus reduce the solar gain in the building considerably. The fully external shading systems are therefore particularly interesting when serious reduction of the cooling is required. An energy comparison with this system as reference case applied in a building with high internal loads and solar gain would lead to the conclusion that all double skin façade systems lead to high-energy consumption.

It is of course very questionable to compare any façade system with reference cases that deliver the highest or lowest energy consumption for that particular façade/building case and then draw the conclusion that double skin façades are ideal or not useful at all. An appropriate comparison would be achieved by taking a reference façade case, which reflects the intended goal of the national energy regulations or a good-practice façade system. This would lead to more balanced conclusions about the impact of a double skin façade on the energy consumption of buildings.

B. Are the assumed parameters chosen in order to deliver conservative results for the energy analysis (i.e. approach from the safe side)?

The assumptions that are made about the functionality of façade components or properties can make a difference to the outcome of the energy analysis. As an example the influence of the functionality of blinds on the energy simulation is discussed in this section. The above whole building analysis contained only a comparison of façade systems with guarantied operation of blinds, i.e. double skin façades systems and façades with internal blinds. Façades with external blind systems were excluded, as limited research is available on how much direct impact the wind has on the functionality of the blinds and how much indirectly on the energy consumption and comfort.

Indeed, movable external shading devices can be more sensitive to wind actions (particularly for high rise buildings) and a BMS system with wind sensor will pull up the blinds when the wind is too strong. In colder climates, snow and ice can cause blinds to be temporarily out of order. These phenomena have direct negative effects on the comfort conditions for the occupants working near the window (some might be sitting in direct sunlight) and also the energy consumption might increase (blinds might pulled up on windy days with high solar radiation). Figure 3 shows a picture of a building where the external shading device was pulled up due to high wind effects during a day with high solar radiation and where people were sitting in direct sunlight and face discomfort, glare problems and higher energy consumption.

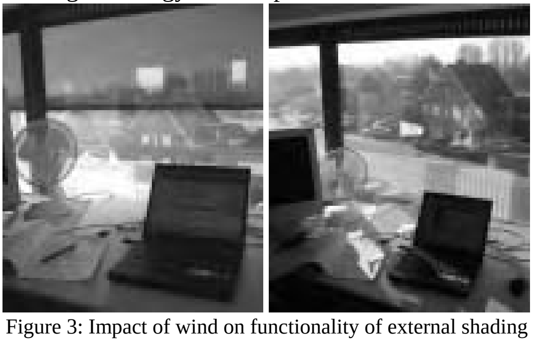

Figure 3: Impact of wind on functionality of external shading system. Left: Comfortable work space. Blinds are down due to intense solar radiation. Right: Blinds are up due to high wind speeds resulting in discomfort and overheating.

Very few researchers take wind effect on externally shaded façades into account in their energy analysis, which results in an overestimation of the functionality of the blind system for both energy and comfort predictions.

C. Are only the best performance criteria highlighted without paying attention to the downfalls of a particular façade system?

When choosing a façade system, a façade designer should always weigh the good performance criteria against the potential failures (and their progressive effects). Some potential problems related to double skin façades (such as condensation risk, integration with HVAC system, solar induced phenomena), and how they can be prevented was discussed in another paper by the same authors [1]. In order to illustrate some consequences inherent to a façade with external shading devices a list is given below (the list is not exhaustive, purely informative and not to be generalised):

- Movable external blind systems can have a smaller design life due to the aggression of different weather parameters such as rain, dirt, snow, ice, wind, temperature variations winter-summer, UV radiation Therefore higher replacement costs have to be considered.
- In cities or nearby main traffic roads, where there is high pollution, external blinds require significantly more cleaning. This has to be taken into account when assessing the long-term maintenance costs of a façade.
- In order to withstand higher wind loads, more robust blinds can be made. However, this will increase the cost and may have undesirable visual effects from the clients point of view (no smooth external façade surface).
- A higher risk for sound effects generated by the wind might appear with external blind systems, such as rattling of slats or flapping of solar screens in the case of light external shading systems. In the case of more robust movable external blind systems, whistling of the wind over the external blinds might occur. This is extremely difficult to predict at the design stage.
- Movable external blind systems can easily cause thermal fracture in the external glazing, which is less likely with systems that do not use external shading devices. As a result heat treatment of the glass is often necessary and therefore an increase in cost has to be taken into account.

The above list illustrates that the selection of specific façade components, which might be ideal to limit solar gains, can have significant negative influences on other performance parameters and/or on the overall cost of the façade.

IV. A MORE HOLISTIC APPROACH TO THE SELECTION OF THE MOST SUITABLE FAÇADE SYSTEM FOR A SPECIFIC PROJECT

Selecting the most suitable façade system at an early design face is one of the most important tasks for the design team of a new project. Ideally a fast decision making tool is used at early design stage to get a first indication of the impact of the façade system on the required façade/building performance parameters. The Massachusetts Institute of Technology Building Design Advisor [5] fulfils such a function by providing architects and building owners with an indication of the impact of different façade types, including double skin façades, on the energy, comfort and daylight performance of a room in a building.

In order to get an overview of the various façade system that may be suitable for the project, the outcome of the fast decision making tool can be tabled in a decision-making matrix. An early decision-matrix highlights some important project criteria and, at the same time, indicates some possible façade configurations (figure 4).

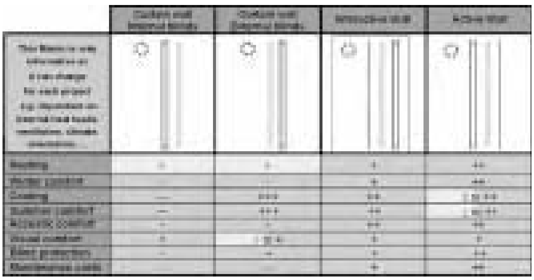

Figure 4: Example of a decision-making matrix for high transparent facades (single story height)

Ideally, the matrix highlights the most important demands of the façade, e.g. requirements inherent to the site location, specific requirements of the client or those set by regulations.

As an example, a possible methodology for the façade selection for a specific project The Corporate Village in Brussels (Belgium) is discussed below for which the following criteria are of main importance (and which are already included in Table 4 above):

- The client and architect expressed the desire for highly transparent façades (fully glazed with clear glass) to ensure maximum availability of daylight and view out.
- The office buildings were to be constructed in a very noisy environment: the main Belgian airport at 3km (Figure 5.a), secondary roads at 400m (Figure 5.a), high way roads and crossing at 700m (Figures 5.a and 5.b), a railway at 300m (Figure 5.b).
- For comfort reasons and energy conservation, solar gain was to be minimised during the summer, as the internal workspace would be an open plan office with limited thermal capacity.
- A fixed overall target budget was to be respected for initial and maintenance costs, i.e. building, façade, HVAC

Figure 5: The Corporate Village in Brussels (Belgium): Design against road traffic, train and air plane noise. Left: West view of the building Airplane noise (Brussels airport) Road noise (secondary roads and highway). Right: South view from building Train noise (Eurostar on railway) Road noise (Highway cross point).

Taking into account the extreme noisy environment, the acoustic performance of the external façade was a very critical parameter at the early design stage. Of all transparent façades, the double skin façades were the only options because of their superior acoustic performance as is demonstrated in Figure 6.

The double skin façade clearly performs much better than the typical curtain wall. Many subcomponents of a DSF will influence the acoustic performance. For instance a larger ventilated cavity of the double skin façade usually results in a higher sound reduction. A 200mm cavity was found to be the ideal compromise between acoustic performance, net-lettable office space and investment cost.

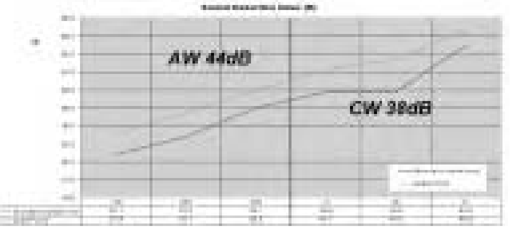

Figure 6: Acoustic sound reduction for an Active Wall ® and a conventional curtain wall

The nearby traffic was expected to produce a higher than normal amount of dust and dirt. In order to reduce the cleaning costs and guarantee the neat appearance of the façade, the design team opted for an Active Wall (a with internal air ventilated double skin façade) above a naturally ventilated or an Interactive Wall, which rely on ventilation with external air. For reasons of high internal loads (PCs, people and lights) in the building, the Active Wall was equipped with high performance glazing in the DGU (high light transmittance and medium solar factor). This way, the required thermal comfort and target energy levels were ensured. Further design optimisation of the façade was done in order to guarantee the many other performance parameters, e.g. minimal risk for condensation during the winter period, resistance against thermal fracture under solar radiation, uniform air flow in the ventilated cavity and many more. It is clear that the decision-making matrix will differ for every new project (other location, different requirements of the client, local regulations). Experience has shown that such a matrix is useful for clients, architects and designers when they have to choose the optimal façade system suitable for their unique project early in the design process.

V. CONCLUSIONS

Due to the architectural demand for high transparent façades, innovative double skin façades are developed of which various performance parameters need to be assessed early on in the design process and for every new specific façade/building configuration.

The use of building energy simulation tools proved to be useful for the calculation of the yearly energy consumption of a building. A comparative study was performed to assess the impact of the façade choice on the whole building energy consumption. For the assessed London office with high internal loads, it was found that a highly transparent double skin façade gives easier compliance to the energy regulations than a conventional façade system with 40% glazing. It was found that it is important to take typical good practice façade configurations as references for energy comparisons rather than façade types that give extremely good or bad energy performances. For façade systems with external shading devices it was discussed that energy calculations are not always trivial to equate as unknown parameters, such as the operability of blinds, might influence the outcome in real life. Many more parameters, which have to be taken into account for the proposal of external shading devices (such as maintenance costs, design life, initial costs, visual effects, sound generation components, thermal fracture) were listed.

Finally, the authors called for a more holistic approach of façade comparison because in most projects not only the energy performance is to be optimised, but many more parameters and sometimes conflicting requirements are more critical to the façade choice. The project Corporate Village in Brussels was used as example to illustrate how the best suitable façade system can be optimised for different performance criteria: acoustic comfort, maintenance, availability of daylight, energy efficiency and architecture.

ACKNOWLEDGEMENTS

The authors would like to thank the engineers at Physibel for the development of upgrades of their software tools with very specific functions for detailed performance assessments on advanced double skin façades.

REFERENCES

[1] De Bleecker H., Zobec M. & Simonella A. (Forth coming) Accurate thermal performance prediction of innovative double skin facades and conflicts with current standards. Sidney: ICBEST 2004
[2] DETR (2001) The Building Regulations 2000. Conservation of fuel and power. Approved Document L2. London: DETR
[3] Physibel (2000) CAPSOL Version 3.3. Computer Program to Calculate Multizonal Transient Heat Transfer. Maldegem: Physibel
[4] Simonella A., Franceschet A., De Bleecker H. & Zobec M. (2003) Carbon emission calculation for non-residential buildings: Integration of daylighting analysis in dynamic energy simulation software. Proceedings of the conference Dynamic analysis and modelling techniques 2003: Ispra
[5] MIT Design Advisor (http://18.80.2.250:8080/Design)
[6] Arons D.M.M. & Glicksman L.R. (2001) Double skin, airflow façades: will the popular European model work in the USA? Canada: Proceedings of ICBEST 2001, Vol. 1:203-207 ASHRAE (1997)
[7] ASHRAE Handbook Fundamentals, Atlanta: ASHRAE
[8] CEN (1996) prEN ISO 13791 Thermal performance of buildings. Internal temperatures of a room in summer without mechanical cooling. General criteria and validation procedures. Brussel: CEN
[9] CIBSE (1999) Environmental design section A3. Thermal Properties of building structures. Guide A. London:
[10] CIBSE ISO (2001) ISO/FDIS 15099 Thermal performance of windows, doors and shading devices Detailed calculations. Geneva: ISO
[11] Lehar M.A. & Glicksman L.R. (2003) A simulation tool for predicting the energy implications of advanced facades. Leuven: Proceedings of Second international building physics conference 2003
[12] Lieb R.D. (2001) Building physical values of double skin façades. Canada: Proceedings of ICBEST 2001, Vol. 1: 51-54
[13] Long, C. (1999) Essential heat transfer. Harlow: Longman
[14] Muneer I., Abodahab N., Weir G. & Kubie J. (2000) Windows in Buildings. Thermal, Acoustic, Visual and Solar Performance. Oxford: Architectural Press
[15] Physibel (1998) Physibel Software Pilot Book. Practical problems solved using the Physibel Software. Maldegem: Physibel
[16] Saelens D., Carmeliet J. & Hens H. (2001) Modeling of air and heat transport in active envelopes. Canada: Proceedings of ICBEST 2001, Vol. 1: 243-247
[17] Van Dijk D. & Bakker L. (2002) Algorithms in WIS on ventilation in gaps. Delft: TNO (Document as part of the WINDAT project. A project supported by DG for Energy and Transport of the European Commission)

EU COST C13 Glass and Interactive Building Envelopes. M. Crisinel, et al. (Eds.). IOS Press, 2007.

Modeling and Simulation of a Double-Skin Façade System

Jan Hensen, PhD, Member ASHRAE
Martin Bartak, MSc,
Frantisek Drkal, PhD,

Starting from a practical design problem related to natural and hybrid ventilation systems, this paper looks at different airflow modeling methods that might be employed to assist in the decision making process of a building design team. The question at hand is whether or not to make use of a double-skin façade system in a new office development. The airflow modeling methods considered are the mass balance network method and computational fluid dynamics (CFD).

The paper gives an overview of the methodology of the design study. The underlying modeling and simulation work is elaborated. The paper finishes with some conclusions, both in terms of the actual performance of the double-skin facade and in terms of the modeling and simulation work.

The main conclusions are that for the foreseeable future the network method is more suited for this type of "everyday" design support work. However there are important areas where the network method in general might benefit from CFD, or vice versa.

I. Introduction

In Europe and elsewhere, fully glazed façade systems are currently very popular with architects and investors. Even in moderate climate zones fully glazed buildings need shading devices in order to reduce cooling loads. External shading devices are much more effective than internal shading devices. However external shading devices are not very popular due to mechanical, cost and aesthetic reasons. An often-used alternative is a shading device positioned within the façade in a ventilated cavity. In the 1970's the climate-window concept was developed, in which the cavity is ventilated with inside air. A more recent development is the double-skin façade concept, as shown in Figure 1, in which the cavity is ventilated with ambient air. If a design team decides for a double-skin façade, a logical next step is to make the cavity an integral part of the natural or hybrid ventilation system; for example by operable office windows which open to the cavity, or by using the cavity for pre-heating fresh supply air during the heating season.

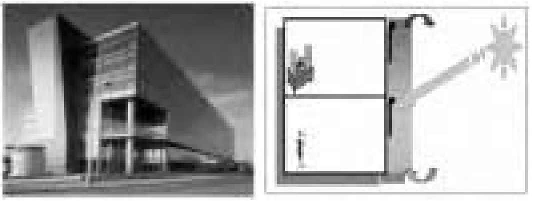

Figure 1: Typical example and principle of double-skin façade.

To predict the performance of a double-skin façade is not a trivial exercise. The temperatures and airflows result from many simultaneous thermal, optical and fluid flow processes, which interact and are highly dynamic. These processes depend on geometric, thermo-physical, optical and aerodynamic properties of the various components of the double-skin façade structure and of the building itself. The temperature inside the offices, the ambient temperature, wind speed, wind direction, transmitted and absorbed solar radiation and angles of incidence – each of which are highly transient - govern the main driving forces. This typically results in highly erratic airflows as indicated in Figure 2.

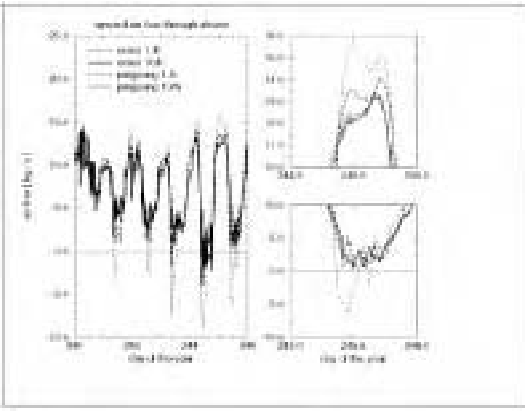

Figure 2: Typical airflow variations in a natural ventilated glazed vertical building structure, such as a double-skin façade. Graphs on the right are blow-ups showing different coupled and de-coupled solutions for temperature and airflow (Hensen 1999)

It is obvious that for such a configuration, computer modeling and simulation is needed to predict the future performance in the real world. Since there are so many parameters and variables involved, it is practically impossible to prepare generally applicable design prescriptions for such a system. Therefore modeling and simulation should be employed to support the design process directly. The methodology involved is basically an iterative process comprising the following main steps.

1. Analysis of the problem and re-expressing the building design in a validated and appropriate simulation model in terms of extent, complexity and time and space resolution levels.
2. Calibration of the model.
3. Performing simulations against relevant inside and ambient boundary conditions during a suitable length of time.
4. Analyzing and reporting of results, perhaps followed by changing the model and further simulations.

This approach is demonstrated in the following sections by means of a design support study for a double-skin façade office development in Prague in the Czech Republic (Hensen and Bartak 2001).

II. Modeling the Double-Skin Façade

The main objective of the study was to generate performance data in support of the design team by predicting the environmental conditions in the double-skin facade, and the resulting cooling loads for the adjacent perimeter offices during extreme summer conditions. The temperatures in the cavity are of interest for the manufacturing and construction methods. The office cooling loads are needed for sizing the HVAC systems. In this case, the design team has actually very little interest in the flow field itself. Since the layout of the building is very regular there is no need to include the whole width or depth of the building. However, the model does need to include the offices adjacent to the façade plus the double-skin façade itself. The stack effect necessitates that the model covers the full height of the building. The simulation period needs to cover at least a full day preceded by several simulation start-up days in order to account for thermal storage effects of the construction. Based on previous studies (e.g. Hensen 1999) time steps of 1 hour are deemed the appropriate temporal resolution.

Although airflow is demonstrably an important aspect of building/ plant performance assessment, the sophistication of its treatment in many modeling systems has tended to lag behind the treatment applied to the other important energy flow paths. The principal reason for this would appear to be the inherent computational difficulties and the lack of sufficient data. In recent times more emphasis has been placed on airflow simulation mostly focused on the following two approaches:

1. Computational fluid dynamics (CFD) in which the conservation equations for mass, momentum and thermal energy are solved for all nodes of a two- or three-dimensional grid inside or around the object under investigation. In theory, the CFD approach is applicable to any thermo-fluid phenomenon. However, in practice, and in the building physics domain in particular, there are several problematic issues, of which the amount of necessary computing power, the nature of the flow fields and the assessment of the complex, occupant-dependent boundary conditions are the most problematic (Chen 1997). This has often led to CFD applications being restricted to steady-state cases or very short simulation periods (see e.g. Haghighat et al. 1992, Martin 1999, Chen 2000).

2. The network method, in which a building and the relevant (HVAC) fluid flow systems are treated as a network of nodes representing rooms, parts of rooms and system components, with inter-nodal connections representing the distributed flow paths associated with cracks, doors, pipes, pumps, ducts, fans and the like. The assumption is made that for each type of connection there exists an unambiguous relationship between the flow through the component and the pressure difference across it. Conservation of mass for the flows into and out of each node leads to a set of simultaneous, non-linear equations, which can be integrated over time to characterize the flow domain.

Obviously there is a tradeoff. The network method is of course much faster but will only provide information about bulk flows. CFD on the other hand will provide details about the nature of the flow field. It depends on the problem at hand, which of these aspects is the more important one.

In the current case the thermal side of the problem is very important. Given the extent of the model and the issues involved, this can only be predicted with building energy simulation. Both CFD and the network method can be integrated with building energy simulation. In case of CFD this is still very much in development although enormous progress has been made in recent times (see e.g. Bartak et al. 2002, Zhai et al. 2002). Integration of the network method with building energy simulation is much more mature (see e.g. Hensen 1991) and more commonly used in practice. The reasons for this are threefold. Firstly, there is a strong relationship between the nodal networks that represent the airflow regime and the corresponding networks that represent its thermal counterpart. This means that the information demands of the energy conservation formulations can be directly satisfied. Secondly, the technique can be readily applied to combined multi-zone buildings and multi-component, multi-fluid (e.g. water and air) systems. Finally, the number of nodes involved will be considerably less than that required in a CFD approach and so the additional CPU burden is minimized.

Based on the above considerations regarding the requirements for the problem at hand and in view of the characteristics of the airflow modeling methods, it was decided to use the network approach fully integrated in a building thermal energy model (Hensen 1991, Clarke 2001). One of the very powerful features of this simulation environment is that it allows modeling of building airflow on different levels of resolution (from user defined air change rates, via mass balance network approach to computational fluid dynamics) and on different levels of integration (e.g. airflow on its own, or coupled with energy balance, and/or coupled with CFD).

As shown in Figure 3, the model comprises a typical 7.5 m wide section of the south side of the building, consisting of a “stack” of 8 zones representing the office zones up to a depth of 5 m behind the façade, and another 7 “stacked” zones representing the double-skin façade itself. These 7 zones are coupled by an airflow network which also includes the inlet opening (modelled by a connection between the bottom cavity zone and outside, i.e. the air temperature and wind pressure in front of the façade) and the outlet opening (a connection between the upper cavity zone and outside, i.e. the air temperature and wind pressure on the roof). It was assumed that the office windows and the shading devices are closed and that effectively there will be no air exchange between the offices and the cavity of the double-skin façade. Solar radiation passes through the double-skin depending on the angle of incidence and the optical properties of the transparent systems. The outer layer of the double-skin façade is single pane clear glass 6 mm thick. The office windows have advanced double glazing with blinds located in the cavity of the double-skin façade. For the case without the double-skin façade, inside blinds were assumed for the office windows. Further details of the model can be found in the appendix.

III. MODEL CALIBRATION

Due to lack of available resources it has to be assumed in this – and many other - design study context that the models and the simulation environment which is being used has been verified (ie the physics are represented accurately by the mathematical and numerical models) and validated (ie the numerical models are implemented correctly). Nevertheless it is critically important to be aware of the limitations of the modelling approach.

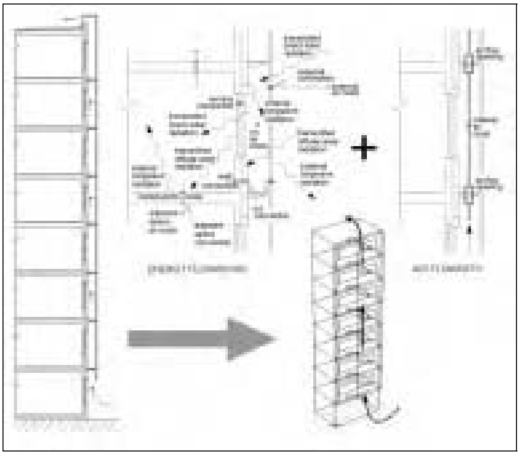

Figure 3: The model of the double-skin façade. On the left: cross-section of the double-skin façade system. Above: schematic representation of the super-imposed thermal and airflow network models. Bottom: graphic feedback from the simulation environment.

For example, when using the network approach it should be realized that most of the pressure-flow relationships are based on experiments involving turbulent flow. Von Grabe et al. (2001) demonstrate the sensitivity of temperature rise predictions in a double-skin façade, and the difficulty of modeling the flow resistance of the various components. There are many factors involved but assuming the same flow conditions for natural ventilation as those used for mechanical ventilation causes the main problem; i.e. using local loss factors ζ and friction factors from mechanical engineering tables. These values have been developed in the past for velocities and velocity profiles as they occur in pipes or ducts: symmetric and having the highest velocities at the center. With natural ventilation however, buoyancy is the driving force. This force is greater near the heat sources, thus near the surface and the shading device, which will lead to non-symmetric profiles. This is worsened because of the different magnitudes of the heat sources on either side of the cavity.

One way forward would be to use CFD in separate studies to predict appropriate local loss factors ζ and friction factors for use in network methods. Strigner and Janak (2001) describe an example of such a CFD approach by predicting the aerodynamic performance of a particular double-skin façade component, an inlet grill.

As discussed elsewhere in more detail (Hensen 1999) another limitation is related to assumed ambient conditions. This concerns the difference between the "micro climate" near a building and the weather data, which is usually representative of a location more or less distant from the building. These differences are most pronounced in terms of temperature, wind speed and direction, the main driving potential variables for the heat and mass transfer processes in buildings! These temperature differences are very noticeable when walking about in the summer in an urban area. Yet it seems that hardly any research has been reported or done in this area. There are some rough models to predict the wind speed reduction between the local wind speed and the wind speed at the meteorological measurement site. This so-called wind speed reduction factor accounts for any difference between measurement height and building height and for the intervening terrain roughness. It assumes a vertical wind speed profile, and usually a stable atmospheric boundary layer.

It should be noted however that most of these wind profiles are actually only valid for heights over 20 z_0 + d (z_0 is the terrain dependent roughness length (m), and d is the terrain dependent displacement length (m)) and lower than 60 . . . 100 m; ie. for a building height of 10 m in a rural area, the profiles are only valid for heights above 17 m, in an urban area above 28 m and in a city area above 50 m. The layer below 20 z_0 + d is often referred to as the urban canopy. Here the wind speed and direction is strongly influenced by individual obstacles, and can only be predicted through wind tunnel experiments or simulation with a CFD-model. If these are not available, it is advised to be very cautious, and to use - depending on the problem on hand - a high or low estimate of the wind speed reduction factor. For example, in case of an "energy consumption and infiltration problem" it is safer to use a high estimate of the wind speed reduction factor (eg. wind speed evaluated at a height of 20 z_0 + d). In case of an "air quality" or "overheating and ventilation" problem it is probably safer to use a low estimate (eg. wind speed evaluated at the actual building height, or assuming that there is no wind at all).

Calibration is a very difficult issue in practice. For existing buildings there are usually no experimental results readily available. In a design context there is not even a building yet. In practice, the only way to calibrate the model is to try to gain confidence by carefully analyzing the predictions and to compare these to expectations or "intuition" based on previous work. Unexpected results are usually the result of modeling errors. In rare – but interesting – cases unexpected interactions take place and – after analyzing these – the simulations may have helped to improve the understanding of the problem. In any event, calibration should not be taken lightly and sufficient resources should be reserved for this activity.

IV. SIMULATIONS

Because of the main interest in the summer conditions the simulations were carried out for an extreme summer day in Prague. The offices inside conditions were for a typical weekday (see the appendix). The simulation period was preceded by five simulation start-up days. All simulations were carried out with 1-hour time steps. In order to generate relevant design information, the following cases have been considered.

A. The building without the double-skin façade and with internal Venetian blinds.
B. The building with the double-skin façade and blinds located in the façade cavity.
C. As B but now assuming that there would be no wind at all.
D. As B but now assuming that the damper in the double-skin façade outlet would be closed.

Case A serves as the reference case. A comparison of case B with case A would show the influence of the double-skin façade as designed. As explained above, Case C is needed in order to show what would happen if there would be no influence of wind, e.g. because of sheltering by neighbouring buildings. Case D would shows what would happen if the outlet damper would be closed, perhaps due to malfunctioning.

V. RESULTS AND DISCUSSION

Figure 4 shows the double-skin air temperature results for cases B and C. These are the air temperatures in the upper part of the double-skin façade, where normally the highest temperatures occur. It is clear that for this building there is not much influence of the wind; i.e. the buoyancy forces are the dominant driving force for the airflow. For both case B and case C, the maximum temperature rise in the double-skin façade is about 12oC above ambient, which will occur in the late afternoon and early evening.

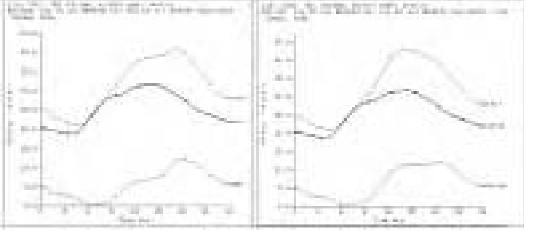

Figure 4: Predicted air temperatures in the double-skin façade during one of the warmest summer days in Prague. Upper lines represent outlet temperatures. Middle lines represent inlet temperatures (ambient). Lower lines represent the temperature rise in the façade. The left graph corresponds to the final design of the double-skin façade with wind forces taken into account. The right graph represents the same situation without taking into account the airflow driving forces due to wind.

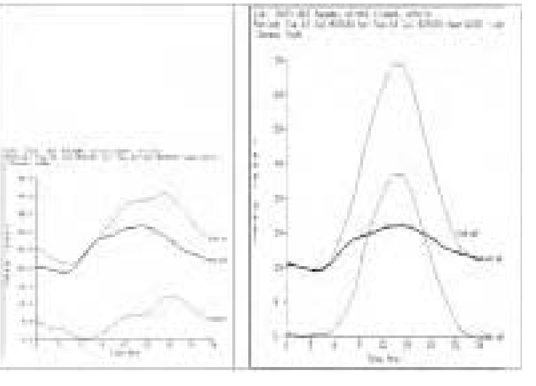

Figure 5: Predicted air temperatures in the double-skin façade during one of the warmest summer days in Prague. Upper lines represent outlet temperatures. Middle lines represent inlet temperatures (ambient). Lower lines represent the temperature rise in the façade. The left graph corresponds to the final design of the double-skin façade. The right graph represents the situation where the outlet damper would be closed

due to malfunctioning or control error. The temperature scales are approximately the same.

As can be seen in Figure 5, the air temperature rise would be considerably higher in case the outlet damper would not be open. In that case the air temperature could rise up to almost 50°C above the ambient temperature, and this would happen in the middle of the afternoon.

Figure 6 shows some results in terms of airflow rate through the double-skin façade for the case B conditions. During most of the day the flow is upward, basically because the average air temperature in the double-skin façade is above the ambient temperature. However during part of the early morning the south façade is in the shade. The thermal capacity of the façade delays the temperature rise of the cavity air relative to the more rapid rise of the ambient air temperature. Thus the average air temperature in the double-skin façade is temporarily lower than ambient. This results in downward air flow through the cavity.

In general, the double-skin façade acts as a thermal buffer in front of the offices. This has three interacting thermal effects for the offices.

1. The air temperature inside the double-skin façade will be higher than ambient during most of the day. This will result in lower conductive heat losses (heating season) and higher conductive heat gains (summer) depending on ambient temperatures and solar radiation levels.
2. The extra outside pane of glass of the double-skin façade will reduce the amount of solar radiation on the inside façade, thus reducing the solar radiation load of the offices due to radiation transmission via the windows.

The double-skin façade allows blinds in the cavity of the double-skin façade as opposed to on the inside of the window, thus reducing the solar radiation load of the offices via the windows.

Which of these three effects is most important at a particular point in time depends on optical and other properties of the structure and complicated dynamic thermal interactions between the façade, temperatures and airflow in the double-skin façade, and outside. As can be seen in Table 1 and Table 2, for the offices adjacent to the façade the result is a reduced maximum cooling load during hot summer days. Of course, in case the outlet damper would be closed, there would be no reduction but an increase in cooling load for the offices.

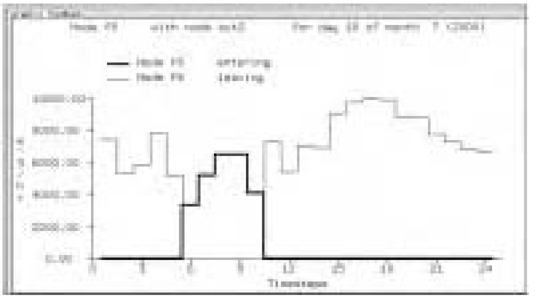

Figure 6: Case B (as designed) airflow rate through the double-skin façade during one of the warmest summer days in Prague. The thin line indicates upward flow in the cavity. The thick line represents downward flow in the cavity. Note that 10000 m3/h corresponds to an average cross-sectional air velocity of about 0.7 m/s in the cavity. Due to smaller cross-sectional areas, this corresponds to about 1.3 m/s in the outlet, and about 2.0 m/s in the inlet opening of the double-skin façade.

As evidenced by Table 1 and Table 2, the cooling load reduction depends on the floor level. It is less for the higher floors because of the higher air temperatures in the cavity of the double-skin façade. This might lead to the suggestion that it would be advantageous to divide the cavity into segments with inlet and outlet openings at various heights. This is however not so easy to predict due to the strong thermodynamic coupling that exists between the airflow and thermal processes in a naturally ventilated double-skin façade structure.

TABLE 1 MAXIMUM SENSIBLE COOLING LOAD FOR THE OFFICE ADJACENT TO THE FAÇADE ON THE TOP FLOOR (I.E. LEVEL 8) DURING ONE OF THE WARMEST SUMMER DAYS IN PRAGUE, AND THE DIFFERENCES RELATIVE TO CASE A (I.E. NO DOUBLE-SKIN FAÇADE)

Case	Maximum sensible cooling load kW	Difference relative to case A		
		W	W/m^2 floor	%
A	3.53			
B	3.29	-240	-6	-7
C	3.32	-210	-6	-6
D	3.65	120	3	3

TABLE 2 MAXIMUM SENSIBLE COOLING LOADS FOR THE OFFICES ADJACENT TO THE DOUBLE-SKIN FAÇADE DURING ONE OF THE WARMEST SUMMER DAYS IN PRAGUE FOR CASE A (WITHOUT DOUBLE-SKIN FAÇADE) AND CASE B (WITH THE DOUBLE-SKIN FAÇADE)

Floor level	**Maximum sensible cooling load**		**Sensible cooling load reduction due to the double-skin façade**		
	Case A kW	**Case B kW**	**W**	**W/m² floor**	**%**
8th	3.53	3.29	250	6	7
7th	3.51	3.24	270	7	8
6th	3.50	3.20	300	8	9
5th	3.50	3.14	360	10	10
4th	3.45	3.08	370	10	11
3rd	3.38	2.95	430	11	13
2nd	3.14	2.67	470	13	13

VI. IN CONCLUSION

The above work shows the advantages of a double-skin façade construction in terms of reducing the cooling load of the adjacent zones especially on the lower floors. Coupling a double-skin façade to a natural or hybrid ventilation system is common but represents challenges as shown in this paper. These are due to the temperature and airflow fluctuations in the façade construction. The airflow is not only highly erratic in magnitude but can even take place in reversed direction.

This paper has shown that to predict the performance of this type of systems constitutes a non-trivial modelling and simulation exercise that should be based on a thorough methodology and good working practice.

When modelling these type of systems it is typically necessary to take into account a large part of the building with dynamic interactions between several zones and ambient conditions. This has consequences for the practically possible level of spatial and temporal resolution which make CFD less appropriate in everyday practical design of these types of systems.

On the other hand this paper has indicated several areas where the network method in general could be improved through separate CFD studies. An example would be to verify and/or improve the network pressure-flow relationships and local loss factors for airflow conditions typical of natural and hybrid ventilation systems. Another area of concern where CFD might be of benefit is the wind pressure distribution on the façade and roof of the building.

A final conclusion from this paper could be that both the network method and CFD have their own advantages and disadvantages for modelling this type of natural and hybrid ventilation systems. Either method can and should be used but at different stages.

REFERENCES

[1] Bartak M, Beausoleil-Morrison I, Clarke J A, Denev J, Drkal F, Lain M, Macdonald I A, Melikov A, Popiolek Z, Stankov P 2002. “Integrating CFD and building simulation,” in Building and Environment, vol. 37, nr. ? (In press.)

[2] Chen Q 1997. ‘‘Computational fluid dynamics for HVAC: successes and failures,’’ in ASHRAE Transactions, vol. 103(1), pp. 178-187

[3] Chen Q and J Srebic 2000. “Application of CFD tools for indoor and outdoor environment design,” Int. Journal on Architectural Science, Vol. 1, nr. 1, pp. 14-29

[4] Clarke J A 2001. “Energy simulation in building design“, 2nd-edition, Butterworth-Heineman, Oxford.

[5] Grabe J von, R Lorenz and B Croxford 2001. “Ventilation of double facades”, in Proc. Building Simulation 2001 in Rio de Janeiro, pp. 229-236, International Building Performance Simulation Association.

[6] Haghighat, F., J.C.Y. Wang, Z. Jiang and F. Allard 1992. “Air movement in buildings using computational fluid dynamics.” Transactions of the ASME Journal of Solar Energy Engineering 114:84-92.

[7] Hensen JLM 1991. "On the thermal interaction of building structure and heating and ventilating system," Doctoral dissertation Technische Universiteit Eindhoven.

[8] Hensen JLM 1999. "Simulation of building energy and indoor environmental quality - some weather data issues," in Proc. Int. Workshop on Climate data and their applications in engineering, 4-6 October 1999, Czech Hydrometeorological Institute in Prague.

[9] Hensen J 1999. “A comparison of coupled and decoupled solutions for temperature and air-flow in a building“, in ASHRAE Transactions, vol. 105:2, pp. 962-969, American Society of Heating, Refrigerating, and Air-Conditioning Engineers.

[10] Hensen J and M Bartak 2001. Design support simulations for the BB Centrum double-skin facade, Report to Sipral a.s., HBPS, Netherlands

[11] Martin P 1999. “CFD in the real world,” ASHREA Journal, nr. 1, pp. 20-25.

[12] Strigner R and M Janak 2001. “Computer simulation of ventilated double-skin façade of the metropolitan library in Brno”, in Proc. 1st Int. Conf. on Renewable Energy in Buildings "Sustainable Buildings and Solar Energy 2001", Brno, 15-16 November, Brno University of

Technology / Czech Academy of Sciences in Prague, pp. 134-137.

[13] Zhai Z, Q Chen, P Haves and J H Klems 2002. "On approaches to couple energy simulation and CFD programs," in Building and Environment, vol. 37, nr. ? (In press.)

Jan Hensen is associate professor in the Building Department, Technische Universiteit Eindhoven, Netherlands. He is also part-time associate professor in the Mechanical Engineering Department, Czech Technical University in Prague, where Martin Bartak is assistant professor and Frantisek Drkal is full professor in environmental engineering.

APPENDIX

A. Geometry

The model comprises 8 stacked thermal zones (named 1flr, 2flr, ..., 8flr according to floor level) which represent the office modules. The dimensions of each office module are: width 7.5 m, depth 5 m, height 3.7 m (except 1st floor which is 4.15 m high). Therefore each office module has a floor area of 37.5 m^2 and a volume of 138.75 m^3. The total building height is 30.05 m. The model comprises another 7 stacked thermal zones (named fcd2, fcd3, ..., fcd8 according to floor level) which represent the double-skin façade construction. The dimensions of each double-skin façade module are: width 7.5 m, depth 0.636 m, height 3.7 m.

B. Constructions

The office façade construction consists from outside to inside of 80 mm insulation + 200 mm concrete. The standardized thermal resistance R is 2.9 m^2K/W or U is 0.32 $W/(m^2K)$. The surface emittance is 0.9 [-], the surface solar absorptance is 0.8 [-]. The roof construction consists from outside to inside of 150 mm insulation + 280 mm concrete. The standardized thermal resistance R is 4.35 m^2K/W or U is 0.22 $W/(m^2K)$. The floors consist of 280 mm concrete.

C. Windows

he double-skin façade outer glazing consists of 6mm clear float with a visible transmittance of 0.87 [-] and a nominal U value of 5.40 $W/(m^2K)$. The direct solar transmittance at 5 angles (0°, 40°, 55°, 70°, 80°) is 0.78, 0.76, 0.72, 0.58, 0.35 [-]. The total heat gain factor at 5 angles is 0.82, 0.81, 0.77, 0.63, 0.40 [-]. The solar absorptance at 5 angles is 0.149, 0.163, 0.173, 0.179, 0.169 [-].

The glazing of the offices towards the double-skin façade consists of double glazing with external blinds and is composed of 5 layers [including air gaps], has a visible transmittance of 0.72 [-] and a nominal U value of 1.60 $W/(m^2K)$. The direct solar transmittance at 5 angles (0°, 40°, 55°, 70°, 80°) is 0.07, 0.03, 0.02, 0.02, 0.02 [-]. The total heat gain factor at 5 angles is 0.09, 0.04, 0.03, 0.03, 0.03 [-]. The solar absorbance at 5 angles for each layer is layer 1: 0.570, 0.551, 0.526, 0.507, 0.507 [-], layer 2: 0.001, 0.001, 0.001, 0.001, 0.001 [-], layer 3: 0.042, 0.017, 0.013, 0.010, 0.010 [-], layer 4: 0.001, 0.001, 0.001, 0.001, 0.001 [-], layer 5: 0.014, 0.006, 0.005, 0.004, 0.004 [-].

D. Operation

Every office zone has infiltration rate of 0.3 ACH continuously. The ventilation rate of the 2nd floor zone until the 8^{th} floor zone is during office hours based on 50 m^3 /(hr.pers) = 187.5 m^3 /hr = 1.351 ACH.

For the office zones the casual gains on working days 7:00–17:00: occupants 233 W sensible + 293 W latent, lights 750 W, equipment 1125 W. There are no casual gains outside working hours.

E. Control

The 1^{st} floor office zone has free floating temperature. The cooling set point is 28°C for the other office zones during working days 7:00–17:00. Free floating temperature outside working hours.

F. Airflow Network

The inlet opening has a cross-sectional area 7 m x 0.2 m = 1.4 m^2. The outlet opening has a cross-sectional area 7 m x 0.3 m = 2.1 m^2. In case of the closed outlet damper, a leakage 7 m x 0.005 m = 0.035 m^2 is assumed. The horizontal openings at each floor level in the double-skin façade are 7 m x 0.6 m = 4.2 m^2.

Node out1 is external node, wind induced pressure, south, at ½ the height of the building = 15 m. Nodes f2, f3, to f8 are nodes in the double-skin façade (number = floor level). Node out2 is external node, wind induced pressure, roof, at height of 30.9 m.

EU COST C13 Glass and Interactive Building Envelopes. M. Crisinel, et al. (Eds.). IOS Press, 2007.

Harmonization of Optical and Thermal Behaviour of Buildings

Aleš Krainer, Živa Kristl
University of Ljubljana, Faculty of Civil and Geodetic Engineering, Slovenia

Design of the living environment has to result from the interactivity of the influences of the location conditions.

Building as part of the ecosystem, which - with the help of high technology - harmonises various influences and conditions in the system, is the aim of the efforts of bioclimatic design of living and working environment. Cicero called it a second world within the world of nature.

Location conditions are formed by the geomorphologic structure: more or less unchangeable, by climatic conditions: changeable and unpredictable, but in a certain sense harmonic, and by behaviour patterns and peoples life habits, which are dependant on the location as the result of creativity and as such changeable but mostly nonharmonic.

Geographical structure has been until now, from the viewpoint of man and his concept of time, firm and unchangeable. But nowadays changes seem to appear, even within these temporal limitations, in the first place as a result of the degradation of physical environment.

Climate conditions change in more or less harmonic cycles, from daily, seasonal and even yearly ones.

The temporal function of cultural activity and creativity is irregular and unstable, and with stopping points in metastable state when their creativity charges are filled up or emptied in unpredictable cycles. (Figure 1)

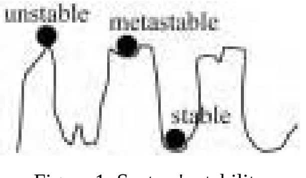

Figure 1: System's stability

The potential of these differences can be the starting point for the design as strategic planning on the level of a building and of its envelope. Stable system can exist only theoretically. In this case there is no exchange between living-working environment and surrounding environment. Metastable system enables and permits possibilities of change with periodic impacts. Nowadays building technology is somewhere in this area. Unstable system is final target of the design of living and working environment. In this case changes are on line in real time. This system is reacting to momentary changes in the outer environment and momentary demands in inner environment. Of course physical properties of different materials and combinations of materials have important influence on the speed of the reaction.

If the demands of the users and the conditions in the natural environment are different and changing, then the response of the building to these conditions and demands has to be dynamic and changeable, too.

This responsiveness can be achieved by automatic control, cybernetic and information technology: over the short-term period by changing the structure of the envelope and over the long-term period by changing the properties of the materials.

Proper functioning of the information system, which controls the exchange of energy and materials, as well as the people's movement, is the condition for creating the possibilities to bring the socio-ecological production - consumption circle (Assimov, 1969) nearer to natural ecological cycles. The functioning of natural ecological cycle is determined by the fact that there is no waste in the system, while all rest is returned into the system. On the other hand the waste practically can not be avoided in the socio-ecological systems at the modern level of technological development. It can often only be reduced.

Technological development demands at least linear growth of the knowledge of controlling the systems for solving these problems, which is generally more demanding than both individual capabilities and readiness for cooperation.

The system is formed by flows of information, energy and matter, and by different functional elements (Krainer, 1993). Thermal and luminous levels and relative humidity, together with air exchange and contacts with the natural environment, depending on psychological, physiological and cultural needs and demands of men, represent information sources that stimulate corresponding responses from the functional elements. Functional elements are integrated and combined into the building. The building should ultimately express a comprehensive and complete socio-ecological system.

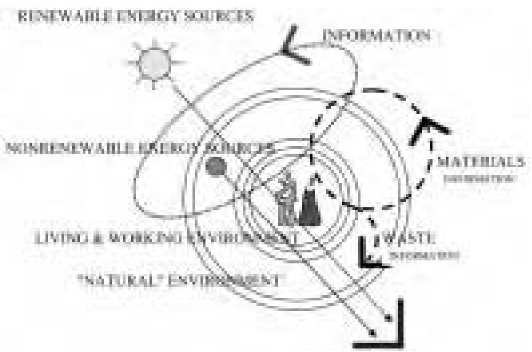

Figure 2: Man made environment in natural environment

The building project has to be structurally and technologically ready for such changes. The keys for the change are on one hand in communications and information systems and on the other hand in minimum use of energy sources, building use and removal, over its complete life cycle.

Two basic starting points lead and direct bioclimatic design strategy of the bioclimaticaly oriented i.e. smart house.

The first starting point is the role of the individual: responsiveness to differing and special demands of an individual person. Throughout the history of mankind the value of the individual has been growing. This fact is directly connected with the level of knowledge and access to the technology. In each period of development men tried to create the best possible specific living conditions. The influences of technology on the assessment of the individual are evident in historic development and in socio-economic relations. The level of individual's tolerances was always a reflection of technological and social development.

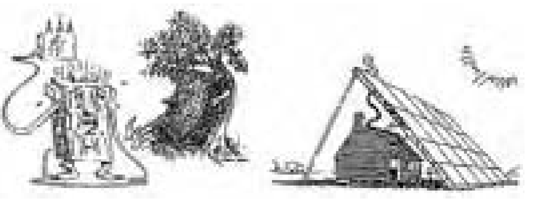

Figure 3: Common sense

The second starting point is common sense. This indicates that a reasonable building is not characterised only by the use of high technology: knowledge well applied has even greater value.

Smart or intelligent handling is organised by two sets of influences. The first set is represented by the user's demands. They are general and individual but both changeable, depending on the life patterns of different groups on different levels (cultural, national, religious etc.) and on particular ways of use. Various kinds of space use should not represent a disturbance in the system but enrichment, although they seem irrational at the first sight. The second set is represented by cyclic and unpredictable changes in the natural environment. They are usually not in accordance with momentary demands and needs of individuals or groups.

By raising the prices of energy, the accuracy and the complexity of interacting influences of user's demands and the natural environment is increasing, too. The use of information technology and intelligent systems can solve these problems. A building is/should be an organised system. In this system interconnected parts and subsystems, management systems, modes of production, storage and emission of energy, and dynamic responses to the outer influences are operating to reach the homeostasis like in a living body.

The area of activity of individual constituents of the system is not strictly limited. The transition points between the elements are never strictly defined. They incorporate both time and place dimensions; they are extensive in time and place. Between the living environment on one side and natural environment on the other, a continuous interface appears. It is formed of various materials, components, elements and the entire building. Their different and changeable combinations represent new generations of building technologies. With dynamic control devices the adaptability of the built environment to the conditions in the outer environment is improving, and the required amount of supplementary energy is diminishing.

The goal of the interface is the regulation of differences between the natural and artificial environment. From the technological point of view, we are in the first place dealing with thermal energy, natural light and air stratification. The level of energy flows needed for maintenance of desired conditions is in inverse proportion to the level of adaptability of the interface.

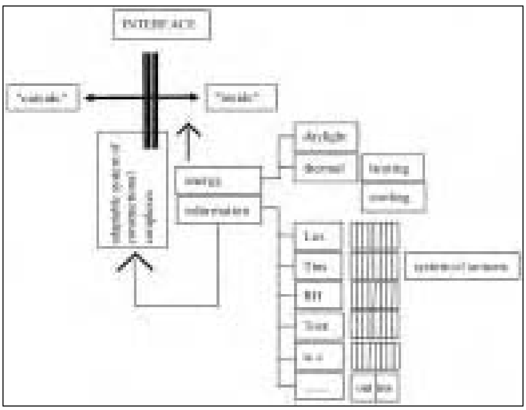

Figure 4: Interface - transparent part

The reasons to construct it are, besides thermal flows and rational use of energy, the enhancement of the space in use, marking of passage of time and use of natural dynamics for stimulation of optimal functioning of human behaviour by the sector of built environment.

To achieve this to as large extent as possible, it is appropriate and natural to use, besides good examples from history, also the possibilities of newly available technologies, control and management systems.

The new interface appears in a contradictive consequence.

One pole represents the requirements of a comfortable living and working environment, assured by a permanent energy flow through the system. The amount of energy is increasing together with the enhanced accuracy of the performance conditions.

The second pole represents loads on the natural environment. The impacts are increasing together with the rise of the standard of living conditions.

The structure of the interface is formed by dynamic control mechanisms.

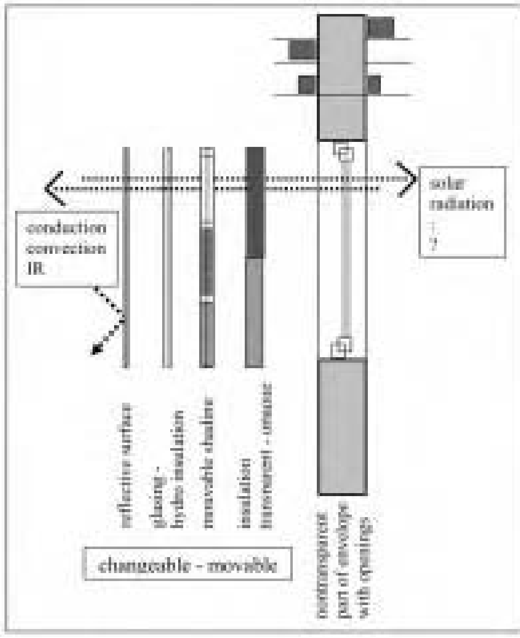

Figure 5: Window: changeable and movable system

Since the pattern of living environments is still rather conservative and there are no larger changes expected in the organisation of life, they will appear in the first place in the structure of the envelope and the selection of materials, assortment and properties. Changes in the structure of the envelope, and in the arrangement and dimensioning of different functional layers, are possible with the use of current technology. This means that they are already available. Changes in the properties of materials are on the other hand a rather longer-term prospect. Materials, which comply with these conditions, are not yet available in sufficient quantities and at reasonable prices.

The guideline is: for the dynamic demands and for changes a dynamic building and dynamic building elements are needed.

The development of new technologies, where one of the aims is energy efficient design of the living and working environment, is not a limitation but a challenge for the architectural design.

From the material point of view these are different constructional complexes and their combinations, from movable insulation and shading devices, to thermal mass, movable transparent and opaque parts of the envelope, to the control of the thermal mass and changeable properties of thermal conductivity and daylight transparency of building materials.

The technological solutions of the transfer and rearranging of the flows of energy and matter, connected to the outer and inner space and to the needs of the users by intelligent informational systems, are nearing the model of kinetic response architecture.

Automated control has opened a new market and the need for: - research and development in the field of analysis, model design and programming

equipment, - the use of new contexts in the existing technologies: devices and machines, and - demand for new products: passive components and elements in buildings as a whole. The markets for microelectronic devices, machine technology, software and the market for adequately adapted conventional building elements (windows, shades, and ventilation devices) are connected through the market of the new living and working environment.

This requires a detailed arrangement of functional elements and complexes, as well as their effective adjustment. Manual control of such a complicated, complex system is not possible.

Information and production technology with clearly defined demands and conditions for their activity must be used.

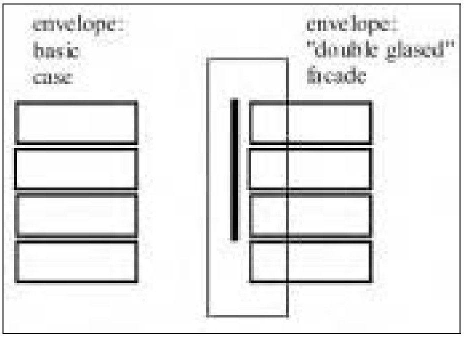

Figure 6: Classical and double envelope system.

One of the guidelines in planning new bioclimatic architecture is to consider the principle of the continuum of place and time in autochthonous buildings and living areas. Conditions in these areas are in some cases regulated, distributed, accelerated or hindered by shifting living and working spaces between closed and open areas in cyclical periods, by opening and closing of shades, and ventilation. They are represented by a mixture of thermal and light flows and man's atavistic contacts with nature, especially in the periods when external conditions are getting nearer to the demands which agree with physiological conditions for comfortable living and working environment.

Systems are as a rule not "classic" building systems from the last century. They are dynamic control mechanisms, which enable the use of as many renewable sources of energy as possible, and the use of natural light. Taking these two parameters into account at forming a built living and working environment is complementary with the principles of man's positive communication with natural environment.

From functioning of space between the outer and inner "glazing system" in double envelope system there are the two basic situations: one with the air space opened in the horizontal and vertical direction and second one with closed air spaces in the defined cross section and many combinations of the two. This intervention is aimed at the control of thermal flows but not at daylight flow.

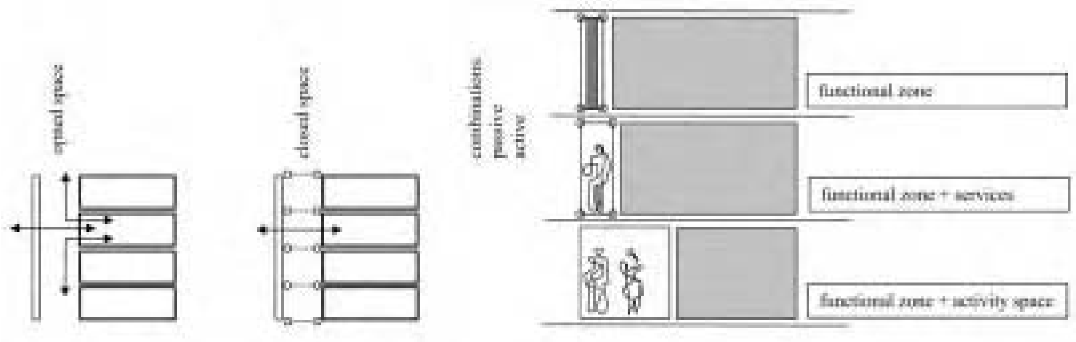

Figure 7: Double envelope functional zone

As far as the space between the inner and outer layer is concerned the first operates as a functional zone: outer ventilated or non ventilated constructional complex, the second serves as cat walk for maintenance and the third as activity space which can be used for different functions from communication to meeting spaces etc. (Figure 7)

Functionally "double envelope" represents enlargement of controlled interface area in the sense of the principle of continuum of time and space concept. It can be used in the endo- and exoskeleton load bearing construction system. Interventions of complex constructional complexes systems can be applied in both load bearing systems.

Introduction of passive techniques in bioclimatic architecture is running on one side on the level of the living space as a complex system, where general activity problems, principles of heating and cooling, daylight, air-stratified ventilation, and physical movements are dealt with. On the other side, we are dealing with the functions of materials, products and systems from the viewpoint of special demands, for example reduction of heat losses by using new materials, aerosols, transparent isolation materials, evacuated glazing, all round and changeable materials, protection against overheating, heat recovery, thermal (heating and cooling) accumulation by traditional materials with new properties, using phase change materials and their combinations with other materials, absorbtivity, emissivity, reflection and spectrally selective properties of surfaces, permeability of glasses and non-transparent parts of the envelope, using the technologies of thin layers and superconductors, optical switching, using thermo-, photo- and electrochromic materials where the control of functions is very important if we want them to operate according to the functional demands and needs, etc.

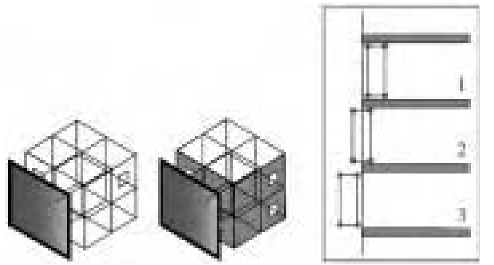

Figure 8: Double envelope system in load bearing construction system

The performance of elements and products can be controlled and adjusted on the level of functioning of selected subsystems, and on the level of automatic and cybernetic functioning of integral systems of living and working environment, starting from an isolated building to a group of buildings or living areas in a closed spatial system and in isolated dislocated buildings in special functional systems.

To ensure the optimal thermal, optical and communication conditions in the environment where these conditions are not assured passively - on the modern stage of development such conditions practically do not exist -, appropriate functional systems have to be formed, and heating energy and light have to be supplied for their functioning. To achieve this by following the ways of functioning of natural ecological systems we use the elements

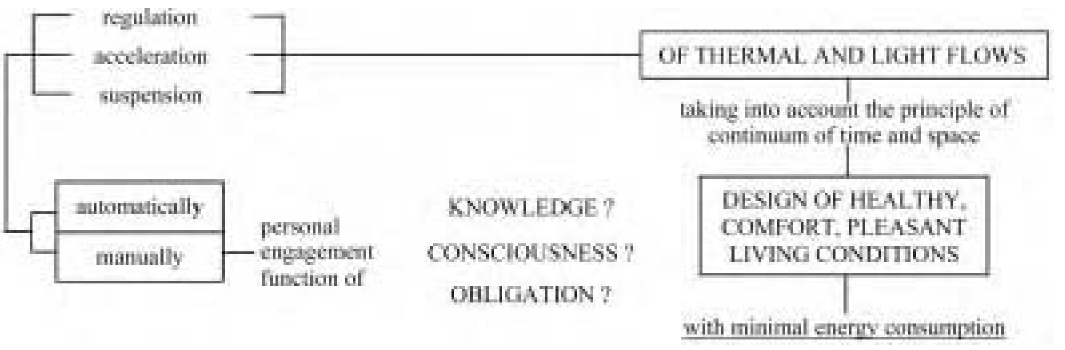

Figure 9: Scheme of influential factors of dynamic opening

and complexes of bioclimatic design.

Manual and learned control was sufficient at a certain stage of development, but the rapid change of living patterns, individual demands and accessible technology have made such control less effective.

Until recently the development was hindered by lack of appropriate control systems. On a building this is manifested by: the thermal control which enables the regulation of thermal flows coming into the building, their distribution inside the building and outflow from the building; movable shades which regulate natural and artificial lighting of spaces inside the building; rearrangement of heat mass and its possible moving or regulation; movable parts of the envelope: non-transparent and transparent; spectrally selective surfaces and changes of properties of conductivity.

Though there will be new and edge technologies included in the smart house which predicts radical changes by the end of the century, the basic shell and the design of the building will not change very much.

The automation of home is now restricted by the compatibility of products. The main problem is represented by mechanical elements and electrical installations. The development of this sphere will influence all the activities, which form a home and will probably lead to changes in life style. Marketing aspirations in the area of automation of home and working environment are still directed towards research and finding out what the owners of such buildings really want. This can, of course, only be one part of market research.

On the other hand it is clear that the main problems will be pollution and degradation of the environment, now and in the future. These problems will direct the market, whether the owners of homes, commercial buildings and production sites will accept it or not. Economic reasons will force them to automate the living and working environment.

High technology incorporated into multifunctional constructional complexes can help to harmonise the diversity of influences and conditions.

New products and technologies enable a total design of the living and working environment, of course in the ecological sense.

New information and automation technologies enable better co-ordination of information and energy flows through the entire system. Today's communication applications are expensive because manufacturers have been unable to agree on a method of communication between these products. Compatible products will be at the top of demand in the future. Potential functions of smart subsystems are limited only by imagination. The main problem is represented by the difficulty of appropriate incorporation of conventional technologies into the system. The skill of producing new corresponding mechanical devices is their limitation.

These systems are not the classical building systems of the last century when thousands years old knowledge and buildings philosophy have been disconnected. They represent dynamic control mechanisms being able to utilise renewable energy sources and natural light. The consideration of these parameters in the design

of built living environment is in accordance with the principles of men's positive communication with his natural environment.

Openings: From the time immemorial mankind has thought that meteorological and cosmic phenomena could affect the functioning of the human constitution and hence people's state of health. In the system man - environment - building the greater part of all processes run through the openings. The system started to operate at the openings. A window is a sign of life. Life means dynamics. Our conceptual problem is an apparent diversity. On one side there is a set of dynamic systems: day - night, season's cycle, weather, sun path, behaviour of inhabitants.

On the other side we wanted to have a final solution, a building where maximum limit is represented by opening and closing of doors and windows.

Solar radiation with daylight is an important factor in the quality of life in the living andworking space.

The reasons are, besides thermal flows and rational use of energy, the enhancement of the space in use, marking of passage of time and stimulation of natural dynamics.

Traditionally the greatest flexibility of the building was expressed in opening and closing the window and sometimes protecting them against direct sunlight. These solutions depended on immovability of the building and its parts.

On the other hand the outdoor environment and men's behaviour are extremely dynamic systems with daily and seasonal cycles of temperature, humidity, wind, precipitation, flora, daylight and sunlight and with men's mobility as a result of behavioural patterns of different groups of inhabitants as functions of their cultural and economic standpoints.

There are not many things found as frequently as windows in buildings. The technology of windows has not changed essentially for many centuries. Still, the window, the opening in the nontransparent part of the envelope, enables the most elegant and direct ways imaginable of using a renewable source of energy nowadays.

Improved design and production of windows, considering the place, geometry, size and structure of frames, wings and transparent parts, are vital contributions to the use of solar energy for heating and cooling, as well as illumination.

Optical and thermal behaviour of the building are inseparable but their analysis, design and control is in most cases made independent. There are many important factors and parameters, which are out of reasonable dimensions of real time systems design. One of the possibilities to harmonise the nonharmonic influences and demands is the use of the fuzzy reasoning. Kosko (1994!) presented three pages of fuzzy products in Japan and South Korea, from video camcorders to sets for cooking time and mode based on steam, temperature, and rice volume!

But none is dealing with the performance and dynamics of the window. We have tried to conceptualise some parts or possibilities of a fuzzy system, which would regulate window performance in real time conditions.

The development of information technology enables new solutions of physical design of the living environment. The interval of tolerance between natural and artificial environment is becoming smaller and smaller with the progress of human race. Manual and trained guidance was sufficient only to certain technologic levels of development. However, with the improved living patterns, demands and technologies, parallel with the decrease of tolerances and the increase of negative charges of environment, manual control just can not be efficient anymore.

It had to be taken under consideration whether to build a stationary, non- responsive building or a dynamic, responsive one. It is the question of building technology. High tech, low tech, no tech, building tech, it is difficult to accept this kind of comparison, but it is unfortunately true. The works of masters (and not only their) throughout the history hardly ever left out the highest technological know-how of the actual period.

Architectonic forms can be lines, planes or volumes: but they must always contain temporal dimension, which represents movement and life.

Building as part of the ecosystem, which with high technology harmonises different influences and conditions in the system, is the aim of the efforts of bioclimatic design of living and working environment.

The architectonic artefact is the interface between the natural environment and the human built environment, adjusted to people's needs considering both his work and life.

The devices are joining the tandem man-envelope. The limitations to the tandem manenvelope were constantly changing, connected to the demands of technological possibilities.

They are nowadays presented by the 3E-slogan ecology, economy and energy. This is mainly a consequence of the problem non-renewable energy sources generate in the last two centuries and not a consequence of some positive evolution.

The flexibility of use, which used to be only the function of place and time, is now also the function of technological possibilities of devices. After the industrial revolution the use of energy in buildings was no longer of interest for the architects. The reason was in cheap and abundant sources of energy for certain social classes where life quality reached a high level.

The other and even more important reason was in the philosophy or in misunderstanding the philosophy of modern movements in architecture, in functionalism of the twenties with its expressionist messages and its recedives.

From prehistoric times security, protection against precipitation of different phases of water, heating and cooling, and daylight were elementary parameters of the creation of living environment. With the development of human race the daylight becomes more and more important factor because it was the only one which could not be completely substituted by an artificial source.

The principle of place and time continuum can be realised by moving the functional zones, which has been known for a long time and by controlling and leading heat and light flows.

The double envelope concept enables extension of the envelope's space in the place and time continuum.

Until recently envelope's devices and mechanisms were regulated by hand. The development of information technology and computer equipment enables one step further: automated control.

The objective is the integral envelope.

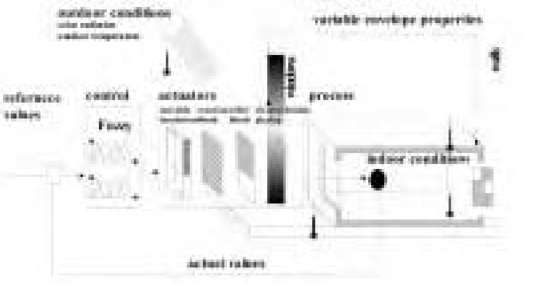

Figure 10

The energy and information flows through transparent part of the envelope are extremely diverse and by rule contradictory. Thermal flows can even run in both directions at the same time depending on radiation wavelengths and are changing permanently. Part of thermal flows depends on temperature differences between inner and outer space, and part of it on short or long wave radiation. This phenomenon is used today to trim thermal and optical responses of glazing: smart windows and surfaces: spectrally selective surfaces. Direct solar radiation on parts of inside surfaces can cause thermal asymmetry. Daylight is welcome in majority of situations, but is many times in opposition to thermal flows in winter and in summertime. Air quality and ventilation depend on number of residents, but also on the outside air quality and temperature difference. Visual connection with the surroundings is mandatory because both space and time dynamics are most important factors not only of comfort but primary of health.

Interventions in this complicated system are very complicated and demanding.

It looks like that possible answer to this problem lies in the fuzzy reasoning. Kosco (1993) wrote that we have only one decision rule: I'll do it if it feels right. In the design process and during the utilisation of the built living environment up to a certain level decisions could be based on feelings. In this cases personal presence and manual operation is necessary. Some experiments show that there are big differences between manual and automatic control (Backer, Radex office building). These differences are based on different reasons, from late response and physiological incapability to follow different processes in the environment to wrong decisions by interventions, for instance opening and closing the windows or solar protection devices.

In the presented figures the first concept of fuzzy system control in a room with two different activities: drawing and reading, during two seasons: winter and summer, and we have used evening red as an example of possible interventions which can be built in the control system.

Four examples of fuzzy system were presented during PLEA97 conference in Kushiro, Japan (Fig. 11).

Variables in the first fuzzy system are intensity of solar radiation as input, stimulus and proportion of night insulation on the window surface as output, response

The input has five fuzzy subsets: radiation is 1. very strong, 2. strong, 3. medium, 4. weak, 5. very weak. The intensity of radiation is in W/m2. The output has also five fuzzy subsets: night insulation is 1. fully opened, 2. nearly fully opened, 3. half opened, 4. nearly closed, 5. closed. The degree of night insulation on the window is in per cent.

They are drawn in Figure 1. The triangles are used because they are simple and illustrative, but it can be bell curves or trapezoids, depending on common sense or engineering judgement.

To define fuzzy rules stimuli are associated with responses. That gives five rules:

Rule 1.: If radiation is very weak, NI is closed.
Rule 2.: If radiation is weak, NI is nearly closed.
Rule 3.: If radiation is medium, NI is half opened.
Rule 4.: If radiation is strong, NI is nearly fully opened.
Rule 5.: If radiation is very strong, NI is fully opened.

These fuzzy rules are like 3D patches. In the presented case they are in the form of pyramid.

Each point on the pyramid base is a product of stimulus and response. The height shows the degree to which the number belongs to the rule patch.

The main advantage of this approach is the possibility of establishing rules of thumb and experience. The real engineering is based on knowledge, and knowledge is rules.

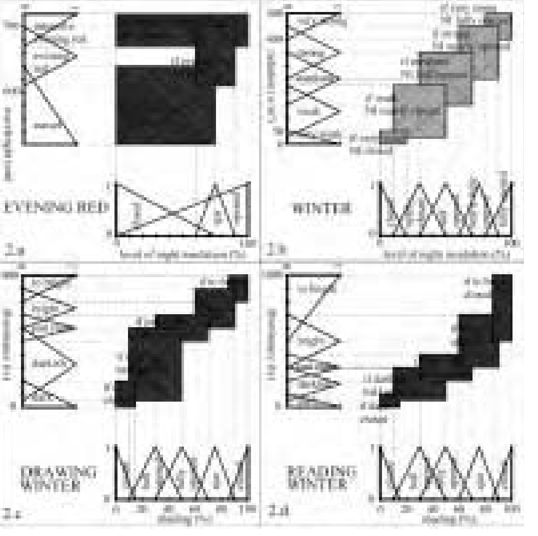

Figure 11: Concept of fuzzy system

The fuzziness in the rules leads to smooth control. Evening red can be watched only from spaces with western orientation. In this case special sensor is actuated, it sends a command, all bus devices listen in, but only the actuator assigned to the movable night insulation element in selected room(s) executed the command in spite of the fact that thermal sensors have different opinion, because outside air temperature is to low and solar radiation power is too small. The information is forwarded on priority bases so the system logic is maintained at all times. In this system infrared cordless switching can be used.

The correct performance of the information system, leading energy and matter flows and the mobility of men is a prerequisite for socio-ecological cycles to approximate natural ecological systems. The application of artificial intelligence (AI) and automation is enabled by the recent developments in information technology and electronics. New technologies enable to shape the system of the smart bioclimatic house, part of which is the interactive envelope.

References

[1] Kosko, B. (1994) Fuzzy Thinking, Flaminco, London, GB.

[2] Birch, S. and Frame, I. (1991) DAYLIGHT version 4.1b, Anglia Polytechnic, GB.

[3] Paassen, A.H.C. and Lute, P.J. (1994), Controlled Ventilation Windows, European Directory of Energy Efficient Building, James&James, London.

[4] Krainer, A., Kladnik, R. (1993) Nove tehnologije za rabo in pretvarjanje energije, C2-353-792-93, Faculty of Arch. & C.E., Ministry of Science and Technology, SI.

[5] Krainer, A., Kladnik, R. (1995) Smart House, Thermodynamics and Optics, P2-5226-0792-95, Faculty of C.E., Ministry of Science and Technology, SI.

[6] Krainer, A., Toward smart buildings, (Building science and environment-conscious design, Module 1: Design principles, 7). London: European Commission, 1993. 84 str., ilustr. IBSN 09525703 7 8, [COBISS-ID 16080389]

[7] Krainer, A., et.al., Research Programme, Renewable energy sources, PO-0504-0792, RS,

[8] Ministry of Higher Education, Science and Technology, 1999-2003.

[9] Krainer, A., et.al., Research Programme Building Constructions, Renewable energy sources, P2-0158, RS, Ministry of Higher Education, Science and Technology, 2005-2008.

EU COST C13 Glass and Interactive Building Envelopes. M. Crisinel, et al. (Eds.). IOS Press, 2007.

Luminous Efficacy Based on Fuzzy Controlled Roller Blind Positioning

Aleš Krainer, Jože Peternelj, Živa Kristl, Vito Lampret
University of Ljubljana, Faculty of Civil and Geodetic Engineering
Chair for Buildings and Constructional Complexes

The knowledge of luminous flux and illuminance phenomena is necessary for proper and qualitative dimensioning and arrangements of openings and thus for comfortable and efficient living environment. In this paper the concept of luminous efficacy of the solar energy as the basis for the control algorithm is taken into account. Luminous efficacy *K* is defined as the ratio of luminous flux to radiant flux, $K = \Phi_V/\Phi_e$. The idea was to design a flexible dynamic building envelope, which will be able to adjust itself to the changeable environmental conditions regarding the inner illuminance requirements. Changes of the opening's geometry are implemented by moving the roller blind. The roller blind is used to control the inside illumination of human-built environment in real time conditions. We realized the concept of the control with fuzzy elements in the control algorithm for automatically adaptable shadow device on the window. For this purpose a model of a real physical system, a test chamber with an opening equipped with movable roller blind on the south side was build. The fuzzy control system manages the roller blind movement, which enables the optimal use of the available solar energy in order to assure the desired internal illumination.

I. INTRODUCTION

Luminous flux Φ_V is a quantity derived from radiant flux Φ_e by evaluating the radiation according to its action upon the standard photometric observer. Consequently, luminous efficacy K is defined as the ratio $K = \Phi_V/\Phi_e$ of luminous flux to radiant flux. Daylight in the building and possible outside view enhance the visual comfort and mean well designed living space offering psychological benefits together with lower conventional energy consumption.

Our aim was to design a flexible dynamic window geometry that will adjust itself to the changeable environmental conditions regarding the internal set-point illuminance. The geometry of changeable window is realized on test chamber, which has a system for automatically adaptable roller blind positioning. Changeable window geometry enables the control of the dynamic illumination response of human-built environment in real weather conditions.

The control concept was first developed through series of experiments, where the luminous efficacy in the building, derived from solar radiation with unshaded window, was observed. Then we investigated the luminous response of the chamber, when the window geometry was alternating. Based on the experiments the design and the optimization of the automatically adaptable roller blind to control the energy flows through window was realized.

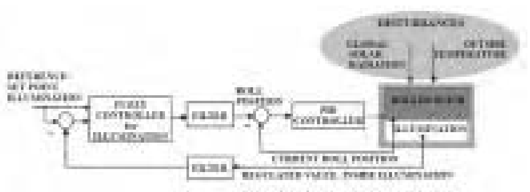

Figure 1: Scheme of the illumination control loop.

The fuzzy logic is incorporated in the controlling system. We emphasized the design of the "illumination" fuzzy controllers. They are of essential importance because they determine the adequate roller blind position and consecutive internal illumination in accordance with the available solar radiation. Such automatic device on windows enables the optimization of visual performance together with efficient use of energy.

II. TEST CHAMBER AND THE MEASURING EQUIPMENT

The fuzzy system for managing and controlling the illumination process with automated reaction of movable roller blind is executed in the test chamber. It is equipped with all the necessary sensors to measure the outdoor and indoor conditions, and with the necessary control equipment. The test chamber was built on the roof of the Faculty of Civil Engineering, UL, Ljubljana (46.0° latitude, 300 m altitude). Its dimensions are 1 m x 1 m x 1 m. The chamber is raised off the ground and the roof is ventilated in order to avoid the overheating caused by direct radiation on the roof. Walls, floor and ceiling are built of lightweight brick blocks. Material properties are shown in Table 1.

TABLE 1: MATERIAL PROPERTIES FOR THE TEST CHAMBER ENVELOPE BUILD OF LIGHTWEIGHT BRICK BLOCKS:

Thermal conductivity k [W/mK]	**Density ρ [kg/m3]**	**Specific heat c [Ws/kgK]**	**Thickness d[m]**	**Absorption coefficient**
0.270	500	0.270	0.010	0.45

The south wall is completely glazed with double-glazing composed of two layers of standard clear glass and air fill, the thickness of wooden frame is 5 cm.

To follow the internal set point illumination with proper reaction of the roller blind regarding the available daylight potential, series of real time measurements are necessary. The measured values for internal and external lighting conditions are:

- direct solar radiation,
- reflected solar radiation measured with pyranomether CM-B (Kipp&Zonnen Delft BV),
- internal illumination measured with luxmeter LUX cell, and
- current position of the roller blind.

The transparent size of the envelope depends on the temporary roller blind position, expressed in percentage of shaded area with regard to the whole glazed area. The displacement sensor measures the exact roller blind position. The test chamber for achieving the desired optical internal conditions with the use of the radiant solar energy contains:

- 1 m^3 physical plant - test chamber - with the necessary measuring equipment.
- Mitsubishi programmable logic controller PLC, which enables the execution of the designed control algorithm.
- Operator panel and personal computer for supervising and managing the process.
- Roller blind with electric engine.

The shading ratio of the window is a time depended parameter and the shading changeability is enabled with the industrial process automation and control equipment, which is incorporated in the test chamber. With this automation the real time experiments are executed with on-line visualization, with data acquisition of all the necessary values for system analysis and with system state alarming. The alternating window geometry is realized with the automatically adaptable roller blind position. The roller blind is an external PVC blind. The alternating position is managed with the aid of the industrial programmable logical controller - PLC. The control algorithm with fuzzy logic is designed in IDR BLOK program environment, which enables PLC to perform the movement of the roller blind to the desired position.

III. THE CONTROL ALGORITHM

Automatically adapting shading ratio of the windows appears as a great opportunity to indirectly control the internal daylight level and consequently the thermal comfort, taking into account new information technology. This process represents inexhaustible possibilities to study alternative control design approach. The illumination control system is functioning with the aid of the control algorithm, designed in the IDR BLOCK environment. The developed control algorithm enables the automatic reaction of the roller blind considering the required set point internal illumination and available solar radiation. With the roller blind alternation the lighting process and partiality also the thermal process in the test chamber is controlled. Light and thermal energy are in direct connection and are inseparable.

The implemented algorithm is synthesized and optimised in IDR BLOK programmable environment and contains fuzzy controllers as alternative approach in control strategy. Different control elements and strategies are included in the scheme: from feed forward open loop control schemes, to closed loop control, using conventional PID and fuzzy controllers that are connected into cascade. Some of these elements are assigned as subroutines to IDR blocks. Because of extremely varying and mostly unpredictable external conditions: the available solar global radiation and the ratio of the direct/reflected radiation, the fuzzy controllers are used. The adequate position of roller blind is appointed with the aid of the fuzzy logic system incorporated in fuzzy controller.

The controlling algorithm is designed to produce suitable signals for the roller blind positioning as a response to changeable external weather conditions in order to harmonize the external available solar radiation with the internal lighting demands. By properly setting of the algorithm parameters, such as parameters of the PID controller, filter time constants, sampling times and priorities of the loops in the control scheme, the manner and the velocity of window geometry alternations as response to the changes of working conditions, are defined. The priority of the optimization is tuning up the fuzzy controller.

IV. THE FUZZY LOGIC IN CONTROL ALGORITHM

Among other possibilities preliminary studies [2,3,5] indicated that only conventional approaches in controlling systems for the window geometry alternation give inadequate results in extremely varying external conditions. Non-linear boundary conditions, time varying characteristic, and complex physical environment are difficult to frame in a mathematical model (e. g. systems of differential equations). One method that simplifies the complex system and tolerates a reasonable amount of imprecision, vagueness and uncertainty during the modelling phase is application of fuzzy logic. Changeable and unpredictable weather regimes during the year stimulated us to develop a control algorithm with fuzzy logic approach. Fuzzy system could represent more appropriate solution and can be designed without precise mathematical model. Illumination fuzzy controller is derived from the knowledge of the real time processes and the control algorithm was designed and optimised using observations of alternations of window geometry and corresponding internal lighting conditions. We observed how the alternation of the window geometry - roller blind positioning - influences the internal lighting. The fuzzy controller was tuned on the basis of trial error experimentation. In fuzzy systems the advantage of reduced complexity is considered. It is achieved as a way of defining nonlinear transition function between the input and output values without the need to specify each numerical value individually. The quality of the developed model can be measured only with regard to the desired reactions of the system in working conditions; the system in use must behave in a desired way. However, no general tuning methods exist to design a fuzzy controller for the observed illuminating process.

Control algorithms with incorporated fuzzy regulators prove better robustness and efficiency in the case of more complicated non-linear and time varying working conditions compared to exclusively conventional approach - PID, PD, I, controllers. An important advantage of forming the fuzzy controller is its design, deriving directly from human reasoning. Fuzzy system, closely related to human reasoning, is based on set of premise-conclusion rules. We want to simulate the behaviour of an operator who manually adapts the movable shadow device by taking into account the internal demands and the external conditions. It is founded on linguistic model, which is expressed with the set of conditional rules, IF-THEN statements. The idea is realised with incorporated fuzzy controller, called “illumination” controller, in the control algorithm to control the inside illumination level. Effective fuzzy control algorithm is obtainable, when the optimal free fuzzy parameters are carried out.

To describe the human behaviour, we have to find out the set of linguistic rules, IF-THEN statements. Although in fuzzy logic the mathematical rules are rigorously considered, one of its advantages is its ability to describe the system linguistically through rule statements. An example of such control rule statement for the roller blind positioning is: “ ***IF*** global solar radiation is low ***AND*** the difference between the desired and measured inside illumination is positive medium ***THEN*** the roll position is very open.”

Several similar rules are used to describe the system-controlled response. Therefore, the basic features for the design and setting the fuzzy controller are:

- Defining the input and output linguistic variables and their corresponding domain.
- Measured values must be defined by fuzzy sets. Fuzzy sets are represented by linguistic terms, and the measured values belong to them with different degrees, called grades of membership. In treating the domain of each variable (inputs or outputs) the fuzzy sets must be properly arranged, as it is pointed in Figure 2.
- Defining the fuzzy logic operators for each IF – THEN sentence, which has essential impact on the final inference and output value?

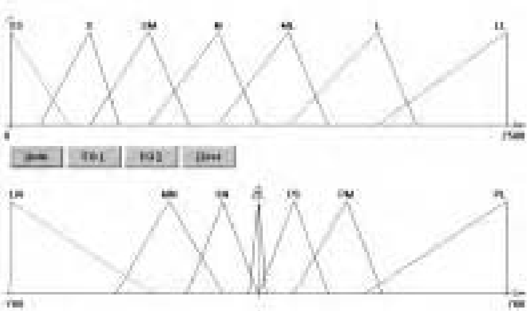

Figure 2: Input values defined with fuzzy sets.

In IF-THEN statements the input and output values expressed with the set of membership functions are combined with the aid of logical fuzzy operators. The input – output correlation is non-linear mapping between two linguistic inputs and one linguistic output and the correlation is graphically represented with the specific 3D surface as is shown in Figure 3.

The actual numerical output value, in our case current position of the roller blind, is located on the 3D shape, depending on the currently measured values of boundary conditions and on the designed fuzzy system.

Illumination fuzzy logic controller determines the roller blind position as output value. The input variables are the measured inside illuminations and the difference between the inside illumination and the set point illumination. All rules of the set of the fuzzy system are evaluated with the aid of the equations to determine the final crisp output value of the fuzzy controller. This is a signal value, which determines the desired position of the roller blind. Fuzzy controllers enable a high level of the system's adaptability to local specifics, appearing in every building. Their functioning is transparent, and they are adjustable to the manner of human thinking and perception processes.

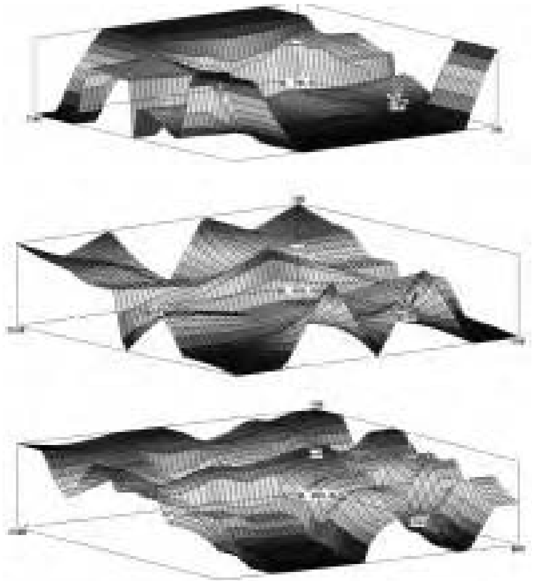

Figure 3. Examples of 3D surface as non-linear mapping between inputs and output as fuzzy controllers for wintertime and summertime illumination regulation.

V. LUMINOUS FLUX AND LUMINOUS EFFICACY

Daylighting is an important and useful strategy in lowering the conventional energy consumption from the cost saving and ecological point of view, and it offers also a psychological benefit. Considerable energy savings result from daylighting, which results in the reduction of the artificial lighting, reduction of cooling loads and offers a potential for reduced heating, ventilation and air-conditioning. The available daylight inside in the building depends on the solar radiation and building geometry. Weather conditions and the level of cloudiness determine the terrestrial total solar radiation and the ratio of diffuse/direct radiation. The solar reflected part depends on the external built environment. Actual daylight illuminance in a room is related to the luminance pattern of the sky and also on the window geometry with regard to the room size dimensions. An important impact on the internal illumination level has the surface properties: absorption, reflection and in the transparent parts of the envelope transmissivity. Luminous flux and luminous efficacy correspond to the solar radiant flux. Spectral distribution of the solar energy is roughly equal to black body spectrum at the temperature of T = 5773 K. The spectral distribution of radiant flux represents the rate at which a body emits radiant energy per unit range of wavelength expressed in watts/nm (1nm = 10-9m), as is presented in Figure 4. [3]

For the purpose of illuminating engineering only the visible part of the total radiant flux is important.

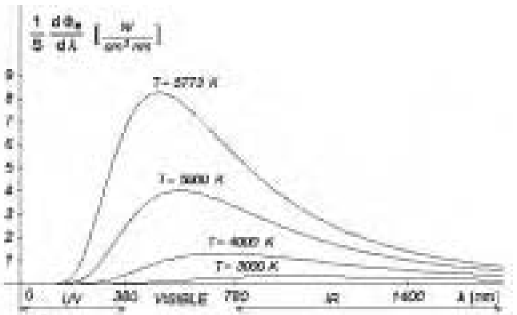

Figure 4: Spectral distribution of radiant flux with respect to wavelength of the emitted radiation. i.e. T = 5773 K, 5000 K, 4000 K and 3000 K.

For the harmonisation of thermal and daylight radiation flows it is necessarily to know what is the effectiveness of the total solar radiation in producing the optical effect. Therefore, the ratio of luminous ΦV to radiant Φe flux is defined as a luminous efficacy K (K= ΦV/Φe). Luminous flux ΦV [lm] is a quantity derived from radiant flux Φe [W] and it is evaluated from the radiant flux Φe [W] with respect to its capacity to evoke the sensation of brightness in human eye regarding the relative luminosity curve for standard observer. In illuminating engineering the same definition is given for the term "light", so it is synonymous for the luminous flux ˜V with unit lumen [lm]. The effectiveness of the given radiant flux Φe in evoking the sensation of the brightens in human eye depends on the spectral distribution Φe/dλ and on the spectral luminous efficacy K(λ) of radiation. Visual sensation has maximum in radiant flux Φ e of wavelength 555 nm, and this corresponds to the peak of standard luminosity curve. Therefore the luminous efficacy K [lm/W] for monochromatic flux is maximum, 685 lumens/1 W.

The wavelengths of the visible light are in the interval 380 nm ≤ λ ≤. 780 nm. Luminous efficacy K of solar radiation is given with the ratio of the luminous flux of the visible light Φ V (380 nm ≤ λ ≤ 780 nm) and the whole solar radiant flux Φ V (0 nm ≤ λ ≈ 2,5 nm). The maximum luminous efficacy of the solar radiation is K = 93 lm/W. This is "overall" luminous efficacy defined as the ratio of the luminous flux output of the total solar radiation to the total solar radiant power, and it approximately corresponds to the black body radiation at a temperature of T = 5773 K.

VI. MEASUREMENTS AND EXPERIMENTS

Internal illumination level is in direct dependence with the given solar radiation and of other design conditions mentioned above. The penetration of the daylight in the test chamber was controlled with the movable shadow device. With proper positioning of the roller blind we try to follow closely the desired internal illumination given as a set point illumination profile. First we observed the solar luminous efficacy in the test chamber during the year, when the roller blind was fully open. Experiments are presented in Figures 5, 6, 7 and 9.

In the figures the outside conditions, such as global and reflected solar radiation, the inside illumination, the luminous efficacy and the position of the roller blind, are shown. When the roller blind is active, the inside illumination is the controlled value, which follows the set point illumination. With automatic positioning of the roller blind the inside illumination is corrected.

The observed luminous efficacy of the solar radiation is based on the measured external global solar radiation and the measured internal illumination. Luminous efficacy [lm/W] presented in these figures is derived from the ratio:

K: Luminous efficacy = (measured inside illumination)[lx]/(measured external solar radiation) [W/m2].

The given external solar radiation is composed of the direct and the reflected component. Figure 5 and 6 present the inside illumination, inside solar luminous efficacy by given solar radiation, when the window is unshaded.

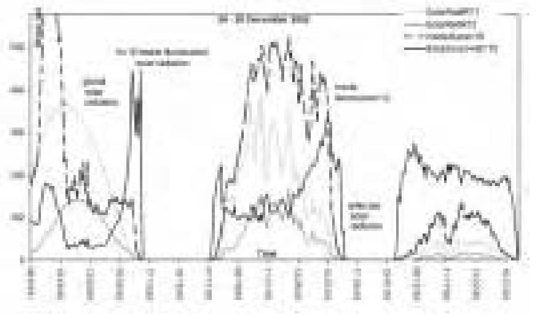

Figure 5: Internal measured daylight illumination, when the window is unshaded. The luminous efficacy in the test chamber is the response to solar radiation, global and reflected. December 24-28, 2002.

It is evident from Figure 5 that the solar luminous efficacy is better in the morning and in the evening, when the solar radiation is low. It is interesting to note that luminous efficacy is high and more even, when the sky is overcast, the light is diffuse and the direct solar radiation during the day is relatively low, in comparison with the clear sky. In the third day the luminous efficacy is very high in spite of low global solar radiation, the sky was completely overcast.

In Figure 6 we can observe the luminous efficacy by a given solar radiation in April, when the window is unshaded. During the first of two days the solar radiation is high, and during the second day the solar radiation is low, because the sky was overcast. The solar luminous efficacy is better in the second day taking into consideration the low solar radiation.

The comparison of the solar luminous efficacy in December and in April shows that it is high in the winter, when the solar radiation is lower and the sky is mostly overcast, as the available solar radiation is diffuse.

We observed further light behaviour and luminous efficacy of the test chamber when the window geometry was automatically adaptable with the aim to follow the set-point illumination profile. With the roller blind positioning the internal illuminations is controlled taking into account the measured solar radiation, global and reflected. The current decisions of proper positioning of the roller blind are defined with the designed “illumination” fuzzy controller.

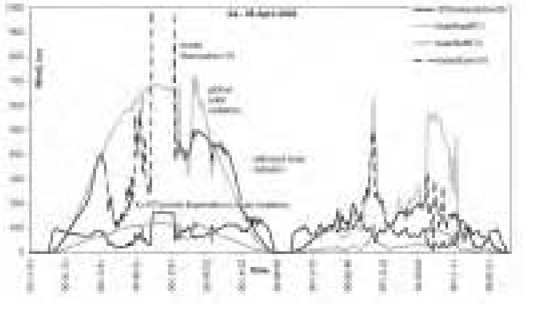

Figure 6: Illumination inside by unshaded window, global and reflected radiation. The luminous efficacy is response to global solar radiation. April 02-05, 2002.

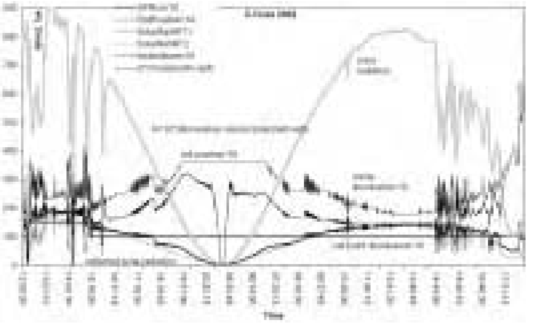

Figure 7: Internal daylight illumination approaches the set-point profile with the automatically adaptable roller blind positioning. The inside luminous efficacy is the response to global solar radiation and to roller blind alternation. June 05-07, 2002.

Typical charts in Figures 7, 8 and 9 are taken from the experiments. They show the measured global and reflected solar radiation, inside illumination, luminous efficacy and roller blind positions. In Figure 7 the controlled inside illumination follows the set point illumination profile. The deviations are in the range of ± 100 lx. The deviations of the inside illuminations from the set point values are in the admissible tolerance. The roller blind alternations are too oscillatory.

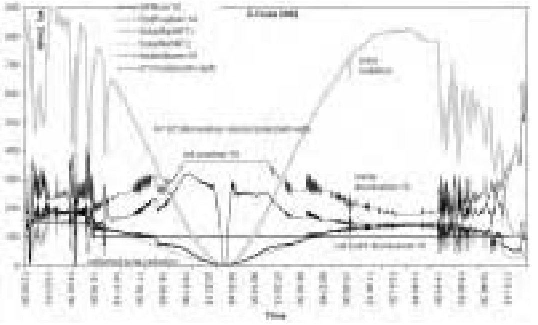

Figure 8: With automated roller blind positioning the illumination set-point value is followed. The inside luminous efficacy corresponds to global solar radiation and roller blind alternation. September 26-27, 2002.

Figure 8 shows the experiment, where the fuzzy system was improved (the membership functions of the input variables are rearranged and their distribution is more dense) and the filter time constants were reset to higher values. With these provisions the roller blind alternations are less oscillatory. In spite of very variable solar radiation the deviations of the inside illumination from the desired values are still in the acceptable range ± 150 lx. The experiment shown in Figure 9 was executed with still more improved fuzzy system. The truth table, where the IF-THEN control rules are framed, is partly corrected. Other logical operators were used in some rules and also the consequent parts of some rules were changed. The deviations of the controlled inside illumination are in the range up to ± 200 lx. This is satisfaction because of the changeable solar radiation and the desired inside illumination profile was changed several times.

From Figure 7, 8 and 9 it is evident that solar luminous efficacy is in close dependence with roller blind alternations. This obvious fact confirms that with automatically adaptable window geometry to outside solar radiation the visual comfort and partly also the thermal comfort are controlled with the use of the renewable energy. Possible oscillations of illumination are in the range of 1000 to 5000 lx or more in a few seconds. Therefore it is difficult to find a well-defined fuzzy model to conduct the roller blind. From these Figures it is also evident, that an illumination fuzzy controller with good designed fuzzy model enables the internal daylight illumination with relatively moderate continuous movement of the roller blind in the area, where the desired value deviates up to ± 200 lx.

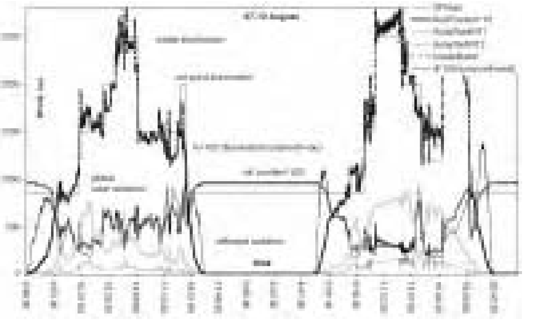

Figure 9: Internal daylight illumination follows the set-point value with the aid of the roller blind positioning – automatically adaptable. The inside luminous efficacy depends on solar radiation and roller blind alternation. August 07-09, 2002.

VII. CONCLUSIONS

The available luminous flux and illuminance in the building is in close dependence with the available solar radiation. It is necessary to assess the quantity and the quality of the available solar radiation for the design and the optimization of the control system, which enables the dynamic response of the transparent parts of the envelope. Daylighting and the internal thermal comfort are essential factors for a good design of the built environment. In this paper the solar luminous efficacy is introduced as observed variable through experiments. The experiments were executed in the test chamber when the window was unshaded and by adjustable window's geometry. The window geometry is automatically adjustable, taking into account the given solar radiation, and it is realized with fuzzy control system.

Luminous efficacy K is defined as the ratio $K = \Phi V/\Phi e$ of luminous flux to radiant flux. It is a quotient, which tells us the real efficacy of the daylight in the sense of internal visual performance taking into account changeable weather conditions. This ratio describes the relationship between the optical and thermal effect of the available solar energy. In the case of ushaded window it was proved that in overcast diffuse sky, when the light is less intense, the luminous efficacy is high. Luminous efficacy in wintertime is also higher than it is in springtime considering the available solar radiation. The diffuse sky means uniform daylight illumination during the day and high luminous efficacy compared to clear sky conditions. Therefore, in such days the shading devices can be fully open.

We made out a window-shading device that adjusts itself to the changeable solar radiation regarding the inner illuminance demands. The roller blind alternation is managed with the fuzzy controller, which contains the control rules directly derived from the observed process. Functioning of the fuzzy controllers is transparent; they are adjustable to the manner of human thinking and perception processes. The design of fuzzy controllers is based on setting up a set of linguistic control rules. The approach is based mostly on experimentation, on real trial error experiments.

The fuzzy control system, which regulates the adaptable roller blind to control the inside illumination, enables the optimal use of the available solar energy for improving the optical and partly also the thermal inside comfort. With the aid of the experiments the fuzzy control system was improved and optimised. The light fuzzy controller, which gives the best controlling performance, assures the inside daylight illumination with moderate continuous movement of the roller blind in the area, where the desired value deviates up to ± 200 lx.

As we simultaneously observed the luminous efficacy in experiments it was proved that internal luminous efficacy value follows the roller blind position. The exceptions are mornings and evenings, when the sun rises or sets and the sky is clear. In these cases the solar radiation is less intense, but the solar luminous efficacy is very high. Therefore, in the mornings and evenings the openings must be unshaded to ensure the biggest solar gain without excessive heat gain in summertime.

REFENCES

[1] Lampret V, Peternelj J, Krainer, A. Luminous flux and luminous efficacy of the black-body radiation-an analytical approximation. Solar Energy 2002; 73(5), 319.

[2] Research project: Smart house: Interaction between dynamic opening and envelope J2-9080-0792-99, Krainer A, FGG, Zupančič B, FE, and Ministry for science and technology, (1997-1999) Ljubljana.

[3] Trobec Lah M, Krainer A. Light and thermal energy coordination in a building with fuzzy logic scheme at dynamically changeable opening – experimentation on real model. The 4th ISES-Europe Solar Congress, Bologna, Italy.

[4] Kladnik R, Krainer A, Perdan R. Light and thermal energy coordination in building. PLEA 1997 KUSHIRO : the 14th International Conference on Passive and Law Energy Architecture 1997, 59-64.

[5] Škrjanc I, Zupančič B, Furlan, B, Krainer, A. Theoretical and experimental fuzzy modelling of building thermal dynamic response, Building and Environment 2001; 36:1023-1038.

[6] Krainer A. Comparative analysis of interactive influence of the geometry and structure of the opening and space on energy balance of the room. Faculty of Civil Engineering, University of Ljubljana, 1990.

EU COST C13 Glass and Interactive Building Envelopes. M. Crisinel, et al. (Eds.). IOS Press, 2007.

Carbon Emissions Calculation for Non-Residential Buildings: Integration of Daylighting Analysis in Dynamic Energy Simulation Software

A. Simonella, A. Franceschet, H. De Bleecker, M. Zobec
Permasteelisa Research & Engineering

This paper highlights the integration of the dynamic daylight simulation software DAYSIM [1] into the transient simulation software TRNSYS [2] in order to predict the energy reduction due to the availability of daylighting and lighting control strategies. The simulation of two different envelope configurations (traditional wall with 40% of glazed area versus a fully glazed curtain wall) fitted in an office room is performed on the basis of real weather data (London). The energy consumption and carbon dioxide emissions of both envelope systems are calculated for various lighting control strategies.

I. Introduction

Electrical energy produces from 30 to 60% more carbon emissions than other types of fossil fuels [3]. Moreover electricity use for artificial lighting represents a significant part of the total energy consumption in non-residential buildings. Different control strategies for artificial lighting can be used in order to minimise the time that the light are switched on. In that way, less electricity consumption for light can be achieved and, at the same time, it results in a lower internal heat gain, which reduces again electricity consumption for cooling. In order to predict this energy reduction, the integration of dynamic daylight simulation software into transient simulation software has to be established.

II. Daylight Integrated In Dynamic Modelling

The authors have opted to use DAYSIM, which is a RADIANCE-based dynamic simulation tool, to calculate the hourly profile of the total indoor illuminance level throughout the year, resulting from the variations in the different sky luminance distribution. In general simplified methods to predict the daylight availability (and the consequent artificial light use) during the year are based on the Daylight Factor approach considering only external diffuse illuminance. This approach does not take into account the direct light part and therefore only approximated results are produced and important parameters such as the influence of the orientation of the façade on the light levels in the building are missing. DAYSIM, instead, calculates the total illuminance distribution, which includes the diffuse and direct part of the daylight spectrum. Moreover, simulating a detailed daylighting model usually requires the detailed description of the sky luminance distribution: high frequency and high quality data, available only from few measurement stations, are thus necessary. But by using DAYSIM, it is possible to produce a detailed sky model elaborating a simple weather data file consisting of direct and diffuse horizontal irradiance, which can easily derive from meteorological databases such as Meteonorm [4]. The results of DAYSIM have been validated [5]. The output from DAYSIM is a data file containing the annual profile of illuminance for predefined points in the building, located at work plane level (0.85m from the floor).

In order to calculate the impact of artificial lighting, energy consumption and heat production on the whole building energy consumption, DAYSIM results have to be imported within a dynamic whole building simulation program for which TRNSYS was chosen (see Figure 1).

TRNSYS is a transient building simulation program that relies on a modular approach to solve large systems of equations described by Fortran subroutines. Each subroutine contains a model for a system component: the subroutine describing the building has to be created by the utility program PREBID [6], then linked with the other components on the user interface and simulation general environment IISiBat [7] (Intelligent Interface for the Simulation of Buildings).

The inputs for the IISiBat environment are then the weather data, the DAYSIM output file and the output file of PREBID. In particular, the DAYSIM file (annual variation of illuminance on the work plane) allows including hourly electricity consumption and internal thermal gains due to artificial light in the overall energy consumption.

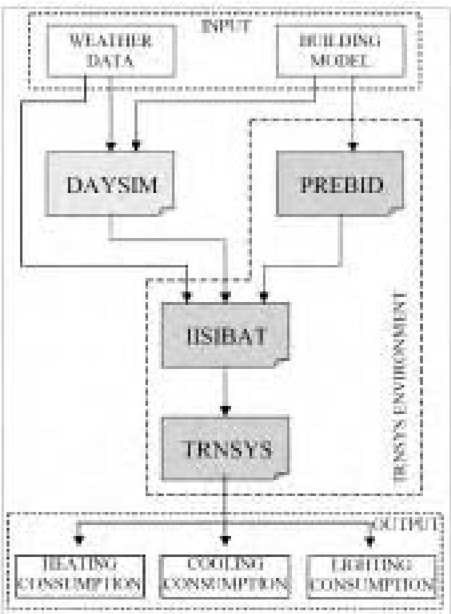

Figure 1: Concept of the integration between the two dynamic simulation software tools.

III. Office Room and Site Description

The integrated methodology is now applied to a typical office room in London (see Figure 2). Two different envelope configurations are fitted in the room: a traditional wall with 40% glazed area versus a fully glazed curtain wall. The room model has the following dimensions: 6.2 x 8.0 x 3.5 m³ (length x width x height) and is situated in the centre of a building surrounded by similar adjacent rooms.

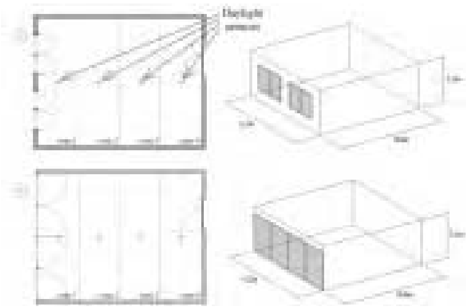

Figure 2: Geometry of the building rooms.

The only façade in contact with exterior environment is south oriented and has two different geometries and two different glazing systems two different geometries and two different glazing systems (see Figure 2). Three external façade types (A, B1 and B2) are researched (see table 1).

The different glazing properties used for the simulation are summarised in table 2. The configuration A has a 40% of glazed area and is set as the traditional case, cases B1 and B2 represent a fully glazed façade, in particular for case B1 a conventional clear glazing system is taken whereas for case B2 a high performance glass is used.The construction data of the walls, floor and ceiling used for the simulations are taken from IEA Annex XII [8] and are summarised in table 3.

The room is situated in London and therefore the weather data file for Kew meteorological station has been derived by means of Meteonorm and is used for both daylighting and energy analysis. For DAYSIM just the hourly direct and diffuse irradiance on horizontal surface have been used where for TRNSYS the same file and additionally the external air temperature is considered.

TABLE 1. FAÇADE TYPE DESCRIPTION

façade type	geometry	glazing system
A	40% transparent surface	clear
B1	100% transparent surface	clear
B2	100% transparent surface	high performance, selective coating

TABLE 2. GLAZING SYSTEMS DATA

building transparent components	area	thermal transmittance	solar factor	visual transmittance
	A [m²]	U [W/m².K]	g [-]	τ_{vis} [-]
A: 4mm clear glass 12mm air cavity 4mm clear glass	6.845	2.8	0.76	0.82
B1: 8mm clear glass 16mm air cavity 8mm clear glass	17.255	2.6	0.69	0.78
B2: 8mm high performance glass (ε=0.04) #2 16mm air cavity 8mm clear glass	17.255	1.4	0.33	0.61

TABLE 3. CONSTRUCTION DATA

building opaque component	area	material	thickness	volumic mass	specific heat	thermal conductivity	total thickness	thermal transmittance	visual reflectance
	A [m²]	-	d [m]	ρ [kg/m³]	c [J/kg.K]	λ [W/m.K]	D [m]	U [W/m².K]	ρ_{vis} [-]
side walls	56,0	plaster brickwork plaster	0.005 0.180 0.005	1300 1100 1300	940 940 940	0.600 0.440 0.600	0.190	1.68	0.50
rear wall	18.4	plaster brickwork plaster	0.005 0.180 0.005	1300 1100 1300	940 940 940	0.600 0.440 0.600	0.190	1.68	0.50
external wall	13.9 (A) 3,1 (B)	fibre cement air cavity mineral wool brickwork plaster	0.010 0.030 0.100 0.120 0.005	1800 - 40 1100 1300	865 - 600 940 940	0.480 R=0.17m²K/W 0.033 0.440 0.600	0.265	0.27	0.50
floor	49.6	carpet mortar mineral wool concrete plaster	0.005 0.050 0.020 0.160 0.010	500 2200 80 2400 1300	1470 1100 600 1100 840	0.100 1.400 0.036 1.800 0.520	0.245	1.03	0.30
ceiling	49.6	plaster concrete mineral wool mortar carpet	0.010 0.160 0.020 0.050 0.005	1300 2400 80 2200 500	840 1100 600 1100 1470	0.520 1.800 0.036 1.400 0.100	0.245	1.03	0.65
frame	0.955 (A) 1,345 (B)	aluminium	0.050	2700	3430	5.0	0,050	5.00	0.70

IV. DAYLIGHTING SIMULATION MODEL

The input for DAYSIM (see Figure 1) is the geometrical model of the office room (containing the material visual properties and the position of lighting sensors) and the weather data file. For AYSIM the visual reflectance for opaque elements (walls, floor, ceiling, etc) and visual transmittance for transparent materials (glazing system) is defined (see table 2). The elements are supposed to be grey. Previously the room has been subdivided in four different zones and in the centre of even/ zone a sensor is positioned at work plane level (0.85m from floor) at different distances from the external fagade. The output file contains the hourly values of the illuminance on the four sensors positions (which is a function of the control strategy for the artificial lighting). The minimum required illuminance level on a work desk for an office is generally 500 lux (from main European standards) and this value has been taken as a limit. The artificial lighting system considered needs 12W/m2, so about 150W per zone [g].

Four different light in control strategies have been considered:

- Occupancy dependent switch 1 one zone: the control has been simulated considering the artificial light profile following the occupancy: all lights are connected together and there is one switch for the whole office;
- Daylight and occupancy dependent switch / one zone: similar to the previous control but in addition the switch will turn off the whole artificial lighting system when in every sensor the illuminance is higher than the minimum required level (500 lux)- 7
- Daylight and occupancy dependent switch 1 four zones: as the previous one but every zone has an independent switch;
- Daylight and occupancy dependent dimmer / four zones: the control will modulate the light intensity of the fixture to compensate the daylight illuminance in order to reach the minimum required illuminance level on the work plane (500 lux). There is one control for every zone.

The name used in the paper to refer to the lighting control strategy is reported in the following table 5.

V. ENERGY SIMULATION MODEL

For the annual energy consumption calculation of the room, the following HVAC controls and internal loads have been chosen (see table 6):

- Heating: set point temperature 20°C and 12°C (during unoccupied periods);
- Cooling: set point temperature max 25°C (no control for unoccupied periods);
- Ventilation: air flow rate 3 Vol/h (during occupied periods)
- Occupancy: 6 people and 6 PCs per room (on Saturday the number of people and PCs is reduced to 2)

The energy consumption and carbon dioxide emission of the rooms with different envelope systems are then calculated taking into account the specific solar and thermal properties of the glazing system and the adopted lighting control strategy.

VI. RESULTS

The room has been divided in four equal zones parallel to the façade. There is a daylighting dependent sensor placed in the middle of every zone as displayed in Figure 3.

The Daylight Factor (DF) variation (shown on Figure 3) has a rapid fall in the first 4m from the façade and then a slower declination towards the bottom of the room. The DF-curve from case A is lower than the one from case B1 due to the lower glazed area of case A. For case B2, the DF-curve is higher than for case A due to the increased transparent area but worse than case B1 due to the solar control coating on the glazing system of B2.

The total lighting consumption, subdivided in the four zones, is shown in Figure 4 for the three room configurations (A, B1 and B2) in function of the different control strategies. The following conclusions can be drawn:

- The total lighting electricity consumption is equal for all three cases when there is no daylight dependent light control.

TABLE 4. GEOGRAPHICAL COORDINATES OF THE SITE AND WEATHER DATA

Station		**Latitude [°]**	**Longitude [°]**	**Site elevation [m]**
Kew-London (UK)		51.28 N	0.19 W	5
Weather data	Time [h]	Direct irradiance [W/m²]	Diffuse irradiance [W/m²]	Air temperature [°C]

TABLE 5. LIGHTING CONTROL STRATEGIES

name	**control strategy**	**zones**
no lighting control	Occupancy dependent switch on/off	One
switch on/off-no zoning	Daylight and occupancy dependent switch on/off	One
switch on/off-zoning	Daylight and occupancy dependent switch on/off	Four
dimmer-zoning	Daylight and occupancy dependent dimmer	Four

TABLE 6. OCCUPANCY, VENTILATION AND SET POINT TEMPERATURES PROFILES

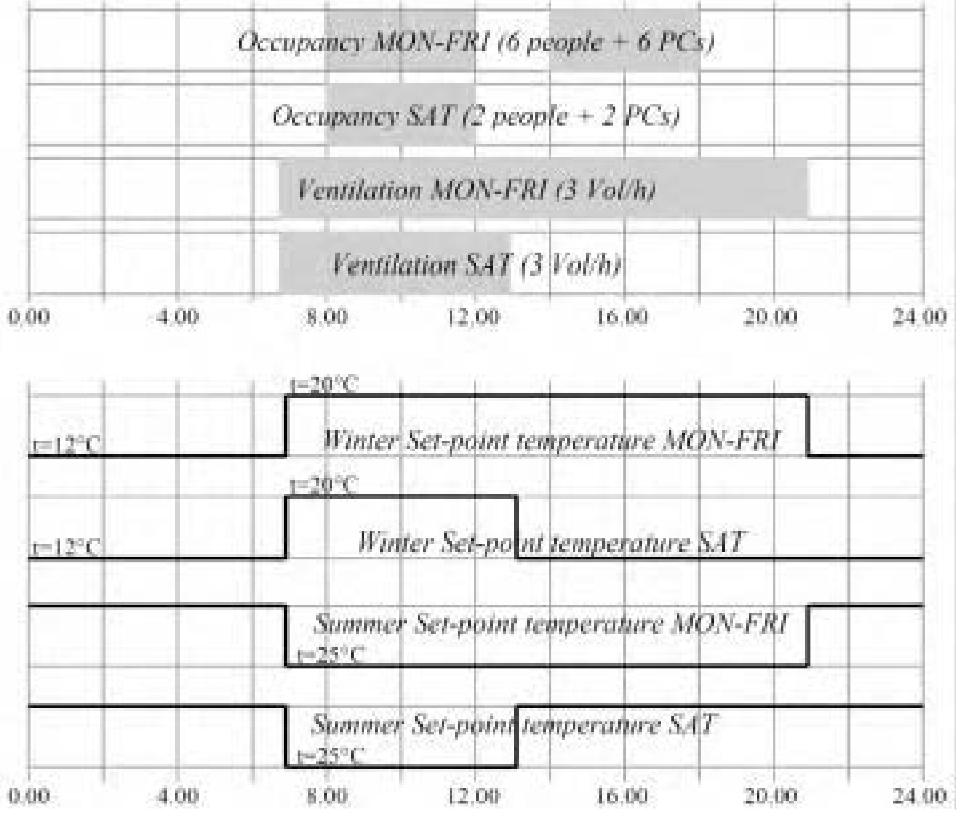

- More refined lighting controls result in considerable less electricity consumption in all cases, which is most significant for the cases B1 and B2 that have higher glazed area.
- It is clear from the results that there is a big benefit of zoning the workspace and using dimmer controls. The combination of using zoning and dimmer controls results in about one fourth of the electricity consumption in comparison with no lighting control.

Additionally the total energy consumption and carbon emissions have been calculated for the three room configurations (A, B 1 and B2) and for the various lighting control strategies. The total yearly energy consumption and carbon emissions (subdivided in heating cooling and lighting) of the office are shown in Figure 5a and 5b respectively. One can clearly notice that for all cases the energy consumption for heating is bigger than for lighting (see Figure 5a). However lighting produces more carbon emissions than heating (see Figure 5b). The reason is that lighting, using an electrical source, has a higher carbon dioxide factor than heating, which uses natural gas (the conversion factors from energy to carbon emissions are 0.19 and 0.44 kg $C0_2$/kWh for respectively gas and electricity [10]). Therefore it is always important to compare carbon emissions when the impacts of different facade system on the building performance are compared.

Figure 6 explains more clearly the differences in heating, cooling and lighting consumption in relation to the reference situation for which no lighting control strategy is applied. One can clearly see from this graph that more sophisticated control strategies are effective in decreasing carbon emissions (cooling and lighting) and that the carbon emissions for heating increases only marginally.

Table 7 represents the energy and carbon emission results from the room configuration where no zoning and a lighting switch on/off is considered. In particular, the impact of the façade geometry (case A, B1 and B2) on the energy consumption is targeted. The following conclusions can be drawn:

- Case B1 compared to case A (same glass type, different percentage of glazing area): The energy consumption for Case B1 with an increased percentage glazed area, results in a lower energy consumption for lighting and heating. However, it is in particular the higher cooling demand that makes that the total carbon emission of Case B1 (fully glazed) is higher than case A (40% glazed).
- Case B2 compared to case B1 (both full height glazing but B2 has high performance glazing):solar controlled glass has a g-value (0.33) that is half of that of normal glass (0.69). The visual transmittance is slightly effected in the other sense i.e. the visual transmittance of the performance glazing is 20% lower than the normal glazing. The differences in characteristics have of course its influence on the overall energy performance of the office: a slightly higher artificial lighting use is found for case B2 but the significant reduction in solar heat gain for case B2 results in an overall carbon emission production which is therefore much lower for B2 than for B1.
- Case B2 compared to case A (different glass type and different percentage glazed area): the heating and cooling consumption are similar in both cases, the artificial lighting use is locase B2 which results in a lower overall carbon emission of the office. Concluding that the façade system of case B2 allows for the architectural choice of a fully glazed façade with an equal overall energy performance than a traditional façade with 40% glazed area.

A significant reduction of energy consumption/carbon emissions is achieved by using zoned lighting scheme and a dimmer lighting control strategy for which the reduction in carbon emission is 1/3 of the initial situation without a daylight dependant control and without zoning. This is due to the reduction of artificial lighting use, which has a double effect: direct in the decrease of electricity consumption for lights fixtures and indirect in the reduction of the internal loads.

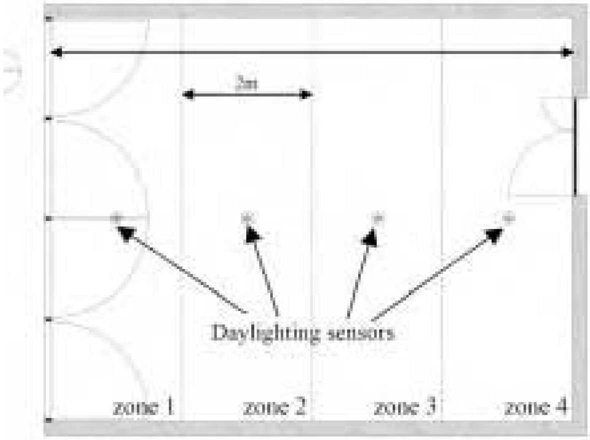

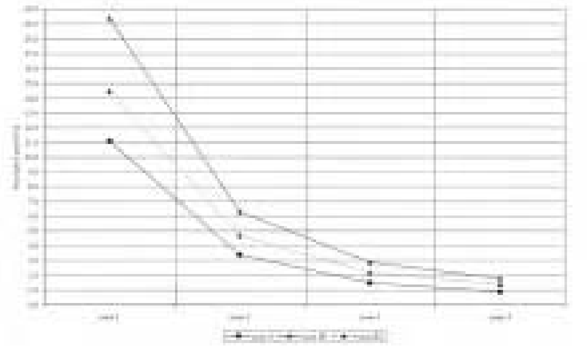

Figure 3: Daylight Factor distribution

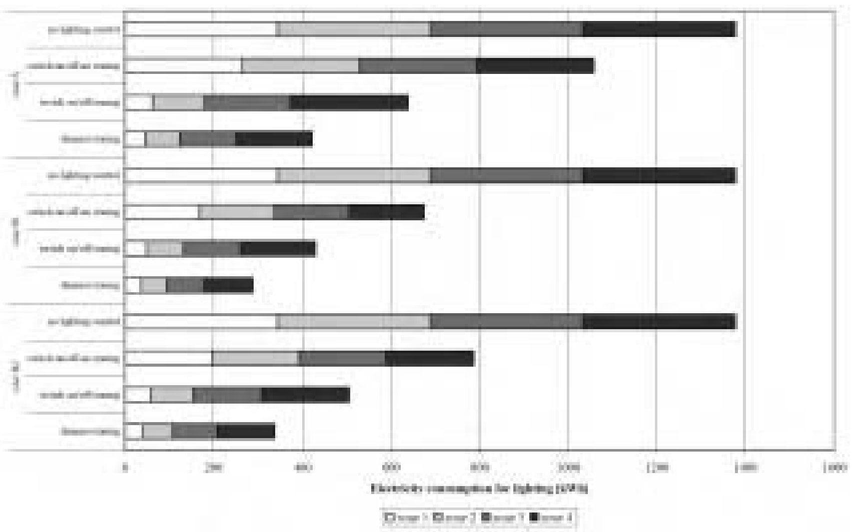

Figure 4: Electricity consumption for different control strategies

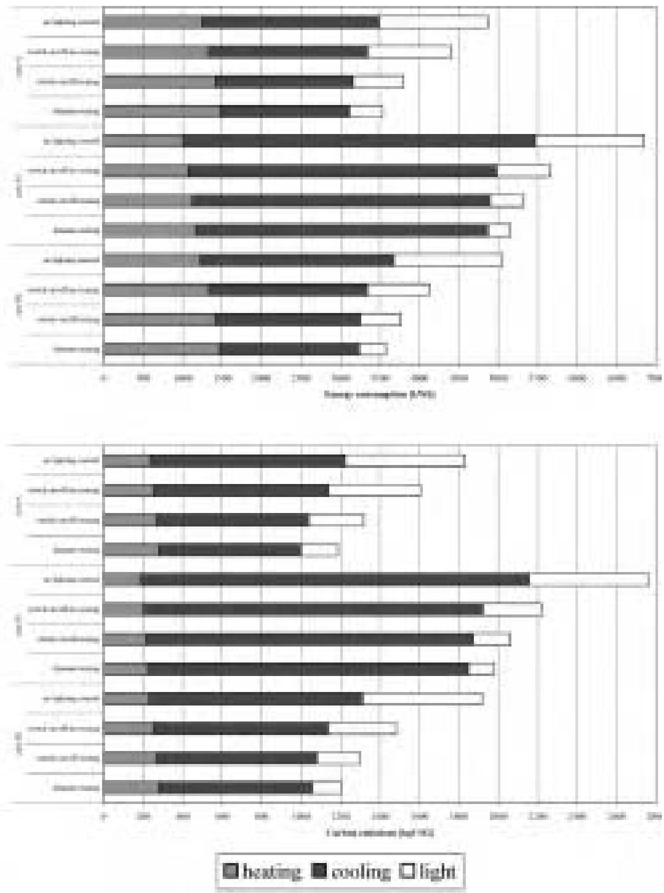

Figure 5a and 5b: Total energy consumption (top) and carbon emissions (bottom)

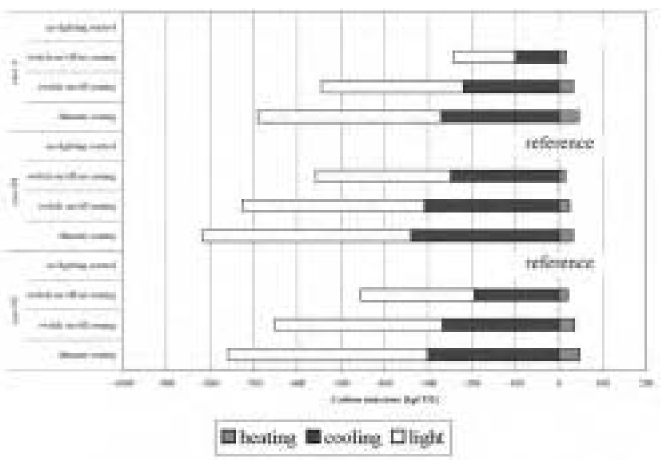

Figure 6: Results in terms of total energy consumption and carbon emissions

TABLE 7. RESULTS FOR THE SITUATION WITH THE SWITCH ON/OFF WITHOUT ZONING CONTROL; DIFFERENCES IN QUANTITIES AND PERCENTAGES FOR THE THREE ROOM CONFIGURATIONS

	energy consumption				carbon emissions			
	heating [kWh]	cooling [kWh]	light [kWh]	total [kWh]	heating [$kgCO_2$]	cooling [$kgCO_2$]	light [$kgCO_2$]	total [$kgCO_2$]
case A (clear glass, 40% glazed)	1328	2018	1058	4404	252	888	465	1606
case B1 (clear glass, fully glazed)	1073	3905	675	5653	204	1718	297	2219
case B2 (solar controlled glass, fully glazed)	1328	2012	786	4127	252	885	346	1484
B1 – A (same glass type, different glass percentage)	-255	1887	-383	1249	-48	830	-168	613
	-19.2%	93.5%	-36.2%	28.4%	-19.2%	93.5%	-36.2%	**38.2%**
B2 – B1 (different glass type, same glass percentage)	255	-1892	111	-1526	48	-833	49	-735
	23.8%	-48.5%	16.4%	-27.0%	23.8%	-48.5%	16.4%	**-33.1%**
B2 – A (different glass type, different glass percentage)	0	-6	-272	-277	0	-2	-120	-122
	0.0%	-0.3%	-25.7%	-6.3%	0.0%	-0.3%	-25.7%	**-7.6%**

TABLE 8. ENERGY SAVINGS (%) USING DAYLIGHT DEPENDANT CONTROL STRATEGIES IN COMPARISON WITH NO CONTROL STRATEGY

energy consumption	**case A**	**case B1**	**case B2**
switch on/off-no zoning	9.5%	17.4%	18.3%
switch on/off-zoning	21.9%	22.2%	25.6%
dimmer-zoning	27.4%	24.7%	29.2%

carbon emissions	**case A**	**case B1**	**case B2**
switch on/off-no zoning	12.3%	19.7%	22.6%
switch on/off-zoning	28.0%	25.4%	32.1%
dimmer-zoning	35.3%	28.4%	37.1%

.

VII. Conclusion

An integration of the daylighting analysis software tool DAYSIM within the dynamic building simulation tool TRNSYS has been established in order to predict the energy consumption of HVAC and lighting equipment. A methodology for lighting control strategy (sensors, controls and zoning) has been worked out to take into account in the dynamic simulations. For the studied office building without lighting control strategy, the artificial lighting consumption represents 20% of the electricity contribution, which is 30% of the total carbon emissions produced for the office.

An appropriate zoning strategy for decentralizing the light groups (in that way not all lights are on hen only needed at the back of the room) have proven to be effective in reducing the yearly electricity demand

The increased glazed percentage of clear glass at the south façade can increase the daylight availability and visual comfort, however can drastically increase the thermal discomfort or the overall energy consumption of the office due to the increased solar heat gain.

A good alternative for highly glazed facades is the use of high performance glazing in a south-facing wall. In that way higher daylight availability was experienced in combination with a lower energy use cooling. For the studied office, the yearly carbon emission production of the office with fully glazed wall (high performance glazing) is less than for a 40% glazed façade.

Further research is currently undertaken to include different blinds management systems.

REFERENCES

[1] DAYSIM – Version 1.3 RADIANCE-based Dynamic Daylight Simulation – User manual written Christoph Reinhart – IRC Institute for Research in Construction – National Research Council – Canada, 2002

[2] TRNSYS Version 15, Solar Energy Laboratory – University of Wisconsin, Madison USA.

[3] National Air Emissions Inventory, UK Greenhouse Gas Inventory, Digest of UK Energy Statistics DTI 1998, Greenhouse Gas Inventory Reference Manual IPCC 1996.

[4] Meteonorm version 4.00 - Meteotest, Bern CH, 1999

[5] [5] C. F. Reinhart, O. Walkenhorst. Validation of dynamic RADIANCE-based daylight simulaions for a test office with external blinds, Energy and Buildings 33 (2001) 683-697.

[6] PREBID Version 4.0 – TRANSSOLAR Energietechnik – Stuttgart, Germany.

[7] IISiBat Version 3.0.CSTB - Sophia Antipolis, France

[8] T. Frank and T.W. Puentener, *Comparison of Six Simulation Codes: DEROB, DYWON, PASSIM, DOE-2.1C, SERI-RES and HELIOSI*, IEA Annex XII (Windows and Fenestration), 1987

[9] ECON19 Energy consumption guide, Energy use in offices Best Practice Programme

[10] Environmental reporting Guidelines for Company Reporting on Greenhouse Gas Emissions June 1999, (Published by the DETR).

EU COST C13 Glass and Interactive Building Envelopes. M. Crisinel, et al. (Eds.). IOS Press, 2007.

Intelligent Building Envelopes Application in the Field of Daylighting

Annemie Wyckmans, Øyvind Aschehoug, Anne Grete Hestnes
Norwegian University of Science and Technology
Faculty of Architecture and Fine Art,

This paper analyses the use of an intelligent building envelope as an instrument to manage the variable and sometimes conflictive requirements posed by daylighting in non-domestic buildings. While proper architectural design is a vital precondition for facing these challenges, in a real-time environment it needs to be supported and enhanced by the performance of the building envelope as an environmentally selective filter. The manner in which the building envelope is able to handle the collection, admission and distribution of daylight indoors determines its successfulness in creating an appealing indoor luminous environment with an efficient use of daylight resources. First a short introduction is given on what the authors believe to be the central characteristic of intelligent building envelopes: adaptiveness to and interaction with the environment, with particular focus on the building occupant. This adaptiveness is then evaluated for its ability to manage the complex set of requirements that arise from the use of daylight in non-domestic buildings with a desirable outcome. The analysis combines and compares a selection of secondary literature sources and built examples in their concrete attempts to create solutions to daylighting challenges. The paper is based on the research results of a Ph.D. to be completed in 2005 at NTNU, Trondheim, Norway.

I. Daylighting Challenges in Non-Domestic Buildings

The appropriate admission and distribution of daylight in non-domestic buildings increases their potential for energy conservation and for providing a healthy and comfortable indoor environment. Appropriateness in this respect depends in the first place on the degree to which architectural form and spatial organisation are adapted to the building's function and to the local climate and site. It however also requires a thorough understanding of the human response to spatial and temporal variations in lighting in the particular climate, site and indoor environment the building occupant is confronted with. Research by (Kuller et al., 1991; 1996) for example shows daylight to exert a profound impact on people's hormones, body temperature, cognitive activity, and mood. The amount and distribution of daylight, its variability and spectral composition, its interaction with surface texture, and the human eye's adaptation to successive and simultaneous contrast are all important in this respect (Valberg, 1998).

"Making better use of available lumens" (Smith, 2004) is also an inevitable premise for successful energy conservation strategies in non-domestic buildings. The use of artificial lighting controls responsive to daylight and user presence is a well-known method to lower artificial lighting energy. As daylight has a higher luminous efficacy than most artificial light sources, such controls are also helpful in lowering internal heat gains in buildings dominated by cooling load. All daylight allowed indoors however produces heat, due to the greenhouse effect. As this heat gain only partially can be avoided, by means of solar shading and blocking of near-infrared radiation (Smith, 2004), an advisable strategy in this respect would be to avoid the admission of superfluous daylight indoors and correspondingly to use the available daylight sources in the most effective manner possible.

Coping with human behaviour forms a third type of challenge for successful daylighting strategies in non-domestic buildings. (O'Connor et al., 1997) reports that during the past few years, human cost has grown to be at least as important, if not more, than energy cost in non-domestic buildings; even a highly energy efficient building does not make up for the slightly reduced productivity of dissatisfied employees. According to (Fontoynont et al., 2002), lighting energy savings in the order of 1 to 2 Euros per m2 and per year are achievable; as this barely equals 1 or 2 hours of salary of an office worker per year for a 10 m2 workplace, a slight reduction in occupant productivity can spoil all expected savings.

II. The Concept of Intelligent Building Envelopes

In the context of building design, the terms intelligent building and intelligent building envelope are frequently used to describe a built form that can meet the demand for steadily increasing functionality at diminishing cost, be it to a varying degree of success. The term intelligent building envelope has become a common denominator for a certain type of built form that uses artificial intelligence to provide the indoor environment with dynamic heating, cooling and lighting, aiming to procure an optimal balance between occupant comfort and energy efficiency. A multitude of definitions however – (Wigginton & Harris, 2002) for example list over 30 definitions of intelligence in the context of building design – opens for rather divergent interpretations as to the manner in which this functionality is to be achieved, and it may be discussed which definition is more appropriate in a given context.

Within the scope of this paper, the intelligence of a building envelope is defined as the ability to adapt to the environment by means of processes of perception, reasoning and action, enabling the envelope to cope with new situations and solve problems that may arise in its interaction with the environment. This instrumental definition is based on the psychological development of intelligent behaviour in humans, where psychical processes of perception, reasoning and action help a subject to solve problems and cope with new situations in a variable and conflictive environment. Its deduction is described in detail in (Wyckmans et al., 2005a;b).

Adaptiveness to the intensity and quality of stimulation exercised by the environment requires for an intelligent building envelope to be able to perceive stimuli in the environment, to choose the most appropriate response according to a set of limitations and priorities, and to execute that response. According to (Hagras et al., 2003), "an essential feature must be its ability to learn and adapt appropriately. For this a system which can adapt and generate its own rules (rather than being restricted to simple automation) is required". In addition, adaptiveness enables the building envelope to communicate with and learn from the people that use the indoor environment on a regular basis, and to optimise the indoor work environment according to the individual occupant's needs and preferences.

III. Adaptiveness in the Context of Daylighting

Given its ability to adapt to the environment by means of perception, reasoning and action, an intelligent building envelope may be expected to fulfil three objectives related to daylighting in non-domestic buildings: to handle a variable environment, conflictive requirements, and human behaviour with a desirable outcome.

A. To handle a variable environment

Indoor daylighting conditions are influenced by a number of environmental factors related to the local climate and site, the built environment, and the building occupant; factors subject to variations the building envelope has no control over. A flexible and adaptive design of material, form and composition can help the building envelope provide an optimal response to a wide range of regular variations, unanticipated events, and changes in priorities and performance criteria that may occur during the envelope's operation. Also changes in the envelope's own performance due to for example the ageing of equipment, the accumulation of dust, and the breakdown of components, need to be accounted for.

Daylight's variability, however, is a desirable quality that should not be filtered out by the building envelope; neither should it be overcompensated by artificial lighting. A study by (Cooper & Crisp, 1984) for example found daylight's variability to be the second most favourable advantage of the use of daylight in buildings. The same study nevertheless simultaneously found daylight's variable intensity to be an important hinder to designers' deliberate involvement of daylight as a light source in buildings. Daylight's influence on the indoor environment thus needs to be kept within acceptable limits, while care should be taken to avoid superfluous compensation of the natural variations that occur in daylighting.

B. To handle conflictive requirements

The use of daylighting in non-domestic buildings brings forth variable and potentially conflictive demands of transparency versus privacy, of openness versus insulation, of access to daylight versus solar shading. Ideally an intelligent building envelope is able to assess these conflicts, make trade-offs according to a prevalent set of priorities, and find a solution optimal to all of the tasks at hand.

Adaptive design provides the building envelope with a diversity of manners in which to perform a certain task, and increases its chances of finding the most favourable solution to a given set of problems. A daylighting strategy may often physically be implemented in several manners; choosing a particular form of adaptation may however give rise to unintended and potentially unfavourable side effects on other parameters. The ability to anticipate the effect of a particular action helps an intelligent building envelope to select the most appropriate solution, i.e. an implementation that combines the elimination of undesirable influences with the most favourable consequences.

C. To handle human behaviour

Information regarding the occupant's needs, preferences and behaviour enables an intelligent building envelope to choose a course of operation more favourable to the occupant, and use the available daylight resources more efficiently to this purpose. Human response to the luminous environment may vary according to individual, cultural and functional preferences and needs, and the particularity of the climate, site and indoor environment the occupant is exposed to. A building occupant may well be satisfied with indoor daylighting conditions even though they do not comply with prevalent lighting recommendations, and vice versa.

Also the building occupant's acceptance of the manner in which an intelligent building envelope manages variations and conflicts in the environment is of the utmost importance to achieve energy conservation. According to (Fitzgerald & Fitzgerald, 1987), "the most probable cause of a system's failure is people. By this we mean the non-acceptance of the system and, therefore, the philosophy and method of going around or 'beating' the system". In a study on user satisfaction with lighting control systems, (Velds, 1999) found the inability to overrule the system to be the users' most important complaint with respect to the systems.

IV. Application of an Intelligent Building Envelope in Daylighting

The fruitful application of an intelligent building envelope in the field of daylighting does not merely involve the building envelope but evidently also includes the entire building and its correspondence to the local climate and site, and to the building program. The authors have however attempted to evaluate the characteristics of an intelligent building envelope apart from the rest of the building. Included are the particular material, form and composition of elements the building envelope uses for its perception, reasoning and action, as well as the nature and degree of their integration or co-operation.

The materials and components used in the building envelope may be application-specific or multi-functional (Figure 1). Multifunctionality in this context refers to the concurrent or successive performance of perception, reasoning, and action functions on the one hand, and different daylighting-related tasks on the other hand. The organisation of functions in autonomous layers or modules may increase their flexibility and reduce interdependency, allowing them to be optimised more easily (Albus, 1999).

The choice of radius in which to perform and coordinate various functions also needs to be given careful consideration, as it affects the efficiency and effectiveness of the building envelope's operation. According to (Clements-Croome, 1997) a fruitful combination would be the decentralised management of perception, reasoning and action functions in modules or zones, linked to a central unit that supervises the overall envelope performance.

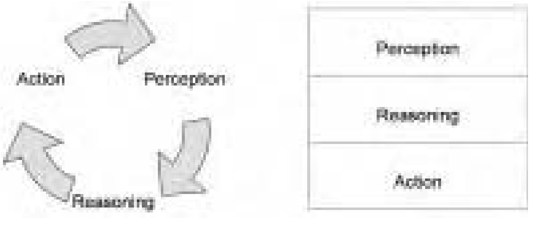

Figure 1: The organisation of perception, reasoning and action as autonomous modules (left) or in onemultifunctional material (afterNeumann, 1999)

A. Perception

Ideally, an intelligent building envelope can perceive environmental factors and correspondent indoor daylighting conditions real-time instead of relying on models, allowing the envelope to fine-tune its operation to environmental conditions. In addition, the envelope needs to monitor the performance of its own component parts in order to ensure optimal operation.

Regarding the building occupant, several parameters need to be taken into account. In the absence of the occupant the operation of the building envelope can be maximised for energy conservation; this requires for the envelope to perceive the occupant's absence and presence, and ideally also includes information regarding the duration of the absence. In the occupant's presence the envelope needs to be able to provide a satisfactory indoor luminous environment. The envelope's perception of daylighting conditions needs to be related to occupant position and view angle. Also the adaptation mechanism of human visual response needs to be taken into account, adapting human visual response to luminance and colour contrasts in the environment and altering its sensitivity and tolerance compared to what may be expected from absolute luminous values.

Perception may occur by means of any device or material that measures or in another way is able to discern environmental conditions. Illustrative examples are:

- Materials sensitive to heat or light;
- Sensors connected to the building envelope or indoor environment;
- Geostationary satellites for remote sensing;
- And a user interface to discern the user's needs and preferences.

1) *Materials*

Materials able to perceive environmental conditions are for example various types of switchable glazing. This type of glazing can perceive the state of a particular environmental control parameter such as incident solar radiation, ambient brightness or indoor air temperature, and automatically adjusts its transmittance of visible or total solar radiation according to the perceived value. In this case, perception is coupled directly to a particular type and degree of response, similar to a reflex action.

2) *Sensors*

Occupancy sensors allow the building envelope to sense the presence and/or absence of the building occupant. Photosensors can be used to perceive illuminance levels in the occupant's visual field. Measurements from various locations can be combined to optimise the data received. An important impediment for the use of photosensors, according to (Ehrlich et al., 2002), is the wide variety in angular and spectral sensitivity they exhibit. Though equipped with a colour-correction filter, photosensors never really manage to simulate human visual response. Furthermore, the perceived illuminance data are influenced by the luminance of all of the surfaces in the sensor's acceptance angle, which complicates proper placement and requires extensive calibration. The correlation between work-plane illuminance and corresponding photosensor signal may in addition vary according to the type of sky conditions (Choi et al., 2005).

3) *Geostationary satellites*

A geostationary satellite can be used to provide the building envelope with information regarding the nature, extension, and density of the cloud cover, water vapour levels, atmospheric pollution, and the corresponding intensity and visibility of the sun. A relatively large amount of calculations and models is needed to relate these data to the local climate and site the building envelope is exposed to. This type of sensing does, however, provide the building envelope with a wide overview of environmental conditions and their development in time. Current and anticipated weather data can be used to predict the optimum heating, lighting and shading strategies for the building envelope. The accuracy and speed of the perceived data however do not suffice for a direct interaction between envelope and environmental variations.

4) *User Interface*

A user interface is in this context a device that allows uni- or bidirectional communication between building envelope and occupant. Design options include a graphical point-and-click interface or natural language processing abilities, written or speech-based, allowing the user to for example request 'more light' or report the experience of glare (Birnbaum et al., 1997; Hoff, 2002; Willey, 1997). A user interface may be mounted on the wall or used as an on-screen control panel via the ordinary computer network; it can also appear as a hand-held control or an infrared remote control device.

The building envelope can deploy a user interface to provide the occupant with information regarding the state of the environment, the various choices the envelope needs to make, and the anticipated outcome of a particular occupant request. Reversely, a user interface enables the building occupant to participate in the formulation of individual comfort level requirements; preferred indoor luminous conditions as well as the manner in which such conditions are to be achieved can be forwarded (Willey, 1997). According to Horvitz however, it is very difficult to design a user interface that can communicate user preferences unambiguously (Birnbaum et al., 1997).

A particular kind of user interface is the smart card unit designed by Kolokotsa et al. The personal card registers occupant preferences and updates them regularly, distinguishing between short-term and long-term preferences. A fuzzy algorithm enables the user to state preferences in natural language form, such as a request for 'more' light. In addition the unit assesses the urgency and accuracy the request is to be executed with: "an occupant who adjusts the control significantly wants a large effect. Hence most people turn the setting down lower than necessary. An occupant who adjusts only very slightly is not interested in a quick response, but in accurate conditions. When an occupant adjusts very often, the control should respond exactly and carefully" (Kolokotsa et al., 2002).

B. *Reasoning*

The successfulness of a building envelope's adaptation to the environment is influenced by its ability to anticipate environmental conditions, learn occupant preferences, and predict the outcome of its own actions. Without these particular reasoning skills, adaptation to the environment typically occurs by means of a reflex action, or "a simple response which follows on directly and inevitably from the stimulus" (Beukers & van Hinte, 1998). Prediction and learning skills however would enable the building envelope not merely to react to its environment, but also to learn the optimal manner in which to respond to new situations, and even to anticipate their occurrence.

As mentioned earlier, human tolerance to luminous conditions may vary according to a number of individual, environmental, and task-related factors, an intelligent building envelope ideally has the ability to learn the needs and preferences of the individual occupant in confrontation with the particular site and indoor environment the occupant is exposed to. The particular nature and extent of control given to the building occupant also need to be considered carefully; while the right type of control increases the occupant's comfort and satisfaction, other types may cause stress and irritation instead (Veitch & Gifford, 1996).

Adjusting envelope operation to occupant preferences may however also involve the admission of additional daylight indoors along with the increased use of artificial lighting, which reduces opportunities for energy conservation. In order to find the most fit strategy within a given set of boundaries and draw inferences between various occupant and energy requirements, an intelligent building envelope ideally has the ability to apply informed prediction. Anticipation of spatial and temporal variations in daylight enables the envelope to assess whether adaptation indeed is required. The ability to predict the main and side effect of its own actions in addition helps the envelope to decide on the appropriate nature, degree and timing of the required adaptation.

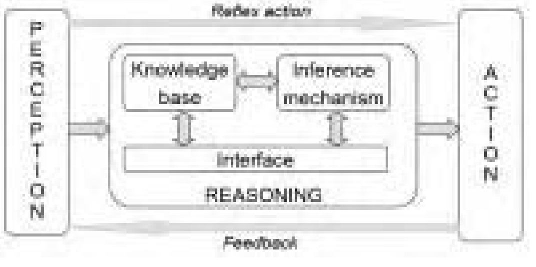

Figure 2: An intelligent building envelope's adaptation to the environment typically involves a knowledge base and an inference mechanism. Particular circumstances may require a 'reflex action' as a direct response to perceived impulses, omitting reasoning.

Prediction and learning skills typically require the deployment of behaviour-based artificial intelligence. Designed to simulate processes of human intelligence, this type of artificial intelligence is able to function effectively in imprecise and uncertain environments. It includes amongst others expert systems, artificial neural networks, fuzzy systems, evolutionary algorithms, and case-based reasoning. A thorough description of the characteristics of each of these systems and their hybrids, as well as an indication of application areas, can be found in (Medsker, 1995).

An intelligent building envelope's adaptation to the environment typically involves a knowledge base and an inference mechanism (Figure 2). A knowledge base may contain the envelope's previous experiences, domain knowledge of human experts, published information, and experimental findings. Real-time data can be used to update the knowledge base to new or altered environmental conditions and make the building envelope more fit for performance in that particular environment. The inference mechanism manipulates the stored knowledge in order to work out appropriate operational strategies. The main advantage of having an architecture that separates the knowledge base from the inference mechanism is the ease of updating the knowledge base without affecting the inference mechanism (Garg, 2001; Medsker, 1995).

The manner in which the interaction between the physical environment, the building occupant and the building envelope is modelled, exerts a strong influence on the successfulness of the building envelope's reasoning skills. According to (Birnbaum et al., 1997) "intelligent systems only perform as well as their representations of the task they are trying to perform and of the world they are trying to perform it in. If these representations are reasonable, then even extremely simple algorithms can result in useful performance. If they aren't then no algorithm, no matter how sophisticated, can yield good performance". Also the speed with which an appropriate response can be produced is of the utmost importance. A time delay may cause the occupant to believe the system is not responding, evoking frustration and the apparent need for continuous user intervention (Vine, 1998).

(Guillemin & Molteni, 2002) tested a shading-device controller using genetic algorithms and fuzzy logic to learn occupant preferences in offline mode, typically during the night. Whenever a user override occurs, the standard operation of the building envelope is switched off temporarily in order to respond to acute user needs. The system also has a built-in wish filter (Figure 3) that assesses the appropriateness of occupant requests. Energetically inappropriate requests are discarded, unless forwarded more than once by the occupant.

(Hagras et al., 2003) describe a hierarchical control system based on evolutionary algorithms and fuzzy systems, able to learn and adapt to occupant behaviour online and in real-time. According to the authors, the system typically uses three minutes to achieve a satisfactory solution whenever the occupant states a particular preference.

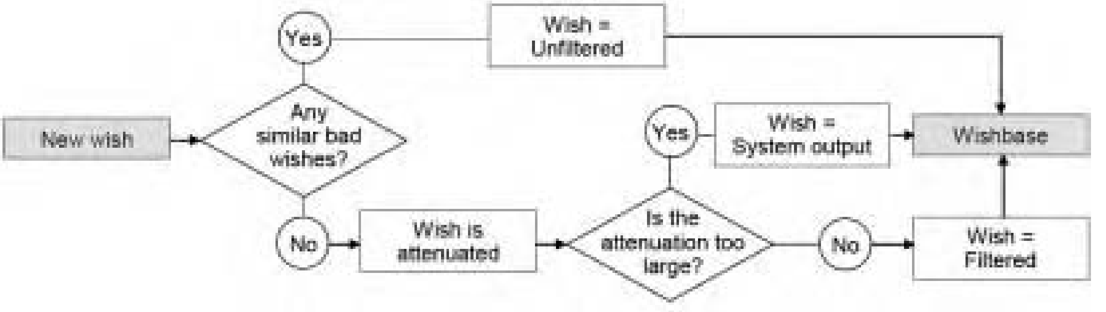

Figure 3: Operation diagram of the “wish pre-processing filter”(Guillemin & Molteni, 2002 p.1093)

C. *Action*

An intelligent building envelope can adapt the material characteristics, form, and composition of its component parts to determine which daylight sources are allowed to influence the indoor environment and how they best be applied to optimise the occupant’s perception of the indoor luminous environment with the most efficient use of daylight resources. Undesirable influences can be prevented, or their outcome altered (Fitzgerald & Fitzgerald, 1987). Important is not only the type of adaptation the envelope undertakes, but also its timing and extent.

Adaptation of the material characteristics, form and composition of its component parts enables the envelope to influence the intensity, distribution, visibility, directionality and colour appearance of light sources in the occupant’s visual field. Adjusting inappropriate luminance ratios in the occupant’s visual field may reduce the risk of glare and transient adaptation, improve the occupant’s perception of the indoor environment, and reduce the need for supplementary artificial lighting. Increasing the amount of reflected light in the indoor environment would enable the building envelope to use the available daylight sources more efficiently and to provide adequate illumination with less incoming daylight. This, however, needs to be balanced against the need for appropriate directionality of indoor lighting for the creation of satisfactory modelling conditions.

In principle, an intelligent building envelope can also manipulate the colour appearance of daylight, for example by redirecting it to surfaces with a strong saturation or chroma. When no particular requirements are stipulated, however, the envelope should attempt to minimise its influence on this parameter, as the nature and variations of daylight’s colour temperature in general are features highly appreciated by the building occupant. Under particular circumstances, though, it might be considered desirable for the building envelope to change the colour appearance of daylight, for example in case of atmospheric pollution.

In addition, an intelligent building envelope can adjust the visibility of light sources and site elements in the occupant’s visual field. The provision of a view to the outdoor environment always needs to be balanced against the occupant’s need for privacy, which may vary according to individual, task-related and environmental factors, the risk of glare, and the prevention of solar heat gain. By allowing particular light sources indoors while others are blocked, redirected or redistributed, the building envelope can choose the light sources with the highest luminous efficacy and accessibility for use in the indoor environment.

A wide range of adaptive envelope materials and other elements is available; the entire range of physical applications would be too extensive to cover. A few illustrative examples will be discussed, grouped according to the nature of adaptation they feature, and the nature of the source that induces it:

- Switchable glazing
- Mechanical daylighting and shading devices
- Pneumatic structures

1) Switchable Glazing

Switchable glazing can change its optical characteristics in response to variations in a specific environmental parameter such as indoor air temperature or an electric charge. The admission and distribution of daylight in the indoor environment can be controlled according to the switching behaviour induced in the glazing, typically between states of high and low transmittance of visible and total solar radiation. Important parameters are adaptation time and the optical characteristics of the low-transmittance state such as glazing colour, the degree of visual contact to the surroundings, and reflectivity. Another discerning characteristic is the type of control parameter used to induce switching.

A built-in control parameter allows the glazing to switch between high and low transmittance states according to a specific environmental condition; examples are thermotropic (thermally activated), gasochromic (solar intensity, indoor air temperature), and photochromic (ambient brightness) glazing. The particular switching point is to be determined during manufacturing, and can not be changed afterwards. This type of glazing thus features a direct link between the perception of a particular environmental stimulus and its automatic response, similar to a reflex action.

Also an external control parameter, typically an electric signal, can be used to adjust transmittance of visible and total solar radiation; an example is electrochromic glazing. The use of voltage as a control parameter enables a more flexible degree and timing of response to environmental conditions. Supplementary cabling may be required to supply the required voltage, however alternative solutions are possible. (Gregg, 1997) for example describes the operation of a photoelectrochromic window, a flexible hybrid combining the advantages of electrochromic and photochromic modules by means of a photovoltaic cell. Thermotropic glazing can be equipped with a resistive heating layer that allows switching between high and low transmittance states at an electric signal as well (Lampert, 2004).

2) Mechanical daylighting and shading devices

Mechanically driven adaptation, for example of Venetian blinds, allows for a high degree of flexibility in timing and degree of response to environmental conditions. Compared to fixed systems however, mechanically driven devices tend to have a higher cost and lower durability. In addition, the continuous movement of envelope components may cause the occupant to experience noise and distraction. The control system also uses additional energy to perform the required form of adaptation.

Figure 4: The use of detail in material, form and composition to minimise the need for adaptation; (left) stepped mirror louvers (Köster, 2003 p.35); (middle) prismatic louvers (Siemens, 1987); (right) functional division of slat angles.

The required frequency and range of adaptation may be minimised by careful use of material and form in the component parts of the daylighting device (Figure 4). Dividing the component parts into modules with a distinct shape and material use can for example provide them with angular or spectral selectivity with regard to specific sources of direct and reflected daylight. The function of component parts may also vary according to their area of operation; the importance of visual contact and glare issues for example is strongly related to a component's position in the occupant's visual field.

3) Pneumatic structures

Adaptation of envelope components may also be driven pneumatically. Particularly the combination of membrane technology and pneumatic drive has come to know interesting applications during the past few years. An important characteristic of membranes in this respect is their flexible form. A particular example is the application of ETFE (Ethyl Tetra Fluoro Ethylene) cushions, where multiple layers of foil are clamped in an aluminium or steel frame; the cushions are self-supporting due to internal pressure. A single cushion can measure up to 25m by 3.5m. The typical U-value of a three-layered ETFE foil cushion lies around 1.95W/m^{2}K; this number can however be reduced to below 0.6W/m2K by means of additional foil layers treated with low-E coating (Tanno, 1997). The inflation of the cushions is maintained by an electrical fan, typically using about 50W per $1000m^2$ (Robinson-Gayle et al., 2001). Compared to glass, ETFE has a similar visible light transmittance and colour rendering properties; its picture rendering qualities however are considerably lower. In addition, the cushions do not provide any acoustic insulation (Robinson-Gayle et al., 2001). Solar shading can be integrated in the cushions by equipping the foil layers with printed patterns. Variable degrees of solar shading can be achieved by pneumatically adjusting the printed inner foil layers (Rittgen, 2001).

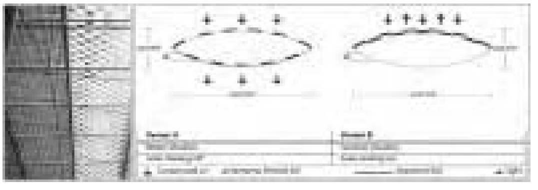

Figure 5 ETFE foil cushions with positive and negative chessboard print for variable solar shading (Rittgen, 2001 p.35; picture: A. Braun, Hameln)

V. Conclusion

The aim of this paper was to examine the potential of an intelligent building envelope as an instrument to manage the variable and sometimes conflictive requirements posed by daylighting in non-domestic buildings. The intelligence of the building envelope was in this context defined as the ability to adapt to the environment by means of perception, reasoning and action, similar to human intelligence. The authors have analysed the particular manner in which each of the perception, reasoning and action skills of the envelope may be expected to improve the occupant's perception of the indoor daylit environment, and how this in turn can be fruitful for energy conservation. After having elaborated these requirements in principle, a range of physical applications has been discussed for their potential to support the kind of adaptation that is expected. In the choice of physical applications, a particular effort has been made to surpass the common mental image of centralised control and mechanically driven shading devices often related to intelligent building envelopes. The majority of physical applications as to yet has not been able to fulfil the stated requirements without undesirable side effects. A particularly interesting development however takes place in the field of nanotechnology, where materials may be produced with a made-to-measure functionality. This would ideally produce materials that may adapt to their environment without the need for mechanical solutions (Neumann, 1999).

References

[1] Albus, J.S. (1999). The engineering of mind. Information Sciences 117:1-18.

[2] Beukers, A.; van Hinte, E. (1998). Lightness: The inevitable renaissance of minimum energy structures. 010 Publishers, Rotterdam.

[3] Birnbaum, L.; Horvitz, E.; Kurlander, D.; Lieberman, H.; Marks, J.; Roth, S. (1997). Compelling Intelligent User Interfaces - How Much AI? Proceedings of the International Conference on Intelligent User Interfaces. Orlando, Florida, USA, pp.173-175.

[4] Choi, A.-S.; Song, K.-D.; Kim, Y.-S. (2005). The characteristics of photosensors and electronic dimming ballasts in daylight responsive dimming systems. Building and Environment 40:39-50.

[5] Clements-Croome, T.D.J. (1997). What do we mean by intelligent buildings? Automation in Construction 6:395-400.

[6] Cooper, I.; Crisp, V.H.C. (1984). Barriers to the exploitation of daylighting in building design: U.K. Experience. Energy and Buildings 6:127-132.

[7] Ehrlich, C.; Papamichael, K.; Lai, J.; Revzan, K. (2002). A method for simulating the performance of photosensor-based lighting controls. Energy and Buildings 34:883-889.

[8] Fitzgerald, J.; Fitzgerald, A.F. (1987). Fundamentals of systems analysis. Using structured analysis and design techniques. John Wiley & Sons, New York, 3rd edition.

[9] Fontoynont, M.; Escuyer, S.; Laurentin, C. (2002). Lighting preferences: role of season, air temperature, daylight quantity, colour of daylight, activity, and architectural constraints. Proceedings of the Visual Environment Symposium, London ,UK, pp.19-20.

[10] Garg, V. (2001). Building automation and energy savings. In Bansal N.K., Cook J. (ed.) Sustainability through building. Omega Scientific Publishers, New Delhi.

[11] Gregg, B. A. (1997). Photoelectrochromic cells and their applications. Endeavour 21(2):52-55.

[12] Guillemin, A.; Molteni, S. (2002). An energy-efficient controller for shading devices self-adapting to the user wishes. Building and Environment 37:1091-1097.

[13] Hagras, H.; Callaghan, V; Colley, M; Clarke, G. (2003). A hierarchical fuzzy-genetic multi-agent architecture for intelligent buildings online learning, adaptation and control. Information Sciences 150:33-57.

[14] Hoff, T. (2002). Mind Design: Steps to an Ecology of Human-Machine Systems. Ph.D. Dissertation, NTNU, Trondheim, Norway.

[15] Kolokotsa, D.; Kalaitzakis, K.; Antonidakis, E.; Stavrakakis, G.S. (2002). Interconnecting smart card system with PLC controller in a local operating network to form a distributed energy management and control system for buildings. Energy Conversion and Management 43:119-134.

[16] Köster, H. (2003). Erweiterung des Landesdenkmalamtes in Esslingen: Neue Wege. Lichtplanung und Fassade. IntelligenteArchitektur 43:34-35.

[17] Küller, R.; Lindsten, C. (1991). Hälsoeffekter vid arbete i fönsterlösa klassrum. Rapport 10. Statens Råd för Byggnadforskning, Stockholm, Sweden.

[18] Küller, R.; Wetterberg, L. (1996). The subterranean work environment: Impact on well-being and health. Environmental International 22(1):33-52.

[19] Lampert, C.M. (2004). Chromogenic smart materials. Materials Today 7(3):28-35.

[20] Medsker, L.R. (1995). Hybrid Intelligent Systems. Massachusetts: Kluwer Academic Publishers.

[21] Neumann, D. (1999). Adaptronics - a Concept for the Development of Adaptive and Multifunctional Structures. In: Janocha, H. (ed.) (1999). Adaptronics and Smart Structures: Basics, Materials, Design, and Applications. Berlin: Springer. pp. 5-12.

[22] O'Connor, J.; Lee, E.; Rubinstein, F.; Selkowitz, S. (1997). Tips for daylighting with windows – The integrated approach. Lawrence Berkeley National Laboratory, PUB-790.

[23] Rittgen, J. (2001). TechnologieCenter der Festo AG in Esslingen: Mehr als Luft. Über das Energiekonzept des neuen Festo TechnologieCenters. IntelligenteArchitektur 31:34-35.

[24] Robinson-Gayle, S.; Kolokotroni, M.; Cripps, A.; Tanno, S. (2001). ETFE foil cushions in roofs and atria. Construction and Building Materials 15:323-327.

[25] Siemens (1987). Product information. Tranreut, Germany.

[26] Smith, G.B. (2004). Materials and systems for efficient lighting and delivery of daylight. Solar Energy Materials & Solar Cells 84:395-409.

[27] Tanno, S. (1997). ETFE foil cushions as an alternative to glass for atriums and rooflights. Proceedings of ICBEST, Bath, pp.357-361. TechnologieCenter der Festo AG in Esslingen: Mehr als Luft... IntelligenteArchitektur 31:29-41.

[28] Valberg, A. (1998). Lys syn farge. Tapir Forlag, Trondheim, Norway.

[29] Veitch, J.A.; Gifford, R. (1996). Choice, perceived control, and performance decrements in the physical environment. Journal of Environmental Psychology 16(3):269-276.

[30] Velds, M. (1999). Assessment of lighting quality in office rooms with daylighting systems. Ph.D. dissertation, Technische Universiteit Delft, The Netherlands.

[31] Vine, E.; Lee, E.; Clear, R.; DiBartolomeo, D.; Selkowitz, S. (1998). Office worker response to an automated venetian blind and electric lighting system: a pilot study. Energy and Buildings 28: 205-218.

[32] Wigginton, M.; Harris, J. (2002). Intelligent skins. Oxford: Butterworth-Heinemann.

[33] Willey, H. (1997). A fuzzy approach to daylight-responsive lighting controls. Presentation to the IEA Task 21 Experts Meeting, Brisbane, October.

[34] Wyckmans, A. (2005). Intelligent Building Envelopes – Architectural Concept and Application in the Field of Daylighting Quality. Ph.D. Dissertation, to be published at NTNU, Trondheim, Norway.

[35] Wyckmans, A.; Aschehoug, Ø.; Hestnes, A.G. (2005). The Intelligent Building Envelope – Concept and Qualifications. Proceedings of Glass in Buildings 2, Bath, UK.

EU COST C13 Glass and Interactive Building Envelopes. M. Crisinel, et al. (Eds.). IOS Press, 2007.

Is Prestressing Control Possible for Tempered Glass Structures?

Fabrice Bernard, Ecole des Mines de Douai – Dpt Génie Civil, Douai, France
Laurent Daudeville, Laboratoire Sols Solides Structures, Grenoble, France

This work deals with the use of glass as a real structural material. An in situ non destructive process is proposed for the control of tempered glass structures, especially in joint zones. A design method is also proposed. It is based on one hand, on a limit state ensuring the structure to be perennial on long duration, and the another hand, on the finite element prediction, on every point of the structure, of both residual stresses due to tempering and stresses due to the mechanical loading. The control method consists, during the life of the structure, in comparing images obtained from photoelastic analyses of the loaded structure, to images obtained from finite element analyses of the structure at the ultimate limit state used for the design.

Keywords: tempered glass, photoelasticity, in situ control, finite elements, residual stresses, ultimate limit state

I. Introduction

The use of glass for civil engineering structures (Figure 1) is strongly penalized. French offices that regulate construction require full-scale tests of any glass structure to be realised (Figure 2) and a relatively large global safety factor (about 7). The global safety factor comes from a coefficient equal to 3.5, classical for brittle materials, that factor includes loading and material uncertainties, multiplied by a coefficient of 2, due to a strength reduction estimated over 50 years. This strength reduction is due to the subcritical crack growth caused by the possible action of water at crack tips [Michalske and Freiman, 1983].

Figure 1: An example of structural glass : tempered beams supporting a glass roof in the Louvre museum

Figure 2: Full scale test of a tempered beam presented in Figure 1

Thermal tempering is a way of reinforcing the glass surface. It not only allows for an increase in the glass tensile strength, since it is necessary to overcome the surface precompression in order to break the material, but also a certain immunity against sub critical cracking, as long as the applied tension does not exceed, in absolute value, the surface precompression.

In the goal of a flexible design method, it would be particularly relevant to have a control method of structures allowing to check with a portable equipment that critical loads are not exceeded. This is particularly important for connection areas where 3D stress states can not generally be obtained from simple calculations.

This article presents a possible non-destructive methodology for in situ control of tempered glass structures. The method is based on an original use of photoelasticity. This technique, developed lengthily thereafter, allows to check if a given stress state is reached.

II. PHOTOELASTICITY OF GLASS

The transparency and the birefringence of glass when it is loaded, are two unique properties in the field of building materials which are proposed to be used in an original way. For that, it is necessary to be able to pass from a photoelastic image to a stress state, and reciprocally. Thereafter, the principles of photoelasticity and polariscopy are explained, then a simulation method of photoelastic images based on the analysis of finite element results is presented. The difficulty comes from the three-dimensional feature of the stress state in the vicinity of joints which makes unusual the photoelastic analysis.

A. Polariscopy and photoelasticity

A plane polariscope is composed of a white or monochromatic (one wavelength) light source and two linear polarizers with crossed axes named the polarizer and the analyser respectively. Two quarter-wave plates can be added in order to obtain a circular polariscope. The glass element to be analysed is positioned between the two polarizers or the two quarter-wave plates (Figure. 3). The light ray, emitted by the source, crosses the first polarizer. It is then constrained to vibrate in a plane normal to the direction of propagation determined by the orientation of the polarizer. The luminous ray is said to be plane or linearly polarized.

If a quarter-wave plate is added, the amplitude of the emergent light vector is constant and the vector extremity draws a circle when the wave propagates: the luminous ray is circularly polarized.

The luminous ray then continues to propagate and meets the glass plate. Glass, like several other non-crystalline transparent materials, is optically isotropic under normal conditions but becomes birefringent, like a crystal, when it is loaded. This phenomenon is called accidental birefringence or photoelasticity [Aben and Guillemet, 1993]. The optical properties of glass can be represented in each point by an ellipsoid of indices whose principal axes coincide with the principal

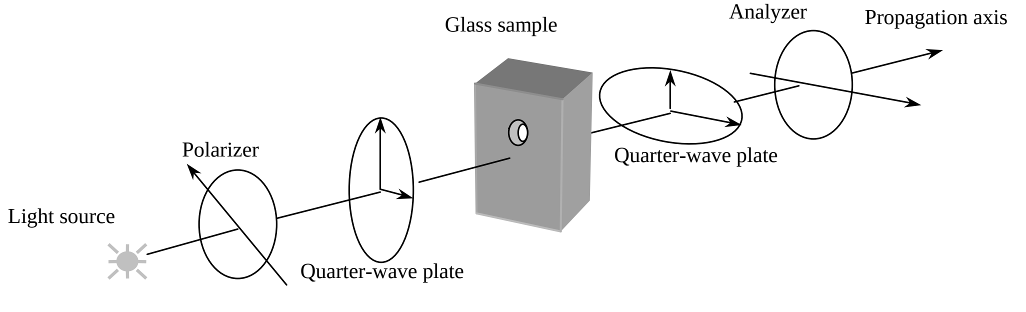

Fig 3: Circular polariscopy

directions of the stresses. So when the luminous ray reaches glass, it is divided immediately into two vibrations whose orientations follow the two secondary principal directions, i.e. the two stress principal directions, in the medium, relative to the plane perpendicular to the axis of light propagation. The third direction does not contribute to birefringence since the propagation velocity of a light ray is not governed by matter alignment along this ray, but by the nature of the medium normally to the ray.

The relative phase retardation Δ which is created between the two vibrations follows the Neumann equations [Aben and Guillemet, 1993]:

$$\begin{cases} \frac{d\Delta}{dx_3} = C(\sigma_1 - \sigma_2) + 2\frac{d\varphi}{dx_3} sin\Delta cot\kappa \\ \frac{d\kappa}{dx_3} = \frac{-d\varphi}{dx_3} cos\Delta \end{cases} \quad (1)$$

κ is such that tan $\kappa = E_2/E_1$ where E_1 and E_2 are the amplitudes of the light vibration along the secondary principal directions ($E_1 > E_2$). σ_1 and σ_2 are the secondary principal stresses (in the plane of the plate, i.e. without taking into account the third direction which does not contribute to birefringence), φ is the angle between the secondary principal directions and the polarizer axes and C is the glass photoelastic constant.

In the case of circular polariscopy, after having crossed glass, the luminous ray propagates through the second quarter-wave plate, whose fast and slow axes are opposed to those of the first quarter-wave plate. The analyzer brings back the two vibrations in the same plane and makes them interfere. The intensity I of the transmitted light is given by:

$$\begin{cases} I = I_0 sin^2 2\varphi sin^2(\Delta/2) & \text{if plane polariscopy} \\ I = I_0 sin^2(\Delta/2) & \text{if circular polariscopy} \end{cases} \quad (2)$$

For a plane polariscopy, this intensity is nil if $\varphi = 0(\pi/2)$ or $\Delta = 0(2\pi)$. In the first case, the dark fringes are named the isoclinics; they correspond to the points where the secondary principal directions are parallel to the directions of the polarizer axes. In the second case, the dark fringes are called the isochromatics. With white light, each phase retardation corresponds to a precise colour. The more numerous the isochromatics the higher the difference between the secondary principal stresses. With circular polarization only the isochromatics appear, preventing the superposition of the two types of dark fringes, which may simplify interpretations of images particularly with monochromatic light.

B. Simulation of the photoelastic images

1) Discussion

The phase retardation Δ depends on the secondary principal stresses, thus on the stress state by the intermediary of the Neumann equations (1).

The resolution of this complete system allows to determine the phase retardation Δ and thus the light intensity. The photoelastic images can be simulated by this way. However, the resolution of the Neumann equations is complex since it is a system of non-linear differential equations with non-constant coefficients. The system is simplified if the angle φ does not depend on the co-ordinate x_3 relative to the direction of propagation of the luminous ray, i.e. if the secondary principal directions remain constant along the optical way. In this latter case, the system (1) becomes:

$$\frac{d\Delta}{dx_3} = C(\sigma_1 - \sigma_2) \quad (3)$$

It is then equivalent to 2D photoelasticity obtained for example with a non holed glass plate loaded in its plane and placed in a polariscope whose axis is normal to the plate. However, in the connection zones of glass structures, the presence of a hole with a possible complex geometry (chamfers) does not allow such an assumption. It is in general impossible to calculate the phase retardation Δ with equation (3) because the shear stress σ_{12} is not constant along the optical way. Thus, the principal directions rotate along the thickness, and the term dφ/dx (eq. (1)) can not be neglected. The Neumann equations (1) have to be entirely considered for the analysis of photoelastic images in joint areas. It is possible to show that system (1) is equivalent to the matrix system (4), obtained from the Maxwell equations of electromagnetism [Aben and Guillemet, 1993]:

$$\frac{d[E]}{dx_3}=-\frac{i\pi C}{\lambda}\begin{bmatrix}\sigma_{11}(x_3)-\sigma_{22}(x_3) & 2\sigma_{12}(x_3)\\ 2\sigma_{12}(x_3) & -(\sigma_{11}(x_3)-\sigma_{22}(x_3))\end{bmatrix}[E]$$

$$\text{denoted: } \frac{d[E]}{dx_3}=M(x_3).[E] \tag{4}$$

[E] is the electrostatic vector field (denoted *E* in the following text), λ is the wavelength of the light ray, σ_{ij} are the components of the stress tensor in the plane perpendicular to the light direction of propagation.

2) Principle

The integration of differential equations (4) can be carried out using a Cranck-Nicholson scheme [Bernard et al., 2004]:

$$\frac{E(x_3+\Delta x_3)-E(x_3)}{\Delta x_3}=M(x_3)\left(\frac{E(x_3+\Delta x_3)+E(x_3)}{2}\right) \tag{5}$$

The expression of the vector *E* at altitude $x_3+\Delta x_3$ is obtained from its value at altitude x_3 (I_d is the identity matrix):

$$E(x_3+\Delta x_3)=\left[I_d-\frac{\Delta x_3}{2}M(x_3)\right]^{-1}.\left[I_d+\frac{\Delta x_3}{2}M(x_3)\right].E(x_3) \tag{6}$$

Thus, the assumption of invariance of the secondary principal directions in the thickness of the plate (invariance of shear in the plane of the plate according to direction 3) can be given up.

The choice of the measurement method (circular or linear polariscopy) gives the initial value of the electrostatic field vector E_0 (eq. (6)) and the final analyzer [Bernard et al, 2004]. The light intensity *I* is equal to the square of the electrostatic field vector *E* and is linked to the phase retardation Δ through the previously given expression. A FORTRAN program, developed in [Bernard, 2001], reads the data file generated by the FE software (stress state in each Gauss point) and calculates:

- the phase retardation in order to compare the predicted isovalues with the images obtained during experiments with white light (in the case of the plane polarized light, the angle φ is obtained from the diagonalization of the stress matrix 2×2 relative to the plate plane),
- or the light intensity in order to compare locations of light extinction (where the intensity is equal to zero) with isochromatics obtained with monochromatic light (only one wavelength).

III. Validation of the Method

A. *Experimental Campaign*

In order to check the validity of the analysis code of photoelastic images, the predicted photoelastic fringes are compared with experimental results. The experimental campaign carried out aims at determining the ultimate loads in joint areas of glass structures. It is indeed in this place that the stress states are the most complex, the validation of the approach will be thus relevant. Figure 4 shows one of the tests carried out.

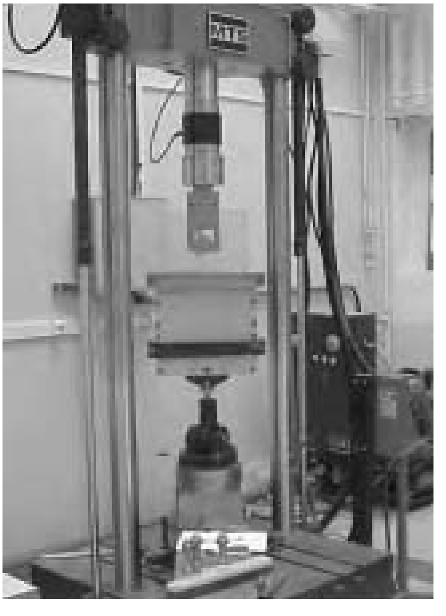

Figure 4: Failure test of a joint

The used MTS testing machine has a loading capacity of 500 kN. Different 350*600 mm^2 glass plates are tested. The glass plate was glued to two metal plates connected to the testing machine frame by means of a knee joint. The mechanical fastener inserted in the hole of the glass plate was embedded in two other plates fixed by means of one pivot joint to the machine horizontal cross-piece. An upwards movement is imposed with a rate of 0.5mm/min. Far from the hole, the stress state is a pure tension. Close to the hole the stress state is three dimensional. The presence of the knee-joint ensures the non-existence of bending and torsion stresses. The loadings is in the plane of the glass plate, as it is the case for structural elements. Experiments were led until failure on both annealed and tempered 19 mm thick glass plates.

Various hole geometries are studied: small, average or large chamfers, small or large diameters (Figure 5, Table 1). The connection is carried out by means of a symmetrical bolt with conical aluminium washers (Figure 6).

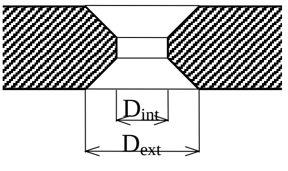

Figure 5: Chamfered hole in the glass plate

Figure 6: Steel connector

TABLE 1: HOLE GEOMETRIES

Hole	**Dint (mm)**	**Dext (mm)**
a1	38	40
a2	54	56
b1	24	40
b2	40	56
c1	30	40

B. Validation of the photoelastic images analysis program

The first step of the validation of the photoelastic images analysis program consists in carrying out a FEM simulation of the tests in order to obtain the stress state in the connection zones.

The assumptions and the validation of this modelling are exposed in [Bernard and al, 2004 and Bernard et al, 2002]. Figure 7 shows the comparison between the photoelastic images visualized during a test for a given loading and a given geometry, with the simulated photoelastic images. The results of simulation are thus similar to the experimental ones.

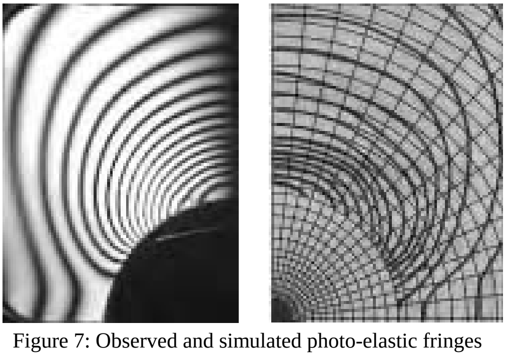

Figure 7: Observed and simulated photo-elastic fringes

IV. APPLICATION OF THE METHOD : IN SITU CONTROL OF JOINTS

Thus, in analysing photoelastic images obtained on existing structures, the stress state can be predicted in the medium. It is also possible to check if the external applied tension exceeds in absolute value the precompression of surface induced by thermal tempering [Zarzycki, 1982]. An ultimate limit state design with this limit state is relevant because tempered glass, whose surface is not under tension, is not subject to subcritical crack growth. In [Bernard, 2001], it is mentioned that for connections areas comprising a hole with large 45° chamfer and large diameter (Φ_{ext} = 56mm), surface is decompressed starting from a load equal to 80kN.

Figure 8 shows the simulated photoelastic images obtained with the load leading to the surface decompression (a) – 80 KN –, as well as this load divided by the classical 3.5 safety coefficient (b) – 23 KN – (the partial coefficient 2 can be removed because the surface is ensured to be in compression), and the failure load divided by 7 (c) – 16 KN – corresponding to the present design method.

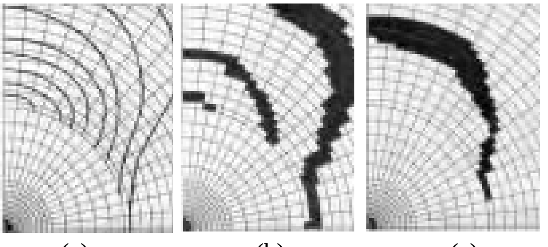

(a) (b) (c)

Figure 8: Simulated photo-elastic fringes beyond the connector at three different load levels

V. CONCLUSION

This work deals with the context of "structural glass", i.e. the use of glass for civil engineering structures.

The lack of knowledge of the long-term mechanical behaviour of glass led to penalize its use for such applications. Full-scale tests and high safety coefficients are required by the offices of control for construction.

The answer to the question asked in the title is surely positive. The use of photoelasticity coupled with a full finite element analysis [Bernard et al., 2002 and 2004] is proposed for the in situ control of glass structures. In addition it is proposed to design tempered glass structures with the ultimate limit state corresponding to the surface decompression. This limit state needs to be calculated by means of finite element predictions of residual stresses due to tempering [Bernard et al., 2002 and 2004]. Such a design method allows to remove the partial safety factor due to the sub-critical crack growth.

The simulation of the photoelastic images, which allows to link stress state and isochromatics, is presented and developed. The originality of the presented work is to account for the three-dimensional feature of the stress state in the zones of connection. The photoelastic images analysis program developed in this study allows the integration of a possible rotation of the secondary principal directions in the thickness of the plate i.e. along the optical way of the light. This method will able to check in situ the stress state of the glass structure, and particularly to know if the glass surface is decompressed or not. It will allow to deliver certificates of guarantee.

REFERENCES

[Aben and Guillemet, 1993].
ABEN H., GUILLEMET C., Photoelasticity of Glass, Berlin, Springer-Verlag, 1993.

[Bernard, 2001]
BERNARD F., Sur le dimensionnement des structures en verre trempé : étude des zones de connexion, thèse de doctorat, Ecole Normale Supérieure de Cachan, 2001.

[Bernard et al., 2002]
BERNARD F., DAUDEVILLE L., GY R., *Sur le dimensionnement des structures en verre trempé*, Revue Française de Génie Civil, Vol. 6, No 7-8, pp.1359-1380, 2002.

[Bernard et al., 2004]
BERNARD F., DAUDEVILLE L., GY R., *Vers une procédure de contrôle des structures en verre trempé*, Mécanique et Industrie, Vol. 5, No 3, pp. 265-273, 2004

[Michalske and Freiman, 1983]
MICHALSKE T.A., FREIMAN S.W., *A molecular mechanism for stress corrosion in vitreous silica*, *J. American Ceramic Society*, Vol. 66, No 4, pp. 284-288, 1983.

[Zarzycki, 1982]
ZARZYCKI J., Les verres et l'état vitreux, Paris, Masson, 1982

EU COST C13 Glass and Interactive Building Envelopes. M. Crisinel, et al. (Eds.). IOS Press, 2007.

Glass in Contact with Different Inserts

Martina Eliášová, Czech Technical University in Prague, Czech Republic
Sébastien Floury, Université Blaire Pascal, Clermont-Ferrand, France
František Wald, Czech Technical University in Prague, Czech Republic

The paper presents experimental observations of glass in contact with inserts of steel, aluminium, polyamide and epoxide resin. Four sets of tests with the different contact materials were carried out in the laboratory of Czech Technical University. Influence of the edge finishing, size and thickness of the glass panel and the corner distance was taken into account. The test results and related FE simulation will allow preparing an analytical prediction model of the contact resistance as well as the bearing resistance of bolted connections.

Keywords: Glass panel, compression, experiments, material of inserts, size effect, edge finishing.

I. Introduction

Modern trends as well as new technologies in production and materials are used in civil engineering. Glass with its new function is one of the most progressive materials nowadays. It is not only the filling but also the load-carrying element. The glass is used for façade systems, roofs of atriums, railing of staircases and over bearing structures.

The structural glass is usually combined with other materials, mostly with steel. There is a lack of knowledge, design rules and procedures, which strengthen use of this attractive material. Designers have limited coherent approach to these problems at present. One of major questions in glass structures design is the connection between the glass components and the joints to the supporting structures. The knowledge in the glass connection is limited even though it is one of the most important parts of the structure.

Glass does not yield, it is a brittle material and its stress concentrations may not be ignored. Ductile material (steel, aluminium) yields if it is locally overstressed and therefore stress concentrations are limited. For glass is important to give an attention to the details and way of their design. Ultimate load depends on the edge finishing, methods of the drilling, bolt positioning and type of the bolts.

II. Experiments

A. Scope of Test

The test set up was prepared to investigate influence of the inserts from different materials on the glass panel resistance. The test results are summarised in tables, Appendix A1, A2, A3. The length of the inserts was studied on tests *Al 90(60,180)/120-15/p-X*, tab. A1. The glass panel's size on tests *Al 90/120(150,180)-15/p-X*, the thickness of glass panel on tests *Al 90/120-15(12,10)/p-X* and the edge finishing on tests *Al 90/120-15/p(s)–X*, tab. A2. The material of insert was studied on tests *Pa (Fe,Ep) 90/120-15/p-X*, tab. A3. The used numbering is adopted to recognize the plates for an analysis. This numbering is given in the following form:

Insert length ↓ ↓ Glass thickness

Al 90 / 120 - 15 / p – number of test

Material ↑ ↑ Glass size ↑ Edges finishing

where: Al = aluminium, Pa = polyamide, Fe = steel, Ep = epoxide resin; insert length: 90 mm, 60 mm, 180 mm; glass size: 120×120 mm, 150×150 mm, 180×180 mm; glass thickness: 10, 12 and 15 mm; edges finishing: p= polished; s = smoothed.

All tests were carried out for annealed float glass. Heat-strengthened and fully toughened glass samples will be investigated in the second step. Totally 81 tests were performed.

B. *Material Tests*

Four point bending tests of glass, Figure 1, were performed for determination of the strength based on standard [ČSN EN 1288-3: 2001]. The thickness of the glass panel was t = 15 mm, test specimen has dimension 1100 x 360 mm.

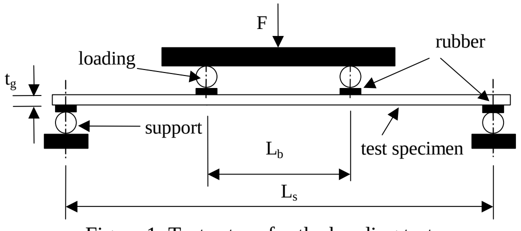

Figure 1: Test set-up for the bending test

The test specimens were loaded to the failure of the glass panel. During the experiment forces and deflections were recorded, Figure 2. Average strength of the single float glass, which was used for next experiments, was $f_{g,t}$ = *67,5 MPa*, Tab. 1.

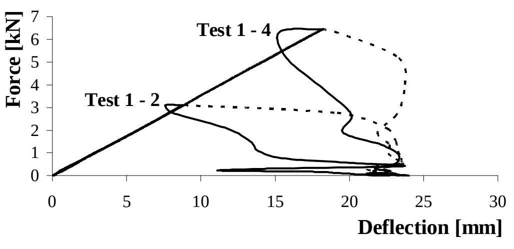

Figure 2: Force – deflection relation of test T1-2, T1-4

The standard coupon tests, [ČSN EN 10002-1: 1994], [ČSN EN ISO 527: 1997] were carried out for inserts to obtain their material properties, Tab. 2.

C. *Test Set-Up*

Glass panels were placed between the inserts and loaded by a force to the failure, Figure 3. Two test machines with the load capacity 400 kN and 1000 kN were used for the experiments. The first one allowed recording force – deformation curve. A transparent box protected the observer against the dangerous glass shards was used, see Figure 4.

TABLE 1:
RESULTS OF FOUR POINT BENDING TEST

Number of test	Stress [MPa]	Deflection [mm]	Young's Modulus [MPa]
1	39,08	7,37	70 413
2	48,39	8,24	76 054
3	85,35	15,51	72 011
4	97,20	18,2	71 048

TABLE 2:
MECHANICAL PROPERTIES OF MATERIALS

Material of inserts	Young's Modulus [MPa]	Poisson's ratio	Tensile strength [MPa]
Aluminium	69000	0,34	265
Polyamide	3500	0,39	76
Epoxide	5700	-	51,5
Steel	210000	0,32	400

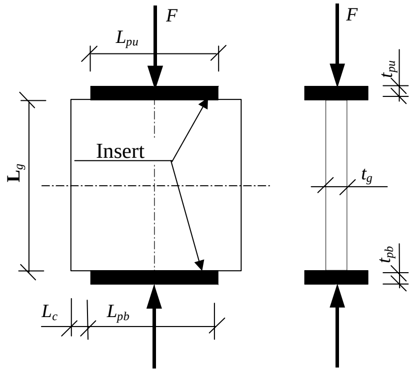

Figure 3: Geometry of the test set-up for the glass in contact under pressure

Figure 4: Transparent box for protection

D. *Measurements*

The shape and thickness of the glass panels and the contact area of inserts were measured before testing. The measured values are summarized in

Appendix Tab. A1, A2 and A3. The edge finishing of the glass panels is taken into account, Figure 5.

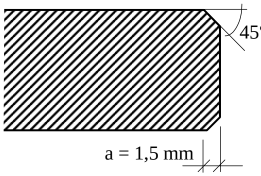

Figure 5: Edge of the glass plate

During the loading of the test specimen an attention was given to the first crack appearance as well as to the shape of the failure in glass panels. Deformations δ of the upper and bottom inserts were measured after the test, Figure 6, and they are recorded in Tab. A1, A2 and A3 in Appendix.

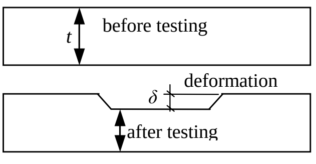

Figure 6: Measurements of the contact plates

III. RESULTS

A. Failure Modes

The failure modes of the glass panel in contact with inserts were observed during the loading stage. It is possible to describe different initial damages according to the shape of the first crack in the glass panel. "The corner crack" is a breaking of the glass panel from the corner of the insert. "The inside crack" is a vertical crack inside the glass panel. "The surface flake" is a scaling of the glass panel's surface. "The edge crack" is the breaking of the glass panel's edge from one insert to the other, see Figure 7a).

Different failure modes were observed at the collapse as well. "The fast failure" is a fast fragmentation of the glass panel into very small pieces of glass. Usually this failure mode was without any initial damages. Next one is "fragmentation" of the panel into big pieces of glass after crack propagation, see Figure 7b). The "cut through the insert" occurred for inserts with Young's modulus lower compared to the tested glass panel, e.g. epoxide resin and polyamide.

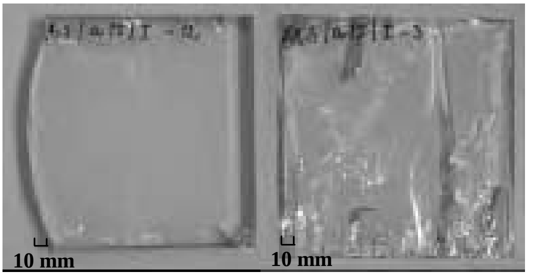

Figure 7a): Edge failure, 7b): Glass with flakes and vertical cracks

B. Resistance

The comparison of the test results may be based on the predicted reduction of the resistance in contact, which is included in the form of joint coefficient β_j. The ultimate resistance can be calculated as

$$F_{red} = \beta_j \, f_{c,u} \, A_i, \tag{1}$$

where β_j is the joint coefficient,
A_i is the contact area of the glass,
$f_{c,u}$ is the characteristic strength of glass in compression and is considered as 500 MPa.

The theoretical resistance F_{theor} $(\beta_j = 1)$ for insert from aluminium is compared to the experimental one F_{exp} in the Figure 8.

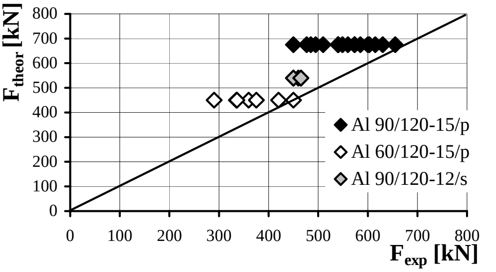

Figure 8: Comparison of the theoretical F_{theor} and experimental F_{exp} resistances

C. Material of Insert

The inserts of steel, aluminium, polyamide and epoxide were tested. The force at the failure is compared for each material at Figure 9. The tests with polyamide and epoxide inserts exhibit similar results due to the similar modulus of elasticity.

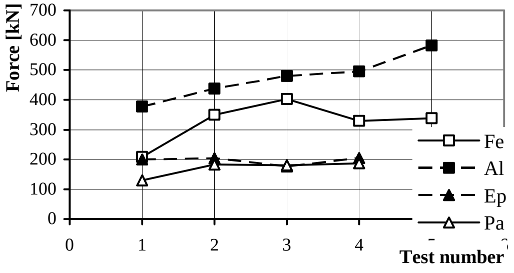

Figure 9: Comparison of the inserts

The evaluation of the joint coefficient β_j for the different material of inserts is shown at Figure 10. Suggested values of joint coefficients, which were determined for glass panel with smoothed edges, are summarized at Tab. 3.

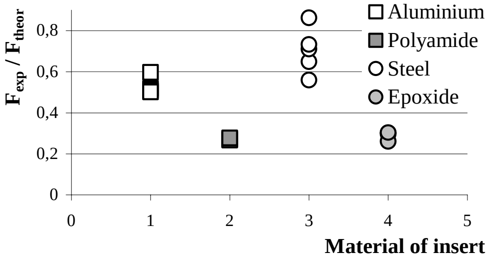

Figure 10: F_{exp} /F_{theor} ratio for different material of inserts

TABLE 3:
JOINT COEFFICIENT FOR DIFFERENT MATERIAL OF INSERTS

Material	Al	Fe	Pa	Ep
Coefficient β_j	0,50	0,55	0,25	0,25

The plastic deformation was developed in the insert under the pressure, see Figure 11.

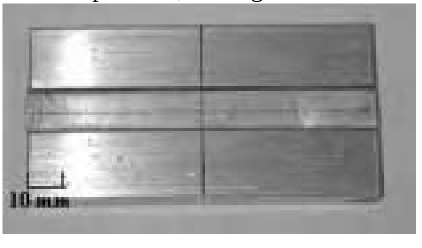

Figure 11: Residual deformation of the aluminium plate

D. Size and Thickness Effect

The glass panels of thickness 10, 12 and 15 mm were tested. The results are compared in Figure 12. Three size of glass panels were examined: 120 x 120, 150 x 150 and 180 x 180 mm. Comparison of results is given in [Floury 2004] and Figure 13.

Resistance was observed by tests in range from 400 MPa to 500 MPa. No influence of glass panel thickness was observed, Figure 12. The maximal forces in compression were at the same level for different size of the glass, joint coefficient β_j varies from 0,65 till 0,75, Figure 13.

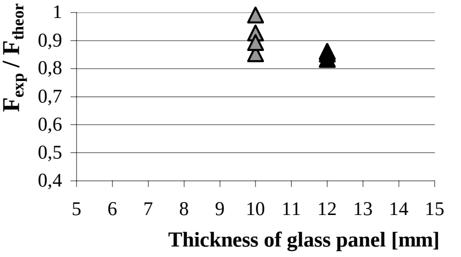

Figure 12: F_{exp} /F_{theor} ratio for different thickness of glass panels

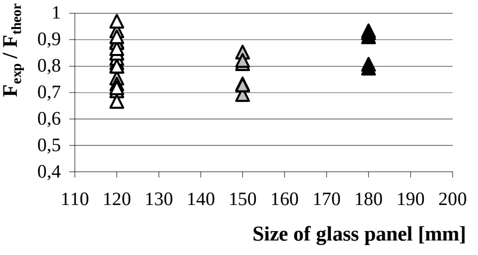

Figure 13: F_{exp} /F_{theor} ratio for different size of glass panels

E. Length of the Insert

Three different lengths of insert from aluminium were tested (60, 90 and 180 mm). The glass panels had the same size and thickness. Maximal reached forces at failure of the glass panels are compared in the graph. Figure 14 shows relation between the maximal forces and measured deformation δ of the inserts. For better understanding the force was recalculated according to the contact area to the stress, see Figure 15.

Behaviour of the 60 mm long inserts was similar to the 90 mm long inserts behaviour. First crack appeared at the corner, then the edge failed and finally the glass panel failed completely. For the 180 mm long inserts, the failure of the glass panel was different. The scales of glass flaked off from the surface of the panel.

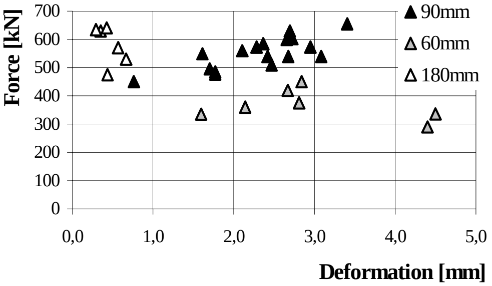

Figure 14: Force – deformation relation for the different length of the contact plate

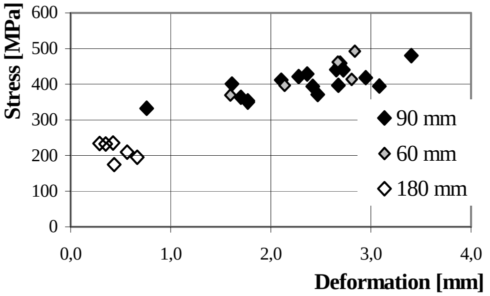

Figure 15: Stress – deformation relation for the different length of the contact plate

F. *Corner Distance*

The size of the insert may be demonstrated also from the point of view of distance between the specimen edge and insert edge L_c, see Figure 3. Results are presented on the Figure 16.

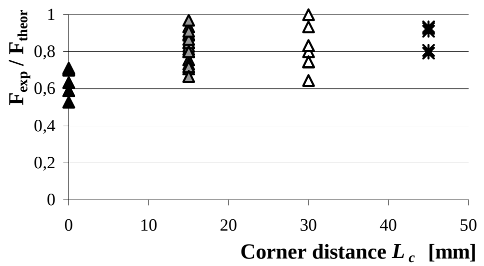

Figure 16: F_{exp} /F_{theor} ratio for different corner distance L_c

G. *Edge Finishing*

Two types of edge finishing were tested: smoothed and polished. Influence of the edge finishing was investigated for aluminium and polyamide inserts, Fig 17.

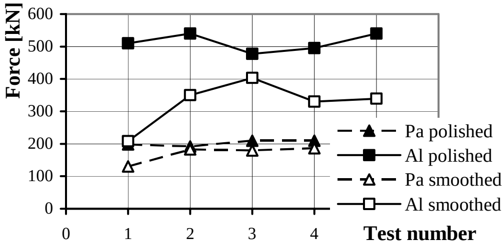

Figure 17: Comparison of the edge finishing

IV. CONCLUSIONS

Four sets of tests were performed to investigate the behaviour of the of float glass in contact with different material. The type of contact material has an impact to the joint resistance. The tests results indicate an influence of the corner distance L_c as well. The influence of the edge finishing was not observed.

The experimentally obtained joint coefficient β_j varies from 0,25 for insert from polyamide up to 0,55 for insert from steel.

Further experiments for fully toughened glass panels and FE method allow to precise contact resistance of glass panel for design. Contact resistance will be used as the first step for the study of bolted connections.

V. ACKNOWLEDGMENT

The research was carried out with financial support of the Czech Grant Agency project No. 103/05/0417. This help is gratefully acknowledged.

REFERENCES

[ČSN EN 1288-3: 2001]
ČSN EN 1288-3: *Glass in building – Determination of the bending strength of glass.* ČNI, 2001.

[ČSN EN 10002-1: 1994]
ČSN EN 10002-1: *Metals : Tensile test.* ČNI, 1994.

[ČSN EN ISO 527: 1997]
ČSN EN ISO 527: *Plastics - Determination of tensile properties.* ČNI, 1997.

[ELIÁŠOVÁ et al. 2003]
ELIÁŠOVÁ, M., WALD, F., SOKOL, Z.: *Bolted connections of glass structures, in Czech*, In: Ocelové konstrukce a mosty 2003, ČVUT Praha, 2003, ISBN 80-01-02747-3.

[FLOURY 2004]
FLOURY, S.: *Glass in Contact*, diploma work Université Blaire Pascal, Clermont-Ferrand, 2004.

Appendix

A 1: Measurements of the glass and contact plates, failure force –material of inserts from aluminium with different length

Test number	Glass		Bottom plate		Upper plate		First cracking [kN]	Failure [kN]	Deformation [mm]	1) Initial, 2) failure modes
	t_g [mm]	b [mm]	t_{pb} [mm]	L_{pb} [mm]	t_{pu} [mm]	L_{pu} [mm]				
Contact material – aluminium, length 90 mm Glass – size 120 x 120 mm, thickness 15 mm Edge manufacturing of glass - polished										
Al 90/120-15/p-1	15.2	120.3	10.1	90.2	10.0	90.2	480	510	2.47	CC, EC
Al 90/120-15/p-2	15.1	120.2	10.0	90.1	10.2	90.2	520	540	2.68	CC, FF
Al 90/120-15/p-3	15.1	119.2	10.1	90.4	10.0	90.3	477	477	1.77	CC, FF
Al 90/120-15/p-4	15.1	119.8	10.1	90.2	10.1	90.3	495	495	1.70	NO, FF
Al 90/120-15/p-5	15.1	120.0	10.0	90.1	10.0	90.2	120	126	0.00	CC, I
Al 90/120-15/p-6	15.2	119.6	10.0	90.1	10.0	90.2	490	540	3.09	PF, PF
Al 90/120-15/p-7	15.2	119.8	9.9	90.1	10.0	90.2	495	549	1.61	NO, FF
Al 90/120-15/p-8	15.1	120.5	10.2	90.2	10.1	90.2	42	42	0.00	CC, I
Al 90/120-15/p-9	15.1	119.8	10.0	90.2	10.1	90.2	530	573	2.28	EC, PF
Al 90/120-15/p-10	15.1	120.3	10.0	90.2	10.1	90.2	540	560	2.11	CC, PF
Al 90/120-15/p-11	15.2	120.4	10.0	90.3	9.9	90.2	540	573	2.95	EC, PF
Al 90/120-15/p-12	15.2	120.2	10.1	90.2	9.9	90.2	600	603	2.73	EC, PF
Al 90/120-15/p-13	15.1	120.5	10.0	90.2	10.1	90.2	570	600	2.66	CC, FF
Al 90/120-15/p-14	15.2	119.8	10.0	90.2	10.2	90.3	450	485	1.77	CC, FF
Al 90/120-15/p-15	15.2	120.4	10.0	90.2	10.1	90.3	525	540	2.42	CC, FF
Al 90/120-15/p-16	15.1	119.7	10.1	90.4	10.0	90.4	575	585	2.37	CC, FF
Al 90/120-15/p-17	15.0	120.3	10.0	90.4	10.0	90.4	450	450	0.76	NO, FF
Al 90/120-15/p-18	15.2	120.3	10.1	90.3	9.9	90.3	620	630	2.70	EC, PF
Al 90/120-15/p-19	15.1	121.0	10.0	90.3	10.1	90.3	600	615	2.69	EC, FF
Al 90/120-15/p-20	15.1	119.6	10.1	90.4	10.0	90.3	650	655	3.41	CC, FF
Contact material – aluminium, length 60 mm Glass – size 120 x 120 mm, thickness 15 mm Edge manufacturing of glass - polished										
Al 60/120-15/p-1	15.2	120.5	10.1	60.2	10.0	60.3	190	215	0.01	PF, IC
Al 60/120-15/p-2	15.1	119.7	10.1	60.4	9.9	60.1	405	420	2.67	CC, PF
Al 60/120-15/p-3	15.1	120.1	10.0	60.1	9.9	60.2	350	360	2.14	CC, FF
Al 60/120-15/p-4	15.1	120.1	10.0	60.0	10.0	60.0	280	335	1.60	CC, FF
Al 60/120-15/p-5	15.2	120.1	9.9	60.0	9.9	60.2	320	450	2.84	CC, FF
Al 60/120-15/p-6	15.1	120.1	10.2	60.0	10.0	60.1	360	375	2.81	CC, FF
Al 60/120-15/p-7	15.0	119.7	10.0	60.1	9.8	60.2	328	336	4.50	CC, I
Al 60/120-15/p-8	15.0	119.7	9.9	60.2	9.9	60.2	-	290	4.40	I
Contact material – aluminium, length 180 mm Glass – size 120 x 120 mm, thickness 15 mm Edge manufacturing of glass - polished										
Al 180/120-15/p-1	15.1	120.1	10.0	180.0	10.0	180.0	-	570	0.57	NO, IC
Al 180/120-15/p-2	15.1	120.2	10.1	180.0	10.0	180.0	-	630	0.35	NO, IC
Al 180/120-15/p-3	15.1	120.2	10.2	180.0	10.0	180.0	-	475	0.44	NO, IC
Al 180/120-15/p-4	15.1	119.6	10.1	180.0	10.0	180.0	-	635	0.29	NO, FF
Al 180/120-15/p-5	15.1	119.8	10.1	180.0	10.1	180.0	-	640	0.43	PF, FF
Al 180/120-15/p-6	15.1	120.1	9.9	180.0	10.0	180.0	-	530	0.67	PF, PF

Notes: 1) Initial damages: EC – edge crack; CC – corner crack; PF – panel flakes

2) Failure modes: PF – panel fragmentation; FF – fast fragmentation; IC – internal crack; CU – insert cut

A 2: Measurements of the glass and contact plates, failure force – material of inserts from aluminium, glass panel with different size and thickness

Test number	**Glass**		**Bottom plate**		**Upper plate**		**First cracking [kN]**	**Failure [kN]**	**Deformation [mm]**	**1) Initial, 2) failure modes**
	t_g [mm]	**b [mm]**	**t_{pb} [mm]**	**L_{pb} [mm]**	**t_{pu} [mm]**	**L_{pu} [mm]**				
Contact material – aluminium, length 90 mm Glass – size 150 x 150 mm, thickness 15 mm Edge finishing of glass - polished										
Al 90/150-15/p-1	15.1	149.6	9.8	90.3	9.8	90.3	480	495	1.80	CC, IC
Al 90/150-15/p-2	15.0	150.1	9.8	90.0	9.9	90.4	435	468	2.15	CC, FF
Al 90/150-15/p-3	15.1	150.5	9.9	90.2	10.0	90.3	375	546	2.90	CC, PF
Al 90/150-15/p-4	15.1	150.2	10.0	90.2	9.8	90.2	525	576	2.90	CC, PF
Al 90/150-15/p-5	15.1	150.5	9.8	90.3	9.9	90.2	435	492	2.10	CC, PF
Al 90/150-15/p-6	15.1	150.4	9.8	90.2	9.8	90.0	445	555	2.15	CC, IC
Contact material – aluminium, length 90 mm Glass – size 180 x 180 mm, thickness 15 mm Edge finishing of glass - polished										
Al 90/180-15/p-1	15.1	180.3	9.9	90.1	9.9	90.1	500	535	3.05	CC, IC
Al 90/180-15/p-2	15.0	180.4	10.0	90.0	9.8	90.1	350	625	2.80	CC, PF
Al 90/180-15/p-3	15.0	180.4	9.9	90.2	9.9	90.0	500	545	2.60	CC
Al 90/180-15/p-4	15.0	180.5	9.9	90.0	9.8	90.0	530	630	3.40	CC
Al 90/180-15/p-5	15.1	180.2	9.9	90.2	9.8	90.0	640	680	3.10	CC
Al 90/180-15/p-6	15.0	180.3	10	90.1	10.0	90.2	475	615	3.30	CC, PF
Contact material – aluminium, length 90 mm Glass – size 120 x 120 mm, thickness 15 mm Edge finishing of glass - smoothed										
Al 90/120-15/s-01	14.6	120.1	10.0	90.2	10.0	90.1	-	208	-	NO, IC
Al 90/120-15/s-02	14.8	120.2	10.0	90.2	9.9	90.2	-	350	-	FF
Al 90/120-15/s-03	14.9	120.0	10.0	90.2	10.0	90.0	210	403	-	PF, PF
Al 90/120-15/s-04	14.8	120.0	10.1	90.1	10.0	90.2	240	331	-	CC, PF
Al 90/120-15/s-05	14.8	120.3	10.0	90.3	10.0	90.1	180	339	-	CC, PF
Contact material – aluminium, length 90 mm Glass – size 120 x 120 mm, thickness 12 mm Edge finishing of glass - smoothed										
Al 90/120-12/s-1	12.2	120.0	9.9	90.2	10.0	90.3	50	75	0	EC, PF
Al 90/120-12/s-2	12.2	120.1	10.1	90.2	9.9	90.3	450	460	1.590	EC, FF
Al 90/120-12/s-3	12.2	120.0	10.0	90.2	10.0	90.2	430	450	1.550	CC, FF
Al 90/120-12/s-4	12.2	119.8	10.0	90.3	10.0	90.2	430	450	1.550	NO, FF
Al 90/120-12/s-5	12.2	119.8	9.9	90.4	10.1	90.4	450	465	2.065	CC, IC
Al 90/120-12/s-6	12.2	119.8	10.0	90.4	9.9	90.3	465	465	1.915	NO, FF
Contact material – aluminium, length 90 mm Glass – size 120 x 120 mm, thickness 10 mm Edge finishing of glass - smoothed										
Al 90/120-10/s-1	10.0	119.6	9.9	90.2	10.0	90.2	-	50	0	PF, IC
Al 90/120-10/s-2	10.0	119.1	10.1	90.2	9.9	90.2	-	45	0	PF, IC
Al 90/120-10/s-3	10.0	118.8	10.1	90.2	10.1	90.2	420	446	4.230	CC, PF
Al 90/120-10/s-4	10.0	119.3	10.0	90.1	9.9	90.1	375	384	2.005	CC, PF
Al 90/120-10/s-5	10.0	119.1	10.1	90.1	10.0	90.1	390	417	2.960	PF, IC
Al 90/120-10/s-6	10.0	119.3	10.0	90.3	9.9	90.2	390	402	2.590	CC, FF

Notes: 1) Initial damages: EC – edge crack; CC – corner crack; PF – panel flakes

2) Failure modes: PF – panel fragmentation; FF – fast fragmentation; IC – internal crack; CU – insert cut

A 3: Measurements of the glass and contact plates, failure force – material of inserts from polyamide, steel, epoxide resin

Test number	Glass		Bottom plate		Upper plate		First cracking [kN]	Failure [kN]	Deformation [mm]	1) Initial, 2) failure modes
	t_g [mm]	b [mm]	t_{pb} [mm]	L_{pb} [mm]	t_{pu} [mm]	L_{pu} [mm]				
Contact material – polyamide, length 90 mm Glass – size 120 x 120 mm, thickness 15 mm Edge finishing of glass – polished, smoothed										
Pa 90/120-15/s-01	14.7	120.0	10.8	90.1	10.8	90.1	-	130	-	PF, I
Pa 90/120-15/s-02	14.7	120.0	10.8	90.2	10.8	90.2	-	183	8.2	EC, I
Pa 90/120-15/s-03	14.8	120.0	10.8	90.2	10.8	90.2	-	180	6.3	PF, I
Pa 90/120-15/s-04	14.8	120.0	10.9	90.0	10.9	90.0	-	187	8.5	PF, I
Contact material – polyamide, length 90 mm Glass – size 120 x 120 mm, thickness 15 mm Edge finishing of glass - polished										
Pa 90/120-15/p-1	15.0	119.7	10.5	90.1	10.5	89.9	192	198	11	I
Pa 90/120-15/p-2	15.0	120.0	10.5	89.9	10.5	90.0	-	192	7	I
Pa 90/120-15/p-3	15.0	120.5	10.5	90.0	10.5	90.0	-	210	-	PF, I
Pa 90/120-15/p-4	15.0	120.0	10.5	90.2	10.5	90.0	-	210	-	I
Contact material – steel, length 90 mm Glass – size 120 x 120 mm, thickness 15 mm Edge finishing of glass - smoothed										
Fe 90/120-15/s-01	14.8	120.0	10.2	90.0	10.0	90.0	120	378	-	EC, PF
Fe 90/120-15/s-02	14.7	120.4	10.0	90.0	10.0	89.9	-	438	-	NO, FF
Fe 90/120-15/s-03	14.8	120.3	10.0	90.0	10.0	98.4	-	480	-	NO, FF
Fe 90/120-15/s-04	14.7	119.9	10.0	89.2	10.0	89.6	90	153	-	CC, PF
Fe 90/120-15/s-05	14.8	119.9	10.0	89.2	10.1	89.6	470	582	-	CC, FF
Fe 90/120-15/s-06	14.8	120.3	8.5	89.1	8.6	89.2	-	495	-	NO, FF
Contact material – epoxide resin, length 90 mm Glass – size 120 x 120 mm, thickness 15 mm Edge finishing of glass - smoothed										
Ep 90/120-15/s-01	14.9	120.2	10.0	89.9	10.1	89.9	-	200	2.7	CU
Ep 90/120-15/s-02	14.9	120.0	10.2	89.9	10.0	89.7	-	204	5.0	CU
Ep 90/120-15/s-03	14.9	120.2	10.0	89.7	10.1	89.7	-	176	3.4	PF, IC
Ep 90/120-15/s-04	14.9	120.1	10.0	90.0	10.0	89.8	-	205	2.6	NO, PF

Notes: 1) Initial damages: EC – edge crack; CC – corner crack; PF – panel flakes

2) Failure modes: PF – panel fragmentation; FF – fast fragmentation; IC – internal crack; CU – insert cut

EU COST C13 Glass and Interactive Building Envelopes. M. Crisinel, et al. (Eds.). IOS Press, 2007.

Design of Glass Members
A Critical Review of the Present Knowledge

Matthias Haldimann
Ecole Polytechnique Fédérale de Lausanne (EPFL),
Steel Structures Laboratory (ICOM), CH-1015 Lausanne, Switzerland

Engineers are currently using various concepts for the analysis and design of structural elements made of glass. There is no general agreement on a certain design concept yet. All available design concepts suffer from more or less severe drawbacks and their applicability is limited to special cases.

The present paper discusses the present knowledge in the field of structural glass design. The aim is not so much to explain every single detail related to the application of the concepts, but at working out the bases and focusing on difficulties and limitations. The paper provides an overview for anyone interested in the topic and aims at serving as a basis for discussions on desirable improvements to current design concepts and for research work on the topic.

Keywords: structural glass, design concept, code, failure prediction, state of knowledge

I. Introduction

In recent years, many research projects have been dedicated to the structural use of glass. Nevertheless, engineers designing load carrying glass elements are in a rather uncomfortable situation when it comes to design concepts:

- In Europe, there is no general agreement on a particular design concept.
- None of the models considers all aspects of the physical behaviour of structural glass elements.
- The applicability of the models is limited to special conditions.
- The physical meaning of important model parameters is obscure and/or several physical aspects are 'hidden' within a single parameter. Some parameters reflect other influences than they are supposed to and therefore depend on the test setup used for their determination.
- The models contain inconsistencies, they give unrealistic results for special cases and different models yield fairly differing results. Several researchers therefore expressed fundamental doubts about the suitability and correctness of common glass design concepts, even for the limited scope that they were developed for.
- No comprehensive safety concept is available to take the particularities associated with the brittle material glass sufficiently into account.

These issues are at the origin of the current unsatisfactory situation and had various negative consequences. Code development in Europe reached a deadlock due to stiff opposition. Confusion and lack of confidence in 'advanced' design concepts hinders the work of engineers. Furthermore, the frequent need for time-consuming and expensive laboratory testing impedes the design process for innovative glass structures.

This paper discusses the present knowledge in the field of structural glass design. The aim is not so much to explain every single detail related to the application of the concepts, but at working out the bases and focusing on difficulties and limitations. The paper provides an overview for anyone interested in the topic and aims at serving as a basis for discussions on desirable improvements to current design concepts and for research work on the topic.

II. State of Knowledge

A. Overview

The methods for the analysis of structural glass elements available today can be divided into three groups:

a) Simple design rules based on allowable stress.
b) Concepts that allow for the calculation of a design resistance based on Weibull theory [Weibull 1951], laboratory tests and correction factors accounting for influences like the action history, the glass panel's surface area, the distribution of stresses within the element and environmental conditions.
c) Design proposals based on alternative approaches like the direct simulation of the growth of a single crack during a glass element's lifetime or the 'classic' (non-Weibull) theory of material resistance.

Some of the more widely used concepts are discussed in more detail in Section C.

B. Terminology

Each section in this chapter uses the notation as it is introduced in the original literature on the concepts discussed. This does inevitably lead to inconsistencies between different sections.

For clarity, some fundamental technical terms and concepts shall be defined here:

Equibiaxial stress:
The two principal stresses are equivalent. In this stress state, the stress normal to a crack is independent of the crack's orientation. An equibiaxial stress state occurs in particular within the loading ring in coaxial double ring testing.

Decompressed surface:
The part of an element's surface where the tensile stress due to loading is bigger that the residual compressive stress due to tempering. On these surface parts, there is a positive effective crack opening stress.

Inherent strength:
The part of the tensile strength that is not due to compressive residual stresses but to the resistance of the material itself. For float glass, this is approximately (even float glass has some compressive residual stresses) the measured macroscopic resistance.

Residual stress due to tempering (σ_{res}):
The residual compressive surface stress that arises from the tempering process. (The term 'prestress' is – although widely used – misleading and therefore not used in the present document.)

Tempered glass:
Glass that has been thermally treated to some extent, i. e. heat strengthened or fully tempered glass.

Uniform lateral load:
Uniformly distributed out-of-plain load.

Weibull distribution:
The two-parameter Weibull probability distribution with the cumulative distribution function given in Eq. (1).

$$\mathrm{F}(\sigma_{\mathrm{f},A_{\mathrm{test}}}) = 1 - \exp\left[-\left(\frac{\sigma_{\mathrm{f},A_{\mathrm{test}}}}{\theta_{A_{\mathrm{test}}}}\right)^{\beta}\right] \tag{1}$$

It is often used to model the inherent strength of glass. $\mathrm{F}(\sigma_{\mathrm{f},A_{\mathrm{test}}})$ is the probability distribution function of the breakage stresses of specimens with the surface area A_{test} exposed to uniform equibiaxial tensile stress. $\theta_{A_{\mathrm{test}}}$ is the scale- and β the shape parameter of the distribution. While the shape parameter is independent from A_{test}, the scale parameter is not.

C. Overview of today's important design concepts

The present chapter briefly presents some glass design concepts currently in use. For detailed information, the reader should refer to [Haas & Haldimann 2004].

C.1. Allowable stress concept

Despite numerous drawbacks, the simplistic approach and the fact that the allowable stress concept is not used in the current building design code generation any more, allowable stress design concepts are still widely used for glass. It is mainly their extreme ease of use and their efficiency that keep these concepts attractive. The general verification format is:

$$\sigma_E \leq \sigma_{\mathrm{adm}} = \sigma_{\mathrm{R}} / \gamma \tag{2}$$

σ_E is the maximum principal stress calculated with the characteristic values of the actions of the most unfavourable design situation, σ_{adm} the allowable stress, σ_{R} the breaking strength in experiments and γ a global safety factor including all uncertainties associated with actions, resistance and modelling.

There is no way of directly considering aspects like the size effect, the target failure probability, the environmental conditions or duration of load effects; they must somehow be 'included' in the recommended σ_{adm} values.

Allowable stress concepts have some important drawbacks:

- They can not consider the actual physical phenomena that govern the mechanical behaviour of glass.
- The scatter and uncertainty is not the same for all influencing parameters. With only one global safety factor, this cannot be accounted for in a sophisticated manner.
- The approach is unsuited for cases where linear superposition of stresses is not possible, e. g. due to geometric non-linearity.
- The transparency and flexibility of the method is very limited. Its application to situations where no or only limited experience is available is problematic.

The German technical guidelines [TRLV 1998] and [TRAV 2003] are well known and widely used examples of design guides based on allowable stresses.

C.2. RWTH Aachen concept

This design concept represents the first European glass design concept that tried to account for the specific properties of glass in an adequate and transparent way. It is compatible with the current partial factor based code generation. Presented to a larger readership in [Sedlacek et al. 1999], the design concept is mainly based on research done at RWTH Aachen, in particular [Blank 1993] and [Güsgen 1998]. The maximum principal design stress is compared to an equivalent resistance as follows:

$$\sigma_{\mathrm{max,d}} \leqslant \frac{\sigma_{\mathrm{bB},A_0,\mathrm{k}}}{\alpha_\sigma(p,\sigma_{\mathrm{V}})\cdot\alpha(A_{\mathrm{red}})\cdot\alpha(t)\cdot\alpha(S_v)\cdot\gamma_{\mathrm{M,E}}} + \frac{\sigma_{\mathrm{V,k}}}{\gamma_{\mathrm{M,V}}} \tag{3}$$

$\alpha_\sigma(p,\sigma_{\mathrm{V}})$	coefficient to consider the stress distribution within the decompressed glass surface; p = uniform lateral load; σ_{V} = residual surface stress due to tempering
$\alpha(A_{\mathrm{red}})$	coefficient to account for the size of the decompressed surface area A_{red} (entire surface area for annealed glass)
$\alpha(t)$	coefficient to consider load duration
$\alpha(S_v)$	coefficient to consider load combination and environmental conditions
$\sigma_{\mathrm{max,d}}$	design value of the maximum first principal stress in the element
$\sigma_{\mathrm{bB},A_0,\mathrm{k}}$	characteristic value of the inherent bending breaking strength in R400 coaxial double ring tests according to [EN 1288-2:2000] (5% fractile, confidence level 0.95, surface area $A_{\mathrm{test}} = 0.24\ \mathrm{m}^2$, stress rate = 2 ± 0.4 MPa/s)
$\sigma_{\mathrm{V,k}}$	characteristic value (5% fractile) of the residual surface stress (called 'prestress' in the RWTH Aachen concept); caution, this is the *absolute value* (positive)!
$\gamma_{\mathrm{M,E}}$	partial factor for the inherent strength
$\gamma_{\mathrm{M,V}}$	partial factor for the residual stress

Determination of some of the coefficients is complex, see [Sedlacek et al. 1999] or [Haas & Haldimann 2004] for details. A modified form of Eq. (3) is proposed for glass beams. The coefficients are defined based on Weibull statistics (cf. Eq. (1)) and many assumptions on load durations, overlapping probabilities, material parameters, lifetime and the like. They are only valid in connection with strength values determined using exactly the indicated test setup and parameters.

C.3. European Draft Code prEN 13474

The design concept of prEN 13474[1] is based on the RWTH Aachen concept, but contains influences from the concepts by Shen and Siebert. The influence of the stress distribution on the glass surface is considered on the action side of the verification equation, the residual surface stress on the resistance side.

The structural safety verification format compares an *effective stress* σ_{ef} with an *allowable effective stress for design* $f_{\text{g,d}}$:

$$\sigma_{\text{ef,d}} \leqslant f_{\text{g,d}} \tag{4}$$

It is interesting to note that the effective stress

$$\sigma_{\text{ef,d}} = \sigma_{\text{max,d}} \cdot \alpha_{\sigma}(q) \tag{5}$$

is defined *independently* from residual stress and that decompression of the whole surface is assumed. For common geometries and support conditions, there are tables and equations to determine $\sigma_{\text{ef,d}}$ in function of the applied load q and the plate dimensions.

The *allowable effective stress* is defined as:

$$f_{\text{g,d}} = \left(k_{\text{mod}} \frac{f_{\text{g,k}}}{\gamma_{\text{M}} \cdot k_A} + \frac{f_{\text{b,k}} - f_{\text{g,k}}}{\gamma_{\text{V}}} \right) \cdot \gamma_{\text{n}} \tag{6}$$

$f_{\text{b,k}}$	characteristic value of the breaking strength (5% fractile); $f_{\text{b,k}} = f_{\text{g,k}}$ for ANG, 70 MPa for HSG and 120 MPa for FTG
$f_{\text{g,k}}$	characteristic value of the inherent strength (5% fractile); $f_{\text{g,k}}$ =45 MPa for soda lime silicate and borosilicate glass
$f_{\text{b,k}} - f_{\text{g,k}}$	the residual stress' contribution to the failure strength; 0 for annealed glass
γ_{V}	partial factor for the residual stress due to tempering (= 2.3 for SLS glass)
γ_{M}	partial factor for the inherent strength (= 1.8 for SLS glass)
γ_{n}	national partial factor (mostly = 1.0)
k_A	factor to consider surface area, defined independently from the residual stress as $k_A = A^{0.04}$
k_{mod}	modification factor to consider load duration, load combination and environmental conditions; many assumptions are made to simplify this to only three values: 0.27 for permanent loads, 0.36 for loads of medium duration (snow, climate loads), 0.72 for short duration loads (wind)

[1]*Important*: This draft code is under revision by the committees CEN/TC 250 ('Structural Eurocodes') and CEN/TC 129 (`Glass in Buildings'). At the time of writing, the non-public working papers differ considerably from the published code drafts [prEN3474-1:1999] and [prEN3474-2:2000]!

C.4. Shen's design concept

This concept has been presented in [Shen 1997] and was adapted to the format of [EN 1990:2002] in [Wörner et al. 2001]. It is mainly a considerable simplification of the RWTH Aachen concept, but the concept to account for tempered glass is very particular, see below. Only two coefficients, both acting on the resistance, are considered and very simple tables are proposed for their values. Residual stresses of tempered glass are accounted for indirectly by these coefficients. The concept is limited to glass panes with continuous lateral support along all four edges and loaded by uniformly distributed out-of plane loads.

The structural safety verification format is:

$$\sigma_{\text{max,d}} \leq \sigma_{\text{k}} \cdot \frac{\eta_{\text{F}} \cdot \eta_{\text{D}}}{\gamma_{\text{R}}} \tag{7}$$

$\sigma_{\text{max,d}}$	design value of the max. principal stress
σ_{k}	characteristic value of the bending strength (conditions like in II. C.2
η_{F}	coefficient for the size of the surface area in tension and the stress distribution
η_{D}	coefficient for the load duration
γ_{R}	partial resistance factor

The factor η_{F} accounts for the surface area and the stress distribution, the factor η_{D} for the load duration. Residual stresses are accounted for indirectly, giving different values of η_{D} and η_{F} for annealed and fully tempered glass respectively. For a combination of loads of different duration, η_{D} has to be calculated individually.

To derive the coefficients, the glass' surface condition and the environmental conditions in structural applications have been assumed to be identical to those in the laboratory tests for the determination of the bending strength. Fully tempered glass is assumed to behave like annealed glass, but with the crack growth coefficient $n_{\mathrm{FTG}} = 70$ instead of 16 for annealed glass. This value is taken from the Canadian Standard [CAN/CGSB 12.20-M89] without further discussion. It has two main drawbacks: (a) Increasing the crack growth parameter has nothing to do with the actual physical phenomena governing resistance of tempered glass. (b) The value of 70 is given in [CAN/CGSB 12.20-M89], but not as the crack growth parameter *n* (although this symbol is used) but for a parameter combining *n* with a constant for the relationship between lateral load and stress in rectangular plates.

C.5. Siebert's design concept

This design concept has been established in [Siebert 1999], based on an analysis of the concepts from RWTH Aachen and Shen. The major modifications with respect to these two are:

- An approach to consider the influence of biaxial stress fields is proposed.
- The residual stress is considered as an action.

The structural safety verification format is:

$$\sigma_{\mathrm{ges,d,max}} \cdot f_{\mathrm{A}} \cdot f_{\sigma} \cdot f_{\mathrm{tS}} \leqslant \frac{\theta}{f_{\mathrm{P}}} \tag{8}$$

$\sigma_{\mathrm{ges,d,max}}$ maximum principal surface stress; $\sigma_{\mathrm{ges,d,max}} = \sigma_{\mathrm{d,max}} + \sigma_{\mathrm{E}}$

$\sigma_{\mathrm{d,max}}$ maximum principal stress due to actions

σ_{E} residual surface stress (compr. = neg.)

f_{A} coefficient for the surface area in tension

f_{σ} coefficient for the stress distribution

f_{tS} factor to consider load duration and relative magnitude of different loads

θ scale parameter of the experimental bending strength Weibull distribution

f_{P} target failure probability coefficient

Residual stress being considered as an action, f_{σ} depends on σ_{E}. f_{A} and f_{tS} are identical to the coefficients in the RWTH Aachen concept: $f_{\mathrm{A}} = \alpha(A)$, $f_{\mathrm{tS}} = \alpha(t) \cdot \alpha(S_v)$.

C.6. Glass Failure Prediction Model (GFPM)

The Glass Failure Prediction Model (GFPM) presented in [Beason 1980] and [Beason & Morgan 1984] is directly based on Weibull theory. According to Weibull, the failure probability of a brittle material can be represented as

$$P_{\mathrm{f}} = 1 - e^{-B} \tag{9}$$

where *B* reflects the risk of failure as a function of all relevant aspects, in particular the surface condition and the stress distribution. For a general case, the GFPM proposes the risk function

$$B = \tilde{k} \int_A \left[\tilde{c}(x,y)\sigma_{\mathrm{eq,max}}(q,x,y)\right]^{\tilde{m}} \,\mathrm{d}A \tag{10}$$

in which $\tilde{c}(x,y)$ is the 'biaxial stress correction factor' (a function of the minimum to maximum principal stress ratio), A the surface area, $\sigma_{\mathrm{eq,max}}(q,x,y) = \sigma(q,x,y)(t_{\mathrm{d}}/60)^{1/16}$ the maximum equivalent principal stress as a function of the lateral load q and the location on the plate surface (x,y). $\tilde{m}$ and $\tilde{k}$ are the so-called 'surface flaw parameters'.[2] Based on this, the following expression for the risk function that is applicable for rectangular glass plates exposed to uniform lateral loads of constant duration is introduced:

$$B = \tilde{k}(ab)^{1-\tilde{m}}\left(Eh^2\right)^{\tilde{m}}\left(\frac{t_{\mathrm{d}}}{60}\right)^{\tilde{m}/16}\tilde{R}\left(\tilde{m},\tilde{q},\frac{a}{b}\right) \tag{11}$$

a and *b* are the rectangular dimensions of the plate ($a > b$), *h* the effective thickness, t_{d} the load duration in seconds, *E* Young's modulus of elasticity (which is taken to be 71.7 GPa). The nondimensional function

$$\tilde{R}\left(\tilde{m},\tilde{q},a/b\right) = \frac{1}{ab}\int_A\left[\tilde{c}(x,y)\tilde{\sigma}_{\max}(\tilde{q},x,y)\right]^{\tilde{m}}\,\mathrm{d}A \tag{12}$$

depends on the value of the surface flaw parameter $\tilde{m}$ and the distribution of nondimensionalized stresses across the surface of the glass. ($\tilde{q} = q(ab)^2/(Eh^4)$ is the nondimensionalized load and $\tilde{\sigma} = \sigma(q,x,y)ab/(Eh^2)$ the nondimensionalized stress.)

The surface flaw parameters $\tilde{m}$ and $\tilde{k}$ can not be measured directly. They are determined from constant load rate tests on rectangular glass plates us-

[2] The tildes are not used in the source. They are required here to avoid confusion with respect to other sections.

ing a rather complex iterative procedure. In order to establish the stress/time relationship at the flaw that caused failure, the failure origin has to be determined visually. From this relationship, the 60 s equivalent failure stress and the corresponding 60 s equivalent failure load is calculated. Then, a set of risk factors, $\tilde{R}\left(\tilde{m},\tilde{q},a/b\right)$, corresponding to each equivalent failure load is calculated for a wide range of assumed values $\tilde{m}$. The best value of $\tilde{m}$ is determined by choosing the one which results in a coefficient of variation of the risk factor closest to 1.0 (= mean value and standard derivation are equal). $\tilde{k}$ can then be calculated using the plate geometry and the mean value of the set of $\tilde{R}\left(\tilde{m},\tilde{q},a/b\right)$ for the best $\tilde{m}$. Both its magnitude and its units are dependent on $\tilde{m}$

C.7. American National Standard ASTM E 1300

The American National Standard [ASTM E 1300-04] provides extensive charts to determine the required thickness of glass plates. Like the Canadian Standard, it is based on the GFPM and uses a target failure probability of $P_{\mathrm{f}} = 0.008$ for the resistance. It applies to vertical and sloped glazing in buildings exposed to a uniform lateral load, made of monolithic, laminated, or insulating glass elements of rectangular shape with continuous lateral support along one, two, three or four edges and of which the specified design loads consist of wind load, snow load and self-weight with a total combined magnitude less than or equal to 10 kPa. It does *not* apply to other applications like balustrades, glass floor panels and structural glass members or to any form of wired, patterned, etched, sandblasted, drilled, notched or grooved glass with surface and edge treatments that alter the glass strength. The verification format is:

$$q \leqslant \mathrm{LR} = \mathrm{NFL} \cdot \mathrm{GTF} \qquad (13)$$

- q uniform lateral load due to actions
- LR ‘load resistance’
- NFL ‘non-factored load’, based on a 3 s load duration
- GTF glass type factor (load-duration dependent)

As an important difference to European design concepts, this verification format is based on loads and not on stresses and does not use any partial factors. The NFL is determined from charts given for various geometries, support conditions, glass thicknesses and monolithic as well as laminated glass. The GTF combines glass type and load duration effects and is given for single panes as well as for insulating glass units.

All charts and values given in [ASTM E 1300-04] are calculated using the GFPM surface flaw parameters $\tilde{m} = 7$, $\tilde{k} = 2.86 \cdot 10^{-53}\,\mathrm{N}^{-7}\mathrm{m}^{12}$, a Young’s modulus of E = 71.7GPa and the effective (not the nominal) glass thickness.

C.8. Canadian Standard CAN/CGSB 12.20

The Canadian National Standard [CAN/CGSB 12.20-M89] deals with soda lime silicate glass panes exposed to a uniform lateral load. As the American National Standard, it is based on the GFPM and uses a target failure probability of 0.8% for the resistance. It is important to notice that unlike the US code, the Canadian standard is based on a 60 s reference duration. This is due to the fact that the 3 s reference duration has only been introduced in the 2003 version of the US code, but the Canadian Standard is based on the 1994 version.

The verification format is based on *lateral pressure* (not stresses) and reads as follows:

$$E \leqslant R \qquad (14)$$

- E combination of all actions (design level = including partial factors)
- R resistance of the pane (design level = including partial factors)

The resistance of a glass plate is given by:

$$R = c_1 \cdot c_2 \cdot c_3 \cdot c_4 \cdot R_{\mathrm{ref}} \qquad (15)$$

The strength coefficients c_1 to c_4 cover the glass surface condition (normally 1.0, 0.5 for sand blasted or etched glass), heat treatment (1.0 for annealed glass; 2.0 for heat strengthened glass, 4.0 for fully tempered glass), load duration (simple table, depends on the glass type and load duration) and *load sharing in* insulating glass units. R_{ref} is the reference factored resistance of glass. The standard gives tabulated values.

Laminated glass may be considered as monolithic glass if the load duration is < 1 min and the temperature < 70°C or the load duration is < 1 week and the temperature < 20°C. For any other condition, laminated glass has to be considered as layered glass (no composite action).

For non-standard cases that are not covered by the tables and factors, more general indications are given. They provide more insight into the underlying assumptions and shall therefore be briefly discussed. The area effect is given by:

$$R_A = R_{\mathrm{ref}} \cdot A^{(-1/\tilde{m})} \tag{16}$$

A is the area of the pane in m^2, $\tilde{m}$ 'varies from about 5 to 7'. The load duration effect is considered by

$$R_t = R_{\mathrm{ref}} \cdot t^{(-1/\tilde{n})} \tag{17}$$

with t being the load duration (in minutes!) and $\tilde{n}$ = 15 for ANG, 30 HSG, and 70 for FTG. It is crucial to notice that $\tilde{n}$ is *not* equal to the exponential crack growth parameter n although the letter 'n' is used in [CAN/CGSB 12.20-M89]. The tilde has therefore been added here to avoid confusion. The standard actually assumes $\sigma \propto R^c$, σ being the 'stress in fracture origin areas', R the uniform lateral pressure and c *a* constant < 1. It is $\tilde{n} = cn$, which means that Eq. (17) is nothing else than a combination of Brown's integral with the proportionality between stress and (uniform lateral pressure)^c found for rectangular plates. This proportionality and the value of c being included in $\tilde{n}$, the tables and equations in the Canadian Standard should not be applied to other geometries, boundary- or loading conditions. For general cases, [CAN/CGSB 12.20-M89] recommends to limit stresses to 25 MPa away from the edges of plates and to 20 MPa on clean-cut edges. These values have to be corrected by the factor for the area effect and – although not explicitly mentioned – most probably also for the load duration.

III. Discussion

After giving an overview of current design concepts, it is now time to identify the main drawbacks, problems and gaps in current glass design concepts. These are the topics where further investigation should be focused on.

The preceding sections have shown that most design concepts are actually variations, extensions or simplifications of others. From a conceptual point of view, there are only two groups: *European concepts* that are based on the RWTH Aachen concept and *North American concepts* that are based on the GFPM. The two approaches are not directly comparable due to conceptual incompatibilities.

A. *Obtaining design parameters from experiments*

A.1. *Surface condition parameters*

For design, it is conservative to assume crack growth parameters that overestimate crack growth. For testing, things are different. The tests currently used to obtain strength related parameters are performed in ambient conditions. This means that the parameters meant to represent the surface condition or some 'material strength'($\tilde{k}$ and $\tilde{m}$ in North American concepts, θ_{test} and β_{test} in European concepts) are inevitably dependent on the surface condition *and* on the crack growth behaviour. This is problematic for at least two reasons:

- The parameters combine unrelated physical aspects – namely the effects of surface condition and subcritical crack growth – in a single value.
- The less crack growth occurs during the tests, the better the parameters will be. If crack growth is faster in in-service conditions than during the tests, design based on the experimentally determined parameters is unsafe.

B. *General design procedure*

The *European procedure* for glass design can be summarized as follows:

- 'Glass strength' data is determined from coaxial double ring tests with a constant stress rate of $\dot{\sigma}_{\mathrm{test}} = 2 \pm 0.4$ MPa/s on flat glass specimens with the surface area $A_{\text{test}} = 0.24\ \text{m}^2$ exposed to uniform equibiaxial tensile stress.

- Although it does not directly reflect the test data, the generally used parameter set is based on float glass samples with intentionally, homogenously scratched (sandblasted) surfaces.
- For design, the strength is based on a single value, the 'characteristic value of the inherent strength'. It is defined as the 5% fractile value (at 0.95 confidence level) of the failure stresses measured in the experiments described above.
  Note: In contrast to usual characteristic resistance values, this one is not a 'real' material parameter. It depends on the geometry and the surface condition of a glass element as well as on the environment and loading (stress history, stress distribution) that it is exposed to. The term 'characteristic value' is therefore somewhat misleading, which is why it is put in apostrophes.
- Crack growth is taken into account by duration of load factors that depend on the loading only. They are based on the empiric two-parameter crack growth relationship $v = S \cdot K_{\text{I}}^n$.
- Some (but not all) differences between the laboratory conditions mentioned above and actual in-service conditions are accounted for using correction factors. Details vary between concepts.
- The glass type is accounted for by adding the absolute value of the residual surface stress due to tempering (multiplied by a 'safety factor') to the allowable tensile stress of float glass.

The *North American procedure* for glass design can be summarized as follows:

- 'Glass strength' data is determined from lateral load tests on rectangular glass plates.
- The parameter set represents weathered windows glass.
- For design, the strength is based on two interdependent parameters called 'surface flaw parameters' $\tilde{m}$ and $\tilde{k}$. Their determination from experimental data is based on the stress history at the visually determined failure origin and a rather complex iterative procedure.
- Only one crack growth parameter is explicitly included in the concept. It is equivalent to the parameter n in European concepts and assumed to be 16.
- Graphs are provided for many common cases. The graphs give loads that a given glass pane can withstand for a certain reference period.
- The glass type is accounted for by multiplying the load resistance calculated for a float glass element by some load duration-dependent glass type factor.[3]

Due to these conceptual incompatibility:

- A direct comparison of European and GFPM-based concepts is a priori not possible;
- It is unclear how the crack growth and surface condition models of both concepts relate to each other;
- It is unclear why the concepts are so different;
- Data obtained in experiments for one concept can not be used for the other.

It would be very interesting to develop a general glass model to overcome these problems. This should as well make it possible to make structural glass design concepts 'converge' towards a single, universal model in the long run.

C. Duration of load effects

C.1. Resistance

Glass strength is time-dependent because of stress corrosion. This time-dependence is 'hidden' within coefficients in the above mentioned design concepts. The underlying assumptions on stress corrosion are not readily visible and shall therefore be shortly discussed. The 'classic' European crack growth parameters have been published in [Kerkhof et. al 1981] and use the ambient condition crack growth parameters from [Richter 1974]. He determined those parameters by optically measur-

[3]In [CAN/CGSB2.20-M89], the glass type factor (called 'heat treatment factor') does not depend on the load duration. But the load duration factor is glass type dependent, which comes to the same thing.

ing the growth of large through-thickness cracks on the edge of specimens loaded in uniform tension. Based on these values, 'design parameters' were chosen in [Blank 1993] and used for the RWTH Aachen design concept. (They actually give substantially higher crack velocities than Richter's measurements.) The European code draft prEN 13474 and the concept by Siebert are directly based on the RWTH Aachen approach and use the same parameters. Shen uses a different approach, see II. C.4.

C.2. Actions

All modern glass design concepts are implicitly or explicitly based on the assumption that crack growth and with it the probability of failure of a crack or an entire glass element can be modelled using the *risk integral*, also known as *Brown's integral*. This integral is obtained by integration of the ordinary differential crack growth equation. Its main implication is that – if the crack growth parameter n is constant – two stress histories $\sigma_{(1)}(\tau)\ \tau \in [0, t_1]$ and $\sigma_{(2)}(\tau)\ \tau \in [0, t_2]$ lead to the same crack growth if

$$\int_0^{t_1} \sigma_{(1)}^n(\tau)\,\mathrm{d}\tau = \int_0^{t_2} \sigma_{(2)}^n(\tau)\,\mathrm{d}\tau. \qquad (18)$$

The risk integral is indispensable for any equivalent stress approach. It does, however, cause two major problems:

- The failure probability at a given point in time is independent of the load applied at that time.
- The risk integral approaches zero when the time of loading approaches zero. The material resistance given by an equivalent stress based model therefore approaches infinity for very short times of loading. This is obviously senseless; it can never exceed the inert strength.

Besides the problems and inconsistencies specific to particular design concepts, these fundamental issues in combination with the fact that resistance parameters vary very much from one test series to another have led to confusion and a general lack of confidence in glass design concepts. The risk integral issues and the high variability of experimentally determined parameters are also the main reasons why some researchers claim that the GFPM (or, more generally, any Weibull distribution based design approach) is fundamentally flawed and unrealistic (e. g. [Reid 1991] [Calderone 2001]).

C.3. How and to what is the duration of load effect applied?

In all concepts, the duration of load effect is considered by a factor that depends on the load duration and sometimes the residual stress *only*. In European concepts, this factor is applied to the allowable maximum or equivalent in-plane principal stress. In GFPM-based concepts, it is applied to the allowable lateral pressure. The limits of applicability of this approach are not indicated or discussed in the concepts.

In view of all aspects that influence the duration of load effect, one would expect the duration of load factor to depend on

- the residual stress
- the action history and action combination,
- the subcritical crack growth model,
- the environmental conditions,
- and the element's geometry (!).

Another issue that can not be accounted for with duration of load factors occurs with tempered glass: As long as the surface is not decompressed, there is no duration of load effect at all. In function of the load, none, all or parts of the surface may be decompressed.

D. How to account for residual stress?

Several concepts 'include' residual stress due to heat treatment in the resistance of the glass. It is however crucial to distinguish residual stress clearly from inherent strength for several reasons, the most important being:

- Subcritical crack growth and all effects that it causes only occur on decompressed surfaces. Factors influencing inherent resistance (the most important being load duration) have no influence on the residual stress.
- The uncertainties and consequently the safety

factors are different for residual stress and inherent strength.

Design concepts that consider residual stress due to heat treatment explicitly use a superposition of residual stress and inherent strength of annealed glass. This approach assumes that the inherent strength is not affected by the heat treatment. There is evidence that the tempering process causes a certain amount of 'crack healing' [Hand 2000] [Bernard 2001]. This assumption can therefore be considered safe (conservative) for design.

From an engineering point of view and to be consistent with modern codes and design concepts for other materials, residual stress should be considered as a *beneficial action*. It is, however, a property of the *material* which means that the *manufacturer* has to guarantee that the specifications (e. g. a minimal residual stress) are met. From this perspective, the residual stress level is part of the product and testing codes, while actions would be part of the design codes.

E. Size effect

As a direct consequence of the use of Weibull statistics, all concepts incorporate a size effect for the resistance of glass elements. Only tensile stress can cause glass failure, even for elements loaded in compression. Parts of the surface that are not exposed to tensile stresses do therefore not contribute to the size effect. The size of the decompressed surface area of tempered glass elements depends – for given geometry and support conditions – on the load and is therefore time-variant. Accurate consideration of this aspect would be complex. European design concepts define the size factor based on the total surface area, which makes it load-independent. The US and Canadian codes multiply the load resistance of annealed glass elements with a factor. As the entire surface of an annealed glass plate is immediately decompressed when loaded, this comes to the same thing.

Sticking to this assumption of a load-independent decompressed surface area, the size effect is:

$$\frac{\sigma(A_1)}{\sigma(A_2)} = \left(\frac{A_2}{A_1}\right)^{1/s} \tag{19}$$

$\sigma(A_1)$ tensile strength of a structural member with surface area A_1 exposed to tensile stress

$\sigma(A_2)$ tensile strength of a structural member with surface area A_2 exposed to tensile stress

s European concepts: Shape parameter of the tensile breaking strength distribution β; GFPM based concepts: surface flaw parameter $\widetilde{m}$

In contrast to what is generally believed, the parameters $\widetilde{m}$ and β do not have the same meaning. It can be shown that $\beta = \widetilde{m}(n+1)/n$. The size effect is quite significant for the ASTM E 1300 value of $\widetilde{m} = 7$, while it becomes almost negligible (at least in comparison to other influences and uncertainties and for commonly used panel sizes) for the value $\beta = 25$ that is generally used in European concepts (see Fig. 1.).

Further investigations are required to answer the following questions:

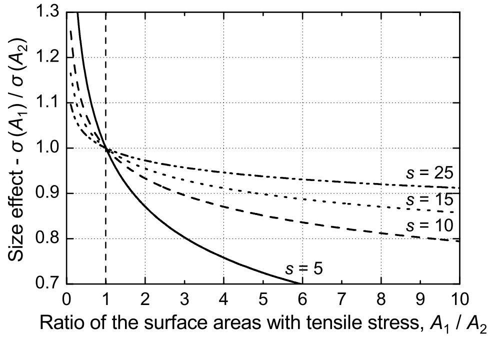

Figure 1: The size effect's dependence on the Weibull shape factor or first surface flaw parameter (using Eq. (19))

- Why do the exponents differ so much between design concepts?
- Is there a feasible way of accurately taking the size effect into account?
- Why do some experiments show little or no relationship between the panel area and the breakage stress? Is this a proof that Weibull

statistics are inadequate for glass modelling? What are the alternatives?

F. Biaxial stress fields

The US and Canadian standards are both based on the GFPM and use the biaxial stress correction factor proposed therein. It depends on the generally load intensity-dependent principal stress ratio and the surface flaw parameter $\widetilde{m}$. Though not explicitly stated, however, resistance graphs as well as the testing procedure use only the fully-developed principal stress ratio to calculate a single biaxial stress correction factor per location, which is then assumed to be valid for all load intensities.

In European glass design concepts, it is mostly assumed that all cracks are oriented perpendicularly to the first principal stress. This assumption is equivalent to assuming an equibiaxial stress field. While this assumption is conservative (safe) for design, it is not conservative when deriving glass strength data from tests. Although it was observed that the strength values measured using four point bending tests (uniaxial) were systematically higher than those measured using coaxial double ring tests (equibiaxial), no approach for the quantification of this effect was available. *Siebert* addressed this issue. He took the view that the biaxial stress correction approach of the GFPM is inappropriate and that a more directly experiment-based approach is required. He developed a special test setup which allows applying any principal stress ratio between 0 and 1 to glass specimens. Using this setup, he established a purely empiric biaxial stress correction factor that depends on the principal stress ratio only and is therefore independent from the surface condition. Further investigations are required to:

- Find out whether and how biaxial stress fields can be accurately considered using a general and entirely fracture mechanics based approach;
- Assess possible simplifications (including the one mentioned above, based on the assumption of a time-independent principal stress ratio) and their limits of validity.

G. Consistency

Current glass analysis and design concepts, especially in Europe, have been developed and improved by numerous researchers over many years. Not astonishingly, this has led to consistency problems. They disturb current users, make it even more difficult to understand the models and give rise to doubts about their suitability. A detailed discussion of all consistency issues would be lengthy and of limited interest in the present context. The unsatisfactory situation shall therefore be illustrated on a single example only.

The calculation of the resistance of a glass plate to lateral loads according to [prEN 13474-2:2000] shall be considered. In this draft code, the ‘characteristic value’ for the inherent strength of glass is given as $f_{g,d} = 45$ MPa. This value was originally defined in [DIN 1249-10:1990], based on coaxial double ring tests[4] on new annealed glass specimens. The surface area A_{test} under uniform tensile stress was 0.24 m^2. A two-parameter Weibull distribution was fitted to the measured failure stresses. The Weibull parameters obtained were $\theta_{A_{test}} = 74$ MPa and $\beta = 6$ (at 0.95 confidence level). The characteristic value is defined as the 5% fractile value of this distribution, which gives the 45 MPa mentioned above. To account for the size effect, $f_{g,d}$ is divided by a size factor k_A given as

$$k_A = A^{0.04} \tag{20}$$

with A being the total surface area of the glass plate. As discussed above, the actual size factor based on Weibull statistics is:

$$k_{A,\mathrm{Wb}} = \left(A / A_{\mathrm{test}}\right)^{1/\beta} \tag{21}$$

A and A_{test} are the decompressed surface areas of the element to be designed and the specimen used to determine the breaking strength. This means:

- A resistance found from a distribution with $\beta = 6$ is combined with a correction factor

[4] The tests were performed according to the German code DIN 52292-2:1986, which has since been replaced by the (essentially equivalent) European code EN 1288-2:2000.

based on $\beta = 25$ (exponent 0.04 = 1/25).

- k_A becomes 1 for $A = 1\ \mathrm{m}^2$, thus assuming that the surface area in the tests leading to $f_{\mathrm{g,d}}$ was 4 times bigger than it actually was. The quantitative effect of this is 6% for $\beta = 25$ and 27% for $\beta = 6$.

H. Are Weibull statistics applicable?

The fit of many experimental data sets to the Weibull distribution is rather bad. Several proposals have been made to address this problem:

- Using a normal or log-normal distribution to represent failure stresses found in experiments and to define some 'characteristic strength value' (i. e. [Fink 2000] [Laufs 2000]). This implies that the weakest-link model (Weibull statistics) is unsuited. The size effect is applied in unaltered form. As it is, however, a direct consequence of the weakest-link model, this is inherently inconsistent and thus problematic.
- Completely abandon statistics and failure probability based design approaches and use the classic theory for the strength of materials, based on zero variability of the strength (i. e. [Calderone 2001] [Jacob & Calderone 2001]).

Both approaches are unsatisfying and can not be readily applied with confidence. The issue clearly needs in-depth investigation.

I. Considering structural redundancy

In general, verification of the reliability against failure is done on an element level. This means that a structure is assumed to fail when one individual load-carrying element fails and in consequence, each individual element has to meet the structural safety requirements. Due to the brittle nature of glass and the high importance of hazard scenarios such as impact or vandalism, this can be problematic for glass structures. The required safety level for the isolated elements is often only achieved at excessive costs. A safety concept that takes structural redundancy explicitly into account and offers quantitative information on such redundancy's influence on required safety levels of components would be of economic and aesthetic interest.

J. Flexibility

A design concept should cover more cases than uniformly distributed out-of plain load. In particular concentrated loads, line loads, stability problems and in-plane loads are frequently encountered in structural glass applications. An engineer using a design concept should be able to easily analyse any load combination and to evaluate non-standard transient or accidental load cases.

K. Proof loading, quality assurance and non-structural measures

Similar to wood, structural efficiency of glass elements suffers from the large uncertainties associated with the material resistance. The large coefficient of variation requires high safety margins for design values. It would therefore be of interest for a design concept to take advantage of measures taken to reduce or accurately quantify the coefficient of variation of resistance parameters. Such measures could be:

- Proof loading of elements or parts of the structure after fabrication or even after erection;
- Quality assurance like direct or indirect (fracture pattern) measurement of the residual stress or visual detection of surface damages;
- Non-structural measures that prevent or limit potential glass surface damage.

L. Design point and target reliability

To define design values for glass resistance, European design concepts generally use

$$P_{\mathrm{f}} = P(R \le R_{\mathrm{d}}) = \Phi(-0.8 \cdot \beta) \qquad (22)$$

from [EN 1990:2002] where R is the resistance, R_{d} the design resistance, β the reliability index and Φ the cumulative distribution function of the standard normal distribution. This means that (a) a predefined influence factor (here –0.8) that may or may not be appropriate for glass is used and (b) resistance is separated from actions, assuming their independence. The reason for the popularity of this simplification is its convenience: it allows the definition of the design resistance independently from the actions. Taking e. g. a target reliability index of $\beta = 3.8$ (according to [EN 1990:2002] for standard buildings and a 50 years service life), Eq. (22) gives 0.0012. Assuming that the glass strength follows the cumulative distribution function $P_f(\sigma)$ known from experiments, the design resistance is simply the 0.12% fractile value of this distribution function.

IV. Conclusions

An overview of today's most commonly used glass design concepts has been given. The main difficulties for the design of structural glass elements have been identified and discussed. Further research work aiming at improving structural glass design should focus on the following aspects:

- Provide an understandable, consistent and flexible model that can be applied not only to special cases but to general conditions;
- The model's parameters should represent only one physical aspect each and be independent of test conditions. Corresponding testing methods providing relevant and accurate model input are required.
- Fundamental questions like the suitability of Weibull statistics and the use of the risk integral need to be required.
- A straightforward way of integrating additional knowledge into the design process should be provided. In particular, models should allow for less conservative design if more data from quality control measures, proof loading or new research is available.

V. Acknowledgements

The author would like to thank Mr. Christoph Haas of Ernst Basler + Partner AG, Zurich, for having been an excellent co-author for the state-of-the-art report [Haas & Haldimann 2004] which is a valuable basis for section II. C. Thanks are also due to Prof. Dr Manfred A. Hirt and Mr. Michel Crisinel of EPFL-ICOM for their ongoing support.

The research on structural glass at EPFL-ICOM is financially supported by the Swiss State Secretariat for Education and Research (SER) and by the Swiss National Science Foundation (SNF). Both contributions are highly appreciated.

References

[ASTM E 1300-04]
Standard Practice for Determining Load Resistance of Glass in Buildings. American Society for Testing Materials, 2004.

[Beason 1980]
BEASON, W. L. *A failure prediction model for window glass*. NTIS Accession no. PB81-148421, Institute for Disaster Research, Texas Tech University, 1980.

[Beason & Morgan 1984]
BEASON, W. L., MORGAN, J. R. *Glass Failure Prediction Model*. Journal of Structural Engineering, Vol. 110, No. 2, pp. 197-212, 1984.

[Bernard 2001]
BERNARD, F. *Sur le dimensionnement des structures en verre trempé: étude des zones de connexion*. LMT Cachan, France, 2001.

[Blank 1993]
BLANK, K. *Dickenbemessung von vierseitig gelagerten rechteckigen Glasscheiben unter gleichförmiger Flächenlast*. Institut für Konstruktiven Glasbau, Gelsenkirchen, 1993.

[Calderone 2001]
CALDERONE, I. J. *The Fallacy of the Weibull Distribution for Window Glass Design*. In Proceedings of Glass Processing Days 2001, 18-21 June, Tampere, Finland, pp. 293-297, 2001.

[CAN/CGSB 12.20-M89]
Structural Design of Glass for Buildings. Canadian General Standards Board, December 1989.

[DIN 1249-10:1990]
Flachglas im Bauwesen - Teil 10: Chemische und physikalische Eigenschaften. DIN, 1990.

[EN 1288-2:2000]
Glass in building - Determination of the bending strength of glass - Part 2: Coaxial double ring test on flat specimens with large test surface areas. CEN, 2000.

[EN 1990:2002]
Grundlagen der Tragwerksplanung. CEN, 2002.

[Fink 2000]
FINK, A. *Ein Beitrag zum Einsatz von Floatglas als dauerhaft tragender Konstruktionswerkstoff im Bauwesen*. Ph.D. thesis, Technische Hochschule Darmstadt, 2000.

[Güsgen 1998]
GÜSGEN, J. *Bemessung tragender Bauteile aus Glas*. Ph.D. thesis, RWTH Aachen / Shaker Verlag, 1998.

[Haas & Haldimann 2004]
HAAS, CH., HALDIMANN, M. *Entwurf und Bemessung von Tragelementen aus Glas – Wissensstandsbericht*. Rapport ICOM 493, Ecole polytechnique fédérale de Lausanne (EPFL), 2004. URL http://icom.epfl.ch/publications/pubinfo.php?pubid=493.

[Hand 2000]
HAND, R. J. *Stress intensity factors for surface flaws in toughened glasses*. Fatigue and Fracture of Engineering Materials and Structures, Vol. 23, No. 1, pp. 73-80, 2000.

[Jacob & Calderone 2001]
JACOB, L., CALDERONE, I. J. *A New Design Model Based on Actual Behaviour of Glass Panels Subjected to Wind*. In Proceedings of Glass Processing Days 2001, 18-21 June, Tampere, Finland, pp. 311-314, 2001.

[Kerkhof et al. 1981]
KERKHOF, F., RICHTER, H., STAHN, D. *Festigkeit von Glas - Zur Abhängigkeit von Belastungsdauer und -verlauf*. Glastechnische Berichte, Vol. 54, No. 8, pp. 265-277, 1981.

[Laufs 2000]
LAUFS, W. *Ein Bemessungskonzept zur Festigkeit thermisch vorgespannter Gläser*. Ph.D. thesis, RWTH Aachen / Shaker Verlag, 2000.

[prEN 13474-2:2000]
Glass in building - Design of glass panes - Part 2: Design for uniformly distributed load. CEN, 2000.

[Reid 1991]
REID, S. G. *Flaws in the failure prediction model of glass strength*. In Proceedings of the 6th Intemational Conference on Applications of Statistics and Probability in Civil Engineering, Mexico City, pp. 111-117, 1991.

[Richter 1974]
RICHTER, H. *Experimentelle Untersuchungen zur Rissausbreitung in Spiegelglas im Geschwindigkeitsbereich 10E-3 bis 5 10E3 mm/s*. Ph.D. thesis, Institut für Festkörpermechanik Freiburg, 1974.

[Sedlacek et al. 1999]
SEDLACEK, G., BLANK, K., LAUFS, W., GÜSGEN, J. *Glas im Konstruktiven Ingenieurbau*. Ernst & Sohn, Berlin, 1999.

[Shen 1997]
SHEN, X. *Entwicklung eines Bemessungs- und Sicherheitskonzeptes für den Glasbau*. Ph.D. thesis, Technische Hochschule Darmstadt, 1997.

[Siebert 1999]
SIEBERT, G. *Beitrag zum Einsatz von Glas als tragendes Bauteil im konstruktiven Ingenieurbau*. Ph.D. thesis, Technische Universität München (TUM), 1999.

[TRAV 2003]
Technische Regeln für die Verwendung von absturzsichernden Verglasungen (TRAV). Deutsches Institut für Bautechnik, January 2003.

[TRLV 1998]
Technische Regeln für die Verwendung von linienförmig gelagerten Verglasungen (TRLV). Mitteilungen des Deutschen Instituts für Bautechnik (DIBt), Berlin, 1998.

[Weibull 1951]
WEIBULL, W. *A Statistical Distribution Function of Wide Applicability*. Journal of Applied Mechanics, Vol. 18, pp. 293-297, Plenum Press, September 1951.

[Wörner et al. 2001]
WÖRNER, J.-D., SCHNEIDER, J., FINK, A. *Glasbau: Grundlagen, Berechnung, Konstruktion*. Springer Verlag, 2001.

EU COST C13 Glass and Interactive Building Envelopes. M. Crisinel, et al. (Eds.). IOS Press, 2007.

Structural Behaviour of Broken Laminated Safety Glass

Alexander Kott, IBK, ETH Zurich, Switzerland
Prof. Thomas Vogel, IBK, ETH Zurich, Switzerland

This research paper reports the experimental and theoretical results of the project "Remaining Structural Capacity of Laminated Safety Glass" at ETH Zurich. The aim of the project is to develop new mechanical models and to control the post breakage behaviour of laminated safety glass (LSG). At first the different stages of failure of LSG and the corresponding definitions are given to explain the different capacities of the structure. In broken LSG the poly-vinyl-butyral (PVB) foil works as tension reinforcement and the upper broken glass layer carries the compression forces. Therefore the mechanical properties of the foil were determined using tensile tests. Bending tests combined with impact tests demonstrate that the different glass types, bearings, the type of initial failure and dimensions of the specimen determine the post breakage behaviour. As observed in these tests the fracture behaviour affects the remaining structural capacity (RSC). Different types of yield lines can evolve from initial cracks. The yield line patterns influence the ultimate load decisively.

Keywords: Failure modes, sandwich structure, viscoelastic stress-strain behaviour, yield line mechanism.

I. INTRODUCTION

With the revolution of the manufacturing process laminated safety glass (LSG) is available consisting of panes of float glass (FG), toughened glass (TG) or heat strengthened glass (HG). The multilayer glass can be used as a structural material, combining even these different glass types. The laminates have to be composed in such a way that after the first crack the interlayer, a Poly-Vinyl-Butyral (PVB) foil holds the pieces together and the whole structure resists. In this way the remaining structural capacity (RSC) can be provided beside the load carrying capacity (LCC). Until now structural engineers conduct costly destructive glass experiments to assess the structural safety.

To avoid these costs a mechanical model has to be developed. Definitions of RSC according to the stage of failure allow to distinguish the different capacities. The stages consider not only the ultimate loads but also the corresponding external works. In the broken LSG the PVB foil works as tension reinforcement and the upper broken glass layers carry the compression forces. The visco elasto plastic stress-strain behaviour of the PVB foil was determined using tensile tests under stationary temperature conditions in a climate chamber. The ultimate failure, which leads to the collapse of the structure, occurs when the compression zone in the yield line fails reaching the compression strength of glass. Temperature, strain level and strain rates are significant parameters that affect the tensile stresses in the thermoplastic polymer. The different yield line mechanisms depend on the actions and the structural supports of the glass specimens. These results were confirmed by experimental tests.

II. THREE STAGES OF LSG

Figure 1 shows a typical LSG consisting of two glass layers and a PVB foil. The glass layers are partially damaged but the PVB foil is intact. Three different stages can be identified due to the type and location of the fracture. The pane is divided into sections classified by these different stages as shown in Figure 1.

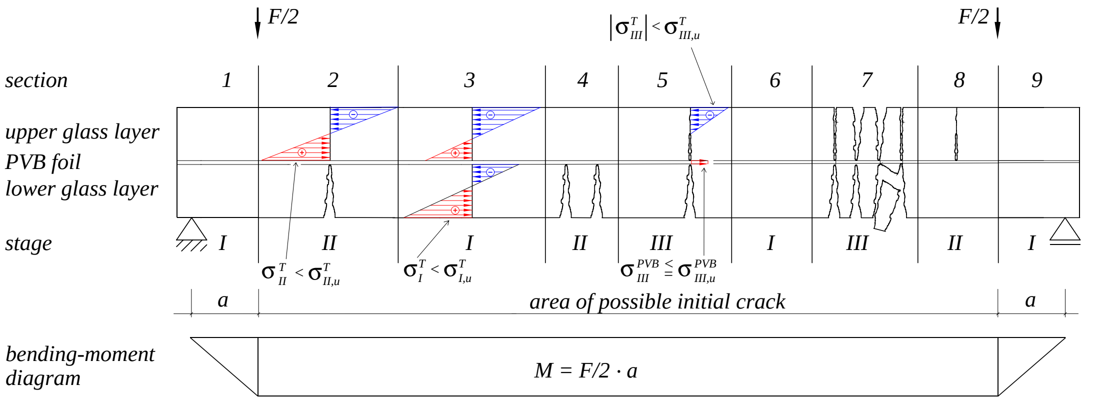

Figure 1: Longitudinal section of a LSG pane divided in sections according to the stages reached.

A. Stage I

In section 3 as long as the pane is unbroken for each uncracked glass layer the hypotheses of Bernoulli can be adopted. Tensional and compression stresses exist only in the glass layers. The modulus of elasticity of the PVB foil can be neglected and the interlayer, as an adhesive joint transfers only the shear stresses. This structural behaviour can be interpreted with the sandwich theory of thick sheets [Stamm 1974]. Finite element methods with volume elements or multi layer elements consider the membrane effects due to large deflections [Bohmann 1999].

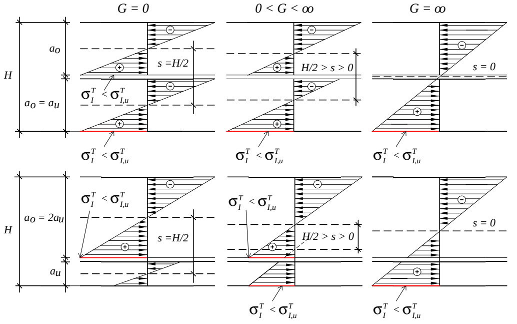

Figure 2: Stress distribution in cross section of equal and unequal glass layers keeping the overall thickness constant.

The problem for these calculations is the unknown shear stiffness, respectively the shear modulus G of the PVB foil.

Time dependency of the loads as well as the influence of temperature can modify the shear modulus [Sobek 2000]. A parametric study of stress distribution depending on the shear modulus in a glass pane explains the location of the first failure.

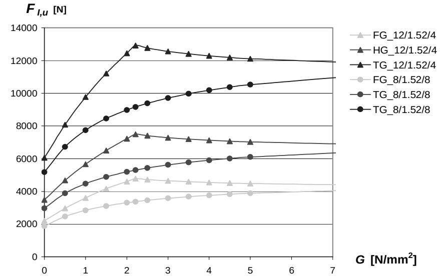

Figure 3: Ultimate loads depending on the shear modulus for two side supported LSG.

The failure appears immediately when the ultimate strength $\sigma^T_{I,u}$ of the glass is reached. As shown in Figure 3 the ultimate loads $F^T_{I,u}$ were calculated with different shear moduli for two side supported glass pane charged by two loads. The static system can be seen in Figure 1. The overall thickness of the LSG is fixed; the partial thicknesses of the glass layers are varied. As shown in Figure 2 the bond can be expressed with the distance $s(G)$ between the neutral axes.

Two extremes can be considered: For the unbonded cross sections the shear modulus of the PVB foil is zero and the distance can be assumed $s(G = 0) = H/2$, independent of the glass layer thicknesses. Unbonded cross sections with equal glass layers have the same stress distributions in both glass layer, therefore the theoretical failure can occur in the lower surface of the upper and lower glass layer respectively. Because, the lower side of the upper layer is protected by the PVB foil the lower glass layer will always break first. For unbonded cross sections with unequal glass layers the thicker layer, which is stiffer, breaks first on the lower side. The other extreme is full bonded cross sections; the distances of the neutral axes in full bonded cross sections reach the minimum of $s(G = \infty) = 0$. In this case the thicknesses of the layers influence not the location of the initial failure. Indeed, always the lower layer will break first. Other cases lie between these two extremes. The graphs in Figure 3 for unequal cross sections are characterised by two shapes. With small shear moduli G the thicker layer breaks first, otherwise with higher shear moduli the lower glass layer fails. The choice of unequal glass layers depending on the shear modulus rises the ultimate load $F^T_{I,u}$ from 15% to 40%.

For specimens hit by an impact, two aspects have to be taken into account. The pane acts as fully bonded and therefore the lower layer breaks first. Even so the upper layer can be destroyed first if the object, which hits directly the upper layer, is stiff enough or if its shape is irregular. Peaks and edges cause singularity.

B. *Stage II*

To explain this stage II also the pane, divided in sections as shown in Figure 1, has to be considered. In stage II the whole load has to be carried by the unbroken layer. The PVB-interlayer serves for two purposes: Firstly the high adhesion of PVB to glass ensures the glass fragments to adhere firmly and secondly the static function of the interlayer remains carrying the bond stresses. As long as the distance between two cracks is sufficiently large, bond stresses can be activated and the sandwich theory can be adopted at least partially, as shown in section 3 of the LSG pane. If one glass layer of a LSG pane is broken, it is important to know the number and size of such stage I sections to predict the ultimate load $F^T_{II,u}$. The tests demonstrate, however, that in LSG panes with TG sheets the distance of adjacent cracks in stage II does not allow intermediate stage I sections. In section 4 it is obvious that the distance between the cracks is too small and the stresses cannot disperse into both glass layers.

C. *Stage III*

The next crack appears in the uppermost sheet in a cross section with already broken lower layers. Therefore a LSG pane switches to stage III and the structure resists although all glass sheets are broken. The PVB foil takes over now a decisive part of the structural function and works as a tension reinforcement. The broken pieces of glass of the upper layer, which continue to be effective in resisting the internal forces, are subjected mainly to compression as shown in Figure 1. Although section 7 is in stage III the cracks are too close to each other and the upper small glass pieces do not firmly adhere to the foil. Therefore the tensile force of the foil cannot be transmitted by bond stresses to the glass. As a consequence, the glass pane acts like a cloth without bending stiffness. For the pane it forms a hinge and if this is simply supported, it falls down. This typical phenomenon can be seen in all simply supported LSG panes of TG sheets, as shown in Figure 4.

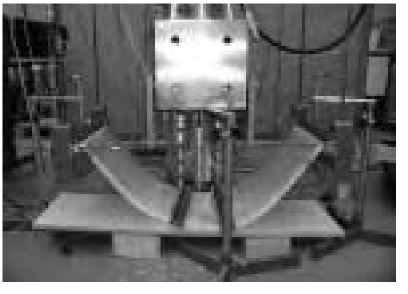

Figure 4: TG pane consisting of two broken glass layers, slipped from the bearings.

The bending stresses of section 5 are distributed into glass layers of section 6, which remains in stage I. Therefore a yield line can be developed in section 5. The calculation of the forces and stresses in the foil as well as in the broken upper layer of this section, satisfying the equilibrium and the material laws, shows that the yield moment increases the distance between the inner forces (called the lever arm of inner forces) [Kott 2004]. This can also be achieved with unequal glass layers. Other possibility to increase the moment is to extend the thickness of the interlayer, as shown in Figure 5. A system of yield lines forming a collapse mechanism is known as a yield line pattern. It is to be noted that a yield line is, in fact, an idealization for a band of intensive cracking. Across to these lines the PVB foil yields. The yield-line method of the theory of plasticity gives an upper bound approach of the ultimate load.

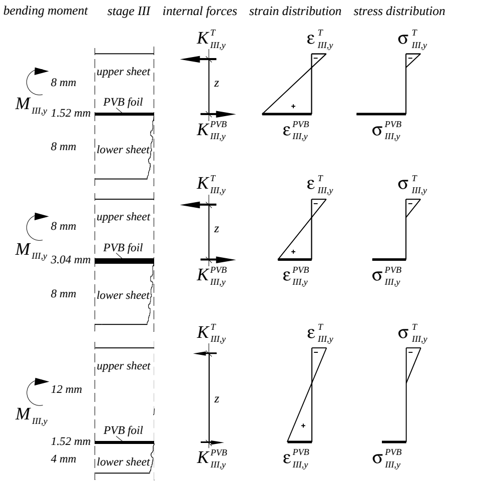

Figure 5: Yield line mechanism in different cross sections; the internal forces as well as vertical distribution of stresses and strains.

The developed mechanism depends on the initial fracture pattern evolved from stage II or I. For the purpose of analysis, the band of intensive cracking is concentrated to a single yield line and all plastic rotation is considered to occur along that line. For estimating a required RSC, energy approach is used, assuming that the total external work W is equated to the total internal work U, as shown in Equation 1.

$$W = U \tag{1}$$

III. REMAINING STRUCTURAL CAPACITY

The remaining structural capacity can be expressed as a ratio of stage II and stage III properties to the according stage I value, either considering load or physical work. According to Equation 2, $RSCR^T{}_{II,F}$ is based on the failure load of the intact sheet and only ultimate loads of the three stages are taken into account. $RSCR^T{}_{II,W}$ in Equation 3, however, is a ratio of the total works. Not only the ultimate forces but also the corresponding deformations are considered.

$$RSCR^T_{II,F} = \frac{F^T_{II,u} + F^T_{III,u}}{F^T_{I,u}} \tag{2}$$

$$RSCR^T_{II,W} = \frac{W^T_{II,u} + W^T_{III,u}}{W^T_{I,u}} \tag{3}$$

According to Equation 4 and 5 the RSC in stage III can also be formulated with similar attributes in the ratios of $RSCR^T{}_{III,F}$ and $RSCR^T{}_{III,W}$ respectively.

$$RSCR^T_{III,W} = \frac{W^T_{III,u}}{W^T_{I,u}} \tag{4}$$

$$RSCR^T_{III,F} = \frac{F^T_{III,u}}{F^T_{I,u}} \tag{5}$$

IV. ACTIONS AND THE RESULTING FRACTURES

The pattern of fracture influences the RSC in stage II and III. In this study four different causes of breakage are explained. Depending upon the type of action LSG can break in completely different ways. The first cause of breakage can be assumed as an impact, which hits the upper side of the upper glass layer. Depending on the dropping height one or more glass layers can break. When the impact is stiff enough or if its shape is irregular the surface of the hit glass layer breaks first, as mentioned in chapter II(a). In the other case the lower glass layer breaks at first. Glass panes hit by an impact act as full bonded sandwiches. In full bonded sandwiches always the lower layer breaks first, as shown in Figure 6.

The second cause of breakage that generates a fracture is the exceeding of the ultimate stress of one glass layer by permanent loads, self weight or snow. As shown in Figure 2, depending on the bond and cross section of the pane the lower or upper layer breaks first.

The third cause, the inclusion of nickel sulphide is widely prevented by the heat soak test. Although a spontaneous failure of one glass layer has to be considered. The initial crack evolved not from the location of the maximum stresses caused by the actions but from the location of the inclusion.

The last cause of breakage, which can be found in particular conditions, is a prefabricated and artificial crack introduced by a glass cutter or another mechanical instrument.

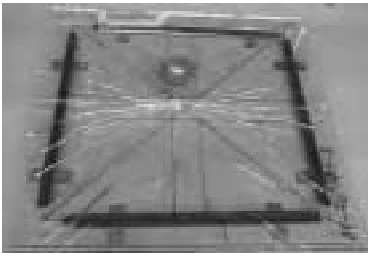

Figure 6: Four side simply supported glass slab damaged by a steel sphere.

V. STRESS-STRAIN BEHAVIOR OF PVB FOILS

As shown in Figure 1, a RSCR in stage III can be achieved, if tension is transmitted by the foil. PVB is a thermoplastic, semi crystalline polymer with a visco elastic-plastic stress strain behaviour. Therefore the stress in PVB depends on three variables as shown in Equation 6:

$$\sigma_{PVB} = \mathrm{f}\left(\varepsilon, \dot{\varepsilon}, T\right) \tag{6}$$

A. Tensile tests

In order to be able to simulate this behaviour and to apply the constitutive laws for the mechanical model, tensile tests were executed under stationary temperature conditions in a climate chamber as shown in Figure 7(a). The details of the experimental set-up are reported in [Kott 2003]. At first, displacement-controlled tests with different temperatures were carried out to determine the material properties taking into account that the glass transition temperature of PVB ranges from 10°C to 15°C. As a consequence, there are in general two types of curves to describe the stress-strain behaviour as shown in Figures 8 and 9. If the experimental temperature is below the glass transition temperature of the thermoplastic, the behaviour is linear elastic until the material reaches the yield point. Due to the plastic deformation, micro cracks can be seen as a white discoloration as shown in Figure 7(b). Finally, before the foil tears apart, the material hardens. If the experimental temperature is above the glass transition temperature, the foil shows no linear elastic behaviour. Instead, the higher the temperature, the larger are the plastic deformations. The influence of the strain rate was investigated at constant temperature. In that tests, the ultimate strength of the foil decreases with lower strain rates. In fact, with higher strain rates the ultimate strain diminishes, too.

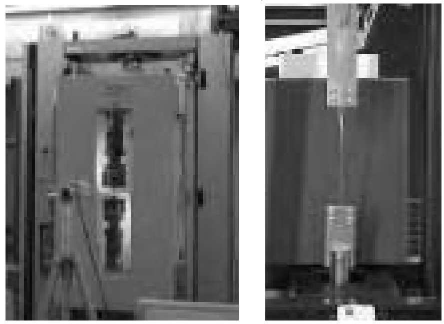

Figure 7: (a) Tensile test of a PVB specimen, (b) PVB specimen with white discoloration in creep test

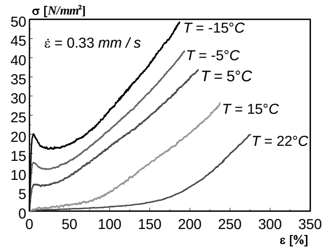

Figure 8: Stress-strain curves, experienced under constant strain rate and different temperatures.

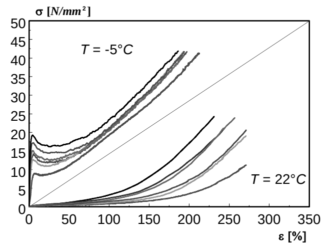

Figure 9: Stress-strain curves, experienced above and below the glass transition temperature depending on the load rate.

B. Tri-linear approach

To determine a computable mechanical behaviour a tri-linear curve is proposed. As shown in Figure 10, the tensile stresses can be calculated with one function and the strain is the only unknown variable. Based on the results of the tensile tests the three gradients and the characteristic stresses can be taken from the created database. The necessary equations are defined in [5].

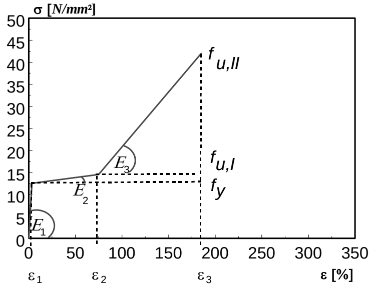

Figure 10: Proposed tri-linear approximation.

C. Creep of the PVB foil

For the verification of the RSC different requirements for the remaining lifetime can be formulated. The lifetime of a VSG pane in stage III is affected decisively by the creep of the foil. In Figure 11(b) the deformation depending on time under constant load and ambient temperature is shown. The constitutive equations most commonly used to describe the creep effects in polymers are based on the Newtonian model (Voigt model) as shown in Equation 7.

$$\varepsilon(t) = \frac{\sigma_0}{E}\left(1 - e^{-\frac{t}{\lambda}}\right) \qquad \lambda = E/\eta \tag{7}$$

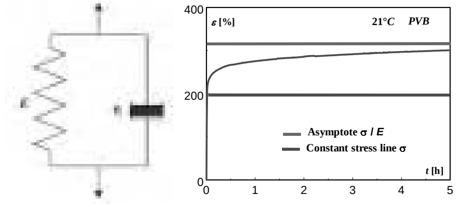

Figure 11: (a) Voigt model for mechanical behaviour of linear visco elasticity [Osswald 1996], (b) creep curve of a PVB specimen under constant tension and constant ambient temperature.

The creep response, i.e. the strain depending on time under constant stress can be modelled by dashpots and springs as shown in Figure 11(a). A more precise model consists of an arbitrary number of Maxwell models connected in parallel called Maxwell-Wiechert model. In this case the Kelvin Model is sufficient under constant loads without strain recovery, because the stress does not relax.

VI. BENDING TESTS

A. Four point bending tests

Four point bending tests were executed with LSG panes of HG, TG and FG as shown in Figure 12(a). The details of the experimental setup are reported in [5]. The first part of the specimens was tested conventionally beginning with stage I. In the other part, to investigate the effects of the actions and of resulting crack patterns, the specimens were damaged by a steel sphere, dropped from a height of two meters. The upper layer broke and the initial crack patterns exhibited the typical form of an impact. To examine stages II and III, damaged specimens were installed in the experimental set-up of the four point bending test.

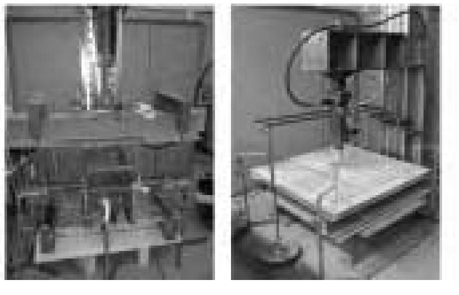

Figure 12: (a) Experimental setup for four point bending test (b) and for point loaded simply supported. square slab.

Varied thicknesses of glass layers and PVB foils were investigated keeping the overall thickness of the cross section constant. The intact LSG panes of equal glass layers (each glass layer 8 mm thick and a PVB foil of 1.52 mm) were loaded in stage I. The velocity of the displacement-controlled test was v = 0.2 mm/s. The load-deflection curve is linear elastic. Therefore the creep effect of the foil can be neglected. The same procedure was repeated with glass panes of unequal glass layers (upper layer of 12 mm, lower layer of 4 mm and a PVB foil of 1.52 mm). As shown in Figure 13, LCC increases with unequal glass layers. The ultimate load $F^{T}_{I,u}$ of the pane with unequal glass layers is 23% higher than the load of panes with equal layers. In sections of equal layers the first failure occurred in the lower sheet. In cross sections of unequal layers, however, the initial crack appears in the thicker upper glass layer.

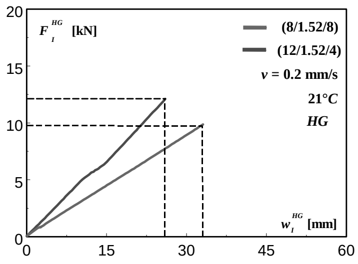

Figure 13: Load-deflection diagram in stage I for specimen with equal and unequal glass sheets.

To avoid the break in the next sheet the system was in the moment of the first break unloaded and a plastic deflection of the pane was observed in stage II. The remaining deformations $w^T_{II,r}$ at the beginning of stage II were evaluated for all glass types. The average elongation of the panes was 19.5 mm in TG, respectively 13.7 mm in HG and 5.5 mm in FG, the respective strains were 1.8% in TG, 1.2% HG and 0.5% in FG. The reason for the elongation could be attributed to differences in form and number of the small fragments of TG or HG as shown in Figure 15(a). Fragments of FG panes were of longitudinal shape as shown in Figure 15(b). Then the specimens were reloaded till the ultimate load $F^T_{II,u}$ was reached. Specimens hit by an impact were also loaded till the ultimate load $F^T_{II,u}$ was reached. The diagram in Figure 14 shows the load-deflection behaviour in stage II for various specimens with glass sheets of 8 mm and a PVB-foil of 1.52 mm thickness. A graph with linear elastic shape for a theoretical monolithic one-glass-pane of 8 mm is also shown in the diagram. $F^{TG}_{II,u}$ is 167% higher than $F^{FG}_{II,u}$ and 71% higher than $F^{HG}_{II,u}$. All failure points lie on a straight line. The curve for the LSG pane of TG sheets is also linear elastic and the ultimate load $F^{TG}_{II,u}$ is more or less the same than the theoretical one. This can be explained by the fracture patterns of the TG sheet. As shown in Figure 15(a) the pane consisting of TG sheets in stage II exhibits a narrow pattern of cracks not leaving relevant stage I sections. Only the upper layer is intact and the whole bending moment has to be carried by the lower glass sheet.

Panes of HG or FG, damaged by an impact, distinguished from those, which were damaged by increasing loads. The panes previously damaged by an impact, however, had more crack patterns with stage I regions.

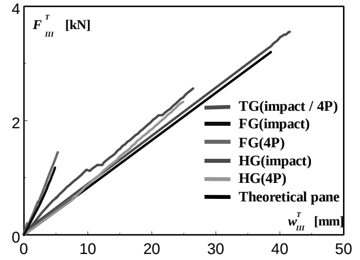

Figure 14: Load-deflection diagram for two specimens in stage II tested in four point bending test.

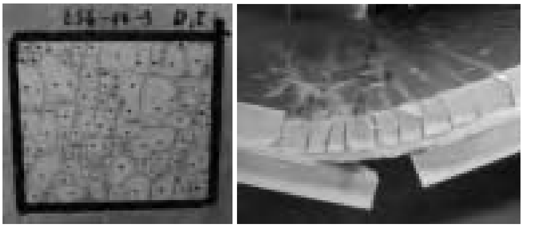

Figure 15: (a) cracks of TG on the lower layer, (b) longitudinal cracks of FG.

At the beginning the graphs show a linear elastic load deflection behaviour. Even so, a phase of crack initiation began accompanied by loud sounds of cracking. When this phase is completed the strain and the load rises up linearly until $F^T_{II,u}$ is reached. The same behaviour was observed with panes of FG sheets, which were also previously damaged by an impact. This phenomenon can be explained as tension-stiffening of glass. A similar behaviour of tension-stiffening can be found in concrete structures. Panes of HG or FG sheets subjected to increasing loads do not show this phase of crack initiation and therefore the load deflection curve is linear. TG and HG panes collapsed immediately reaching stage III. The whole pane was in section 7, as shown in Figure 1 and mentioned in chapter II(C). Also FG panes of equal glass layers exhibited localized section 7 and the panes collapsed immediately. FG panes of unequal glass layers or with thicker foil resists after the second failure. After the force $F^T_{II,u}$ was reached and the last intact glass layer was broken a yield line mechanism depending on the initial crack patterns began to develop. Figures 18(a,b,c) show three different yield line mechanisms in two side supported LSG. The ultimate load $F^{T}_{III,u}$ of panes with yield lines completely perpendicular to the principle stresses is the highest as shown in Figure 16. The panes damaged by the sphere have not the possibility to transfer the compression forces in the centre of the pane, where the sphere hit the pane.

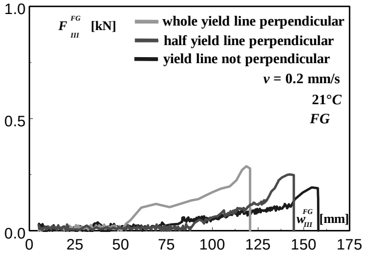

Figure 16: Load-deflection diagram for simply two side supported LSG panes with three different yield line mechanisms in stage III.

The surface of the hit layer is completely destroyed and a compression zone cannot be found. It is to be noted that to develop a perfect perpendicular yield line a notch was introduced by a glass cutter. The artificial crack appears also perpendicular to the principle stresses after hitting the pane with a rubber hammer. Also here the panes were installed into the set-up. Considering the cross-section, tests showed that the ultimate load $F^{T}_{III,u}$ increases by enforcing a larger lever arm of the internal forces by unequal glass thicknesses and by the extension of the thickness of the foil. Finally, all four point bending tests showed that yield line mechanisms were necessary to reach stage III.

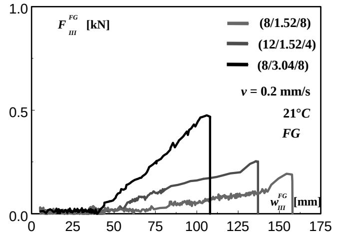

Figure 17: Load-deflection diagrams for LSG panes with similar yield line but different cross-sections.

B. *Tests with simply supported slabs*

The bearings have a decisive part in a structural system to carry the loads. Therefore in yield line theory the bearings influence the yield line patterns. In addition to the four point bending tests other bending tests with square slabs simply supported were conducted. Both spans were 0.90 m long and the cross sections of the FG slabs consist of two 8 mm glass layers and a 1.52 mm PVB foil.

The span/thickness ratio can be calculated as 513. The specimens were loaded in the centre of the slab by a concentrated load F^{FG}_{I} until the lower layer broke. The graph in the corresponding load-deflection diagram in Figure 19 is not linear. Then the specimens were un- and reloaded until the ul-

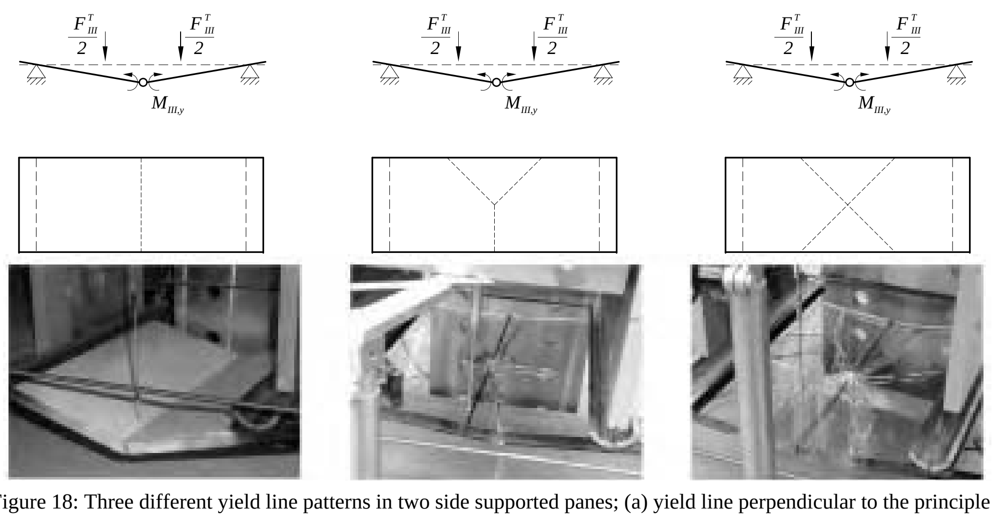

Figure 18: Three different yield line patterns in two side supported panes; (a) yield line perpendicular to the principle stresses; (b) half yield line perpendicular to the principle stresses, (c) four yield lines crossing the centre.

timate load $F^{FG}_{II,u}$ was reached. The loads increase nonlinear due to the high values of the deflections and the span/thickness ratio. This effect can be observed in stage I as well as in stage II. A remaining deformations $w^{T}_{II,r}$ at the beginning of stage II was observed, as shown in Figure 20. Finally in stage III all specimens developed yield line patterns as shown in Figures 19(b,c). Not all slabs were tested in this way. A specific number of specimens were first of all hit by an impact, as shown in Figure 6. Depending on the dropping height one or both glass layers broke. Also here the damaged specimens were installed in the experimental set-up to test them in stage II and/or III. In the following three different modes shows the different yield line patterns of a square slab. As shown in Figure 21(a), the slab in mode 1 resists the induced load developing yield line patterns in form of a circular fan. Specimens of collapse mode 2 with yield lines in form of fans in the corners have the smallest ultimate load $F^{FG}_{III,u}$, as shown in Figure 20. The collapse mode with the minimum ultimate load $F^{FG}_{III,u}$ is the proper value for the calculation of RSC. Therefore collapse mode 3, which is also possible, is not the proper one. The smallest ultimate load of mode 2 is not the exact solution but this approximation is quite accurate. In general in stage III the yield line theory is applicable to glass slabs of LSG that are reinforced uniformly by a PVB foil.

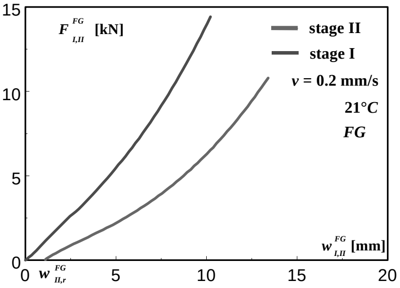

Figure 19: Load-deflection diagrams for four side simply supported LSG slab in stage I and II

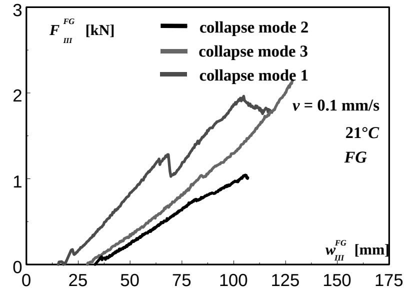

Figure 20: Load-deflection diagrams for four side simply supported LSG slab with three different yield line mechanisms in stage III.

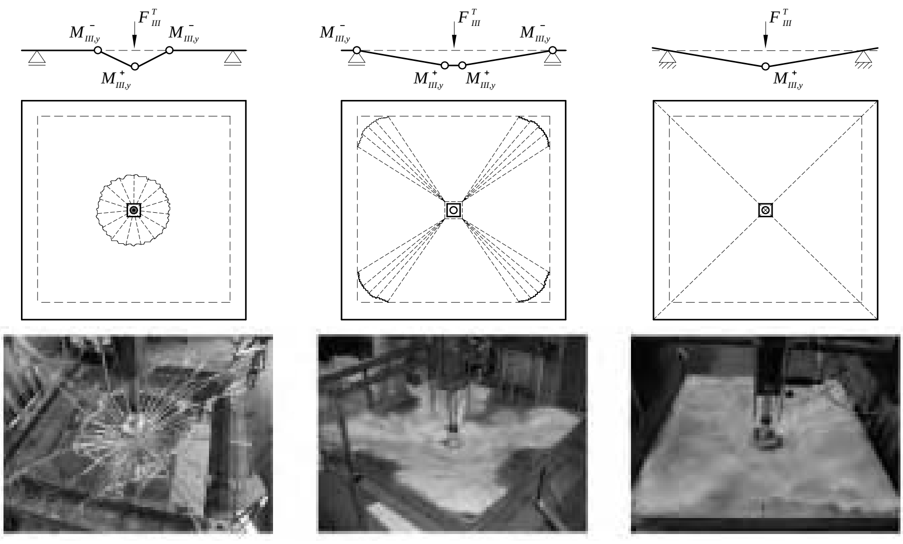

Figure 21: Three different yield line patterns in simply supported square slabs, (a) mode 1; circular fan, (b) mode 2; corner levers in form of fans, (c) mode 3; yield lines from the slab centre to the four corners.

VII. CONCLUSIONS

Three stages were proposed to determine the structural safety of a glass structure. With the corresponding ultimate forces and virtual works it is possible to give statements about the remaining structural capacity according to the degree of damage. The four point bending tests as well as tests with simply supported glass slabs combined with impact tests have shown that with unequal glass sheets the load carrying capacity in stage I and the remaining structural capacity in stage III can be increased. Remaining structural capacity in stage III exists in all glass structures of laminated safety glass only if the initial cracks patterns form yield line patterns. Therefore laminated safety glass of toughened glass simply supported in two sides as well as in four sides has no RSC in stage III. The ultimate collapse occurs when the glass on the surface of the upper layer fails by compression. Then the foil tears or the pane slide from the bearing. The ultimate moment of resistance at the yield line can be determined taking into account the material laws of the glass and the PVB foil. Finally the total collapse in stage III of a glass structure can be determined from the yield line patterns using the equations of equilibrium. As a result the ultimate load in stage III can be found to estimate the RSC. In future, bending tests with point fixed glass plates have to be carried out. The resulting types of yield lines have to be discussed. Also other enhancements like interlayer with other material laws or interlayer with matrix of glass fibre have to be investigated.

VIII. ACKNOWLEDGMENT

The presented research project is part of the European COST action C13 and supported by the Swiss Federal Office for Education and Science. All test specimens were delivered by the Swiss branch of Pilkington AG free of charge. Both contributions are highly appreciated.

REFERENCES

[Stamm 1974] Stamm, K., Witte, H.; *Sandwich-konstruktionen*; Springer-Verlag; Wien, New York 1974.

[Bohmann 1999] Bohmann, D.; *Ein numerisches Verfahren zur Berechnung von Verbundglasscheiben*; Shaker Verlag; Aachen 1999.

[Sobek 2000] Sobek, W., Kutterer, M., Messmer, R.; *Untersuchungen zum Schubverbund bei Verbundsicherheitsglas*; Bauingenieur Bd. 75, Heft 1, Januar 2000; pp. 41-46.

[Kott 2004] Kott, A., Vogel, T.; *Safety of laminated glass structures after initial failure*; Structural Engineering International 2/04.

[Kott 2003] Kott, A., Vogel, T.; *Remaining Structural Capacity of Broken Laminated Safety Glass*; Glass Processing Days 2003; Tampere (Finland) 15. – 18.06.2003; pp. 403-407.

[Osswald 1996] Osswald, T., Menges, G.; *Materials Science of Polymers for Engineers*; Carl Hanser Verlag; München, Wien, New York 1996.

NOTATIONS

Upper case letters:

$F^T_{i,u}$	Ultimate load in stage *i* for glass type T (*i*=I, II, III)
$K^T_{III,y}$	Internal forces in the yield line in stage III
$M_{III,y}$	Ultimate moment of resistance in stage III
$RSCR^T_{i,W}$	Remaining structural capacity ratio of external works in stage *i* for glass type *T* (*i*=II, III)
$RSCR^T_{i,F}$	Remaining structural capacity ratio of ultimate forces in stage *i* for glass type *T* (*i*=II, III)
$W^T_{i,u}$	Physical work in stage *i* for glass type *T* (*i*=I, II, III)
U	Internal work in the yield line

Lower case letters:

$w^T_{II,r}$	Plastic deflection in stage II for glass type T

Greek letters:

σ^{PVB}_{III}	Tensile stress in the PVB foil in stage III
$\sigma^{PVB}_{III,u}$	Ultimate tensile stress in the PVB foil in stage III
σ^T_I	Tensile stress for glass type T in stage I
$\varepsilon_{III,y}$	Strains in the yield line in stage III
$\sigma^T_{I,u}$	Flexural strength for glass type T in stage I
σ^T_{II}	Tensile stress for glass type T in stage I
$\sigma^T_{II,u}$	Flexural strength for glass type T in stage II
σ^T_{II}	Tensile stress for glass type T in stage II
σ^T_{III}	Compressive stress for glass type T in stage III
$\sigma^T_{III,u}$	Ultimate compressive stress for glass type T in stage III

Superscripts:

FG	Float glass
HG	Heat strengthened glass
TG	Toughened glass
T	Glass types (FG, HG or TG)

Subscripts:

F	Load
r	Residual
u	Ultimate
W	External work
I,II,III	Stage I, II or III

EU COST C13 Glass and Interactive Building Envelopes. M. Crisinel, et al. (Eds.). IOS Press, 2007.

Proposal for a Code Calibration Procedure

Jørgen Munch-Andersen, Danish Building and Urban Research, Hørsholm, Denmark
Randi Kruse Vestergaard, NIRAS - Consulting Engineers and Planners A/S, Allerød, Denmark

A method for estimating the strength parameters of the Weibull distribution and the power in Brown's integral from full-scale experiments with rectangular glass panes loaded uniformly at different load rates is proposed.

Knowing the parameters, it is possible to estimate the load capacity of a glass pane subjected to any load history. Provided accurate load histories (load as a function of time during the service life) for e.g. wind and snow loads are available this enables fairly simple and very accurate estimates for the load capacity of a glass pane for different load types.

The method is applied to permanent load and Danish snow load in order to demonstrate the consequences.

Keywords: Weibull distribution, parameter estimation, code calibration, duration of load

I. INTRODUCTION

The use of glass for structural purposes suffers from insufficient knowledge of the properties of glass and the nature of the loads. It is therefore difficult to formulate simple and accurate code requirements for load bearing glass structures.

A measure of the failure probability can be obtained if loads and strength are sufficiently described by statistical distributions. Two properties inherent in glass make it difficult to deal with the safety level. One is the damage accumulation that causes the strength to become severely dependent on the load duration, the other a significant size dependency. The established models for these phenomena, Brown's integral and the Weibull distribution, requires estimates for several parameters. However, different methods to estimate these parameters lead to very different values.

The large deflections of glass panes add to these difficulties, because calculation of damage accumulation for variable load has to be made on stress level.

This paper deals with determining the parameters in Brown's integral and the Weibull distribution using results from full-scale experiments with glass panes simply supported along the four edges and loaded at different rates. The advantage of this method is that uncertainties about the models for size effect and damage accumulation becomes less important because the experimental results used for calibration of the models originates from specimens of the same size, and with the same support and loading conditions as the real glass panes.

If the parameters are determined from idealised test set-ups, e.g. double ring tests, possible weaknesses of the theoretical description will significantly increase the uncertainty for real glass panes.

The paper also discusses how simple rules for designing glass panes can be achieved. As a part of this an estimated load history for snow loads have been applied to simulated panes with strength parameters determined from the full-scale experiments. This enables accurate estimates of the load capacity for snow load. The method can of course also be used for other load types.

This paper is based on an idea outlined in [Munch-Andersen & Ellum, 1995] and developed in a MSc-thesis [Vestergaard, 2004]. Somewhat similar methods are described in [Beason & Morgan, 1984] and [Grüters et al., 1990].

II. DEFINITIONS

The well-known Brown's integral is used to describe the damage in an area of the glass pane due to the load history up to time T.

$$K(T) = \int_0^T \sigma(t)^n \, dt \,. \tag{1}$$

K is somewhat related to the fracture mechanics parameter K_I, see e.g. [Simiu et al., 1984].

The equivalent 1 second stress is defined as the constant stress that, when it acts for 1 second, causes the same damage as the real stress does during the time T. It can be determined from $K(T)$ as

$$\sigma_{e,1\mathrm{sec}} = (\tfrac{1}{1\mathrm{sec}} K(T))^{1/n} \tag{2}$$

The Weibull distribution can only yield for the strength of an area with a constant stress field. In particular it deals with the size-effect, which is caused by the fact that the probability of the presence of a severe micro-crack is increased when the size of the area is increased. The distribution of the 1 second strength $f_{1\mathrm{sec}}$ can be written as

$$F(f_{1\mathrm{sec}}) = 1 - \exp\left[-\left(\frac{f_{1\mathrm{sec}} - a}{(A/A_0)^{-1/k} b} \right)^k \right] \tag{3}$$

where a is a minimum strength (which is often assumed to be zero), b is related to the average 1 second strength, k is the size parameter, A is the actual area and A_0 is a reference area for which b is determined.

K is closely related to the variance for which reason k can be estimated from tests with only one size of test specimens. A small value means large size-effect and variance. The influence of the parameters is illustrated in Figure 1.

It should be noted that the Weibull distribution presupposes that the strength of two neighbouring areas is uncorrelated.

The 'weakest link of a chain' analogy is often used to explain the Weibull distribution. The ratio A/A_0 replaces the number of links in the chain.

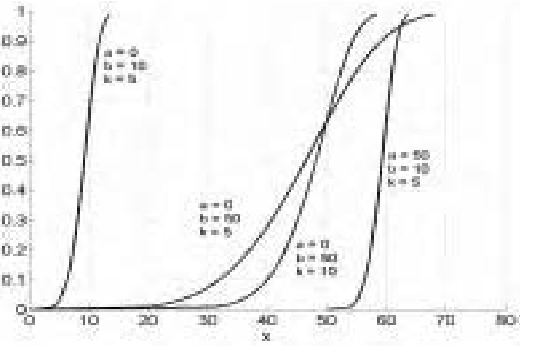

Figure 1: Influence of the parameters a, b and k on the distribution function of the Weibull distribution for A/A_0 = 1 and a, b and x in kPa.

III. OUTLINE OF METHOD

The method is based on physical and simulated experiments with rectangular glass panes, which are exposed to uniformly distributed load increased at a constant rate d until failure. Since glass is linearly elastic, the stress history $\sigma(t)$ at any point of the pane can be quite accurately calculated by means of a FEM programme when the load rate d, the failure load p_f and the time to failure T is known. Also the equivalent $\sigma_{e,1\mathrm{sec}}$ at any point can be determined for an assumed value of n.

In the simulated experiments the pane was divided into a number of sub-areas in which the stress field was assumed to be constant. The strength of each sub-area was assumed to be Weibull distributed. For an assumed set of strength parameters (a, b, k) the 1 second strength of each sub-area was simulated by means of a random number.

Load was applied at a constant rate and $\sigma_{e,1\mathrm{sec}}$ was calculated for each sub-area at each load step. Failure occurs when $\sigma_{e,1\mathrm{sec}} > f_{1\mathrm{sec}}$ in any of the sub-areas. This failure determined the load capacity of the simulated pane.

This procedure was repeated for a large number of simulated panes. Then the distribution function for the failure load was estimated and compared with the results from the experiments. In the present study the strength parameters were determined so that the square of the difference between the

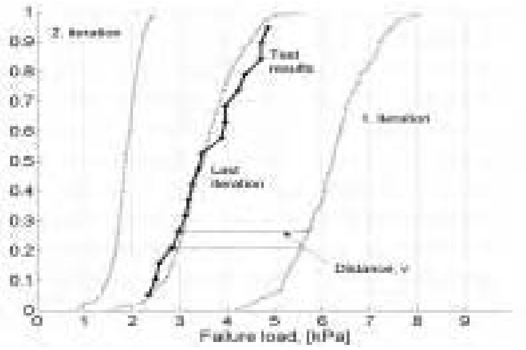

Figure 2: Distribution of failure loads from test results and simulated tests. The estimated strength parameters of the Weibull distribution are taken as the values that minimise the square distance between the distributions.

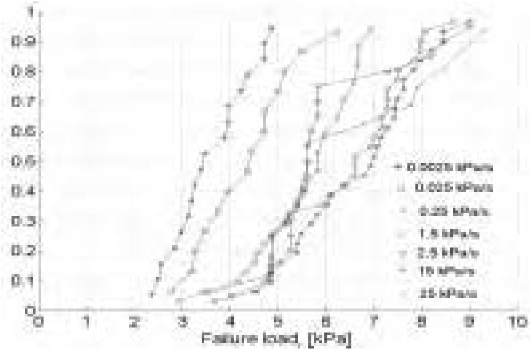

Figure 3: Tests results from [Johar, 1981 & 1982] plotted as distribution functions for the failure load for each loading rate. Tests are carried out at normal room conditions.

Simulated and the measured distribution of the failure loads are minimised, see Figure 2. More sophisticated methods, like maximum likelihood estimation, could also be used.

It should be noted that the resulting distribution of the failure loads will not be a Weibull distribution. A LogNormal distribution might be a good approximation. This is the distribution type usually used to describe material strengths.

In principle the power *n* in Brown's integral could be estimated from experiments with only one loading rate, because the different failure loads causes a slight time dependency of *a* and *b* in the Weibull distribution. However, a reliable estimate requires physical experiments carried out at different loading rates, *d*. Then *n* can be included in the estimation.

IV. Experimental results

This study was based on thorough test series by [Johar, 1981] and [Johar, 1982] with 6 mm thick glass panes 1.5 m × 2.4 m. They were loaded at constant rates ranging from 0.0025 kPa/s up to 25 kPa/s. This caused the time to failure to range from less than 1 second to about 30 minutes. There are about 20 tests for each loading rate. The results used for this study are shown as distribution functions in Figure 3.

For the slower loading rates it is seen that the failure load decreases with the loading rate as would be expected from Brown's integral. For loading rates above about 1 kPa/s, the experiments indicate that this effect is significantly reduced as the strength distribution is almost independent of the loading rate.

The estimation is therefore divided into two parts, one for loading rates up to 0.25 kPa/s and one for the faster rates.

The reduction is most obvious for the rates 1.5 kPa/s and 15 kPa/s, because the distribution of the results for 2.5 kPa/s and 25 kPa/s is seen to be quite awkward. The results for loading rates 2.5 and 25 kPa/s is not included in the analysis further on in this paper.

Results from experiments where the failure occurs at the edge cannot be used directly as the failure mechanism at the edge is different. Using the information that the strength of the internal part of the pane is larger than the failure value requires use of statistical methods for censored samples. This was not attempted in this study, but it was proved that the estimated parameters became almost the same if the results from panes with edge failure were excluded or were included without correction.

V. DETAILED PROCEDURE

6. The pane was divided into $m \times m$ sub-areas. The values m = 5, 10, 15 and 20 were used.

2. A set of strength parameters (a, b, k, n) was assumed.

Step 3 was performed for each sub-area.

3A. The relation between the load p and the largest principal stress σ_1 at the centre point was established by means of a FEM programme, taking large deflections into account. This was done for 25 load steps, allowing for sufficiently accurate determination of the stresses by linear interpolation.

3B. The (p, σ_1) relation was transformed to a (t, σ_1) relation by means of the known loading rate and $t = p/d$.

3C. Equivalent stresses $\sigma_{e,1\text{sec}}$ for each load step were determined by Eq. (2) from the (t, σ_1) relation and the assumed n. Hereby a (t, $\sigma_{e,1\text{sec}}$) relation was established.

Step 4 was repeated many times (200 - 1000) with new simulated panes and for each relevant loading rate

4A. The 1 second strength, $f_{1\text{sec}}$, for each sub-area was simulated by generating a random number x between 0 and 1. $f_{1\text{sec}}$ was then calculated from Eq. (3) as $x = F(f_{1\text{sec}})$.

4B. The time to failure for which $\sigma_{e,1\text{sec}} = f_{1\text{sec}}$ was found for each sub-area from the (t, $\sigma_{e,1\text{sec}}$) relation from step 3C.

4C. The sub-area with the shortest time to failure was identified and the failure load $p_{f,i}$ was calculated by multiplying that time by the loading rate d.

5. The simulated failure loads for each loading rate was ranked and the square of the distance between all the experimental results and the simulated distribution for the corresponding loading rate was calculated.

6. New sets of parameters were assumed and the procedure from step 3C was repeated until a good approximation was reached, i.e. a small square distance. If n is unchanged, the repetition can start at step 4.

VI. RESULTS OF ESTIMATION

A. Low loading rates

The results for the slower loading rates, 0.0025, 0.025 and 0.25 kPa/s, were used for this analysis. The parameters (a, b, k, n) were estimated when they were all free, see Table 1, and for n = 16, see Table 2. Also the number of sub-areas was varied. All numbers in Tables 1 and 2 are determined for 500 simulated panes for step 4 and b refers to A_0 = 1 m^2.

TABLE 1:
ESTIMATED PARAMETERS FOR LOADING RATES BELOW 1 KPA/S WHEN ALL PARAMETERS ARE FREE.

m, no of sub-areas = $m \times m$	5	10	15	20
n, power in Brown's integral	11.7	11.4	11.6	11.3
a, minimum strength, MPa	26.3	25.3	0.0	3.2
b, strength parameter, MPa	55	47	74	70
k, size parameter	3.9	3.9	6.2	6.0

TABLE 2:
ESTIMATED PARAMETERS FOR LOADING RATES BELOW 1 KPA/S WHEN n = 16 IS CHOOSEN.

m, no of sub-areas = m, $\times$ m	5	10	15	20
n, power in Brown's integral	16	16	16	16
a, minimum strength, MPa	3.5	0.0	0.4	0.3
b, strength parameter, MPa	72	68	68	67
k, size parameter	6.2	6.2	5.8	6.4

When all parameters were free, it was seen that n became a very stable value around 11.5, significantly smaller than the values usually quoted which range from 16 to 20, depending i.a. on humidity. It was further seen that the other parameters for m = 5 and 10 were quite different from those for m = 15 and 20. A supplementary investigation showed that if a was assigned the value zero, k and b approached the values found for m = 15 and 20, where a was close to zero.

It should also be mentioned that for m = 10 the number of simulations affected a, b and k significantly. Using either 200 or 1000 simulations in stead of 500 changes the estimates to numbers close to those quoted for m = 15 and 20 in Table 1. The high value for a found in a few cases was likely to be a statistical coincidence.

When n = 16 was chosen as a fixed value, it is

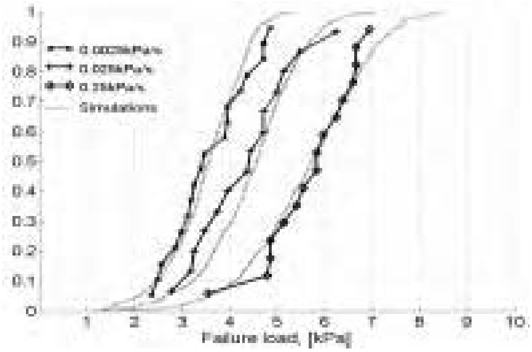

Figure 4: Estimated distribution functions compared with experimental data for loading rates below 1 kPa/s when all parameters are free (n ~ 11) and *m* = 15.

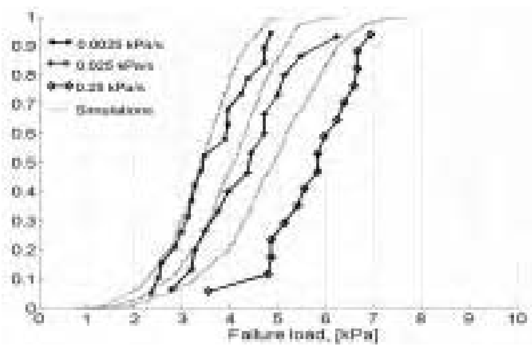

Figure 5: Estimated distribution functions compared with experimental data for loading rates below 1 kPa/s when *n* = 16 is chosen and *m* = 15.

seen from Table 2 that *a* became close to zero and the size parameter equalled the higher values in Table 1. Comparing Figures 4 and 5 shows that the approximation was much less satisfying for *n* = 16 than when *n* was free. The values obtained for *m* = 15 are used henceforth.

B. *High loading rates*

The difference in the failure load depending on the load duration was dealt with by estimating a different value of *n* for each loading rate but common values for *a*, *b* and *k*. This was done for m = 15 and 500 simulations. The estimated values for *n* are given in Table 3.

The value of *n* increased significantly between 0.25 and 1.5 kPa/s. The high values were so high that the time dependency could be ignored for practical purposes. (For *n* approaching infinity only the maximum load mattered, the usual assumption for most other materials). The approximation was good as can be seen from Figure 6.

TABLE 3:
ESTIMATED VALUES FOR *n* WHEN PARAMETERS FOR ALL LOADING RATES ARE USED AND *n* IS ALLOWED TO DEPEND ON THE RATE AND ALL OTHER PARAMETERS ARE ASSUMED INDEPENDENT OF THE RATE.

Loading rate	*n*
0.0025 kPa/s	13.0
0.025 kPa/s	12.1
0.25 kPa/s	17.7
1.5 kPa/s	52.2
15 kPa/s	50.0

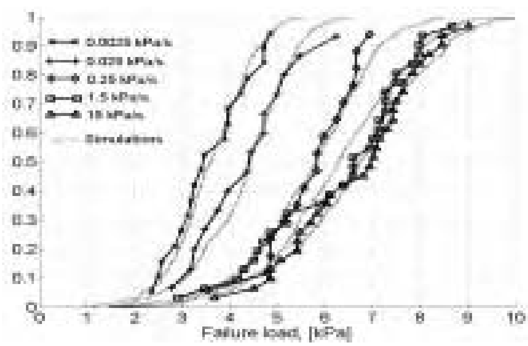

Figure 6: Estimated distribution functions compared with experimental data for all loading rates when *n* is estimated separately for each loading rate.

For the three lower rates *n* was on average higher than 11.6. The reason is that due to statistical uncertainties *a* became significantly larger than zero for this estimation. This also affected the other estimated parameters so they took values somewhat different from the stable values in Table 1. Other estimations indicated that the average would approach 11.6 if *a* was given the value zero.

VII. APPLICATIONS

Having estimated the parameters of the Weibull distribution and the power *n* in Brown's integral, a stochastic model for the strength of a glass pane was established. It can be used to estimate the failure probability by simulation for any load history, *q(t)*. This can be done very much similar to the Detailed procedure described above.

A. Constant load

The procedure can be used to estimate a distribution function for the load capacity of a glass pane subjected to constant load q_T acting for the time *T*. These distributions can be used to derive a relation between the characteristic load capacity of a glass pane and the duration of the load.

The simulation procedure for constant load was slightly different from the simulated tests, where the load was increased until failure. The way to handle this was, for each simulated glass pane, to increase q_T gradually until failure occurred after precisely the time *T*. Results from the simulations is shown in Figures 7 and 8 for n = 11.6 and 16.

The characteristic 5% fractiles of the load capacity and material strength are given in Table 4.

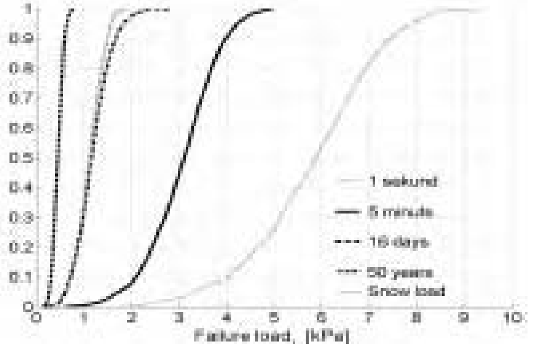

Figure 7: Distribution of load capacity for constant loads q_T for n =11.6 and *T* equal to 1sec, 5 min, 16 days, and 50 years. The capacity for estimated Danish snow load is shown, too.

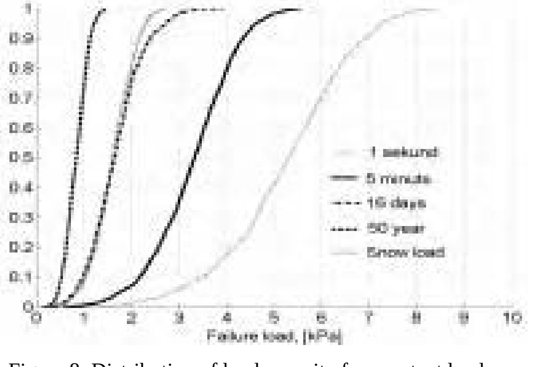

Figure 8: Distribution of load capacity for constant loads q_T for n = 16 and *T* equal to 1 sec, 5 min, 16 days, and 50 years. The capacity for Danish snow load is shown, too.

TABLE 4
ESTIMATED CHARACTERISTIC LOAD CAPASITIES AND MATERIAL STRENGTHS FOR DIFFERENT DURATIONS OF LOAD.

T	1 sec	5 min	16 days	50 years
n = 11.6	3.3 kPa 45 Mpa	1.7 kPa 25 MPa	0.6 kPa 12 MPa	0.3 kPa 8 Mpa
n = 16	2.9 kPa 41 Mpa	1.8 kPa 27 MPa	0.8 kPa 14 MPa	0.4 kPa 10 MPa

It is seen that the relative decrease with increasing duration was smaller for the strength than for the load capacity. This should be regarded when using the values to estimate k_{mod} values. The coefficient of variation was 25% independent of the duration.

B. Variable load

When the load varies over time, as most loads do, it becomes more complicated to estimate $\sigma_{e,1sec}$, but if the load history *q(t)* is known, the principle is almost the same as described above.

When the load history was applied to a sufficient number of simulated panes, the failure probability could be estimated from the number of failed panes. This did not, however, enable estimation of the coefficient of variation of the strength.

An estimate that included the coefficient of variation was achieved by applying a load factor α to the load history and then for each simulated pane, by determining the highest value of α that did not cause failure. The variation of α was then a measure for the variation of the strength.

1) Snow load

The load history for snow is the snow load as a function of time during each of the major snow packs during the service life, $q_1(t)$, $q_2(t)$,…, $q_N(t)$ and 0 the rest of the time. A snow pack is defined as the period from the first day where the ground is covered by snow until it has all melted away again.

The load history was modelled by three stochastic parameters:

1. The peak load $q_{max,i}$ during snow pack *i*.
2. The number of snow packs during service life T_s (50 years).
3. The equivalent duration $t_{e,i}$ of each snow pack, see below.

The distribution of the *peak load* was taken as the distribution of the yearly maximum ground snow load used for the Danish code for actions [DS 410:1998]:

$$F(q_S) = \exp\left(-\exp\left(-\frac{q_S - 415\,\text{Pa}}{124\,\text{Pa}}\right)\right) \qquad (4)$$

The characteristic 98% value was 900 Pa.

The return time for snow packs with this distribution of the maximum load was obviously 1 year. The *number of snow packs* during the service life T_s was therefore modelled as a Poisson process with the parameter $T_s \times 1$ year^{-1}.

The *equivalent duration* of a snow pack is defined as the time that the peak load $q_{max,i}$ should act in order to cause the same damage K (defined by Eq. (1)) as the real load during the snow pack.

Similar damage means that the contribution to the equivalent stress $\sigma_{e,1sec}$ in all parts of the pane for the actual and the simulated snow pack must be similar. Due to the non-linear load-stress relation this requires that the load level is representative. Because the contribution to the damage from loads below say 90% of $q_{max,i}$ was very small, it was judged that using the peak load to estimate $t_{e,i}$ was sufficiently accurate.

The equivalent time was estimated from an estimation of the ground snow load during all snow packs for 32 years at two Danish locations. The locations were that far apart that major events could be considered independently, so that the data represented 64 years. The distribution of the major peak loads agreed well with the distribution in the code, Eq. (4).

Figure 9 shows the run of the load during a snow pack and the equivalent constant load by which it is represented.

$t_{e,i}$ is determined for all snow packs during the 64 years for which $q_{max,i} > 400$ Pa. By inspection it is seen from Figure 10 that $t_{e,i}$ was significantly higher for snow packs with $q_{max,i} > 700$ Pa than for the others. Because correct estimation was most important for the higher loads, the estimate was

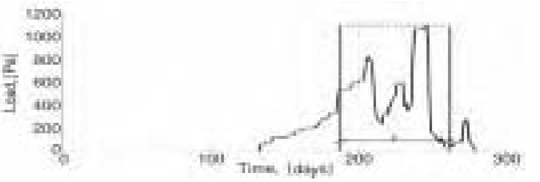

Figure 9: The load during an (exceptionally long) snow pack and the equivalent load represented by $t_{e,i}$ and $q_{max,i}$.

based on the incidents with $q_{max,i} > 700$. Unfortunately, there were only four of these incidents. The duration was therefore assumed independent of the load and was modelled as a LogNormal distribution with parameters estimated from the four incidents. The mean value was somewhat dependent on the power n in Brown's integral. It is about 11 days for $n = 11.6$ and 8 days for $n = 16$.

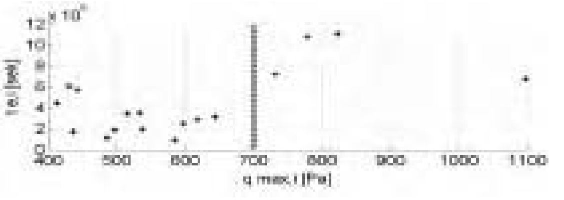

Figure 10: The relation between peak load $q_{max,i}$ and the logarithm of estimated equivalent duration $t_{e,i}$ in seconds for $n = 11.6$.

Simulated snow load histories could then be applied to simulated glass panes. For each simulation the snow load was multiplied by a load factor α which was increased until failure occurred. Hereby the distribution of the load capacity $\alpha\, q_{max}$ could be found (q_{max} was the largest peak load during the service life so the distribution of q_{max} was the usual snow load in the code). The distribution of $\alpha\, q_{max}$ is shown in Figures 7 and 8 for two values of n. The 5% fractile represents the characteristic load capacity for Danish snow loads.

The lower part of the distribution was seen to be very similar to the distribution for constant load for 16 days, but the coefficient of variation was smaller. A sound conclusion about k_{mod} for snow requires calculation of partial coefficients with and without duration of load effects. This might be done in line with [Sørensen et al., 2003].

VIII. Conclusions

A model for estimation of the statistical distribution of the load capacity of simply supported rectangular glass panes subjected to any load history is suggested. The input parameters in the models are estimated from tests with rectangular glass panes which means that only severe shortcomings of the assumed models for strength (Weibull) and damage accumulation (Brown) will affect the load capacity.

Considering the limited number of test results available, these models appear to give a satisfying description of the test results.

The estimated parameters for the Weibull distribution (3) conform quite well with other estimates. It appears that the minimum strength a should be taken as zero and that the size dependency k is about 6. (The latter is assigned the value 25 in the proposal for a CEN standard for the design of glass. This value means that the size dependency becomes insignificant).

The parameter n in Brown's integral (1), which governs the damage accumulation (or Duration-of-Load effect) deviates significantly from the expected n ~ 16-20. The estimated n = 11.6 means that the Duration-of-Load (DoL)-effect is much more severe than usually anticipated. This estimate is based on tests lasting no more than an hour, thus there is a crucial need to carry out tests with real size glass panes subjected to constant load and with expected time to failure of 1 month - 10 years.

The estimation of n also showed that for short duration loads - like wind - there seem to be no DoL-effect. Also this should be investigated more closely.

The reliability of all the estimated parameters should be improved by carrying out more tests, including other glass thicknesses and other areas and aspect ratios. The model should in principle be applicable to all shapes of panes and uneven load distributions. This should also be confirmed be experiments.

A principle for stochastic modelling of snow load is also described. The principle requires knowledge of the run of the ground snow load during major snow packs. The necessary parameters are estimated for Danish circumstances. The interpretation to code format need further work.

Acknowledgement

The study on which this paper is based [Vestergaard, 2004] is supervised by L. O. Nielsen, Department of Civil Engineering, Technical University of Denmark, P. Friis Hansen, Department of Mechanical Engineering, Technical University of Denmark and the first author.

References

[Beason & Morgan, 1984]
BEASON, W. L., MORGAN, J. R. Glass failure prediction model. J. of Structural Engineering, Vol 110, no 2. 1984

[Sørensen et al, 2003]
SØRENSEN, J. D., STANG, B. D., SVENSSON, S. *Effect of load duration on timber structures in Denmark.* In ICASP9 - the 9th International Conference on Applications of Statistics and Probability in Civil Engineering, July 6-9, 2003, San Francisco, California, USA.

[DS 410:1998]
Code of Practice for Loads for the Design of Structures. DS 410 (4.1). Dansk Standard. 1999.

[Grüters et al, 1990]
GRÜTERS, H.,HACKL, K., WILLMS, H. *Stress and strain analyses of rectangular plates for large deformations, Part 2, Calculation of fracture probabilities in rectangular plates under area load.* Glastech. Ber 63, no 4. 1990.

[Johar, 1981]
JOHAR, S. *Dynamic fatigue of flat glass. Phase II*. Ontario Research Foundation. Department of Metals, Glass and Ceramics. Mississagua. 1981.

[Johar, 1982]
JOHAR, S. *Dynamic fatigue of flat glass. Phase III*. Ontario Research Foundation. Department of Metals, Glass and Ceramics. Mississagua. 1982.

[Munch-Andersen & Ellum, 1995]
MUNCH-ANDERSEN, J., ELLUM, J. C. *Glass in the building envelope - a review* (In Danish). Danish Building Research Institute (SBI Bulletin 107). Hørsholm, 1995.

[Simiu et al, 1984]
SIMIU, E. et al. *Ring-on-Ring Tests and Load Capacity of Cladding Glass*. U.S. Department of Commerce. National Bureau of Standards. Gaithersburg, 1984.

[Vestergaard, 2004]
VESTERGAARD, R. K. *Strength of glass Constructions* (in Danish). Master Thesis. Dept. of Civil Eng., Technical University of Denmark. 2004.

EU COST C13 Glass and Interactive Building Envelopes. M. Crisinel, et al. (Eds.). IOS Press, 2007.

To Increase the Residual Bearing Capacity of Glass with a Local Reinforcement

Jürgen Neugebauer
Institute of Structural Design, University of Technology, Graz, Austria

A requirement of overhead glazing constructions is that they have a minimum residual bearing capacity. Wide spanned broken laminated glass with a continuous or a discrete support has a risk of falling down. The solution is to fix the laminated glass to the substructure. Wire-cloth or other synthetic fabrics are embedded in the PVB-interlayer or the synthetic resin, near the edges were the glass is supported. The fabric can be fixed to the glazing beads or to the glass fittings with special connections.

Keywords: reinforcement, residual bearing capacity

I. Introduction

Residual bearing capacity is defined as the resistance against a collapse of a broken system. In glass technology this definition is used in connection with the carrying behavior of laminated glass or laminated safety glass, which is already destroyed by load effect or spontaneous break of one or more glass panels. [Wörner et al. 2001]

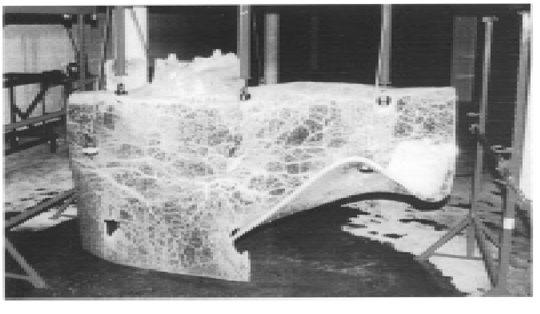

Figure 1: Example of a broken glass [Bauen mit Glas, 2002]

II. Static of broken glass

The principal concept for increasing the residual bearing capacity for continuously supported glass panes is to fix the glass to the supports. In the case of damage the glass panes cannot fall down. Therefore the values of the horizontal (membrane) forces at the support have to be computed, to be able to design the fixation.

In the case of a discrete supported glass pane the correlation between the forces at the support and the membrane forces in the glass in the area around the glass hole are needed.

A. Horizontal forces by continuous support

The initial system is an unbroken laminated glass pane with the length *l* simply supported only on two edges. Figure 2 shows a sketch of the static systems of the glass panel. The sketch is structured into the initial system, the deflected static system, the system with tension cracks and the static system of a cable.

The load q is increased from zero. At the supports, only vertical (A_v or B_v) reactions result if small deformations are assumed, see in Figure 2 (a). With a further load increasing up to the fracturing load the theory of the small deformations cannot be assumed any longer. It is a change from the theory of small deformations to the theory of large deformations. At the supports, vertical (A_v or B_v) and horizontal (A_h or B_h) reactions result, see in Figure 2 (b).

At the moment of the fracture there is a change in carrying behavior. The bending moment decreases and the traction increases, and at the supports larger horizontal (A_h or B_h) reactions result, see in Figure 2 (c) [Sobek et al. 1999].

The PVB (polyvinyl butyral) interlayer stretches near the cracks. Dependent on the load the forces of static system can be in an equilibrium. But with a higher load q a further deformation is possible. With this further deformation of the system, the stretch of the foil can be so large, that the system can transfer no more bending moment to the supports and the static system of a broken toughened glass changes to that of a cable system see in Figure 2 (d).

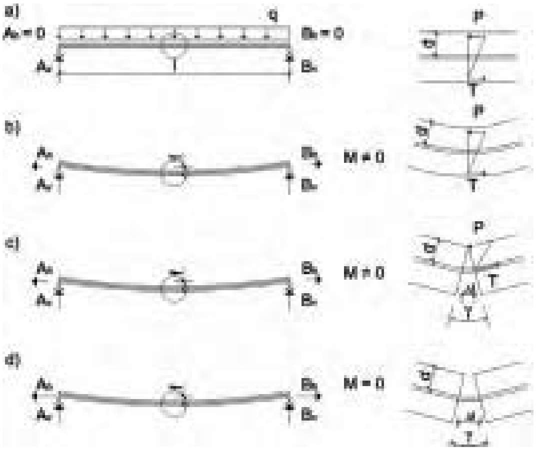

Figure 2: Load carrying systems of continuously supported glass

In the case where this deflection of the static system of a cable is the smallest the largest horizontal force results. Further stretching of the foil due to non linear effects causes an enlargement of the deflection *f* and thus a decrease of the horizontal bearing force (A_h or B_h) .

These horizontal forces tend to pull the glass out of the supporting system.

B. Horizontal forces by discrete support

With point load supported glass panes, the stress maxima are concentrated in the range of the glass fittings. The load *q* over the whole area is increased from zero to the fracturing load. At the moment of the fracture there is a change in carrying behavior, a change from small to large deformations and from pure bending moment to bending moment and traction. The traction membrane force is concentrated near the supports, see Figure 3.

These membrane forces result in a ring of traction around the hole, which causes an expansion of the hole. If the deformations at the hole edge are too large, the broken glass panel can slide out of the glass fittings.

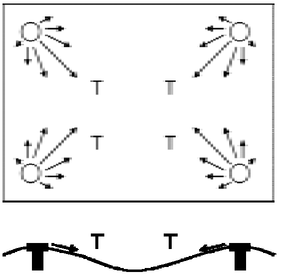

Figure 3: Load carrying systems of discretely supported glass

III. Concept of the Reinforcement

A. Continuous support

The principal concept for increasing the residual bearing capacity is the fixation of the glass with a fabric to the substructure. A fabric is embedded into the PVB-interlayer between the glass panes near the edges, and one side of the fabric protrudes of the glass. The projecting fabric is cast into a plastic fastening batten, or is welded to the metal profile. Into that fastening border holes for the screws are drilled, and with these screws the border is fastened to the support profile. In order to handle thermal deformations the holes must be bored with a larger diameter. A squeeze-free storage for the unbroken glass panel must be ensured. The grip is supposed to become effective only in case the glass breaks.

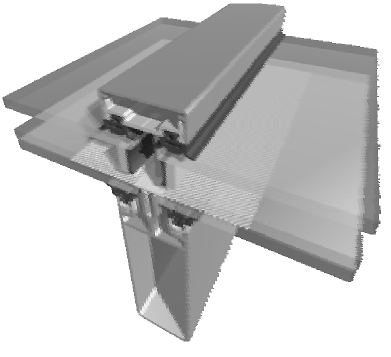

Figure 4: Concept for continuously supported glass

B. Discrete support

The function of the reinforcement is similar to that in reinforced concrete. The expansion of the glass hole due to the membrane forces is hampered by the reinforcement. A round fabric is embedded into the PVB-interlayer between the glass panes around the glass hole. The fabric is cast into a plastic hollow shaft or welded to a metal hollow shaft. The height of this core is slightly smaller than the total thickness of the structure and the outside diameter is slightly smaller than the hole diameter. The inside diameter results from geometry of the glass holder. In order to handle all movements of the glass cladding a squeeze-free fixation of the glass pane must be ensured.

Figure 5: Concept for discretely supported glass

IV. MATERIALS OF THE REINFORCEMENT

To be able to select the correct material used for the reinforcement, the production conditions must be considered. Furthermore it is important that the materials used are themselves chemically compatible. Only with the knowledge of the boundary conditions a sound connection between the glass and the fabrics on the one hand and between the fabric and the support on the other hand, can be reached.

The production of a laminated safety glass takes place at a temperature of 140°C, and a pressure of 14 bar, therefore the fabric must have a temperature resistanc of approx.140°C. [Leicht und Glasbau, 2002]

The fabrics should possess a high measure of transparency due to a requirement of the architects to the glass.

The thickness of the fabrics cannot be more than 1,0 mm due to the generally used thickness of the PVB-interlayer with thickness of 1,52 mm.

TABLE 1:
REINFORCEMENT MATERIALS

MATERIALS	TENSILE STRENGTH	FUSING TEMPERATURE
fabrics	N/mm²	°C
glass fibre	3400	400
polyamide	400-700	225
polyester	600	220
wire	450-750	600-1200

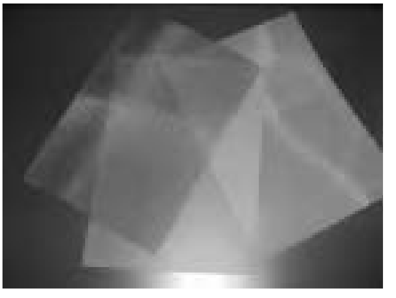

Figure 6: Reinforcement materials (fabrics)

V. TESTS AND RESULTS

A. Continuous support

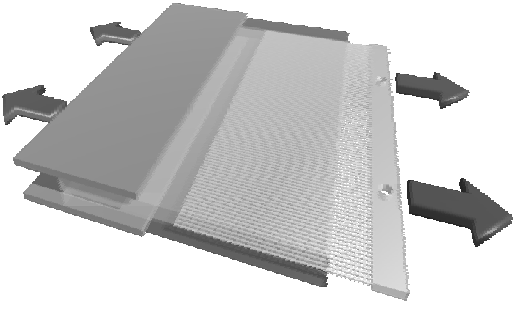

Figure 7: Testing concept for the traction tests

For the horizontal forces which tend to pull the glass out of the supporting system a sound fixation has to be developed. To be able to design the fixation it is required to get values for the load resistance of the different materials. It is important to find out which is the weakest member of this composition of glass, fabric and the fastening profile. With simple traction tests it is possible to get the fracturing load of the weakest member and information of the fracturing behaviour of this system

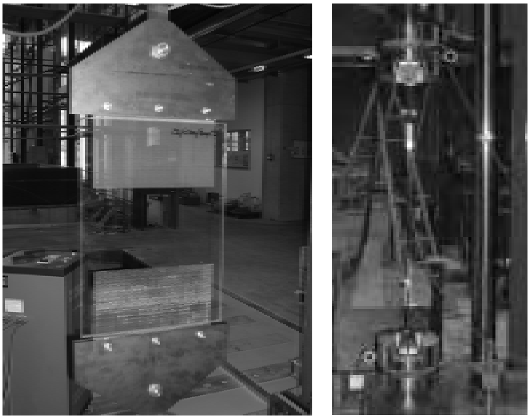

Figure 8: Test set up in the laboratory

In the laboratory the traction test series were done with a cylinder press, see in the Figure 8. In the test set up a laminated glass with two 6 mm float glass with a width of 360 mm and a height of 500 mm for the test objects were used. In the PVB-interlayer the wire-cloth and the syntactic fabrics were embedded at both sides of the testing object. The upper position was the carrying side with a strong wire fabric and the lower side was the testing side. The size of each fabric was 300 mm in the length and 200 mm in the width. At the testing side fabrics with different materials, different diameters of the threads and different mesh openings were arranged. The fabrics were glued with a synthetic resin to two small steel profiles on both sides of the fabrics. With three bolds the profiles were fixed to two bigger steel plates on both sides, see in Figure 8. Two big bolds were the fixation to the hydraulic press. With this symmetrical testing set up only axial forces are ensured.

The load deformation diagram in Figure 9 shows the result of a test series with a wire-cloth. The threads had a diameter of 0.5 mm and a mesh opening of 1.6 mm. The result of this test was a fracturing load of approximately 20.0 kN. The crack was in the space between the glass and the fastening profile, it was a fracture of the fabric itself, as shown in Figure 10.

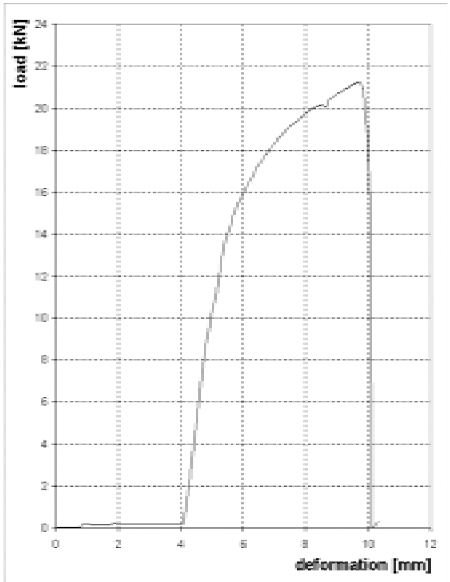

Figure 9: Load deformation diagram of the traction test with a wire-cloth

Figure 10: Broken wire-cloth

In the load deformation diagram, see in Figure 11, the result of the test series with a polyamide fabric is shown. The threads had a diameter of 0.3 mm and the mesh opening was 0.5 mm. In the Figure 11 is an oscillating curve before the fracturing load with approx. 8.5 kN was reached. The reason is, that the bond between the PVB-interlayer and some threads has gone lost (Figure 12).

After the maximum load was reached the oscillating curve was the breakage of the polyamide fabric thread by thread.

The result of the test series with a polyester fabric see in the load deformation diagram in Figure 13. The threads had a diameter of 0.35 mm and the mesh opening was 1.18 mm. The result of this test was a fracturing load of approximately 8.5 kN, it was a breakage of the polyester fabric itself. The crack was in the space between the glass and the fastening profile, see in Figure 14.

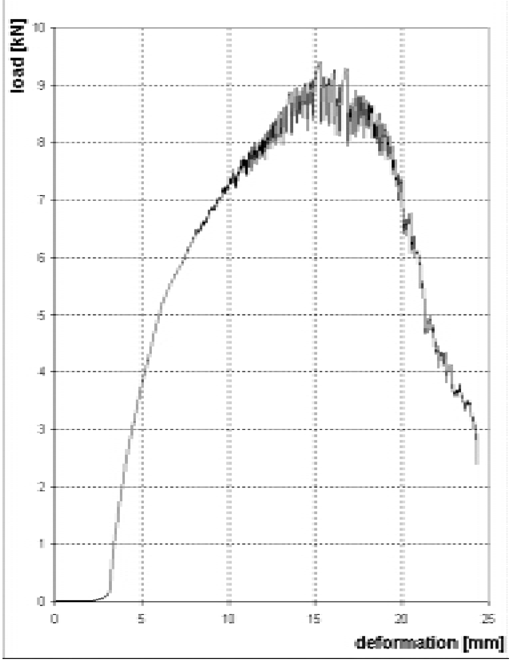

Figure 11: Load deformation diagram of the traction test with a polyamide fabric

Figure 12: Broken polyamide fabric

With these testing results with the different materials it is possible to say, that the less deformable wire-cloth (approx. 6 mm), is better than synthetic fabrics with deformations in the space between the fastening profile and the glass of more than 10 mm.

To prevent a collapse of glazing system, it is a requirement to ensure that the glass panes can not slip out of their supports. With an opening of more than 10 mm, as with synthetic fabrics, a slip out of the supporting system is possible.

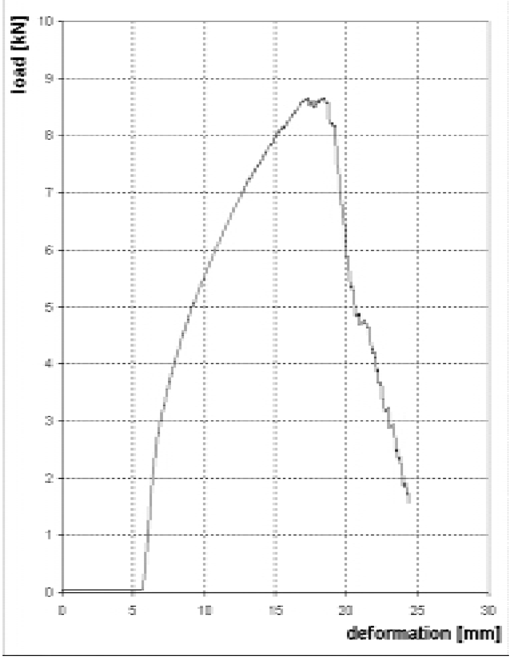

Figure 13: Load deformation diagram of the traction test with a polyester fabric

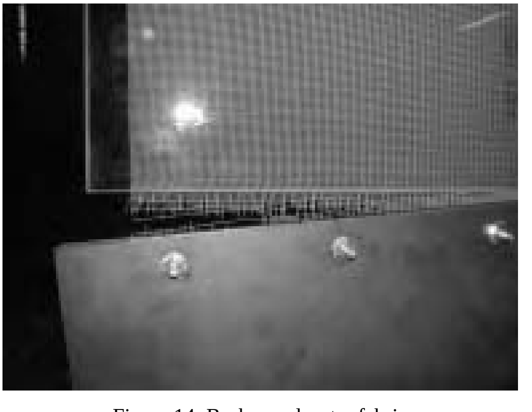

Figure 14: Broken polyester fabric

B. Discrete support

To get information of the behaviour of the broken laminated glass around the glass hole, pressure test series were prepared. The concept of these tests was, to get the maximum force where the glass fitting is pulled out of the glass. The goal of these series was, to get the difference in the residual bearing capacity between the laminated glass system without and with reinforcement.

In the test set up a laminated glass with two 6, 8 and 10 mm toughened glass panes with a 30 mm hole in the middle were used. The laminated glass with a size of 600 mm in both directions is supported on a frame, as shown in the Figure 16. A glass fitting with a diameter of 60 mm was used.

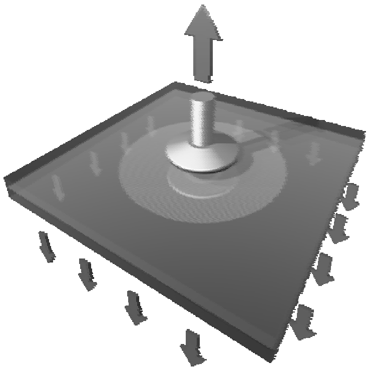

Figure 15: Testing concept for the pressure tests

Figure 16: Test set up in the laboratory without reinforcement

The reinforcement with a diameter of 200 mm and a hole in the middle with a diameter of 30 mm was embedded in the PVB-interlayer around the glass hole (see Figure 17). For the test series different materials with different diameters of the threads and different mesh opening were used.

The results of these test series without a reinforcement one can see in the Figure 18. As a function of the thickness of the laminated glass the load deformation diagram shows the fracturing load of the glass with approx. 4.0 kN up to approx. 11,5 kN.

Figure 17 Test set up in the laboratory with reinforcement

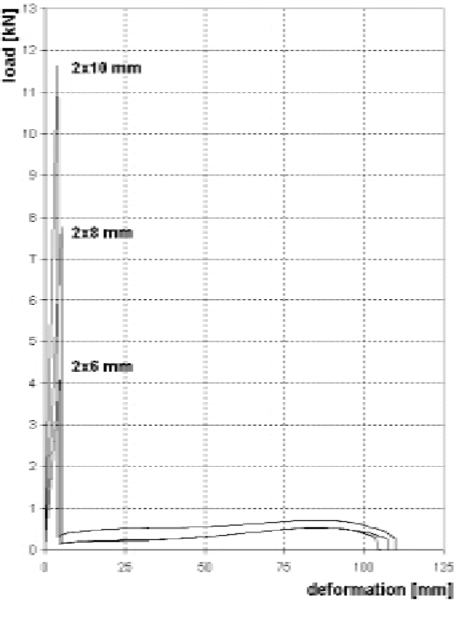

Figure 18 Load deformation diagram of the system without reinforcement

An important fact is, that the load maxima with which the glass is pulled out of the glass fitting was with approximately 0.5 kN and with a deformation of approx. 90 mm in all cases of the glass thickness nearly the same. The maximum force for the residual bearing capacity depends on the extensional stiffness of the PVB-interlayer.

Figure 19 Result of the system without reinforcement

In the first test set up a laminated glass with reinforcement two 6 mm toughened glass panes with a 30 mm hole in the middle were used.

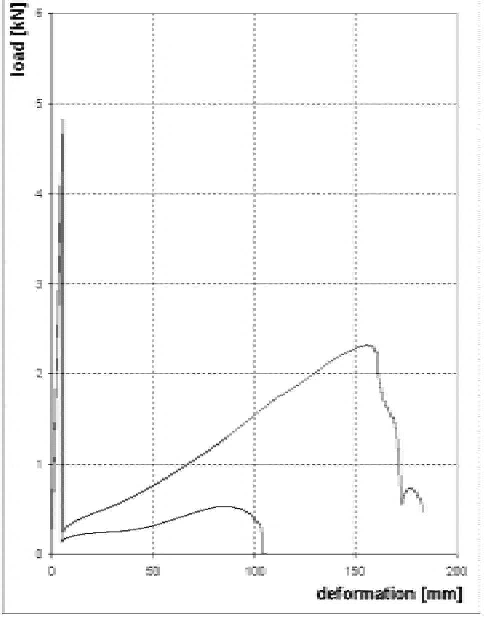

Figure 20: Load deformation diagram of the system with and without a reinforcement of a 2x6 mm laminated glass

The Figure 20 shows a comparison of the test result of a 2x6 mm laminated glass without and with reinforcement. The fracturing load of the test with reinforcement was, with approx. 4.5 kN, a little bit higher than the result of the system without a reinforcement. The load where the glass is pulled out of the glass fitting was with approx. 2.3 kN, and the deformation was approx. 140 mm. The value was more than 4 times higher than the load where the glass is pulled out of the glass fitting of the system without reinforcement. The residual bearing capacity was increased by a factor of 4.

Figure 21 Result of the system with reinforcement

The comparison of the two pictures, in Figure 19 the system without reinforcement and picture in Figure 21 the system with reinforcement, shows the different shapes of the broken glass. With the reinforcement the broken glass gets more bending stiffness around the glass hole and the shape changes from a funnel to a bowl.

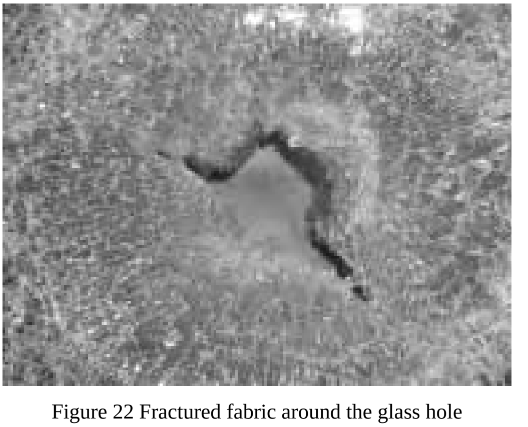

Figure 22 Fractured fabric around the glass hole

Figure 22 shows the glass hole after the glass fitting was pulled out. One can recognize that the collapse occurred by the fracture of the fabric due to the membrane forces.

VI. Summary and Prospects

With the proposed construction it is possible to design wide spanned laminated glass simply supported on two sides. By point load supported glazing it will be possible to use laminated toughened glass with its high bending stress resistance. The goal is that the broken glass (in all qualities - float glass, heat strengthened glass, or toughened glass) remain fixed and is prevented from falling down.

The future research will concentrate on an optimization process of this system.

VII. Acknowledgment

The work in this paper was primarily conducted with the support of Prof. Gernot Beer from the Institute of Structural Analysis at the Graz University of Technology and the industry partner Herbert Maierhofer Glastechnik GmbH (St. Marein/Mürztal, Austria).

References

[Bauen mit Glas, 2002]
Bauen mit Glas, Information für den Bauherrn, Architekten und Ingeniure, Wirtschaftsministerium Baden-Württemberg, .2002

[Leicht und Glasbau, 2002]
Bemessung von Glaskonstruktionen, Institut für Stahlbau, Holtbau und Flächentragwerke, Technische Universität Graz, 2002.

[Sobek et al. 1999]
W.SOBEK, F. MAIER, M. KUTTERER, *IL Forschungsbericht 1/99,"Mutifunktionale Glassysteme", Bewehrtes Verbundsicherheitsglas, 1/99* Universität Stuttgart, 1999.

[Wörner et al. 2001]
WÖRNER, SCHNEIDER, FINK, *Glasbau, Berechnung, Konstruktion,* Springer Verlag, 2001.

EU COST C13 Glass and Interactive Building Envelopes. M. Crisinel, et al. (Eds.). IOS Press, 2007.

Inelastic Material Behaviour of Soda-Lime-Silica Glass

Frank Schneider, Darmstadt University of Technology, Statics and Dynamics of Structures, Darmstadt, Germany
J.-D. Wörner, Darmstadt University of Technology, Statics and Dynamics of Structures, Darmstadt, Germany

The inelastic material behaviour of thermally toughened and heat strengthened Soda-Lime-Silica glass at room temperature was investigated. A four-point bending test configuration was used. The delayed elastic deformations were measured and reveal a significant time-dependent behaviour. The possible origin such as sub-critical crack growth, ion diffusion or absorption of water molecules is discussed briefly. The aim of the study is a better understanding of the nature of glass itself, in order to use this brittle material as a structural member in the field of civil engineering according to appropriate safety requirements.

Keywords: inelastic material behaviour, Soda-Lime-Silica glass, creep

I. INTRODUCTION

Glass is one of the oldest materials used by mankind and the applications in the field of civil engineering increase successfully since many years. Nevertheless, the understanding of the non-crystalline solid as a state of matter is still poor. Especially the long term behaviour and the influence of long duration loading on the glass structure and the material strength have to be investigated and verified. Therefore, a brief summary of the constitution of glassy materials will be given in the next paragraph of this paper before the experimental results are discussed**.**

II. THE GLASS MATERIAL

A. Chemical composition

Glasses used in structural applications consist mainly of SiO_2. In the crystalline form of SiO_2 each Si-atom is surrounded tetrahedrally by four O-atoms (Figure 1), whereby each O-atom is connected to two neighboured tetrahedras and therefore counts to ½ in the chemical formula. The three-dimensional network formed of the crystalline structure exhibits equal bond angles between its composites. In the glassy state these angles vary slightly and the periodicity of the crystalline lattice, i.e. the long-range order, is lost [Greaves, 1997]. Therefore, glassy materials are characterized by a certain short-ranged order of the nuclei, but without long-range order, as it can be found in the regular lattice of a crystal.

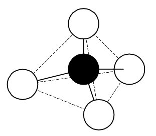

Figure 1: Si-O_2 tetrahedra [Wörner, 2001]

Pure-fused silica is difficult to produce economically due to a very high softening temperature of around 1200°C. By adding oxides such as NaO_2 and CaO_2 the glass transition range of the modified glass, like the most common Soda-Lime-Silica Glass, is lowered to about 550°C. The added oxides enter the network as cations. The radical oxygen breaks the covalent bond of the SiO_2 network apart into two groups of $Si\text{-}O^-$ connected by a weaker polar bonding.

B. The structure of glass

Despite many other solids, glass does not have a crystalline structure on microscopic scale. At room temperature the molecules have a disordered arrangement like a fluid, but they are rigidly bound like in a solid. Structurally, non-crystalline solids are similar to fluids, but the entire network is rigid. This state is called an amorphous solid or a glass. Therefore, glass is rather more a state of matter, than a special material with a certain chemical composition. The glass state does not fit into the classical classification of substances by three states of aggregation. It is an own class halfway between fluids and solids. Because of this, glass is sometimes called a frozen super-cooled liquid. These misnaming has led to the legend that antique windowpanes would very slowly flow downwards under there own weight [Zanotto, 1998].

Theoretically every material independent on its chemical composition can achieve the glassy state, if crystallization can be prevented by cooling the melt very fast. The molecules have no time to move into the ordered crystalline arrangement until the melt solidifies. Due to the increasing viscosity during the cooling process the molecules remain in this metastable frozen-in non-equilibrium condition. In this sense a solid can be defined as a liquid with a very high viscosity [Scholze, 1988]. A glass-forming melt has a tendency to achieve this super-cooled condition especially easy. The temperature Tg, at which the glass transition takes place, and the achieved material properties depend on the chemical composition and also cooling rate. By cooling slowly the material has more time to relax during solidification, the transition occurs at lower temperatures and the glass is more dense. This phenomenon is technically used by the production of thermally toughened glass.

C. Strength and material properties

The material properties are determined by the glassy state. Its characteristic brittle behaviour results from this disordered structure. Plastic deformations, i.e. the slip of molecular layers observed in a crystalline metal, cannot occur. A tensional loading leads to stress concentration at any surface crack and finally to a spontaneous brittle fracture without plastic deformations at the crack-tip. Therefore the technical strength of the glassy material extremely depends on the condition of the surface in the tension zone and is some orders of magnitudes lower than the expected theoretical strength of the atomic bonds. To overcome this deficit it is possible to prestress the glass by heating it above Tg and cooling it rapidly afterwards. The result is a residual stress state with compression at the surface and tension in the interior. Depending on the surface compression achieved the glass can be classified as toughened glass or heat strengthened glass. Usually, anorganic glass as an amorphous material is treated to be both ideal linear-elastic and isotropic. Nevertheless, small inelastic deformations could be measured in a bending test. After unloading from a long term loading, the glass specimens exhibit a remaining deformation of up to 1% of the instant elastic one. Subsequently, during a recovery phase the inelastic deformations mostly disappeared.

III. EXPERIMENTAL PROCEDURE

A. Specimens

The test specimens consist of 6 mm thick glass plates. Every plate is 1 m long and 0.1 m wide. Altogether nine specimens have been investigated in this preliminary study. Six of the specimens are made of toughened glass and three of heat strengthened glass.

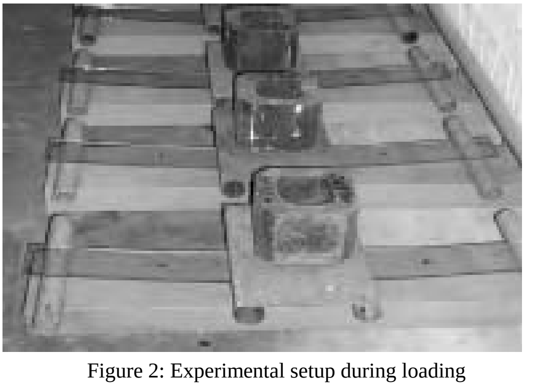

Figure 2: Experimental setup during loading

B. Experimental procedure

A four-point bending test configuration with a span of 0.91 m was used to apply a static load P. Tree different loading levels have been applied to the test specimens in order to achieve the maximum tensile stress showed below in Table 1. The increasing inelastic deformation was measured manually each day after temporary unloading each specimen. A mobile rigid frame was installed above the supports and the deflection was measured in the middle of the span by a digital dial gage (Figure 3). Afterwards the loading was applied to the specimen again. Every specimen was loaded at room temperature for a period of seven days at all. During the subsequent 101 days recovery period the decrease of the deformation was measured similarly.

TABLE 1:
LOAD LEVELS AND NUMBER OF SPECIMENS

Glass type	applied tensile stress [N/mm²]	degree of utilization [%*]	Number of specimens
toughened glass	120	100	2
toughened glass	100	83	2
toughened glass	70	58	2
Heat strengthened glass	70	100	3

* based on the characteristic value of the bending strength

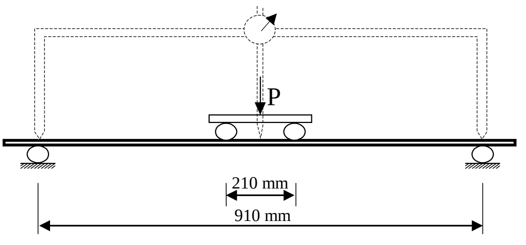

Figure 3: Schematically experimental setup of four-point bending testResults and Discussion

C. Experimental results

The experimental results reveal a significant time-dependent behaviour. During the loading period an increasing delayed-elastic deformation was observed. After seven days loading, the inelastic deformation grew up to 1% of the instant elastic one. Subsequently, during the 101 days recovery phase the deformations mostly disappeared. Therefore no viscous flow is observed. For that reason it is more accurate to speak about a delayed elastic behaviour.

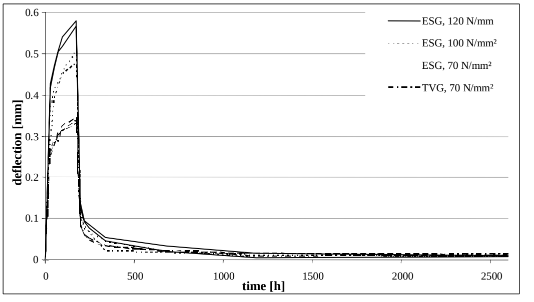

Figure 4: Measured deflection during a 2600 h time period

D. Discussion

Two out of three of the heat strengthened glass sheets failed during the loading period. The remaining did not exhibit a significant different behaviour to the equally loaded toughened glass sample. The delayed-elastic deformation is proportional to the applied load, i.e. the achieved stress, as illustrated in Figure 4. Therefore, an influence of the load-level is not evident.

Visco-elastic flow of glass, as it is observed in the glass transition range, can be excluded as a possible reason for the observed behaviour at room temperature [Gy, 1994], [Duffrène, 1999]. A probable explanation could be the growth of sub-critical crack inside the initial tension zone, which weakens the material [Gy, 1999] and could give an explanation for the failure of two out of three heat strengthened glass specimens after a certain load period. This static fatigue could also lead to a time dependant decrease in the material strength and should be considerate in the design of load bearing glass members. Even the recovery phase could be explained by cracks-healing after unloading. At the other hand, no significant differences exist between the evolution of the delayed deformations based on the instantaneous elastic one, neither between the different load levels, nor between toughened glass and heat strengthened glass, i.e. the value of the residual stress state (Figure 5). An influence of the overall stress state on the growth of cracks is not identifiable, which could be expected if sub-critical crack growth causes the observed behaviour. Furthermore, the curvature in Figure 5 leads to the assumption of a linear viscoelastic material behaviour.

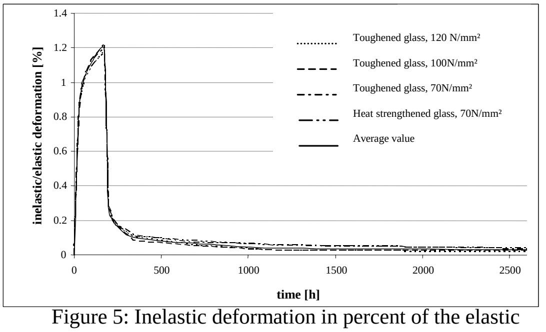

Figure 5: Inelastic deformation in percent of the elastic deformation.

In technical literature alternative explanations, such as ion diffusion [Holloway, 1973], [Kahnt, 1996], switches in atomic bonds of the SiO_2 network [Pelletier, 1999] and absorption of water molecules [Franeck, 1983] are also frequently discussed. The idea of water molecules entering the tensioned glass surface and after unloading generating the observed deformations by acting like a wedge needs further investigations.

A slow diffusion of cations in the glass structure is the most probable explanation. Due to external stress sodium ions get slowly squeezed out of their initial position to an energetically more favourable place in the lattice. After removing the load the ions move back into their original position, thus an explanation of recovery phase could be given. A time-depending decrease of the material strength is not expected in this case. The determination of the ultimate bending strength has not been performed by now, due to the small amount of similar specimens and load conditions and the expected scattering of the results. Furthermore, a combination of two ore more of the discussed mechanisms could be responsible for the effect. The dominant mechanism can not clearly be identified using the current test setup.

A viable rheological model will be developed to describe the behaviour in the next chapter.

E. Rheology

The general constitutive equation of a linear viscoelastic material can be written in the form of a hereditary integral

$$\sigma(t) = \int_0^t \Phi(t-\bar{t})\dot{\varepsilon}(\bar{t})d\bar{t}\ . \qquad (1)$$

For any applied strain history ε(t) the achieved stress σ(t) can be calculated easily if the relaxation modulus Φ(t) is known. At the other hand, the analogue equation

$$\varepsilon(t) = \int_0^t \Psi(t-\bar{t})\dot{\sigma}(\bar{t})d\bar{t} \qquad (2)$$

can be used to describe the strain for a particular stress. The creep compliance function Ψ(t) can be obtained by fitting the parameters of the assumed rheological model to the results of a performed creep experiment. Therefore, a average curve of the measured delayed elastic deformations illustrated in Figure 5 is calculated as a basis of the fit. Subsequently, an adequate rheological model composed of linear elastic springs ($\sigma=E*\varepsilon$) and linear viscous dashpots ($\sigma=\eta*\varepsilon$) has to be chosen. A single Maxwell or Kelvin Element does not describe the observed characteristics of the viscoelastic behaviour sufficiently. For that reason, a chain of three Kelvin solids in series is used.

$$\varepsilon(t) = \varepsilon_1(t) + \varepsilon_2(t) + \varepsilon_3(t) \qquad (3)$$

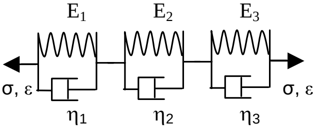

Figure 6. Kelvin chain

The total strain is the sum of the strains of each Kelvin element (Figure 6), thus the creep compliance Ψ(t) is:

$$\Psi(t) = \sum_{i=1}^{3} w_i(1-e^{-\frac{t}{\tau_i}}) \qquad (4)$$

Whereby w_i represents weighting factors and $\tau_i=\eta_i/E_i$ is the retardation time of any Kelvin solid. Nevertheless, the elements and its parameters can not directly be related to any physical mechanism. A similar behaviour could be described by three parallel Maxwell elements and its particular parameters. The equations of the Maxwell model are more convenient if a strain is applied and the stress-relaxation is measured. Nonetheless, both models are equivalent.

An equal approximation can be done by the b-function, which represents a continuous distribution of relaxation times. In this case the creep compliance Ψ(t) has the form

$$\Psi(t) = (1 - e^{-\left(\frac{t}{\tau}\right)^{b}}) \quad (5)$$

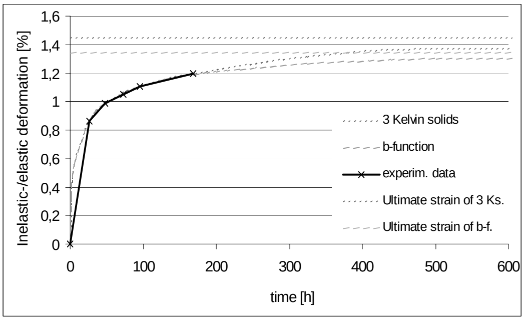

Figure 7: Inelastic deformation, approximation by rheological models and ultimate value

Figure 7 illustrates the average values of the inelastic deformation during the loading period and the approximations by the Kelvin chain and the b-function. Furthermore, the calculated limit of the ultimate deformation $\varepsilon(t=\infty)$ is presented for both models and the increasing inelastig deformation is extrapolate to 600 h.

TABLE 2:
PARAMETERS OF THE RHEOLOGICAL MODELS, LOADING PERIOD

	Kelvin Chain			b-function
	1	2	3	
weighting factor*	0.389	0.294	0.317	b=0.408
relaxation time [s]	10^4	10^5	10^6	87957
relaxation time [h]	2.78	27.78	277.78	24.43
Ultimate strain [%]	1.44			1.34

TABLE 3:
PARAMETERS OF THE RHEOLOGICAL MODELS, UNLOADING PERIOD

	Kelvin Chain			b-function
	1	2	3	
weighting factor*	0.637	0.237	0.127	b=0.288
relaxation time [s]	10^4	10^5	10^6	7820054
relaxation time [h]	2.78	27.78	277.78	5.57
ultimate strain [%]	1.16			1.17

* in case of the b-function the value of the parameter b

The same procedure can be performed for the unloading period. The parameters given in Table 2 and 3 enable someone to describe the deformations in both cases mathematically.

F. Restrictions

The deflection could not be determined immediately after the removal of the load. The delay between unloading and measuring was approximately one minute, but the delay-time differs slightly, dependent on the quantity of the applied dead load. For that reason, a short term creeping-effect could not be acquired and the time period between unloading and measuring the deflection was not exactly equal.

Sufficient statistical information could not be ensured, due to the small number of test specimens. Nevertheless, a tendency can be deducted. An improved test assembly with an enlarged numbers of specimens and detailed investigations to comprehend the different influences is planed for the future.

G. Further investigations

A test series of 30 samples of toughened glass is planned to be carried out. Each glass specimen will be investigated on its material behaviour, e.g. Young´s Modulus, weight, dimension, surface compression, etc. before and after the long term loading test. In addition the transparency of the specimens will be determined before and after the loading to prove cracks inside the glass directly, as illustrated in Figure 8 schematically. A laser diode will be used as an intense light source and a photo sensitive diode (PSD) will gauge the intensity of the received signal. Eight samples will remain unloaded for the whole test period to exemplify as a reference.

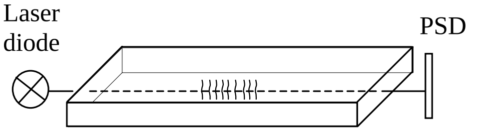

Figure 8: Schematic illustration of the transmission detection test setup

An advanced measurement device, namely laser triangulation, has been developed to increase the accuracy of the test method and detect short time creep. The deformation will be determined by a laser-optical device (Figure 9). A laser beam above the support will be deflected at the surface of the glass. The rotation φ of the support, which is directly related to the deflection by a simple linear equation, is measured by a position sensitive detector continuously, even during loading and unloading. Finally, the bending strength of every specimen will be determined.

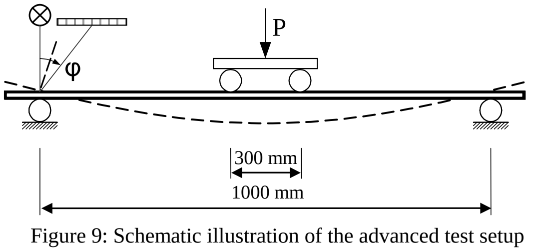

Figure 9: Schematic illustration of the advanced test setup

Four specimens will remain in an immersion bath during the whole test period to investigate the influence of the water. Furthermore, the detection of water molecules inside the glass structure, e.g. by infrared-spectroscopy and microwave-irradiation will be investigated. Unfortunately, first tests performed at the Darmstadt University of Technology department of Physics did not show sufficient results. One possible reason for that are the different bonding conditions in physical and chemical bonded water compared to bulk water. The influence of ion-diffusion will be analysed by studying specimens of pure Silica-glass, which does not include oxides in the glass structure. If no significant delayed elastic behaviour can be observed in pure Silica-glass, the effect in Soda-Lime-Silica glass can be related to that.

In the investigated glass specimens, the inelastic part of the deformation is very small and for that reason difficult to verify. To visualize the inelastic deformations more easily it is projected to study the reaction of glass-fibre bundles, 6 m in length, under static tensile load. Due to its high strength and small cross-section measurable deformations can easily be achieved. Preliminary investigations exhibit a noticeable delayed deformation of about 30 % of the instant elastic one after 24 hours loading. Subsequently, during a 24 hour recovery phase the deformations mostly disappeared. A small remaining deformation can be explained by the failure of single fibres in the bundle. Unlike bulk glass, fibres exhibit an axial orientation of the SiO_2 network due to the manufacturing process. Nevertheless, the achieved results are promising and will be carried on in the future.

IV. Conclusion

Thermally toughened glass was tested. The increase of the inelastic deformation is measured by a digital dial gauge. More accurate measurements by laser triangulation sensors are planned for the future. The value of the evidenced delayed elastic deformation is small, compared to the instantaneous elastic one. Nevertheless, it could affect the safety of permanently loaded units, e.g. externally prestressed members. The origin of the observed behaviour is not completely understood at present. Time depended material behaviour at room temperature of glass is frequently attributed to viscose flow. Sub-critical crack growth inside the initial tension zone, ion diffusion, switches in atomic bonds of the SiO_2 network or absorption of water molecules are more likely the reason of the observed inelastic deformation. To understand the origin of that behaviour and the consequence for the safety requirements further investigations have to be carried out.

REFERENCES

[Greaves, 1997]
GREAVES, G.N., *Local structure, microstructure and glass properties. Journal of Non-Crystalline Solids*., Vol. 222, pp. 13-24, 1997

[Wörner, 2001]
WÖRNER, J.-D., *Glasbau-Grundlagen, Berechnung, Konstruktion,* Berlin Heidelberg New York, Springer, 2001

[Zanotto, 1998]
ZANOTTO, E., *Do Cathedral Glasses Flow?* Am. Phys. Vol. 66, pp. 392-396, 1998

[Scholze, 1988]
SCHOLZE, H., *Glas - Natur, Struktur und Eigenschaften*, Berlin Heidelberg New York, Springer, 1988

[Gy, 1994]
GY, R.., *New insights into the viscoelasticity off glass. Journal of Non-Crystalline Solids*, Vol. 175, pp. 103-117, 1994

[Duffrène, 1999]
DUFFRÈNE, L., *Viscoelastic behaviour of a soda-lime-silica glass: inadequacy of the KWW function*, Journal of Non-Crystalline Solids, Vol. 215: pp. 208-217, 1999

[Gy, 1999]
GY, R., *Creep and Recovery of a Thermally Tempered Glass Plate at Room Temperature*, Glass Processing Days 13-16 June 1999

[Holloway, 1973]
HOLLOWAY, D.G., *The Physical Properties of Glass,* London, Wykeham, 1973

[Kahnt, 1996]
KAHNT, H., *Ionic transport in Glasses*, Journal of Non-Crystalline Solids, Vol. 203, pp. 225-231, 1996

[Pelletier, 1999]
PELLETIER, J.M., *Evidence for a residual elastic modulus in inorganic glasses by mechanical spectroscopy,* Journal of Non-Crystalline Solids, Vol. 258, pp. 119-130, 1999

[Franeck, 1983]
FRANEK, H. J., *Reaktionen zwischen Glasoberfläche und Wasser bzw. wässrigen Lösungen*, Glastechnische Berichte Vol. 56 No. 6/7, pp. 165-175, 1983

EU COST C13 Glass and Interactive Building Envelopes. M. Crisinel, et al. (Eds.). IOS Press, 2007.

Glass Strength in the Borehole Area of Annealed Float Glass and Tempered Float Glass

Jens Schneider, Senior Engineer
Schlaich Bergermann und Partner, Stuttgart, Germany

Thermal stresses of tempered glass in the area of typical boreholes were estimated using Narayanaswamy's structural relaxation model implemented in a Finite-Element-Code (ANSYS 5.5.2). Surface stresses were measured for samples with holes of different float glasses (soda-lime-silica-glass, borosilicate glass) from different commercial tempering processes. The bending strength in the borehole area of the samples and of annealed (float) glass samples was determined using a modified coaxial double-ring bending test. Results are compared and evaluated on a statistical basis. It is shown that the characteristic glass strength of tempered glass in the borehole area is not lower than in the "infinite area" given in European standards. From the results it is also assumed that crack healing plays an important role for the bending strength of tempered float glass.

Keywords: glass strength, tempered glass, numerical modelling, tempering process, structural glass, photoelastic measurements

I. Introduction

In many facade applications, structural glass is fixed in holes with glass fittings. Finite-element calculations show that the tensile stresses in such glass panes mostly have their maximum in the area of the chamfers of holes, for usual dimensions and bending from wind loading [BATHE 1990, SCHNEIDER 2001].

Thus, it is important to determine the glass strength in the hole area for the structural design of the glass. The glass strength very much depends on the surface condition influenced by the drilling process and - for tempered glass - the amount of temper stress. Because of sub-critical crack growth and the stress concentration in the hole area, annealed float glass is usually inadequate for this applications. For tempered glass, the qualitative distribution of thermal stresses in the borehole area was calculated in [LAUFS 2000, SEDLACEK 1999] with a viscoelastic model but only little quantitative data about their influence on the glass strength was given.

In [CARRE 1997, CARRE 1999] the amount of thermal stresses at the edges of tempered glass was re-calculated by means of photoelastic measurements and their influence on the glass strength was compared with the results of bending tests.

In this investigation the same methodology was used for the borehole area. First, photoelastic methods (*Laser-Gasp®*, Epibiaskop, [ABEN 1993]) were used to determine the surface stresses in the "infinite" area of tempered samples with holes from different commercial tempering processes. Then, 3-D finite-element calculations for symmetrical and asymmetrical holes in tempered glasses were done to calculate temper stresses in the borehole area using *Narayanaswamy's* structural relaxation model that is implemented in ANSYS [ANSYS 1999, DUFFRENE 1997, GY 1994, NARAYANASWAMY 1971, NARAYANASWAMY 1978, SCHERER 1986, SOULES 1987]. In a parameter study for different apparent heat transfer coefficients, the amount of temper stresses in the "infinite" and in the borehole area was then re-calculated with the FE-models. Finally, tempered samples and identical annealed test samples (samples before tempering) were tested in a modified coaxial bending test [DIN EN 1288, SCHNEIDER 2001] to determine the bending strength at the edges or chamfers of the holes.

II. HOLE GEOMETRY AND TEMPER STRESS DISTRIBUTION IN THE HOLE AREA

For architectural glass, usually two types of holes are used: cylindrical and conical holes. The diameter of the holes depends on different types of glass fittings.

Table 1 shows the geometry of the holes from the three producers A, B and C, the number of tested samples and stress rates for the tests (see chapter III). All samples had a nominal thickness of 10 mm and were stored in a box outside in the same conditions for approx. 3 months after drilling. Figure 1 shows a typical test sample after the drilling process, figure 2 the breaking pattern of the glass after the bending test.

Table 2 shows the results of the measured thickness of all samples from the different test series. It is interesting to note that the thickness of all soda-lime-glasses just meet the allowable lower tolerance given in the standards (10 mm – 0,2 mm = 9,8 mm). This is important for stress calculations from bending.

Table 3 shows the measured surface compression stresses for all tempered samples from producer A and B (soda-lime-glass) in the “infinite area” in comparison with numerical results at the edges/ chamfers of the holes. For the numerical calculations, the apparent heat transfer coefficient was re-calculated iteratively from the mean value of the surface stress from photoelastic measurements in the “infinite area” of the samples. *Apparent* means that the effects from heat radiation were neglected in this study as they are of minor influence for the given thickness. It resulted in 150 W/m²K for series A and in 200 W/m²K for series B. In the borehole area, a different heat transfer coefficient was applied. It was reduced by 50 W/m²K (100 W/m²K and 150 W/m²K, respectively) considering the results of stress measurements in the borehole area from [LAUFS 2000]. For both cylindrical and conical holes it was assumed to be constant in the hole area. This is not strictly true for conical holes where a division in three parts (infinite area, cone area, cylindrical area) could be made. Figure 3 shows typical results of 3-D tempering simulations for a cylindrical and a conical hole of test series A. For calculations with borosilicate glass, the heat transfer coefficient was assumed to be 500 W/m²K which is the maximum for air quenching achievable [SCHERER 1986]. The surface stress of borosilicate glass could not be measured due to the different stress optical coefficient of the glass.

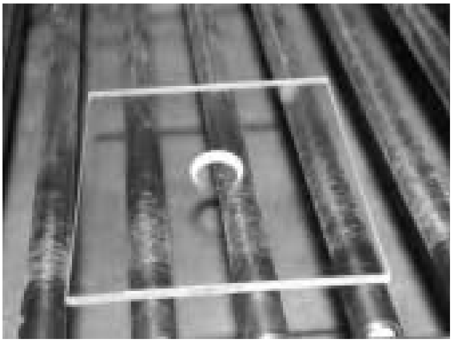

Figure 1: Typical test sample after drilling process (tempered soda-lime glass)

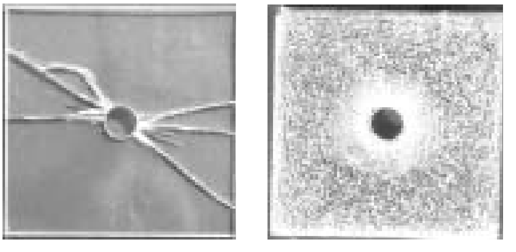

Figure 2: Breaking pattern of test samples after coaxial double ring bending test,
left: float glass, right: tempered glass

Results from table 3 and figure 3 show, that the surface compression stress near the chamfers of the holes is slightly higher than in the infinite area (approx. 10% to 15%) but that - for the chosen heat transfer coefficients - inside the holes in the centre (half the thickness of the pane) the surface stress is lower. Also, on the surface, close to the holes, in an area of about half the thickness of the pane, compression stresses are slightly lower than in the infinite area of the pane. Here tangential membrane stresses at the edges of the holes use some of the surface stresses to get in equilibrium. Similar results were obtained in [LAUFS 2000, SEDLACEK 1999]. Therefore, the glass strength for bending in the area of the holes should be approximately equal to the strength of the infinite plate. For in-pane loading with maximum stresses in the centre of the holes glass strength should be lower.

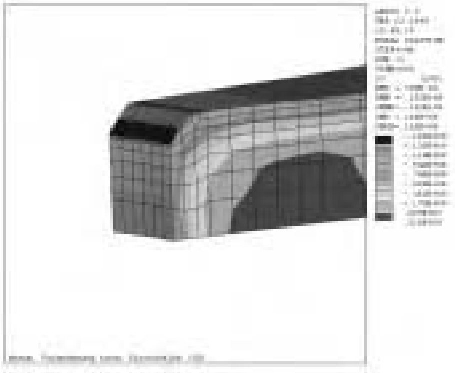

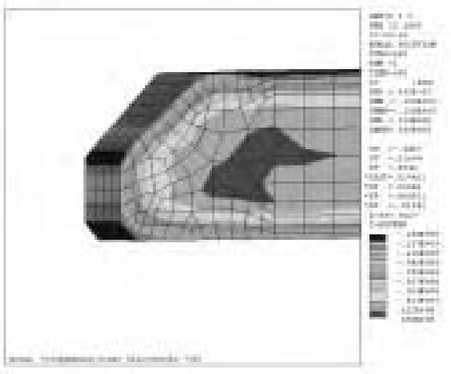

Figure 3: Test series A: Principal compression stress at the edge of a hole (glass thickness 10 mm).
Above: cylindrical hole ∅ 46 mm (for symmetry reasons, only one half of the thickness was modelled),
Below: conical hole ∅ 57 - 46 mm, [N/m²]

TABLE 1:
TEST SERIES AND GEOMETRY OF HOLES TESTED

pr.	test series / type (F= annealed float glass, E= tempered float glass)		nominal thick-ness [mm]	number of sam-ples	stress rate [MPa·s^{-1}]	con. (CO) or cyl. (CY) part under tension	hole dia-meter [mm]	hole geometry
A	A.F1 A.E1 A.F2 A.E2	conical hole with chamfer, diamond drilled, soda-lime-silica-glass	10	40 39 43 39	2,0	CY CO	57 (con. part) 46 (cyl. part)	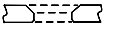
	A.F3 A.E3, A.F4 A.E4 A.F5 A.E5	cylindrical hole with chamfer, diamond drilled, soda-lime-silica-glass	10	30 30 30 30 33 36	0,2 2,0 20,0		46	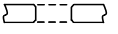
	A.F6 A.E6	cylindrical hole without chamfer, water-jet drilled, soda-lime-silica-glass	10	30 33	2,0		46	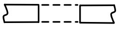
B	B.F1 B.E1 B.F2 B.E2 B.F3 B.E3 B.F4 B.E4 B.F5 B.E5 B.F6 B.E6	conical hole with chamfer, diamond drilled, soda-lime-silica-glass	10	35 33 33 32 31 30 31 32 32 33 31 31	0,2 2,0 20,0 0,2 2,0 20,0	CY CO	32 (con. part) 22 (cyl. part)	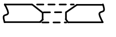
C	C.F1 C.E1 C.F2 C.E2 C.F3 C.E3	cylindrical hole with chamfer, diamond drilled, borosilicate glass	10	31 29 29 29 29 29	0,2 2,0 20,0		40	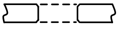

TABLE 2:
MEASURED THICKNESS OF ALL SAMPLES

Test Series	no. of samples	maximum value [mm]	minimum value [mm]	mean value [mm]	standard deviation [mm]	coeff. of variation [-]
A	413	9,97	9,78	9,86	0,03	0,004
B	384	10,08	9,75	9,93	0,08	0,008
C	183	10,25	9,95	10,07	0,06	0,006

TABLE 3:
SURFACE STRESSES OF TEMPERED GLASSES, MEASURED BY PHOTOELASTIC MEASUREMENTS VS. COMPUTED SURFACE STRESSES AND COMPUTED STRESSES AT THE CHAMFER

Test Series	no. of samples	measured mean value [MPa]	**infinite area** measured standard dev. [MPa]	5%-fractile [MPa]	**infinite area** computed surface stress [MPa]	**hole area** computed stress at edge/ chamfer [MPa]
A	207	127	17	98	130	152
B	191	160	8	146	150	166
C	-	n.a.	n.a.	n.a.	50	55

III. EXPERIMENTAL EVALUATION OF THE BENDING STRENGTH IN THE BOREHOLE AREA

A. Test set-up

To avoid all uncertainties of the theoretical determination of the glass strength caused by the surface condition after the drilling process and by the tempering process, the experimental set-up shown in figure 4 was used. The advantage of this set-up is a constant distribution of tensile stresses at the edge or chamfer of a hole so that the maximum surface flaw and/ or minimum temper stress will always be detected. The different types of holes in annealed and tempered soda-lime-glass and borosilicate glass from table 1 were tested at different stress rates. Figure 5 shows the boundary conditions of a finite-element-model of the test. Figure 6 shows the stress distribution of the principal tensile stress around the hole.

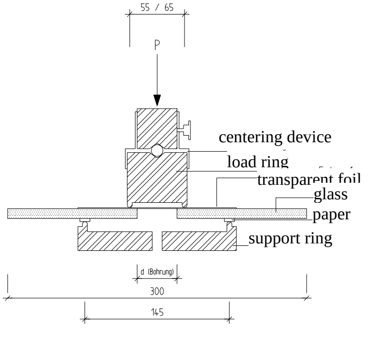

Figure 4: Section of experimental set-up: Modified coaxial double-ring bending test [mm]

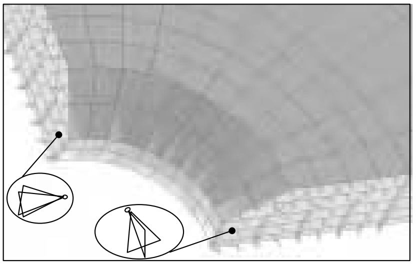

Figure 5: Finite-element model of the coaxial double ring bending test for a conical hole with static boundary conditions (1/4 of a sample, symmetry)

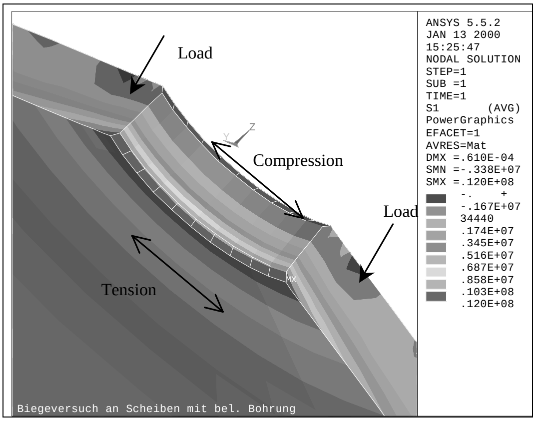

Figure 6: Stress distribution at the chamfers of a cylindrical hole in a coaxial double-ring bending test

B. Test results

Failure occurred at the edges or chamfers for nearly all test samples. Table 5 gives the results of the bending strength. 5%-fractiles were calculated for a 95% confidence interval [PLATE 1993]. Note that a logarithmic normal distribution was used instead of a Weibull-distribution to calculate fractiles, because the evaluation of the experimental data for both float and tempered glass clearly showed that a Weibull-distribution – especially for low fractiles - does not fit the data as well as a logarithmic normal distribution (Figures 7, 8).

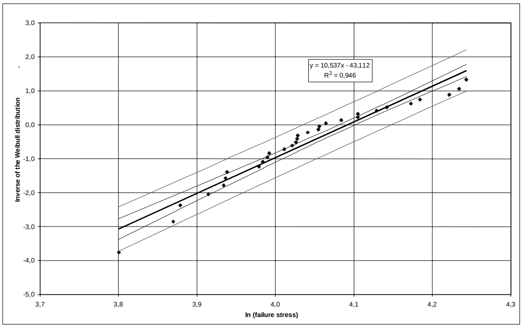

Figure 7: Fit of failure stress of series A.F4 to the Weibull distribution with linear regression and confidence intervals

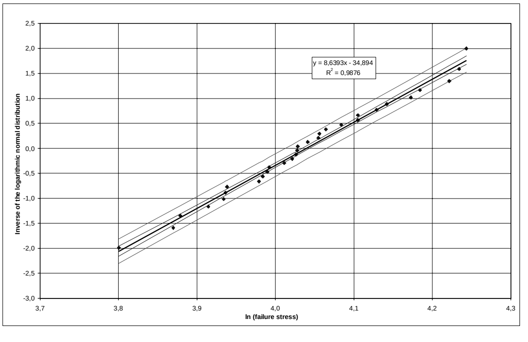

Figure 8: Fit of failure stress of series A.F4 to the logarithmic normal distribution with linear regression and confidence intervals

TABLE 5:
BENDING STRENGTH AT THE EDGES/ CHAMFERS OF ANNEALED AND TEMPERED GLASS WITH HOLES

Test Series		stress rate [$MPa \cdot s^{-1}$]	mean [MPa]	standard deviation [MPa]	coefficient of variation [-]	5% fractile [MPa]
A.F1	annealed	2,0	59,5	4,6	0,08	49,8
A.F2		2,0	56,7	6,1	0,11	44,3
A.F3		0,2	51,5	4,6	0,09	41,5
A.F4		2,0	57,1	6,3	0,11	43,4
A.F5		20,0	66,6	6,2	0,09	53,4
A.F6		2,0	45,8	9,4	0,21	25,3
A.E1	tempered	2,0	193,2	14,9	0,08	162,1
A.E2		2,0	167,3	11,2	0,07	143,9
A.E3		0,2	173,0	11,1	0,07	146,1
A.E4		2,0	185,5	8,8	0,05	166,3
A.E5		20,0	187,9	10,0	0,05	166,7
A.E6		2,0	195,2	14,6	0,07	163,8
B.F1	annealed	0,2	61,3	6,2	0,10	48,3
B.F2		2,0	67,3	6,5	0,10	52,9
B.F3		20,0	67,5	6,1	0,09	54,4
B.F4		0,2	79,0	12,6	0,16	52,2
B.F5		2,0	94,9	11,3	0,12	70,8
B.F6		20,0	105,6	10,7	0,10	82,9
B.E1	tempered	0,2	204,2	10,1	0,05	182,6
B.E2		2,0	215,8	8,1	0,04	198,5
B.E3		20,0	221,4	10,6	0,05	198,2
B.E4		0,2	234,6	14,0	0,06	204,2
B.E5		2,0	250,1	16,4	0,07	214,6
B.E6		20,0	265,2	13,9	0,05	236,4
C.F1	annealed	0,2	42,5	3,0	0,07	36,1
C.F2		2,0	45,3	5,0	0,11	34,5
C.F3		20,0	54,9	5,3	0,10	42,9
C.E1	tempered	0,2	163,0	10,6	0,06	145,6
C.E2		2,0	167,7	10,0	0,06	140,1
C.E3		20,0	177,2	11,6	0,07	151,9

C. *Discussion of the results*

For float glass, the bending strength mainly depends on the drilling process. Holes manufactured by producer A show lower mean values than glasses without holes from literature (approx. 60–120 MPa, [FINK 2000, LAUFS 2000, SCHNEIDER 2001]) but 5 %-fractiles are in the range of the bending strength defined in the standards (45 MPa, [DIN 1249]) because the scattering is very low. So the drilling process reduces the mean value but at the same time reduces scattering. Only for holes drilled with water-jet without a chamfer, mean values and 5 %-fractiles are significantly lower which corresponds to bigger surface flaws at the edges resulting from this drilling process [WÖRNER 2001].

Glass of producer B gives higher values and even 5 %-fractiles are higher than 45 MPa. This phenomenon could be explained by the different drilling process or by a "better" basis glass; the origin of the soda-lime-glasses of both producers A and B were unknown. It is also interesting with the results from series B that significantly lower values result from holes with the cylindrical part under tension for both float and tempered glass. A reason for this could be that in this drilling process the driller goes through the whole plate from the conical side and the chamfer on the cylindrical side is done in a second process. This could cause bigger surface flaws. The holes from producer A are drilled from both sides simultaneously.

Float glass from borosilicate glass (producer C) shows lower values than the soda-lime float glasses which is in contrast to results from literature [EXNER 1982]. The reason for this could also be the drilling process.

For all tempered glasses, the bending strength in the hole area is higher than the 5 %-fractile defined in the standards (120 MPa, e.g. [DIN 1249]) - even for tempered borosilicate glass although the amount of temper stress was significantly lower than for soda-lime-glass due to a lower thermal expansion coefficient. It is not possible to clarify if the higher compression stresses at the edges/ chamfers calculated in the numerical models (Figure 3) are the reasons for the relatively high bending strength. Also a – for glass - very low scattering of the test results causes higher 5 %-fractiles, so both effects cannot be separated.

From the difference in the results from different stress rates, the crack propagation factor N for sub-critical crack growth could be calculated for the annealed glasses and compared to data from literature. It resulted in approx. N=17 for series A and C and N=21 for series B. Usual values for annealed soda-lime-glass are N=18 and for annealed borosilicate-glass N=30. For tempered glasses, sub-critical crack growth only occurs at stresses above the temper stress. As design stresses of tempered glasses are well below the temper stress, the determination of the crack propagation factor for tempered glasses is not interesting from an engineering point of view.

It is interesting to note for holes drilled with water-jet (test series A.F6 and A.E6, table 5) that after tempering the bending strength is in the same range as for holes drilled with diamond drillers whereas before tempering this samples showed the lowest values. It is assumed that crack healing originating from the tempering process plays an important role for the glass strength of tempered glass [DANNHEIM 1991, LAWN 1993, STAVRINIDIS 1983, WIEDERHORN 1970].

IV. CONCLUSION AND FURTHER RESEARCH

Results show that finite-element-calculations in combination with photoelastic measurements give a good approximation about the qualitative distribution of temper stresses in the borehole area. Parameter studies and strength tests can be used where the heat transfer coefficient is unknown. For more detailed numerical simulations of thick glasses the effect of heat radiation, especially in the in the holes, should be considered.

Simulations show that temper surface stresses at the chamfers of holes are at least as high as in the "infinite" part of the plate whereas the surface stresses are presumably lower in the centre part of the holes. This was corroborated by the results of the bending strength. Still, it could be shown by the comparison of the bending strength of annealed glasses and tempered glasses (identical samples, annealed or tempered) that the influence on the scattering of the bending strength caused by a variation of the temper stresses from the technical process and caused by the surface condition of different drilling processes cannot be identified separately. Therefore, only with the large number of test samples and bending tests, design values for engineers can be calculated on a statistical basis for different glasses, drilling and tempering processes. In this study, the bending strength in the borehole area of tempered glass was higher than the 5%-fractile for tempered glass according to German or European standards (120 MPa) for all glasses and tempering processes.

Samples of a soda-lime-silica glass with water-jet drilled holes gave the lowest strength values for float glass but reached the same strength as diamond drilled holes for tempered glass for an identical basis glass and tempering process. Therefore it is assumed that crack healing while tempering plays an important role for tempered glass strength.

Further research should concentrate on crack healing from tempering, glass strength for in-plane loading and the interaction of glass fittings with glass for the determination of load-bearing capacity of glazing systems.

REFERENCES

[ABEN 1993]
ABEN, H., GUILLEMET, C., *Photoelasticity of Glass*, Springer, Berlin 1993

[ANSYS 1999]
ANSYS 5.5.2, *Theory Reference 4.6: Viscoelasticity*, Eigth Edition, 1999.

[BATHE 1990]
BATHE, K.J., *Finite-Elemente-Methoden*, Berlin, Springer, 1990.

[CARRE 1997]
Carré H., *Le verre trempé, un nouveau matériau de structure*. Cahiers du CSTB, Livraison 385, Cahier 3003, 1997.

[CARRE 1999]
CARRÉ H., DAUDEVILLE, L., *"Load-bearing capacity of tempered structural glass"*, Journal of Engineering Mechanics, Vol. 125 (1999) No. 8, pp. 914-921.

[DANNHEIM 1991]
DANNHEIM H., OEL H.J., PRECHTL W., *"Einfluß der Vorspannung auf die Oberflächendefektentstehung bei thermisch vorgespannten Flachgläsern"* Glastechnische Berichte, Vol. 54 (1981) No. 10, pp. 312-318.

[DIN 1249]
DIN 1249-10, Flachglas im Bauwesen, *Chemische und physikalische Eigenschaften*. Berlin, Beuth, 1990.

[DIN EN 1288]
DIN EN 1288-5, Glas im Bauwesen - Bestimmung der Biegefestigkeit von Glas – Teil 5, *Doppelring-Biegeversuch an plattenförmigen Proben mit kleinen Prüfflächen.* Berlin, Beuth, 2000.

[DUFFRENE 1997]
DUFFRÈNE L., GY R., *"Viscoelastic constants of a soda-lime-silica glass"* Journal of Non-Crystalline Solids, Vol. 211 (1997), pp. 30-38.

[EXNER 1982]
EXNER G., LINDIG O., *"Bestimmung des Widerstandswertes der Spannungsrißkorrosion n an Borosilicatglas DURAN"*, Glastechnische Berichte, Vol. 55 (1982) No. 5, pp. 107-117.

[FINK 2000]
FINK A., *Ein Beitrag zum Einsatz von Floatglas als dauerhaft tragender Konstruktionswerkstoff.* Dissertation (PhD-thesis), Institut für Statik, Technische Universität Darmstadt, 2000.

[GY 1994]
GY R., DUFFRÈNE L., LABROT M., *"New insights into the viscoelasticity of glass"* Journal of Non-Crystalline Solids, Vol. 175 (1994) pp. 103-117.

[KURKJIAN 1963]
KURKJIAN C.R., *"Relaxation of torsional stress in the transformation range of a soda-lime-silica glass"*, Physics and Chemistry of Glasses, Vol. 4 (1963) No. 4, pp. 128-136.

[LAUFS 2000]
LAUFS W., *Ein Bemessungskonzept zur Festigkeit thermisch vorgespannter Gläser.* Dissertation (PhD-thesis), Lehrstuhl für Stahlbau der RWTH Aachen, Shaker-Verlag, 2000.

[LAWN 1993]
LAWN B., *Fracture of brittle solids.* 2nd edn., New York, Cambridge University Press, 1993.

[NARAYANASWAMY 1971]
NARAYANASWAMY O.S., *"A Model for Structural Relaxation in Glass"*, J. Am. Ceram. Soc., Vol. 54 (1971) No. 10, pp. 491-498.

[NARAYANASWAMY 1978]
NARAYANASWAMY O.S.: *"Stress and Structural Relaxation in Tempering Glass"*, J. Am. Ceram. Soc., Vol. 61 (1978) No. 3, pp. 146-152.

[OEL 1984]
OEL H., HELLAND G., DANNHEIM H., *"Thermisches Vorspannen von Glasscheiben"*, Glastechnische Berichte, Vol. 57 (1984) No. 1 pp. 1-6.

[ÖKSOY 1994]
ÖKSOY D., PYE L.D., BOULOS E.N., *"Statistical analysis of viscosity-composition data in glassmaking."* Glass Science & Technology, Vol. 67 (1994) No. 7, pp. 189-195.

[PLATE 1993]
PLATE E.J., *Statistik und angewandte Wahrscheinlichkeitslehre für Bauingenieure.* Berlin, Ernst & Sohn, 1993.

[SCHERER 1986]
SCHERER G.W., *Relaxation in Glass and Composites.* New York, Wiley, 1986.

[SCHNEIDER 2001]
SCHNEIDER J., *Festigkeit und Bemessung punktgelagerter Gläser und stoßbeanspruchter Gläser.* Dissertation (PhD-thesis), Institut für Statik Technische Universität Darmstadt, 2001.

[SCHNEIDER 2004]
SCHNEIDER J, *"Glass Strength in the Borehole Area of Annealed Float Glass and Tempered Float Glass"*, The International Journal of Forming Processes (IJFP), Special Issue on Glass (2004), in print

[SEDLACEK 1999]
SEDLACEK G. LAUFS W. *"Stress distribution in thermally tempered glass near the edge, corner and hole, part 2: Distribution of thermal stresses."* Glass Science & Technology, Vol. 2 (1999), pp. 42-48.

[SOULES 1987]
SOULES T.F., BUSBEY R.F., REKHSON S.M., MARKOVSKY A., BURKE M.A., *"Finite Element Calculation of Stresses in Glass Parts Undergoing Viscous Relaxation"*, J. Am. Ceram. Soc., Vol. 70 (1987) No. 2, pp. 90-95.

[STAVRINIDIS 1983]
STAVRINIDIS B., HOLLOWAY D.G., *"Crack Healing in Glass."* Phys. and Chem. Glasses, Vol. 24 (1983) pp. 19-25.

[WIEDERHORN 1970]
WIEDERHORN S.M., TWONSED P.R., *"Crack Healing in Glass."* Proc. 72nd Ann. Meeting, The Am. Ceram. Soc., 1970, p. 486-489.

[WÖRNER 2001]
WÖRNER J.D., SCHNEIDER J., "Glass Strength of Annealed an Tempered Structural Glass in the Area of Drilled holes." *Proc. 7^{th} Glass Processing Days Tampere Finland*, 2001, p. 193 – 198.

EU COST C13 Glass and Interactive Building Envelopes. M. Crisinel, et al. (Eds.). IOS Press, 2007.

Buckling-related Problems of Glass Beams

Jan Belis and Rudy Van Impe
Laboratory for Research on Structural Models, Ghent University

At different research institutes in and outside Europe, research is in progress to find pieces of the structural glass puzzle. At Ghent University, the focus is on glass beams.

In the present contribution, the authors want to highlight some experiences of the past and current activities concerning buckling problems of glass beams. It is the authors' opinion that at the current state of technological development, glass beams with a rectangular cross-section are by far the most realistic starting-point. Such geometry implies a slender cross-section, which is sensitive to lateral-torsional buckling.

Some concepts are compared in order to deal with lateral torsional buckling of laminated glass beams.

By means of experimental tests on monolithic glass beams and numerical simulations on corresponding models, it has become clear that stability (buckling) instead of strength can be the limiting factor of the load-carrying capacity of glass beams, especially if strengthened or tempered glass is used.

It is also shown that prevention of buckling can increase the load-bearing capacity considerably. Several configurations for buckling prevention are proposed and compared, varying from fixed local supports to continuous supports comparable to elastic foundations. In many cases, the elastic sealants used to connect the beam to the supported glass plates suffice to realize the desired buckling prevention. This support is not brought into account in today's practice.

Keywords: glass, beams, buckling, laminate

I. Introduction

The material glass is developing towards a very popular all-round building material, able to fulfil an infill, cladding and structural role. The structural use of glass in the sense of primary load-carrying components however, lacks design recommendations , codes and standards.

Although some researchers are currently experimenting with alternative geometries, the basic (and actually by far the most-used) glass beams have an approximately rectangular cross-section. In many cases this cross-section is quite slender, which makes it rather sensitive to lateral torsional buckling.

II. LATERAL TORSIONAL BUCKLING

A. General

In the scarce literature on load-bearing glass beams, the failure mechanism that is usually examined is brittle fracture due to exaggerated tensile stresses at the edge. These stresses are induced by simple bending along the strong axis, so the beam is supposed to deform only in its own plane. In experiments described in literature [Hess 2000], [Veer et al. 2001], precautions are taken in order to prevent lateral torsional buckling: lateral supports are provided along the length of the beam, excluding any out-of-plane movement.

Due to the slenderness of the rectangular cross-section, however, the risk of instability –especially lateral torsional buckling- increases [Kasper et al. 2003], [Belis et al. 2003], [Luible 2004]. In favour of general comprehensibility, lateral torsional buckling is briefly illustrated in Figure 1, in which the combined action of out-of-plane displacement u, in-plane displacement v and torsion angle φ due to a post-critical in-plane load P is indicated.

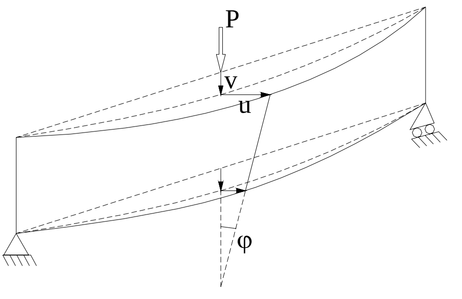

Figure 1: Principle of lateral torsional buckling of a beam

Lateral torsional buckling can be the factor that limits the load-bearing capacity instead of fracture due to in-plane bending.

B. *Structural Analysis*

Numerical analyses are performed with the finite elements software Abaqus [HKS 2002]. The mesh and element type have been chosen after an optimisation study.

The numerical analysis of lateral torsional buckling can be performed on different levels of complexity, which are briefly explained below.

1) Elastic buckling analysis

The most simple approach is the elastic analysis, which assumes the glass to be perfectly straight, free of any residual stresses, and without set-up imperfections (e.g. loading eccentricity, initial inclination,…).

Analytical expressions for the elastic buckling approach can be found in literature, e.g. in [Timoshenko et al. 1961].

The elastic buckling load (theoretical critical load) and the corresponding buckling modes can be determined using elastic buckling analyses, which are basically eigenvalue calculations.

2) Non-linear buckling analysis

The buckling analysis becomes more realistic – and more complex– when realistic imperfections are taken into account. Non-linearity covers geometrical aspects like initial shape imperfections and loading eccentricity, as well as material-related aspects like residual stresses and visco-elastic interlayer behaviour. Only a few authors have published data on some of these parameters, so values should be adopted with care and only for a corresponding area of applicability [Laufs 2000], [Luible 2004], [Belis 2004.1]. Wherever possible, more data should be collected in a systematic way.

3) "Buckling strength" analysis

Some glass beams can show considerable lateral displacements without glass fracture when the critical buckling load has been reached. In that case, the glass beam failed due to lateral torsional buckling, but is still able to carry a load which is slightly higher than the critical load: the limited post-critical stability can offer some residual load-bearing capacity.

To indicate this phenomenon using the expression "buckling strength" is rather confusing, since it refers at the same time to an instability phenomenon (buckling) as well as to a material characteristic (strength). The authors would prefer to replace the expression "buckling strength" with "post-buckling strength".

4) Material properties

a) Glass

The glass is modelled as a linear elastic material in both the elastic and the non-linear analysis. At normal serviceability conditions regarding to temperature and time, this is in good correspondence with experimental results. The assumed values of 70 GPa for Young's module and 0.23 for Poisson's ratio are also generally accepted.

b) Interlayer

The material chosen for the adhesive layers in the numerical work is polyvinyl butyral (PVB), because it is probably the most common interlayer material at present. This polymer shows a more complex, visco-elastic behaviour with sensitivity to creep under long-term loadings and temperature-dependent reologic properties. The PVB properties used in the simulations can e.g. be adopted from [Van Duser et al. 1999].

For eigenvalue calculations the time effect plays no role, so "instantaneous values" are used for the PVB material properties. They are displayed in Table 1:

TABLE 1. PROPERTIES OF BUTACITE ACCORDING TO [VAN DUSER ET AL. 1999]

G_0	471 MPa
E_0	1310 MPa
ν_0	0.391 [-]

Hence that these values correspond only to the Butacite type, which can vary from other types of PVB.

For non-linear analyses, a real relaxation curve can be followed [Van Duser et al. 1999], [Luible 2004], [Belis 2004.1].

c) Boundary conditions

The beam is supported by fork bearings, which exclude any lateral displacement or sideways rotation of the cross-sections above the supports. Loading takes place as a concentrated load at mid span, because this loading case can be simulated as a reference in destructive experiments without too many practical problems. This concentrated load is divided equally amongst the different glass leafs in order to avoid initial eccentricity.

III. LAMINATED GLASS BEAMS

A. General

From a safety point of view, the practical use of monolithic glass beams is limited to some cases of glass fins used as stiffeners for glass facades. In general, laminated beams are obligatory for reasons of residual strength and avoidance of falling glass pieces, especially when they are used to support floors or roofs.

The actual structural component is a composite of glass alternated with transparent interlayers, usually PVB or resin. Although the total thickness of the composite can be higher compared to monolithic sections and the slenderness is possibly reduced, a study of the buckling behaviour of laminated glass beams seems very useful here too.

B. Parameters

The following geometric parameters are taken into account:

1) Span

The span of the beams is varied in a range from 2m to 4m. The authors are aware of the fact that standard production limits allow lengths up to 6m, but taking into account the relatively high cost of such specimens, lengths are limited to more “affordable” beams in order to allow comparative experimental tests in a later phase. The span-parameter is varied with incremental steps of 0.10 m.

2) Height

The height parameter is expressed in relation to the span. The aspect ratio is based on the acceptability of the dimensions and on the perception of built examples. The three aspects ratios that are withheld are 0.10, 0.15 and 0.20 times the span.

3) Glass thickness

The basic assumption is that only glass leafs with a load-bearing function are taken into account, which means that eventual thin glass panes with a solely protective function are abandoned. The following series of standard production thicknesses is implemented in the parametric study: 8, 10, 12 15 and 19 mm.

In this study, a laminated beam consists always of two identical glass layers interconnected by PVB. In the following, the value of the thickness of a beam consisting of e.g. two panes of 10mm will be referred to with “10mm”, even if the total glass thickness comes to 20mm.

4) Interlayer thickness

The standard production thickness of PVB interlayers is 0.38 mm. The combination of several stacked layers allows multiplication of this value. This is in particular useful for glass panes that have been subjected to thermal treatments, since residual stress-caused shape imperfections need to be intercepted by the thickness of the PVB when laminated beams are composed.

C. “Ideal” laminated beams

1) Parameter combination

The results of the analyses can be put in a series of three-dimensional graphs, representing the values of the critical load P_{cr} corresponding to different combinations of span and thickness for a given aspect-ratio of the height [Belis 2004.2].

A quick growth of the critical load is noticed when the thickness increases. Moreover, a steady decrease of P_{cr} becomes visible for higher values of the span. A less important influence of the height parameter can be mentioned. More details on the study of "ideal" laminated glass beams can be found in [Belis 2004.2].

2) Buckling or fracture?

For practical purposes, it is very useful for designers to know which failure mechanism is more critical: instability or strength. The results for the buckling loads are compared to the loads which cause tensile bending stresses that correspond to the strength of different types of glass. The strength of glass is a complex characteristic, which should be applied with great care and with respect to the type of glass, the way the glass element is used (as a beam or as a plate), the finishing of the edges, etc. A good overview is given in [Haas et al. 2004]. As an example, some design values are given of the own strength (i.e. the failure stress minus the pre-stress) of toughened glass according to [Laufs 2000], [Haas et al. 2004] in Table 2:

TABLE 2.

DESIGN VALUES FOR THE OWN STRENGTH OF GLASS, USED AS DIFFERENT STRUCTURAL COMPONENTS, ACCORDING TO (LAUFS 2000)

Glass used as	Strength [MPa]
Plate	17.1
Beam	18.3

In the example of a beam with 2m span and 0.2m height, values of the buckling loads are clearly higher than loads corresponding to fracture due to in-plane bending. For this geometry, it seems that buckling will not even happen for float glass.

However, the authors want to draw the reader's attention to the fact that until now a perfect geometry and instantaneous material properties are assumed. Results will change considerably for beams with realistic geometric imperfections and long-term effects. The picture is different for beams with higher values for span and height.

For thermally treated glass with the given ideal geometry, failure will always be due to buckling. The bending strength is only of importance in case of float glass.

3) Variation of PVB thickness

Curves for different PVB thicknesses showed analogous results. More of interest is the comparison of the effect of the interlayer thickness on the buckling loads. A higher thickness seems to cause a slight augmentation of the critical load. This effect is more accentuated for higher beams. However, again the authors remind the reader of the initial assumptions of perfect geometry and instantaneous material properties made here.

D. Imperfect laminated beams

Two major imperfections have been taken into account: shape imperfections and temperature/time effects.

1) Shape imperfections

Shape imperfections have been implemented in the FE model, based on the first buckling eigenmode. A range of amplitudes has been tested, in order to characterise the influence on the buckling load.

The results are of major importance. For reasonable shape imperfections –i.e. with amplitudes smaller than or equal to 1/400 of the span– the critical load is reduced to 75% of the value corresponding to "perfectly" shaped beams.

2) Temperature effects

The visco-elastic behaviour of PVB has been mentioned before. The main consequences in a structural context are creep and temperature dependency.

Practical values of Young's module and Poisson's ratio are derived from a Williams-Landell-Ferry equation. These values allow to estimate the structural behaviour under a load of long duration.

The effect is important: Buckling loads drop to only one quarter of their instantaneous value. It should be clear however, that this may vary when other types of PVB than Buctacite are used.

3) Combined effect of shape imperfections and long term loadings

Taking the two previous parameters together results in a quite realistic modelisation of glass beams. On the long term, the critical load drops to only 16% of its initial value. For more details the reader is referred to [Belis 2004.1].

IV. MONOLITHIC EQUIVALENTS FOR LAMINATED BEAMS?

A finite elements model of a laminated glass beam would initially be three dimensional, as was the case in the previous chapters. In this research in which a considerable amount of calculations is made, parametric studies last for the order of magnitude of one day. For this reason, alternative numerical models have been sought in order to reduce the required computing time.

Two different approaches are mentioned briefly below.

A. *First approach - Virtual stiffness*

1) Principle

The laminated beam is considered to be a fictitious beam: an imaginary monolithic section made of a homogeneous and isotrope material. The bending stiffness of this fictitious beam represents the combined effect of the bending stiffness of the glass, the deformation of the PVB, and the duration of loading. It is called the “virtual stiffness” E’I’, in which E’ represents the virtual Young’s modulus and I’ the virtual second moment of area.

The virtual bending stiffness is found from the comparison of the theoretical deflection of the fictitious monolithic material and the deflection of the laminate measured in the experiments

$$E'I' = \frac{11}{768}\frac{FL^3}{u_{midspan,experimental}} \qquad (1)$$

With Equation 1, the virtual bending stiffness can be determined on the basis of a four-point bending test, since both the force F and the deflection can be measured accurately.

By means of bending tests on laminated glass specimens, measured deformations and loadings are used to calculate the overall bending stiffness of the laminated glass beam.

In certain cases, the necessity of experimental tests can be replaced by a theoretical expression for bending of laminated glass sections, as proposed by Hooper [Hooper 1973]. The bending at mid span, valuable for four-point bending, is given by:

$$u_{midspan,theoretical} = \frac{11}{384}\frac{PL^3K_3}{E_gI} = \frac{11}{768}\frac{FL^3K_3}{E_gI} \qquad (2)$$

(For the calculation of the factor K_3 the reader is referred to [Hooper 1973].)

The good correspondence between theoretically and experimentally obtained Young’s moduli validates this operation.

The virtual bending stiffness can then be calculated as follows:

$$E'I' = \frac{E_gI}{K_3} \qquad (3)$$

Since I’ follows directly from the geometry of the glass beam, E’ can be obtained easily from equation (3). The virtual Young’s modulus found can directly be imported as a material property of a single layer shell finite elements model.

The stiffness of the interlayer and the corresponding structural behaviour of laminated glass beams is influenced by temperature conditions and duration of loading. The tests are performed at a constant room temperature and at different speeds of loading. The loading duration has been taken into account by performing continued bending tests during more than a daytime.

Next, the virtual stiffness is implemented in the finite elements computer model, built with ordinary single-layer Lagrange shell elements.

Due to the simplicity of the elements chosen, exaggerated computing times are avoided, even if very fine meshes are used. Since the basic numerical model properties are obtained experimentally, the accordance between numerical and experimental results for bending out-of-plane are very good.

2) Limitations

The virtual stiffness model works well for out-of plane bending of the geometries tested. However, when the focus is on buckling of glass beams, in-plane and out-of-plane bending combined with torsion have to be dealt with simultaneously. In most proposed expressions for lateral torsional buckling, torsional stiffness and bending stiffness are data that need to be inserted separately.

In an analogous way, virtual torsional stiffness properties can be determined experimentally in the laboratory.

In-plane bending experiences no significant influence of the presence of interlayers, since their bending stiffness is negligible. This means that the stiffness of the virtual monolith equals the actual in-plane bending stiffness as discussed above. Finding a suitable law to determine a correct balance between the two to unify them into one value that is needed in buckling expressions, is a difficult problem that has not been solved at this moment.

In principle the virtual stiffness model can be used to study second order effects as well. It does not allow, however, to include material non-linearity: residual stresses in a shell elements model cannot correctly simulate the residual stresses which are present in the different glass panels of a laminate. The simulation of visco-elasticity of the interlayer is limited to a single elastic value, corresponding to a fixed temperature or load duration.

B. Second approach - Laminated shell elements

1) Principle

Special shell elements with laminated section properties can be used in Abaqus [HKS 2002]. Properties and dimensions of the different glass and interlayers can be inserted in the program and connected to the laminated shell elements. The model is built with one set of elements, that is virtually planar, but which has the internal mechanical properties of the laminate.

2) Limitations

Like most simplified methods, this one too has its limitations regarding boundary conditions and applicability.

A direct consequence of working with laminated shell elements, is that shear deformations of the soft interlayers cannot be taken into account. The model will only give realistic results for loading cases where straight cross sections of the laminate will stay straight during and after deformation.

In terms of practical applications, the model could be useful for elastic buckling simulations of beams under normal or low temperature conditions, but above all for short-term loadings. As confirmed in many codes on laminated glass, long-term loadings coincide with considerable shear deformations in the laminated glass as a whole and in the interlayer in particular.

On the level of complexity of the numerical simulations, the same remarks are valid as for the virtual stiffness model (cfr. Supra).

V. Monolithic Glass Beams

A. General

The authors are aware of the fact that for practical applications, laminated glass beams will often be required. Since laminates consist of several individual glass panes held together with transparent interlayers, it is useful to examine single panes first. In the following chapter, the focus will be on the effect and relevance of common structural devices in the context of avoidance of lateral torsional buckling. Even if the obtained buckling loads for single and laminated beams may differ considerably, the general principle of buckling prevention stays valid for laminated glass beams as well.

Glass fins, which are meant to take horizontal loads acting on a glass façade, are often designed as a monolithic piece. In relation to wind pressure, which can be considered perpendicular to the surface it is acting on, the horizontal or vertical glass stiffeners will act like beams. For reasons of completeness, the authors mention that lateral torsional buckling could also occur to that kind of structural glass components.

B. Parameters

Basically, the same geometric parameters of span, height and glass thickness are used in the analysis as those already mentioned in §III.B (cfr. Supra). However, the range of these properties was rather limited, as will become clear below. Especially for the study of buckling prevention, extra parameters were introduced, like the type, number and position of lateral supports (cfr. Infra).

C. “Ideal” monolithic glass beams: possible actions in order to avoid buckling?

Most of the time a glass roof, ceiling or floor is connected to glass beams by means of point-wise fixations like bolted connections, or continuous elastic joints like sealants. Generally, such joints are applied to avoid a direct glass-on-glass contact and to introduce forces in a smooth way into the beam. However, both point-wise and continuous fixations fulfil a very important secondary structural role, which is often not counted on in the structural designing process. The horizontal support against out-of-plane movements of the beam, as realised at the same time by such joints, is of underestimated structural importance. Without any horizontal support, the compressed rim of the beam can buckle out-of-plane at a lower critical value of the applied load.

Numerical and experimental analyses show clearly that the overall load-bearing capacity of glass beams can be increased significantly when elastic joints are applied, as demonstrated in [Belis 2003].

However, caution is needed since most, but not all combinations of lateral restraints of the compressed rim result in a synergetic improvement of the total load-bearing capacity of the beam. Moreover, the numerical part published there covers only the elastic buckling analysis, which does not take the initial shape imperfections etc. into consideration (Cfr. Supra). In spite of this, a good correspondence was found with the analytical (elastic) expressions. A reason could be a very limited amplitude of the initial shape imperfections (“global bow”) of the tested glass specimens.

In the numerical simulations, small models (span x height x thickness = 1000 mm x 100 mm x 50 mm) are used as well as larger models (2100 mm x 400 mm x 10 mm). Loads are applied point-wise at mid span as well as uniformly distributed along the upper rim.

In order to simulate the effect of a continuous elastic joint with a varying stiffness, a continuous spring support along the upper rim is modelled. The spring stiffness k could be understood as the ability of the elastic joint to resist against lateral displacements of the glass beam.

A basic structural sealant is used in the experiments to realise the elastic joint. Different stiffnesses of the joint are simulated by testing connections at different stages of the curing process. A relationship is found between spring stiffness and curing time, so experimental results could be linked to numerical values.

Experimental results show that even a weak continuous connection results in a remarkable gain of buckling load, which is in complete agreement with numerical results.

Elastic joints, which connect glass beams with its superstructure, have an important positive effect on the buckling load. Especially for beams with a slender cross-section, the overall load-bearing capacity can be improved considerably.

Even joints with a relatively low stiffness, like e.g. sealants at a rather early stage in the curing process, can influence the results in a positive way. More details are given in [Belis 2003].

Results for “imperfect” glass beams covering second-order effects are not available yet, but they will be published by the authors soon.

VI. CONCLUSIONS

Geometric parameter analyses have been performed on “ideal” laminated beams, consisting of two glass layers and one PVB interlayer. The influence of the basic dimensions of the whole composite beam have been examined in a range that is relevant to practice.

The parameter that influences the buckling load most is the glass thickness. To a lesser extent, the height of the beam plays a similar role. Longer spans increase the buckling risk.

Elastic buckling of ideal glass beams seems to be the failure mechanism for beams with a slender cross-sections and a long span in case they are composed of thermally treated glass (heat-strengthened or fully tempered).

The buckling risk is considerably higher when imperfections are taken into account. Especially the “weakening effect” of PVB under long term loadings or under higher temperatures are important. Moreover, the influence of initial shape imperfections (which are present for fully tempered glass in particular) is not to be neglected. An important reduction factor has to be taken into account on computing the lateral torsional buckling load of realistic laminated glass beams.

Elastic joints, which connect glass beams with its superstructure, have an important positive effect on the buckling load. Especially for beams with a slender cross-section, the overall load-bearing capacity can be improved considerably.

VII. ACKNOWLEDGEMENT

The authors wish to acknowledge their colleagues at the Laboratory for Research on Structural Models, as well as Solutia and Glaverbel for their interest and support. In addition, Dr. Andreas Luible is acknowledged for his critical review and valuable comments.

REFERENCES

[Belis et al. 2003]
BELIS, J., VAN IMPE, R., LAGAE, G. AND VANLAERE, W., *Enhancement of buckling-load bearing capacity of glass beams by means of lateral restraints*, Struct. Eng. Mech., Vol. 15(5), pp. 495-511, 2003.

[Belis et al. 2004.1]
BELIS, J., VAN IMPE, R., DE MEESTER, B., LAGAE, G., KATNAM, K., "Stability Approach of the Dimensioning of Glass Beams", ISAAG International Symposium on the Application of Architectural Glass, Munich, 15-16 november 2004.

[Belis et al. 2004.2]
BELIS, J., VAN IMPE, R., LAGAE, G., "Parametric approach of buckling of load-bearing glass beams", Proceedings of ASEM'04 Advances in Structural Engineering and Mechanics, paper published on CD-ROM, pp. 1599-1608, Seoul, 2004.

[Haas et al. 2004]
HAAS, C., HALDIMANN M., *Entwurf und Bemessung von Tragelementen aus Glas – Wissensstandsbericht*, ICOM rapport 493, Lausanne, 2004.

[Hess 2000]
HESS, R., *Glastraeger*, vdf Hochschulverlag AG an der ETH Zürich, Zürich, 2000.

[HKS 2002]
HKS, *Abaqus User's Manuals version 6.3,* Hibbitt, Karlsson & Sorensen, USA, 2002.

[Hooper 1973]
HOOPER, *On the bending of architectural laminated glass,* International Journal of Mechanical Science, Vol. 15, pp. 309-329, 1973.

[Kasper et al. 2003]
KASPER, R., SEDLACEK, G., Structural use of glass beams, Glass Processing Days, pp. 312-315, Tampere, 2003.

[Laufs 2000]
LAUFS, W., *Ein Bemessungskonzept zur Festigkeit thermisch vorgespannter Gläser*, Schriftenreihe Stahlbau – RWTH Aachen Heft 45, Shaker Verlag, Aachen, 2000

[Luible 2004]
LUIBLE, A., *Stabilität von Tragelementen aus Glas*, dissertation, Thèse N° 3014(2004), EPFL, Lausanne, 2004

[Timoshenko et al. 1961]
TIMOSHENKO, S.P., GERE, J.M., *Theory of elastic stability*, McGraw-Hill Book Company, Inc., New York, Toronto, London, 1961.

[Van Duser et al. 1999]
VAN DUSER, A., JAGOTA, A., BENNISON, S.J., "Analysis of Glass Polyvinyl Butyral Laminates Subjected to Uniform Pressure", *J. Eng. Mech.*, april issue, pp. 435-442, 1999.

[Veer et al. 2001]
VEER, F., RIEMSLAG, TING, "Structurally efficient glass laminated composite beam", Glass Processing Days, pp. 363-367, Tampere, , 2001.

EU COST C13 Glass and Interactive Building Envelopes. M. Crisinel, et al. (Eds.). IOS Press, 2007.

Stability of Laminated Glass Beams

Ruth Kasper and Gerhard Sedlacek
RWTH Aachen – Institute of Steel Construction, Germany

The following paper summarizes the actions and the results of a research project concerning the behaviour of laminated glass beams.

Keywords: glass, laminated glass, glass beams, material data of PVB-foil, analytic calculation method

I. INTRODUCTION

Beams consisting of single glass panels either laminated glass panels are popular elements in modern architecture (Figure 1). The mechanical viewpoint is focused on the stability of laminated glass beams that is influenced by the behaviour of the interlayer. The interlayer is mostly consisting of PVB-foils that have a time and temperature dependent material characteristic.

Figure 1: Example

The stability behaviour of steel beams can be described by buckling curves. Buckling curves include geometrical and material imperfection and are based on tests or calculations. Buckling curves are evaluated by using the ultimate load carrying capacity.

The use of buckling curves is not appropriate for glass beams, in particular for beams consisting of laminated glass, as the ultimate load carrying capacity of a laminated glass beam depends on the loading rate and loading duration caused by the visco-elastic material properties of the PVB-foils. Additionally the influence of loading with different loading durations (e.g. self weight and wind load) can not be taken into consideration.

Caused by these reasons a design concept and a calculation method based on the theory second order have been developed to take the mentioned aspects into account [Kasper 2005].

II. PROBLEM AND PROCEEDING OF THE RESEARCH PROJECT

The idea of the calculation model was to describe the sandwich with equivalent stiffness I_z^{eq} (second moment of area) and I_T^{eq} (torsional stiffness). I_z^{eq} and I_T^{eq} depend on the actual PVB-foil-stiffness $G_F(t,T)$ that is influenced by the temperature and loading duration. The global behaviour of the beam can be described with the elastic bending and torsional theory. I_z and I_T of a beam consisting of a single glass panel can be replaced by the equivalent values I_z^{eq} and I_T^{eq}.

The proceeding of the research project was divided into the following steps:

1. Small scale tests to determine the time and temperature depending behaviour of the PVB-foil.
2. Original size lateral torsional buckling tests with beams (single glass panels and laminated glass panels).
3. Solving the equations of the elastic bending and torsional problem to describe the

buckling behaviour, the deformation of the beam in the space and to determine the additional stress determinant M_z^{II} of second order theory.

4. Application of the extended bending and torsional theory to determine the equivalent stiffness I_z^{eq} and I_T^{eq} of the glass sandwich and to calculate the stress distribution over the sections caused by M_z^{II}.
5. Numerical analysis to verify the theoretical model.
6. Development of a design concept which take into account different loading durations.

The investigations were focused on the load carrying behaviour of laminated glass beams with a visco-elastic interlayer. That is why no evaluation concerning the resistance of the glass has been carried out.

III. Properties of the PVB-foil

A. Introduction

The interlayer of laminated glass beams is mostly consisting of PVB-foils. PVB-foils have a significant visco-elastic material behaviour that is characterised by a time and temperature dependent material stiffness. Because of too little test results [Sobek 1998, Duser 1999, Schuler 2003] further tests were necessary to receive available data for the evaluation of the lateral torsional buckling tests with laminated glass beams.

B. Testing and results

A new test method has been used for the determination of material data. The test specimens were laminated glass panels (1100 mm x 360 mm). Comparable specimens are normally used for four-point-bending tests to determine the bending strength of glass [DIN EN 1288-3]. Compared with other test methods the advantage of the used test method is that the evaluated material data are based on a larger surface.

The test specimens were distorted to a constant angle ϑ. The torsional moment M_T was measured over the time. By using the equations derived by the extended bending and torsional theory the effective PVB-foil shear stiffness $G_F(t,T)$ could be determined depending on the angle ϑ and the torsional moment M_T. The tests have been carried out for different loading durations (up to 60 h) and different temperatures (-10°C up to 40°C) (Figure 2).

Figure 2: Test set-up for torsional tests

The evaluation of the test results shows the following:

1. The shear stiffness $G_F(t,T)$ depends highly on the temperature during the first hour of loading (Figure 3 and 4). After a loading duration longer than e.g. 20 hours the influence of temperature is anymore existing (Figure 5).

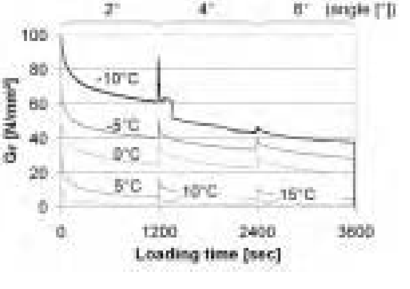

Figure 3: $G_F(t,T)$ (Variation of the angle and the temperature) – loading duration 1 h (T = -10°C–15°C)

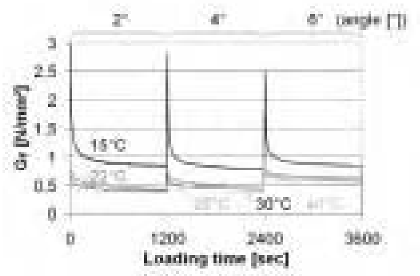

Figure 4: $G_F(t,T)$ (Variation of the angle and the temperature) – loading duration 1 h (T = 15°C–40°C)

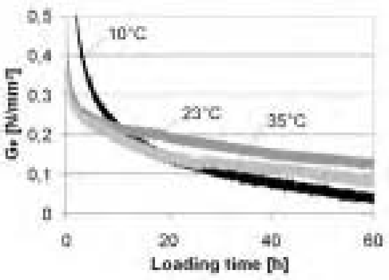

Figure 5: $G_F(t,T)$ (Variation of the temperature) – loading duration 60 h

2. The scatter of the PVB-foil shear stiffness $G_F(t,T)$ for a constant temperature was significant (Figure 6). The test results of repeated tests with one test specimen (equal test conditions) showed also a scatter (Figure 7). The shear stiffness $G_F(t,T)$ was not influenced by the order of the tests.

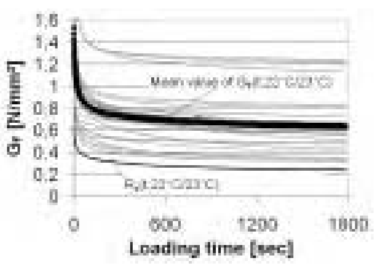

Figure 6: $G_F(t,T)$ – Statistical evaluation of all test results (T = 23°C)

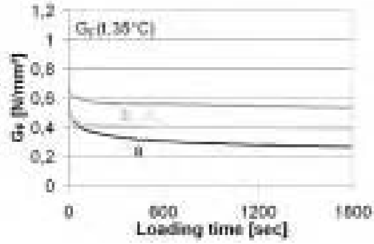

Figure 7: $G_F(t,T)$ – Repeated loading of one test specimen (T = 35°C)

3. The effective shear stiffness $G_F(t,T)$ was influenced by the temperature at the beginning of the tests. A following change of the temperature had only an influence on the relaxation time and not on the effective value of $G_F(t,T)$ (Figure 8)

.

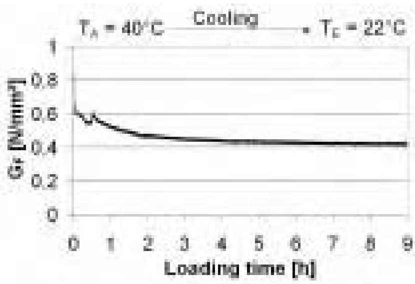

Figure 8: $G_F(t,T)$ – loading duration 9 h

C. Numerical description of the visco-elastic behaviour

For numerical simulations the visco-elastic behaviour can be described by using a prony series consisting of exponential elements. Additionally the property of the thermorheological simplicity can be used. Thermorheological simplicity means that the time-dependent material properties must be determined for one reference temperature T_{Ref} ("master curve"), e.g. a prony series, and can be converted to all further temperatures by using a shift function (e.g. William-Landels-Ferry) (Figure 9).

Shift function $$a_s = \frac{\tau(T)}{\tau_{Ref}(T_{Ref})}$$

WLF-equation $$\log a_s(T) = -\frac{C_1(T - T_{Ref})}{C_2 + (T - T_{Ref})}$$

with

C_1, C_2: calibration constants

τ: relaxation time at temperature T

τ_{ref}: relaxation time at the reference temperature T_{Ref}

[Duser 1999] gives the elements of a prony series for a reference temperature T_{Ref} evaluated by small scale tests and the coefficients for the shift function of William-Landels-Ferry for PVB-foils.

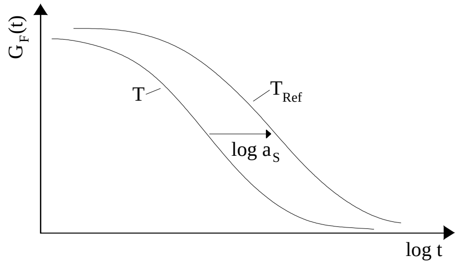

Figure 9: Principe of the time shift

For one specimen tested between -10°C and 40°C the theoretical approach has been applied. Figure 10 shows the test results for all measured temperatures represented in a logarithmic scalation.

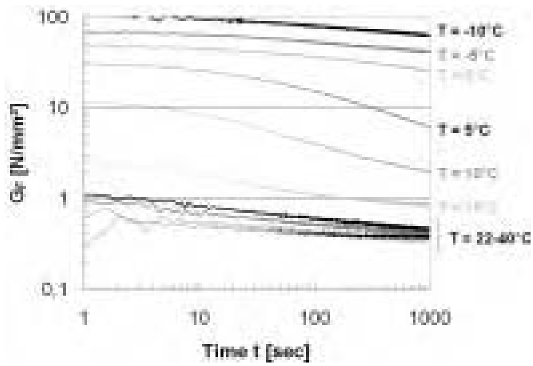

Figure 10: $G_F(t,T)$ (Variation of the angle and the temperature) – loading duration 1 h – logarithmic scalation

By using the shift function of Williams-Landel-Ferry (WLF) calibration constants have determined for the temperatures between 10°C and 40°C. Figure 11 shows the results of the calibration. The reference temperature was chosen to T_{Ref} = 22°C. In the temperature field near to the glass temperature (T_g = 10°C-15°C) the calibration constants had to be modified and the thermorheological simplicity was not valid.

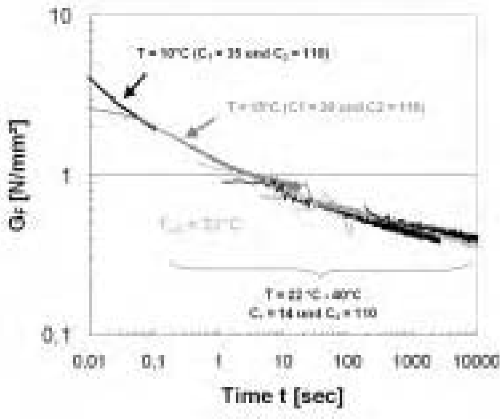

Figure 11: Application of the thermorheological simplicity on the test results

D. Conclusions

The test results can be used for further calculation of laminated glass panels with the interlayer PVB. The tests showed that the material properties of PVB scatter in a large range and that a temperature dependency after a loading duration longer than 10 h is not useful.

The tests and the evaluation of the results showed that numerical material descriptions can be used only with defined restrictions (e.g. temperature field and loading duration).

A comparison with existing test results showed that the formula of [Sobek 1998] give a good approach to describe the time and temperature behaviour for $T > T_g$. The formula is written as:

$$G_F(t,T) = 0{,}008 \cdot (100 - T) - 0{,}0011 \cdot (50 + T) \cdot \log(t)$$

with

T: temperature [°C]

t: time [sec]

IV. Lateral torsional buckling behaviour of glass beams

A. Introduction

For the investigation of the lateral torsional buckling behaviour of laminated glass beams tests with single glass panels as well as laminated glass panels have been carried out.

The tests with single glass panels were useful to assess the functionality of the test set-up and to verify the used finite element model. The advantage of this approach was that the test results could be evaluated without the influence of the PVB-foil. The results of this investigations are not demonstrated in this paper.

In the second step lateral torsional buckling tests with laminated glass have been carried out. The loading rate v_B [mm/sec] and the loading duration have been varied.

B. Testing and evaluation

For lateral torsional buckling tests the applied load F has to follow vertically and horizontally the load application point during the test. Caused by the restraints of the testing machine in Aachen the problem was solved by a test set-up with supports which can move horizontally whereas the load application point was horizontally fixed. At both ends of the beams the rotation about the vertical axis (z-axis), the rotation about the beam-axis (x-axis) and the horizontal displacement were free (Figure 12). During the tests the vertical deformation of the load application point, the horizontal deformations of the supports, the inclination at midspan and the strains at midspan were measured (Figure 13).

A disadvantage of the test set-up was that the results could not directly compared with the analytic solution based on second order theory caused by the changed boundary conditions.

Figure 12: Boundary conditions of the test set-up

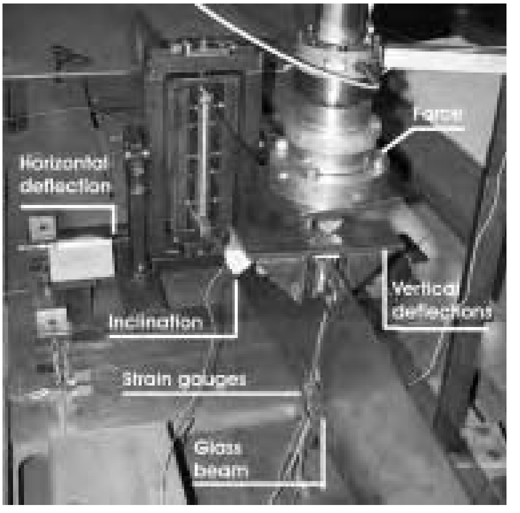

Figure 13: Test set-up of the lateral torsional buckling tests

The beam was loaded by controlling the displacement of the force application point. The lowest possible loading rate was v_B = 0,04 mm/sec. The fastest loading rate was chosen to v_B = 1,0 mm/sec. By reaching the highest load level, perceptible from the moment when the load augmentation was stopped, the displacement of the force application point has been stopped and the system was de-loaded with the same loading rate. Caused by the high slenderness of the beams the load capacities were mostly determined by the deformation of the system and not limited by the resistance of the material. This course of action was called “short time loading”. For the “long time loading” the augmentation of the displacement at midspan was stopped before the highest load level was reached. The displacement was fixed and the augmentation of the inclination, the horizontal deformations of the support and the strains at midspan were measured. The measured temperature during the tests was 23°C.

The evaluation has been made in two different ways (Figure 14). First, the tests were analyzed with a finite element simulation with an estimated elastic shear modulus $G_F(t,T)$=cte. This has been done for two different times: beginning and any time during the test. The load-deformation-curves and the load-stress-curves of the tests and the simulation have been compared (Figure 16) and the estimated shear modulus $G_F(t,T)$ have been compared with the results of the small scale tests. Second, the evaluation of the tests has been made by using the results of the small scale tests. The $G_F(t,T)$-formula of Sobek was modified in the way that a formula for $G_F(t,23°C)_{upper}$ and $G_F(t,23°C)_{lower}$ was reached (Figure 15). With these formulas a $M_{ki}(t,23°C)$-curve or rather $F_{ki}(t,23°C)$-curve could be calculated numerically and compared with the highest load levels and the load levels depending on the time.

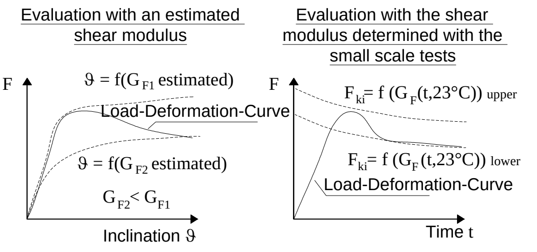

Figure 14: Evaluation of the test results

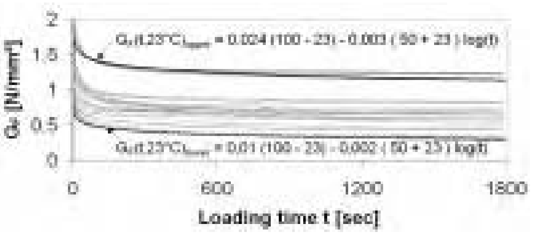

Figure 15: Modification of the $G_F(t,T)$-formula of [Sobek 1998]

Figure 16 shows an example for the evaluation method with the estimated shear modulus $G_F(t,T)$. Figures 17 and 18 show examples for the evaluation method with the $M_{ki}(t,23°C)$-curves based on $G_F(t,T)_{upper}$ and $G_F(t,T)_{lower}$ for short and long time loading.

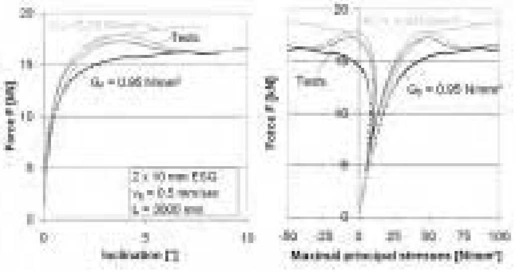

Figure 16: Test results (short time loading) – evaluation with an estimated $G_F(t,T)$-value

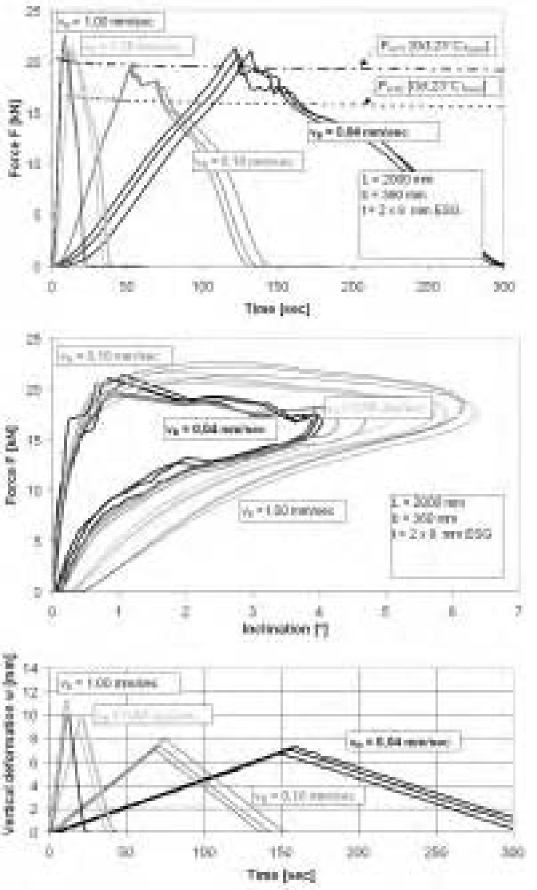

Figure 17: Test results (short time loading)

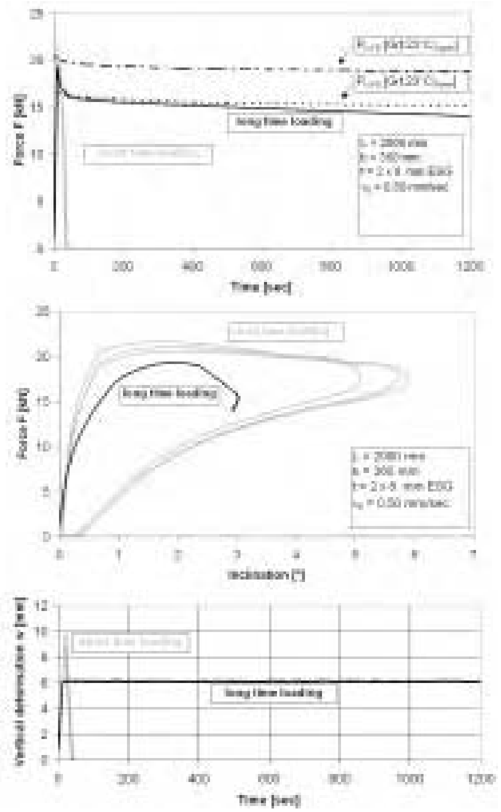

Figure 18: Test results (long time loading)

C. Conclusions

The investigations showed that the shear modulus $G_F(t,T)$ evaluated on the basis of the small scale tests was related to the results of the lateral torsional buckling tests. The loading capacities of the laminated glass beams were influenced by the loading rate: the higher the loading rate the higher was the loading capacity. This phenomenon can be explained by the relaxation time of the PVB-foil that is lower than the loading rate.

The test specimens have been used for several tests. By measuring the imperfections of the beams before testing it could be identified that the imperfection of the beam became larger after repeated testing.

The evaluation with the finite element simulation showed that the buckling behaviour could be described by using an elastic shear modulus $G_F(t,T)$.

V. Elastic Bending and Torsional Problem of a Beam Subjected to Bending

A. Introduction

The problems of stability and second order theory can be solved on the basis of the potential [Roik 1972]. The stability solution gives a value for the elastic critical moment M_{ki} of a perfect beam subjected to bending without any imperfections (Figure 19). In reality this value can not be reached caused by geometric imperfections of the beam. But M_{ki} must be known to limit the loading. To determine the realistic deformations and the stresses in the beam additionally a solution for the deformations must be evaluated. This can be done on the basis of second order theory applied on an imperfect beam with the initial imperfections v_0 and ϑ_0 (Figure 19).

For the calculation of the stresses in the section based on second order theory the stress resultants $M_y^{Th.I.} = M_y^{Th.II.}$ and $M_z^{Th.II.} = M_z^{Th.I.} \cdot \vartheta$ must be taken into account.

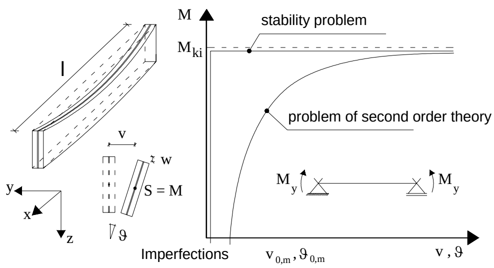

Figure 19: Stability problem and stress problem

Exemplary the solutions have been found for the load cases shown in Figure 20.

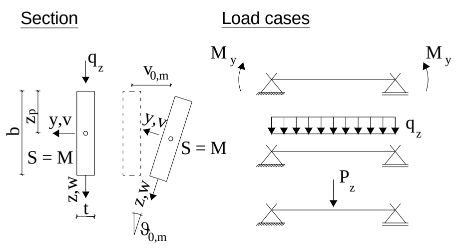

Figure 20: Load cases

The potential can be written as:

$$\Pi = \frac{1}{2}\int_0^{\ell}\left\{E \cdot I_z \cdot v_{,xx}{}^2 + E \cdot I_y \cdot w_{,xx}{}^2 + G \cdot I_t \cdot \vartheta_{,x}{}^2\right\}dx$$
$$-\frac{1}{2}\int_0^{\ell}\left\{-2 \cdot M_y(x) \cdot v_{,xx} \cdot \vartheta - q_z(x) \cdot z_p \cdot \vartheta^2 + 2 \cdot q_z(x) \cdot w\right\}dx$$
$$-\frac{1}{2}\sum_j \left\{P_{z_j} \cdot \left(2 \cdot w - z_{p_j} \cdot \vartheta(x_j)^2\right)\right\}$$

For the solution the deformations have been attempt sinusoidal.

$$v(x)^{Th.II} = a_1 \cdot \sin\left(\frac{\pi}{\ell}x\right)$$
$$w(x)^{TH.II} = a_2 \cdot \sin\left(\frac{\pi}{\ell}x\right)$$
$$\vartheta(x)^{Th.II} = a_3 \cdot \sin\left(\frac{\pi}{\ell}x\right)$$

B. Elastic critical moment

The following formulas give the solution for the elastic critical moments for the considered load cases.

M_y = cte:

$$M_{ki} = \frac{\pi}{\ell}\sqrt{E \cdot I_z \cdot G \cdot I_t}$$

q_z = cte and "P_z at midspan":

$$M_{ki} = M_y = \frac{1}{c_1} \cdot N_{ki}\left(\frac{1}{2} \cdot \frac{c_2}{c_1} \cdot z_p + \sqrt{\left(\frac{1}{2}\frac{c_2}{c_1} \cdot z_p\right)^2 + \frac{G \cdot I_t}{E \cdot I_z} \cdot \left(\frac{\ell}{\pi}\right)^2}\right)$$

Table 1 gives the accompanying coefficients.

Tab 1: Coefficients c_1 and c_2

Load case	c_1	c_2
q_z	$\frac{2}{3} + \frac{2}{\pi^2}$	$\frac{8}{\pi^2}$
P_z	$\frac{2}{\pi^2} + \frac{1}{2}$	$\frac{8}{\pi^2}$

C. Deformations based on second order theory

The deformations based on second order theory were evaluated by assuming sinusoidal initial imperfections v_0 and ϑ_0:

$$v_0(x) = v_0 \cdot \sin\left(\frac{\pi}{\ell}x\right)$$
$$\vartheta_0(x) = \vartheta_0 \cdot \sin\left(\frac{\pi}{\ell}x\right)$$

The solutions for the deformations v and ϑ of second order theory are:

My = cte:

$$\vartheta(x)^{Th.II} = \frac{\frac{M_y^2}{E \cdot I_z} \cdot \vartheta_0 + \left(\frac{\pi}{\ell}\right)^2 \cdot M_y \cdot v_0}{G \cdot I_t \cdot \left(\frac{\pi}{\ell}\right)^2 - \frac{M_y^2}{E \cdot I_z}} \cdot \sin\left(\frac{\pi}{\ell}x\right) \quad (6.2)\ (6.3)$$

$$v(x)^{Th.II} = \frac{\frac{G \cdot I_t}{E \cdot I_z} \cdot M_y \cdot \vartheta_0 + \frac{M_y^2}{E \cdot I_z} \cdot v_0}{G \cdot I_t \cdot \left(\frac{\pi}{\ell}\right)^2 - \frac{M_y^2}{E \cdot I_z}} \cdot \sin\left(\frac{\pi}{\ell}x\right)$$

qz = cte and "Pz at midspan":

$$\vartheta(x)^{Th.II} = \frac{\vartheta_0\left(\frac{c_1^2 \cdot M_y^2}{E \cdot I_z} - c_2 \cdot \left(\frac{\pi}{\ell}\right)^2 \cdot M_y \cdot z_p\right) + c_1 \cdot \left(\frac{\pi}{\ell}\right)^2 \cdot M_y \cdot v_0}{G \cdot I_t \cdot \left(\frac{\pi}{\ell}\right)^2 - \frac{c_1^2 \cdot M_y^2}{E \cdot I_z} + c_2 \cdot M_y \cdot z_p \cdot \left(\frac{\pi}{\ell}\right)^2} \cdot \sin\left(\frac{\pi}{\ell}x\right)$$

$$v(x)^{Th.II} = \frac{c_1 \cdot \frac{G \cdot I_t}{E \cdot I_z} \cdot M_y \cdot \vartheta_0 + c_1^2 \frac{M_y^2}{E \cdot I_z} \cdot v_0}{G \cdot I_t \cdot \left(\frac{\pi}{\ell}\right)^2 - \frac{c_1^2 \cdot M_y^2}{E \cdot I_z} + c_2 \cdot M_y \cdot z_p \cdot \left(\frac{\pi}{\ell}\right)^2} \cdot \sin\left(\frac{\pi}{\ell}x\right)$$

The coefficients c_1 and c_2 are given in table 1.

VI. SANDWICH SOLUTION BASED ON THE EXTENDED BENDING AND TORSIONAL THEORY

For the use of the equations derived by elastic bending and torsional theory for laminated glass beams, formulas for the second moment of area I_z^{eq} and the torsional stiffness I_T^{eq} are needed. For a monolithic section the formulas are known:

$$I_z = \frac{b \cdot t^3}{12}$$

$$I_t = \frac{b \cdot t^3}{3}$$

By using the "Extended bending and torsion theory" [Roik 1970, Scarpino 2002, Völling 2000] an equivalent stiffness I_z^{eq} and I_T^{eq} of the sandwich can be determined depending on the shear modulus $G_F(t,T)$ of the interlayer. To this end the basic degree of freedoms for monolithic sections were augmented by additional degrees of freedom due to the sandwich characteristics. Figure 21 shows the degree of freedoms of a monolithic section and the additional degree of freedoms of the sandwich for bending and torsion which have been used to solve the equations. The equations have been solved separately for bending and torsion for a laminated glass with two and three glass panels [Kasper 2004]. An extension of the solution is also possible for a laminated glass with more than three glass panels.

Figure 21: Basic and additional degree of freedom for bending and torsion

The equivalent torsional stiffness I_t^{eq} depends only on the geometry and the material characteristics of the sandwich. The second moment of area I_z^{eq} depends additionally on the type of loading and the length of the beam.

Beneath the equivalent stiffness I_z^{eq} and I_T^{eq} the solution gives also the needed equations for the evaluation of the torsional tests and calculation of the stress distribution caused by $M_z^{Th.II.}$.

The proceeding and the solutions are explained in detail in [Kasper 2005].

VII. Numerical Investigation

The numerical simulation for proving the theoretical model has been done with the FEM-program ABQAQUS. The glass and the PVB-foil have been modelled with 8-node-volume-elements. The material properties are for both materials (glass and PVB) elastic. The model was apart from the boundary conditions identically with the model used for the evaluation of the tests. Here, the force application point could move horizontally and the supports were fixed horizontally. The simulation has been carried out in two steps:

Step 1: Buckling of the system to determine the lowest eigenvalue and the associated eigenform.

Step 2: The displacements of the determined eigenform were scaled (e.g. L/1000) to the perfect beam. A geometric non-linear calculation has been carried out to determine the load-deformation-curves.

The theoretical model has been checked for single and laminated glass panels. The geometry of the beam (section values and length) as well as the stiffness of the interlayer have been varied. Figure 22 and 23 show exemplary a comparison between the finite element simulation and the theoretical model for single and laminated glass panels.

The theoretical model reach an good agreement on the numerical results for loading smaller than 80% of M_{ki}.

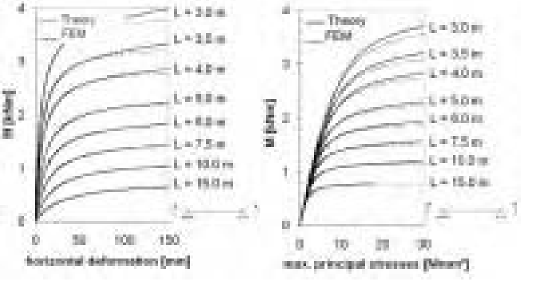

Figure 22: Comparison of the numerical results with the theoretical results (single glass panel, t = 10 mm, b = 500 mm)

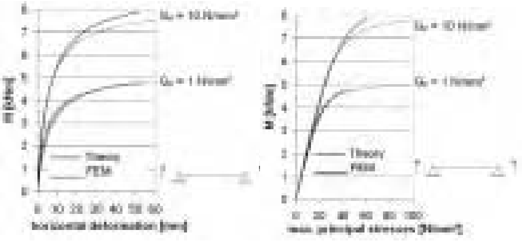

Figure 23: Comparison of the numerical results with the theoretical results (laminated glass panel, t = 2 x 8 mm, h = 1,52 mm, b =300 mm, l = 3000 mm)

VIII. DESIGN CONCEPT

The application of glass beams gives the problem that the loads are not active for the same loading durations. E.g. laminated glass beams in roof structures are loaded by the self loading of the glass construction and additionally by wind loading. For self loading the PVB-foil shear stiffness $G_F(t,T)$ is at the time $t = \infty$ equal to zero independent of the actual temperature. For wind loads with short loading duration the PVB-foil shear stiffness $G_F(t,T)$ can be chosen to e.g. 0,4 N/mm². Figure 24 shows the design model to take into account different loading duration with different effective shear modulus $G_F(t,T)$.

1a: The beam is loaded with the self weight of the structure M_1. At the beginning the effective shear modulus is $G_F > 0$.

1b: The deformations and stresses caused by self loading can be determined directly for the time $t = \infty$ with $G_F = 0$.

2: Before loading the system with e.g. wind loading, the system is de-loaded. For the de-loading curve the effective shear modulus is $G_F > 0$.

3: For the common effect of self loading + wind loading (M_2) the system with the new initial imperfections v_1 and ϑ_1 must be taken into account.

The imperfections v_1 and ϑ_1 can be determined with the following conditions:

$$v(M_1, v_0, \vartheta_0, G_F = 0) + v_0 \overset{!}{=} v(M_1, v_1, \vartheta_1, G_F > 0) + v_1$$
$$\vartheta(M_1, v_0, \vartheta_0, G_F = 0) + \vartheta_0 \overset{!}{=} \vartheta(M_1, v_1, \vartheta_1, G_F > 0) + \vartheta_1 \qquad (8.5)$$

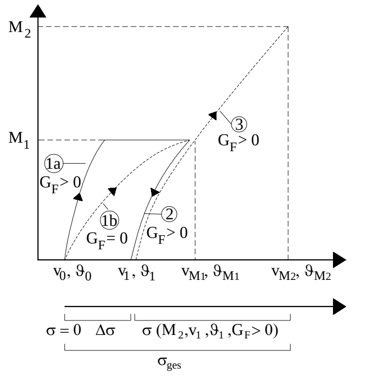

Figure 24: Consideration of loads with different loading duration

The theoretical analyse of different load cases (different moment distribution over the beam) can also be done by using the theoretical formulations. The critical moment must be limited to:

$$\frac{M_1}{M_{ki,1}} + \frac{M_2}{M_{ki,2}} < 0{,}8$$

The calculation procedure is shown in Figure 25.

IX. SUMMARY AND PROSPECTS

The paper summarizes the results of the DFG-project “Laminated glass beams” and the thesis “Tragverhalten von Verbundglasträgern”. The work shows possibilities for the design of laminated glass beams which can be applied also on columns or shear fields consisting of laminated glass.

The theoretical model can be extended for further load cases, e.g. restraint beams.

The advantage of the theoretical model is that an application for several interlayer is possible and an optimizing parameter studies can easily done. In opposite to buckling curves the serviceability of the structure can be analyzed directly. This is useful caused by the high slenderness of glass beams where the application is often limited by large deformations.

The used testing method (torsional tests) is a very simple possibility to determine the material data of different interlayer by using original size test specimens. The testing data can also be used for the design of laminated glass plates.

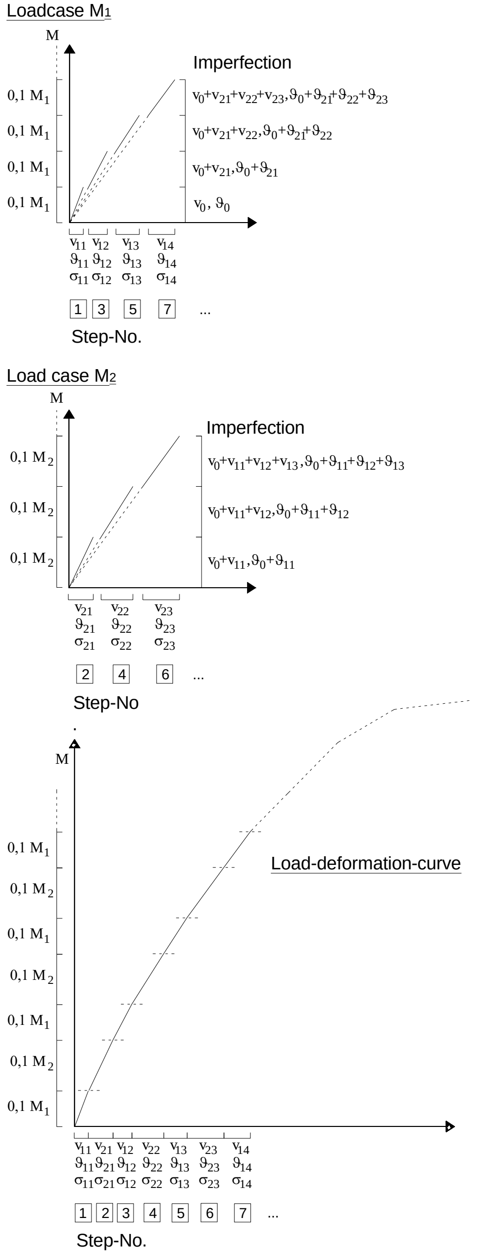

Figure 25: Consideration of loads effecting different stress resultants along the x-axis of the beam

X. Acknowledgment

The project has been carried out by the financial support of the “Deutsche Forschungsgesellschaft” (DFG). Saint Gobain Deutschland GmbH gave the test specimens.

References

[DIN EN 1288-3] Glas im Bauwesen: Bestimmung der Biegefestigkeit von Glas. Teil 3 Prüfung von Proben bei zweiseitiger Auflagerung (Vierschneiden-Verfahren). September 2000

[Duser 1999] Duser Van Alex, Jagota Anand, Bennison Stephen J.: Analysis of Glas/Polyvinyl Butyral Laminates subjected to uniform pressure, Journal of Engineering Mechanics, April 1999

[Kasper 2005] Kasper, Ruth: Tragverhalten von Glasträgern. Dissertation 2005

[Roik 1970] Roik, K.; Sedlacek; G.: Erweiterung der technischen Biege- und Verdrehtheorie unter Berücksichtigung von Schubverformungen, 1970, Die Bautechnik 47 Heft 1, S, 20-32.

[Roik 1972] Roik K, Carl J, Lindner J: Biegtorsionsprobleme dünnwandiger Stäbe. Ernst & Sohn 1972

[Scarpino 2002] Scarpino, P.: Berechnungsverfahren zur Bestimmung einer äquivalenten Torsionssteifigkeit von Trägern in Sandwichbauweise. Diplomarbeit RWTH Aachen, 2002, unveröffentlicht.

[Schuler 2003] Schuler C: Einfluss des Materialverhaltens von Polyvinylbutyral auf das Tragverhalten von Verbundsicherheitsglas in Abhängigkeit von Temperatur und Belastung. Dissertation 2003 TU München Lehrstuhl für Stahlbau

[Sobek 1998] Sobek W, Kutterer M, Messmer R: Bauen mit Glas - Rheologisches Verhalten von PVB im Schubverbund, Forschungsbericht 4/98, Universität Stuttgart, Institut für leichte Flächentragwerke, April 1998

[Völling 2000] Völling, B.: Berechnungsverfahren für Balken und Platten in Sandwichbauweise nach der erweiterten Biegetheorie. Diplomarbeit RWTH Aachen, 2000, unveröffentlicht.

EU COST C13 Glass and Interactive Building Envelopes. M. Crisinel, et al. (Eds.). IOS Press, 2007.

Contribution to the Use of Reinforced Glass Loaded on its Strong Axis

Klaus Kreher, EPFL – IBOIS, Lausanne, Switzerland

Due to loading on the strong axis of glass panes, different fracture mechanical behaviour has to be admitted than due to the loading on the weak neutral axis. Existing models to describe the structural safety of glass can not easily be adopted.

The load-bearing of reinforced glass panes varies with the degree of prestressing due to increasing residual stresses of heat strengthened glass. Ductile load carrying-behaviour is achieved by using reinforced heat strengthened glass.

This article offers a model to calculate the stresses of I-Beams with and without the appearance of cracks (Mode I and II) and the load-bearing behaviour of the adhesive joint of reinforced glass, such as distances between cracks, number of cracks and load introducing length.

Safety-considerations taking into account the load carrying-behaviour of reinforced glasses with different residual stresses due to heat strengthening are shown.

Keywords: reinforced glass, strong neutral axis

I. Introduction

Glass loaded on its strong axis offers excellent stiffness and load-bearing.

In reinforcing the stressed edge, the load-bearing varies to ordinary glass-panes. The panes do not collapse in a fragile way anymore; fractures appearing during loading preview the collapsing of a pane and an important post cracked load capacity can be achieved.

This offers the opportunity to modify the safety-considerations used for glass design and to increase the allowed stressing of glass.

The post-cracked load capacity is largely dependent on the quality of the used glass. Depending on the quality of the glass (residual stresses due to heat-strengthening, e.g. annealed glass, heat-strengthened glass, fully tempered glass), the ductility and the mode of failure of the panes change. As a result of its failure mode, annealed glass without internal prestressing offers the highest remaining load-carrying potential after the first crack appeared. This ductility, and thus the structural safety, diminishes with an increasing degree of internal prestressing due to thermal treatment. Heat-strengthened glass (with various degrees of prestressing, various residual stresses) shows a decrease in remaining load-carrying capacity with an increasing degree of prestressing until it fails in a brittle mode as fully toughened glass does.

In order to define the stressing of the glass, a calculation-method had to be developed taking into account the appearance of cracks and the deviation of strains and stresses.

This paper shows equations by solving the differential equations of a pulled slab to calculate the stressing of the glass, the adhesive and the reinforcing-material, which is suggested to be glued on the glass. The material stressing due to bending is transformed into a pulled slab.

Based on a slab model, the forces applied on the structure can be calculated as it is shown in [1] taking into account the non-cracked and the cracked structure.

II. Definition of the Material Stressing

To obtain the structural safety the most stressed parts of the structure have to be focused on. On both sides of a crack the adhesive and the reinforcing-material show a maximum stressing. A model based on the differential equations of the non-rigid bond is defined in order to calculate the loading-peaks of the adhesive joint and the material loading itself. The characteristic values of the non-rigid bond, such as the number and distances between cracks and the load introducing length, can be defined.

The slab-model is based on the following infinitesimal part with the shown forces:

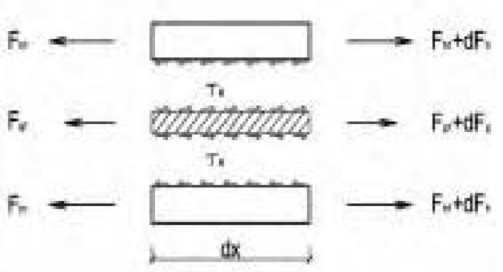

Figure 1: Infinitesimal part of the slab model with its forces

The indices *g* is for material glass, *h* for the reinforcing material and *kl* for the adhesive (non-rigid bond).

III. SUGGESTIONS

The differential equations are developed under suggestion of the following hypothesis:

- All materials have constant surfaces,
- All materials offer linear elastic material bearing,
- The stress-distribution is uniform in all cuts,
- The deformations are little and suggested for theory of 1st order,

The following strains can be defined:

$$\delta_h^{'} = \frac{d\delta_h}{dx} = \varepsilon_h \text{, strain of reinforcing material} \qquad (1)$$

$$\delta_g^{'} = \frac{d\delta_g}{dx} = \varepsilon_g \text{, strain of the glass} \qquad (2)$$

Horizontal equilibrium is:

$$2dF_h + dF_g = 0 \qquad (3)$$

$$2dF_h - 2\tau_{kl} \cdot b_{kl} \cdot dx = 0 \rightarrow 2\tau_{kl} \cdot b_{kl} = 2\frac{dF_h}{dx} \qquad (4)$$

The stresses after Hook`s law are:

$$\sigma_h = E_h \cdot \varepsilon_h = E_h \cdot \delta_h^{`} \qquad (5)$$

$$\sigma_g = E_g \cdot \varepsilon_g = E_g \cdot \delta_g^{`} \qquad (6)$$

Integration offers the internal forces as:

$$F_h = \int_{A_h} \sigma_h \cdot dA_h = E_h \cdot A_h \cdot \delta_h^{'} \qquad (7)$$

$$F_g = \int_{A_g} \sigma_g \cdot dA_g = E_g \cdot A_g \cdot \delta_g^{'} \qquad (8)$$

The difference between the materials displacements δ_h and δ_g are:

$$\delta = \delta_h - \delta_g \qquad (9)$$

The derivative shows the strain difference:

$$\delta^{'} = \delta_h^{'} - \delta_g^{'} \qquad (10)$$

(7) and (8) calculate $\delta_h^{'}$ and $\delta_g^{'}$:

$$\delta^{'} = \frac{F_h}{E_h \cdot A_h} - \frac{F_g}{E_g \cdot A_g} \qquad (11)$$

The second derivative is the equivalence to the stressing of the non-rigid bond:

$$\delta^{''} = \frac{dF_h}{dx \cdot E_h \cdot A_h} - \frac{dF_g}{dx \cdot E_g \cdot A_g} = b_{kl}\tau_{kl}\left(\frac{1}{E_h \cdot A_h} + \frac{2}{E_g \cdot A_g}\right) \qquad (12)$$

Taking into account a law for the bond $\tau_{kl}(\delta)$, which was evaluated by testing, the differential equations of the non-rigid bond in relation to the material stressing can be defined as the following:

$$\delta^{''} = a \cdot \delta + b \qquad (13)$$

The non-rigid bond can be described with the following equation:

$$\tau(\delta) = \tau_a + k \cdot \delta \qquad (14)$$

The factor *k* is to define the elasticity of the adhesive.
The constant value τ_a needs to be $\tau_a > 0$.

IV. THE NON-RIGID BOND FOR THE SLAB-MODEL

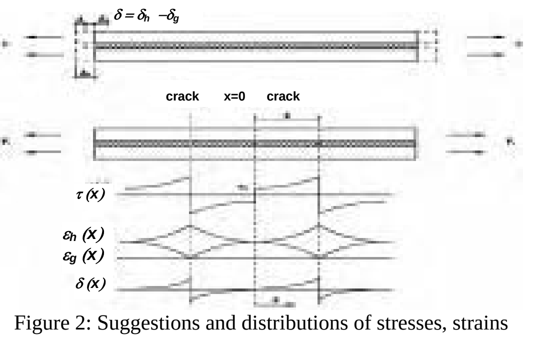

Figure 2: Suggestions and distributions of stresses, strains and differences of the material displacements

According to the infinitesimal part, the distributions of the displacements for the whole slab are:

$$\delta_h(x) = \int_0^x \varepsilon_h(x)dx \tag{15}$$

$$\delta_g(x) = \int_0^x \varepsilon_g(x)dx \tag{16}$$

The difference between the displacement is:

$$\delta(x) = \delta_h(x) - \delta_g(x) \tag{17}$$

At *x=0* the force in the reinforcing material is:

$$F_{h_0} = \sigma_{h_0} \cdot A_h = E_h \cdot \varepsilon_{h_0} \cdot A_h \tag{18}$$

For the whole length of the slab it can be written:

$$\Delta F_h(x) = b_{kl} \cdot \int_0^x \tau_{kl}(x) \cdot dx \tag{19}$$

With

$$\Delta F_h(x) = \Delta\varepsilon_h(x) \cdot E_h \cdot A_h \tag{20}$$

and

$$\Delta\varepsilon_h(x) = \frac{b_{kl}}{E_h \cdot A_h} \cdot \int_0^x \tau_{kl}(x) \cdot dx \tag{21}$$

the distribution of the strains can be defined as the following:

$$\varepsilon_h(x) = \varepsilon_{h_0} + \frac{b_{kl}}{E_h \cdot A_h} \cdot \int_0^x \tau_{kl}(x) \cdot dx \tag{22}$$

Equally, the glass parameters can be written:

$$F_{g_0} = \sigma_{g_0} \cdot A_g = E_g \cdot \varepsilon_{g_0} \cdot A_g \tag{23}$$

$$\Delta F_g(x) = \Delta\varepsilon_g(x) \cdot E_g \cdot A_g \tag{24}$$

$$\Delta F_h(x) + \Delta F_g(x) = 0 \tag{25}$$

$$\Delta\varepsilon_g(x) = -\frac{2 \cdot b_{kl}}{E_g \cdot A_g} \cdot \int_0^x \tau_{kl}(x) \cdot dx \tag{26}$$

$$\varepsilon_g(x) = \varepsilon_{g_0} - \frac{2 \cdot b_{kl}}{E_g \cdot A_g} \cdot \int_0^x \tau_{kl}(x) \cdot dx \tag{27}$$

The differences of the material strains

$$\Delta\varepsilon(x) = \varepsilon_h(x) - \varepsilon_g(x) = \varepsilon_{h_0} - \varepsilon_{g_0} + b_{kl}\left(\frac{1}{E_h \cdot A_h} + \frac{2}{E_g \cdot A_g}\right) \cdot \int_0^x \tau_{kl}(x) \cdot dx \tag{28}$$

can be shown in relation to the stresses due to the non-rigid bond:

$$\delta''(x) = b_{kl}\left(\frac{1}{E_h \cdot A_h} + \frac{2}{E_g \cdot A_g}\right) \cdot \tau_a + b_{kl}\left(\frac{1}{E_h \cdot A_h} + \frac{2}{E_g \cdot A_g}\right) \cdot k \cdot \delta \tag{29}$$

$$\delta(x) = \int_0^x \Delta\varepsilon(x) \cdot dx \tag{30}$$

Besides this equation, the difference of the displacements is related due to the non-rigid law of the bond. This allows developing the differential equation for the non-rigid bond for the slab model:

$$\delta''(x) = b_{kl}\left(\frac{1}{E_h \cdot A_h} + \frac{2}{E_g \cdot A_g}\right) \cdot \tau_a + b_{kl}\left(\frac{1}{E_h \cdot A_h} + \frac{2}{E_g \cdot A_g}\right) \cdot k \cdot \delta(x) \tag{31}$$

A. *Solution of the differential equation*

The solution for this linear homogenous differential equation of second order with constant coefficient can now

$$y''(x) - c_0 \cdot y(x) = r \tag{32}$$

can be found with the following basic functions:

$$y_{ho} = e^{\lambda x} \tag{33}$$

the characteristic solution

$$\lambda^2 - c_0 = 0 \tag{34}$$

and the real solution:

$$\lambda_{1,2} = \pm\sqrt{c_0} \tag{35}$$

With linear combination the basic solution is:

$$y = c_1 \cdot e^{\lambda_1 x} + c_2 \cdot e^{\lambda_2 x} \tag{36}$$

The particular solution can be found by approach of the right part of the equation:

$$y_{pa} = c_3 \tag{37}$$

and defining the constant to:

$$c_3 = -\frac{r}{c_0} \tag{38}$$

The solution for the difference of the displacements is:

$$\delta(x) = c_1 \cdot e^{\lambda_1 x} + c_2 \cdot e^{\lambda_2 x} - \frac{\tau_a}{k} \tag{39}$$

with:

$$\lambda_{1,2} = \pm\sqrt{b_{kl}\left(\frac{1}{E_h \cdot A_h} + \frac{2}{E_g \cdot A_g}\right) \cdot k} \tag{40}$$

B. Definition of constants with boundary conditions

To define the constants the known values can be evaluated and the equations solved. The two different states "not cracked" and "cracked" have to be taken into account.

At $x=0$ is

$$\delta(0) = c_1 + c_2 - \frac{\tau_a}{k} = 0 \tag{41}$$

for a non cracked slab can also be defined:

$$\delta'(0) = \pm\lambda \cdot (c_1 - c_2) = 0 \tag{42}$$

Introducing the length s which is the equivalent to the needed length to introduce the force into the glass (defined by tests) it can be written:

$$\delta'(s) = \lambda \left\{c_1 \cdot e^{[\lambda \cdot s]} - c_2 \cdot e^{-[\lambda \cdot s]}\right\} = \varepsilon_{h_{II}} \tag{43}$$

For a cracked cut, a further compatibility condition can be chosen. The whole force has to be taken by the reinforcing material:

$$\delta'(s) = \varepsilon_{h_{II}} = \frac{F_{hrII}}{E_h \cdot A_h} \tag{44}$$

Solving the system of equations the constants are defined to:

$$c_1 = c_2 = \frac{\tau_a}{2 \cdot k} \tag{45}$$

C. Defining the load introducing length

The load introducing length s can be calculated in transforming:

$$e^x - e^{-x} = 2 \cdot \sinh(x) \tag{46}$$

and

$$ar\sinh(x) = \ln\left(x + \sqrt{x^2+1}\right) \tag{47}$$

to:

$$s = \frac{1}{\lambda} \cdot \ln\left[\frac{\frac{F_{hrII}}{E_h \cdot A_h} \cdot k}{\tau_a \cdot \lambda} + \sqrt{\left(\frac{\frac{F_{hrII}}{E_h \cdot A_h} \cdot k}{\tau_a \cdot \lambda}\right)^2 + 1}\right] \tag{48}$$

D. Solution

The stressing of the bond along the slab model can be calculated to:

$$\tau(x) = \frac{\lambda^2}{b_{kl} \cdot \left(\frac{1}{E_h \cdot A_h} + \frac{2}{E_g \cdot A_g}\right)} \cdot \left(c_1 \cdot e^{\lambda \cdot x} + c_2 \cdot e^{-\lambda x}\right) \tag{49}$$

with defined constants:

$$\tau(x) = \frac{\tau_a}{2} \cdot \left(e^{\lambda \cdot x} + e^{-\lambda \cdot x}\right) \tag{50}$$

The strains of the materials are:

$$\varepsilon_h(x) = \varepsilon_{hII} - \frac{\frac{1}{E_h \cdot A_h}}{\left(\frac{1}{E_h \cdot A_h} + \frac{2}{E_g \cdot A_g}\right)} \cdot \lambda \cdot \left[c_1 \cdot \left(e^{\lambda \cdot s} - e^{\lambda \cdot x}\right) - \left(c_2 \cdot e^{-\lambda \cdot s} - e^{-\lambda \cdot x}\right)\right] \tag{51}$$

and

$$\varepsilon_g(x) = \frac{\frac{2}{E_g \cdot A_g}}{\left(\frac{1}{E_h \cdot A_h} + \frac{2}{E_g \cdot A_g}\right)} \cdot \lambda \cdot \left[c_1 \cdot \left(e^{\lambda \cdot s} - e^{\lambda \cdot x}\right) - \left(c_2 \cdot e^{-\lambda \cdot s} - e^{-\lambda \cdot x}\right)\right] \tag{52}$$

With defined constants:

$$\varepsilon_h(x) = \frac{F_{hrII}}{E_h \cdot A_h} - \frac{\frac{1}{E_h \cdot A_h}}{\left(\frac{1}{E_h \cdot A_h} + \frac{2}{E_g \cdot A_g}\right)} \cdot \lambda \cdot \left[\frac{\tau_a}{2 \cdot k} \cdot \left(e^{\lambda \cdot s} - e^{\lambda \cdot x}\right) - \frac{\tau_a}{2 \cdot k} \cdot \left(e^{-\lambda \cdot s} - e^{-\lambda \cdot x}\right)\right] \tag{53}$$

and

$$\varepsilon_g(x) = \frac{\frac{2}{E_g \cdot A_g}}{\left(\frac{1}{E_h \cdot A_h} + \frac{2}{E_g \cdot A_g}\right)} \cdot \left[\frac{\tau_a}{2 \cdot k} \cdot \left(e^{\lambda s} - e^{\lambda x}\right) - \frac{\tau_a}{2 \cdot k} \cdot \left(e^{-\lambda s} - e^{-\lambda x}\right)\right] \cdot \left[\begin{array}{l} \frac{\tau_a}{2 \cdot k} \cdot \left(e^{\left[\frac{\tau_a}{2k}\left(e^{\lambda s} - e^{\lambda x}\right) - \frac{\tau_a}{2k}\left(e^{-\lambda s} - e^{-\lambda x}\right)\right] s} - e^{\left[\frac{\tau_a}{2k}\left(e^{\lambda s} - e^{\lambda x}\right) - \frac{\tau_a}{2k}\left(e^{-\lambda s} - e^{-\lambda x}\right)\right] x}\right) - \\ \frac{\tau_a}{2 \cdot k} \cdot \left(e^{-\left[\frac{\tau_a}{2k}\left(e^{\lambda s} - e^{\lambda x}\right) - \frac{\tau_a}{2k}\left(e^{-\lambda s} - e^{-\lambda x}\right)\right] s} - e^{-\left[\frac{\tau_a}{2k}\left(e^{\lambda s} - e^{\lambda x}\right) - \frac{\tau_a}{2k}\left(e^{-\lambda s} - e^{-\lambda x}\right)\right] x}\right) \end{array}\right] \tag{54}$$

E. Width of cracks and completed crack distribution

A completed crack distribution can be admitted when the following relation is achieved:

$$s \le a_{r,\min} \le 2s \quad (55)$$

This shows that a maximum number of cracks can be calculated in relation of the load introducing length.

The theoretical width of a crack is defined to:

$$b_r = 2 \cdot \delta(a) \quad (56)$$

V. Safety considerations

To design reinforced glass panes loaded on their strong axis, the design at the limit state of cracking governs the dimension (thickness of the panes) in relation to the post cracked load capacity. The author suggests a minimum of two cracks appearing before collapsing of the structure and a minimum ratio for post cracked load capacity of 1.5 (ultimate load / load of first crack).

The influence of the thermal treatment of the glass is also shown in [1].

Figure 3 shows the relation of post cracked load capacity in relation to glass with different residual stresses due to thermal treatment.

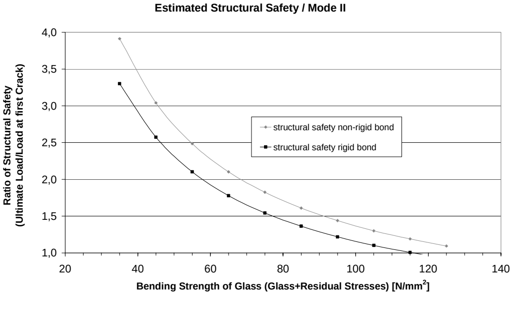

Figure 3: Post cracked load capacity in relation to glass with different residual stresses due to thermal treatment

VI. Conclusion/Example

The load-bearing of glass panes loaded on their strong axis can be improved by reinforcing the stressed edge. In relation to the residual internal stresses due to thermal treatment of the glass, the post cracked load capacity varies.

To be able to calculate the loading peaks at the limit state of cracking, the stresses of glass, reinforcing material and adhesive need to be known.

The calculation method shown in this paper offers the opportunity to define these values to insure the design and the structural safety of reinforced glass panes loaded on their strong axis.

An estimation of the structural security taking into account the glass quality and failure of the reinforcing material shows good correlation with testing-results. Figure 4 shows the estimated structural safety (*ultimate load/load at first crack*; with: *rigid* and the real *non-rigid* bond; *testing-results: points* and *line of linear correlation*) and the corresponding stresses due to bending, calculated with the shown model.

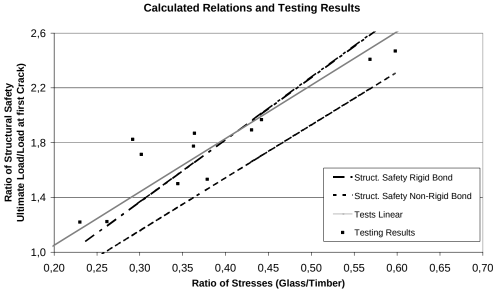

Figure 4: Correlation between testing-results and calculated values

Figure 5 shows a tested girder of heat strengthened glass reinforced by timber.

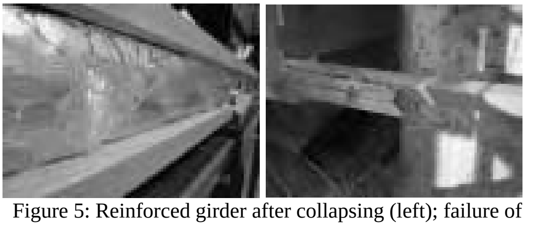

Figure 5: Reinforced girder after collapsing (left); failure of the reinforcing timber-slab (right)

Reference

[Kreher 2004]
KREHER, K., *Tragverhalten und Bemessung von Holz-Glas-Verbundträgern unter Berücksichtigung der Eigenspannungen im Glas*, These Nr. 2999, IBOIS, EPFL

EU COST C13 Glass and Interactive Building Envelopes. M. Crisinel, et al. (Eds.). IOS Press, 2007.

Stability of Load Carrying Elements of Glass

Andreas Luible, SCHMIDLIN AG, Aesch, Switzerland
Michel Crisinel, EPFL – ICOM, Lausanne, Switzerland

Glass is a material, that is able to resist very high compression stresses and which has special architectural appeal because of its transparency. For this reason, there is a growing trend to extend the use of glass sheets to load carrying elements such as beams, columns and shear panels. Due to their high slenderness and high compression strength, such load carrying elements tend to fail because of instability. The main objective of the research work is the experimental and theoretical study of the fundamental stability problems (column buckling, lateral buckling, plate buckling) for single layer and laminated glass.

Based on stability tests, the load carrying behaviour of simple and laminated glass in the foreseeable dimensions of application was examined and analytic and numeric models were developed. To simulate the buckling behaviour of laminated glass elements, the time and temperature-dependent behaviour of the PVB interlayer was modelled with viscoelastic finite elements.

The main objective of the work is to discuss possible design methods for single layered and laminated glass elements by means of the test results, the developed models and the parametric study.

Keywords: glass, stability, load carrying glass elements, buckling, second order

I. INTRODUCTION

Modern architecture demands for more slender and lighter structures. Glass is a material that has been used for a long time in windows as a filling material and has much to offer in this regard due to its very high compressive strength and transparency. For this reason, there is a growing trend to extend the use of glass to load carrying elements such as columns, beams and panels.

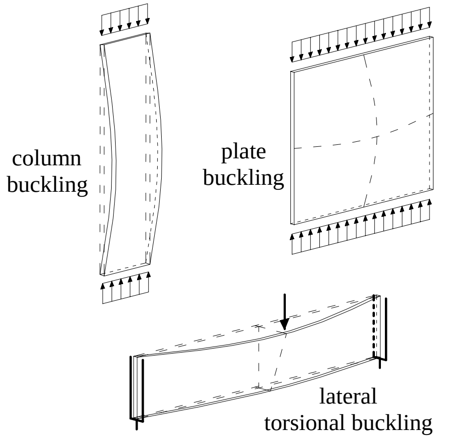

Figure 1: Stability problems.

Due to their high slenderness, such elements tend to fail because of instability (e.g. column buckling, lateral torsional buckling or plate buckling) (Figure 1).

At present little knowledge exists about the load carrying behaviour of glass structural elements, and existing design methods for other materials (i.e. steel) cannot be directly transferred to glass panels, since the influence of the following aspects on the behaviour of glass must be investigated in a different manner:

- production tolerances (i.e. glass thickness)
- initial deformations,
- the visco-elastic Poly-Vinyl-Butyral interlayer (PVB) used for laminated safety glass,
- the ideal elastic material behaviour without plastic deformability, and

- the ultimate breaking stress in glass, which depends on the embedded compressive surface stress due to the tempering process, the degree of damage of the glass surface and the load duration.

With this in mind, the main objectives of the research project were:

- The theoretical and experimental study of the load carrying behaviour of glass elements which may fail due to lack of stability.
- Discussion of possible design methods for the three main stability problems (column buckling, lateral torsional buckling and plate buckling).

II. Study of the Parameters with the Most Important Influence on the Buckling Behaviour

The dispersion of the **glass thickness** and the **initial deformation** of glass panels were measured for more than 200 test specimen from two different glass manufacturers.

The thickness t of annealed flat glass panels differs from the nominal value because glass manufacturers try to save material in making the most use of the thickness tolerances specified by the codes. The real glass thickness is often less than the nominal value, therefore reducing the moment of inertia of the cross section and, thus the buckling strength. The aforementioned measurements confirmed that the values follow a normal distribution. The 5% percentile value is 97.61% of the nominal glass thickness.

The initial geometric deformation w_0 (Figure 2) of flat glass, which is mainly caused by the tempering process was measured with a taut steel wire. For the measurements the glasses were supported in such a way that the deformation due to the dead load has no influence on their initial deformation. The results confirmed that non-tempered annealed flat glass has a very low initial deformation (< *1*/2500) while heat-strengthened and fully toughened glass can have a sinusoidal initial deformation up to *1*/300 of the length L. The nominal thickness of the glasses have an influence on the statistical distribution but for design in practice the simplified assumption of one single distribution might be sufficient. Laminated safety glass showed the same results. The measured values followed a normal distribution with a 95% percentile value of *1*/386. However maximum initial deformations depend strongly on the quality of the furnace and can therefore vary between different glass manufacturers.

III. Column Buckling

A. Introduction

Stability problems can be divided into two categories (Figure 2). The first includes perfect members that are subjected to an increasing load, where instability occurs suddenly when a critical load $N_{cr,K}$ is reached. The second more realistic category covers members with imperfections in the linearity of the bar (i.e. initial deformations w_0) and/or an eccentricity e of the applied load where the critical load can never be obtained. An increasing load N leads to disproportional increasing deformations already under very small loads until the strength of the material or a maximum deformation is exceeded (imperfect column buckling). The maximum load N_K is the point where the maximum stresses in the material due to the lateral deformations are reached. For the design of structural elements under compression, the fundamental study of the difference between the critical load $N_{cr,K}$ and the maximum load N_K is necessary.

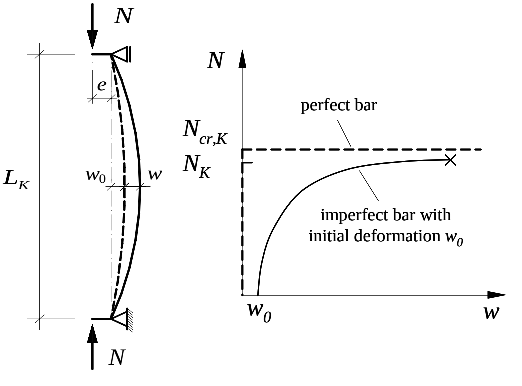

Figure 2: Eccentrically loaded bar with initial deformation w_0.

B. Buckling Models for Glass

1) Single Layer Glass

The load carrying behaviour of single layered glass can be described using a second order differential equation [Hirt et al. 1998] for a bar with a length, L_K, under axial compression, N, the bar is pinned at the ends, has an initial sinusoidal deformation w_0 and the load is applied with an eccentricity, e. The solution for the elastic critical buckling load is given by:

$$N_{cr,K} = \frac{\pi^2 EI}{L_K^{\ 2}} \quad \text{with: } I = \frac{bt^3}{12} \tag{1}$$

and the geometrical slenderness is defined as:

$$\lambda_K = \pi\sqrt{\frac{EA}{N_{cr,K}}} = \pi\sqrt{\frac{E}{\sigma_{cr,K}}} \tag{2}$$

The maximum deformation is given by:

$$w = \frac{e}{\cos\left(L_K / 2\sqrt{N/N_{cr,K}}\right)} + \frac{w_0}{1 - N/N_{cr,K}} \tag{3}$$

and the maximum surface stress can be determined as:

$$\sigma = \frac{N}{A} \pm \frac{N}{W}\left[\frac{e}{\cos L_K/2\sqrt{N/EI}} + \frac{w_0}{1 - N/N_{cr,K}}\right] \tag{4}$$

2) Laminated Safety Glass

The PVB interlayer in laminated glass behaves like a shear connection between the glass layers. The load carrying behaviour can be described using elastic "sandwich" theory [Zenkert 1997] or by means of a finite element model [ANSYS 2002] where the PVB interlayer can either be represented by elastic or visco-elastic elements [Van Duser et al. 1999].

The critical buckling load of a two layer elastic "sandwich" (Figure 3) with a width b is given by [Stamm et al. 1974]:

$$N_{cr,K} = \frac{\pi^2(1+\alpha+\pi^2\alpha\beta)}{1+\pi^2\beta}\ \frac{EI_S}{L_K^{\ 2}} \tag{5}$$

For a laminated safety glass with two glass layers:

$$\alpha = \frac{I_1 + I_2}{I_S}; \beta = \frac{t_{PVB}}{G_{PVB}\ b(z_1+z_2)^2}\ \frac{EI_S}{L_K^{\ 2}} \tag{6}$$

$$I_i = \frac{bt_i^3}{12}; I_S = b(t_1 z_1^2 + t_2 z_2^2) \tag{7}$$

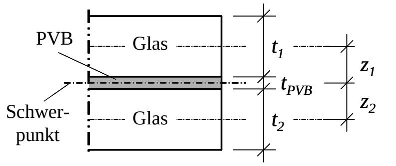

Figure 3: Laminated safety glass with two glass layers.

For a laminated safety glass with three glass layers and symmetrical cross section (Figure 4)

$$\alpha = \frac{2I_1 + I_2}{I_S} \tag{8}$$

$$\beta = \frac{t_{PVB}}{2G_{PVB} b\, z_1^{\ 2}}\ \frac{EI_S}{L_K^{\ 2}} \tag{9}$$

$$EI_S = 2Ebt_1 z_1^{\ 2} \tag{10}$$

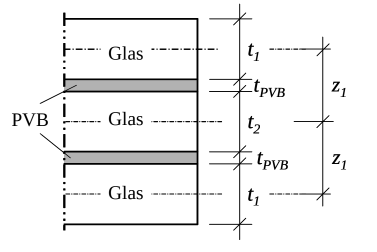

Figure 4: Laminated safety glass with three glass layers and symmetric cross section.

The geometrical slenderness is defined as

$$\lambda_{K,Sandwich} = \frac{L}{\sqrt{\frac{I_S}{A}\frac{1+\alpha+\pi^2\ \alpha\beta}{1+\pi^2\ \beta}}} \tag{11}$$

C. Experimental Investigation

A total of 80 displacement- and load-controlled column buckling tests were carried out (Figure 5).

1) Single Layered Glass

a) Test Results

The differential equation solution (Eq. (3)) showed good agreement with the test performance of single layered glass (Figure 6). The initial fracture occurred always on the tensile surface and, in most cases, within a distance of about three times the glass thickness from the glass edge (Figure 7).

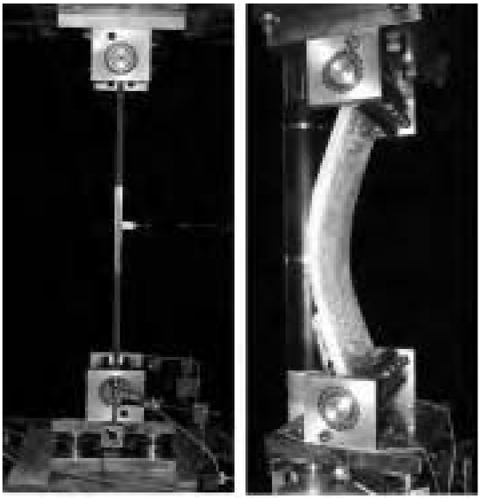

Figure 5: Test setup column buckling tests.

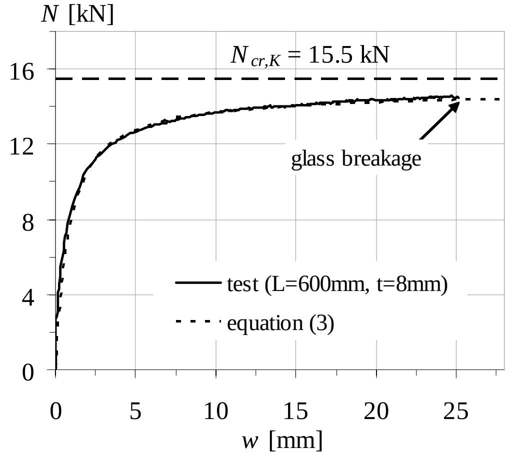

Figure 6: Test result single layer glass.

b) Load carrying Behaviour

The study of the load carrying behaviour showed that the glass thickness t, the initial deformation w_0 and the load eccentricity e have the most important influence on the maximum load. Due to the high compressive strength of glass, the buckling strength of a glass element under compression, with the dimensions applied in building construction ($L > 300$ mm, $t < 19$ mm, initially deformed) is always limited by the maximum tensile strength [Luible 2004].

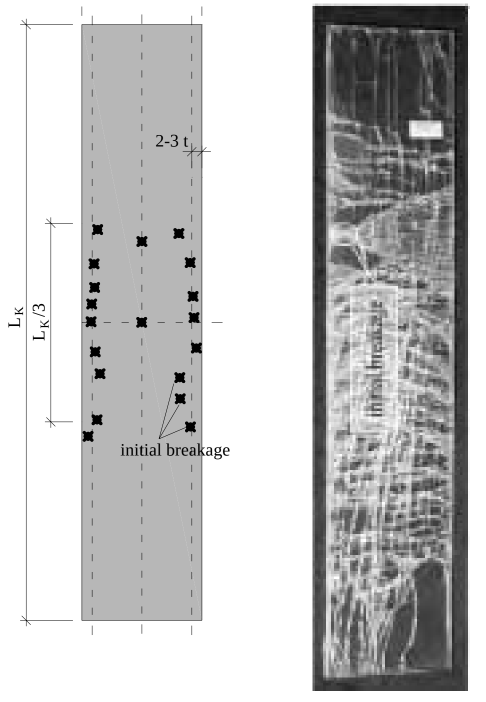

Figure 7: Initial breakage spots of 19 column buckling tests on single layered glass.

The initial breakage can occur on the whole glass surface and depends on the “frozen-in” compressive surface stress in addition to the tensile strength of the annealed float glass as mentioned above. But the study showed that the weakest point of the glass surface can simplistically be assumed to be at the point of the highest tensile stress.

2) *Laminated Safety Glass*

a) Test Results

The results of finite element models with linear visco-elastic elements representing the PVB-interlayer showed good agreement with the column buckling test results (Figure 8).

b) Load carrying Behaviour of Laminated Safety Glass

Simulations with the visco-elastic model under different temperatures and loading speeds demonstrated the effect of the interlayer on the load carrying capacity of laminated safety glass columns. In practice, the visco-elastic modelling of the PVB is complicated and may be simplified by an elastic model instead [Booker et al. 1974].

Parametric studies showed that the influence of the shear transfer by the PVB depends on the shear stiffness of the interlayer (which is a function of the temperature and the load duration), but also on the glass geometry (length, thickness of glass and PVB) [Luible 2004]. An improvement of the maximum load, comparing to a similar glass without PVB interlayer, is marginal for long-term loading and temperatures higher than 25°C. From an economical and safety point of view, a shear connection might therefore only be taken into account for short-term loading like wind or impact.

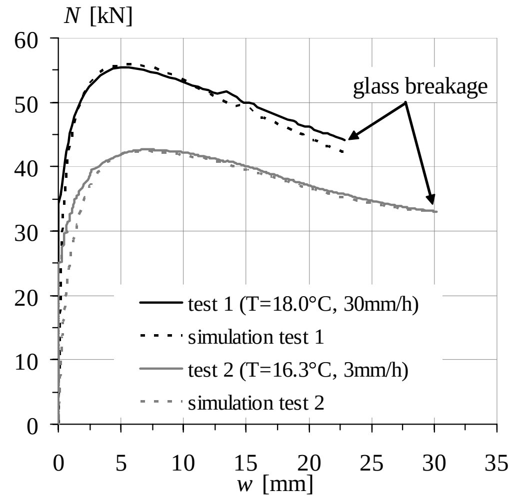

Figure 8: Test result laminated safety glass.

D. *Synthesis for Design*

1) Single Layer Glass

To simplify the design of compression members (e.g. steel columns) **column buckling curves** are commonly used. The same approach can be applied to compressive glass elements. In contrast to steel, however, the slenderness ratio for glass must be based on the maximum tensile strength, since the compressive strength of glass is not limiting its buckling strength. Unfortunately, simulations of column buckling curves for glass elements based on a slenderness ratio showed large variations for different tensile strength. Therefore, in contrast to steel, it appears unpractical to establish column buckling curves for glass using this approach. Column buckling curves might still be determined based on the geometric slenderness (Eq. (2)), which results in a family of curves for different tensile strengths. Additional lateral loads and end moments can be taken into account by means of interaction formulas similar to the design of compressive steel members. It was found, however, that for short glass panels these interaction formulas can lead to uneconomic solutions [Luible 2004] [Luible et al. 2004].

A more suitable approach for design might be a direct calculation of the maximum tensile stress in the compressed glass member by means of **elastic second order equations** (e.g. Eq. (4)) followed by a comparison of the this tensile stress to the design value of the tensile strength of glass. The calculation must be carried out with a reduced glass thickness (e.g. 97.61% of the nominal glass thickness) and a reasonable assumption for the initial deformation (e.g. $w_0 = L_K/400$) [Luible 2004] [Luible et al. 2004].

2) Laminated Safety Glass

For the design of a compressed laminated safety glass element, the visco-elastic behaviour might be simplified by the above mentioned elastic approach. The same methods as described for single layered glass can be applied to laminated safety glass elements. The maximum tensile stress for a given load *N* might be calculated either with a numerical model or an analytical sandwich model that takes into account second order effects (eg. Eq.(4)). For further simplification, the sandwich cross section may be replaced by an effective monolithic cross section with the effective thickness t_{eff} given by:

$$t_{eff} = \sqrt[3]{\frac{12\, I_s (1+\alpha+\pi^2 \alpha\, \beta)}{b\ \ (1+\pi^2 \beta)}} \qquad (12)$$

IV. LATERAL TORSIONAL BUCKLING

A. *Introduction*

Lateral torsional buckling is a limit state of structural stability, where a beam is loaded with pure bending and the deformation is a combination of lateral deflection and twisting. In glass structures this type of stability failure can occur, for example in beams or swords used as stiffeners in facades.

B. Lateral Torsional Buckling Models

1) Single Layer Glass

The critical torsional buckling moment (bifurcation buckling) of a beam with a rectangular cross section can be calculated with:

$$M_{cr,D} = C_1 \frac{\pi^2 EI_z}{L_D^{\,2}} \left[\sqrt{C_2 z_a + \frac{GK\, L_D^{\,2}}{\pi^2 EI_z}} + C_2 z_a \right] \qquad (13)$$

The factors C_i and z_a take into account different boundary conditions, different bending moments and the distance between the centre of gravity and the point where the load is applied [Hirt et al. 1998]. Due to their rectangular cross-section, warping torsion may be neglected in glass beams (Figure 9).

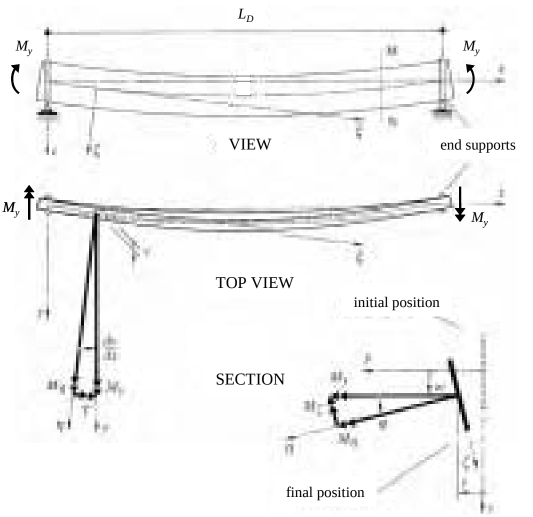

Figure 9: Lateral buckling with end moments.

Similar to column buckling the lateral torsional buckling resistance is not limited by the critical torsional buckling moment $M_{cr,D}$. Due to imperfections of the beam the lateral deformation and twisting start already to increase under very small loads and the lateral torsional buckling resistance is reached when the maximum stresses in the beam exceeds the material resistance. Bifurcation buckling (e.g. Eq.(13)) over-estimates the real lateral torsional buckling resistance.

To describe the real load carrying behaviour, analytical and numerical models (finite element method - FEM) were developed. It was found, that the numerical model is more suitable to describe the load carrying behaviour due to the slender geometries of glass beams, than analytical models based on the linear elastic beam theory [Luible 2004].

2) Laminated Safety Glass

The critical lateral torsional buckling moment of laminated safety glass may also be calculated using Eq. (13), where the lateral bending stiffness EI_z and the torsional stiffness GK are replaced by a equivalent stiffness, $EI_{z,eff}$ and GK_{eff}, to take into account the composite action of the PVB interlayer in laminated safety glass [Luible 2004].

$$EI_{z,eff} = EI_s \left(\frac{\alpha\beta\pi^2 + \alpha + 1}{1 + \pi^2 \beta} \right) \qquad (14)$$

with

$$I_S = h(t_1 z_1^2 + t_2 z_2^2) \qquad (15)$$

For α and β see Eq. (6).

$$GK_{eff} = GK_{glass1} + GK_{glass2} + GK_{comp} \qquad (16)$$

with

$$GK_{comp} = GI_S \left(1 - \frac{\tanh \frac{\lambda h}{2}}{\frac{\lambda h}{2}} \right) \qquad (17)$$

$$I_S = 4 \left(\frac{t_1 + t_2}{2} + t_{PVB} \right)^2 \frac{t_1 t_2}{t_1 + t_2} h \qquad (18)$$

$$\lambda = \sqrt{\frac{G_{PVB}}{G} \frac{t_1 + t_2}{t_{PVB}\, t_1 t_2}} \qquad (19)$$

To study the lateral torsional buckling behaviour of a glass beam composed of laminated safety glass with imperfections a finite element model [ANSYS 2002] was developed (Figure 10).

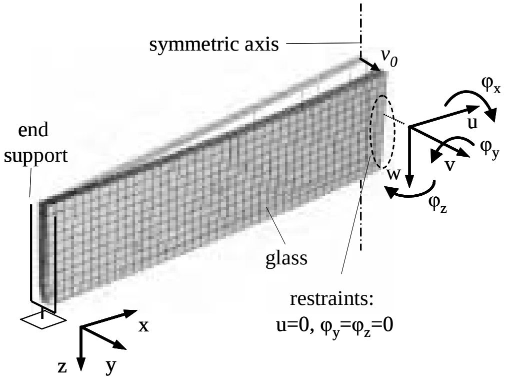

Figure 10: FEM-Modell laminated safety glass.

Only half of the glass beam was modelled because of the symmetrical system. The glass layers were modelled with shell elements and the PVB interlayer with volume elements. The applied initial deformation was a scaled shape of the first eigenform of the considered system.

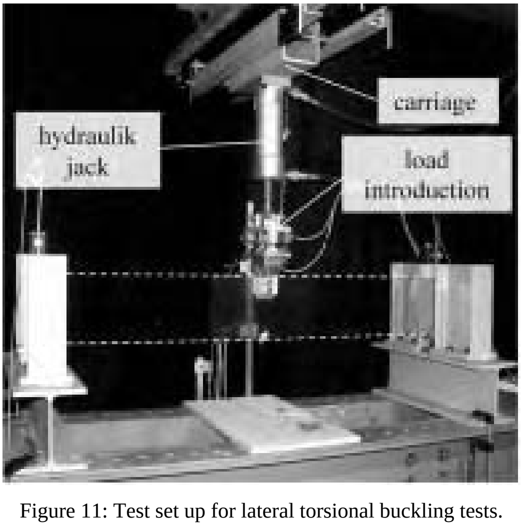

Figure 11: Test set up for lateral torsional buckling tests.

C. *Experimental Investigation*

1) *Test Setup*

For the test setup a simply supported beam was subjected to a concentrated load at mid-span. The main difficulty was the load application that had to to follow the lateral displacement of the upper edge of the glass beam. The hydraulic jack and the load introduction device were therefore fixed on a carriage (Figure 11).

In Figure 12 a deformed single layered glass beam is shown.

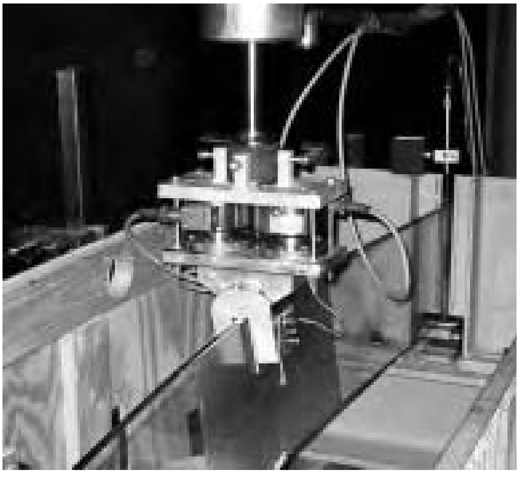

Figure 12: Buckled glass beam.

2) *Main Results*

Seventy-nine lateral torsional buckling tests on single layered and laminated safety glass were carried out.

a) Single Layer Glass

The results of the tests showed a good agreement with the numerical simulation. Similar to column buckling, the maximum force in the test approaches the critical buckling load $F_{cr,D}$.

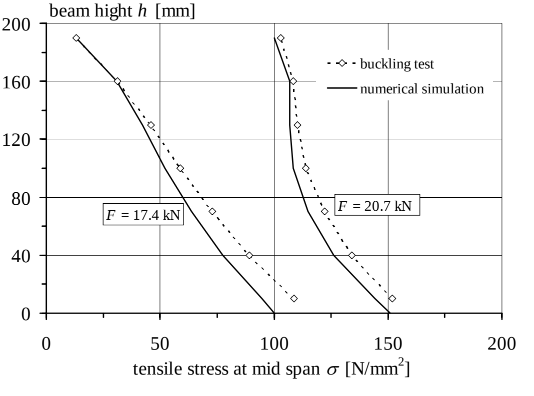

Figure 13: Tensile stress distribution on the glass surface.

During the test the stress distribution on the glass surface was controlled with strain gauges and compared with the numerical simulation (Figure

13). It could be seen that the stress distribution is non linear over the beam height *h*. The more the lateral displacement increased this non linear effect became stronger.

The breakages patterns of all tests were analyzed and it was seen that three typical modes for the initial breakage can be identified (Figure 14):

a) initial breakage on the corner of the glass edge
b) initial breakage on the lateral glass surface in a certain distance from the glass edge
c) initial breakage on the glass edge almost in the middle.

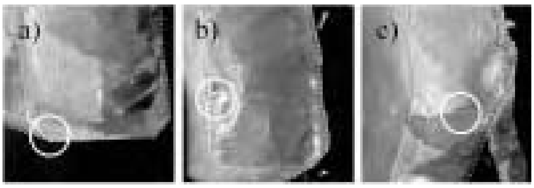

Figure 14: Three different breakage modes.

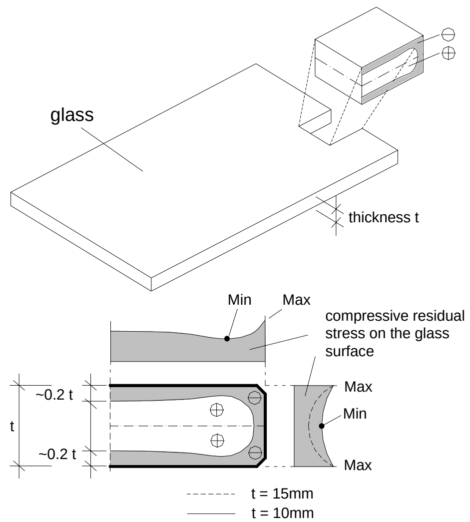

Figure 15: Distribution of compressive residual stresses on the glass surface near glass edges.

Breakage mode b) and c) can be explained by taking into consideration that the residual stresses of tempered glass near the glass edges can be lower than the residual stresses in the middle of the glass surface [Laufs 2000.2] [Bernard 2001]. These points with minimum residual stresses are located in the middle of the glass edge and at a certain distance from the glass edge on the lateral glass surface – exactly where the initial breakage occurred (Figure 15).

b) Laminated Safety Glass

The buckling tests confirmed that the load carrying behaviour of a laminated safety glass is characterised by the visco-elastic behaviour of the PVB interlayer (Figure 16). The temperature and the load duration therefore have an important influence on the lateral torsional buckling resistance of a laminated glass beam.

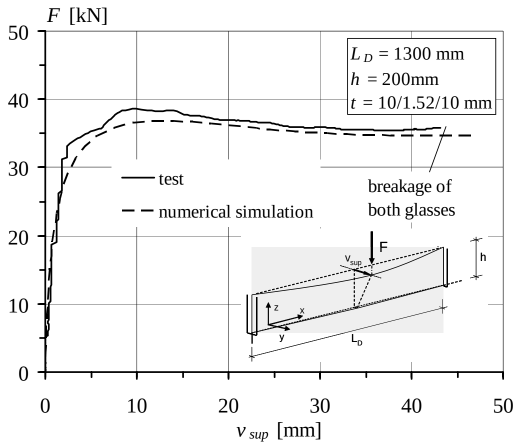

Figure 16: Test result laminated safety glass.

D. Synthesis for design

The study of the load carrying behaviour showed that the dispersion glass thickness *t*, the initial deformation of a glass beam, the composite action due to the PVB interlayer and the tensile strength of glass have the most significant influence on the lateral torsional buckling resistance of a glass beam. Due to the high compressive strength of glass the tensile strength of glass is determinant for the buckling resistance. In practice, the visco-elastic behaviour of the PVB interlayer can be simplified by an elastic interlayer with equivalent shear modulus, G_{PVB}. Figure 17 shows the influence of an elastic interlayer on the buckling strength. It was found, that for realistic values of G_{PVB} (< 5 N/mm^2) monolithic behaviour of the glass beam cannot be achieved.

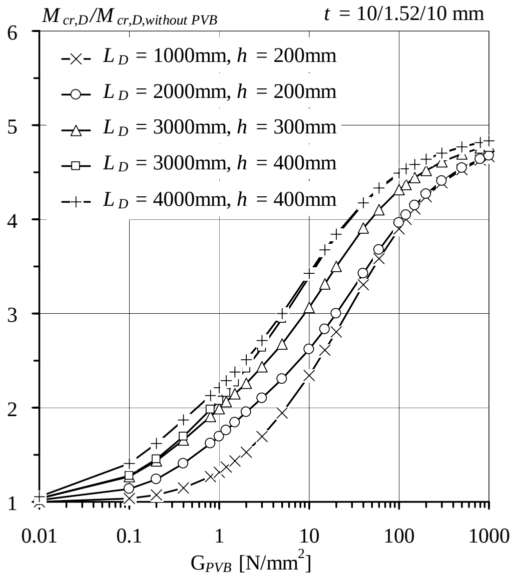

Figure 17: Influence of the shear behaviour.

The buckling resistance is reached when the maximum stress in the glass beam is equal to the tensile strength at one of the three critical points (breakage modes) mentioned above. For a simplification in practice, the tensile strength of the entire cross section may be taken as the minimum of the tensile strength at these three critical points to determine the lateral torsional buckling resistance. The maximum stress in the glass beam has to be calculated with a suitable model that takes into account second order effects and the non linear stress distribution in the cross section.

1) Design methods

The lateral torsional buckling resistance of a glass beam may either determined with a suitable model (e.g. FEM) or with buckling curves. The development of buckling curves was studied in this research work [Luible 2004] by means of the developed FEM models.

2) Buckling curves

To determine buckling curves a slenderness ratio $\bar{\lambda}_D$ and a reduction factor were defined. In contrast to steel, these are based on the tensile strength, since the compressive strength does not limit the buckling strength:

$$\bar{\lambda}_D = \sqrt{\frac{\sigma_{p,t}}{\sigma_{cr,D}}} = \sqrt{\frac{2\sigma_{p,t} I_y}{M_{cr,D} h}} \quad (20)$$

Where $\sigma_{p,t}$ the is the tensile strength of the glass and $\sigma_{cr,D}$ is the critical lateral torsional buckling

The critical lateral torsional buckling moment $M_{cr,D}$ may be calculated with Eq. (13). For the design of a laminated safety glass the equivalent lateral bending stiffness $EI_{z,eff}$ (Eq.(14)) and the equivalent torsional stiffness GK_{eff} (Eq. (16)) might be used. The reduction factor χ_D in a buckling diagram is a function of the slenderness ratio:

$$\chi_D = f\left(\bar{\lambda}_D\right) \quad (21)$$

Hence the maximum bending moment M is:

$$M = \sigma \frac{2I_y}{z} = \chi_D \sigma_{p,t} \frac{2I_y}{z} \quad (22)$$

For different types of loading, glass geometries, shear modulus of the PVB interlayer, and initial deformation, v_0, reduction factors were generated and plotted in buckling diagrams (i.e. Figure 18).

These diagrams may serve as a preliminary orientation in determining lateral torsional buckling curves for glass. The main results are:

- It is possible to define lateral torsional buckling curves for glass based on the tensile strength.
- Existing buckling curves for example for steel structures can not be transferred to glass.

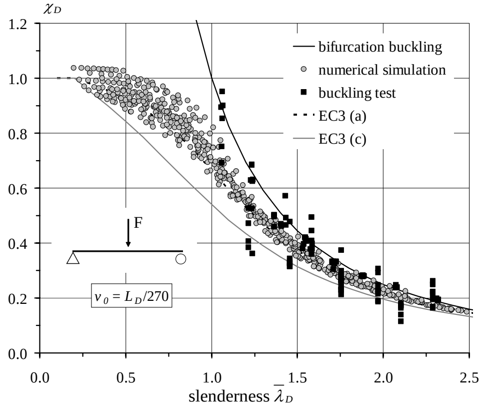

Figure 18: Simulated reduction factors for a concentrated load at mid span compared to buckling tests.

- It might be useful to determine several buckling curves, depending on the composition of the glass (single layer, laminated safety glass), the type of loading and the initial deformation.

- Further studies with additional systems are necessary (i.e. systems with intermediate lateral support or with partial restraint of the beam by structural silicon joints).
- Buckling curve (c) in Eurocode 3 [EN 1993-1-1:1993] may be used as a conservative approach for design of glass elements since all simulations results lay above this curve.

V. Plate Buckling

A. Introduction

When a plate simply supported along its edges is subjected to compression or shear forces in its middle plane the stability phenomenon of plate buckling can occur. The load carrying behaviour is a deformation *w* perpendicular to the middle plane that comes along with a distortion of the cross section of the plate (Figure 19).

The main difference compared to other stability problems is, that the critical buckling load $N_{cr,P}$ is not necessarily the ultimate load of the plate. The buckled element may sustain greater loads than the critical buckling load due to additional membrane stresses in the plate. Therefore initial out of plane deformation are less important. In glass structures this type of stability failure can occur in glass walls or shear panels.

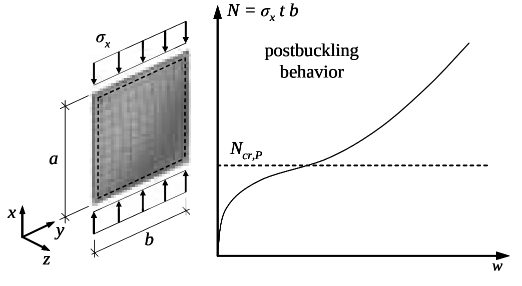

Figure 19: Plate buckling.

B. Plate Buckling Models for Glass

1) Single Layer Glass

The critical buckling load may be calculated with analytical models based on linear elastic bending theory. However, due to post-critical buckling behaviour, the critical buckling load $N_{x,cr,P}$ is not a criterion for the ultimate strength and thus most of these analytical models are not suitable for design.

$$N_{x,cr,P} = \left(\frac{mb}{a} + \frac{a}{bm}\right)^2 \frac{\pi^2 E t}{12\left(1-\nu^2\right)} \left(\frac{t}{b}\right)^2 \tag{23}$$

To study the load carrying behaviour of a buckled glass plate in a more realistic manner (including post-critical buckling) a FE model with shell elements was created. [Luible 2004].

2) Laminated Safety Glass

The critical buckling load $N_{x,cr,P,VSG}$ of laminated safety glass may be determined using linear elastic sandwich theory [Zenkert 1997].

$$N_{x,cr,P,VSG} = \left(\frac{mb}{a} + \frac{a}{mb}\right)^2 \frac{\pi^2 D}{b^2} \frac{\frac{(D_1+D_2)}{D}\left[\left(\frac{mb}{a}\right)^2+1\right] + \frac{Ab^2}{\pi^2 D_s}}{\left[\left(\frac{mb}{a}\right)^2+1\right] + \frac{A}{\pi^2 D_s}} \tag{24}$$

with

$$D = D_1 + D_2 + D_s \tag{25}$$

$$D_i = \frac{E t_i^3}{12(1-\nu^2)} \tag{26}$$

$$D_s = \frac{E t_1\, z_1^2 + E t_2\, z_2^2}{1-\nu^2} \tag{27}$$

$$A = \frac{G_{PVB}(z_1+z_2)^2}{t_{PVB}} \tag{28}$$

where

z_1, z_2: distance between the centre of gravity of the total cross section to the centre of gravity of the glass layer (Figure 3)

t_i: thickness of the corresponding glass layer

N_x: pressure force per unit length ($N_x = \sigma_x\, t$)

D: plate stiffness applied to a unit width b

For the investigations of the plate buckling behaviour a FE model was developed instead since analytical models are not suitable to describe the load carrying behaviour of a laminated safety glass. The cross section in this model consisted of shell elements for the glass layers and volume elements for the PVB interlayer similar to the FEM for lateral torsional buckling. The load introduction and boundary conditions were applied by means of additional nodes, which were coupled with the element nodes. For symmetrical deformations of the plate only one fourth was modelled with the corresponding boundary conditions in the symmetric axis (Figure 20).

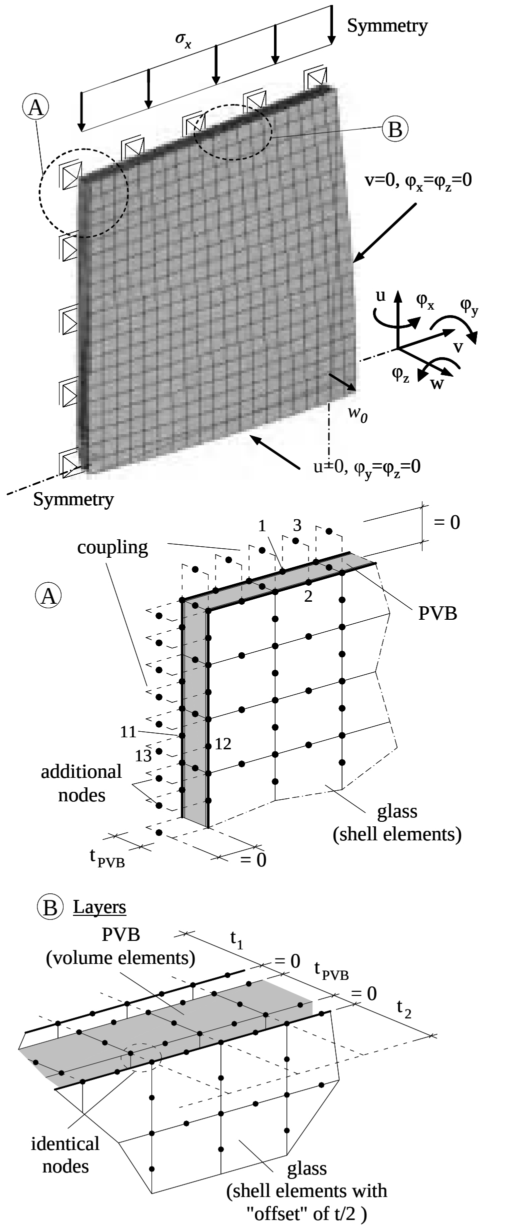

Figure 20: Finite element model for plate buckling (reduced model for symmetrical deformations).

C. *Experimental Investigation*

1) Test setup

The test setup corresponds to a square plate with four hinged edges. The load introduction in the two horizontal glass edge was achieved with aluminium supports that allow a free rotation of the edge and include a reinforced PTFE interlayer to reduce friction.

The vertical glass edges were supported with neoprene profiles (Figure 21).

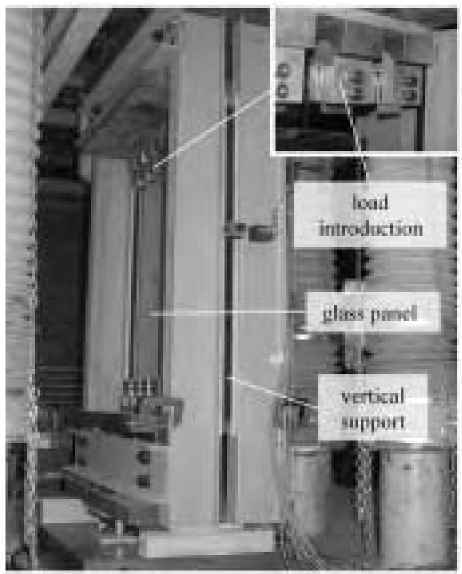

Figure 21: Plate buckling test setup.

2) Main results

A total of 9 plate buckling tests on single layered glass and 6 tests on laminated safety glass were carried out.

a) Single Layer Glass

The load carrying behaviour of the tested glass plates demonstrated the typical plate buckling behaviour with a load capacity higher than the critical buckling load, $N_{cr,P.}$ (Figure 22). The stiffness of the tested plates corresponds well with the model where the load is introduced by a constant edge displacement, *du*. Due to plastification of the aluminium interlayer close to the glass edges, however the measured deformation, *w*, in the centre of the plate is higher than in the model. Below the critical buckling load the curves differ more than in the post buckling region where they are almost identical.

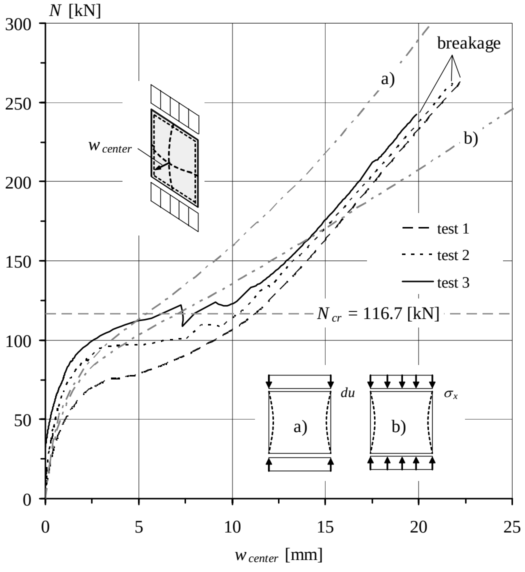

Figure 22: Plate buckling test on heat strengthened glass.

In all tests the initial breakage occurred on the glass surface under tensile stress and in a region close to the glass corners (Figure 23).

Figure 23: Buckled glass plate.

This is due to the maximum principle tensile stress which is moving as a function of the applied load in the corners of the buckled glass plate as it can be seen in the numerical simulation (Figure 24) [Luible 2004].

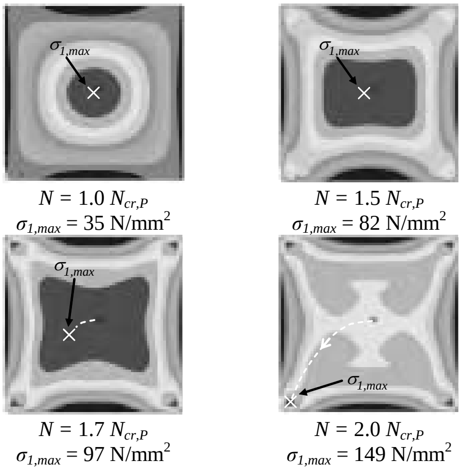

Figure 24: First principle stress on the glass surface.

The study of the load carrying behaviour demonstrated that the dispersion of the glass thickness, the boundary conditions, the tensile strength of the glass surface and the initial deformation have the most significant influence on the buckling strength. For loads lower than the critical buckling load the initial deformation has an influence, on the buckling strength.

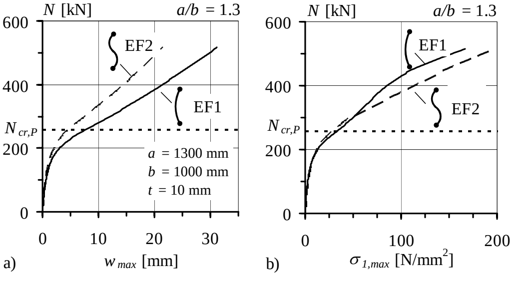

Figure 25: Influence of the buckling shape.

Studies with different initial deformations (applied as a multiple of the eigenform (EF1, EF2)) showed, that the shape of the buckled glass plate may have an influence on the buckling resistance (Figure 25) as well since the maximum tensile stress determines the buckling strength and not the stiffness of the plate. This important criterion has to be taken into account for glass when for example, the initial deformation does not correspond to the first eigenform (EF1) or when a so called "snap through" of the plate may occur [Luible 2004].

b) Laminated Safety Glass

Tests on laminated safety glass elements demonstrated the influence of the PVB interlayer on the buckling strength. The comparison with the simulations confirmed that a composite action can be activated, but the shear modulus of the PVB has to be relatively high to create a noticeable increase in buckling strength. Even for short time loading and low temperatures the influence is not as high as it is for column buckling or lateral torsional buckling. Therefore the assumption of a monolithic behaviour of a laminated safety glass in buckling overestimates the real buckling resistance. The shear stiffness of the PVB interlayer has to be taken into account. In all tests with laminated safety glass both glass layers broke at the same time. Due to the high stored energy, the breakage pattern of heat strengthened glasses was almost as fine as it normally appears for toughened glass.

D. Synthesis for design

1) Design methods

Investigations of possible design methods for buckling of glass panels showed that it is important to know the distribution of the maximum tensile stress on the glass surface. Therefore, analytical models are not precise enough. A more precise approach may be by means of a FEM calculations presented in [Luible 2004]. In practice, glass panels are usually supported by soft interlayer materials, hence the assumption of restrained edges as it is often the case for steel plates overestimates the real buckling strength. A conservative simplification for design of glass panels are non constrained vertical edges (y-direction, Figure 19) and a load application by a constant compressive force on the horizontal glass edge. For loads lower than the critical buckling load a reasonable assumption for the initial deformation has to be made. FEM calculations are often too fastidious in practice; therefore the possibility of developing design aids (e.g. buckling curves) was studied.

2) Buckling curves

The slenderness ratio and the reduction factor for plate buckling of glass panels were both based on the maximum tensile strength $\sigma_{p,t}$ and defined as:

$$\bar{\lambda}_P = \sqrt{\frac{\sigma_{p,t}t}{N_{cr,P}}} \tag{29}$$

$$\rho = \frac{\sigma_p}{\sigma_{p,t}} = \frac{N_{x,P}}{\sigma_{p,t}t} \tag{30}$$

Reduction factors for different types of loading, glass geometries, initial deformations w_0 and boundary conditions were generated with FE model and plotted in buckling diagrams (e.g. Figure 26).

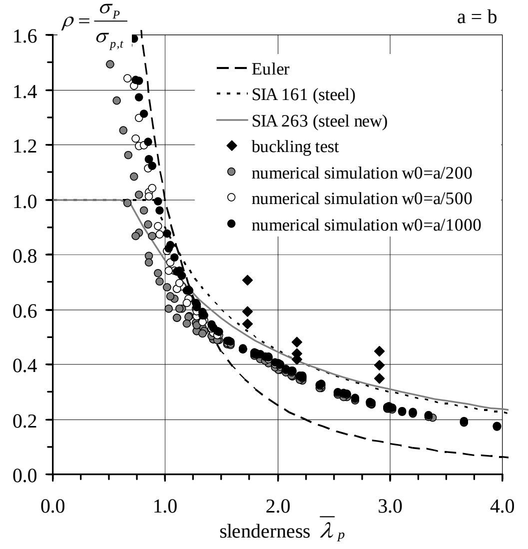

Figure 26: Simulation of reduction factors.

These simulation results are a first step towards a future definition of plate buckling curves for glass panels. The main results are:

- It is possible to define plate buckling curves for glass panels based on the tensile strength.
- For a slenderness ratio > 1.5 the curves are independent of the initial deformation.
- For a slenderness ratio < 1.5 the initial deformation has an influence on the buckling strength and therefore the curves have to be defined as a function of the initial deformation.
- The buckling curves for glass are below existing design curves in steel construction due to the different boundary conditions assumed.

Buckling curves for steel are therefore not suitable for glass.

VI. Conclusions

Stability is an important design criterion for load carrying glass elements. It was shown in the studies of this research work that the main influences on the buckling resistance of a load carrying glass element are the dispersion of the glass thickness, the initial deformation, the tensile resistance of the glass surface and the composite action due to the PVB interlayer in laminated safety glass. Residual stresses near the glass edges have to be known exactly in order to determine the realistic tensile resistance. Near the glass edges the residual stress of tempered glass is normally less than in the centre of the glass panel. The assumption of a tensile strength that is based on breakage tests carried out in the middle of the glass surface overestimates therefore the real load bearing capacity.

One of the main differences as compared with other materials is that the tensile strength limits the buckling strength.

A suitable design method for column buckling of glass elements seems a second order stress analysis. On the contrary, this approach is not suitable for lateral torsional buckling and plate buckling for which buckling curves are more appropriate. One of the main differences as compared with buckling curves in steel structures is that the slenderness ratio the reduction factors must be based on the maximum tensile strength of glass.

VII. Acknowledgment

The work in this paper was primarily conducted with the support of the Swiss National Science Foundation (SNF) and the industry partners *Glas Trösch* (Bützberg, Switzerland) and *Verre Industriels SA* (Moutier, Switzerland).

References

[ANSYS 2002] ANSYS, Release 6.1, SAS IP, Inc, 2002.

[Bennison et al. 2002] BENNISON, S. J., SMITH, C. A., VAN DUSER, A., JAGOTA, A., Structural Performance of Laminated Glass Made with a "Stiff" Interlayer, Glass in Buildings, ASTM STP 1434, V. Block, ed., ASTM International, West Conshohocken, PA, 2002.

[Booker et al. 1974] BOOKER, J.R., FRANKHAM, B.S., TRAHAIR, N.S., Stability of Visco-Elastic Structural Members, Civil Engineering Transactions, pp. 45-51, The Institution of Engineers, Australia, 1974.

[Hirt et al. 1998] HIRT, M. A., BEZ, R., Stahlbau: Grundbegriffe und Bemessungsverfahren, Ernst & Sohn, Berlin, 1998.

[Laufs 2000.2] LAUFS, W., Ein Bemessungs-konzept zur Festigkeit thermisch vorgespannter Gläser, Schriftenreihe Stahlbau RWTH Aachen, Shaker Verlag, Aachen, 2000.

[Luible 2004] LUIBLE, A., Stabilität von Tragelementen aus Glas, Thèse EPFL 3014, Ecole polytechnique fédérale de Lausanne (EPFL), Lausanne, 2004.

[Luible et al. 2004] Luible, A., Crisinel, M., Buckling Strength of Glass Elements in Compression, Structural Engineering International, Vol. 14, No. 2, IABSE, Mai 2004.

[Stamm et al. 1974] STAMM, K., WITTE, H., Sandwichkonstruktionen - Berechnung, Fertigung, Ausführung, Springer Verlag, Wien, 1974.

[Van Duser et al. 1999] VAN DUSER, A., JAGOTA, A., BENNISON, S., J., Analysis of Glass/Polyvinyl Butyral Laminates Subjected to Uniform Pressure, Journal of engineering mechanics, Vol. 125, pp. 435-442, 1999.

[Zenkert 1997] ZENKERT, D., The Handbook of Sandwich Construction, Engineering Materials Advisory Service Ltd., United Kingdom, 1997.

EU COST C13 Glass and Interactive Building Envelopes. M. Crisinel, et al. (Eds.). IOS Press, 2007.

Fastening of Glass Panes with Undercut Anchors – FEA and Experimental Investigations

Peter Hof, Darmstadt University of Technology,
Statics and Dynamics of Structures, Darmstadt, Germany
Jens Schneider, Schlaich, Bergermann und Partner, Stuttgart, Germany

Undercut anchors were so far seldom used in glass due to brittleness and the risk of subcritical crack growth. The use of tempered glass in combination with a special drilling-process and -geometry of the undercut holes now made it possible to develop a system that allows this method of fastening glass panes. In a parameter study of 3-D numerical tempering simulations with *Narayanaswamy's* structural relaxation model, the amount of residual stress in the area of the undercut hole was estimated. Temper stresses were compared to surface stresses in the "infinite" area that were measured by photoelastic methods. Pull-out tests and shear-off tests of anchors from annealed and tempered glass were performed and results compared to the numerical results. Both prove that a significant residual compression stress from tempering exists in the undercut area. Finally load bearing tests showed the performance of the system.

Keywords: Glass panes, Undercut Anchors, Pull-out test, heat-transfer coefficient

I. INTRODUCTION

Glass is one of the oldest materials used by mankind and the applications in the field of civil engineering increase successfully since many years. Nevertheless, the understanding of the non-crystalline solid as a state of matter is still poor.

Undercut anchors are a relatively young but successful method of fastening. Today, they are mainly used in concrete, stone or ceramics. The idea is to drill an "undercut" borehole and fix the anchor in the undercut area with a special mechanism (Figure 1, 2 and 3). In concrete, the anchors are drilled after the setting of the concrete, usually to fix steel elements. They can sustain very high loads. Applications for undercut anchors in combination with stone or ceramics are usually facade panels. Here, they guarantee a simple but powerful way of fastening with one main advantage: invisibility of the anchor from the outside of a facade pane. For these applications, the undercut holes are drilled in each pane automatically with CNC-drilling machines at a very high accuracy. In glass, the use of undercut anchors was so far problematic due to the extreme brittleness, subcritical crack growth in glasses and the stress concentration in the undercut area.

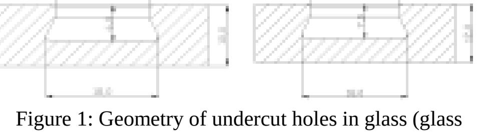

Figure 1: Geometry of undercut holes in glass (glass thickness 10 mm and 12 mm)

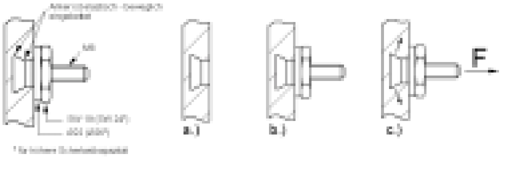

Figure 2: Anchor system

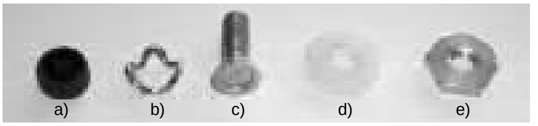

Figure 3: Details of the anchor system: a) plastic cap, b) curved steel part (steel snake), c) screw with conical head, d) plastic washer, e) nut

After some years of research, *Fischerwerke* in Waldachtal, Germany, developed a special drilling process, geometry for the undercut holes and plastic interlayer between steel anchor and glass [Fischer 2000]. In combination with tempered or heat strengthened glass it is now possible to fasten glass panes with undercut anchors. 3-D numerical tempering simulations and pull-out and shear-off tests of anchors from annealed and tempered glass show that a significant residual compression stress from tempering exists in the undercut area. For the numerical tempering models with the finite-element-code ANSYS 5.6 [Ansys 1999], material data and relaxation constants from [Carré 1999] were used to perform a parameter study with different heat transfer coefficients in the undercut area whereas the apparent heat transfer coefficient in the “infinite” (surface) area of the tempered samples was approximated from photoelastic measurements of the surface stress of 10 mm and 12 mm tempered glass samples. These samples and annealed samples were used in pull-out tests of anchors. These tests were simulated in 3-D numerical models with glass, anchor and plastic interlayer to calculate failure stresses. Finally, from the glass strength of the annealed samples and the tempered samples, the apparent heat transfer coefficient in the undercut area could be approximated from a parameter study.

II. Numerical Tempering Simulation

A. Finite-Element modelling

The thermal stresses for glass plates with undercut holes were calculated by simulating the tempering process with the finite-element program ANSYS 5.6. The theories of viscoelasticity and structural relaxation as described by *Narayanaswamy* [Narayanaswamy 1971, 1978] are implemented in ANSYS. Glass plates of the thickness 10 mm and 12 mm were examined. The glass plates are cooled from an initial temperature of 670 °C to 20 °C by forced convection on both sides.

A 3-D FE-model of the glass plate was constructed using the ANSYS FE code. Due to the rotational symmetry only a part of the glass plate is modelled. ANSYS SOLID90-elements were used to calculate the distribution of temperature over the duration of cooling. Afterwards these elements were replaced by ANSYS SOLID95-elements to calculate stresses. The test specimens consist of 6 mm thick glass plates. Every plate is 1 m long and 0.1 m wide. Altogether nine specimens have been investigated in this preliminary study. Six of the specimens are made of tempered glass and three of heat strengthened glass.

B. Cooling parameters and Material properties

The cooling parameters and the material properties of the glass, e.g. the viscous and structural relaxation times, were obtained from *Carré* [Carré 1999]. The thermal conductivity and the specific heat of the glass were considered to be constant and not to vary with the temperature as suggested by *Carré*. The thermal conductivity was set to l = 1,05 W/(mK) and the specific heat to cp = 980,4 J/(kgK).

The only unknown parameter of the tempering process simulation is the apparent heat transfer coefficient. The heat transfer coefficient is apparent, as the heat radiation influence was neglected in this study. With photoelastic measurements (Laser-Gasp, Strainoptics, U.S.A) it is possible to obtain the tempering stresses at the free surface of glass samples. The surface compression stress of the 10 mm and 12 mm glass plates was found to be approx. 100 MPa for all tempered samples. Calculations were carried out to identify the apparent heat transfer coefficient that leads to a surface compression stress of 100 MPa. Good results could be obtained with a heat transfer coefficient of 135 W/(m²K) at the free surface. It is difficult to measure the tempering stresses within the area of the undercut hole. To get qualified results for the stress distribution therefore the heat transfer coefficient in the area of the undercut hole was varied between 20 W/m²K and 135 W/m²K.

C. *Parameter study*

The stresses resulting from thermal tempering were calculated for an apparent heat transfer coefficient at the free surface of 135 W/(m²K) and 20, 40, 60, 80, 100, 120, 135 W/(m²K) in the undercut area. The distribution of the principal compressive stresses for heat transfer coefficients of 20, 60 and 135 W/(m²K) in the area of the hole are shown in Figure 4. Figure 4 also shows the path along which the stresses were calculated. The principal compressive stresses along this path are plotted in Figure 5.

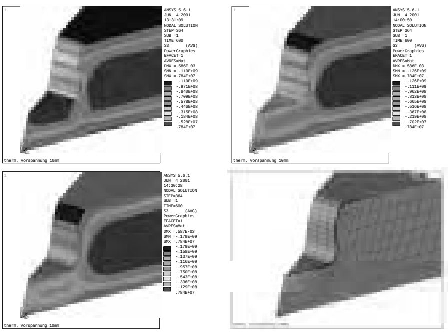

Figure 4: Principle compression stress for heat transfer coefficient of 20, 60 & 35 W/(m²K) in the borehole area (135 W/(m²K) at free surface), nodes of a path along the borehole

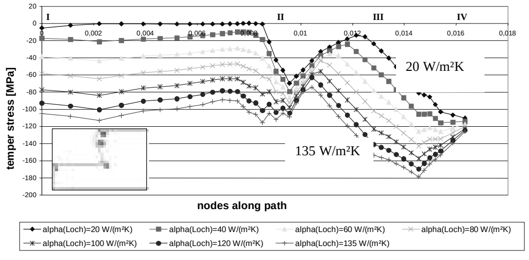

Figure 5: Computed principal stresses (compression) for different heat transfer coefficients in the borehole area (135 W/(m²K) at the free surface) along the path in Figure 4.

III. Determination of the Heat-Transfer Coefficient in the Undercut Area

A. *Pull-out tests*

Pull-out tests with annealed (float)-glass and tempered glass were performed (Figure 6). Specimens of 300 mm x 300 mm for each glass type and thickness were tested. In a Finite Element Analysis (FEA) (Figure 7) these tests were simulated to calculate failure stresses in the undercut area. Special contact elements between the glass surface and plastic material were used to simulate a realistic load distribution. From the results and the crack origins of annealed glass, the failure stress could be identified for each specimen. It was proved to be almost the same as the glass strength in the borehole area of annealed glass with drilled holes [Schneider 2001].

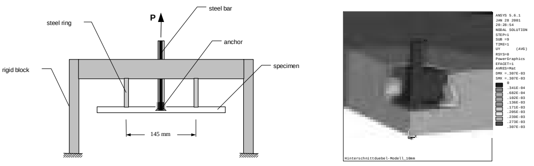

Figure 6: Section of test set-up (pull-out tests), FE-simulation of pull-out tests (glass, anchor and plastic interlayer)

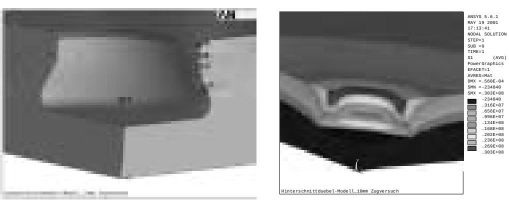

Figure 7: Crack origins (A to E) for tests with annealed (float) glass, stress distribution in the undercut area (principal tension stress) for failure load [Block 2001]

It was difficult to locate the exact crack origin for tempered glasses but due to an almost linear behaviour, the stress distribution in tempered glass could be calculated from failure loads with the FE-model. Presuming that the glass strength of tempered glass results in an addition of the inherent (annealed) glass strength and the temper stresses (no crack healing), a vector addition of the failure stresses of annealed glasses and the temper stresses for different heat transfer coefficients along the path of Figure 4 could be made to identity the temper stresses and heat transfer coefficient that fit the failure load results of tempered glass (Figure 8, approx. 60 W/(m²K)). ote that stresses at the top edge of the chamfer (IV) equal to almost zero whereas significant tension stresses cause failure in tempered glasses in the oblique area (II-III) due to lower temper stresses there.

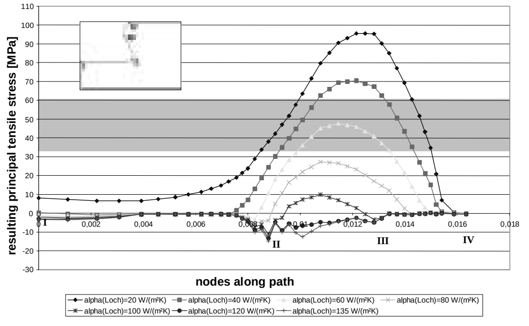

Figure 8. Resulting principle tensile stresses on the surface of a 10 mm tempered glass for different heat transfer coefficients, grey area: failure range of annealed glass, pull-out test

B. *Shear-off tests*

Additionally to the pull-out tests shear-off tests were made. The specimens were the same as described for the pull-out tests. The test set-up is given in Figure 9. Because of the steel snake as shown in Figure 3 it was necessary to divide the simulation of the test in two models. The models differ in the angle between the load-direction and the direction of the steel snake (Figure 10).

The screw and the steel snake were modelled as a quarter for each part of the steel snake. So the resulting tensile stresses differ in value and distribution. The stresses for the two models are shown in Figure 11 for a glass thickness of 10 mm. As shown only half of the drilling and the anchor system is simulated because of symmetric reasons. The results of the principle tensile stresses are given in Figure 13 for the model 1. The results are calculated separately for two paths (Figure 12). One path called edge, at the edge of the model and one called middle, which is set in the area of the maximum stresses beside the screw.

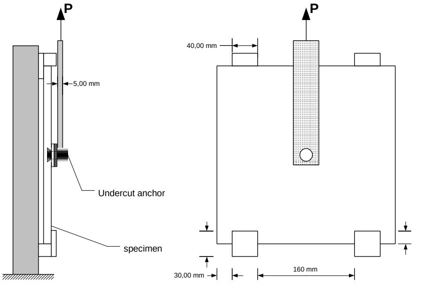

Figure 9: Test set-up, shear-off test

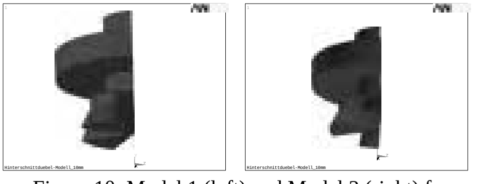

Figure 10: Model 1 (left) and Model 2 (right) for Shear-off test

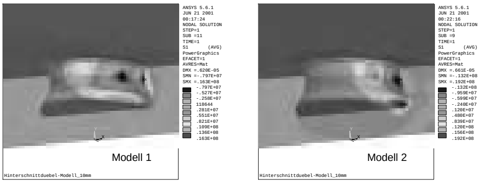

Figure 11: Tensile stresses for the shear-off test for the two models.

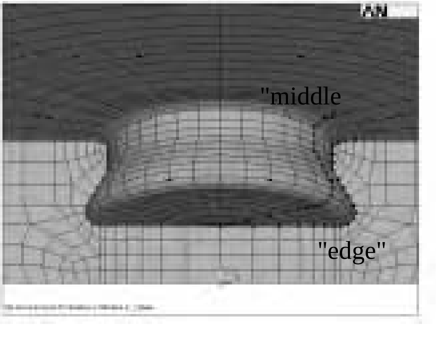

Figure 12: Paths edge and middle

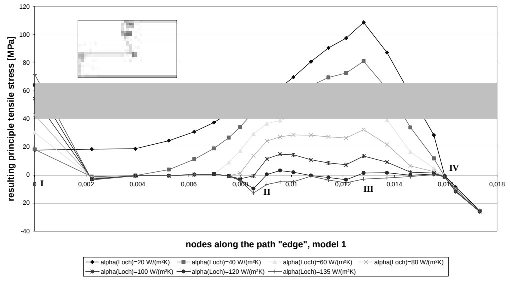

Figure 13a: Resulting principle tensile stress on the surface of a 10 mm tempered glass for different heat transfer coefficients, grey area: failure range of annealed glass, shear-off test, model1, path edge

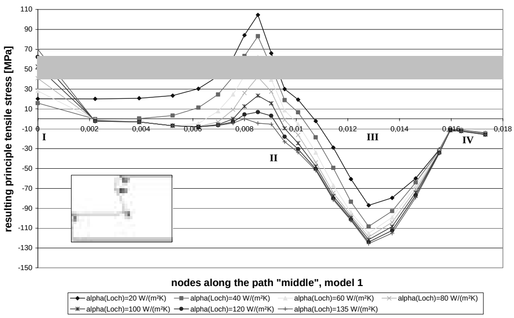

Figure 13b: Resulting principle tensile stress on the surface of a 10 mm tempered glass for different heat transfer coefficients, grey area: failure range of annealed glass, shear-off test, model 1, path middle

C. *Results*

With consideration of the pull-out test and the shear-off test for both examined thicknesses, the apparent heat transfer coefficient could be identified to be always in the range of 60 ± 20 W/(m²K) for different commercial glasses and tempering processes. The results of the pull-out test deviate less than the results from the shear-off tests. For this heat transfer coefficient, the whole undercut area is under compression (Figure 5) to prevent subcritical crack growth.

IV. Full Scale Tests

As further investigations full scale test were examined. The specimens were tested in the dimension from 1200 x 2200 mm² up to 1200 x 4000 mm². The glass types varied from tempered glass with 10 mm and 12 mm, to laminated safety glass made of tempered and heat strengthened glass. Different numbers of fittings for the different dimensions of the glass specimens were taken. The tests were done by loading the glass specimen using an airbag with air compression. The load was kept constant for a certain span of time at defined load steps. For each load step the displacement of several points of the specimens were taken. The test set-up is shown in Figure 14. The results for the compression load test were satisfying and lead to the possibility to use the tested specimens up to 100 m high buildings with an safety factor of 3,0 (for this load case). The suction test gave inferior results. Especially the high loads at the edges of buildings from wind suction allow the use only up to 8 m at the moment.

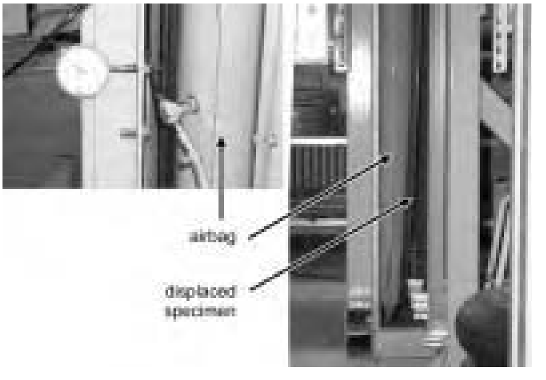

Figure 14: Full scale load bearing tests

V. Conclusion and Further Research

Fastening of glass panes with undercut anchors is a possibility for tempered glass. A special geometry of hole and anchor, a plastic interlayer and very accurate CNC-drilling are required. Numerical results show that apparent heat transfer coefficients (neglecting the heat radiation influence) of 60 ± 20 W/(m²K) in the undercut area are realistic for commercial glasses and tempering processes preventing subcritical crack growth due to surface compression stresses in the whole undercut area. Photoelastic measurements in the undercut area should be made to validate the results. Moreover, full scale load capacity tests proofed the performance of the anchor system. Further researches deal with a new circlip instead of the curved steel for a higher load bearing capacity.

REFERENCES

[Aben, 1993]
ABEN, H., GUILLEMET, C., *Photoelasticity of Glass*, Springer, Berlin 1993

[Ansys 1999]
ANSYS 5.5.2, *Theory Reference 4.6: Viscoelasticity*, Eigth Edition, 1999

[Bathe 1990]
BATHE, K.J., *Finite-Elemente-Methoden*, Springer, Berlin 1990

[Block 2001]
BLOCK, C., *Bestimmung der Festigkeit von Glas im Bereich einer Hinterschnittbohrung*. Studienarbeit am Institut für Statik, TU Darmstadt, 2001, unpublished

[Carré 1999]
CARRÉ, H.; DAUDEVILLE, L., *"Load-bearing capacity of tempered structural glass"*, Journal of Engineering Mechanics, Vol. 125 (1999), No. 8, pp 914-921

[Fischer 2000]
ARTUR FISCHER GMBH & CO. KG, *Informationsblatt über Glasbefestigung mit Hinterschnittanker FZP-G*, Edition 4/2000

[Laufs 2000]
LAUFS, W., *Ein Bemessungskonzept zur Festigkeit thermisch vorgespannter Gläser*. Dissertation (PhD-thesis), Lehrstuhl für Stahlbau der RWTH Aachen, Shaker-Verlag, 2000.

[Narayanaswamy 1971]
NARAYANASWAMY, O.S., *A Model for Structural Relaxation in Glass*, J. Am. Ceram. Soc., Vol. 54 (1971) No. 10, pp 491-498

[Narayanaswamy 1978]
NARAYANASWAMY, O.S.: *Stress and Structural Relaxation in Tempering Glass*, J. Am. Ceram. Soc., Vol. 61 (1978) No. 3, pp 146-152

[Scherer 1986]
SCHERER, G.W., *Relaxation in Glass and Composites*. Wiley, New York 1986.

[Schneider 2001]
SCHNEIDER, J.: *Festigkeit und Bemessung von Glas: Punktgelagerte Verglasungen, Dynamisch beanspruchte Verglasungen bei weichem Stoß*. Dissertation (PhD-thesis), Institut für Statik TU Darmstadt, 2001.

[Soules 1987]
SOULES, T.F., BUSBEY, R.F., REKHSON, S.M., MARKOVSKY, A., BURKE, M.A., *Finite Element Calculation of Stresses in Glass Parts Undergoing Viscous Relaxation*, J. Am. Ceram. Soc., Vol. 70 (1987) No.2, pp 90-95

EU COST C13 Glass and Interactive Building Envelopes. M. Crisinel, et al. (Eds.). IOS Press, 2007.

Point Bearing Elements Research Investigations

Ruth Kasper and Gerhard Sedlacek
RWTH Aachen – Institute of Steel Construction, Germany

Point bearings are a popular element of modern glass constructions. On the one hand point bearings are elements that can be used to design transparent buildings, on the other hand point fixings allow for a good failure resistance after breakage of a laminated glass panel.

Due to the brittle behaviour of glass the knowledge about the rupture process in the glass hole and the influence of the point bearing geometry is important. The article gives an overview on the investigated research projects of the RWTH Aachen, the results as well as the proposed methods to solve the design problem "point bearing".

Keywords: glass, design, point-fixings

I. Introduction

Figure 1 shows an transparent roof structure made of point supported glazing.

Figure 1: Example

Point fixings possess different geometries and materials to avoid contact between glass and steel. The geometry of the hole can be cylindrical or conical (Figure 2). Besides the general static system these parameters have an influence on the stress concentration around the glass holes caused by loading.

Figure 2: Types of point-fixings

The quality of the stress concentrations can be determined with finite element methods by modeling the hole, the geometry of the point-fixing and the stiffness of the separating materials. The results can be manipulated by variation of several parameters. Following this, finite element analysis are not useful for this application without any verifying tests. To ensure a safe design of point-supported glazing a method needs to be developed that takes into account the individual behavior of the types of point-fixings.

Generally, the material used for point-supported glazing is thermally toughened or heat strengthened glass. Thermally treated glasses possess a higher material resistance and can bear the concentrated stresses near to the holes. The material resistance near to the hole has been analyzed by [Laufs 2000, Carre 1996, Schneider

2001]. The investigations included breakage tests (Figure 3), numerical modelling of the distribution of the pre-stressing and measuring of the pre-stressing, both near to the hole. The latter has been done by using optical measurement devices. Therefore the material resistance of the hole of tempered glass is known. Figure 4 shows the distribution of the pre-stressing of a conical hole.

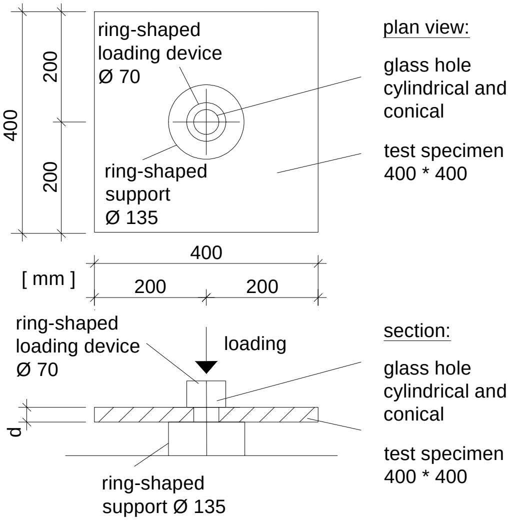

Figure 3: Breakage tests at glass holes

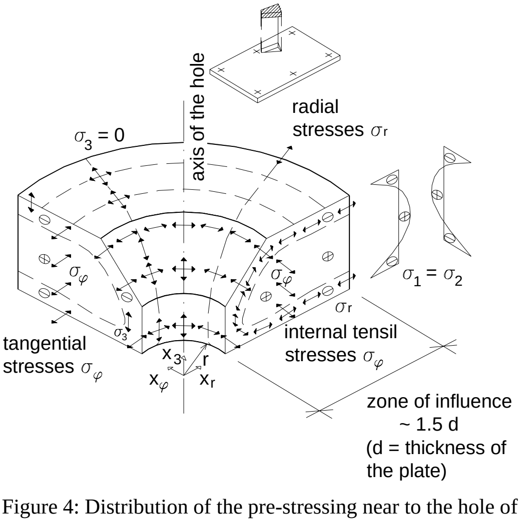

Figure 4: Distribution of the pre-stressing near to the hole of tempered glass

In the frame of actual research investigations of the University of Aachen three different methods have been analyzed and evaluated. All design concepts are based on small-scale tests. With the aid of the small-scale tests force-stress-characteristics for each type of point-fixing could be developed.

Design concept 1 uses the developed force-stress-characteristics for the calibration of simplified finite element models. The functionality of this method has been proofed [Wolf 2004, Kasper 2004].

Design concept 2 contains the proposition that the quantity of the stress concentration is depending on the reaction forces at the point-fixings, but the numerical investigation showed that this proposition is not valid [Wolf 2004].

Design concept 3 is based on the hot-spot method used in the field of steel constructions. The adaptability on point-fixings has been analyzed and the evaluation showed that further investigations are necessary for the validation [Wolf 2004].

In the following the execution of the tests for the development of the force-stress-characteristics are described. Furthermore the results of the examination of the different design methods are summarized.

II. Development of Force-Stress-Characteristics for Point-Fixings

The force-stress-characteristic of point fixings depends on the geometry of the test specimen and the geometry of the point-fixings. Here, a standard point-fixing is used exemplary to show the usability of the concept.

The force-stress-characteristic of point-fixings has been developed for test specimen with the size of 400 mm x 400 mm. The thickness of the test specimen was 10 mm. The tests specimens were line-supported on two opposite sides (Figure 6). The specimens were loaded under 4 different angles. Figure 5 shows the test set-up and the different loading directions. During the tests strain gauges measured the strain at several points (Figure 6).

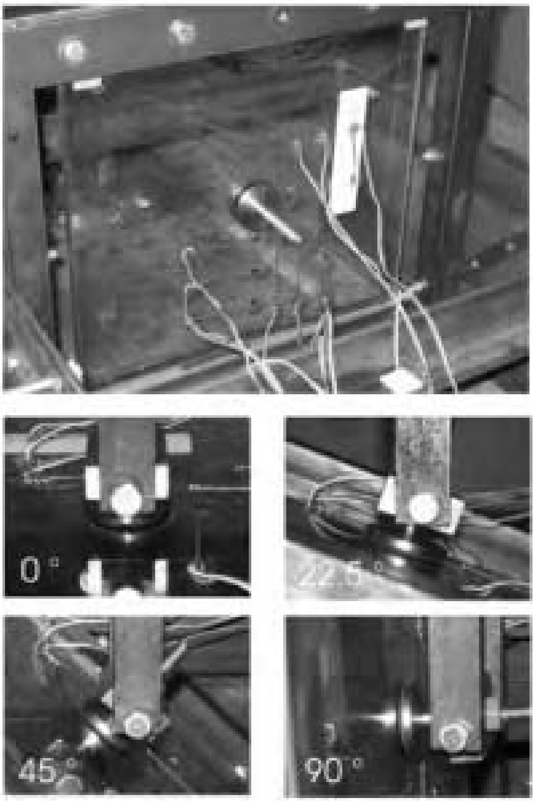

Figure 5: Test set-up and loading directions of the small-scale tests

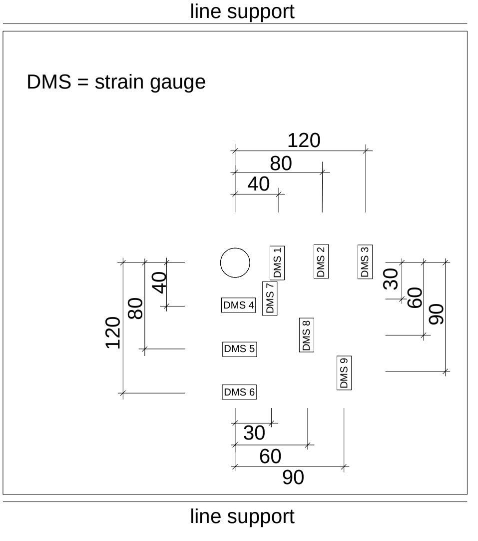

Figure 6: Strain measurements and static system

The evaluation of the test results (force-strain-curves) has been based on finite element calculations. For the finite element model volume elements and contact approaches were used. Figure 7 shows details of the finite element model.

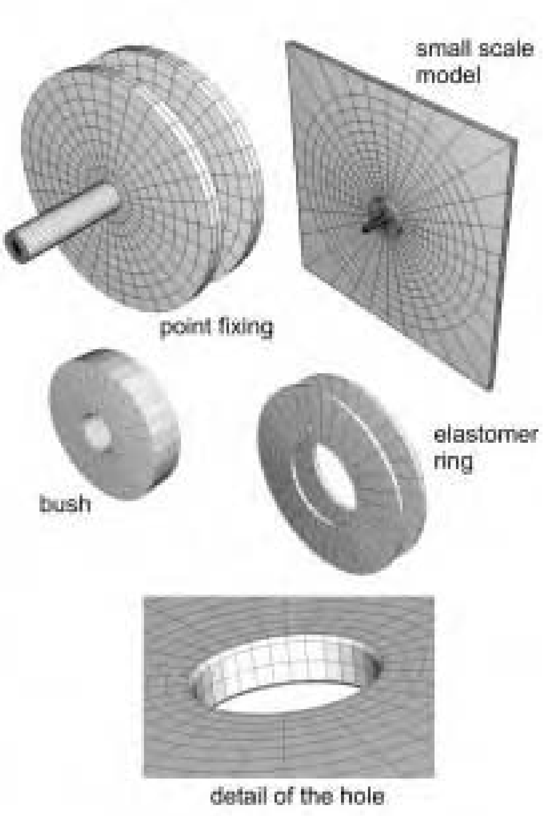

Figure 7: Details of the finite-element-model

The model's calibration has been done by variation of the E-Modulus of the separating materials and by comparing the measured as well as the calculated strains. For each loading direction a data sheet has been developed. The data sheet shows the comparison between the measured and the calculated values on the different paths, the distribution of the principal stresses and the maximum stress concentration next to the hole. Table 1 shows an abstract of the data sheet for the loading direction of 0°. Analogous data sheets for each loading angles have also been developed.

TABLE 1:
DATA SHEET WITH STRESS-STRAIN-CHARACTERISTIC FOR THE LOADING DIRECTION OF 0°

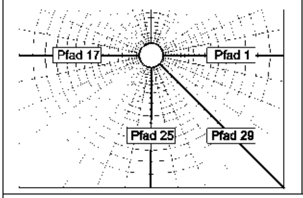

Load F = 2500 kN

Eccentricity e = 0 mm

E-Modulus bush

E = 350 N/mm²

E-Modulus elastomer ring E = 25 N/mm²

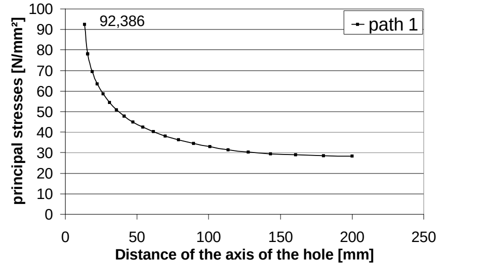

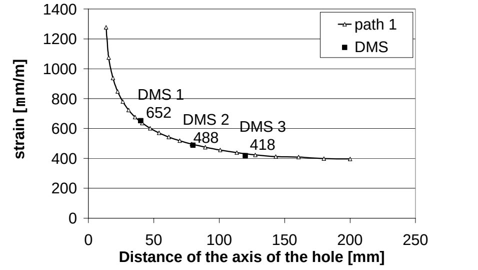

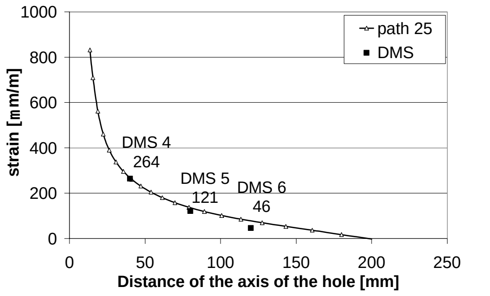

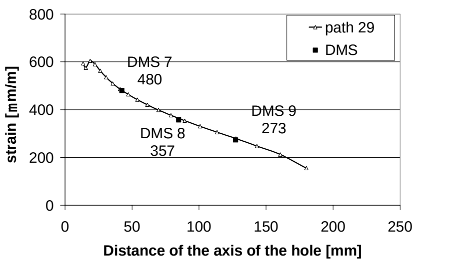

III. TEST OF DESIGN CONCEPT 1 - USING FORCE-STRESS-CHARACTERISTICS FOR THE CALIBRATION OF SIMPLIFIED FINITE ELEMENT MODELS

For the verification of this design method further original size tests were executed. The proceeding was the same as for the small-scale tests. The tests were made for two different geometry: 1000 mm x 1000 mm with 4 point-fixings and 2000 mm x 1000 mm with 6 point-fixings. The test specimens were loaded with a single load at midspan.

The original size tests were also evaluated with finite element calculations: the results show that the discrepancies between the measured and the calculated strain values are higher than for the small-scale tests. Reasons for this can be imperfections of the test set-up.

The next step was the use of simplified models calibrated with the aid of the data sheets including the force-stress-characteristics. If the model confirms the results or gives higher stress-concentrations next to the hole, the model can be used for the design of the point-supported glass panel. After the results of the original size tests were confirmed with the simplified model.

Table 2 and table 3 compare the results of the stress concentration of the calibrated and a simplified model. For the simplified model also volume elements were used but the contact approach was neglected. The results show that it is possible to determine the stress concentrations of large scale components with a model which has been calibrated on the basis of small scale tests.

TABLE 2: COMPARISON BETWEEN THE STRESS CONCENTRATIONS (CALIBRATED MODEL AND SIMPLIFIED MODEL) - SMALL SCALE TESTS

	Calibrated model	Simplified model	Ratio
E-Modulus elastomer ring	E = 25 N/mm²	E = 10 N/mm²	[-]
0°	92,4 N/mm²	95,9 N/mm²	1,04
22,5°	89,7 N/mm²	90,2 N/mm²	1,01
45°	75,9 N/mm²	75,1 N/mm²	0,99
90°	46,5 N/mm²	55,2 N/mm²	1,19

TABLE 3: COMPARISON BETWEEN THE STRESS CONCENTRATIONS (CALIBRATED MODEL AND SIMPLIFIED MODEL) - LARGE SCALE TESTS

	Calibrated model	Simplified model	Ratio
E-Modulus elastomer ring	E = 25 N/mm²	E = 10 N/mm²	[-]
1000 mm x 1000 mm with 4 point supports	53,5 N/mm²	62,5 N/mm²	1,17
2000 mm x 1000 mm with 6 point supports			
Hole at the edge	8,8	9,98	1,134
Hole in the corner	88,4	93,5	1,058

IV. TEST OF DESIGN CONCEPT 2 - "THE STRESS CONCENTRATION NEXT TO THE HOLE DEPENDS ON THE REACTION FORCES AT THE POINT-FIXING"

It can be easily shown that this thesis is not valid. For the demonstration the calibrated finite element model was used. The system is statically determined and the eccentricity of the point-fixing is equal to zero, which means that only vertical reaction forces exist. The geometry of the system is varied and the system is loaded with a uniformly distributed loading. The quantity of the loading is determined in that way that the vertical reaction forces are equal to 1250 N for each system.

The results are shown in Table 4. The maximum principal stresses vary between 31,4 N/mm² and 46,5 N/mm². That means that the stress concentration does not depend only on the quantity of the reaction force but also on the global proportions of the plate. For comparison the stress concentration for the centrical loaded (0°C, F = 1250 N) small scale test specimen is 46,2 N/mm².

The results show that the thesis is not useful and the quantity of the stress concentration is influenced by further parameters.

TABLE 4 RESULTS OF NUMERICAL STUDY FOR DESIGN CONCEPT 2

System	Geometry	Span	q	A_x and A_y	A_y	$\sigma_{max,hole}$
	[m]	[mm]	[N/mm²]	[N]	[N]	[N/mm²]
1	1,0 x 1,0	800	0,005	0	1250	31,4
2	1,25x1,25	1050	0,0032	0	1250	35,3
3	1,5 x 1,5	1300	0,00222	0	1250	37,7
4	2,0 x 1,0	900	0,0028	0	1250	46,5

V. TEST OF DESIGN CONCEPT 3 - "HOT SPOT METHOD"

The hot-spot method is used, for example, for designing details of steel constructions. The stress concentrations due to welds or details are taken into account by the aid of stress concentration factors. It is sufficient to determine the global stresses near to the detail and to multiply the stress with the stress concentration factor.

The first question to answer is: Is it possible to determine a reasonable stress distribution over the plate without a detailed point-fixing? The plate is modeled without holes and one node in the geometrical center of the hole is restrained in vertical direction. Depending on the number of elements the global stress distribution is equal to the stress distribution of the model with a detailed point fixing (Figure 8 and 9). Consequently it is possible to verify a geometrical stress that is more or less independent of the modeling of the point fixing.

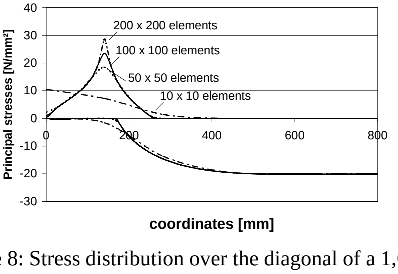

Figure 8: Stress distribution over the diagonal of a 1,0 m x 1,0 m plate depending on the number of elements

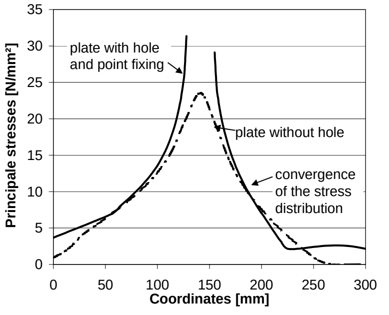

Figure 9: Comparison between stress distribution of the simplified model and the detailed model next to the hole (1,0 m x 1,0

Figure 10 shows the influence of the plate size on the stress distribution in the area of the point fixing. The scaled illustration makes clear that the form of the stress concentration is not only depends on the geometry and the materials of the point fixing but also on the geometry of the plate.

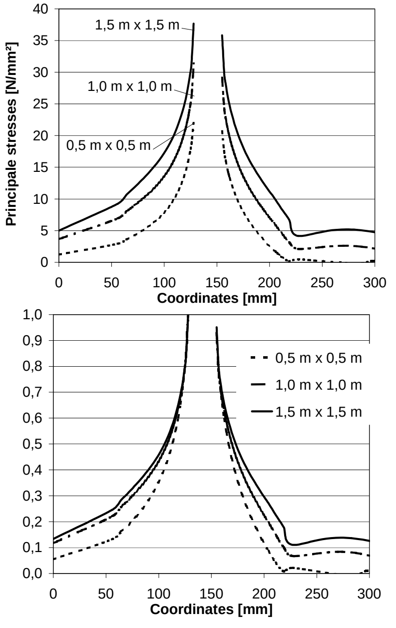

Figure 10: Comparison between the stress distribution next to the hole for different sizes of the plate (non-scaled and scaled illustration)

Furthermore the investigations have shown that the stress concentration factor not only depends on the size and the geometry of the plate but also on the kind of loading (existent distributed loading near to the point fixing).

VI. SUMMARY AND PROSPECTS

The paper shows different possibilities for the design of point-supported glazing. The design based on force-stress-characteristic is already a proved possibility for the specification of the behaviour of point-fixings. With further research investigations the possibility of the application of the "hot-spot" needs to be analyzed to define the different parameters.

VII. ACKNOWLEDGMENT

The investigations could be done by the support of the "Fachverband Konstruktiver Glasbau (FKG) e.V.".

REFERENCES

[Carre 1996] Carre, H: Etude du comportement a la rupture d'un materiau fragile precontraint : le verre trempe. These 1996.

[Kasper 2004] Kasper, R ; Sedlacek G : Bemessungskonzept für punktförmig gelagerte Scheiben. FKG - Arbeitskreis Punktgestützte Gläser. 8. Forschungsvorhaben 2004.

[Laufs 2000] Laufs, W: Ein Bemessungskonzept zur Festigkeit thermisch vorgespannter Gläser. Promotion 2000.

[Schneider 2001] SCHNEIDER, J.: Festigkeit und Bemessung von Glas: Punktgelagerte Verglasungen, Dynamisch beanspruchte Verglasungen bei weichem Stoß. Dissertation (PhD-thesis), Institut für Statik TU Darmstadt, 2001.

[Wolf 2004] Wolf, H : Experimentelle und numerische Untersuchung von punktförmig gehaltenen Glasscheiben im Hinblick auf ein Bemessungskonzept. Diplomarbeit 2004 Lehrstuhl für Stahlbau RWTH Aachen (not published)

EU COST C13 Glass and Interactive Building Envelopes. M. Crisinel, et al. (Eds.). IOS Press, 2007.

Pre-design of Discretely Supported Glass under Uniform Loading with the Help of Interpolation

Jürgen Neugebauer
Graz University of Technology – Institute of Structural design, Austria

In the planning process it is helpful that rectangular glass panels under uniform loading can be designed very fast. Furthermore it is important to check the results of a FE calculation.

A calculation of many different discretely supported glass panels under an uniform load with the value *q=1,0 kN/m²* with the help of the FE method results in values of stresses and deformations. The insertion of these values in a 3D-diagramm, results in a surface of results of stresses or deformations. For a pre-design this surface of the shape of a hyperbolic paraboloidal shell is exact enough. A linear interpolation in this surface is very easy.

With a short number of input data, such as the distance in direction length, the distance in direction across or the thickness of the glass panel, it is possible to interpolate the results of stress in this shape. The interpolation results must be calibrated with other influences for example with the diameter of the the hole and the distance of the hole to the edges and with the shore hardness of the rubber at the support.

Keywords: interpolation, discrete support, glass fitting

I. Introduction

For a finite element calculation there are many different parameters to be defined, on the one hand geometrical parameters such as the size or the thickness of the glass pane, and on the other hand parameters of the different materials such as the glass, the rubber or the steel of the glass fitting.

For results a lot of time is needed, which in some cases does not exist. A concept to shorten the design time is desirable. Furthermore it is important to check the computed results of a FE method calculation. A possibility is, to check all the input data, and to believe the computed results. Another possibility is, to check the results itself, with calculated results one gets in another way.

II. Stresses and Deformations

A finite element calculation results in values for the stresses and values for the deformations of each point of the glass pane. In Figure 1 to Figure 3 see the results of a finite element calculation. The results are the principal stresses σ_1 and σ_2 and the deformation w.

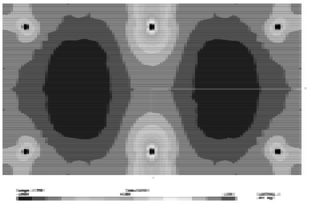

Figure 1: Results of the principal stresses σ_1

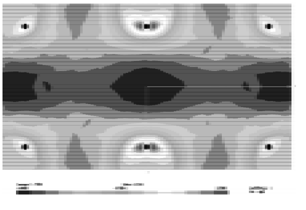

Figure 2: Results of the principal stresses σ_2

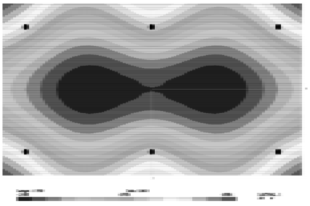

Figure 3: Results of the deformation *w*

One can see that the maximum of the stresses σ_1 are located in the area around the hole and the maximum of the principal stresses σ_2 are located in the middle of the glass pane. The maximum deformation is in the middle of the glass pane. In most cases the maximum of principal stresses are located around the hole.

III. DIFFERENT STATIC SYSTEMS

The most used glass panes are rectangular. For this type it is possible to separate the static systems by the numbers of the glass fittings, see in Figure 4. The results of a calculation of the principal stress σ_1, see in Figure 5, shows that there is a big difference between the results of the system with 4 and system with 6 glass fittings. By a further increase of the number of the supports the difference between the results is little. One can reduce the problem to three kinds of rectangular glass panes with 4, 6 and 8 glass fittings, see in Figure 4.

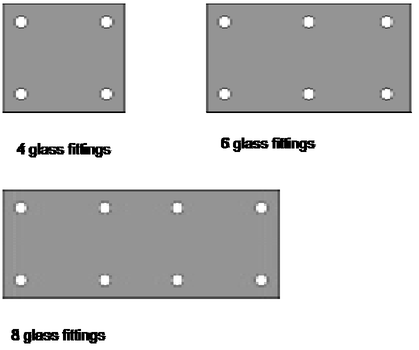

Figure 4: Different static system of point load supported glass panes

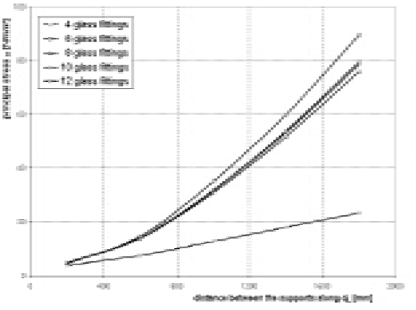

Figure 5: Results of the principal stresses σ_1 with different numbers of glass fittings

IV. INPUT DATA

The basic idea for the interpolation is to define different geometrical sizes, analyse them, and interpolate in between the different values.

The geometrical input data required for the interpolation are the distance in direction length d_L the distance in direction across d_C and the thickness see in Figure 6.

The materials are defined with the elasticity modulus $E = 70000\ N/mm^2$ and the Poisson´s ratio $\nu = 0.23$. These values for the materials are constant values in the interpolation process.

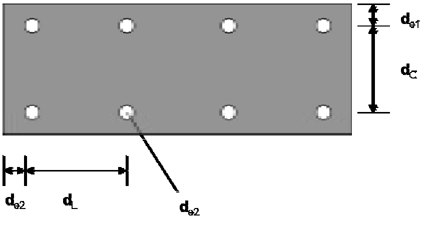

Figure 6: Input data of the glass pane

d_C	distance between the glass fitting in direction across [mm]
d_L	distance between the glass fitting in direction length [mm]
d_H	diameter of the glass hole [mm]
d_{e1}	distance to the edge in direction across [mm]
d_{e2}	distance to the edge in direction length [mm]

V. Interpolation of Principal Stresses

The results of the principal stresses of different calculations with different geometries are able to be drawn into diagrams. The diagrams for the different static systems are shown in Figure 7 to Figure 9. An important fact is that the graphs of the results in the different static systems are nearly straight. With this fact a linear interpolation in between them is possible. Coefficients depending on the numbers of glass fittings are created in table 1 to table 3.

The basis for the calculation of the maximum principal stresses is the equation (1). Depending on the numbers of the glass fittings the coefficient *C* has to be chosen out of table 1 to table 3. Interim values can be interpolated linear. The interpolation is based on a fixed diameter of the hole, a fixed distance to the edges and a fixed shore hardness of the rubber at the supports.

For the calculations the thickness of the glass pane was assumed to be *h=10 [mm]* and the diameter of the hole was d_H*=30 [mm]*. The distance to the edges were given with $d_{e1} = 100$ *[mm]* and $d_{e2} = 110$ *[mm]*. The load was given with *q=1.0 [kN/m²]*. For the rubber at the supports the shore hardness was assumed to be 20 *[-]*. The results of the principal stresses are drawn into the diagram shown in Figure 7 to Figure 9. For all other geometrical input data one can multiply the interpolated result with the coefficients *(c_1, c_2, c_3)*. These influences are dealt with later. With the assumption of theory of small deformations one can do a linear static calculation.

$$\sigma_{\max} = \frac{C}{h_{ef,\sigma i}{}^{2}} \cdot q \cdot c_1 \cdot c_2 \cdot c_3 \cdot 1E6 \qquad (1)$$

σ_{max}	maximum principal stress [N/mm²]
C	coefficient dependent on the numbers of glass fittings [mm²]
q	uniform load on the glass pane [N/mm²]
c_1	coefficient depending on the influence of the diameter of the hole [-]
c_2	coefficient depending on the influence of the distance to the edge [-]
c_3	coefficient depending on the influence of the shore stiffness of rubber [-]
$h_{ef,\sigma i}$	fictive thickness of the glass pane for the verification of the stresses [mm]

A. Point load fixation with 4 glass fittings

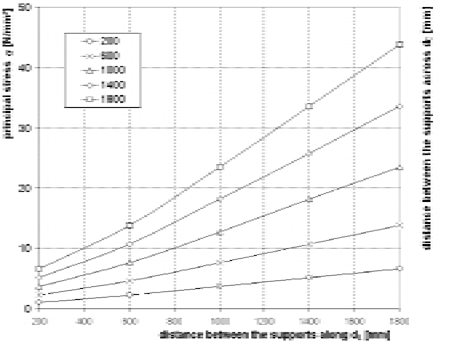

Figure 7: Principal stress σ_1 of a glass pane with 4 glass fittings

TABLE 1:
COEFFICIENT **C** FOR 4 GLASS FITTINGS

dC/dL	200	600	1000	1400	1800
200	0,11	0,23	0,37	0,52	0,66
600	0,23	0,46	0,77	1,08	1,39
1000	0,37	0,77	1,28	1,82	2,35
1400	0,52	1,08	1,82	2,58	3,36
1800	0,66	1,39	2,35	3,36	4,38

B. Point load fixation with 6 glass fittings

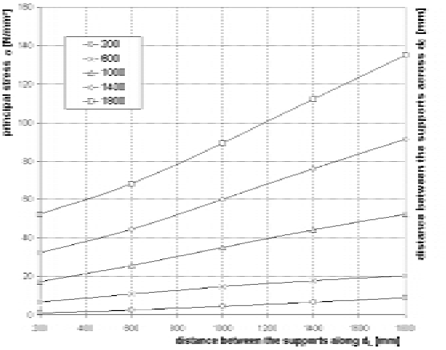

Figure 8: Principal stress σ_1 of a glass pane with 6 glass fittings

TABLE 2:
COEFFICIENT **C** FOR 6 GLASS FITTINGS

dC/dL	200	600	1000	1400	1800
200	0,11	0,67	1,73	3,24	5,22
600	0,26	1,09	2,55	4,46	6,83
1000	0,45	1,48	3,51	6,01	8,94
1400	0,67	1,78	4,43	7,59	11,21
1800	0,89	2,02	5,25	9,12	13,49

C. *Point load fixation with 8 glass fittings*

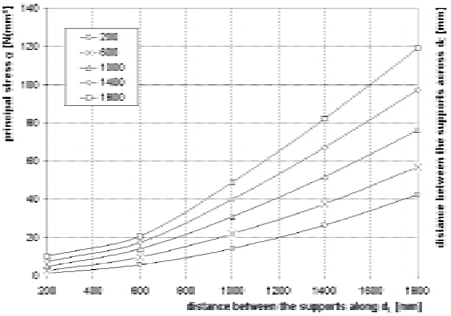

Figure 9: Principal stress σ_1 of a glass pane with 8 glass fittings

TABLE 3:
COEFFICIENT **C** FOR 8 GLASS FITTINGS

dC/dL	200	600	1000	1400	1800
200	0,11	0,57	1,42	2,64	4,24
600	0,26	0,97	2,18	3,75	5,68
1000	0,49	1,38	3,10	5,17	7,61
1400	0,75	1,75	4,01	6,69	9,72
1800	1,03	2,06	4,88	8,20	11,90

VI. INTERPOLATION IN 3D-DIAGRAMM

It was shown, in the earlier chapters, that the lines of the results for the principal stresses σ_1 are nearly straight. It is possible to create a 3D-diagram, like a coordinate system – (*x, y, z*). The coordinate x is the distance in direction lengthwise and the coordinate *y* is the distance in direction across. In the direction *z* the results of the maximum principal stress of the glass pane are plotted in. The sum of all these values results in a shape of a hyperbolic paraboloidal shell.

With this fact it is possible to make a linear interpolation between the different distances in direction lengthwise and cross.

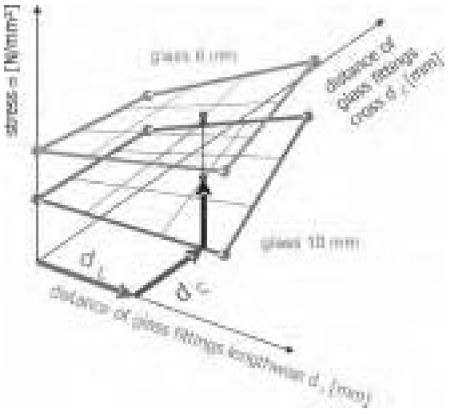

Figure 10: 3D-concept of the interpolation

This concept is easy to implement it into a program such as Excel. With a calculation of results at the corners of the 3D-surface all other geometrical possibilities can be obtained by a interpolation in between them, see in Figure 10.

VII. APPROXIMATION OF THE DEFORMATION

The idea was, to model beams in the line of the supports with the unit width of *b=1 [mm]* and the height of the thickness of the glass pane. It is possible to arrange these beams in a special way to get a good approximation for the deformation. One can see the assembling of these beams for the different number of glass fittings in Figure 16, 18 or 20. The load *q [N/mm²]* of for the uniform load of the glass pane is equal to the load *q [N/mm]* of the beam, due to the unit width of *b=1 [mm]*.

For a beam there are three basic possibilities for their support behaviour. A free supported beam on both sides is the first possibility. The second is a beam restrained on one side and hinged on the other side. The third beam is fixed on both sides see in Figures 11 to 13. For the beams it is also possible to have a projecting end on the hinged supported side, see in Figure 14 and 15.

$$w = \frac{5}{384} \cdot \frac{q \cdot d^4}{E \cdot I} \tag{2}$$

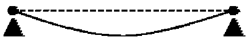

Figure 11: Hinged supported beam

$$w = \frac{2}{369} \cdot \frac{q \cdot d^4}{E \cdot I} \tag{3}$$

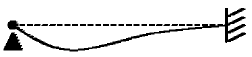

Figure 12: One side hinged supported and the other side restrained supported beam

$$w = \frac{1}{384} \cdot \frac{q \cdot d^4}{E \cdot I} \tag{4}$$

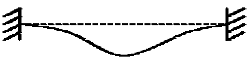

Figure 13: Restrained supported beam

$$w = \frac{1}{16} \cdot \frac{q \cdot d^4}{E \cdot I}\left(\frac{5}{24} - \frac{d_e^2}{l^2}\right) \tag{5}$$

Figure 14: Hinged supported beam with projecting ends

$$w = \frac{1}{384} \cdot \frac{q \cdot d^4}{E \cdot I} \tag{6}$$

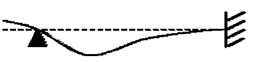

Figure 15: One side hinged supported and the other side restrained supported beam with a projecting end

With these values one is able to compute each deformation of each beam in both directions. The concept of the approximation is to sum up each deformation of each beam. The possibilities of the assembling for the different numbers of supports will be shown in the following.

A. Point load fixation with 4 glass fittings

For a glass pane with 4 supports it is the sum of the deformations both directions (along and across) of hinged supported beams with projecting ends, (Figure 14).

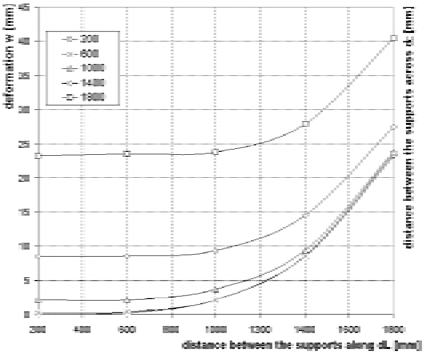

Figure 15: Deformation of a glass pane with 4 glass fittings

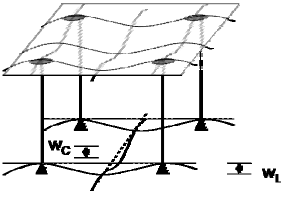

Figure 16: Approximation concept of a glass pane with 4 glass fittings

$$w = w_L + w_C$$
$$w = \frac{q \cdot d_L^4}{16 \cdot E \cdot I} \cdot \left(\frac{5}{24} - \frac{de_2^2}{d_L^2}\right) + \frac{q \cdot d_C^4}{16 \cdot E \cdot I} \cdot \left(\frac{5}{24} - \frac{de_1^2}{d_C^2}\right) \tag{7}$$

w	deformation [mm]
q	load on the beam [N/mm]
d_L	distances between the glass fittings along [mm]
d_C	distances between the glass fittings across [mm]
E	elasticity modulus [N/mm²]
I	moment of inertia [mm^4]
d_e	projecting end (distances to the edge) [mm]

B. Point load fixation with 6 glass fittings

For a glass pane with 6 supports it is the sum of the deformations along of a one side hinged supported beam with projecting end (Figure 12) and across a hinged supported beam with projecting ends (Figure 14).

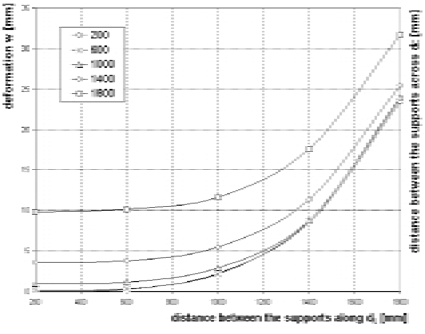

Figure 17: Deformation of a glass pane with 6 glass fittings

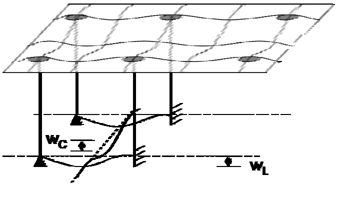

Figure 18: Approximation concept of a glass pane with 6 glass fittings

$$w = w_L + w_C$$
$$w = \frac{2 \cdot q \cdot d_L^4}{369 \cdot E \cdot I} \cdot + \frac{q \cdot d_C^4}{16 \cdot E \cdot I} \cdot \left(\frac{5}{24} - \frac{de_1^2}{d_C^2} \right) \tag{8}$$

C. Point load fixation with 8 glass fittings

For a glass pane with 8 supports it is the sum of the deformation along of a one side free supported and the other side restrained supported beam (Figure 12) and the deformation across of a hinged supported beam (Figure 11). The values were modified slightly, see in equation (9).

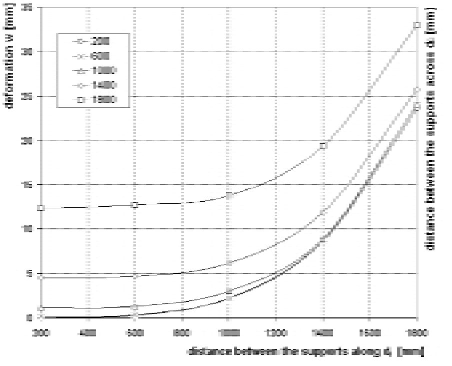

Figure 19: Deformation of a glass pane with 8 glass fittings

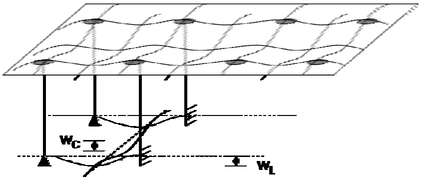

Figure 20: Deformation of a glass pane with 8 glass fittings

$$w[mm] = w_L + w_C$$
$$w = \frac{2{,}5 \cdot q \cdot d_L^4}{369 \cdot E \cdot I} \cdot + \frac{4{,}5 \cdot q \cdot d_C^4}{384 \cdot E \cdot I} \cdot \tag{9}$$

VIII. Influence of the Thickness

For glazing systems a single glass or a laminated glass is possible. For a single glass the definition of the thickness is trivial. In the case of a laminated glass one has to consider a composite cross section. It is possible, to arrive at a simple solution using the concept of a virtual thickness. With this trick one can compute laminated glass in the same way as a single glass. How it goes, is shown in the following equations [Bucar et al., 2002].

$$h_{ef,w} = \sqrt[3]{h_1^3 + h_2^3 + 12 \cdot \Gamma \cdot I_s} \tag{10}$$

$$\mathrm{h}_{1,\mathrm{ef},\sigma} = \sqrt{\frac{\mathrm{h}_{\mathrm{ef,w}}^3}{\mathrm{h}_1 + 2 \cdot \Gamma \cdot \mathrm{h}_{\mathrm{s},1}}} \tag{11}$$

$$h_{2,ef,\sigma} = \sqrt{\frac{h_{ef,w}^3}{h_2 + 2\cdot\Gamma\cdot h_{s,2}}} \qquad (12)$$

with

$$\begin{aligned} h_s &= 0,5\cdot(h_1+h_2)+h_v \\ h_{s,1} &= h_s\cdot h_1/(h_1+h_2) \\ h_{s,2} &= h_s\cdot h_2/(h_1+h_2) \\ I_s &= h_1\cdot h_{s,1}^2 + h_2\cdot h_{s,2}^2 \end{aligned}$$

h	thickness of the glass pane [mm]
h_1	thickness of the glass pane 1 of a laminated glass with two glass panes [mm]
h_2	thickness of the glass pane 2 of a laminated glass with two glass panes [mm]
$h_{ef,w}$	virtual thickness for the verification of the deformation [mm]
$h_{1ef,\sigma1.}$	virtual thickness of the glass pane 1 for the verification of the stresses [mm]
$h_{2ef,\sigma2.}$	virtual thickness of the glass pane 2 for the verification of the stresses [mm]
h_v	thickness of the PVB-interlayer [mm]

The shear transmission factor Γ is given with:

$$\Gamma = \frac{1}{1+9,6\cdot\frac{E}{G}\cdot\frac{I_s\cdot h_v}{h_s^2\cdot a^2}} \quad 0\le\Gamma\le 1 \qquad (13)$$

with

$$\begin{aligned} I_s &= h_1\cdot h_{s,1}^2 + h_{s,2}^2 \\ h_s &= 0,5\cdot(h_1+h_2)+h_v \\ h_{s,1} &= h_s\cdot h_1/(h_1+h_2) \\ h_{s,2} &= h_s\cdot h_2/(h_1+h_2) \end{aligned}$$

E…	elasticity modulus [N/mm²]
G…	shear modulus in respect to the boundary conditions, see in table 1 [N/mm²]
a…	length of the shorter side of the glass pane [mm]
l_v…	span length (distance between the glass fittings) [mm]

TABLE 4:
SHEAR MODULUS G IN N/mm²

temperature in the PVB-interlayer	loading duration		
	short-time	mid	always
< 25°C	0,75	0,5	0,01
≥ 25°C	0,5	0,25	0,01

TABLE 5:
LOADING DURATION – LOAD TYPE

loading duration	load type
short-time	wind
mid	climatic load
always	dead load

These equations can be simplified with an assumption of two extreme shear transmission behaviours, in a carrying behaviour of full bond between the glass panes for short load durations and without a full bond for long load durations.

If there is a system with a full bond it is the following equation:

$$h_{ef,w} = h_{ef,\sigma} = \Sigma h_i \qquad (14)$$

If there is a system without bond it will be the following equations:

$$h_{ef,w} = \sqrt[3]{\Sigma h_i^3} \qquad (15)$$

$$h_{ef,\sigma i} = \sqrt{\frac{\Sigma h_i^3}{h_i}} \qquad (16)$$

h_i	thickness of each glass pane [mm]
$h_{ef,w}$	virtual thickness for the verification of the deformation [mm]
$h_{1ef,\sigma i.}$	virtual thickness of each glass pane for the verification of the stresses [mm]

IX. INFLUENCE OF THE DISTANCE OF THE HOLE TO THE EDGE

To get the influence of the distance $d_{e1}$of the hole to the edge on the principal stresses, calculations were done. The distance to the edge $d_{e1}$was varied from 40 mm to 200 mm. With these values of the diagram the interpolated results can be calibrated for another distances to the edge.

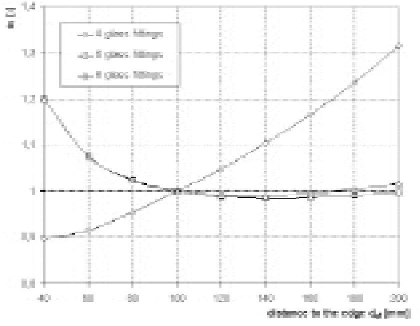

Figure 21: Result of a glass pane with 8 glass fittings

X. Influence of the Shore

To get the influence of the shore hardness of the supports on the principal stresses, calculations were done. The shore hardness was varied from shore 20 to shore 100. With these values of the diagram the interpolated results can be calibrated for another shore hardness of the rubber at the supports.

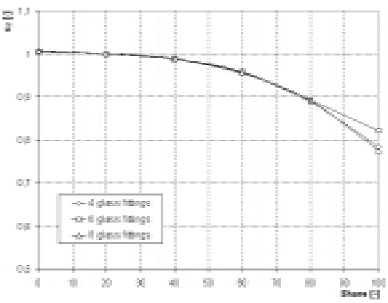

Figure 22: Result of a glass pane with 8 glass fittings

XI. Influence of the Diameter of the Hole

To get the influence of the diameter d_H of the hole on the principal stresses, calculations were done. The diameter d_H of the hole was varied from 30 mm to 70 mm. With these values of the diagram the interpolated results can be calibrated for another diameter of the hole.

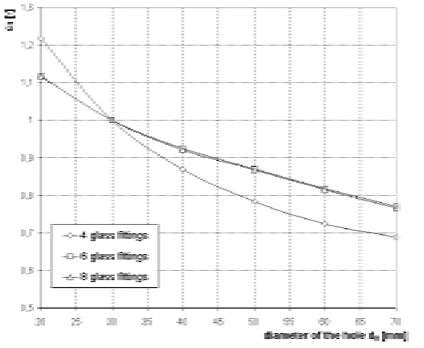

Figure 23: Result of a glass pane with 8 glass fittings

XII. Conclusion and Prospects

With this concept of the interpolation it is possible, to pre design point load supported glass panes very easily. Further it is possible to check the results of finite element calculations, to be sure that the calculations did what you wanted.

XIII. Acknowledgment

This paper was created with the help of Prof. Gernot Beer from the Institute of Structural Analysis at the Graz University of Technology.

References

[Bucar et al., 2002]
Ö. BUCAR, C. SCHULER, A. MEYER, A. FRIED, *Bauen mit Glas, VDI Bericht 1527zur Berücksichtigung der Verbundtragwirkungbei VSG mit PVB-Zwischenschichten.*

EU COST C13 Glass and Interactive Building Envelopes. M. Crisinel, et al. (Eds.). IOS Press, 2007.

Glued Joints in Glass Structures

Frank Wellershoff, Gerhard Sedlacek
Institute of Steel Construction, RWTH Aachen University, Germany

ABSTRACT. In facade engineering the potential of glued joints of glass members is not exploited except in structural sealant glazing systems. In other technical fields the application of glued joints is already state of the art, even in safety relevant parts. A further development of glued glass joints in facades can therefore be expected in the near future.

To state the potential, but also the risks in using glued joints the chemical and physical background is described. This includes the chemical principles of bonding forces and the physical principles of the deformation behaviour of polymer materials.

To allow the development of new glued joints the behaviour of high modulus adhesives under variable loads and different environmental conditions has to be tested. Test results of point supports with epoxy or acrylic adhesives, tested in compliance with the aging and loading conditions of the European Technical Approval for Structural Sealant Glazing Systems, are shown. Furthermore results of linear overlapping supports with Polyurethanes and Acrylics under short-term loads and long-term loads are presented. In compliance with the Eurocode, the ultimate limit state as well as the serviceability of glued joints must be verified. For the development of appropriate design concepts, which can be implemented in corresponding standards, suitable computation methods need to be verified. The calculation of the hyper elastic deformation behaviour of polyurethanes with FE-Methods using energetic models is explained and shown exemplarily. The calculation of deformations under long-term loads with logarithmic functions, which have been calibrated by tests, are explained and verified with respect to their accuracy.

Keywords: joints, gluing, adhesives, glass

I. INTRODUCTION

The accredited use of glued joints in glass structures is today restricted to structural sealant glazing facades with linear glued joints, consisting of silicon adhesives [ETAG 002]. These joints are allowed to transmit forces acting to the single façade element only. In mechanical engineering glued connections are already applied to safety relevant parts. In modern cars the windows are used to stiffen the car body. The stiffening forces are transmitted by glued connections with high modulus polyurethanes.

However, that the potential of glued glass joints is not entirely exploited in civil engineering. Possible applications of glued glass joints could be point supports or linear bearings which:

- carry single façade elements
- transmit stiffening forces
- connect elements to plates, columns or beams

Adhesives for the above mentioned applications have to be as stiff as possible, but able to equalize different temperature elongations between the components. Further the adhesive must be resistant to environmental conditions like temperature, humidity and UV- radiation.

II. BASIC PRINCIPLES

A. *Characterisation of Adhesives*

1) General molecular structures

Adhesives are polymer materials that consist of simple monomer units recurrently chained to macromolecules. The atoms in each macromolecule are chemically bonded and the macromolecules are physically or chemically bonded to each other and intertwining is inevitable.

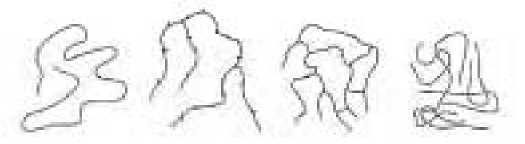

Figure 1: molecular structure of polymers [Ehrenstein 1999]

2) Classification

Polymers can be classified according to their thermo-mechanical properties.

a) Thermoplastics

Relatively weak intermolecular forces keep molecules in a thermoplastic together, so that the material softens when exposed to heat, but returns to its initial condition when cooled. Thermoplastic polymers can be repeatedly softened by heating and then solidified by cooling - a process similar to the repeated melting and cooling of metals. Most linear and slightly branched polymers are thermoplastics. All the major thermoplastics are produced by chain polymerisation.

b) Thermosets

A thermosetting plastic solidifies or "sets" irreversibly when heated. Heating cannot reshape Thermosets. Thermosets usually are three-dimensional networked polymers with a high degree of cross-linking between polymer chains. The cross-linking restricts the motion of the chains and leads to a rigid material.

c) Elastomers

Elastomers are rubbery polymers that can be stretched easily to several times their unstretched length and which rapidly return to their original dimensions when the applied stress is released.

Elastomers are cross-linked, but have a low cross-link density. The polymer chains still have some freedom to move, but are prevented from permanently moving relative to each other by the cross-links.

B. Deformation behaviour of Adhesives:

1) Deformation shares

Under external forces three different deformations, which have to be superimposed, could be identified:

- A) Spontaneous elastic deformation (spontaneous reversible) according to changed valence bond angles of atoms in chemical bonding.
- B) Time dependent viscoelastic deformation (time dependent reversible) according to stretched molecular chains.
- C) Time dependent viscous deformation (time depending irreversible) according to movement of molecular chains.

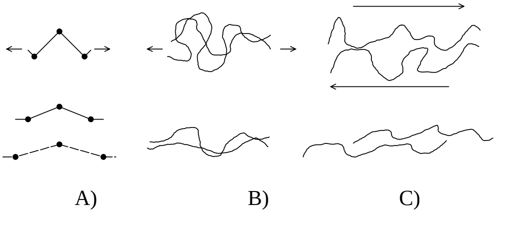

Figure 2: Deformation shares

2) Rheological models

To describe the time depending deformation behaviour of polymers different rheological models are developed and can be classified:

a) Linear viscoelatic models

Under linear vicoelasticity the time depending yieldingness depends only on the material temperature but not on the stress.

Some common used models are explained in the following:

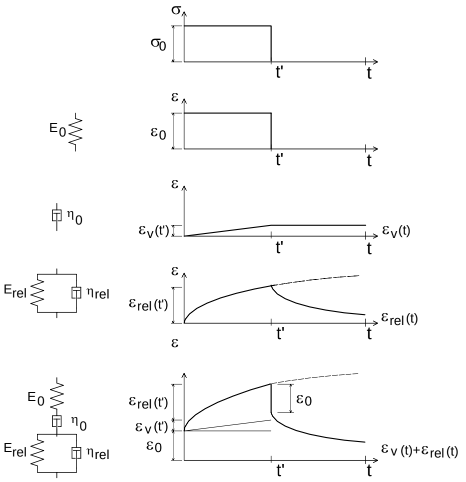

Figure 3: Burgers-Model (Four-Parameter-Model)

The strain function for the Burgers Model is:

$$\varepsilon = \varepsilon_0 + \varepsilon_v + \varepsilon_{rel}$$
$$= \frac{\sigma_0}{E_0} + \frac{t \cdot \sigma_0}{\eta_0} + \frac{\sigma_0}{E_{rel}} \cdot \left(1 - e^{-t/\tau}\right) \text{with } \tau = \frac{\eta_{rel}}{E_{rel}} \qquad (1)$$

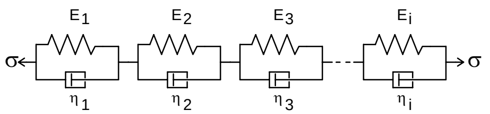

Figure 4: Generalized Kelvin-Voigt-Model

The strain function for the generalized Kelvin-Voigt-Model is:

$$\varepsilon = \left(\sum_{i=1}^{n} \frac{1}{E_i} \cdot \left(1 - e^{-t/\tau_i}\right) \right) \cdot \sigma_0 \quad \text{with} \quad \tau_i = \frac{\eta_i}{E_i} \qquad (2)$$

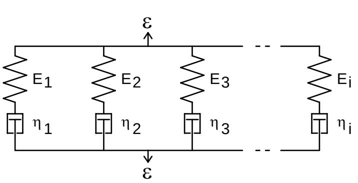

Figure 5: Generalized Maxwell-Model

The stress function for the generalized Maxwell-Model is:

$$\sigma = \left(\sum_{i=1}^{n} E_i \cdot e^{-t/\tau_i} \right) \cdot \varepsilon_0 \text{ with } \tau_i = \frac{\eta_i}{E_i} \qquad (3)$$

b) Non linear visoelastic models

In these models the young's modulus E or the shear modulus G depend on the load duration, the temperature of the material and the value of the applied stress.

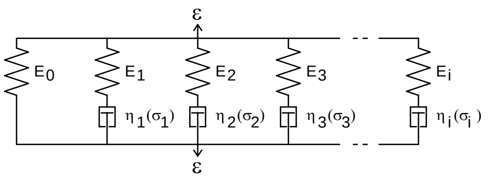

Figure 6: Deformation Model

For the solution of the differential equation of the deformation model the non-linear function for each damping element must be calculated. Optimised results are verified with 20 parallel Maxwell-Elements. As analytic solutions are nearly impossible, numerical methods are developed [Lewen 1991].

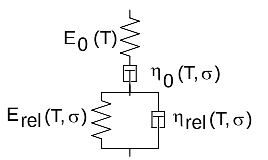

Figure 7: Modified Burgers-Model

The strain function for the modified Burgers-Model is:

$$\varepsilon_{ges} = \frac{\sigma_0}{E_0(T)} + t \cdot \frac{\sigma_0}{\eta_0(T,\sigma)} + \frac{\sigma_0}{E_{rel}(T,\sigma)} \cdot \left(1 - \exp\left(- \frac{E_{rel}(T,\sigma)}{\mu(T,\sigma) \cdot (1 - \nu(T,\sigma))} \cdot t^{(t - \nu(T,\sigma))} \right)\right) \qquad (4)$$

3) Super positioning

The linear viscoelasticity is the basis for linear accumulation of loads and deformations.

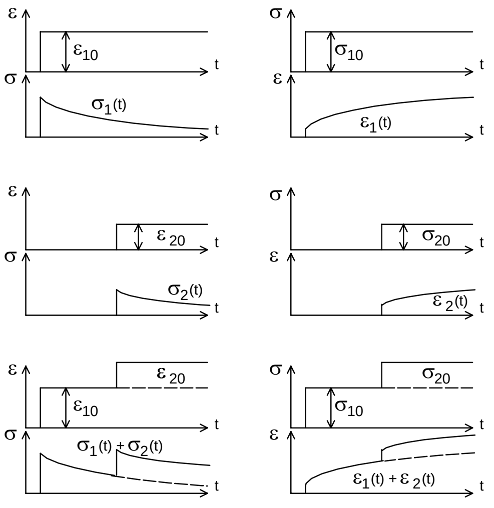

Figure 8: Boltzmann's superposition

Left: If the strain ε_{10} is causing the stress $\sigma_1(t)$ and the strain ε_{20} yields to the stress $\sigma_2(t)$, than the strain $\varepsilon_{10}+\varepsilon_{20}$ is leading to the stress $\sigma_1(t)+\sigma_2(t)$.

Right: If the stress σ_{10} is causing the strain $\varepsilon_1(t)$ and the stress σ_{20} yields to the strain $\varepsilon_2(t)$, than the stress $\sigma_{10}+\sigma_{20}$ is leading to the strain $\sigma_1(t)+\sigma_2(t)$.

4) *Corresponding principle*

All solutions based on the theory of linear elasticity (plate theory, beam theory) could be used with linear viscoelatic materials. In this case the time and temperature depending behaviour of the materials must be considered.

C. Glass as an assembly part in glued connections

The characteristics of the glass surface must be considered if higher bonding forces to an adhesive are desired.

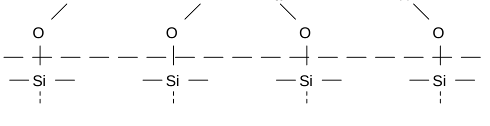

Figure 9: Glass surface

The surface consists of silicon atoms saturated with OH-groups and some metal ionic (e.g. Na).

In glued glass joints chemical bonding with silanized bonding agents are very common. On one side the bonding agent owns a reactive group for the glass surface and on the other side a reactive group for the adhesive [Röder 1996].

The hydrolysis of the silane to a silanol is enabled by the humidity on the glass surface.

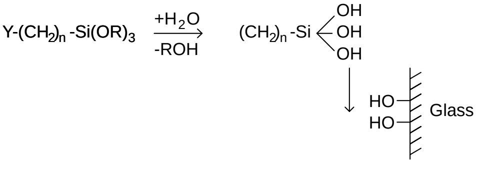

Figure 10: Hydrolysis

After the hydrolysis the bonding happens in two steps:

- Hydrogen bonds arise between the OH-molecules of the silanol and the glass surface.
- By splitting of water some hydrogen bonds change into chemical SI-O-SI bonds.

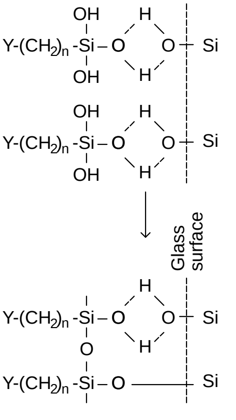

Figure 11: Atomic Bonding at the glass surface

III. GLUED POINT BEARINGS

A. Test set up

1) *Test specimen*

Stainless steel cylinders are glued to thermally toughened glass panes. The maximum surface roughness of the cylinders was R_{max} = 6.9 µm and the thickness of the adhesives was d = 0.5 mm.

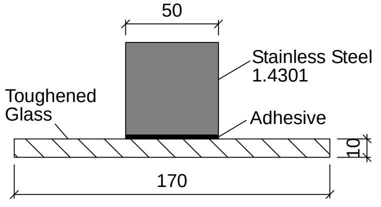

Figure 12: Glued point bearings / test specimen

2) Adhesives

For the described purpose of point supports under various environmental conditions a producer of technical adhesives proposed the adhesives to be tested.

- *Epoxi* (Delo Duopox 1895) is a silane modified two-component epoxy adhesive.
- *UV-Acrylate* (Delo Photobond 4436) is a toughened one-component acrylate where the initial polymerisation is applied by UV-radiation.

TABLE 1: ADHESIVE CHARACTERISTICS

	Epoxy	*UV-Acylate*
Young's modulus	3200 N/mm²	
Shore A		83
α_t	6 x 10^{-5}	8 x 10^{-5}
Operating Temp.	-40°C - + 100°C	-30°C - + 120°C

3) Tensile test set up

The glass panes were fixed with a steel ring D = 70 mm and tensile forces were applied to the point bearings with a rate of 500N/s.

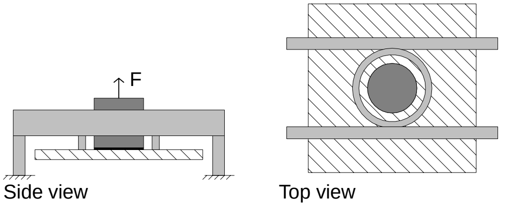

Figure 13: Tensile test

4) Shear test set up

A steel fork supported the point bearings and the glass panes were pushed out with a force rate of 500N/s.

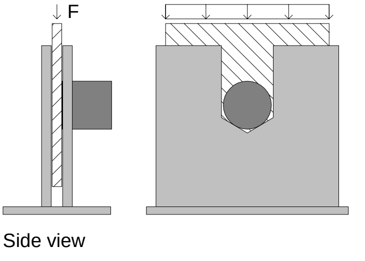

Figure 14: Glued point bearings / shear test

B. Results

1) Initial strength

The characteristic strength before aging F_c (5% quantile; significance level 95 %) is a mayor input variable for fatigue tests. Therefore larger numbers of test specimen are tested without aging.

TABLE 2: INITIAL STRENGTH / TENSILE TEST

		Epoxy	*UV-Acylate*
N		16	11
F_{min}	[kN]	1.074	10.38
F_{max}	[kN]	4.38	31.71
F_{mean}	[kN]	2.72	22.07
Standard deviation	[kN]	0.98	6.37

TABLE 3: INITIAL STRENGTH / SHEAR TEST

		Epoxy	*UV-Acylate*
N		12	12
F_{min}	[kN]	2.77	19.40
F_{max}	[kN]	7.43	23.18
F_{mean}	[kN]	5.12	21.55
Standard deviation	[kN]	1.55	1.02

The mean values F_{mean} of these specimen indicate a higher initial strength of the connection with the *UV-Arylate.* This is most likely due to the better stress balancing behaviour of the *UV-Arylate*. This theory is supported by the breakages pattern of the stiffer *Expoxy*-specimen in the shear tests, where the glass surface is cracked like a shell.

2) Tensile Strength after fatigue load

Cycle loads according to [ETAG 002] were applied before the ultimate limit load was tested.

- Phase 1: 100 cycles with 0.1 F_c – 1.0 F_c
- Phase 2: 250 cycles with 0.1 F_c – 0.8 F_c
- Phase 3: 5000 cycles with 0.1 F_c – 0.6 F_c

F_c characteristic tensile strength

TABLE 4: STRENGTH AFTER FATIGUE LOAD / TENSILE TEST

		UV-Acylate
N		4
F_{min}	[kN]	14.26
F_{max}	[kN]	23.59
F_{mean}	[kN]	19.69
Standard deviation	[kN]	3.92

The value F_{mean} decreases by 12.1%, however with only four specimen tested this effect is not statistically proved.

3) *Strength after UV-Radiation*

The test specimen were stored in an aging chamber and illuminated with UV-A light (320 – 400 nm) for 21 days. The radiated power of the lamp was 162 W/m² at the beginning and 80 W/m² at the end of the aging period and therefore higher than the postulated power of 50 W/m² [ETAG 002].

TABLE 5: STRENGTH AFTER UV-RADIATION / SHEAR TEST

		Epoxy	*UV-Acylate*
N		4	4
F_{min}	[kN]	8.50	0.00
F_{max}	[kN]	21.34	8.52
F_{mean}	[kN]	12.29	5.03
Standard deviation	[kN]	6.06	3.62

Although the *UV-Acylate*-specimen need UV-radiation to initialize the polymerisation the strength of these specimen decrease extremely by UV- aging. On the other hand the *Epoxy*-specimen showed higher strength values after UV-aging. This could be evoked by the temperature in the UV- chamber that might have enabled a degradation of residual stresses which arose during the polymerisation process.

4) *Strength after Immersion in water*

In this aging scenario the specimen were stored in 45°C hot demineralised water for 28 days [1].

TABLE 6: STRENGTH AFTER IMM. IN WATER/TENSILE TEST

		Epoxy	*UV-Acylate*
N		5	5
F_{min}	[kN]	1.94	0.00
F_{max}	[kN]	2.53	5.82
F_{mean}	[kN]	2.27	3.38
Standard deviation	[kN]	0.25	2.11

TABLE 7: STRENGTH AFTER IMM. IN WATER / SHEAR TEST

		Epoxy	*UV-Acylate*
N		3	3
F_{min}	[kN]	4.18	0.95
F_{max}	[kN]	6.29	2.68
F_{mean}	[kN]	5.31	2.09
Standard deviation	[kN]	1.07	0.99

Comparable to the UV-aging the strength of the *UV-Arylate*-specimen decreased and the strength of the *Epoxy*-specimen is not negatively influenced.

5) *Strength after Immersion in water under high temperature*

After immersion in demineralised water (28d, 45°C) four specimen (two with each adhesive) were heated to 80°C for two hours. Only one *Epoxy*-specimen did not delaminate by heating and reached a maximum force of 11.6 kN in the shear test. Higher temperature is apparently the limiting environmental condition for the tested connections. Different temperature elongations between the stainless steel and the adhesives is assumed to be the reason for the delamination.

C. *Conclusions*

Both of the two investigated connections are not suitable for the dedicated application in facades. The *UV-Arylate*-specimen showed substantial aging effects due to UV-radiation or immersion in water and both specimen types (*UV-Arylate* and *Epoxy*) delaminate when heated up to 80°C.

Better results could be expected with a toughened *Epoxy*-Adhesive and a larger application thickness which could balance stresses due to temperature elongations.

IV. LINAR GLUED JOINTS

A. Tested Adhesives

- *PU-1* (Sikaflex 265) and *PU-2* (SikaTack HM) are 1-component adhesives on polyurethane basis. Both react with the air humidity by polyaddition to an elastomer.
- *PU-3* (Sika 250 HMA-1) is a 1-component adhesive with an hot melting component. Under the application temperature of 80°C this component is melted and enables a good handling of the adhesive. After cooling this adhesive shows a direct stiffness according to the melting component. The maximum stiffness is reached by the polyaddition.
- *Acrylat* (SikaFast-5211 VP) is a fast hardening 2-component adhesive.

TABLE 8: APPLICATED ADHESIVE THICKNESS

	PU-1	PU-2	PU-3	Acrylate
Thickness [mm]	3.1 – 3.6	2.9 – 3.1	3.0 – 3.3	1.8 – 2.0

B. Tests with short-term loads

1) Test specimen

Thick steel bars in double sided connections are used to exclude not desired stress peaks, which could occur in one sided overlapping specimen due to the bending moment generated by the eccentricity.

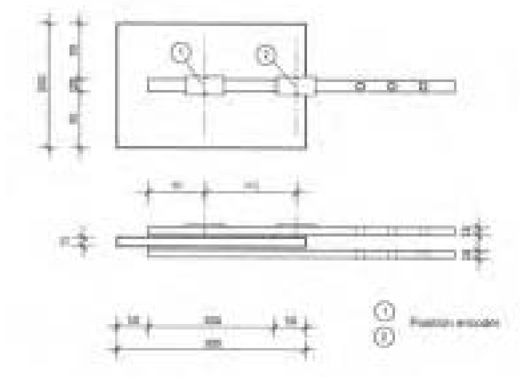

Figure 15: Test specimen for short time loads

2) Test set up

The test specimen are fixed in a steel frame and the force direction was controlled along the bond-line with a slide bearing and a pin joint.

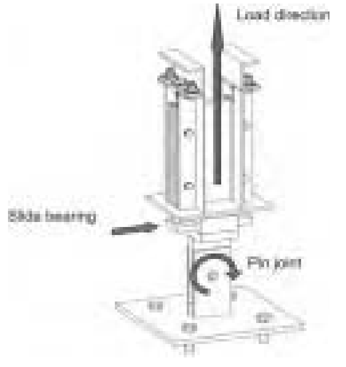

Figure 16: Double splice test set up for short-term loads

3) Test results

a) Ultimate limit tests

The ultimate limit tests were conducted with a constant stress rate of $\Delta\tau$ = 0,05 N/mm²s and different temperatures of the adhesives. The shear strain tan γ and the shear modulus G are calculated with:

$$\tan\gamma = \frac{v}{d} \tag{5}$$

$$G = \frac{\tau}{\tan\gamma} \tag{6}$$

v Displacement

d adhesive thickness

The tested polyurethanes and the *Acrylate* are much stiffer than the *Silicone* (DC 993) that is usually used in structural sealant glazing systems.

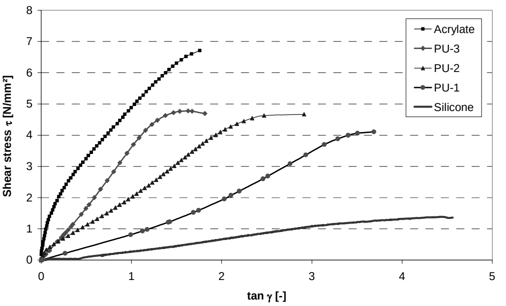

Figure 17: Stress-strain relation / $\Delta\tau$=0,05 N/mm²s / T = 23°C

TABLE 9: ELASTIC SHEAR MODULUS $G_{ELASTIC}$
ULTIMATE SHEAR STRESS $\tau_{ULTIMATE}$

	PU-1	PU-2	PU-3	Acrylate
$G_{elastic}$ (measured, $\Delta\tau$=0,05 N/mm²s)	0.83	2.1	3.3	33
$G_{elastic}$ (producer information)	0.84	2.5	3.3	-
$\tau_{ultimate}$ (measured $\Delta\tau$=0,05 N/mm²s)	4	4.7	4.7	6.7
$\tau_{ultimate}$ (producer information)	(4.5)	(4.0)	(5.0)	(8.0)

The stiffness of *PU-1* is not affected by temperatures between 20°C and 80°C but with increasing temperature the ultimate shear stress decreases.

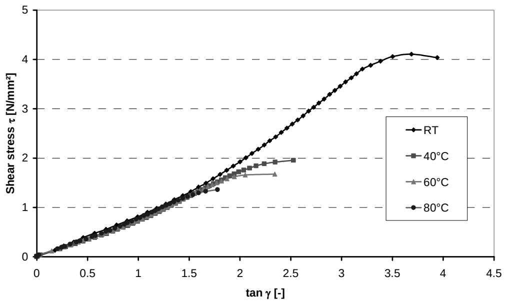

Figure 18: PU-1; stress-strain relation / Δτ=0,05 N/mm²s
T = 23°C; 40°C; 60°C; 80°C

In Figure 19 the melting point of the melting component in *PU-3* can be detected. Between room temperature and 40°C is a shift in the stiffness.

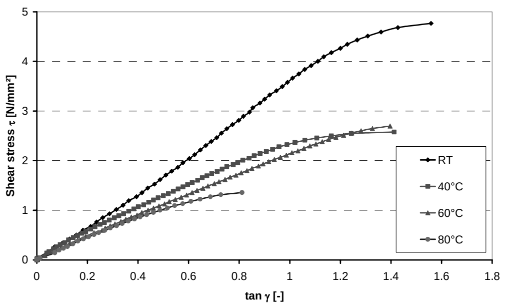

Figure 19: PU-3 ; stress-strain relation / Δτ=0,05 N/mm²s
T = 23°C; 40°C; 60°C; 80°C

The stiffness of *Acrylate* decreases extremely between room temperature and 40°C. This indicates its transitions temperature.

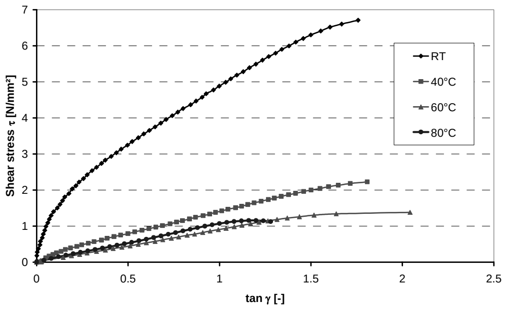

Figure 20: Acrylate; stress-strain relation / Δτ=0,05 N/mm²s
T = 23°C; 40°C; 60°C; 80°C

b) Dynamic tests

A significant characteristic is the dynamic modulus G_{dyn}:

$$G_{dyn} = \frac{\tau_{\max} - \tau_{\min}}{\tan\gamma_{\max} - \tan\gamma_{\min}} \qquad (7)$$

Although the stiffness of *PU-1* and *PU-2* showed no relevance to temperatures in the ultimate limit tests the dynamic modulus decreases with rising temperature. The relevance of the frequency is of secondary importance.

TABLE 10: DYNAMIC SHEAR MODULUS G_{DYN}

	PU-1 [Hz]				PU-2 [Hz]			
	0.1	0,25	0.5	1.0	0.1	0,25	0.5	1.0
23°C	1.1	1.09	1.09	1.15	2.5	2.54	2.54	2.56
40°C	0.92	0.91	0.93	0.94	1.78	1.78	1.76	1.85
60°C	0.88	0.87	0.87	0.92	1.44	1.44	1.44	1.45
80°C	0.86	0.83	0.82	0.82	1.25	1.26	1.28	1.29

4) Numerical Methods in FE Applications

For the design of glued joints with finite elements different material models were developed to consider the viscoelastic behaviour of adhesives. Efficient energetic models were developed by MOONEY and RIVLIN or by OGDEN. In both models the same basic energy approach is used:

$$U = \sum_{m=1}^{N}\sum_{n=1}^{N} C_{m,n}(I_1 - 3)^m \cdot (I_2 - 3)^n \qquad (8)$$

I_1, I_2 — invariants of the CAUCHY-GREEN deformation vector; they describe the deformation-energy relation.
$C_{m,n}$ — material parameter
N — order

With N=3 the approaches are:

- MOONEY-RIVLIN:

$$U = C_{10}(\mathrm{I}_1 - 3) + C_{01}(\mathrm{I}_2 - 3) + C_{11}(\mathrm{I}_1 - 3)(\mathrm{I}_2 - 3) \quad (9)$$

- OGDEN:

$$\mathrm{U} = \sum_{n=1}^{3} \frac{\mu_n}{\alpha_n}(\lambda_1^{\alpha_n} + \lambda_2^{\alpha_n} + \lambda_3^{\alpha_n} - 3) \quad (10)$$

The viscous stress tensor can be calculated with:

$$\sigma_{m,n} = \frac{\partial \mathrm{U}}{\partial \varepsilon_{m,n}} = \frac{\partial \Phi}{\partial \varepsilon_{m,n}} \quad (11)$$

U deformation energy

$\varepsilon_{m,n}$ deformation tensor

The identification of the material parameters in these models is the mayor task that is usually solved in two steps:

- Experimentally examination of the material behaviour in suitable tests that represent the real application load (stress and time) as good as possible (tensile tests, shear tests, compressive tests etc.)
- Determination of the unknown parameters by fitting the model response to the test data. The stability of the solutions to changes in the test data and the valid range of the identified parameters are important verification criteria's.

For the adhesive *PU2* the following values are determined by fitting the measured shear-stress-strain relation.

- MOONEY-RIVLIN:

$C_{10} = C_{01} = 0{,}5247977$, $C_{11} = 0$

- OGDEN:

$\mu_1 = 11{,}9431$, $\mu_2 = 19{,}1102$, $\mu_3 = 10{,}9421$,
$\alpha_1 = 0{,}10877$, $\alpha_2 = 0{,}12035$, $\alpha_3 = 0{,}0956804$

An alternative linear-elastic description is:

$$E \cong 6 \cdot (C_{10} + C_{01}) = 6{,}5 N / mm^2$$

C. Creeping Tests

1) Test set up

Long-term loads are e.g. those due to self weights. Although the load could be multiplied by mechanical transformation the maximum load is limited. Therefore the length of the bond line was decreased to 50 mm. All other geometric parameters were the same as in the test series for short-term loads. The dead weight of 50 kg steel blocks were transmitted with a see-saw. Before a test specimen was stretched in the steel frame the resulting force on the passive side of the see-saw was adjusted to the volitional value.

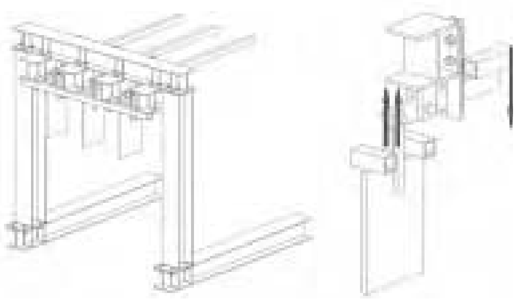

Figure21: Creeping test steel frame

2) Test data and numerical approximations for design

A usual approximation for the time yieldingness is:

$$I = \frac{\tan\gamma}{\tau} = B \cdot t^{\alpha} \quad (12)$$

I time depending yieldingness

B, α material parameters

A linear curve in a double logarithmic scale is typical for the time depending shear strain of polymers under permanent load.

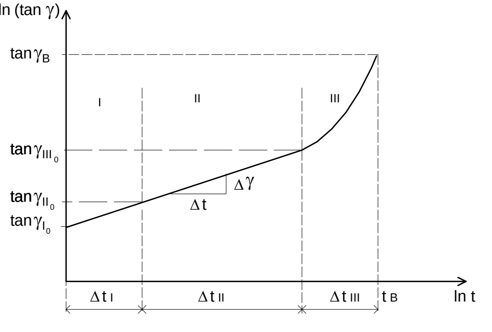

Figure 22: characteristic values in creeping tests

$\gamma_{I_0}, \gamma_{II_0}, \gamma_{III_0}$ shear strain at the beginning of the deformation regions I, II, III

$\Delta t_I, \Delta t_{II}, \Delta t_{III}$ time in the regions I, II, III

γ_B, t_B ultimate limit values

For design purpose the level γ_{III_0} should not be reached, because the failure of the connection is initialized at this level.

In the following graphs the parameters B and α are determined for the tested adhesives for different temperatures.

The test specimen S3 (PU-1; 20°C; τ=1.0 N/mm²) failed after 40 h. in this case the parameters B and α are calculated with the deformation in the first 30 h.

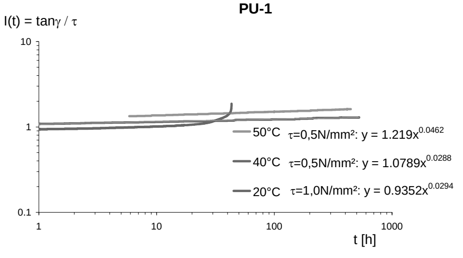

Figure 23: PU-1 / creeping measurement and numerical approximation

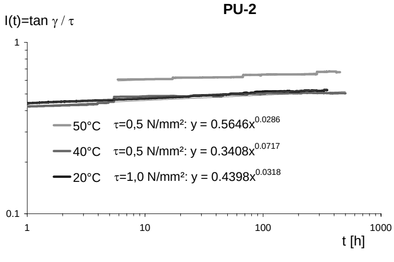

Figure 24: PU-2 / creeping measurement and numerical approximation

The test specimen S2 (Arylate; 20°C; τ=1.0 N/mm²) failed after 5 h and test specimen S5 (Arylate; 40°C; τ=0.0 N/mm²) failed after 150 h. The parameters B and α are calculated with the deformation in the first 4 h and 100 h.

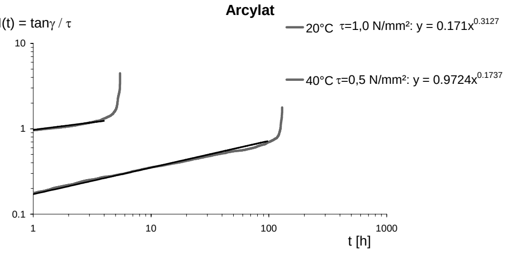

Figure 25: Acrylat / creeping measurement and numerical approximation

V. Acknowledgment

Special thanks to the companies SIKA, Switzerland and DELO, Germany. They sponsored the adhesives and provided us with their product information and their experiences.

References

[ETAG 002-P 1: 2001]
European Organisation for Technical Approvals; *Guideline for European Technical Approval for Structural Sealant Glazing Systems; Part 1, Supported and Unsupported Systems*, Brussels 2001

[Ehrenstein 1999]
Ehrenstein, G.W.: *Polymer-Werkstoffe, Structur Eingeschaften Anwendungen*, 2. Auflage, Hanser Verlag 1999

[Lewen 1991]
Lewen B.: *Das nichtlinear viskoelastische Verhalten von Kunststoffen am Beispiel der Zeit- Temperatur-Verschiebung und der Querkontraktionszahl*, Dissertation, Institut für Kunststoffverarbeitung, RWTH Aachen, 1991

[Röder 1996]
Röder, T.: *Klebstoffkonstruktionen in Verbindung mit Kfz. Verglasungen* , 4. Fachkongress Innovatives Bauen mit Gas, Bauzentrum München 1996

EU COST C13 Glass and Interactive Building Envelopes. M. Crisinel, et al. (Eds.). IOS Press, 2007.

Glass Façades of Mid-rise Steel Buildings under Seismic Excitation

Charalambos C. Baniotopoulos, Institute of Steel Structures, Department of Civil Engineering, Aristotle University of Thessaloniki, GR-54124 Thessaloniki, Greece

Konstantinos T. Chatzinikos, Institute of Steel Structures, Department of Civil Engineering, Aristotle University of Thessaloniki, GR-54124 Thessaloniki, Greece

The present research work intends to propose a methodology that will provide engineers aiming to design glass facades of mid-rise steel buildings with the appropriate know-how regarding their performance under dynamic loadings. As a matter of fact, modern structural codes dictate that non-structural elements of buildings, which in case of failure may cause risks or - from a serviceability point of view - negatively affect the building, have to be verified to resist along with their supports the design actions with regard to dynamic loadings. Within such a framework, the glass facades were analysed applying well-known finite element method analysis software packages [Computers & Structures 1998] [Ansys Inc. 2002]. The analysis was performed for seismic loadings. In particular, the seismic analysis was carried out in two steps. The first step was to generate time history inter-storey drifts by imposing to the steel frame structures time history accelerations derived from accelerograms of a reference earthquake (c.f. the Athens 1999 earthquake). The second step was to develop and apply as input, drift or load histories for the seismic analysis of the glass facade under investigation [Truman et al. 1996], [Chatzinikos, Baniotopoulos 2003]. The proposed methodology is illustrated in the final part of the paper by means of a numerical application.

Keywords: aluminium, glass, curtain wall, seismic, building facade, dynamics

I. INTRODUCTION

During the last decades, the use of glass facades being the envelope of mid-rise steel buildings is very common in modern construction. The development of modern and sophisticated curtain wall systems improved their reliability. However, the curtain wall systems are extremely vulnerable to natural (i.e. wind pressure, earthquakes, temperature variations) and human actions. Moreover, glass used in infill panels is exceptionally brittle. These facts render the detailed and well-documented structural analysis of glass facades a necessity.

The fact though, is that modern structural codes do not pay the proper attention to the assessment of the integrity and serviceability of non-structural elements and in particular, of curtain wall systems and their connections to the steel buildings [Baniotopoulos, Wald 2000] [Ivanyi, Baniotopoulos 2000]. Most modern building codes contain requirements to accommodate movements of non-structural elements due to lateral forces during an earthquake so as to minimize building envelope damage. In particular, modern seismic codes incorporate inter-storey drift limitations on the primary load-bearing structure for seismic forces. However, they do not provide engineers with a methodology for the modelling and the verification of glass facades and their supports to resist the design seismic actions [CEN 1998] [OASP 1999].

The intention of the present research work is to contribute to such a pilot methodology that will provide engineers aiming to design curtain walls with the appropriate technique regarding curtain wall modelling and performance during a seismic event. The modelling and analysis of the curtain wall systems has been performed using well-known finite element method software packages (e.g. ANSYS and SAP2000). The use of two different software packages for the same models using the same basic assumptions and the comparison of the obtained results makes the analysis more reliable.

The research effort has been developed in two steps. The first step was to model a typical mid-rise steel load-bearing structure with moment resisting and braced frames. At this step, the presence of the glass facade has not been taken into account apart from its dead load and mass, which have been properly distributed in the load-bearing structure model. The purpose of this analysis was to generate time history inter-storey drifts and load histories as input data for the seismic analysis of the glass facade. The aforementioned input data has been generated by imposing to the steel load-bearing structure time history accelerations derived from accelerograms of a reference earthquake (for the case at hand the Athens 1999 earthquake).

The second step was to use the generated input data for the seismic analysis of a standard curtain wall system together with its supports to the primary load-bearing structure. The curtain wall system has been modelled in detail so that the analysis to achieve a good level of reliability.

II. GEOMETRY – MATERIAL PARAMETERS

The modelled steel structure is a six-storey office building. Each floor is 3m high and the total height of the building is 18m high. The resisting structure comprises six moment resisting frames and two braced frames parallel to the Y-Z plane and six moment resisting frames and two braced frames parallel to the X-Z plane. The plan of the building was considered to be square with dimensions 42x42 m. The distance between two consecutive bays parallel to the Y-Z plane and parallel to the X-Z plane is 6m. The finite element method model of the steel load-bearing structure is presented in the following figure.

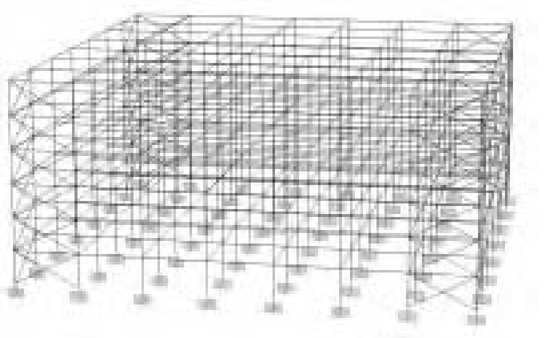

Figure 1: Steel load-bearing structure model

The structure consists of IPE300 beams on the upper level and of IPE360 on the other levels. The columns are HEA320 for the lower two levels, HEA260 for the next two levels and HEA200 for the upper two levels. The braces are all QHS100x10 sections. In order to implement an integrated analysis of the steel frame structure it was necessary to take into account the dead load, the live load and the wind loading applied to this structure. The selection of the sections used to model the steel structure was based on a preliminary design regarding the aforementioned loadings according to Eurocodes 1 and 3 [CEN 1993] [CEN 1995].

The curtain wall consists of a grid of vertical and horizontal aluminium elements with dimensions 1.2x1.0 m. The vertical elements (mullions) are rigidly supported to the main load-bearing structure at every floor (at every 3.0 m) and they are 6.0 m high. The transoms are pin-connected at their edges to the mullions and their length is 1.2 m. All degrees of freedom were constrained at the connection of the curtain wall with the steel frame.

The glass panels are supported along their perimeter by the aluminium elements and they were meshed so as to obtain more accurate results. The curtain wall model is presented in Figure 2.

The materials that were simulated for the purposes of the analysis models are steel, aluminium and glass.

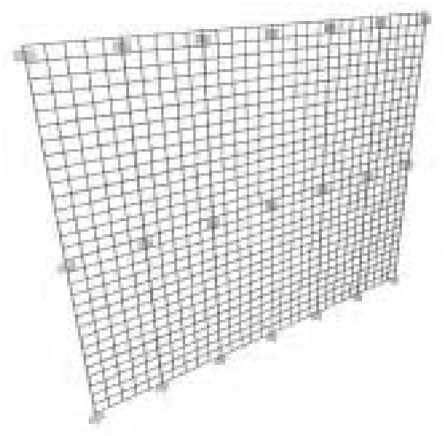

Figure 2: Curtain wall model

The modulus of elasticity for steel is $2.0x10^5$ MPa and the mass density is 7900 kg/m^3. Steel behaviour was considered to be linear-elastic, since the load-bearing steel structure was designed so as not to exhibit non-linear or plasticity effects.

The modulus of elasticity for aluminium is $7.0x10^4$ MPa and the mass density is 2700 kg/m^3. The stress-strain curve used to simulate aluminium behaviour of the alloy used, is presented in Fig.3 and it is designed based on the following formula proposed by Ramberg-Osgood [Baniotopoulos et al. 1998]:

$$\varepsilon = \frac{\sigma}{E} + 0.002 * \left(\frac{\sigma}{\sigma_0}\right)^n \qquad (1)$$

ε is the strain that corresponds to stress σ

σ is the stress

E is the modulus of elasticity

σ_0 is the actual 0.2% proof stress and

n is the index of curvature of the stress-strain relation

The two terms in this expression are the elastic and plastic strain respectively. The role of the index n is to control the curvature of the knee of the curve and depends on the aluminium alloy used. The actual 0.2% proof stress corresponds to a value of plastic strain equal to 0.002. For the analysis, 6082-T4 alloy was employed, the index n of which equals to 6.7, the σ_0 and the ultimate stress σ_u equal to 110 and 205 MPa respectively [Mazzolani 1985] [Dwight 1998] [CEN 1999].

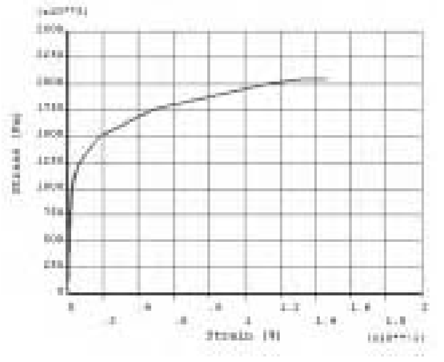

Figure 3: The aluminium stress-strain relation

The glass behaviour is extremely brittle and exclusively elastic. The modulus of elasticity of glass is $7.0x10^4$ MPa and the mass density is 2700 kg/m^3.

III. EARTHQUAKE GROUND MOTION

A time history analysis of the steel load-bearing structure was performed based on the 9 September 1999 Athens earthquake accelerogram, which derived from the acceleration records of the aforementioned earthquake. The records used refer to longitudinal and transversal direction. Each record represents the value of ground acceleration in the corresponding direction and the recording time step was 0.005 seconds. The duration of the earthquake was about 39 seconds and the strong ground motion lasted 5.5 seconds. By the term strong ground motion we mean ground acceleration values over 0.05g. The peak ground acceleration was 0.264g (2.590 m/sec^2) and 0.303g (2.970 m/sec^2) for the longitudinal direction and the transversal direction respectively. The graphs of the longitudinal and transversal acceleration versus time are shown in Figures 4 and 5. The vertical component of the reference earthquake has not been taken into consideration in the time history analysis because it was considered to be not significant.

The Athens 1999 earthquake was chosen because it was a disastrous seismic event and its characteristics are typical of earthquakes occurring in Greece.

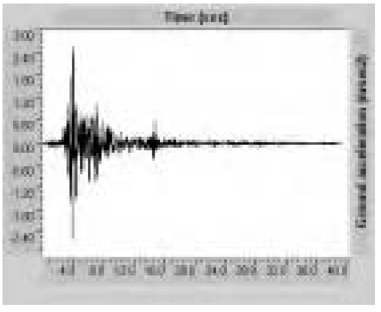

Figure 4: Time history of longitudinal ground acceleration

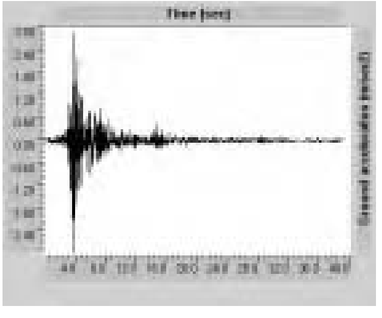

Figure 5: Time history of transversal ground acceleration

IV. MODELLING ASSUMPTIONS

All the floors are concrete (14 cm thick) over metal deck and therefore, were modelled as rigid diaphragms at the vertical axis. The rigid diaphragm assumption can be achieved in both software packages by using appropriate diaphragm constraints. By doing so, all the nodes of the plane of each floor belong to a diaphragm and therefore have the same displacements along the axes x and y. Furthermore, the floor masses were assumed to be concentrated at the centres of mass for each floor.

Both columns and beams were modelled using two-node beam elements with 6 degrees of freedom at each node. The columns were fixed at the foundation and the beams rigidly attached to the columns at their joints. The bracings were assumed to be pin-connected to the frame structure.

The loads were distributed to the beam elements as uniformly distributed loads, such that each beam element carries one-quarter of the load of its respective bays. The curtain wall dead load was distributed to the outer beams such that one-half of the load of each panel is carried by the upper beam element and one-half by the below beam element. The elements of the load-bearing frames have been considered massless and their masses were calculated and added at the mass discretizaton points.

Dead load masses including the self-weight of the steel structure, the load of the concrete deck and the load of the glass panels of the facade, have been considered to produce inertia forces.

The mass discretizaton at joints was done so as to simulate the structure in such a way that the distribution and the magnitude of the developing inertia forces between the real structure and the model to be close enough. The discretizaton depends on the movement of the structure. For the given seismic movement the horizontal and transversal translational masses were distributed at the mass centres of each floor. The analysis did not take into account any vertical translational masses. The amplitudes of the masses are given in Table 1 (in Ns^2/m^4).

TABLE 1: MASS DISTRIBUTION AT EACH FLOOR

	Concrete deck	Dead load	Façade	Total mass
Roof	629,36	33,1	7,71	670,17
Floor5	629,36	47,84	15,41	692,61
Floor4	629,36	50,32	15,41	695,09
Floor3	629,36	52,8	15,41	697,57
Floor2	629,36	55,59	15,41	700,36
Floor1	629,36	58,39	15,41	703,16

The damping coefficient of the structure was assumed to be 4% as the Greek Anti-Seismic Structural Code and Eurocode 8 dictate for steel structures with bolted connections for concentric braced steel frames [CEN 1998] [OASP 1999].

V. MODAL ANALYSIS OF THE STEEL FRAME

The modal analysis of the steel frame structure has been performed so that its vibration characteristics (natural frequencies and mode shapes) to be determined. The modal analysis can also be the basis for a more detailed dynamic analysis of the structure such as the time-history analysis is. Within this framework, the generalized eigenvalue problem has been treated, which is described by Equation (2):

$$[K]\{\phi_i\} = \omega_i^2[M]\{\phi_i\} \qquad (2)$$

[K] is the stiffness matrix of the structure
φ_i is the mode shape i
ω_i is the eigenvalue of mode i and
[M] is the mass matrix of the structure

The first 10 periods for SAP2000 and ANSYS model are shown in Table 2. The modal participating mass factors for each mode are shown in Table 3. It is quite clear that the first 4 translational modes contribute for more than 90% to the total response of the structure.

TABLE 2: MODAL PERIODS

Mode	SAP2000 (sec)	ANSYS (sec)	difference
1	0.9222	0.9265	0.47%
2	0.8422	0.8292	1.57%
3	0.3056	0.3066	0.31%
4	0.2794	0.2742	1.91%
5	0.1694	0.1694	0.02%
6	0.1547	0.1511	2.36%
7	0.1231	0.1229	0.14%
8	0.1121	0.1098	2.12%
9	0.1018	0.1016	0.16%
10	0.0911	0.0894	1.89%

TABLE 3: MODAL PARTICIPATING MASS FACTORS

Mode	Period	Individual mode (%)		Cumulative sum (%)	
		UX	UY	UX	UY
1	0.9222	0.00	77.61	0.00	77.61
2	0.8422	77.08	0.00	77.08	77.61
3	0.3056	0.00	15.91	77.08	93.52
4	0.2794	15.21	0.00	92.29	93.52
5	0.1694	0.00	4.08	92.29	97.60
6	0.1547	4.35	0.00	96.64	97.60
7	0.1231	0.00	1.33	96.64	98.93
8	0.1121	1.49	0.00	98.13	98.93
9	0.1018	0.00	0.64	98.13	99.57
10	0.0911	0.90	0.00	99.03	99.57

VI. TIME HISTORY ANALYSIS OF THE STEEL FRAME

The time-history analysis has been employed in order to determine the dynamic response of the steel frame structure subjected to earthquake loading, which is a time-varying loading. This way the time-varying deformations and forces of the steel frame structure have been calculated at the joints of the steel structure with the glass facade.

The aforementioned results of the time-history analysis have been derived from the time integration and solution of the following dynamic equilibrium equations of motion:

$$[M]\ddot{u}+[C]\dot{u}+[K]u = F(t) \qquad (3)$$

[M] is the mass matrix of the structure
[C] is the damping matrix of the structure
[K] is the stiffness matrix of the structure
$\ddot{u},\dot{u},u$ are the acceleration, velocity and displacement of the structure and
F(t) is the time-varying load vector

In SAP2000 a transient (time-history) analysis has been performed. The program solved the dynamic equilibrium equations of motion for the complete structure using the standard mode superposition method of response analysis. The mode superposition method summed factored mode shapes (eigenvectors) from the modal analysis to calculate the response of the structure. The time integration step used for the time-history analysis was 0.005 sec., which was the time step given by the Athens earthquake accelerographic data.

After retrieving and elaborating the time-history analysis results, the maximum displacements, maximum storey drifts and the time when they occurred were determined. The peak displacement was presented at the roof (3.18 cm along the x-direction and 4.54 cm along the y-direction). The maximum storey-drift along the x-direction was presented between the first and the second floor 3.91 seconds after the start of the earthquake excitation and had a value of 0.76 cm. The maximum storey-drift along the y-direction was presented between the third and the fourth floor 4.32 seconds after the start of the earthquake excitation and had a value of 1.07 cm. The maximum displacements and inter-storey drifts along x and y direction are presented in Table 4.

TABLE 4: MAXIMUM DISPLACEMENTS AND INTER-STOREY DRIFTS

	earthquake direction x		earthquake direction y	
	displacements (cm)	maximum drift (cm)	displacements (cm)	maximum drift (cm)
ROOF	3,18	0,49	4,54	0,63
FLOOR5	2,67	0,66	4,05	0,87
FLOOR4	2,20	0,69	3,39	**1,07**
FLOOR3	1,75	0,65	2,51	0,88
FLOOR2	1,13	**0,76**	1,46	0,86
FLOOR1	0,49	0,70	0,63	0,80

Eurocode 8 dictates that for building having non-structural elements composed of brittle materials (e.g. glass) attached to the main load-bearing structure, the following limit shall be observed:

$$d_r v \leq 0.005h \tag{4}$$

d_r is the design inter-storey drift

h is the storey height and

v is a reduction factor, depending on the importance class of the building

Assuming that the design inter-storey drifts are the drifts deriving from the time-history analysis and v equal to 0.5 (recommended value for importance class III buildings), then the drift limit in meters is:

$$d_r \leq 0.03 \tag{5}$$

The inter-storey drift values obtained from the time-history analysis of the main load-bearing structure are in good accordance with the aforementioned drift limit, since the maximum value obtained is 1.07 cm.

VII. ANALYSIS AND DESIGN OF THE CURTAIN WALL

The horizontal and vertical aluminium elements were simulated by two-node beam elements with six degrees of freedom at each node. Common industrial sections have been considered for the mullion-transom aluminium structure. Such section is presented in Fig.6. The section properties (area, moments of inertia) have been calculated with the aid of well-known design tools (such as AutoCAD).

The glass panels were simulated by four-node shell elements with six degrees of freedom at each node and they were properly meshed in order to obtain more accurate and reliable results. The shell elements have both bending and membrane capabilities and their thickness is 12mm.

Mass density was issued for both aluminium and glass in order to calculate the inertia loads.

The curtain wall is symmetrical in two axes. We took advantage of the symmetry, hence only a part of the curtain wall has been analysed.

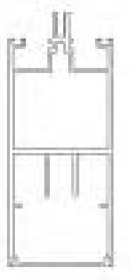

Figure 6: Typical load-bearing aluminium section

The results generated by the time-history analysis of the steel frame structure can be used further as input either for computational analysis of curtain wall systems or for laboratory testing of the aforementioned systems. In the present research effort, the time-history displacements of the floors were used as input data at the joints of the curtain wall with the steel frame structure for a time-history analysis.

In ANSYS a transient (time-history) analysis has been performed, in order to take into account possible effects of geometry and material nonlinearities. The time integration step used was 0.02 sec. The input data considered the displacements at the first 20 sec, when the displacements are significant.

The results of this time-history analysis have been derived from the time integration and solution of the dynamic equilibrium equations of motion (3), which were also used for the time-history analysis of the steel frame.

After retrieving and elaborating the time-history analysis results, the maximum displacements of the glass facade were determined and in particular the displacements of the glass facade in the transversal direction were examined. The conclusion of the processing of the aforementioned results showed no significant displacements of the glass facade in regard to the movement of the main load-bearing steel structure. The deformed shape of the glass facade is presented in Figure 7.

Figure 7: Deformed shape of the glass facade

The time history of the longitudinal displacement at the roof height level is presented in Figure 8.

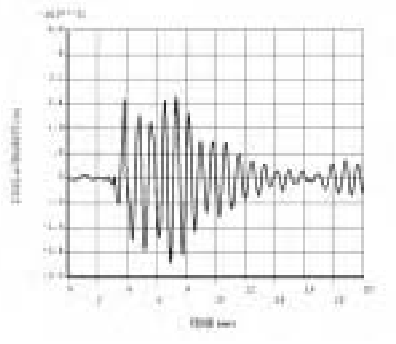

Figure 8: Time history of roof longitudinal displacement

VIII. CONCLUSIVE REMARKS

The curtain wall systems are in general analysed and designed empirically. The present research work intends to contribute to a pilot methodology that will provide engineers aiming to design curtain walls with the appropriate know-how regarding curtain wall performance during a seismic event. In order to achieve the previously mentioned objective, the research effort has been developed in two steps. A time-history analysis of the steel load-bearing structure has been employed in order to generate input drift history to be applied at the curtain wall system. The computed values are the displacements of the joints of the mullion-transom system. After elaboration of the aforementioned values the relative displacements along the axes were extracted and compared to the restrictions dictated by Eurocode 8. More specifically, the maximum inter-storey drift rises to 1.07 cm, whereas Eurocode 8 defines that the limit in the case investigated is 3.0 cm [CEN 1998]. Furthermore, no significant displacements of the glass facade has been present in relation to the movement of the main load-bearing structure. It is noteworthy a similar methodology for the design of glass facades under wind loading has been recently proposed [Chatzinikos, Baniotopoulos 2005].

IX. ACKNOWLEDGEMENT

The authors acknowledge with thanks the financial support of part of the present research activity by the Greek General Secretariat of Research and Technology (G.S.R.T.): Concerted Programme Renewable Energy Sources & Energy Saving E11: PhotoV-AluE – "Research, Development and Certification of Large Dimensions Aluminium Structural Members with Incorporated Modern Technology Photovoltaic Elements and Innovative Grid Connected Power Inverters, aiming to their Effective Application into Building Construction".

REFERENCES

[ANSYS Inc. 2002]
ANSYS Inc., *Theory Reference,* 2002.

[Baniotopoulos et al. 1998]
Baniotopoulos C. C., Koltsakis E., Preftitsi F., Panagiotopoulos P. D., *Aluminium Mullion-Transom Curtain Wall Systems: 3D F. E. Modelling of their Structural Behaviour,* Proc. ISCAS 4th Intern. Conf. on Steel and Aluminium Structures, pp. 433-440, Helsinki 1998.

[Baniotopoulos, Wald 2000]
Baniotopoulos C. C., Wald F. (eds.), *The Paramount Role of Joints into the Reliable Response of Structures: From the Classic Pinned and Rigid Joints to the Notion of Semi-rigidity,* Kluwer, Dordrect, 2000

[Chatzinikos, Baniotopoulos 2003]
Chatzinikos K. T., Baniotopoulos C. C., *On the Performance of Glass-Aluminium Curtain Wall Systems of Mid-rise Buildings During Seismic Events,* Proc. Of the 10th Inter. Conf. On Metal Structures, Timisoara, 2003

[Chatzinikos, Baniotopoulos 2005]
Chatzinikos K. T., Baniotopoulos C. C., *Glass - Aluminium Facades in Steel Buildings: Analysis of their Per-*

formance under Dynamic Loadings, Proc. of 4th Eurosteel Conference, Maastricht, 2005 (in print)

[Computers & Structures 1998]
Computers & Structures, Inc., *SAP2000 Integrated Finite Element Analysis and Design of Structures: Analysis Reference*, 1998

[Dwight 1998]
Dwight J., *Aluminium Design and Construction*, E & FN Spon, 1998

[CEN 1995]
European Committee for Standardization, *Eurocode 1 – Actions on structure,* 1995.

[CEN 1993]
European Committee for Standardization, *Eurocode 3: Design of steel structures – Part 1-1:General rules – General rules and rules for buildings,* 1993.

[CEN 1998]
European Committee for Standardization, *Eurocode 8 – Part 1: Design of structures for earthquake resistance – General rules, seismic actions and rules for buildings,* 1998.

[CEN 1999]
European Committee for Standardization, *Eurocode 9 – Part1-1: General rules and rules for buildings,* 1999.

[Ivanyi, Baniotopoulos 2000]
Ivanyi M., Baniotopoulos C. C. (eds.), *Semi-rigid Joints in Structural Steelwork,* Spinger, Wien, 2000

[Mazzolani 1985]
Mazzolani F. M., *Aluminium Alloy Structures,* Pitman Publishing Ltd., London, 1985

[OASP 1999]
Organization for Anti-Seismic Protection – Greece, *Greek Anti-Seismic Structural Code,* 1999.

[Truman et al. 1996]
Truman K. Z., Pantelides C. P., Behr R. A. and Belarbi A., *Comparison of linear and non-linear seismic drift histories for mid-rise steel frames,* Engineering Structures, Vol.18, No.8, pp. 577-588, 1996.

EU COST C13 Glass and Interactive Building Envelopes. M. Crisinel, et al. (Eds.). IOS Press, 2007.

Design, Engineering, Production & Realisation of Glass Structures for 'Free-Form' Architecture

Mick Eekhout, Professor Product Development at the Delft University of Technology & Director of Octatube Space Structures, Delft, The Netherlands

Structural designers are confronted in the last decade with architectural spatial schemes that greatly benefited from the aid of computer-operated design and modelling programs like Maya, Rhino and 3D-Studio Max. These architectural designs are referred to as 'Fluid or Liquid Designs' or 'Blob Designs'. They contain sculptural building forms in arbitrary geometrical forms, which cannot be developed mathematically, or to be generated easily, even by computer. These building forms do not have a systematic and recognisable repetitive structure, either.The gap between architects and structural engineers seems to open wide at first in each project and an even larger gap appears between architects, technical designers on the one hand and co-engineers, producers, co-makers, sub-contractors and builders a little later in the same project. In the structural glass building parts, with its tight tolerances and high degree of prefabrication an enormous effort is necessary in the engineering phase to define accurately all individually shaped building components. This will definitely transform 'production' into 'co-engineering & production'.

Keywords: blob, free-form architecture, glass, engineering, management

I. Introduction

The second half of the 20th century has witnessed the development of a number of spatial and systemised lightweight structures: shell structures, space frames, tensile structures, cable net structures, pneumatic structures, folded plate structures and 'tensegrity' structures. Most of these structures were developed by dedicated pioneers in the 1950-ies who designed, analysed and built impressive amounts of ever new concepts: Felix Candela, Frei Otto, Max Mengeringhausen, Richard Buckminster Fuller, Zygmunt Makowski, Walter Bird, Peter Rice et all [Eekhout 1989]. The common basic idea was to minimize the amount of material consumed, and in order to attain this, extensive intellectual investments in man hours were necessary. Computer analysis programs assisted the accurate analysis of complex geometries of the components in these three-dimensional though – in our current view - highly regular 3D-structures. Thanks to the further development of accurate analysis programmes based on non-linear structural behaviour these 3D-structures can now be designed by structural engineers all over the world. They reached a status of accepted and mature technology. Peter Rice (or rather: R.F.R) introduced the intricate use of structural glass in buildings in the 1980-ies, based on regularity and systemization in the Serres of La Vilette, Paris in 1986 [Rice et al. 1995].

In the newest trend the forms of digital baroque buildings are non-rectilinear, non-repetitive and in their conceptual stage only derived as clay-modelled sculptures, as it were, either by making concepts really in clay or by modelling and generating them in a similar way on the computer. Computer rendering programs like 3D design 'Maya' nowadays are able to juggle and generate all kinds of geometric forms, including the ones without any regularity in its geometric patterns. In the conceptual design stage, architects usually do not look for geometrical repetitive forms and systemised structural schemes or behaviour at the same time, but design like artists a totally new building with a mega-surprise for the entire world. Structural engineers are initially paralysed when they have to develop a load bearing structure in the contours of these geometrical forms in order to materialise the structural concept of the building's envelope. The same is valid for building technical engineers working these designs out more elaborately onto the level of shop drawings. The question is how to reconcile this 'Computer Supported Sculpturalism' with sound structural design and industrial prefabrication principles in a proper balance that revitalises the excellent and extensive experiences of 20Th century 3D-lightweight structures. This should happen already in the conceptual stage, so that both existing know-how and experience are activated and the cost prices of these buildings are less of a surprise. The relation between pre-design principle and post-design application is at stake here. Principles were conquered and gained by pioneers and scientists later, while architects, acting as composers, but sometimes with the elitarism of prima ballerinas, do as they like in both surprising and pleasing society at the same time. It raises the question of relationship between principles and applications.

II. 'Liquid Design' Architecture after Gehry's Guggenheim

Out of the blue came the Guggenheim museum in Bilbao, opened in 1997. Perfectionist American design blended with a Spanish way of building. But after the opening of this Museum designed by Frank O. Gehry the world was amazed. It really boosted the 'Liquid Design' era. Gehry designs his buildings in clay as sculptures. The model that satisfies him most is measured electronically and fed into a geometrical computer program. Gehry's office in Santa Monica uses the French Dassault-based program Catia for this purpose, developed for engineering aeroplanes. By then the enlarged clay geometry is fixed and the building is tendered as a total package. Then the subscribing main-contractors have to find sub-contractors who are willing to engineer, produce and built the building parts exactly as designed by Gehry. Subcontractors have to buy the Catia program as well in order to detail the global geometry as given in the main design. From this 3D-Catia model the construction and composition of all elements and components of each different building part, taken care of by each sub-contractor, is derived and fixed, especially when these elements and components have to be prefabricated.

Figure 1: Guggenheim Museum Bilbao, Frank O. Gehry

Gehry was also responsible for the design of the glass roof over the D.G.Bank in Berlin, built by Gartner. This type of experimental architecturally complex geometries can not at all be built by differently thinking building parties, as is usually the case. In case of unequal distribution of 'say & duty', the producing parties will pay these projects out of their own pockets, which means a short popularity of the architectural approach and many frustrations amongst participants in the building processes who get the blame and not the glory. Hence the nickname 'Fluid Design Nightmares' amongst producers.

III. Higher degree of co-operation: collaboration

A free-form geometry involving all building parts of the building design leads automatically to a

very accurate co-operation, rather collaboration between the building team partners, much higher and more intense than ever experienced before. It takes for most of the concerned architects a number of projects to agree with this and to change their usual distance to the production & building phase and work towards an integrated approach of all building team parties concerned. The building team is to be defined as the sum of all participating architects, designers, advisors, main contractor, building managers, component designers, sub-contractors and producers involved in the project.
One could define four major stages:

- Design of the building and its components
- Engineering of the building parts (elements, components and site parts)
- Productions of elements and assembly to components
- Building on site and installation of prefab components

Each of the 4 stages has its own characteristics of taking design considerations ands assuring quality of the building as the end product being a composition of the different building parts, installed on the building site by different building team partners. The phase of design of the building and its components will be the global domain of the architect and his advisors. In 'Liquid Designs' the tendency is for standard products to become systemized and for building systems to become special project systems. The need for special components will increase because of the special geometry of the building, influencing the form and position of each composing element/component. The tendency towards individualisation can be described as: *'Industrialisation in lots of one'*.

IV. Co-engineering, Production and Installation

Different building team parties are involved engineering their own production. These engineering activities all have to be based on the central 3D-mother CAD model. This model is the basis for the engineering of the total building. The keeper of this model is indispensable in the office and will become a crucial factor in each co-engineering company. Despite computers, in-house logistics will be depending on one master-engineer only!

For the co-ordination and integration of the different co-engineering parties in the building team two clearly distinct modus operandi can be followed:

Separate Model*:* Every party works on his own program, taking the basic data from the mother model. The problem will then how to check the quality of these separate computer drawings and outputs and how to relate them to the common details, where two or more building parts are joined, each to be worked out by a separate building party. In the Netherlands the steel construction engineers work with Strucad or X-steel, while façade engineers work with Autocad 2000 or 14. The two systems are not compatible. Installation engineers use other programs. Checking of the different results is extremely difficult and mistakes only appear on the building site. The architect does not check any drawing in its dimensions. This traditional pattern is not satisfactory at all.

Collaborative Model: Each party works on the 3D-CAD mother model successively as it is allowed 'slot time' (like aeroplane traffic coordination). During the start the situation is fixed and detailing and modifications of elements and components can be fed in. The whole is to be worked through. The end situation will be fixed and communicated to all building parties. After the proper closing off of the slot time of one party, check and certification by the model keeper, the next is allowed his slot time. Simultaneous work on the 3D model by more than one engineering sub-contractor is not allowed, as it will lead to confusion and possible legal problems thereof. Gehry enforces the use of Catia in his projects. But now different teams in the engineering department of one producing company could be working with different programs. This will lead to mistakes and confusion. So a plea is made towards the development of an universal 3D-computer program to be used by all corresponding building team members, capable of handling the conceptual design, the presentations, the overall building design drawings, the static analysis, the engineering co-ordination drawings, the shop drawings up to the quantity lists. After each of the building-directed engineering contributions of all participants, regular geometrical checking has to be done. Neglect of this will lead to large problems in the integration and co-ordination of the engineering, in production and installation and hence, much effort has to be spent here. Liability is also at stake here. Four building parties are able to execute this: the architect, the building technical engineer, the building contractor and the geodetic surveyor. Each option has its advantages and disadvantages. Each proposed party has to realise assort of forward or backward integration.

V. Case 1: Galleria, Wilhelminahof Metro Station Rotterdam, Tender 1995

The first of the Dutch Blob buildings was a design of Zwarts and Jansma for a railway station crossing a tramway in Rotterdam-South: the Wilhelmina-pier. The design of the main structure contained steel trees with thicker and thinner branches in varying heights. The tips of the top branches were covered with a triangulated glass roof, in a hilly, undulating form. The architects and the engineers ABT had thought of a nodal system to suit the many different corners in which the glass panels had to be fixed.

ABT was smart enough to have a series with informative talks with national and international specialist-companies to check the validity of the design and the price level. The international parties declined. We made a material proposal for an alternative node which would enable the steel riggers to accurately position the tops of the steel top rods supporting the glass nodes. The secret was the surveying of the exact location of the centre lines of the corners of the triangular glass panels. For all components of the roof: both steel and glass are produced simultaneously in different factories and from theoretical drawings. The silicone seams between the glass panels are 10 to 15 mm at the most. Disapproval already happens when there are larger differences in seam widths than 2-3mm. That was thought to be the wizardly domain of the glass subcontractor. We had thought out a logistic ‘modus operandi’, which led to continuous 3D surveying of all installed components, adjusting them to exactly the required level and X,Y,Z position.

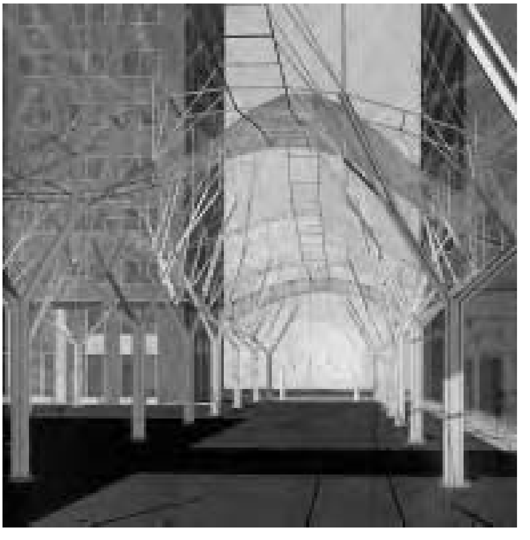

Figure 2: Rendering of the Galleria in Rotterdam
(image: courtesy of the architects Zwarts & Jansma)

With these components we drafted our price and were very astonished that we were the lowest bidder at 12 million guilders. Alas the architect and engineers had grossly underestimated the complexity of the design realisation, despite the warnings that had sounded form the pre-talks. The budget appeared to be only 4 million guilders. The architects and engineers were dismissed and architect Cees Dam designed a flat glass lean-to roof which met the budget but was not worth publishing here.

VI. CASE 2: DG BANK BERLIN, OCTATUBE'S DESIGN ALTERNATIVE 1998

The design by Frank O. Gehry called for a triangular network in the form of the body of a whale, to be constructed in stainless steel solid square rods, in triangulated form, to be covered with double and triple glazing panels. The nodes in finger form with all fingers having different vertical and horizontal directions. This was an extremely difficult job as all nodes were different, all bars were different and all panels were different.

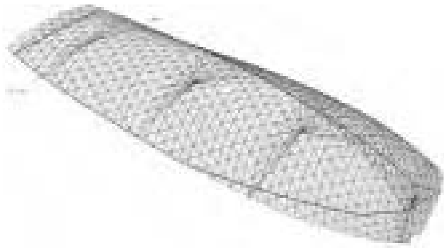

Figure 3: Alternative geometry for the DG Bank by Octatube

The Octatube alternative design consisted of hollow spherical cast nodes and tubular CHS members, all in stainless steel. The nodes were to be drilled in the exact direction. The length of the tubes would form the desired spatial envelope. The drawings show the illustrations. The tendering process resulted in a contract for Gartner in the original design at a dangerously low price, for which they suffered badly. The company is now taken over by Permasteelisa. The building has been completed in 2000. The accuracy, high degree of workmanship and finish of materials posed incredible high demands. The result has the quality of watchmakers accuracy, though!

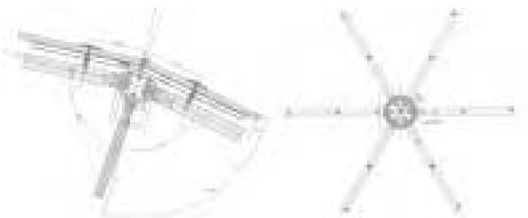

Figure 4: Alternative detailing by Octatube

VII. CASE 3: MUNICIPAL FLORIADE PAVILION BY ASYMPTOTE ARCHITECTS, HOOFDDORP NL

The competition winning design of Asymptote Architects, New York, originally contained a building volume in an arbitrary form with two sloped all glass surfaces. In a later planning phase this glass roof was partly replaced by aluminium panels. Over both roof surfaces water is running continuously down, as a sign of the Dutch water-rich culture. The architects refer in their publications to 'the Hydra Pier'. There are three remarkable technical experiments.

The first experiment consists of the water filled frameless glass pond sized 5x12m², designed as a continuous curved glass volume filled with water, containing in its summit around 1.400mm of water. The target for development was to realise the laminated glass panels in 2D-, 2,5D- and 3-D glass frameless suspended glass. These panels were 1 x 1.4m in size. The still standing challenge of production was an experimental route of an initial thermal dual deformation into a 3D-form, subsequent (certified) chemical treatment, liquid lamination of the duo panels, testing these and comparing them with the theoretically calculated end results. Due to high costs and long replacement time the client choose for polygonal flat panels of 12.12.4 fully pre-stressed glass.

Figure 5: Glass pond of the Municipal Pavilion

The second experiment contained cold deformed laminated glass panels, produced flat en bent by first fixing them on the four corners like the habit for spider glass and pressing two double points pushing outward on the upper and lower chord of the 2x2m² glass panels. The cold bent camber achieved was 80 mm over 2m side lengths. Bending stresses rose up to 35N/mm², while the allowable stresses including wind bending had a maximum of 55 N/mm². The cold bent panels had to be combined with hot bent monolithic panels for the smaller curvatures.

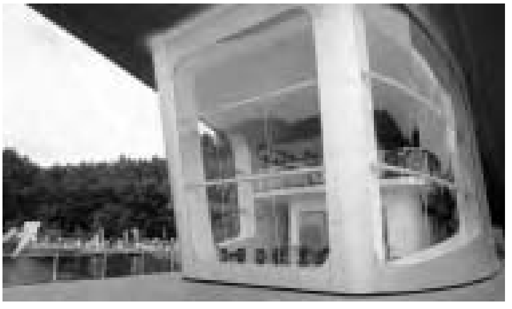

Figure 6: Cold deformed laminated glass panels

The third experiment were 3D aluminium panels in the two outer corners of the roof. To this end an experimental route was followed of drafting a Maya file CAD/CAM, machining polystyrene blocks to the desired mould shape, smoothening tem with epoxy filled glass fibre weave, cast off with fibre reinforced concrete. After curing the concrete mould was covered with 5 mm aluminium sheet, in a 300mm water basin with an explosion loading of TNT, which subsequently was brought to explosion into the mould. After this global forming, the edged were checked on a timber model, the edges were fitted and welded on and the panels were smoothened and coated by air spray. The fitting on the site and sealing the 10 mm gasket in between finalised the production and installation of these 14 panels. Industrialisation in lots of one. For the next project the Japanese adage of 'half the time, half the effort and half the price' will be the target.

Figure 7: Roof with the 3D aluminium panels

VIII. Case 4: Front Façade Town Hall Alphen aan den Rijn, NL

This design of architect Erick van Egeraat and ABT engineers is a pre-runner of Liquid Design Architecture. The main load bearing structure has not a single piece of repetition. Octatube was selected for the engineering, production & installation of the frameless glazing façades. This building has a façade of frameless glass panels, fully screened with graphical motives of trees, leaves and flowers in quite an ad hoc fashion. The panels are supported by elliptical façade mullions 75x150 and 110x220 up to 20m height, spaced at around 1.8m, with glass support nodes in between. The high yield, slender hot rolled elliptical mullions are excellent in freestanding use of frameless glazing. Their use in Quattro façades, either vertically or horizontally and suspended from the roof, is a standard system. The glass panels, around 850 pieces, are all unique in form and print design. The glass panels have been screened on surface 2 and have a low E coating on side 3. Most of the panels are 10.12.10 double glazed units in fully-tempered clear glass panels; the roof panels have laminated lower panels 6.6. All panels are fully tempered.

Figure 8: Exterior of the Town Hall with its triangulated and printed glass panels

In the 'semi-Blob' geometry, parts of the façade are conical upward and downward, cylindrical, spherical, anti-clastical and only some parts are straight. Because of the geometrical differences between lining of the façade mullions and glass panels, the columns are positioned in varying angles to the glass panels. The glass connectors are irregular. Not one of the 90 mullions is equal to another. In the anti-clastical surface (roughly 10x10m²) the rectangular glass panels are twisted and the elliptical mullions have up to 9 bents in their longitudinal axis, which are cut and welded on jigs in the factory straight from the engineering drawings. They fitted perfectly.

At the double curved back of the building around 500 glass panels are installed, all of them in model form (i.e. non-rectangular) due to the at random form of the intersecting bays, called the 'spaghetti strips'. The design called for a twisted glass panel. In the first development and engineering phase of 6 months a timber window firm tried to develop stepped glass windows and suitable details to that purpose. After they gave up, Octatube brought forward a simple but fitting solution. The idea was to get rid of the window frames, and to use only double glass panels composed of two panes of fully tempered glass, laminated in panels under angles less than 80 degrees. The individual glass panels were to be warped slightly. The maximum size of 900 mm width and 1800 mm length was to be warped for 40 mm perpendicular on its surface. This was done by cold deformation. Tests in the Octatube laboratory showed that this was feasible. Static analysis of the tensions by bending showed that only 10 to 20% of the maximum tensions were used in bending. The stresses in the sealant were acceptably low and the sealant manufacturer gave his guarantee as usual. This was the first time in the history of Octatube that cold forming of insulated glass was performed in a solution much more simple than the original glazed timber window frame solution.

Figure 9: The so-called 'spaghetti-strips' of cold formed glass panels

But this type of 'Liquid Design' architecture required the utmost of the engineering department: triple the time consumption of a regular project, including many problems with the matching of other building parts. An intensive collaboration was required in the final design stage, which took place after tender, involving all building parties. Opening of the town hall matured in June 2002.

IX. Case 5: Rabin Center in Tel Aviv

Architect Moshe Safdie designed a memorial building for Yitzhak Rabin wit two special halls on top: a Library and a Great Hall, overlooking the Ayalon valley in Tel Aviv. The form the roofs resembles the wings of a (peace) dove. The tender, elaborated by Over Arup of New York, contained a random steel structure with open profiles and a concrete cladding to be constructed at the initiative of the sub-contractor. We tendered for a more systemized space frame and GRP covered foam cladding on top as a variation on the tender specification and a wild alternative idea of a load-bearing structure of a mega-sized GRP sandwich construction, able to span the 30x20m² size of the wings in one go. Initially the foam core was thought as 800 to 1000mm thick polystyrene and 10 mm glass fiber reinforced polyester. The wild alternative was 25% more expensive but a clean and structurally very straightforward construction, which was extremely convincing. The architect spoke about *"an amazing solution"*. We received a pre-engineering contract which contained a redesign in Maya of the design of the Great Hall in its overall design and its composing details, based on our propositions. We also made 4 real size material prototypes of the two alternatives. As a result of this pre-engineering contract, the prices dropped considerably. At the moment we have started with the engineering of the 30x20m² free spanning GRP sandwich construction with quite an intensive experimental route in front of us to test the bonding of the 200mm PIR foam core and the two GRP skins, specially in the 8m long cantilevering wing tips where fatigue due to changing wind loadings is suspected and the danger of punching-through of the steel columns supporting the front sides of the wings, is immanent. We agreed with the architect that Octatube as the specialist will solely do the redesign on a 3D-model in an appropriate computer program (Maya), the engineering in (AutoCAD with Pro-engineer) and the obligatory productions, assemblies and installations on site. As a result of all previous experiments, failures and new experiences with liquid design buildings as described above, the current process promises to be an adequate set-up. We are supported by an internationally recognized architect who unconditionally backs us, but remains critical as a designer on the quality of the outcome.

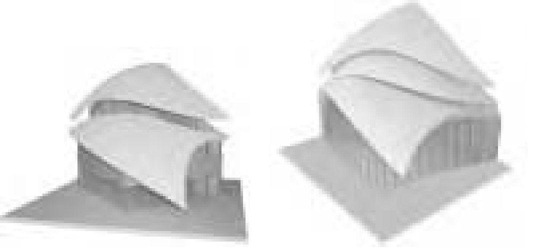

Figure 10: Model of the Library (left) and the Great Hall (right)

REFERENCES

[Eekhout 1989] Mick Eekhout, *Architecture in Space Structures,* 010 Publishers, Rotterdam, 1989, ISBN 9064500800

[Rice et al. 1995] Peter Rice, Hugh Dutton, *Structural Glass,* E&FN Spon, London, 1995, ISBN 0419199403

[Cook 1999] Peter Cook, *Archigram, Revised Edition,* Princeton Architectural Press, New York, 1999, ISBN 1-56898-194-5

[Gomez et al. 1996] Gomez, Coll, Melero, Burry, *La Sagrada Familia De Gaudi al Cad,* 1996

[Berkhout 2000] Guus Berkhout, *The Dynamic Role of Knowledge in Innovation*, Delft University Press, 2000, ISBN 90407207701

[Eekhout 1992] Mick Eekhout, *Between Tradition and Technology,* Publicatiebureau Bouwkunde, 1992, ISBN 9052691134

[Eekhout 1997] Mick Eekhout, *POPO, Procesorganisatie voor productontwikkeling,* Delft University Press, 1997, ISBN 904071631-5

[Zwarts & Jansma 2003] *Zwarts & Jansma Architecten, 52°21"N 04°55'51"E,* NAi uitgevers, Rotterdam, 2003, ISBN 9056623028 (English edition: ISBN 9056623036)

[Nijsse 2003] Rob Nijsse, *Glass in Structures,* Birkäuser, Basel, 2003, ISBN 3764364394

EU COST C13 Glass and Interactive Building Envelopes. M. Crisinel, et al. (Eds.). IOS Press, 2007.

Glass Canopy for the Office Center of the DZ Bank in Berlin

Rudolf Hess,
GLASCONSULT, Structural Engineering of Glass Constructions,
8142 Uitikon, Switzerland

A building located on the "Pariser Platz" in Berlin, was designed by the famous architect Frank 0. Gery and completed in 1999. Covering the main entrance is an interesting glass canopy measuring a total length of 14.30 meters and a cantilever of 1.50 meters without any support structures such as girders or hangers.

This paper, including an introduction about the building, describes the structural analysis of the glass canopy and the complicated attachment devices. A special analysis was performed to ensure that, in the case of failure of all the glass sheets, the remaining structure would be supported by the PVB layers.

The impact tests, carried out on an actual canopy in order to obtain the "declaration of consent" from the authorities of Berlin, are described in detail.

Keywords: glass canopy, cantilever, support structure, structural analysis, attachment devices, PVB-layer, impact test

I. Introduction

At the Pariser Platz, a historical place in the center of Berlin, a multifunctional office center with conference area and independent apartment house was built on behalf of the DG Bank, today named DZ Bank. By building this finance- and service center, the DZ Bank wanted to demonstrate their unique solidarity with the city.

The original building, Pariser Platz 3, was constructed as nobility residence of the count of Rohdich. In the temporal circuit of the empire establishment of 1871, the traditional baroque building was demolished and a new building was erected from 1878 to 1880. As part of the modernisation of Berlin as German capital after the fall of the Berlin wall in 1989, the reconstruction of the area of the Pariser Platz was a particular challenge. For the initiators of the building it was clear that for this exposed location particular demands would be required. Therefore an international competition was initiated by inviting eight internationally famous architects. The international jury unanimously chose the design of architect Frank O. Gehry. Frank O. Gehry founded the office Gehry & Associates, Inc in 1962. Over 90 awards in the field of architecture and furniture design were granted to him to date; the most prestigious in this impressive series is the Pritzker prize in 1989. Gehry particularly became famous with the museum building in Bilbao and recently with the Disney Hall in Los Angeles.

Figure 1: Façade facing Pariser Platz

In the near future, the building of the DZ Bank-will be flanked on the east side by the academy of arts and on the west side by the new building of the embassy of the United States of America. Gehry's success was, to "interpret" historic elements, without copying the history. The façade is not spectacular but it shows an exquisite well-proportioned elegance (Figure 1). Typical of this façade are the large windows and the relatively broad glass balustrades. The windows are partially sliding windows with complicated closing mechanism. The main entrance is discreetly covered by a glass canopy which is subject of this paper (Figure 1 and 3).

Entering the building the visitor discovers a six story Atrium. The light enters through a light glass construction (glass sky). The "glass floor" of the ground floor allows the view to the basement, where the casino and a further conference room is located. The back part of the atrium is a construction in the shape of a mussel, clad in stainless steel (Figure 2). The curved bimorph form is partially glazed and used as an auditorium for up to 100 participants. The new location of the DZ Bank is a place of encounter. In the atrium, a forum serves for an extensive array of events. The separation between office and residential area is created through an atmosphere in which the glass lifts connect the floors. The building went into operation in the course of the year 1999.

Figure 2: glass sky, glass floor, conference room

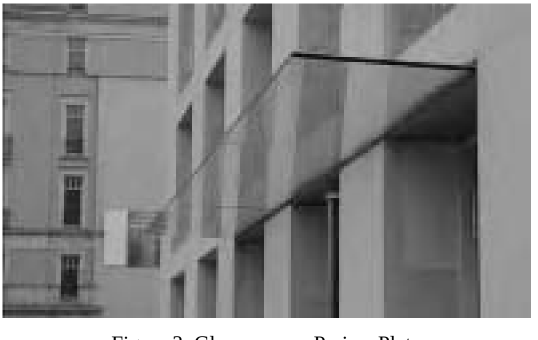

Figure 3: Glass canopy Pariser Platz

II. Glass canopy facing Pariser Platz

The glass canopy measures 14.30 m in length and a free cantilever of 1.45 m (Figure 3). The top lies approximately 4.15 m over the level of the entrance floor.

A. Concept

Specific to this canopy is that neither suspensions nor porters (swords) are available (Figure 3). The cantilevering glass roof is restrained in the steel-girder construction behind the façade from natural stone. The original concept anticipated an entire glass depth of 2.25 m i.e. 1.50 m cantilever and 0.75 m restrained in the façade construction. This concept with additional modifications and improvements is presented in Figure 4.

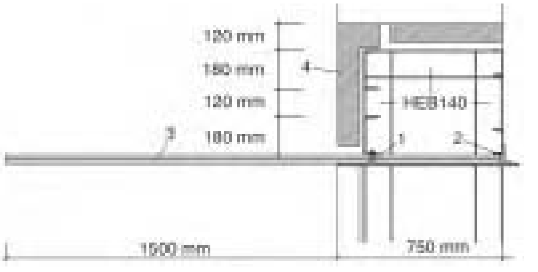

1 suspension M12 approximately every 500 mm
2 UNP with neoprene 5 mm shore 70-80
3 glass 3 x 12 mm heat strengthened glass, PVB 3.04 mm
4 natural stone

Figure 4: Original concept of the glass canopy (revised)

A first approximate analysis considering a restraint cantilevered beam of 1m width yielded a glass thickness of 3 x 12 mm tempered glass.

In the project stage, and in the phase of invitation to tender, the glass roof was intended to be constructed as one element of 14.30 m length and 2.25 m width. As a matter of fact, the glass roof was offered by the general contractor with these measurements, still in unaware of the static behaviour and the exact glass construction.

From the beginning, it was clear that for such an overhead construction only laminated glass could be used. The engineers responsible for the glass static proposed a construction with a laminated glass with three panes, considering that the use of three panes increases the safety at a possible break.

The original concept according to Figure 4 shows a fastening of the glass to the existing steel girders of the façade construction. In the front area, the pane should be suspended with screws M12 mm every 500 mm. The screw heads would have been welded to the lower stainless steel plate, in order to hide the suspension from the underside view. For this purpose holes of 40 mm would be required in both lower panes and 20 mm in the upper pane. In the back part the pane would be fastened by a UNP-profile with a neoprene layer of at least 5 mm. The main disadvantage of this concept was that the façade construction was already erected at time of the installation of the glass canopy (Figure 5).

Figure 5: Steel-girder construction of the façade

Six pairs of support consisting of HEB 140 (Figure 4) therefore would have to penetrate the glass roof. For this concept glass slots would have been necessary, which would be unfavourable from the point of point of view of the concentrated stresses.

A float glass plant is basically able to produce glass sheets of 3.21 m width and normally a length of 6.0 m. Theoretically the production of a pane of 14.3 x 2.25 m would have been possible. However a length of over 6 m would require a special production process. On the contrary, it was clear that no supplier could prestress a glass of 14.3 x 2.25 m nor produce a laminated glass of this size. This is due not only to fabrication but also to handling constraints.

The building owner and the architect however still insisted in the construction proposed of one piece of 14.30 m length. There was no other solution, than to subdivide the canopy in longitudinal direction into several parts.

According to the concept in Figure 4, given a glass depth of 2250 mm it would have been possible to manufacture glass up to a length of 3800 mm. This would have yielded a division in longitudinal direction in at least four elements. Such a subdivision was basically refused by the architect. However after lengthy negotiations, the architect agreed to a subdivision into three parts, such that the gaps between the individual elements would be situated in the middle of the large pillars (Figure 1 and 3).

Gaps of a maximum width of 15 mm between the elements was accepted, resulting in a center piece of 5.48 m length and two edge elements of 4.395 m each leading to a total length of 14.3 m. As a consequence the largest piece to be delivered measured 5.48 x 2.25 m. At the time of the construction, laminated glasses of this size with heat strengthened or tempered glass was not available, at least not in Europe.

Therefore another solution of the restraint had to be found, so that the depth of the glasses could be reduced. A supplier was found who could deliver laminated glass with a total thickness of 70 mm with heat strengthened glass (HSG) or tempered glass (TG) up to the measurements of 1670 x 7000 mm. With a modification at the production plant, the same supplier was able to increase the width to 1700 mm.

With a depth of 1.7 m and a cantilever of 1.5 m only 200 mm were available for the restraint of the glass sections. After negotiations with the client and the architect a reduction of the cantilever length could be achieved from 1.50 m to 1.45 m. With this reduction a depth of 250 mm to restraint the glass could be realized.

The engineers responsible for the glass construction developed a concept whereby the glass was clamped between two steel plates and covered with elastomer stripes of approximately 5 mm thickness, bolted together with chrome steel screws (Figure 6).

The lower steel plate (5) could be used over the whole depth of 250 mm. The canopy has a slope of 2% against the façade. The upper plate (4) had to be shortened by 200 mm, in order to allow a drainage system in longitudinal direction. In Figure 7 the system of the restraints of the glass structure is presented enlarged.

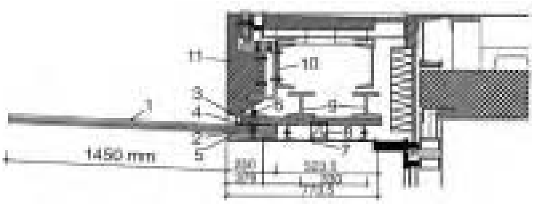

1 3 x12 mm glass PVB 4 x 0.76
2 Neoprene 50 x 5 mm Shore 75
3 Flat steel plate 700 x 40 mm
4 Flat steel plate 200 x 8 mm
5 Plate 250 x 15 mm St 52
6 bolts CNS M16 every 330 mm
7 stainless steel 2 mm
8 installation Light
9 Girder HEM 120
10 Girder UNP 240
11 natural stone

Figure 6: Final solution of the construction of the glass canopy

First it was considered to weld a RHS tube of about 1000 mm length on to the upper steel plate (4) every 300 mm and to fasten these tubes to the girders UNP 240, which are a part of the façade construction. As a consequence of the lever mechanism heavy loads would have been transferred to the girders UNP 240; the front girder would have experienced a bending force downwards and the back girder one upwards. The large forces mentioned above were not considered in the static calculation of the steel-girder construction of the façade, which was already erected at that stage. The two girders UNP 240 (10) s. Figure 6 and 7 could not support the large forces from the glass canopy. Therefore a separate construction had to be found for fixing it.

Two additional steel girders HEM 120 (9) were introduced as continuous beam over five spans similar to the UNP 240 (10) positioned above. The upper steel plate of the construction (4) was welded on to a plate of 40 mm thickness and 700 mm depth (3), which was welded to the steel girders HEM 120, thus no additional loads were transferred to the girders UNP 240.

The final analysis was performed by means of the method of finite elements using the computer program [CEDRUS3+]. Thereby the construction of the restraint was modelled in an exact way. Due to the cantelever forces the glass is held within the restraint by the elastomer supports (2) and (4) in Figure 7 the forces acting in opposite directions. From the Shore hardness of the neoprene the compression modulus could be determined and as a result the spring constants for both plate supports. At an assumed Shore hardness of 70, a width of the neoprene stripe of 50 mm and a thickness of 5 mm a compression modulus of 159.5 MPa could be determined according to [Angst & Pfister 1996]. The stiffness of the bolts was considered in the spring constant.

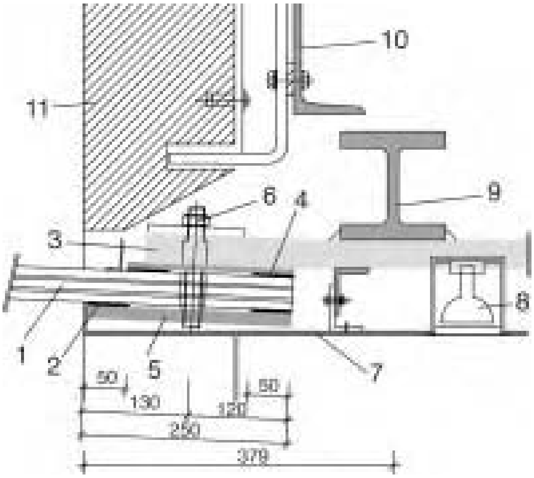

1 3 x 12 mm glass PVB 4 x 0.76 each
2 Neoprene 50 x 5 mm Shore 75
3 Flat steel plate 700 x 40 mm
4 Flat steel plate 200 x 8 mm
5 Plate 250 x 15 mm St 52
6 bolts CNS M16 every 330 mm
7 stainless steel 2 mm
8 installation Light
9 Girder HEM 120
10 Girder UNP 240
11 natural stone

Figure 7: Detail of the restraint construction

B. *Structural Analysis*

The glass thickness of 3 x 12 mm found in the preliminary analysis was adopted. Whether TG or HSG was still undecided.

1) Normal loads :

Proper weight 0.90 kN/ m^2

Snow load for Berlin according to code [DIN 1055 Teil 5 1990] 0.75 kN/ m^2

Both for the load case proper weight as well as proper weight + snow no composite between the individual glass panes was considered (layered construction). Own experiences and tests years ago have shown, that the compound effect is lost fast due to long term loads [Hess 1988].

a) Maximum edge stresses:

- proper weight: σ_{max} = 13.6 MPa
- proper weight + snow: σ_{max} = 25.0 MPa

The allowable stress for TG is 50 MPa and for HSG 29 MPa. Thus the stresses are below the allowable limits. In addition, the case was investigated where a pane of the construction is broken due to mechanical damage for instance.

The load capacity is guaranteed for this case only through two panes (no composite effect).

- proper weight: σ_{max} = 20.7 MPa
- proper weight + snow: σ_{max} = 38.0 MPa

The stresses are below the allowable stress of 50 MPa for tempered glass. For the load case proper weight + snow the allowable stress of 29 MPa for HSG is exceeded. With a strength of 70 MPa for HSG the safety margin amounts to 1.8, which can be considered as sufficient.

Finally the extreme case is investigated, where both the upper as well as the lowest pane is broken due to mechanical damage. The remainder load capacity must be guaranteed through the medium pane alone. For this case only the influence of the proper weight is considered.

The maximum stress amounts to 41 MPa. This is smaller than the allowable stress of 50 MPa for tempered glass. With a strength of 70 MPa for HSG the safety margin amounts to 1.7, which can be considered as sufficient for this extreme case.

b) Maximum Deflections

For the load case proper weight the deflection at the outer edge, without considering composite effect can be determined to 21.3 mm, this corresponds to a value of 1/ 115 of the span width (double of cantelever span). The canopy was installed with a slope of 2 %, so that the drainage can flow against the building. The deflection for the load case snow under neglect of the composite effect yields a value of 17.8 mm, together with the proper weight a total of 39.1 mm corresponding to 1/ 74 of the span width, which lies within the allowable limit. The effective deflection at the outer edge for the load case proper weight + snow under consideration of the slope amounts to 11.2 mm, the canopy is still sloped towards the façade.

The above analyses for the normal load cases have shown that the canopy can be realized with TG as well as with HSG.

2) Extreme load cases :

By order of the Berlin authorities, the impact of a steel ball of 4.0 kg with a minimal drop height of 3.0 m had to be investigated, whereby the following both cases were considered:

- Impact at the free edge in the middle of the plate
- Impact at the free edge in the plate corner

By means of equivalent static load method according to [Pilkey 1994] static calculations were accomplished. Since these load cases are short term loads, full composite (monolithic construction) is considered. The load case proper weight was superimposed. Separate calculations were performed for the panes of 4.395 m and 5.48 m.

a) Maximum stresses:

The resulting stresses for the governing case totals: σ_{max}= 28.3 MPa.

On demand of the Berlin senate authority the impact should occur under consideration of an existing snow load. Therefore the above-mentioned stress is superimposed with the stresses from proper weight + snow, without composite effect. This yields an entire stress of 54 MPa. This stress lies above the allowable stress of TG of 50 MPa as well as the one for HSG of 29 MPa. If the stress is compared with the strength of 120 MPa for TG and 70 MPa for HSG, safety factors against failure of 2.2 and 1.3 respectively are found. These values are sufficient for these unusual load cases.

b) Maximum deflections:

For the impact at the free edge in the middle of the plate the deflection totals at the outer edge 16.1 mm and for the impact in plate corner 24.3 mm. This corresponds to a value of 1/ 180 and 1/ 119 respectively of the span width. Superimposing the this deflection with the deflection of proper weight + snow, neglecting the composite effect, total values of 26.2 mm and 34.4 mm respectively are found. These values have indeed only academic character.

These calculations have shown that also for the extreme load cases, the canopy can be realized with TG as well as with HSG. For the determination of the stresses in the upper and the lower steel plates of the restraint system as well as for chrome steel screws the load case impact is governing, likewise for the remaining fastening constructions.

The determination of the forces in the screws were performed with a modified FE-Model. It turned out that a screw CNS M 16 was necessary every 330 mm. The screws were prestressed up to about 70%.

Furthermore a calculation was accomplished for the case that all three panes of the laminated glass would be broken. A model was assumed, whereupon the complete failure occurs near the restraint, the pane revolving as a hinge around the point O (Figure 8). Through the complete failure of the glass, the remainder load capacity is guaranteed only through the PVB-folios.

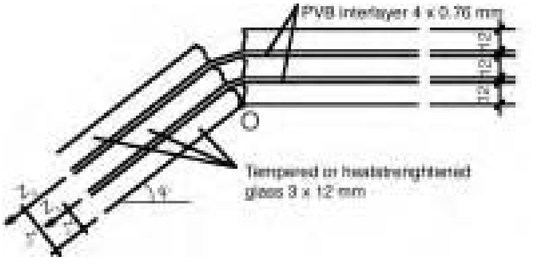

Figure 8: Failure of all glasses (hinge effect)

In the case of the failure of all panes using the model in Figure 8 the safety against rupture of the PVB can be determined as follows:
Assumed strength of PVB 20 MPa
Cantilever span a= 1.45 m
PVB thickness t_i 4 x 0.76 mm= 3.04 mm each
Tensile forces in the folios due to the proper weight g for the worst case where the glass stays in horizontal position $\varphi = 0°$ (Figure 8)

$$M_{rupture} = \frac{g \cdot a^2}{2} = \frac{0.9 \cdot 1.45^2}{2} = 0.95 \text{ kN/m}$$

From the strain plane through point O it can be determined:
$M_O = Z_1 \cdot h_1 + Z_2 \cdot h_2$
Assuming $Z_2 = 2 \cdot Z_1$:
$M_O = Z_1 \cdot (h_1 + 2 \cdot h_2)$
and from $M_O = M_{rupture}$

$$Z_1 = \frac{M_{rupture}}{h_1 + 2 \cdot h_2} = \frac{0.95}{0.0135 + 2 \cdot 0.0285} = 14.48 \text{ kN/m}$$

$Z_2 = 2 \cdot Z_1 = 26.95$ kN/m

The stresses in the PVB can now be determined to :

Folio 1 : $\sigma_1 = \dfrac{Z_1}{t_1 \cdot 1000} = \dfrac{14480}{3040} = 4.8$ MPa

Folio 2 : $\sigma_2 = 2 \cdot \sigma_2 = 9.6$ MPa

With an average strength of 20 MPa of the PVB a safety factor of 2.1 can be determined in interlayer 2. The safety in interlayer 1 is accordingly double. A global safety factor of 2.1 can be considered as sufficient for the extreme case of the failure of all panes.

C. Declaration of consent

In Germany a declaration of consent has to be applied for constructions which are not regulated. The canopy under consideration was such a structure, therefore an application had to be turned in at the Berlin senate-authority. Besides the presentation of a detailed structural analysis, impact tests using a 1:1 mockup were required. To reduce the costs of the tests, the authority allowed, that the tests be carried out with a body of 2 m length instead of the largest effective length of 5.48 m. The panes of 2.0 x 1.70 m were erected on a special steel structure, where the restraint was modelled exactly. The requirement was, that if all the glass panes failed, that the glass or glass pieces should not fall on to the busy entrance area. For the tests a steel ball of 4.0 kg was used. Two panes were available, one laminated glass with 3 x 12 mm TG and second with 3 x 12 mm HSG, with 4 x 0.76 mm PVB interlayer. The glass was loaded first with sandbags to simulate the snow load of 0.75 kN/ m^2 (Figure 9).

Figure 9: Mock-up for the impact tests at the construction site

At the first test with tempered glass with a drop height of 3.0 m the lowest pane broke (Figure 10).

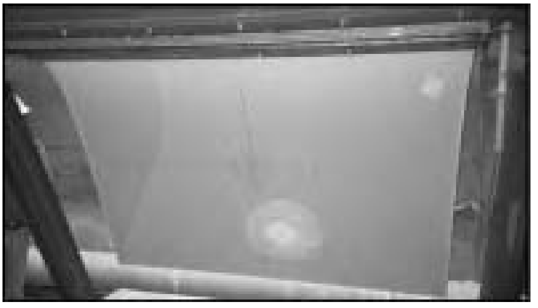

Figure 10: Failure of the lowest pane TG, drop height 3.0 m

The other two panes remained intact. Only after an impact with a drop height of 10 m all three glasses failed (Figure 11).

Figure 11 Failure of all panes TG after an impact from 10 m

Figure 11 clearly shows, that the destroyed pane remained in a position under a certain angle, thereby the sandbags slipped away. The considerations previously presented, that the pane is held only by the PVB-interlayers, were confirmed. The pane remained in this position.

Figure 12: Broken TG forced into vertical position

The panel was pressed subsequently by force into the vertical position (Figure 12).

After the first tests with the glass assembly of 3 x 12 mm TG the analogous test series with 3 x 12 mm HSG were carried out. At the first test with a drop height of 3 m no failure occurred. After several throws with different drop heights only the upper pane was destroyed (Figure 13).

Figure 13: Test HSG (failure uppermost pane)

Only at an impact with a drop level of 10 m all panes failed. The PVB-interlayer was to be held again in the position under an angle of approximately 30 degrees (φ in Figure 8). Thereby the sandbags slid slowly down (Figure 14). The formerly made considerations, that the pane is still held only by the PVB- interlayers, was confirmed here again.

Figure 14: Test HSG (failure of all panes)

Subsequently the glass assembly was pressed into the vertical position and left for some days. The weight had to be supported by the PVB-interlayer only (Figure 15). The folios withstood these loads, no failure of the PVB occurred. The stresses could be the determined as 0.21 MPa which is far below the strength of the material.

Figure 15: Test HSG pressed into vertical position

After these successful tests, the declaration of consent was given orally by the participants of the Berlin authority on site. The variant HSG was preferred because the pane did not brake at an impact level of 3 m. The written declaration of consent was presented later including a series of additional requirements. Most of them could be fulfilled relatively easy. The only requirement that could not be fulfilled was that the front girder HEM 120 (Figure 6 and 7) should only have a maximum deflection of 0.5 mm. The purpose of this requirement was that the glass should not be stressed additionally through the deflection of the steel girder. It could be shown that this concern was excessive. A mathematical proof yielded, that under the load proper weight + snow with consideration of the stiffness of the steel plate of 40 mm thickness (Figure 7) the deflection was 2.45 mm. These deflections of the girders were considered as external loads in a finite element analysis of the glass plate. Both cases, monolithic as well as layered were investigated. With the layered system a maximum stress of 26.4 MPa resulted, bellow the allowable stress of 29 MPa. The monolithic approach leads to larger bending moments, but smaller stresses, namely 12 MPa. As an extreme case, the stress is determined for the bending moment obtained from monolithic system with the resistance of the layered systems. A value of 34 MPa was obtained. This value for the extreme conservative approach lies only slightly above the allowable stress of 29 MPa, it might hardly appear. With the presentation of these calculations, the requirement mentioned above was withdrawn by the authorities.

III. Glass Canopy on the Building Side Behrenstrasse

Two additional canopies illustrating the same principle with smaller cantilevers and reduced lengths were realized on the building side of Behrenstrasse (Figure 16).

Figure 16: Glass canopies at the building side facing Behrenstrasse

The larger canopy has a cantilever span of 1.20 m and the smaller one of 0.90 m.

Despite the smaller cantilever size the same glass thickness and the same concept as on the Pariser Platz building side were applied.

The reason was architectural considerations and to avoid having to go through additional declaration of consent.

The process of fastening the glass panes was essentially simpler than for the canopy on the Pariser Platz building side.

IV. Acknowledgment

The following partners took part in the building construction concerning the glass canopy:

Building owner:
Pariser Platz 3 property Ltd.& Co building KG
10117 Berlin, Germany

Project management:
DG real estate management company GmbH
Frankfurt, Germany
and
HINES, property management Ltd., Berlin, Hines real estate Ltd.
10117 Berlin, Germany

Architect:
Frank O, Gehry& Associates Inc.
Santa Monica, California, USA

General contractor and site supervision:
Müller-Altvatter, building enterprise Ltd. & Co.
10117 Berlin, Germany

Structural Steel for the fixing of the canopy
Ingenieurbüro Dr. Janßen
33739 Bielefeld / Germany

Glass static and construction:
GLASCONSULT, Structural engineering of glass constructions,
8142 Uitikon/ Zurich Switzerland

Glass delivery:
Bischoff glass technology
75015 Bretten Germany

Erections of canopies:
Aepli& Co metal contractor
9201 Gossau / Switzerland

REFERENCES

[DIN 1055 Teil 5 1990]
Lastannahmen für Bauten; Schneelast und Eislast 1990

[CEDRUS3+]
Finite Element Program Scheiben / Platten Cubus Inc, Zurich

[Angst & Pfister 1996]
Katalog Schwingungs- und Schallschutztechnik 1996 Techniche Informationen.

[Hess 1988]
Zürcher S-Bahn/ Bahnhof Stadelhofen Teilprojekt 5, Glasüberdeckung Perrondach, Technischer Bericht, 15. Dec 1988.

[Pilkey 1994]
Formulas for stress, Strain and Structural Matrices 1994 John Wley& Sons Inc. New York, ISBN 0471527467

EU COST C13 Glass and Interactive Building Envelopes. M. Crisinel, et al. (Eds.). IOS Press, 2007.

All-Glass Staircase, Notting Hill, London

Wilfried Laufs, Werner Sobek Ingenieure, Stuttgart, Germany

To bring direct day-light into a domestic housing staircase area in London, an all-glass staircase has been built, where all treads are purely made of glass. The following article describes the design, detailing, calculation and construction of the staircase, which was also tested for sufficient strength and post-failure security aspects.

Keywords: all-glass staircase, glass testing

I. Introduction

Staircases next to walls without windows might be dark and non-spectacular. If the staircase is yet to be constructed, why not use glass as the leading construction material, acting as the primary structural element. The following article describes such an all-glass staircase, which was designed and constructed in Notting Hill, London, in 2003 according to Figure 1. It is meant to give a practical example of the capacity of modern glazing, combined with structural as well as detailing knowledge within the field of structural glass engineering.

II. Structural Concept and Detailing

A. Global Structural System

To keep opaque structural material to a minimum, each tread was designed as an individual C-section, cantilevering out from the adjacent wall, where a hidden pair of steel beams spans across from concrete floor to concrete floor level with sufficient bending and torsional capacity, see Figure 2.

B. Glass Tread Profile

Each C-profile is composed of three flat laminated glazing panels, rigidly glued to each other by means of acrylic bond, see Figure 3. For aesthetic clarity, the 90° corners of the C-section were chamfered to 45° at adjacent glass mitred joint edges before toughening and lamination. As internal temperature load cases are small ($\Delta T \sim 10$ K only) and very little UV-light is hitting the intermediate bonding layers, acrylic bond was chosen as a suitable material instead of a PVB-interlayer. To achieve a good grip on each tread, non-slippery lines of ~0.5 mm depth were manufactured into the top surface (water jet).

Figure 1: All-glass staircase Notting Hill, London

C. Construction

In order to avoid a direct steel-glass contact, but still transfer all support forces from the glass treads into the main steel support structure within the wall, a “shoe-connection” detail was developed according to Figure 4. A two-component resin was squeezed as the compatible intermediate mortar material between the glazing and mild steel flat profiles of the support (Figure 4), in addition to some distant-holding plastic support pads locally.

Figure 2: Global structural system of glass stair (during construction)

Each glass tread was bonded together and fixed into its steel shoe. Each shoe was then bolted to the main steel beam in the wall, with options to adjust tolerances both vertically and horizontally. Neoprene pads (t = 3mm) were placed underneath each bolt to guarantee some spring behaviour against impact (abrupt steps); also shims can be added to align each tread in its exact final position.

Figure 3a: All-glass tread C-section

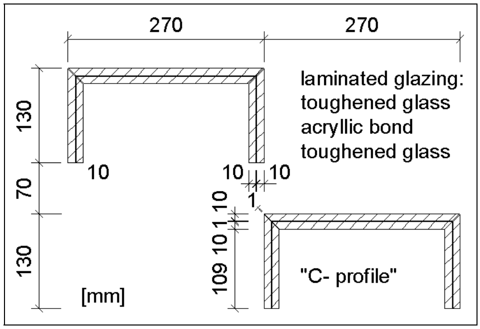

Figure 3b: All-glass tread C-section

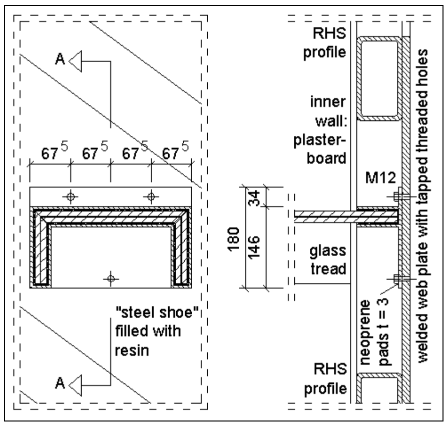

Figure 4: Glass “shoe support” construction detail; all edges polished

D. Structural Calculations

A load case according to Figure 5 was considered relevant, which two persons (100 kg each) crossing each other’s way on the stair and stepping onto one tread at the same time, where a dynamic amplification factor of 1.5 was assumed.

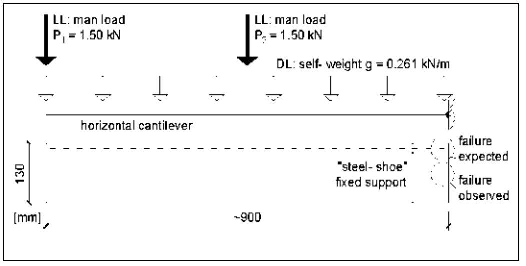

Figure 5: Structural system and relevant loading per tread

Assuming linear-elastic theory, the above loading would lead to a maximum un-factored upper tensile stress of max $\sigma_1 = M/\ W_{1\ yy\ upper}$ = 2.13 kNm / 390585 cm³ ~ 5.5 N/mm² (with full shear interaction of the bonding layers) and $\sigma_2 = M/\ W_{2\ yy\ lower}$ = 2.13 kNm / 57772 cm³ ~ 37 N/mm² (with no shear interaction) respectively, with $\sigma_{allowable}$ = 50 N/mm² > 37 > 5. One might expect the primary crack to start from the area of highest tensile stresses at the top, but as will be explained further down, this was not the case under high loads during every test.

III. TESTING

A. General

As for most of modern glass constructions with primary load-carrying function, both strength and durability tests for regular usage as well as post-failure security tests for accidental cases need to be performed to satisfy all safety aspects and learn about the glass stair treads behaviour by means of 1:1 testing.

B. Ultimate limit state (static)

Breakage of toughened glass usually is in the order of 120 to 200 N/mm² for short-term loading and would be expected at the area of highest tensile stresses. However, due to the unknown exact support condition (shoe with resin), where local pressure peaks or friction may occur, a 1:1 testing series was performed. A first glass tread with support shoe was tested, where the load P1 (see Figure 5) was increased in steps of 25 kg sand bags each (one bag per minute) up to failure (see Figure 6). The tip deflection at the free cantilever end was measured with results according to Figure 7. Due to a lack of budget, the shoe support itself was bolted to a non-rigid steel frame, simulating the wall behind, which also deflected under loading. Nevertheless, a rather linear load-deflection curve was obtained, with the first crack coming from the centre of the left flange at 835 kg loading. The loading could be further increased, until the second glazing panel on the left flange side failed. The partially broken tread kept in place until at a 925 kg loading the system collapsed as a whole.

Figure 6: Testing set-up with sand-bag loading for P_1 (top); primary crack at centre of inner laminate of flange (bottom)

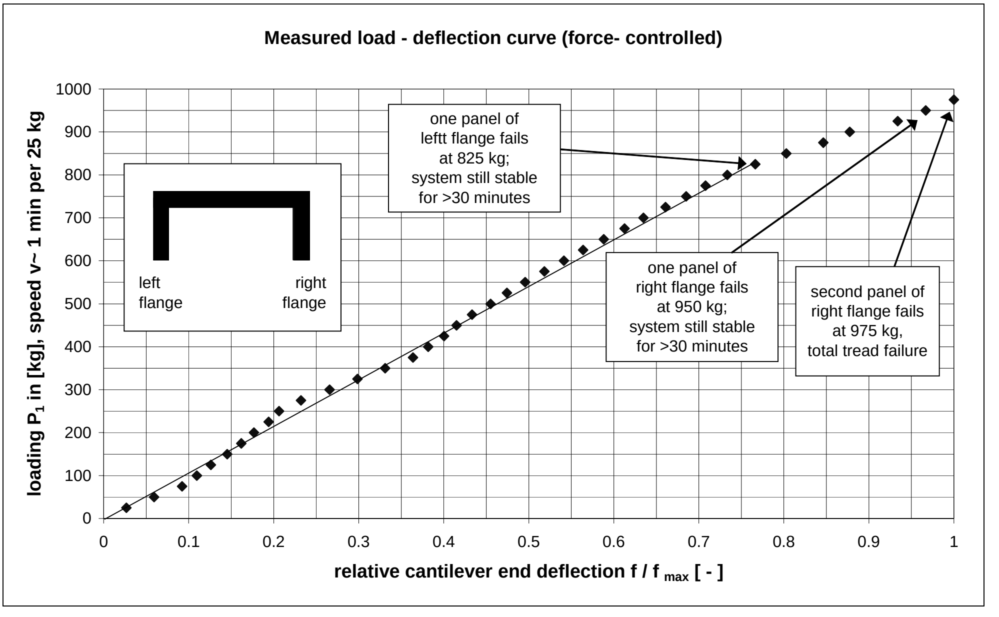

Figure 7: Indicative force – deformation behaviour of test rig with glass tread

Test	Breakage force	Breakage stress		comment
[no]	P_1 [kN]	Full shear interaction [N/mm²]	no shear interaction [N/mm²]	
1	825	19	129	first crack
2	1250	29	196	at collapse
3	1125	26	176	at collapse

Table 1: Theoretical breakage stresses

However, as a system strength rather than a glass strength was tested within the steel shoe system test set-up, *Table 2* cannot be taken directly for design, which is much rather achieved by 1:1 testing here, with 825 kg >> 2* P_1 = 300 kg for short-term ultimate loading conditions.

C. Ultimate limit state (dynamic impact)

To examine the glass tread under possible abrupt high impact loads, a drop test was carried out using a 25 kg weight landing on the end of the tread and dropped from a height of 4 m. No glass or joints failed (Figure 8).

D. Serviceability limit state (long-term durability)

As the glass strength might decrease with time and the steel shoe system needs to be durable, a cycle test was performed with the same test rig by loading the tread with 300 kg and measuring a tip deflection f_0, and mounting an electric motor with an eccentric cam which applied f_0, simulating the 300 kg load (approximately two people on one tread). The motor was left running 830 rounds per minute for approximately 10 hours (498000 cycles). This simulated an average family of 4, each using the stairs 4 times a day for 40 years (up and down). There was no breakdown of any of the joints, laminate or resin observed.

Figure 8: Drop test with a 25kg weight landing on the end of the tread, $\Delta H \sim 4m$, no failure

E. Post-Failure security

To learn about remaining capacities of partially broken steps, both panels of one flange were broken on purpose by hammer. As shown in Figure 10 and Figure 11, the tread was still able to fully carry one person for at least 10 minutes. Here, the acrylic bonding appears to be advantageous compared to the usual PVB-interlayer or resin products for laminate safety glazing: the fine broken glazing pieces stick to each other and still transfer compressive forces at the bottom of each flange for a long time and keep the C-section working under loading. Therefore, if one glass panel breaks, each laminate would stay in position long enough for a person to step on adjacent unbroken steps to be safe. In this context, it has to be added that the glass stair did not have to perform in case of fire, as there are other escape routes in the house. Therefore, fire resistance was not tested.

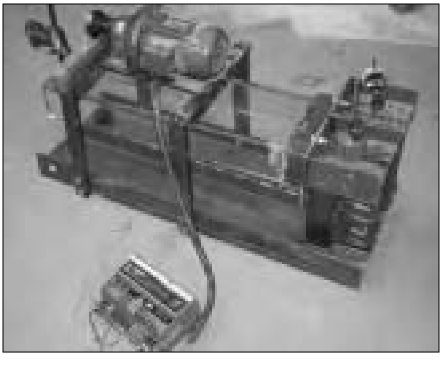

Figure 9: Testing set up for cycling test

Figure 10: Both panels of one flange broken, tread still carries one person

Figure 11: Sufficient post-failure security observed

IV. SUMMARY

As shown above, a modern all-glass-stair construction is capable to carry high ultimate short-term loads as well as give a long-term durability for many years. Testing the system as a whole is recommended to find the true failure modes and learn from the broken system in terms of its post-failure capacity and breakage behaviour. In this case, even a partially broken tread can still carry a person long enough to walk down the staircase. The presented glass tread (Figure 12) represents a new generation of structural glazing applications and appears to be the first of its kind.

V. ACKNOWLEDGEMENTS

Client: Chris Shirley, Notting Hill London

Structural concept and Engineering: Whitbybird London, Wilfried Laufs / Will Stevens

Construction and testing: Peter Collins, Hourglass Havant Hampshire

Figure 12: Finished glass tread and balustrade (not touching the treads)

EU COST C13 Glass and Interactive Building Envelopes. M. Crisinel, et al. (Eds.). IOS Press, 2007.

Glass House Badenweiler

Hans Schober, Hannes Gerber, Jens Schneider, Senior Engineers
Schlaich Bergermann und Partner, Stuttgart, Germany

For a connecting structure between two bath houses at *Therme Badenweiler*, Germany, an all glass structure was designed and built. The glass house consists of vertical glass columns (l =7,60 m) and horizontal glass girders (l = 6,20 m) to support the vertical and horizontal loads of the facade. The roof structure is supported by glass beams (l = 6,20 m) that are formed according to the bending moment and are suspended by a steel cable within a channel in the laminated glass. The glass structure and all details were worked out diffident to include the new structure within the ambiance.

Keywords: glass structure, glass beams, glass columns, glass design

I. Introduction

The last part of the modernisation of *Therme Badenweiler* was the renovation of the *Lindebad*, a famous building designed 1957 by Prof. Linde. To connect the old *Marmorbad* with the *Lindebad*, we designed a small all-glass structure with maximum transparency. All structural elements, girders, columns and beams are made of tempered laminated safety glass.

II. Situation

A light, decent structure with a maximum of transparency was selected to guarantee a structure that preserves the independence of the old *Mamorbad* and the “new” *Lindebad* in the centre of Badenweiler. The all-glass structure consists of a 6,20 m wide and 7,60 m long glass façade and 6,20 m wide and 7,80 m long glass roof.

Figure 1: The small glass house between *Marmorbad* and *Lindebad*

The slope of the roof (2%) is to the back side of the roof to prevent a gutter at the front side. The width of 6,20 m between the old and new part made it possible to use glass beams and girders without joint as the typical size of float panes is 3,20 m x 6,00 m. The shape of the roof beams is formed according to the moment diagram of a simple beam. They are pre-stressed by means of steel cables from stainless steel. These are used to decrease the tension stresses in the glass and to improve the post-breakage behaviour of the beams [Bucak 2003]. The beams are stiffened horizontally by the roof glazing (insulating glass, 10 mm tempered glass/ 2 x 10 mm laminated heat strengthened glass) that spans between the beams. Small steel T-Profiles were introduced in the other direction between the roof glazing to improve its post-breakage behaviour as the roof may be stepped on for cleaning reasons. In Germany, building authorities insist on breaking all glasses of an insulating glass unit for testing the post-breakage behaviour.

The horizontal façade girders are supported and stiffened by vertical glass columns. The façade grid size includes the glass door to ensure a structure without a door frame. The top of the façade is connected to a stainless steel frame with fin windows to ensure natural air vent.

III. Facade Structure

The façade structure consists of three horizontal glass girders and five vertical glass columns. The horizontal girders are made of three panes of 10 mm tempered laminated safety glass. They run horizontally with a width of 280 mm whereas the vertical columns with a width of 260 mm and a length of 2300 mm for each section span between them. The columns are connected to the girders by a small stainless steel box so that vertical and horizontal loads can be transferred. This small box is glued to the girders by a structural silicone sealant. An additional steel bolt was included and glued in with a 2-component epoxy mortar to prevent additional tests for the glued connection by the building authorities. The complete horizontal force could be transferred by the bolted connection without using the sealant.

The façade columns consist of laminated safety glass, two panes of 15 mm tempered glass. Our original design used three panes where the edge of interior pane should be set back to prevent a destruction of all three panes at a time from the edge. The authorities nevertheless insisted on having a scenario of a complete destruction of all three panes a column. Therefore, the steel frame on top of the façade was strengthened and the columns were reduced to two panes. Now the frame is strong enough to carry the loads although a complete column is destroyed.

The façade panes have a four side support for wind pressure from the columns and the girders, wind suction is transferred through glass fittings at the corners. The glass fittings are connected to the glass girders through the small steel box. The horizontal glass girder is connected to the existing structures of *Mamorbad* & *Lindebad* by mounting parts that are fixed to the walls with anchors.

Figure 2: Interior view of the glass house and the façade

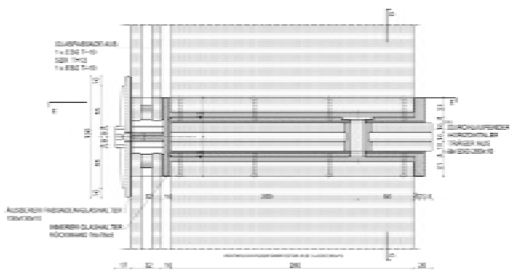

Figure 3: Detail connection façade column – façade girder with small stainless steel box

The top end of the façade is a stainless steel frame of flats 20 mm x 80 mm with included fin windows. This frame is also used to support the roof glazing. The vertical loads from the frame are supported by the glass columns by simple contact. In case of a complete destruction of a façade column, the deformation of the façade girder above the destroyed column is greater than the deformation of the steel frame. So vertical loads are transferred by the steel frame to the next columns. The horizontal girder only has to transfer self-weight and the load of two column parts as a maximum but no additional loads from the roof structure. A safety calculation with reduced safety factors showed the reliability of the system.

IV. ROOF STRUCTURE

The glass roof structure consists of four glass beams of laminated glass (each three panes of tempered glass, 10 mm outer panes, 15 mm inner pane) in a distance of 1,70 m and with a span of 6,20 m between the existing buildings (Fig. 4, 5). To decrease the tension stresses in the glass beam and to improve the post-breakage behaviour of the beams, a stainless steel cable runs in a small channel in the bottom of the laminated glass (open spiral strand 1x37, diameter 10 mm). This channel simply results from letting the inner pane of the laminated glass stand back. The cable is anchored in a stainless steel box at the edges of the glass beams. The gap between the box and the glass is filled by a two-component epoxy mortar (Fig. 6).

Figure 4: Interior view of the roof structure

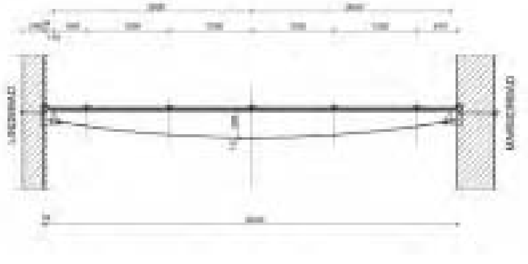

Figure 5: Roof girder

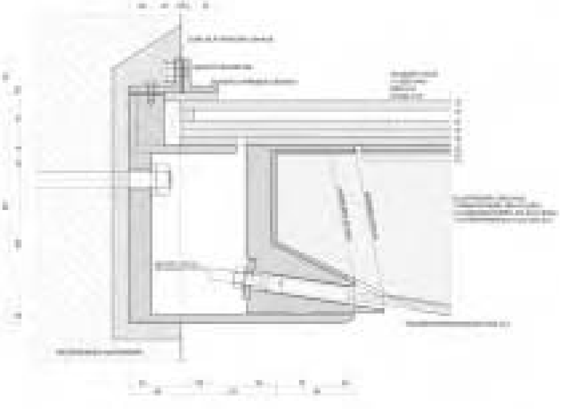

Fig 6: Glass beam support and cable bracing

The steel boxes are supported by steel consoles that are fixed in the walls with anchors. The insulating glass units of the roof (top layer 10 mm tempered glass, bottom layer laminated heat strengthened glass, 2 x 10 mm) spans between the beams. To ensure a post-breakage behaviour of the glass after a complete breakage of all three glasses that was demanded by the building authorities, small steel T-Profiles were placed in the joints between the insulating glasses perpendicular to the glass beams. This results in a four-sided supported of the panes. The crack pattern of four-side supported glasses with the cracks perpendicular to the principal stress isochores ensures a much better post-breakage behaviour than the crack pattern of a two-side supported glass. Two-side supported glasses usually have a crack pattern where all cracks are in the centre of the panes which leads to a “hinge” and the pane slips off the supports.

V. DESIGN

A. Global Structural Analysis

The internal forces of the system were studied with a global structural model to ensure that the interaction between roof and façade structure is acquired realistically. Especially the fail-safe scenarios with a complete failure of single glass columns can only be simulated in such a global model (Figure 7).

Figure 7: Global structural system

The load transfer between the steel frame of the façade and the glass columns was simulated by non-linear springs that only transfer compression. The stiffness of the springs was adapted to the material parameters of the EPDM-interlayer. So the load distribution between the frame and the still intact glass columns - which depends on the stiffness and the deformation of the different partners - could be simulated realistically. The loads on the structure were taken from the German load design code DIN 1055. Different load cases with and without safety factors had to be calculated to account for the different safety concepts for glass (global safety concept), steel (partial safety factors) and the failure scenarios.

B. Local Stress Concentrations

The local design for stress concentrations in the glass elements was done by using detailed Finite-Element-Models [Schneider 2001]. The finite-element-model of the bolted connection in the façade girders and the notch of the girder at the supports is showed in Figure 8.

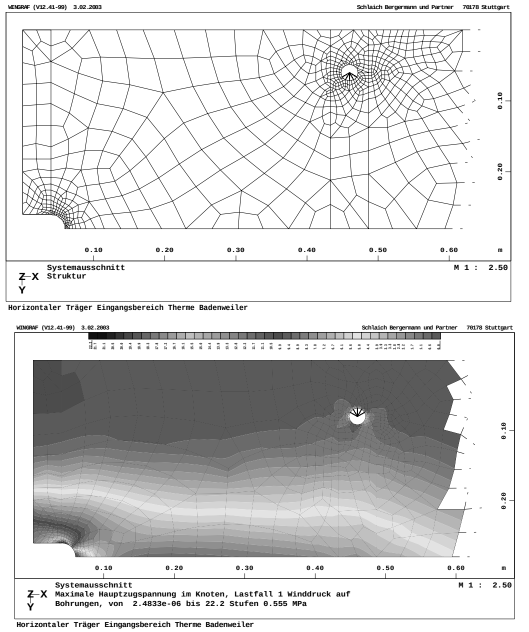

Figure 8: FE-Model of a façade girder detail

For roof-panes, the controlling load case is usally the concentrated load of a person on the pane. In Germany, the load to be applied for a glass pane is 150 kg on an area of 10 cm x 10 cm at the moment. Moreover, it has to be assumed for the design that the top glass layer failed and the load is only transferred by the bottom laminated layer. The shear connection between the glass panes by the PVB-interlayer must not be considered for that load [TRLV 1998, Wörner 2001]. Figure 9 shows the stress distribution in the bottom glass layer for this load case. Finally, the impact load and post-breakage behaviour of a falling person on the roof has to be proved. This was done by using results of similar tests on glass panes with four-side support [Bucak 2003].

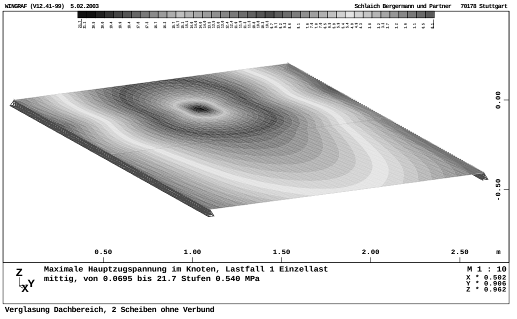

Figure 9: Stress Distribution in the bottom glass layer of the roof pane

C. *Stability Analysis*

The stability analysis of the glass columns and the glass beams (lateral buckling) were also done by using finite-element models, neglecting the shear stiffness of the PVB-interlayer. For the columns, a simple column (EULER type II) was calculated. The imperfection of the column was assumed to be l/300, which means 7,7 mm for the given length of 2300 mm. Research at the EPFL in Lausanne [Luible 2002] showed that this value is realistic for tempered glasses. Calculations showed a sufficient safety even for the failure of one of the two panes. As explained in section *A*, the whole structure is nevertheless capable of a total failure of a column.

The stability analysis of the roof beams were done using a finite-element-model of the beam with realistic boundary conditions and the steel cable suspension. The resulting deformations from the first eigenvalue of stability failure were calculated with a dynamic analysis (Fig. 10). These deformations were scaled to a maximum of l/300 and applied to the model as an imperfection by means of node deformations. The deformed system was now calculated with the unfavourable load cases. Again, the shear stiffness of the PVB-interlayer was neglected and the failure of two of the three panes was also considered. Calculations showed that the glass beams are not suspected to stability failure.

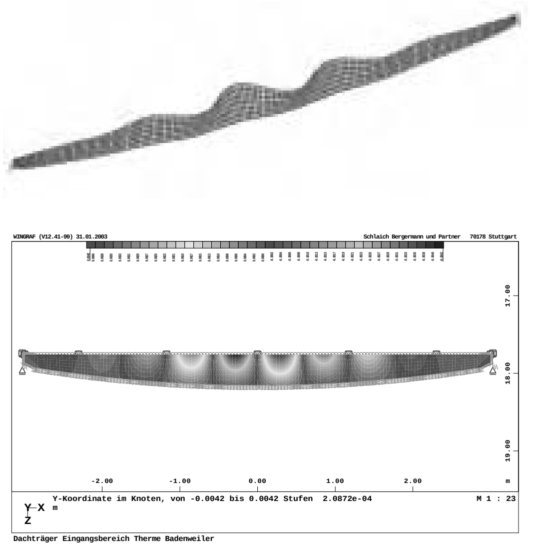

Figure 10: Lateral buckling eigenform of the roof girder and resulting stress distribution

VI. Safety and Redundancy Concept

First of all, the whole structure is designed to use laminated safety glass for all structural glass elements to make a total collapse of an element unlikely. The design values for the bending strength of glass were taken from the German design code for linear supported glass [TRLV 1998]. The values base upon a global safety concept:

- tempered glass: 50 MPa
- heat strengthened glass: 29 MPa,
- laminated safety float glass in the overhead area: 15 MPa,
- laminated safety float glass in the overhead in insulating glass panes after collapse of the top layer: 25 MPa.

Moreover, as explained in the respective chapters, different failure scenarios of the glass columns and the glass beams were analysed. The structure is capable of a total collapse of a column; the post-breakage behaviour of the glass beams with a steel cable suspension was tested for similar structures [Bucak 2003] and showed good results even after the collapse of all panes.

The post-breakage behaviour of the roof panes after impact of a falling person was improved by using a four-side support which showed acceptable results in comparable tests [Bucak 2003].

To prove the behaviour of the glass beams under impact load of a falling person on the roof, a simplified mass-spring-mass-spring model was used to calculate static equivalent load (= 38 kN) from the dynamic soft body impact [Schneider 2001]. This load results in a maximum principal tension stress of 66 MPa for the tempered glass which is acceptable for the extreme load situation.

VII. Final Remark

This small project shows that all-glass structures require very detailed engineering design. This does not only affect the local stress analysis but also a stability analysis and a safety concept. Due to a lack of consistent design codes for structural glass, the engineer is challenged to get most of the knowledge from research results.

VIII. Project Partners

Client:
Staatliches Vermögens- und Hochbauamt Freiburg Germany

Architect:
Architektengruppe F70, Freiburg, Dipl.-Ing. (FH) Spathelf

Construction
Hunsrücker Glasveredelung Wagener, Kirchberg, Germany

Checking engineer:
Prof. Dr.-Ing. J.-D. Wörner, Darmstadt, Germany

Expert's report on roof structure:
Prof. Dr.-Ing. Ö. Bucak, Munich, Germany

References

[Bucak 2003]
Bucak, Ö, *Gutachterliche Stellungnahme zur Glasdachkonstruktion beim Bauvorhaben Therme Badenweiler*, June 2003, unpublished

[BÜV 2001]
BÜV-Empfehlung für die Bemessung und Konstruktion von Glas im Bauwesen, Der Prüfingenieur (2001) Vol. 4

[Luible 2002]
Luible, A., *„Auf Biegen und Brechen"* tec21 (2002), Vol. 12

[Schneider 2001]
SCHNEIDER, J.: *Festigkeit und Bemessung von Glas: Punktgelagerte Verglasungen, Dynamisch beanspruchte Verglasungen bei weichem Stoß*. Dissertation (PhD-thesis), Institut für Statik TU Darmstadt, 2001.

[TRLV 1998]
Technische Regeln für die Verwendung von linienförmig gelagerten Verglasungen (TRLV), Fassung September 1998, Mitteilungen Deutsches Institut für Bautechnik 6/1998.

[Wörner 2001]
Wörner, J.D., Schneider, J., Fink, A. *Glasbau.* Springer-Verlag, Berlin, 2001

EU COST C13 Glass and Interactive Building Envelopes. M. Crisinel, et al. (Eds.). IOS Press, 2007.

Designing Double Glazed Façade Constructions

Olavi Tenhunen, Helsinki University of Technology, Espoo, Finland
Sini Uuttu, Lumon Oy/ Parvekenikkarit Oy, Vantaa, Finland
Aki Vuolio, Helsinki University of Technology, Espoo, Finland

Useful data of materials, loads, design methods, breakage causes and maintenance for designing double glazed façade constructions have been introduced.

Keywords: double skin, facade, glass

I. Characteristics and Methods

The characteristics of the facade have to correspond to the demands. The demands must be presented so that by designing and implementing according to those demands the wanted result is gained. The properties may be defined at different levels. The profile of the demands may be different in each building. The minimum demands are given in laws and regulations. The methods for rating and classifying have to be such that it is possible to prove the fulfilment of all the important property requirements. A comparison with the demands is sensible only when the demands are given in advance.

II. Structures

A. General

Movements of the structure have to be born in mind during the design and the implementation. Drying of wood, hardening of concrete, strain, creep, increasing and varying stresses in the course of the erection and movements because of the temperature variations keep the structure in movement all the time. The order of the assembly also affects the result especially in the facade.

Figure 1: Cantilever beams as a supporting structure

Figure 2: Suspended structure

Figure 3: Vertical frames as a supporting structure

B. Metal structures

The frame of the outer glass skin is usually made of aluminium, hot dip galvanized steel, stainless steel or weathering steel. Gratings are made of hot dip galvanized steel, stainless steel or aluminium.

Hot dip galvanizing is usually more economic against corrosion of steel than painting of equal protecting ability. Directions for design are presented in the standard EN ISO 14713. Also zinc coated cold rolled products are used.

The insulated wall is usually constructed of light non-bearing wall elements. The frame of the elements is often made of steel sheet profiles. Webs of the steel sheet studs are often perforated for diminishing thermal conductivity. Surface of the element is usually metal or glass, but may be also more sensitive material, because it is sheltered by the outer glass skin.

Paint coated, enamelled or COR-TEN steel sheet products can be used in visible surfaces of the intermediate space (cavity) of the double façade. If painted in the factory the PVDF coating is preferred. Polyester paint is recommended for powder painted products.

Stainless steel may be used in bearing structures, door and window structures, lists, gratings and fixings (screws, bolts, nuts, washers, expansion bolts and fixing plates on the concrete). Chromium nickel steel of low carbon percentage 1.4307 (AISI304L) is usually good enough. If the building is situated quite on the shore of the sea, it is maybe reasonable to use stainless steel with molybdenum content 1.4404 (AISI316L), because it tolerates better chlorides of the sea water. Bigger content of nitrogen increases a resistance to the climate corrosion.

Aluminium bars used in constructions are strengthened by alloying. Extruded profiles are commonly made of alloys EN AW-6060 [EN AW – Al MgSi] and EN AW-6063 [EN AW - Al Mg0,7Si], which have good physical properties and which are very suitable for anodizing. EN AW-6005A [EN AW – Al SiMg(A)] is an alloy suitable for anodizing with a little more strength. EN AW-6082 [EN AW – Al Si1MgMn] is intended specially for constructions, but is not so suitable for anodizing. The most common of the weldable structural alloys is EN AW-7020 [EN AW – Al Zn4.5Mg1]. The physical properties of alloys and the tolerances of products are given in the standard EN 755-1…9. Because the tolerances in facades are minor, the standard EN 12020-1…2 can be followed. Aluminium structures in double glazed facades are usually ready-made products belonging to a facade system.

Weathering steels with high phosphorus content (e.g. COR-TEN A, phosphorus 0.07…0.15% and COR-TEN B, phosphorus 0…0.35%) have the best corrosion resistance. Granted impact resistance, however, requires low content of phosphorus (<0.025%) and sulphur (<0.020%) (e.g. COR-TEN B-D).

When different materials are combined, different behaviour in temperature variations and under varying loads have to be kept in mind.

C. Glass structures

Four different types of glass are classified according to the strength: annealed float glass, heat-strengthened glass according to the standard

EN 1863-1, thermally tempered (also called fully tempered or toughened) glass according to the standard EN 12150-1 and laminated glass according to the standard EN ISO 12543. The single plies of laminated glass are glued to each other with membranes of polyvinyl butyral (PVB) and may be of any kind of float glass. All these types of glass may be used as a single glass pane or joined to an insulating glass unit. Quality classes and minimum requirements are presented in the standard EN 572-2.

Emissivity of float glass is 0.84 (property to radiate long wave heat radiation, proportion to the emission of the black body, which has the emissivity of 1). Lower values are possible to get by coating. If the emissivity is not more than 0.20, the glass is called Low E glass.

The most advanced glasses for regulation of solar radiation are chromogenic glasses, which change their properties depending on the sunlight (photochromic) or surroundings temperature (thermochromic or thermotropic) or which are activated by electric current.

Coatings of metal or metal oxide usually conduct electric current. The resistance gets them to warm up. If the coating is on the innermost glass pane of the insulation glass unit and electric current is switched on the coating, 90% of the heat radiates into the room.

Fire-resistant glasses may be used in facades to stop the spreading of smoke or fire. Fire-resistant glasses form a unity with all the surrounding structures. These glasses are classified by entity (E- classes), heat radiation (EW-classes) and heat insulation (EI-classes).

There is not any kind of glass that would be the best for all purposes. Even in the same building several kinds of glasses may be used depending on the cardinal points, local climate and needs of heating, cooling, light, shading and appearance.

The cut edge of the glass pane has to be as smooth as possible. Untreated edges can be used only in inaccessible places. The strength of the glass pane can be increased by grinding edges. At Helsinki University of Technology, the edge strengths of glasses with different edge treatments were examined with 80 glass bars of the size 8 mm x 30 mm x 320 mm. Following are microscope photos from the edges of the glass bars.

Figure 4: Cut edge of the annealed float glass

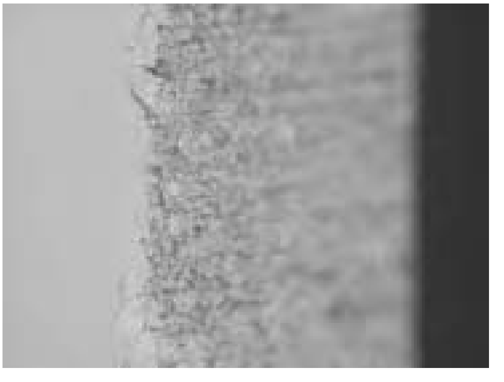

Figure 5: Arrissed edge of the annealed float glass

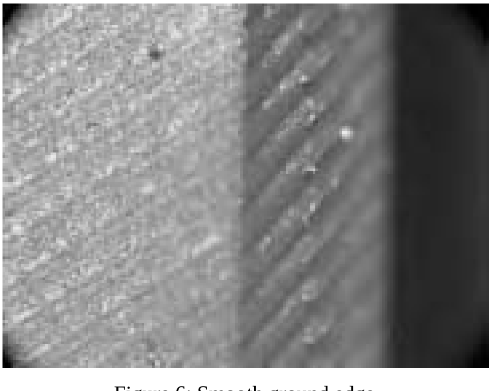

Figure 6: Smooth ground edge

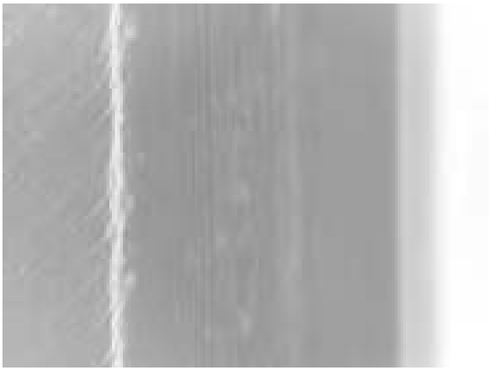

Fig 7: Polished edge

Results of the tests are in the table below.

TABLE 1:
EDGE STRENGTH ACCORDING TO THE TESTS

Edge treatment	Tensile strength at the edge N/mm^2	Corresponding temperature difference ΔT °C
Annealed float glass, arrissed edge	35	16
Annealed float glass, smooth ground edge	46	22
Annealed float glass, polished edge	55	26
Heat-strengthened glass, smooth ground edge	125	94
Heat-strengthened glass, polished edge	141	101
Tempered glass, smooth ground edge	160	145
Tempered glass, polished edge	187	159

If these values are used, the small amount of samples and the required safety level (safety factors) must be considered.

According to the measurements done by Helsinki University of Technology, the biggest temperature variations during 24 hours on the inner surface of the outermost glass pane in a double glazed facade were over 40°C. Temperature at the edge of the pane was at any time not more than about 10°C lower than in the middle of the pane and not more than 16°C higher.

III. LOADS

A. Wind load

The determination of wind load is a fundamental task in structural design of façade structures. It is done in compliance with part 2-4 of Eurocode 1, when the structures are designed in accordance with the European CEN design standards.

In the particular case of double glazed facades, an important design aspect is the consideration of the wind actions during execution. The reference wind load during execution may be taken as about 75 % of the characteristic value, which corresponds to a wind speed with a return period of 10 years. It is important to note, however, that even though the reference load may be reduced in the design for the temporary situation, the combination of the aerodynamic factors may be more unfavourable temporarily during execution than in the final situation.

B. Other loads

Other loads to consider include

- Permanent loads from the self-weight of the glasses and the frame structures as well as service equipment, lighting fixtures, shades etc.
- Snow load, if the facade contains horizontal surfaces where snow may accumulate.
- Vertical imposed loads, if the facade frame carries the loads from a service platform.
- Horizontal imposed loads from human impact for structures working as safety barriers. Façade structures within a certain height from the floor level need to be designed for these loads if otherwise there is a risk of a person falling down.
- Thermal loads resulting from temperature differentials between structures and temperature differentials within a structure.
- Internal loads in the design of insulating glass units.
- Actions in accidental situations, such as fire, explosion or earthquake, may sometimes need to be considered.

IV. Structural Design of Glass Panes in Facades

A. General

Recently, parts 1 (1999) and 2 (2000) of the European standard proposal prEN 13474 dealing with the structural design of glass panes, have been published. Part 1 of the standard proposal presents general basis of design and part 2 covers the design for uniformly distributed loads. The exact contents of the design code may be changed considerably before the final approval of the EN standard. However, the draft versions already provide useful information about the design of glass structure, as accurate design methods have been lacking so far in many countries. The principles of fracture mechanics are combined with the Weibull statistics to determine the strength of glass. The geometrical non-linearity induced by the so-called membrane effect is taken into account in the formulas for four-edge supported rectangular panes. The membrane effect arises when the deflection of a glass pane exceeds about half of the pane thickness. As the deflections become large, the use of linear theory, that has been generally used before the introduction of the new code proposals, leads to overestimation of stresses and deflections so that the design may become significantly conservative.

The strength of glass is dictated by the geometry and distribution of surface flaws. In addition, glass has a lower strength against long-term than short-term loading because of the slow sub-critical crack propagation known as static fatigue. Therefore, the design strength is influenced by the duration of the load, size of the pane and the distribution of tensile stresses. For heat-strengthened and tempered glass, the strength is the sum of the compressive prestress at the surface and the tensile strength of float glass.

The design is carried out by using limit state method in accordance with EN 1990 and other Eurocode standards. The strength verifications are made in the ultimate limit state. The required level of structural safety of glass structures is now determined in the same manner as for other structural materials, and it depends on the consequences of possible failure. The introduction of the national partial factor in the design code provides a possibility for national adjustment of the safety level, since historically the levels of structural safety for glass design have differed notably from country to country. The serviceability limit state design comprises checking that specified service limits, concerning usually the displacements and vibration of the structure, are not exceeded. The exact serviceability requirements are not outlined in the design code proposals, so they should be adopted by the designer based on national or other regulations and guidelines.

B. Insulating glass units

Insulating glass units (IGU's) usually consist of two or three parallel glass panes that are connected to each other by the spacer and sealants at the edges, so that there is an insulating, hermetically closed cavity between the panes. The width of the cavity is typically 12 mm or 15 mm, but also widths of 6 mm and 9 mm are sometimes used. The cavity contains air or, to improve insulating capacity, some other gas like argon or krypton.

As the gas in the cavity may be assumed to satisfy the Boyle's law of ideal gases

$$\frac{p \cdot V}{T} = \text{(constant)}$$

a change in its temperature T causes a change in the pressure p, and vice versa, when the volume V is fixed. On the other hand, the pressure acting on the panes makes the panes to deform and thus induces a change in the volume V, which makes the problem non-linear. The membrane effect further complicates the problem when the deflections of the panes become large. The pressure inside the cavity depends also on the ambient atmospheric pressure: when the ambient pressure drops, an overpressure develops inside the cavity, and vice versa. The climatic effects arising from variations of atmospheric pressure and temperature may result in considerable internal loads for IGU’s, especially for small-sized units.

The panes of an IGU may be single or laminated, and the individual plies may be normal float, tempered or heat-strengthened glass. Each pane is designed in accordance with the rules given for the specific type of glass. Relatively complicated calculations are required in the design of IGU's according to the code proposals. The difficulty is determining the load applied to the panes, considering the internal loads, load sharing between the panes and several load combinations with varying duration. In the design code proposals, a hand calculation method is presented for the design of continuously supported IGU's consisting of two glass panes. For the design of IGU's consisting of three or more panes, finite element (FE) analysis with fluid elements modelling the cavity may be used to determine the stresses and deflections. The FE modelling is advisable also for the design of curved IGU's or when the support conditions are exceptional.

V. FACTORS CAUSING BREAKAGE OF GLASS PANES IN FACADES

A. General

The probability of failure seems still to be much higher for glass structures than for structures of other materials. Often the breakage is spontaneous in nature and the exact reason for it cannot be specified easily. It should be noted, that despite exact formulas for strength verification are given in the design codes, it is not possible to determine the level of structural safety for glass structures as accurately as for other load-bearing structures. This is due to the fact that the strength of glass depends almost entirely on the flaws on its surface, so the variation of strength between panes is large. Therefore, the strength may deteriorate significantly during the life cycle of a glass structure, if flaws more critical than expected in design occur e.g. as a consequence of contacts with sharp objects.

The potential actions that may induce failure are presented below divided into three groups.

B. Actions allowed for in the design code

The main load, that the glass panes in facades are designed for, is wind. It can be shown that when a glass pane is designed in accordance with the design code drafts prEN 13474-1 and -2, the failure probability due to wind load is lower than required from normal load-bearing structures belonging to reliability class CC2 of EN 1990. This means, practically, that glass panes, that are properly designed, manufactured, installed, used and maintained, do not break due to wind load.

For internal loads of IGU’s a slightly higher probability of failure is allowed, as the strength verification is made only in the serviceability limit state instead of the ultimate limit state. Still, a breakage of an IGU due to internal loads alone is extremely rare occasion.

C. Actions not allowed for in the code

In the design code, the strength of glass signifies the tensile strength at the central area of the pane, corresponding to the so-called ring-on-ring test method where the strength is determined. The tensile strength at the edge of the pane, however, is usually significantly lower than the one specified in the design code and it depends strongly on the quality of the edge finish. Although the influence of reduced strength has not been at all allowed for in the design code proposals, notable tensile stresses may occur at the edges of the pane as a consequence of e.g. temperature differentials within the glass pane, membrane effect of thin plates subjected to wind loads and displacements of the supporting structure when the joint between the glass and the support is rigid enough to transfer stresses as in structural glazing.

Critical thermal stresses occur when the temperature at the middle areas of the pane is higher than at the edges. That may be the case, if the central areas of the pane become hot due to solar radiation while the edges behind the glazing beads remain cool, or if the pane is otherwise partially shaded. Thermal effects are most significant in coated glasses as they absorb more heat than clear glasses. In the northern climate, the inner panes of IGU's may become subjected to high edge stresses in cold weather, if the edge profile conducts heat and consequently makes the temperature at the edges of the pane lower than in the central areas.

It is evident that in many cases the failure probability due to thermal stresses is higher than due to loads considered in the design code. The edge strength of a glass pane can be improved by using either heat-strengthened or tempered glass instead of normal float glass or by improving the quality of edge finish of the pane.

D. Defects in material, design, execution or use

Most of the failures of glass structures in facades are consequences of some kind of defect or negligence either in material technique, design, execution or use. Because of the slow sub-critical crack propagation of glass, the failure may take place long after the initial flaw has been induced.

Tempered glass is sometimes sensitive to two specific problems related with the material, namely excessive pre-stresses and nickel sulphide (NiS) inclusions. There are no upper limits for the pre-stress in the standards for tempered glass, but it is recommended that the pre-stress should not be much higher than 110 MPa to minimize spontaneous breakages and to guarantee the intended safe failure pattern. The higher risk of failure caused by nickel sulphide inclusions may be eliminated almost totally by using heat soaked tempered glass.

As glass does not possess any plastic deformation capacity, even a small error in the design or installation may lead to a total failure of a structure. The designer should be especially careful with the details. The joints between glass and its metal frame must be designed in a way that the glass-to-metal contact is not possible. Therefore, adequate clearances need to be arranged so that the displacements of the frame, thermal movements and the tolerances in the manufacture and mounting are all allowed for. The materials for sealings and bushings must be correctly selected, so that adequate resistance to environmental conditions, such as UV radiation and variations in temperature, is ensured.

The installation of the panes and the supporting frame requires great accuracy as tolerances are much smaller than in construction usually. During the construction stage there is a high risk of degradation of the glass surface, and hence a notable decrease in strength, caused by e.g. accidental impacts of sharp objects or spatters from welding. Therefore, the pane should be properly protected at the construction site.

During the use of the glass structure, particularly the maintenance and service work near the glass panes may induce initial flaws that could later cause a spontaneous breakage. For example, impacts by service trolleys may be detrimental to the glass pane.

VI. ISSUES ON EXECUTION

No specific one of the various types of supporting structures has turned out to be overwhelmingly good. It depends more on a personal choice of an architect which type is chosen. However, both designers and contractors emphasize that the supporting structure of the double-skin façade should be erected as an independent structure from the floor slabs because of the totally different tolerances. The supporting structure can be connected to a column instead of the intermediate floor's edge. In this way the possible movements of the intermediate floors will not have an effect on the supporting structures of the double-skin façade. This kind of structure is shown in fig 8. The cantilever bracket is hidden under the service platform.

The supporting structure should be designed with adjustable joints in every direction. The suspended structure gives these adjustment possibilities in all directions. However, the rigidity of this type of supporting structure under the erection phase is still causing some problems.

Figure 8: Double-skin structure connected to an I-section column

Figure 9: The completed structure of fig 8 seen from outside.

Rough weather (rain, snow, wind, cold) is often hindering the construction work of double-skin façades. The benefit of pre-glazed elements is that the glazing can be performed in standard conditions and standard temperature. The typical glue (sealant) used in the joints requires a minimum temperature of + 5°C. The construction site is also less jammed. On the other hand there is a risk that pre-glazed elements will be damaged during transport.

The double-skin façade projects in Finland involve a lot of different parties (owner, client, architect, structural designer, façade designer, main contractor, façade contractor, workshops, glass manufacturer, HVAC-designer etc). The responsibilities of each party are sometimes unclear. This leads easily to delays and misunderstandings. It is important that all these parties work together from the beginning and divide responsibilities clearly. A very common problem is that plastering and levelling works are not completed when the aluminium profiles are erected. Fresh plaster and concrete in contact with aluminium profiles will induce corrosion. Early determination of requirements, criteria and delivery lots specified in cooperation with experts is the key for a successful progress of a double-skin façade project. Especially experts of building physics and glass structures and manufacture are needed.

VII. Issues on Fire and Maintenance

After the flashover in the fire situation, the room temperature becomes so high that even tempered glasses break. Spreading of the fire in the intermediate space of the double skin facade depends on the openings and on the depth of the space. The fire of 2 MW through the 1 m^2 opening to the intermediate space needs about 2 m^2 openings at the top and bottom of the intermediate space to keep 20 m high, 10 m wide and 0.4 – 1.0 m deep intermediate space smokeless. [Hietaniemi et al. 2002]

The most common maintenance work in the double glazed facade is washing. It can be minimized by avoiding outside details that corrode, catch dirt or form water streams, and by using self-cleaning glasses. Maintenance has to be taken into consideration as early as possible. For outside washing the mobile cranes or the service cages may be used. Crane locations, use of the cage and necessary structures have to be designed. For inside washing the service platforms or service cages have to be used. It is necessary to fit the service platforms with handrails or other barriers or lifelines. Maintenance may be easier if there are sockets for electricity and also wall taps and hose connections for water in the intermediate space. The space has to be so deep that it is possible to do maintenance works taking into account also Venetian blinds. Fittings on the gratings make the walking difficult. Fittings on the insulated external wall may hinder opening of the doors and windows. Diagonal bars in the space may be harmful for using the service cage.

Figure 10: The service cage for the maintenance of the intermediate space.

REFERENCES

[Hietaniemi et al. 2002]
HIETANIEMI, J., HAKKARAINEN, T., HUHTA, J., KORHONEN, T., SIISKONEN, J., VAARI, J., *Ontelotilojen paloturvallisuus, Ontelopalojen tutkimus kokeellisesti ja mallintamalla.* Espoo 2002: VTT, Vuorimiehentie 5, PL2000, 02044 VTT, VTT Tiedotteita 2128. 125 s. + liitt. 63 s. ISBN 951-38-5953-3. ISSN 1235-0605. (in Finnish).

[Mäkeläinen et al. 2002]
MÄKELÄINEN, P., TENHUNEN, O., VUOLIO, A., LINTULA, K., VILJANEN, M., BERGMAN, J., HÄNNINEN, J., ALINIKULA, T., PALMI, P., *Kaksoisjulkisivun suunnitteluohjeet.* Espoo 2003: Helsinki University of Technology, Laboratory of Steel Structures, P.O. Box 2100, FIN-02015 HUT. Publications 26. 166 p. ISBN 951-22-6649-0. ISSN 1456-4327. http://www.hut.fi/Yksikot/Rakennus/Teras/Julkaisut/jsarj.html. (in Finnish).

[Tenhunen, O. 2003]
TENHUNEN, O., *Metalli-lasirakenteisen kaksoisjulkisivun materiaalien soveltamiskriteerit.* Espoo 2003: Helsinki University of Technology, Laboratory of Steel Structures, P.O. Box 2100, FIN-02015 HUT. Publications 28. 104 p. + appendices 43 p. ISBN 951-22-6780-2. ISSN 1456-4327. http://www.hut.fi/Yksikot/Rakennus/Teras/Julkaisut/jsarj.html. (in Finnish).

[Uuttu, S. 2001]
UUTTU, S., *Study of Current Structures in Double-Skin Façades.* Espoo, 21.8.2001: Helsinki University of Technology, Department of Civil and Environmental Engineering, Laboratory of Steel Structures, Master´s Thesis. http://www.hut.fi/Yksikot/Rakennus/Teras/Tutkimus/tproj_mela.htm

[Vuolio, A. 2003]
VUOLIO, A., *Structural Behaviour of Glass Structures in Facades.* Espoo 2003: Helsinki University of Technology, Laboratory of Steel Structures, P.O. Box 2100, FIN-02015 HUT. Publications 27. 127 p. + appendices 34 p. ISBN 951-22-6843-4. ISSN 1456-4327. http://www.hut.fi/Yksikot/Rakennus/Teras/Julkaisut/jsarj.html

[Keski-Rahkonen, O. 1998]
KESKI-RAHKONEN, O., *Breaking of Window Glass Close to Fire,* Fire and Materials, Vol 12, pp. 61-69, 1998.

[SFS-ENV 1991-2-4, 1995]
Eurocode 1: Basis of design and actions on structures. Part 2-4: Actions on structures. Wind actions.

[prEN 1990, 2001]
Eurocode: Basis of structural design. Draft, January 2001.

[prEN 13474-1, 1999]
Glass in building – Design of glass panes – Part 1: General basis of design. Draft, January 1999.

[prEN 13474-2, 2000]
Glass in building – Design of glass panes – Part 2: Design for uniformly distributed loads. Draft, February 2000.

EU COST C13 Glass and Interactive Building Envelopes. M. Crisinel, et al. (Eds.). IOS Press, 2007.

Shaping Glass Plate Structures

Ture Wester
Royal Danish Academy of Fine Arts, School of Architecture, Copenhagen, Denmark

Buildings using glass sheets in the load carrying structure is not a new idea. The large and elegant Victorian palm houses from the time of the industrial revolution often used glass sheets as a bracing element for a steel lattice structure. This very appropriate way of using glass in the primary structure has unfortunately disappeared. Glass is recently very slowly being reintroduced as a structural element for beams, walls, columns, as member in steel trusses etc, but very few projects seem to use glass according to its unique properties. Because of the special structural behaviour of glass it seems that optimal shaping of the structures is essential in order to reduce stresses in general and concentrated stresses in particular. The paper will discuss these properties and express the morphological consequences for the shaping, faceting and detailing of structures that are made from glass and other similar types of tiles. A number of Nature's solutions and of projects and ideas will be discussed.

Keywords: cost, glass, morphology, plate structures, shaping, duality.

I. Glass in Nature

Glass (SiO_2 being the main component) is widely used in nature as a material for skeletal force-resistant structures. Organisms like e.g. Radiolaria [Haeckel 1887] and Glass Sponges (Fig. 2) are examples of morphologically highly sophisticated structural configurations. However, these strutures do not use glass sheets. They are built from clusters of specules in such a way that they are comparable to fibre-glass. Nature discovered a long time before we did, that fibre-glass in every way (strength, elasticity, reliability, fragility etc.) is a far better building material than plane glass. The best option for the structural use of glass seems therefore to be as fibres, and it would be of great interest to try to use glass fibre in structures far more extensively than today where it normally appears as reinforcement for plastics and cements, only. But when we talk about the use of glass in building structures we usually mean transparent plane or curved glass

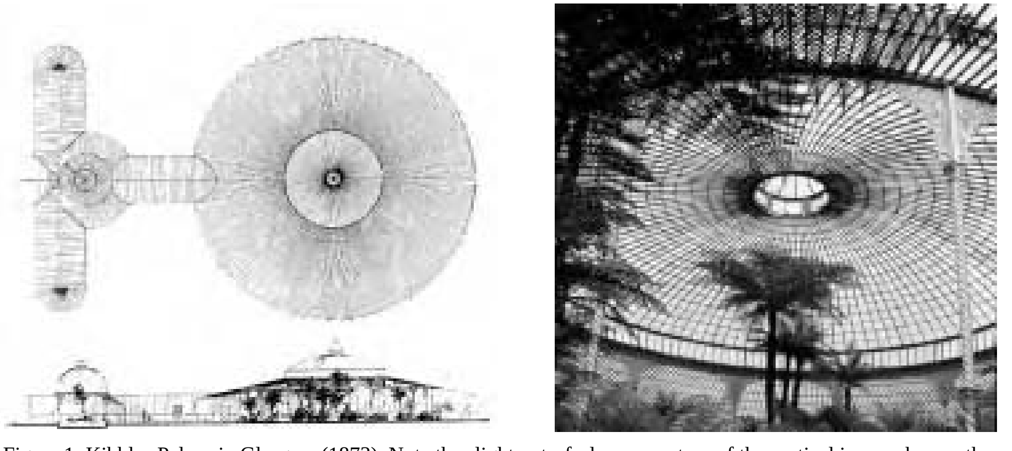

Figure 1: Kibbles Palace in Glasgow (1873). Note the slight out-of-plane curvature of the vertical iron arches on the right photo. This indicates the bracing action of the glass panels.

sheets. However, in nature we find structures built from calcite plates which have almost similar general mechanical properties as glass e.g. coccolithophores [Winter et al.] and seaurchins [Wester 1983] see Fig. 3. Among these we might find inspiration for efficient use of plane glass for structural purposes. Material Properties of Plane Glass

II. Material Properties of Plane Glass

For structural use it is evident to consider tempered or hardened glass as this has much better properties than plain untreated glass. In order to discuss the morphological possibilities for glass structures, it is not necessary to go into details in the field of Material Science. In order to get a rough idea of the properties of plane hardened

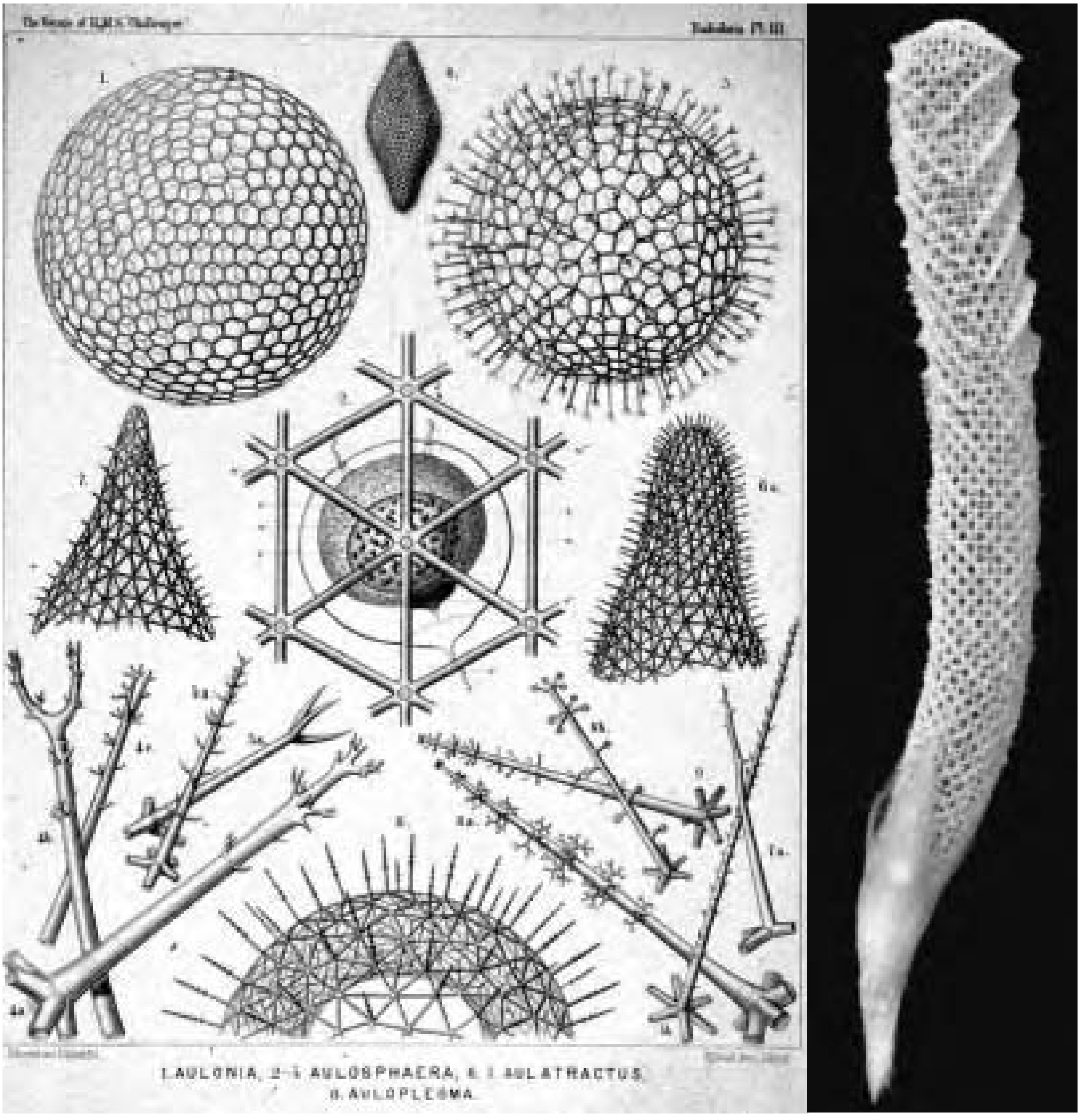

Figure 2: The siliceous marine plankton Radiolaria (left) and a deep sea Glass Sponges (right) show examples of Nature's way of using fibre-glass for its skeletal structure

glass, we can compare it to some well known structural materials:

- It has double the strength of mild steel for compression, but half the strength for tension.
- Its rigidity (E-value) is one third of that of steel, or approximately as aluminium, or 5 times higher than that of wood.
- Thermal expansion, which is important in case of transfer of forces between glass and e.g. the metal frame, is typically 75% of steel or 30% of aluminium, i.e. closest to steel.
- The specific gravity is one third of steel, or approximately the same as aluminium, or 4 times the value for timber.
- The maximum working temperature, i.e. without losing much strength is as for aluminium or half of that of steel.
- The "Achilles' heel" of glass is its brittleness. One of the most appropriate ways to reduce this problem is to laminate two or more glass sheets together. As failure will normally only affect one layer, the other layer(s) must hold enough carrying capacity to prevent failure or the forces must be able to rearrange in the structure until the glass element is replaced.

III. Pure Plate Action

In a similar way of stabilizing a pure lattice (bar-and-node) structure by tension and compression, a pure plate structure (plane plates hinged together along shear lines) can be stabilized by the transfer of shear forces across the shear lines. The well known characteristic pattern for lattice action is the triangle while it is a 3-valent vertex for plate action (Fig. 4). These two configurations are geometrical duals in our 3-dimensional space, i.e. if inter-connected vertices are substituted with equally intersecting planes, a triangle becomes a 3-valent vertex and vice-versa [Wester 1983]. This duality can be extended to the level of statical properties as rigidity, forces and elasticity [Wester 1987].

As it is not the purpose of this paper to go into detail about this, but some of the relevant general results are as follows (see also "further reading"):

A single-layer triangulated structural configuration can only be rigid as a pure lattice structure, and it is rigid if closed (like a ball), even that there are some special non-convex exceptions. The facets are not structurally active and may be removed. Only nodes and bars are needed.

A single-layer structural configuration with only 3-branched vertices can only be rigid as a pure plate structure, and it is rigid if closed (here are also some special non-convex exceptions).

A single-layer configuration which is neither fully triangulated nor fully 3-branched cannot be rigid as a pure plate or as a pure lattice structure, but is rigid (with similar exceptions as above) as a

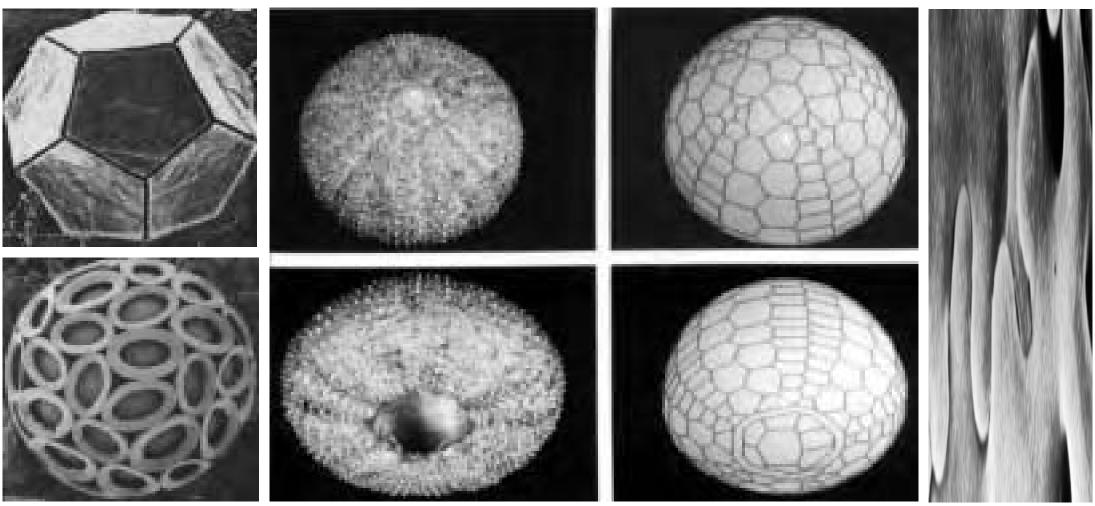

Figure 3: Left column: microscopic coccolithophores (Nishida). Center: macroscopic sea-urchins in a natural and computer version, showing 3-branched vertex pattern which is significant for pure plate action. Right: SEM of the teeth-like shear-resistant suture between plates in a sea-urchin

combined lattice and plate structure, even it may be a sensitive structure.

Pure lattice structures are characterized by having concentrated internal forces in bars and nodes, hence well suitable for the use of strong materials as e.g. steel. Pure plate structures distribute the internal forces along the whole length of the shear lines and the total surface of the plates. Distributed forces are of course much better for the use of glass and other similar two-dimensional structural elements.

This knowledge, embedded in the structural duality, enables plate structures to be generated just as complex as lattice structures are today - in a very simple way. The geometrical transformation, which has the quality to preserve all structural data, is called Polar Reciprocation, and is thoroughly explained in [Cundy et al. 1961] while the structural transformation is explained in [Wester 1987]. In order to handle the geometrical and structural duality, a computer program has been developed, see [Wester]. This method of dual transformations has been used in a number of projects made by the author in collaboration with architects, artists and students, as discussed below.

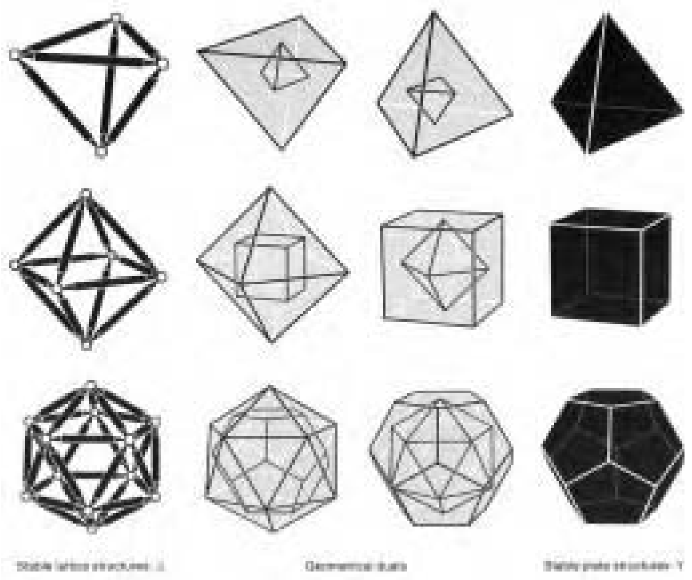

Figure 4: Structural duality follows the well-known geometrical duality. The triangulated polyhedra (tetra-, octa- and icosahedra) are stable by pure lattice action (axial forces in the bars), while the 3-branched (tetra-, hexa- and dodecahedron) are stable by pure plate action i.e. transfer of shear forces across the intersecting lines

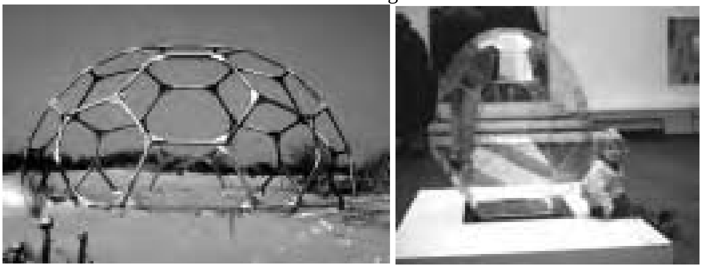

Figure 5: The Bella Dome is a polyhedral pure plate structure with plates as open rigid frames. The openings might be adequately closed by plane glass, which then will overtake the plate action. In fact the wooden frames could then be eliminated, leaving a pure glass plate dome as indicated at the right. This seems to be the ultimate solution for glass structures.

IV. BELLA DOME

Originally the dome in Fig. 5 was suspended from a roof in Bella Centre in Copenhagen for a building exhibition, and later placed on the ground as shown. This 12m diameter and 6m high dome is a class II, frequency 4 of the Cube (or Octahedron) family and is designed by the author in collaboration with architect T. Ebert, Copenhagen. The plate units are rigid closed frames and made from 68*68 mm timber, bevelled on one side to fit the adjacent frame. The triangular frame-knees are made from 19 mm plywood, depressed and glued.

The intention was to open up the plates as much as possible. The open rigid frame structure is strong enough for the original indoor use, but not strong enough as an outdoor structure. The idea was therefore to strengthen the open wooden frames by adding glass plates. In this situation the wooden bars would act as the casement for the glass, and the glass would, as it is much stiffer than the frame, overtake the plate action almost completely.

V. MUSEUM LOUNGE

The very regular polyhedral shapes as the above are often considered 'too mathematical and too regular' and not fit for good architecture. However, these polyhedral shapes may easily be altered to something more appropriate and interesting from an architectural as well as a structural point of view.

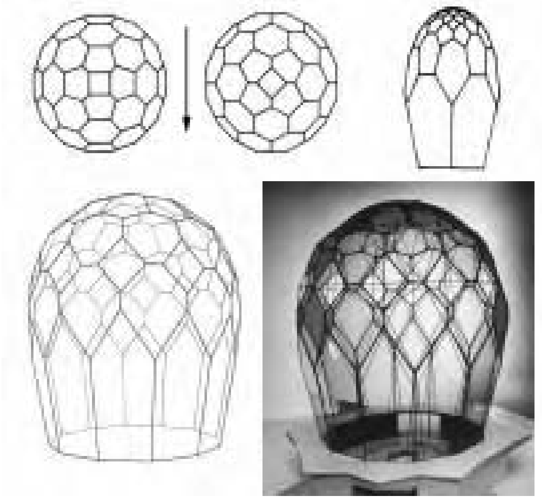

Figure 6: Upper row: class I, frequency 4 cube breakdown has for uniform load in the direction of the arrow an efficiency of 38% (100% is perfect shape for the load). b: The same polyhedron rotated 45 degrees shows an increase of the efficiency to 50%. It is interesting to notice that a spherical polyhedron has a different efficiency when it is rotated. c: Now, the polyhedron is manipulated into a much more interesting configuration and, at the same time, the efficiency has increased to 75%. Lower row: Further manipulation led to the final shape, and finally the physical model.

By geometrical manipulations, CADual can produce a number of different shapes and facets. At the same time it can evaluate the actual configuration from a statical point of view. For given loadings, it can determine the efficiency of the structure, i.e. how close the shape is to the equally loaded kinetic net. This enables an interactive design process, dealing with shapes, faceting and structural behaviour. Fig. 6 shows a procedure for generating structurally and architecturally improved configurations.

The final project was designed in collaboration with the Danish sculptors M. Jørgensen and G. Steenberg for an architectural competition. It was considered whether the glass covering should be structurally active or not, but even if it was absolutely possible, it was chosen to brace the plates by steel rods. Still it gives an appropriate configuration for plane glass used as structural elements.

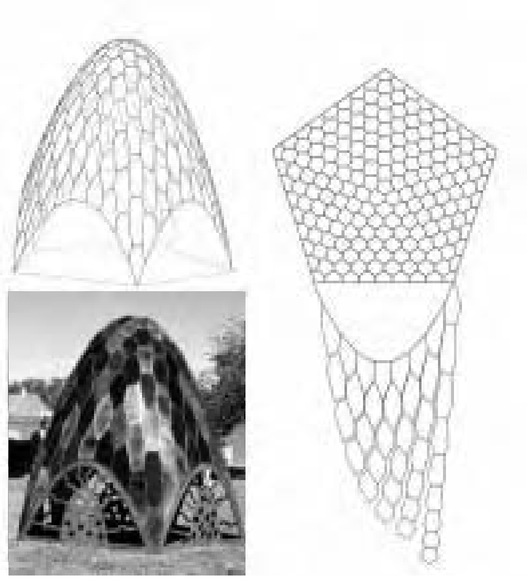

Figure 7: The ceramic dome Pentagonia, the computer model and the cutting pattern for the clay.

VI. PENTAGONIA CERAMIC DOME

This project is based on plane ceramic tiles, which have qualitatively similar properties as glass.

Pentagonia (Fig. 7) is a single layer plate dome-shaped sculpture, 2.8m high and made from 10 to 15mm thick ceramic tiles, its name is derived from the regular pentagonal top tile and ground plan. The thickness of the tiles is greater than needed from a structural point of view but is necessary to prevent warping of the tiles during firing of the clay. To produce the sculpture, clay slabs of the required thickness were cut directly to the cutting pattern generated by CADual. An ordinary sand/cement mortar was used to connect the ceramic tile plates together. Ceramic artists Esben Madsen and Gunhild Rudjord created the form - a paraboloid of revolution - in collaboration with the author. CADual indicated that this form is ideal to resist uniform vertical load - as is close to the distribution of the self-weight of the structure.

As ceramic tiles is in every way are much weaker than glass, it shows at the same time an almost ideal shape and faceting for a pure plate pure glass structure. The investigations by CADual show that shape, faceting and structural properties of Pentagonia makes this configuration quite unique and very appropriate for glass structures. It seems to be the first time that this configuration has been suggested and statically documented. The closest seems to be Gaudi's visionary work with kinetic nets and ceramic tiles [Zerbst 1987], even Gaudi used reversed chain curves and did not use the tiles as structural elements.

VII. Palm House Project

The Pentagonia concept for an ideally shaped glass structure was used as a basis for the final examination project by two B.Sc.(eng.) students [Ohannessian et al. 1991]. The project shows a 30

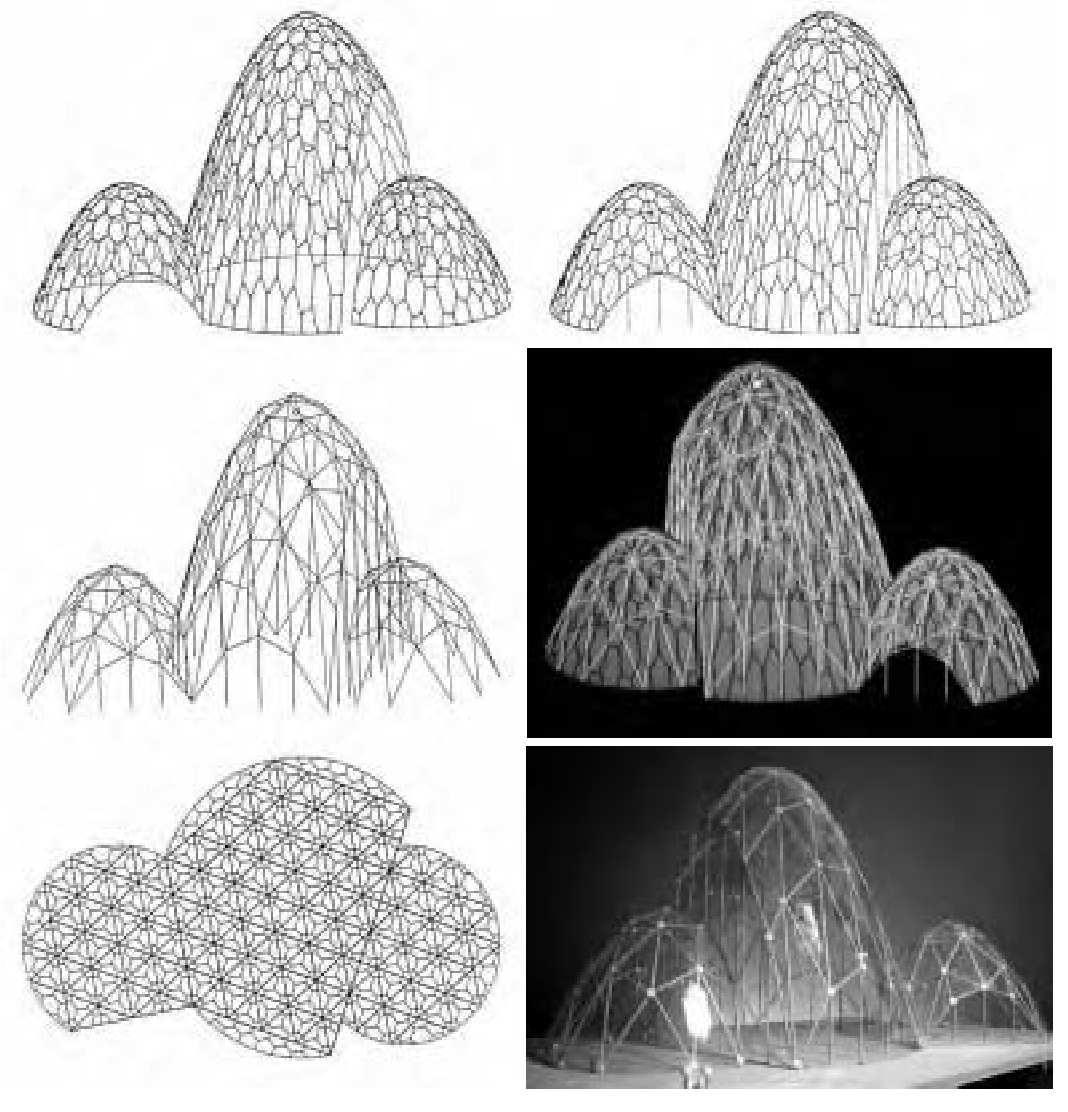

Figure 8: Palm House project. Note the perfect regular pattern for the horizontal projection of the structure

m high botanical glass house (Fig. 8). In order to secure the glass plate structure from progressive collapse in case of breakage of a single glass sheet, the 3-branched fine-meshed glass structure was complemented by a triangulated coarse-meshed steel lattice structure. Both the steel nodes and the glass planes follow the same theoretical paraboloid of revolution with the steel nodes on the surface and the bars inside, whilst the glass plates are all external intersecting tangential planes to the same surface. The apparently quite complicated geometry is generated extremely easily by the Dual Method on CADual.

A well-known problem when building together doubly curved facetted shells are matching along intersections, but the combination of equivalent paraboloids fit perfectly together without awkwardly shaped facets along the intersecting lines. As the glass is a part of the structure and as it is relatively heavy, it is important that the shape is optimised for its self-weight, hence the parabolic form. In the case of wind load on the smooth and aero-dynamic shape combined with the relatively large self-weight, the total efficiency of the shape will only slightly decrease.

As the lattice structure is only introduced for emergency reasons, it can be constructed quite slender.

The structural design showed that all the glass plates might be cut from long glass strips of 2 m width, which is very relevant for glass production. The static analysis resulted in 12mm hardened glass which was laminated on 3 mm soft glass.

The connection between the glass plates was suggested as cogged which is directly inspired by the toothed join between the plates of the sea-urchin.

VIII. Market Hall Project

The same two students continued their studies and finished their M.Sc. with a project [Ohannessian et al. 1993] which was a continuation of the palm house. This time they chose a 16 m tall and 45 m long market hall roof as a different type of combined glass plate and steel lattice structure (Fig. 9). The main parabolic shape is the same as before, but in this structure, the steel and glass structure works intimately together as one structural envelope. The geometry shows quadri-lateral plane plates, four-branched nodes which

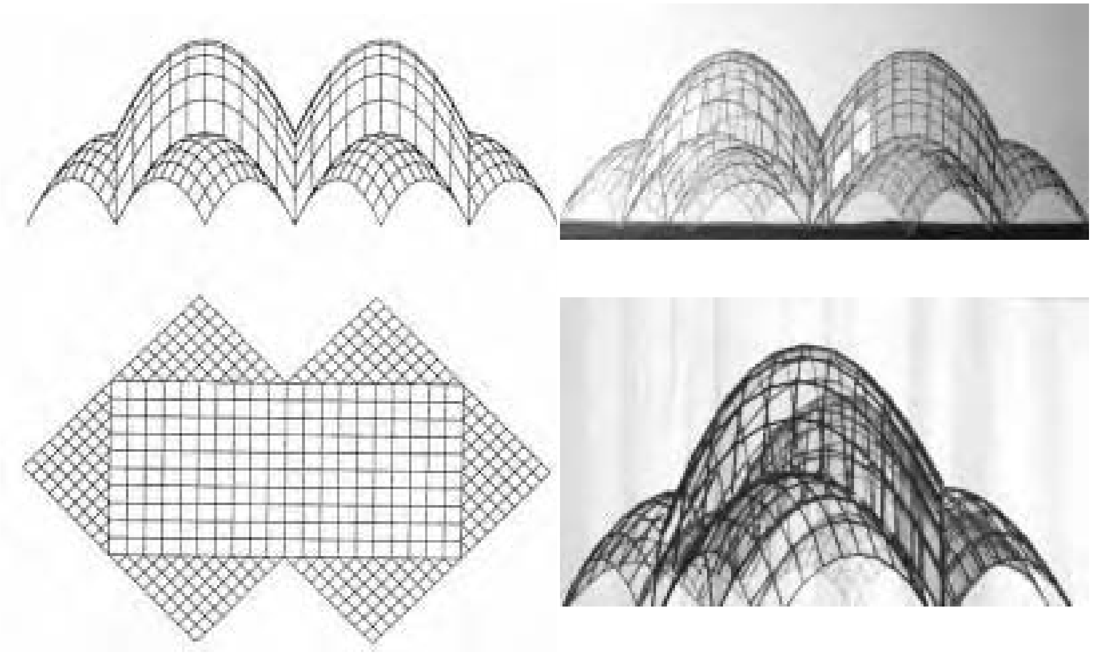

Figure 9: Market Hall project. Note that the horizontal projection creates perfect squares. This project has structural similarities to Kibbles Palace as shown in Fig.1.

give a projection of perfect squares. The hardened glass plates, cut from a 2 m wide glass strip, was calculated to be of 8 mm thickness, laminated with 3 mm ordinary glass. Because of the necessary transfer of forces between glass and steel bars, and because of the different thermal expansion of these two materials, a friction connection as a steel plate fitting with an elastomer as lining and fastened by a prestressed bolt was suggested as a realistic possibility.

IX. CONCLUSION

The projects described in this paper are connected to the author's research on the concept of structural duality and plate action. It has been fascinating to see that these overlooked concepts have led to a deeper insight into Nature's structures as well as suggestions for new and appropriate morphological design and computation of structures made by plane glass sheets.

FURTHER READING

- *A Geodesic Dome-Type Based on Pure Plate Action* , paper in the International Journal of Space Structures, Vol.5 Nos 3 & 4. Special Issue on Geodesic Forms, edited by T.Tarnai, 1990
- *Structural Morphology and Natural Structures* Paper in Evolution of Natural Structures, Part 9. Edited by M.Hilliges. SFB 230, University of Stuttgart and Tübingen, Germany, 1994
- *The Fabulous Paraboloid*: Dual Transformation as a Design Method, paper in *Katachi U Symmetry*, pp. 323-330, Springer Verlag Tokyo 1996
- *The Structural Morphology of Basic Polyhedera*, article in J.F. Gabriel (ed) *Beyond the Cube*, pp. 301-342, John Wiley & Sons, Inc. NY, 1997

REFERENCES

[Cundy et al. 1961]
CUNDY, H.M. AND ROLLET, A.P., *Mathematical Models*, Tarquin Publications, Oxford University Press, 1961

[Haeckel 1887]
HAECKEL, E., *Report on the Radiolaria* collected by H.M.S. Challenger expedition during the years 1873-1876, by Vol. XVIII, 1887

[Ohannessian et al. 1991]
OHANNESSIAN, P, GRUNNET, N., Projektering af en Glasskivekuppel (The Design of a Glass Plate Dome). Final examination project (B.Sc.eng.) at the Danish Engineering Academy, Lyngby, Denmark. In Danish. 1991

[Ohannessian et al. 1993]
OHANNESSIAN, P., GRUNNET, N., Samvirkning mellem Gitter- og Skivekonstruktioner (Co-operation between Plate and Lattice Structures). Final examination project (M.Sc.eng.) at the Danish Technical University, Lyngby, Denmark (in Danish) 1993

[Wester]
WESTER, T., *CADual: Computer Aided Duality*. Royal Academy of Fine Arts, Copenhagen. This software was made for DOS 3.11 and has special requirements for printer etc. This means that it will not run in Windows. Please contact the author for further information.

[Wester 1983]
WESTER, T., *Structural Order in Space*. Royal Danish Academy of Fine Arts. Copenhagen, Denmark, 1983

[Wester 1987]
WESTER, T., *The Plate-Lattice Dualism*, paper in the Proceedings of the IASS Colloquium on Space Structures for Sports Buildings, edited By Lan & Zhilian. Elsevier Applied Science, London, 1987

[Winter et al. 1994]
WINTER, A., SIESSER, W. G. (eds), *Coccolithophores*, Cambridge University Press 1994

[Zerbst 1987]
ZERBST. R., *Antoni Gaudi*. pp.80-81. Taschen Verlag Köln 1987

EU COST C13 Glass and Interactive Building Envelopes. M. Crisinel, et al. (Eds.). IOS Press, 2007.

Construction Practice in Glass Structures

Philip Wilson, Malishev Wilson Engineers, London, UK

The paper gives a summary of various key principles that should be applied to the design of glass elements. Consistency in design can be achieved more easily where there are well-established codes of practice, but the situation with glass is that currently no design standards exist and engineering judgement needs to be applied from first principles. The information in this paper gives an insight into the design of glass structures and might be useful to the practicing engineer as a guide to initial design and detailing. Where there is uncertainty it would always be wise to base the final design on test results.

The application to design problems is referenced to built projects where glass acts as a structural material, starting with early work at Dewhurst Macfarlane and Partners on annealed glass beams, then entire structural frames.

I. Introduction

Glass, being a brittle material, fails abruptly without first yielding or permanent deformation. Failure always results from a tensile component of stress. A key principle is that of redundancy in the event of sudden failure of an element or leaf of glass, due to impact loading or spontaneous fracture by impurities inherent in glass, and to design to avoid the possibility of collapse disproportionate to the cause of breakage. The consequences of such a breakage should be considered and it is often necessary to laminate to provide redundancy.

II. General Principles

A. Soda-lime glass

There are many different glasses produced using chemical compositions appropriate to their application. The majority of sheet glass used in the construction industry is soda-lime glass. This glass has generally a green tint due to the presence of iron in the mix used to lower the melt temperature and to reduce float glass production costs. Some of the properties of soda-lime glass are given in Table 1.

TABLE 1:
PROPERTIES OF SODA-LIME GLASS

Density	2500 kg/m^3
Refractice Index	1.52
Hardness (MoH scale)	6
Youngs Modulus	70 kN/mm^2
Poisson’s ratio	0.23
Coefficient of thermal expansion	7.75 x 10^{-6}/°C

The viscosity of glass increases very rapidly with decreasing temperature. The term glass transition temperature (T_g) has been given to the approximation when glass changes instantly from an infinitely mobile fluid to an elastic solid and is also noted as the ‘annealing point’ as defined in Table 2.

TABLE 2:
TEMPERATURE DATA

Strain point	510°C
Annealing point	555°C
Softening point	740°C

B. Design stresses

The design thickness of glass should be the minimum tolerance allowed for monolithic glass. Standards of production in the UK set the design thickness of 12 mm thick glass as 11.7 mm and for 15 mm and 19 mm thicknesses the design thickness would be 14.5 mm and 18 mm respectively.

The properties of glass have been known for some time, notably the publication by E B Shand

[Shand 1958]. The forthcoming Eurocodes (prEN 13474-1, Glass in Building [prEN 13474-1], currently in draft form, obtained data from 740 samples of 6 mm thick annealed glass from 30 batches from 9 different float plants over Europe tested for bending strength. The range of failure stresses, between 30 N/mm^2 and 120 N/mm^2, was very wide, with a mean of 70 N/mm^2, and no significant variation between different suppliers. Based on these data, the draft Eurocode gives the following characteristic strengths (strength exceeded by 95% of samples tested):

TABLE 3:
CHARACTERISTIC STRENGTHS

Annealed	45 N/mm^2
Heat strengthened	70 N/mm^2
Toughened	120 N/mm^2

For the TIF Yurakucho canopy tests were carried out at City University, London, where the load and reactions for a three-point bending tests were applied to the glass sample through holes in bearing rather than edge loading. Failure in each test was at the extreme fibre and not at the point of loading which may often be the case. Results showed a mean strength of toughened glass as 160 N/mm^2.

A guide to allowable stresses for initial design of glass for short duration loads, based on unfactored loads and using simple elastic formulae, can be taken as the mean failure strength with a factor of safety of 3. The allowable stress for annealed glass can be assumed as 23 N/mm^2 and toughened glass as 53 N/mm^2.

C. *Annealed glass*

Standard thicknesses, in mm, are 3, 4, 6, 8, 10, 12, 15, 19, and 25. Typically the maximum sheet size is 3.0 m x 6.0 m, but 3.2 m x 8.0 m is possible, and larger by special order.

Annealed glass is subject to stress corrosion cracking under long duration loads. This phenomenon is due to chemical corrosion at the tips of surface micro-cracks caused by the action of water, which elongate the crack. There is a threshold stress below which stress corrosion cracking is no longer a significant factor and this is taken as 7 N/mm^2.

Another phenomenon to which annealed glass is vulnerable is thermal shock. This causes cracking due to internal stresses resulting from temperature differences between different parts of the same sheet of glass. The critical temperature difference has been found to be 33°C. The possibility of thermal shock is greatest where parts of the glass are in shadow, within the frame rebate for example, while other parts are exposed to direct sun. If thermal shock is found to be a problem then the glass needs to be specified as heat-strengthened or toughened.

D. *Heat strengthened and toughened glass*

Annealed glass can be tempered by re-heating the glass, to a temperature around 650°C, and then rapidly cooling the outside surface in a carefully controlled manner. The cooling prestresses the outside skin and greatly enhances the capacity of the extreme fibres to resist tensile stress. The magnitude of stress, referred to as ‘residual’ are determined largely by the rate of cooling. Toughened glass is often specified to have a minimum residual surface stress of 100 N/mm^2, and heat strengthened glass to have a minimum residual surface stress of between 40-50 N/mm^2.

Glass thickness for heat strengthening follows annealed glass up to a maximum thickness of 12 mm. For toughened glass all thicknesses are possible although 25 mm thick glass is difficult to toughened adequately. Maximum sheet size depends on the furnace used, and is normally 2.14 m wide and 4.5 m long. Larger tempering furnaces are available up to a maximum of 3.0 m x 6.0 m.

To minimise the risk of spontaneous shattering due to nickel sulphide inclusions, toughened glass may be specified to be heat soaked following toughening. Heat soaking would take place at a temperature of around 280°C. It is important to note that, while heat soaking will minimise the risk of spontaneous shattering, there is still some small residual risk. This spontaneous shattering due to nickel sulphide inclusions is caused by the rapid cooling during toughening inhibiting the phase change of nickel sulphide crystals. It is therefore a phenomenon that is a problem for toughened glass, but not for heat-strengthened glass, where the cooling rate is slower.

E. Laminated glass and interlayers

Interlayers are either in sheet materials, such as PVB (PolyVinylButrly) or polyurethane, or liquid cast resins. The design thickness of a laminated glass depends on the duration of load and the temperature. Following the guidance of the Canadian Code (CAN/CGSB 12.20-M89, Structural design of glass for buildings) [CAN/CGSB 12.20-M89]**,** leaves in glass should be treated as composite only under wind loads and at temperature less than 70 °C. For all other situations, the glass should be treated as two separate leaves, with the load divided between the leaves in proportion to their stiffness. The performance of an interlayer, whether tacting as a composite or layered, is related to the T_g. Generally, when designing in laminated glass, it should be assumed that, under serviceability conditions, when deflection is usually the design criterion, both sheets are acting. When checking for robustness with one sheet failed, the stress in the remaining sheet is important, but not its deflection.

III. CONNECTIONS

In order to go beyond the production limits of a single sheet of flat glass, to support a span of over 5.0m, a connection which links a series of elements becomes necessary and this joint becomes the critical area in the design of the glass structure.

The designer's choice of connection type is based on various criteria, notably strength requirements, adequate tolerance for construction, cost, method of fabrication and aesthetics. The transfer of load through a bearing connection makes use of the high strength capacity of glass and minimises the depth and complexity of the connection. Alternative connections such as friction grip connections result in deeper sections to achieve sufficient moment capacity with a greater number of parts to install on site. However, the bearing detail requires a high level of machining precision in the fabrication of both metal and glass elements.

A. Edge bearing connections

The load transfer between the horizontal glass beam and glass fin is by bearing through an acetal, acrylic or nylon block. The overlaping beam and fin allow for redundancy in the event of failure of a single element. The 'mortise and tenon' joint detail is borrowed from timber construction. An example of this type of construction is the glass conservatory for Tregardock Cottage, Cornwall (1996). The glass beams are each 4.0 m long, and made of 10 mm annealed sheets of triple compound glass. The joint with the 2.2 m vertical fin is similar to a timber 'mortise and tenon' joint, with the two side wings of the beam resting on the two side wings of the fin. This is an adequate method because the joint is not required to resist moment, and the lateral stability is provided through the attachment to the building.

Figure 1: Tregardock Cottage, Cornwall

B. Hole bearing connections

This solution were first developed for the glass canopy of the Yurakucho subway station at the Tokyo International Forum (1996) and followed with the façade of the Samsung Jong-Ro Building (1997) in Seoul, Korea.

The glass canopy is 4.2 m wide with a cantilever span of 11 m. As the maximum length of toughened sheets of glass available at that time in England was 5 m, a series of laminated toughened beams with leaves 19 mm thick are joined together by a bearing connection through holes in each of the beams. The number of beams that overlap increases towards the support, in line with the bending moment and force in each pin connection.

Figure 2: TIF Yurakucho canopy

The key to the design was the method of transferring force at the connections, to ensure that the bearing areas were sufficient and accurately fabricated to prevent high stress concentrations, which would cause failure. The process of toughening the glass puts the whole surface of the glass into compression, including the internal surface of the holes provided. Detailed analysis of the stresses, by using conventional formulae with stress concentration factors, or by finite element analysis, or by physical testing with strain gauges, allows the stress around holes to be accurately determined

Initial tests at a University laboratory on a 48 mm diameter hole in a 19 mm thick toughened glass sample with the load applied in pure tension gave a mean failure capacity of 77 kN. These results compared well with predication by elastic analysis of stress concentrations around holes and led to full scale testing of single and laminated glass beams.

The interlayer material used was a UV cured acrylic resin. Before the glass beams were shipped out to site each individual toughened glass element was fully tested to three times working load.

A similar technology was used for the 50 m x 50 m façade of the Samsung Jong-Ro Building in Soeul, to create 12m long beams. The upper part of the façade is supported by horizontal laminated, toughened glass beams made of two 19 mm thick leaves, which span 12 m between columns. The lower part to the foyer is supported by similar vertical beams made of two 15 mm thick leaves. The weight of the glass is supported by steel hangers.

Figure 3: Full scale testing of glass beam

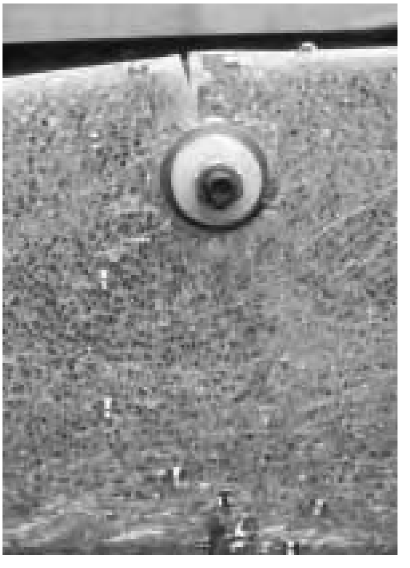

Figure 4: Stress concentrations around hole

Figure 5: Horizontal glass beams span 12m

Load was transferred through square edges holes in contrast to chamfered holes for the Yurakucho canopy.

In order to determine the distribution of load through bushes in laminated glass, tensile tests were carried out an representative samples. With the highest tolerance drilles holes in glass and machined fittings the load sharing between the leaves was 60% to 40% and at worst 85% to 15%. The importance of tight fitting bushes in true circular holes in glass is a major factor in determining the load capacity.

Figure 6: Tensile tests in laminated glass and square edged holes

Other projects where the principle of carrying load through holes in glass include the Transport Stack, Discovery Centre, Birmingham (2000) and the staircase to the Fleming Gallery, London (2001).

Figure 7: Transport Stack, Discovery Centre, Birmingham

Figure 8: Glass sided staircase, Fleming Gallery, London

C. Friction grip connections

These were first pioneered by Pilkington Glass and have been used for many years with single-ply toughened glass. For the Glass Reading Room of the Arab Urban Development Institute in Riyadh, Saudi Arabia (1998) a solution was found to friction-grip laminated glass and overcome the problem of interlayer creep relaxing the bolt tension and hence losing the friction in the long term.

The cube is 8 m x 8 m x 8 m and has no internal structure. Toughened glass beams 2.67 m in length formed of two 15 mm thick leaves were joined using friction grip connectors to create portal frames which carry the glazing loads and provide stability. Because of the high forces that arise when the bolts are tightened, an aluminium spacer of low temper yet creep-resistant was inserted between the glass leaves at the connection.

Figure 9: Glass cube, AUDI, Riyadh

We have found that for these connections attention to detail at manufacturing stage is vital. Key things to watch for are: the steel surfaces at the friction connection must be milled perfectly flat; the fibre gaskets must be used only once and should be made of semi-flex vulcanised fibre; the thickness of aluminium must be carefully matched to the edge tape thickness to provide 5-10% compression to the tape; the joint must be clamped during UV curing of the resin.

Figure 10: Detail of roof construction

D. Compression plates

The use of glass plates in compression presents the possibility of withstanding high loads. The concept of stacked glass plates for a structure over 30 m high was first concieved for the Construction Tower competition (2000). The tower reached 100 ft and comprised 2000 sheets of 15 mm thick annealed glass. Tests on the flatness of glass plates was carried out to determine whether high points could cause the glass to fracture. The structure was both robust and durable as it could withstand breakage of multiple sheets. Chosen as the winning entry the project was never built.

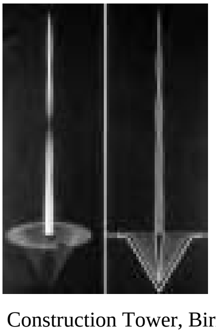

Figure 11: Construction Tower, Birmingham

The same concept was, however, applied to the construction of three stacked glass structures for The Bullring, Birmingham. Internal glass fins and beams restrain the structure from overturning, with all vertical load taken through the annealed glass plates.

Fig 12: Glass and Water feature, St Martins Square, The Bullring, Birmingham

IV. FUTURE DEVELOPMENT

Early tests on double-overlap joints using a cast resin interlayer gave positive results in the short-term. The average failure shear stress of 3.0 N/mm^2 was found to be greater than the figure of 1.1 N/mm^2 reported by the manufacturer. However, creep tests of the resin interlayer, at an elevated temperature of 60°C, gave a poor performance with a delay period of 100 hrs and failure of the sample after 120 hrs, with an applied constant stress of less than 0.1 N/mm^2. The reason for failure can be understood when realised that the T_g for resin interlayers is only 17°C and approximately 20°C for PVB interlayers. The test results were conclusive, under the conditions set, in indicating that the resin laminate overlap joint would not be suitable for the proposed structural design. However, the composite performance of laminates are of special interest to the manufacturers, with DuPont now marketing a higher grade material, Sentry Glas-Plus, of higher stiffness and a T_g of 55°C.

V. Summary

The selection of the connection method depends largely on the tolerance of production processes available. The transfer of load through a bearing connection requires a high level of precision in fabrication.

The work carried out over the last decade has shown that, with suitable attention to detail in both design and construction and by the provision of redundancy by using laminated glass where appropriate, glass can be used as a structural material with adequate safety.

VI. Acknowledgment

Each of the projects mentioned draws upon personal experience while working at Dewhurst Macfarlane and Partners. For that experience I would like to thank Tim Macfarlane for his direction and guidance. Thanks are also due to John Hodgson and Mark Leddra, both at F A Firman (Harold Wood) Ltd, who acted as fabricators for many of the projects, for showing willingness to experiment when it was never sure there would be a definite job.

References

[Shand 1958]
SHAND, E.B., *Glass Engineering Handbook*, 2nd Edition, McGraw-Hill Book Company, New York, USA, 1958.

[CAN/CGSB 12.20-M89]
Structural Design of Glass for Buildings, CAN/CGSB 12.20-M89, Canadian General Standards Board, Canada, 1989.

[prEN 13474-1]
Glass in Building – Design of Glass Panes – Part 1: General basis of design, DRAFT, 1999.

EU COST C13 Glass and Interactive Building Envelopes. M. Crisinel, et al. (Eds.). IOS Press, 2007.

COST Action C13 Glass and Interactive Building Envelopes
Working Group 3 Structural Aspects of Glass

Working Group 3 Activity Report

Michel Crisinel, Chairman COST C13 WG3
Ecole polytechnique fédérale de Lausanne (EPFL)
Steel Structures Laboratory (ICOM) CH-1015 Lausanne, Switzerland

This report gives an overview of the scientific activity of the COST C13 Working Group 3 "Structural Aspects of Glass" of the Action COST C13.

I. WORK ORGANIZATION

The work of the group was prepared during the second and third Management Committee meetings in 2001 and formalized at the fourth Management Committee meeting in Bled (SL) in September 2001 together with the two other working groups WG1 (Architecture and design integration) and WG2 (Quality of interior space). Seven subsequent Working Group 3 meetings took place between November 2001 and April 2005. Contacts were established between the three working groups through the Management Committee meetings, the Workshop in Graz (AT) and the final conference in Bath (UK).

II. LIST OF WORKING GROUP 3 MEETINGS

Preparation		
0.1. Copenhagen (DK)	22-23 January 2001	
0.2. Bath (UK)	7-8 June 2001	
0.3. Bled (SL)	17-18 September 2001	
Meetings		
1. Lausanne (CH)	8-9 November 2001	19 participants
2. Lausanne (CH)	12-13 September 2002	24 participants
3. Graz (AT) *Workshop*	23-24 October 2003	14 participants
4. Prague (CZ)	11-12 March 2004	18 participants
5. Aachen (DE)	2-3 July 2004	14 participants
6. Thessaloniki (GR)	8-9 October 2004	16 participants
7. Bath (UK) *Final Conference*	6-8 April 2005	15 participants

III. LIST OF MEMBERS

The following alphabetic list includes the members, delegates, substitutes, guests, hosts and experts who have participated at least one time in a Working Group 3 meeting.

Name	Country	e-mail
Lambis Baniotopoulos	Greece	ccb@civil.auth.gr
Henry Bardsley	France	Henry.Bardsley@rfr.fr
Andrea Bassetti	Switzerland	aba@luechingermeyer.ch
Pierre Bays	Switzerland	
Jan Belis	Belgium	jan.belis@ugent.be
Fabrice Bernard	France	bernard@ensm-douai.fr
Uwe Bremen	Switzerland	
Michel Crisinel *Chairman 2003-2005*	Switzerland	michel.crisinel@epfl.ch
Laurent Daudeville	France	daudevil@hmg.inpg.fr
Mick Eekhout	The Netherlands	m.eekhout@octatube.nl
Martina Eliasova	Czech Republic	eliasova@fsv.cvut.cz
Michael Fiedler	Austria	michael.fiedler@uibk.ac.at
Sébastien Floury	France	
Martin Fucik	Czech Republic	
Wolfgang Gollner	Austria	wolfgang.gollner@fh-joanneum.at
Matthias Haldimann	Switzerland	matthias.haldimann@epfl.ch
Rudolf Hess	Switzerland	r.hess@uitikon.ch
Jacqueline Houpert	France	jacqueline.houpert@eiffel.fr
Ruth Kasper	Germany	ruth.kasper@stb.rwth-aachen.de
Alexander Kott	Switzerland	kott@ibk.baug.ethz.ch
Klaus Kreher	Switzerland	klaus.kreher@gmx.de
Wilfried Laufs *Chairman 2001-2003*	Germany	wilfried.laufs@gmx.net
Stephen Ledbetter *Chrm Manag. Comm.*	United Kingdom	s.r.ledbetter@bath.ac.uk
Andreas Luible	Switzerland	andreas@luible.name
Tapio Leino	Finland	tapio.leino@vtt.fi
Daniel Meyer	Switzerland	dme@luechingermeyer.ch
Jørgen Munch-Andersen	Denmark	jma@by-og-byg.dk
Jürgen Neugebauer	Austria	office@nemaglas.com
Robert Nijsse	The Netherlands	r.nijsse@abt-consult.nl
Olga Rio	Spain	rio@ietcc.csic.es
Christian Schaur	Austria	christian.schaur@uibk.ac.at
Frank Schneider	Germany	schneider@iwmb.tu-darmstadt.de
Jens Schneider	Germany	j.schneider@goldfisch-fra.de
Olavi Tenhunen	Finland	olavi.tenhunen@hut.fi
Sini Uuttu	Finland	sini.uuttu@lumon.fi
Margarita Vyzantiadou	Greece	
Frantisek Wald	Czech Republic	wald@fsv.cvut.cz
Frank Wellershoff	Germany	f.wellershoff@permasteelisa-ce.de
Ture Wester	Denmark	ture.wester@karch.dk
Philip Wilson	United Kingdom	pwilson@dewmac.com

IV. List of oral contributions during the meetings

1. Lausanne (CH), 8-9 November 2001

Lambis Baniotopoulos (GR)	Response of the aluminium-glass facades under performance
Henry Bardsley (FR)	Development of a limit state design method
Laurent Daudeville (FR)	Failure analysis of joints in structural glass
Michael Fiedler (AU)	Analysis and design of glass structures
Wilfried Laufs (DE)	Glass stability members – design examples and possible future design concepts
Stephen Ledbetter (UK)	Glass/adhesive composite members
Andreas Luible (CH)	Stability of glass load-carrying elements
Tapio Leino (FI)	Faults and damages on glass envelopes
Jørgen Munch-Andersen (DK)	Thoughts about code format and load duration factors
Robert Nijsse (NL)	Strength of glass is a surface determined property, project: Glass bridge Hoofddorp
Jens Schneider (DE)	New experimental results and finite-element-design of single-point fixed plates
Olavi Tenhunen (FI)	Constructions of the Finnish double skin facades
Frank Wellershoff (DE)	Columns, beams, shells / recent projects and research program
Ture Wester (DK)	Innovative Morphological Design of Glass Plate Structures
Philip Wilson (UK)	Bearing detail for the Yurakucho canopy in Tokyo

2. Lausanne (CH) 12-13 September 2002

Olavi Tenhunen (FI)	Measurements in Double Skin Façades and Tests for Specifying Edge Strength of Glass Panes
Ture Wester (DK)	Force Follows Form or The Ignored Importance of Shaping Glass Structures
Jacqueline Houpert (FR)	Built examples of modern steel- glass facades
Andreas Luible (CH)	Stability of Glass Elements and Load Introduction
Klaus Kreher (CH)	Glass and Wood in Structural Glazing – Crack-Distribution in Reinforced Glass
Alexander Kott (CH)	Remaining Structural Capacity of Broken Laminated Safety Glass
Robert Nijsse (NL)	New Glass Connections for a House in Avalon / France
Fabrice Bernard (FR)	Numerical modelling of temper pre-stresses around boreholes
Jens Schneider (DE)	Glass Connections
Frank Wellershoff (DE)	In-plane glass corner connections
Rudolph Hess (CH)	Experiments on glass girders

3. *Graz (AT), Workshop, 23-24 October 2003*

Uwe Bremen (CH)	Modern glass façade case studies: conception, practical design and construction
Ruth Kasper (DE)	European standardisation in structural glass design
Alexander Kott (CH)	Current research activities in Europe
Mike Eekhout (NL)	Research in the structural use of glass
Zenkner & Handel (AT)	Glass structural aspects of several projects

4. *Prague (CZ), 11-12 March 2004*

Lambis Baniotopoulos (GR)	Design of glass facades of steel buildings under dynamic loadings, response of facades in seismic areas
Frank Schneider (DE)	Inelastic behaviour of glass
Sini Uuttu (FIN)	Study of Current Structures in Double-skin Facades
Henry Bardsley (FR)	Connections between the building envelope and the structural framework
Jürgen Neugebauer (AT)	Fastening glass at the sub-construction
Mike Eekhout (NL)	Development in frameless glass connections in experimental projects
Ruth Kasper (DE)	Point bearing elements - Research investigations
Andrea Bassetti (CH)	Geschäftshaus Elsässertor: a case study

5. *Aachen (DE), 2-3 July 2004*

Jan Belis (BE)	Buckling-related problems of glass beams
Jürgen Neugebauer (AT)	Special fixation of the laminated safety glass
Andreas Luible (CH)	Stability of load-carrying glass elements
Ruth Kasper (DE)	Lateral torsional buckling of laminated glass beams
Jürgen Neugebauer (AT)	Pre design of discrete supported glass with the help of interpolation

6. *Thessaloniki (GR), 8-9 October 2004*

Margarita Vyzantiadou (GR)	Interaction of glass and steel - examination of function and morphology by the use of fractal geometry
Stephen Ledbetter (UK)	Cladding structure interaction

V. Presentations at the Final Conference, Bath (UK), 6-8 April 2005

List of papers presented by WG3 members

Mick Eekhout (NL)	Zappi' structures and constructions in 'blob' architecture
Andreas Luible/ Michel Crisinel/ (CH)	Plate buckling of structural glass panels
Matthias Haldimann (CH)	Fracture mechanics modelling and time-dependent reliability of structural glass elements
Martina Eliasova/ Frantisek Wald (CZ)/ Sébastien Floury (FR)	Resistance of glass in contact with different materials
Jürgen Neugebauer (AT)	Broken laminated glass has a risk of falling down
Alexander Kott/ Thomas Vogel (CH)	Structural behaviour of broken laminated safety glass
Frank Wellershoff/ Gerhard Sedlacek (DE)	Glued joints in glass structures
Mauro Overend (UK)	Optimising connections in structural glass
Philip Wilson (UK)	Construction of all-glass structures with external glass frames
Rudolf Hess (CH)	Glass canopy for the office centre of the DZ Bank in Berlin
Michel Crisinel/ Thomas Vollmar (CH)	Glass façade elements with internal fluid flow
Frank Wellershoff/ Gerhard Sedlacek (DE)	Employing the glazing for the stabilization of building envelopes

VI. Short Term Scientific Missions (STSM)

Two short term scientific missions took place in 2004:

Name	**Institution**	**Host Institution**	**Period**
Martina Eliasova	CTU Prague (CZ)	EPF Lausanne (CH)	01–30/06/2004
Konstantinos Chatzinikos	Univ Aristotle, Thessaloniki (GR)	EPF Lausanne (CH)	02–14/12/2004

Martina Eliasova

- Introduction to the main topics of the research of the Steel Structures Lab ICOM: stability, safety and risk analysis of glass structures,
- evaluation of experiments of glass elements under compression,
- discussion about the experimental work in laboratory: initial fracture and related stresses, measurement stresses on the surface of tempered glass,
- participation in experiments of glass beams,
- presentation of a seminar to the Steel Structures Lab members on *experiments on glass members in compression including the behaviour of glass in contact.*

Konstantinos Chatzinikos

- Contribution to the experiments conducted at the Steel Structures Lab ICOM on the structural behaviour of glass elements with internal fluid flow,

- presentation of a seminar to the Steel Structures Lab members on *glass-aluminium facades under seismic and wind loadings*.

VII. INTERNET COLLABORATION

A collaborative website (MS SharePoint) to facilitate the exchange of information and knowledge within WG3 has been established and maintained at EPFL–ICOM. The access is restricted to WG3 members and guests. The presentations given at meetings, the scientific papers published in the Final Report and additional technical resources in connection with the activity of WG3 are available on this website. The complete document exchange of the process of writing, reviewing and publishing the scientific part of the Final Report was made by means of the collaborative website.